

YMP-023-R5
04/02/98

YUCCA MOUNTAIN SITE CHARACTERIZATION PROJECT TECHNICAL DATA INFORMATION

(Check one): ACQUIRED DATA (complete Parts I and II)
Data Tracking Number (DTN): _____

DEVELOPED DATA (complete Parts I, II and III)
Data Tracking Number (DTN): MO9901MWDGFM31.000

PART I Identification of Data

Title/Description of Data: GEOLOGIC FRAMEWORK MODEL VERSION GFM3.1 (THESE DATA SUPERSEDE DATA PREVIOUSLY IDENTIFIED BY DTN: MO9804MWDGFM03.001)

Principal Investigator (PI): CLAYTON, R W
Last Name First and Middle Initials

PI Organization: M&O/WCFS

Qualification Status: Q Non-Q Accepted Governing Plan: SCP

SCPB Activity Number(s): 8.3.1.4.2.3.1

WBS Number(s): 1.2.3.9.5

PART II Data Acquisition/Development Information

Method: REVIEWED BY QAP-SIII-2, REVIEWERS: DAVID C. BUESCH AND RICHARD W. SPENGLER, SOFTWARE: EARTHVISION VERSION 4.0, PROCEDURE: QAP-SIII-3, SCIENTIFIC NOTEBOOKS.

Location(s): VICINITY OF YUCCA MOUNTAIN

Period(s): 9/1/1998 to 1/6/1999
From: MM/DD/YY To: MM/DD/YY

Sample ID Number(s): _____

data cartridge located in file cabinet

PART III Source Data DTN(s)

<u>GS940708314211.035</u>	<u>GS950108314211.003</u>	<u>GS950108314211.006</u>
<u>GS950108314211.001</u>	<u>GS950108314211.004</u>	<u>GS950208314211.013</u>
<u>GS950108314211.002</u>	<u>GS950108314211.005</u>	<u>GS950408314211.018</u>

Comments

CA0005
9902040045 980930
PDR WASTE
WM-11 PDR

Checked by: _____ Signature _____ Date _____

YMP-023-R4
08/31/95

**YUCCA MOUNTAIN SITE CHARACTERIZATION PROJECT
TECHNICAL DATA INFORMATION
CONTINUATION SHEET**

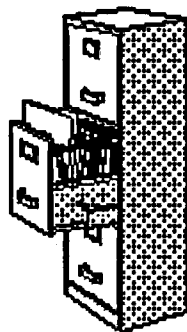
Page 2 of 2

Source Data DTN(s) (continued)

GS950408314211.019
GS950408314211.020
GS950408314211.021
GS960908314224.020
GS970208314224.005
GS970808314221.002
GS970808314224.016
GS981108314224.005
MO9811MWDGFM03.000
SNF40060198001.001
SNF40060298001.001

YUCCA MOUNTAIN SITE DESCRIPTION

BOOK 1 SECTIONS 1,2,3



RECIEVED WITH LETTER DATED 9/30/98
FILE CODE 102.8 ACCESSION # 9902040045

WBS: 1.2.3.9
QA: L

**Civilian Radioactive Waste Management System
Management & Operating Contractor**

BOOK 1 - SECTIONS 1, 2, 3

YUCCA MOUNTAIN SITE DESCRIPTION

B00000000-01717-5700-00019 REV 00

September 1998

**INFORMATION COPY
LAS VEGAS DOCUMENT CONTROL**

Prepared for:

U.S. Department of Energy
Yucca Mountain Site Characterization Office
P.O. Box 30307
North Las Vegas, Nevada 89036-0307

Prepared by:

TRW Environmental Safety Systems Inc.
1261 Town Center Drive
Las Vegas, Nevada 89134-6352

Under Contract Number
DE-AC08-91RW00134

LAS VEGAS DOCUMENT CONTROL
INFORMATION COPY

Disclaimer

This report was prepared as an account of work sponsored by an agency of the United States Government. Neither the United States nor any agency thereof, nor any of their employees, makes any warranty, expressed or implied, or assumes any legal liability or responsibility for the accuracy, completeness, or usefulness of any information, apparatus, product, or process disclosed, or represents that its use would not infringe privately owned rights. Reference herein to any specific commercial product, process, or service by trade name, trademark, manufacturer, or otherwise, does not necessarily constitute or imply its endorsement, recommendation, or favoring by the United States Government or any agency thereof. The views and opinions of authors expressed herein do not necessarily state or reflect those of the United States Government or any agency thereof.

CONTENTS

	Page
1. GEOGRAPHY AND DEMOGRAPHY	1.1-1
1.1 SITE LOCATION AND DESCRIPTION	1.1-1
1.2 POPULATION DISTRIBUTION	1.2-1
1.3 REFERENCES	1.3-1
1.3.1 Documents Cited	1.3-1
1.3.2 Regulations	1.3-2
2. NEARBY INDUSTRIAL, TRANSPORTATION, AND MILITARY FACILITIES ...	2.1-1
2.1 INTRODUCTION	2.1-1
2.2 NEARBY FACILITIES AND ACTIVITIES WITHIN 8 KILOMETERS (5 MILES)	2.2-1
2.3 NEARBY FACILITIES AND ACTIVITIES GREATER THAN 8 KILOMETERS (5 MILES)	2.3-1
2.4 NEARBY TRANSPORTATION ROUTES	2.4-1
2.5 EVALUATION OF POTENTIAL ACCIDENTS	2.5-1
2.6 REFERENCES	2.6-1
2.6.1 Documents Cited	2.6-1
2.6.2 Codes, Standards, and Regulations	2.6-2
3. GEOLOGY	3.1-1
3.1 INTRODUCTION	3.1-1
3.1.1 Regulatory Framework	3.1-2
3.1.2 Key Observations of the Geologic System	3.1-3
3.1.3 Methods of Investigation	3.1-5
3.2 REGIONAL GEOLOGIC SETTING	3.2-1
3.2.1 Tectonic Setting	3.2-1
3.2.1.1 Walker Lane Domain	3.2-2
3.2.1.2 Basin and Range Domain	3.2-2
3.2.1.3 Inyo-Mono Domain	3.2-3
3.2.2 Regional Stratigraphy and Lithology	3.2-3
3.2.2.1 Pre-Cenozoic Rocks	3.2-4
3.2.2.1.1 Precambrian Rocks	3.2-4
3.2.2.1.2 Paleozoic Rocks	3.2-5
3.2.2.1.3 Mesozoic Rocks	3.2-11
3.2.2.2 Cenozoic Rocks	3.2-13
3.2.2.2.1 Tertiary Rocks	3.2-13
3.2.2.2.2 Quaternary Rocks and Sediments	3.2-18
3.2.3 Regional Structure and Tectonic Deformation	3.2-20
3.2.3.1 Compressive Tectonics of the Yucca Mountain Region ...	3.2-20
3.2.3.2 Extensional Tectonics of the Yucca Mountain Region	3.2-26

CONTENTS (Continued)

	Page
3.3 REGIONAL TECTONIC MODELS	3.3-1
3.3.1 Elements and Constraints	3.3-1
3.3.1.1 Yucca Mountain Faulting	3.3-2
3.3.1.1.1 Vertical Axis Rotation	3.3-4
3.3.1.1.2 Basaltic Volcanism	3.3-5
3.3.1.2 Crater Flat Faulting	3.3-6
3.3.1.3 Bare Mountain Fault	3.3-8
3.3.1.4 Eastern Structural Boundary of Crater Flat Basin	3.3-9
3.3.1.4.1 Calico Hills	3.3-9
3.3.1.4.2 Areas East and North of Calico Hills	3.3-10
3.3.1.5 Tectonic Implications of Eruptions in the Southwestern Nevada Volcanic Field	3.3-10
3.3.1.6 Pahute Mesa Faulting	3.3-12
3.3.1.7 Tectonic Stress and Strain in the Yucca Mountain Region .	3.3-12
3.3.2 Evaluation of Tectonic Models	3.3-15
3.3.2.1 Crater Flat-Prospector Pass Caldera Model	3.3-16
3.3.2.2 Simple Shear or Detachment Models	3.3-19
3.3.2.3 Pure Shear Models	3.3-26
3.3.2.4 Lateral Shear Models	3.3-29
3.3.3 A New Tectonic Model for Yucca Mountain	3.3-32
3.4 QUATERNARY STRATIGRAPHY AND SURFICIAL PROCESSES	3.4-1
3.4.1 Regional Physiographic Setting	3.4-1
3.4.1.1 Structural Setting	3.4-1
3.4.1.2 Climatic Setting	3.4-2
3.4.2 Physiographic Setting of Yucca Mountain and Vicinity	3.4-3
3.4.2.1 Description of Major Landform Elements Around Yucca Mountain	3.4-3
3.4.2.2 Influences on Geomorphology	3.4-5
3.4.2.2.1 Tectonics/Faulting	3.4-5
3.4.2.2.2 Volcanology	3.4-5
3.4.3 Surficial Geology	3.4-6
3.4.3.1 Surficial Geologic Mapping in the Yucca Mountain Area ..	3.4-6
3.4.3.2 Geochronology	3.4-8
3.4.3.3 Quaternary Stratigraphy	3.4-10
3.4.3.3.1 Quaternary Deposits, Soils, and Geomorphic Surfaces	3.4-10
3.4.3.3.1.1 Alluvial Deposits and Geomorphic Surfaces .	3.4-11
3.4.3.3.1.2 Colluvial Deposits (Qcu)	3.4-18
3.4.3.3.1.3 Eolian Accumulations on Geomorphic Surfaces	3.4-20
3.4.3.3.1.4 Spring Deposits (late? to middle Pleistocene)	3.4-20
3.4.3.4 Origin of Secondary Carbonate	3.4-20

CONTENTS (Continued)

	Page
3.4.3.4.1	History of the Issue of the Existence of a Potentially Adverse Condition 3.4-21
3.4.3.4.2	Calcite Deposits along Faults, Fractures, and at the Surface 3.4-22
3.4.3.4.2.1	Field Data 3.4-22
3.4.3.4.2.2	Mineralogic and Textural Data 3.4-22
3.4.3.4.2.3	Major- and Trace-Element Data 3.4-24
3.4.3.4.2.4	Stable Isotope Data 3.4-25
3.4.3.4.2.5	Radiogenic Tracer Isotope Data 3.4-26
3.4.3.4.2.6	Paleontological Data 3.4-28
3.4.3.4.2.7	Possibility of Perched Water 3.4-28
3.4.3.4.2.8	Data Pertaining to a Hypogene Origin 3.4-29
3.4.3.4.2.9	National Academy of Sciences' National Research Council Findings 3.4-29
3.4.3.5	Comparison of Regional Quaternary Stratigraphies 3.4-30
3.4.3.6	Distribution of Quaternary Deposits in the Yucca Mountain Area 3.4-31
3.4.4	Paleoenvironmental History of Yucca Mountain 3.4-33
3.4.5	Erosion at Yucca Mountain and Vicinity 3.4-38
3.4.5.1	Erosion and Deposition in the Present Climate 3.4-38
3.4.5.2	Quaternary Erosion on Volcanic Land Forms 3.4-39
3.4.5.3	Erosion Rates at Yucca Mountain 3.4-40
3.4.5.3.1	Hillslope Erosion Rates from Dated Colluvial Boulder Deposits 3.4-41
3.4.5.3.1.1	Cation-Ratio Dating of Hillslope Boulder Deposits 3.4-41
3.4.5.3.1.2	In Situ Cosmogenic Nuclide Dating of Hillslope Boulder Deposits 3.4-42
3.4.5.4	Hillslope Stripping (Erosion) During the Q5 Interval 3.4-44
3.4.5.5	Evolution of Fortymile Wash 3.4-45
3.4.5.6	Incision in Valleys that Directly Overlie the Repository ... 3.4-47
3.5	SITE STRATIGRAPHY 3.5-1
3.5.1	Introduction 3.5-1
3.5.2	Criteria for Differentiating Volcanic Rock Units 3.5-3
3.5.2.1	Lithology, Mineralogy, Geophysical Logs, and Rock Properties 3.5-4
3.5.2.2	Geochemical Criteria 3.5-11
3.5.2.3	Borehole Geophysical Log Characteristics 3.5-13
3.5.3	Stratigraphic Descriptions 3.5-18
3.5.3.1	Pre-Cenozoic Rocks 3.5-19
3.5.3.2	Pre-Lithic Ridge Volcanic Rocks 3.5-19
3.5.3.3	Lithic Ridge Tuff 3.5-19

CONTENTS (Continued)

	Page
3.5.3.4 Dacitic Lava and Flow Breccia	3.5-20
3.5.3.5 Crater Flat Group	3.5-20
3.5.3.5.1 Tram Tuff	3.5-20
3.5.3.5.2 Bullfrog Tuff	3.5-21
3.5.3.5.3 Prow Pass Tuff	3.5-22
3.5.3.6 Calico Hills Formation	3.5-23
3.5.3.7 Paintbrush Group	3.5-24
3.5.3.7.1 Topopah Spring Tuff	3.5-25
3.5.3.7.2 Pah Canyon Tuff	3.5-25
3.5.3.7.3 Yucca Mountain Tuff	3.5-26
3.5.3.7.4 Tiva Canyon Tuff	3.5-26
3.5.3.8 Post Tiva Canyon-Pre-Rainier Mesa Tuffs	3.5-27
3.5.3.9 Timber Mountain Group	3.5-27
3.5.3.9.1 Rainier Mesa Tuff	3.5-27
3.5.3.9.2 Ammonia Tanks Tuff	3.5-28
3.5.3.10 Younger Basalt	3.5-28
3.5.3.11 Surficial Deposits	3.5-28
3.5.4 Correlation of Lithostratigraphic, Hydrogeologic, and Thermal-Mechanical Units	3.5-29
3.6 SITE STRUCTURAL GEOLOGY	3.6-1
3.6.1 Introduction	3.6-1
3.6.2 Geologic Mapping: Structural Framework	3.6-3
3.6.2.1 History	3.6-3
3.6.2.2 Approach	3.6-4
3.6.2.3 Site Area Structure	3.6-4
3.6.2.3.1 Hierarchy of Faulting	3.6-4
3.6.2.3.2 Structural Domains	3.6-5
3.6.2.3.3 Timing of Deformation	3.6-12
3.6.2.3.3.1 Stratigraphic Relations Across Faults	3.6-13
3.6.2.3.3.2 Angular Discordance Across Unconformities	3.6-15
3.6.2.3.3.3 Vertical-axis Rotations	3.6-18
3.6.2.3.3.4 Fault Slip Analyses	3.6-18
3.6.2.3.3.5 Sequential Joint Formation and Relation to Site Scale Structural Evolution	3.6-19
3.6.2.3.4 Summary of Timing of Deformation	3.6-21
3.6.2.4 Central Block Structural Framework	3.6-22
3.6.2.4.1 Prominent Intra-block Faults in the Central Block-Distribution and Geometry	3.6-23
3.6.2.4.1.1 Ghost Dance Fault	3.6-23
3.6.2.4.1.2 Sundance Fault	3.6-24
3.6.2.4.1.3 Diabolus Ridge Fault	3.6-26

CONTENTS (Continued)

	Page
3.6.2.4.2	Structural Geology of the Yucca Crest Sub-block 3.6-27
3.6.2.5	Site Scale Geophysical Investigations of Yucca Mountain Structure 3.6-30
3.6.3	Fractured Rock Mass Studies 3.6-33
3.6.3.1	Types of Fracture Studies 3.6-34
3.6.3.1.1	Fracture Data from Surface Exposures 3.6-34
3.6.3.1.2	Fracture Data from Subsurface Exposures in the Exploratory Studies Facility 3.6-35
3.6.3.1.3	Fracture Data from Boreholes 3.6-36
3.6.3.2	Comparison of Data Collection Methods 3.6-37
3.6.3.3	Fracture Attributes of Lithostratigraphic Units 3.6-37
3.6.3.3.1	Tiva Canyon Tuff 3.6-37
3.6.3.3.2	Lithostratigraphic Units Equivalent to the PTn Hydrogeologic Unit 3.6-38
3.6.3.3.3	Topopah Spring Tuff 3.6-40
3.6.3.3.4	Calico Hills Formation 3.6-42
3.6.3.3.5	Bullfrog Tuff 3.6-42
3.6.3.4	Fracture Intensity 3.6-42
3.6.3.5	Fracture Connectivity 3.6-43
3.6.3.6	Structural Controls on Fracture Network Properties 3.6-44
3.6.3.6.1	Fracture Intensity Near Fault Zones 3.6-44
3.6.3.6.2	Links Between Discontinuous Faults and the Fracture Network 3.6-46
3.6.3.7	Spatial Variability of Fracture Properties 3.6-47
3.6.3.8	Correlation of Small Scale Structures from the Surface to the Subsurface 3.6-49
3.6.3.9	Structural Evidence for Fast Hydrologic Pathways from Studies of ³⁶ Cl 3.6-50
3.6.4	Structural Model for Yucca Mountain 3.6-51
3.6.4.1	Descriptive Structural Model 3.6-52
3.6.4.2	Genetic Controls on Structural Geometry 3.6-57
3.7	SITE GEOENGINEERING PROPERTIES 3.7-1
3.7.1	Introduction 3.7-1
3.7.1.1	Stratigraphic Framework For Testing 3.7-1
3.7.1.2	Geographic Distribution of Data 3.7-4
3.7.1.3	Use of Data for Three-Dimensional Rock Properties Modeling 3.7-4
3.7.2	Rock Structure 3.7-5
3.7.2.1	Rock Structural Data from Surface Mapping, Underground Mapping and Geophysical Studies 3.7-5
3.7.2.2	Rock Structural Data From Boreholes 3.7-7
3.7.2.2.1	Core Recovery 3.7-7

CONTENTS (Continued)

	Page
3.7.2.2.2	Rock Quality Designation 3.7-8
3.7.2.2.3	Rock Weathering 3.7-9
3.7.2.2.4	Rock Hardness 3.7-10
3.7.2.2.5	Fracture Data 3.7-10
3.7.2.3	Potential Key Blocks in Underground Excavations 3.7-11
3.7.3	Laboratory Properties of Intact Rock 3.7-12
3.7.3.1	Physical Properties 3.7-12
3.7.3.1.1	Density and Porosity 3.7-12
3.7.3.1.2	Mineralogy 3.7-13
3.7.3.2	Thermal Properties 3.7-16
3.7.3.2.1	Thermal Conductivity 3.7-16
3.7.3.2.2	Thermal Expansion 3.7-19
3.7.3.2.3	Heat Capacity 3.7-23
3.7.3.3	Mechanical Properties 3.7-24
3.7.3.3.1	Static and Dynamic Elastic Constants 3.7-24
3.7.3.3.2	Compressive Strength 3.7-26
3.7.3.3.3	Unconfined Compressive Strength 3.7-26
3.7.3.3.4	Confined Compressive Strength 3.7-28
3.7.3.3.5	Tensile Strength 3.7-29
3.7.3.3.6	Shear Strength 3.7-29
3.7.3.3.7	Time-Dependent (Creep) Behavior 3.7-29
3.7.3.3.8	Hardness 3.7-30
3.7.3.3.9	Correlations and Parametric Effects for Mechanical Properties 3.7-30
3.7.3.3.10	Mechanical Properties of Fractures 3.7-32
3.7.4	Rock Mass Properties 3.7-33
3.7.4.1	Rock Mass Classification 3.7-34
3.7.4.2	Rock Mass Thermal Properties 3.7-38
3.7.4.3	Rock Mass Mechanical Properties 3.7-40
3.7.4.3.1	Rock Mass Strength 3.7-40
3.7.4.3.2	Rock Mass Elastic Moduli 3.7-43
3.7.5	In Situ Stress Conditions 3.7-44
3.7.6	Excavation Characteristics of the Rock Mass 3.7-46
3.7.6.1	Excavation Methods 3.7-46
3.7.6.2	Excavation Characteristics 3.7-48
3.7.6.2.1	Rock Bolt Load 3.7-48
3.7.6.2.2	Portal Girder Deformation 3.7-49
3.7.6.2.3	Steel Set Deformation 3.7-49
3.7.6.2.4	Installed Ground Support versus Rock Mass Quality Projections 3.7-49
3.7.7	Engineering Properties of Surficial Material 3.7-50
3.7.7.1	Surficial Sedimentary Deposits 3.7-50
3.7.7.2	Surface Soil Investigations 3.7-50

CONTENTS (Continued)

	Page
3.9.4 Eruptive and Subsurface Effects of Basaltic Volcanism	3.9-12
3.9.4.1 Analog Studies of Eruptive Centers	3.9-12
3.9.4.2 Effects of Basalt Intrusions on Silicic Tuffs	3.9-13
3.9.5 Volcanic Hazard Calculations	3.9-15
3.9.5.1 Recurrence Rate	3.9-15
3.9.5.2 Disruption Probability	3.9-15
3.9.5.3 Probability of Magmatic Disruption of a Repository	3.9-17
3.9.5.4 Probabilistic Volcanic Hazard Assessment	3.9-17
3.10 SEISMICITY AND SEISMIC HAZARDS	3.10-1
3.10.1 Earthquake Record	3.10-2
3.10.1.1 Prehistoric Earthquake Record	3.10-2
3.10.1.2 Historical Earthquake Record	3.10-3
3.10.2 Historical Seismicity of the Yucca Mountain Region	3.10-3
3.10.2.1 History of Seismographic Network Monitoring	3.10-4
3.10.2.2 Historical Seismicity Catalog for Yucca Mountain	3.10-5
3.10.2.3 Significant Earthquakes and Earthquake Sequences	3.10-7
3.10.2.4 Areas of Significant Seismicity	3.10-12
3.10.3 General Features of the Instrumental Seismicity in the Southern Great Basin	3.10-15
3.10.3.1 Seismogenic Depths	3.10-15
3.10.3.2 Focal Mechanisms	3.10-16
3.10.4 Seismicity in the Vicinity of Yucca Mountain	3.10-17
3.10.4.1 The 1992 Little Skull Mountain Sequence	3.10-18
3.10.4.2 Earthquakes in the Rock Valley Area	3.10-19
3.10.4.3 1995-1996 Microearthquakes at Yucca Mountain	3.10-20
3.10.5 Induced and Triggered Seismicity	3.10-20
3.10.5.1 Earthquakes Triggered by Underground Nuclear Explosions	3.10-21
3.10.5.2 Other Triggered Earthquakes	3.10-21
3.10.5.3 Lake Mead Area	3.10-22
3.10.6 Prehistoric Earthquakes at Yucca Mountain	3.10-23
3.10.6.1 Prehistoric Earthquake Data	3.10-23
3.10.6.2 Fault Slip Rates	3.10-26
3.10.6.3 Timing of Surface-Displacement Events and Possible Distributive Rupture Scenarios	3.10-28
3.10.6.4 Displacements Per Event	3.10-31
3.10.6.5 Rupture Length Constraints	3.10-32
3.10.6.6 Recurrence Intervals	3.10-34
3.10.6.7 Magnitude Distribution	3.10-35
3.10.6.8 Descriptions of Known and Suspected Quaternary Faults in the Yucca Mountain Region	3.10-37
3.10.7 Relevant Earthquake Sources	3.10-56

CONTENTS (Continued)

	Page
3.10.8 Estimation of Vibratory Ground Motion	3.10-57
3.10.8.1 Key Seismologic Parameters	3.10-58
3.10.8.2 Strong Motion Attenuation in Extensional Regimes	3.10-61
3.10.8.3 Little Skull Mountain Earthquake Ground Motions	3.10-63
3.10.8.4 Scenario Earthquake Modeling Project	3.10-64
3.10.8.5 Ground Motion Characterization Supporting the Probabilistic Seismic Hazard Analyses Project	3.10-67
3.10.9 Probabilistic Seismic Hazard Analyses	3.10-70
3.10.9.1 Probabilistic Seismic Hazard Analyses Methodology	3.10-71
3.10.9.2 Seismic Source Characterization for Vibratory Ground Motions	3.10-73
3.10.9.3 Vibratory Ground Motion Hazard	3.10-78
3.10.9.4 Fault Displacement Characterization	3.10-79
3.10.9.5 Fault Displacement Hazard	3.10-81
3.10.10 Deterministic Seismic Hazard Analysis of Potential Type I Faults at Yucca Mountain	3.10-82
3.10.10.1 Methods	3.10-83
3.10.10.2 Deterministic Magnitudes-Ground Motions and Revised Potential Type I Faults	3.10-84
3.11 NATURAL RESOURCES	3.11-1
3.11.1 Introduction	3.11-1
3.11.1.1 Objectives	3.11-1
3.11.1.2 Regulations and Regulatory Guidance	3.11-1
3.11.1.3 Previous Project Studies	3.11-2
3.11.1.4 Assumptions, Methods, and Procedures	3.11-3
3.11.1.5 Quality Assurance Procedures Used	3.11-4
3.11.2 Metallic Mineral Resources	3.11-4
3.11.2.1 Introduction	3.11-4
3.11.2.1.1 Purpose	3.11-4
3.11.2.1.2 Previous Work	3.11-5
3.11.2.2 Methods of Study	3.11-7
3.11.2.2.1 Literature Search	3.11-7
3.11.2.2.2 Field Work	3.11-7
3.11.2.2.3 Sample Analysis	3.11-8
3.11.2.2.4 Statistical Analysis of Geochemical Data ..	3.11-8
3.11.2.2.5 Petrographic and Mineralogic Work	3.11-9
3.11.2.2.6 Remote Sensing	3.11-9
3.11.2.3 Metal Mining and Prospecting History	3.11-10
3.11.2.4 Metallic Mineralization in Southern Nevada/California ..	3.11-11
3.11.2.5 Mining and Prospecting in the Yucca Mountain Conceptual Controlled Area	3.11-12

CONTENTS (Continued)

	Page	
3.11.2.6	Metallic Mineral Assessment of the Yucca Mountain Conceptual Controlled Area	3.11-12
3.11.2.6.1	Identified Metallic Resources in the Yucca Mountain Conceptual Controlled Area . . .	3.11-12
3.11.2.6.2	Evaluation of the Yucca Mountain Conceptual Controlled Area for Undiscovered Metallic Mineral Deposits .	3.11-14
3.11.2.6.3	Models of Potential Metallic Mineral in the Yucca Mountain Conceptual Controlled Area	3.11-14
3.11.2.6.4	Commodities and Deposit Types Not Considered	3.11-16
3.11.2.6.5	Comparison of the Geology of the Yucca Mountain Conceptual Controlled Area with Mineralized Areas in the Region	3.11-16
3.11.2.6.5.1	Stratigraphy	3.11-16
3.11.2.6.5.2	Structure	3.11-17
3.11.2.6.5.3	Alteration	3.11-18
3.11.2.6.6	Geophysics	3.11-20
3.11.2.6.6.1	Metallic Mineral Exploration Strategy . . .	3.11-21
3.11.2.6.7	Remote Sensing	3.11-24
3.11.2.6.8	Geochemistry	3.11-25
3.11.2.6.8.1	Trace Element Frequency Distributions . . .	3.11-25
3.11.2.6.8.2	Statistical Analyses	3.11-27
3.11.2.6.8.3	Specific Mineralogic, Lithologic, and Trace Element Associations in the Yucca Mountain Conceptual Controlled Area	3.11-33
3.11.2.6.8.4	Mercury and Gold in Surface Calcrete, Silica, and Fault Gouge	3.11-35
3.11.2.6.8.5	Trace Elements in Fumarolic Deposits, Paintbrush Tuff	3.11-37
3.11.2.6.8.6	Veins in Tertiary Volcanic Rocks in the Subsurface	3.11-40
3.11.2.6.8.7	Pyritic Tuff	3.11-45
3.11.2.6.8.8	Gold and Gold Pathfinders in Paleozoic Carbonate Rock	3.11-50
3.11.2.6.9	Uranium at Yucca Mountain	3.11-52
3.11.2.7	Conclusions	3.11-55
3.11.2.8	Summary	3.11-56

CONTENTS (Continued)

	Page
3.11.3 Industrial Rocks and Minerals Resources	3.11-59
3.11.3.1 Methodology for Industrial Minerals Assessment	3.11-59
3.11.3.2 Industrial Rocks and Minerals Classifications (Models) ..	3.11-59
3.11.3.3 Industrial Minerals in the Great Basin	3.11-60
3.11.3.4 Industrial Rocks and Minerals at Yucca Mountain	3.11-61
3.11.3.4.1 Barite	3.11-61
3.11.3.4.1.1 Barite Occurrences at Yucca Mountain ...	3.11-61
3.11.3.4.1.2 Economics of Barite Resources at Yucca Mountain	3.11-61
3.11.3.4.2 Building Stone	3.11-62
3.11.3.4.2.1 Building Stone Occurrences at Yucca Mountain	3.11-62
3.11.3.4.2.2 Economics of Building Stone Resources at Yucca Mountain	3.11-62
3.11.3.4.3 Clay	3.11-63
3.11.3.4.3.1 Clay Occurrences at Yucca Mountain	3.11-63
3.11.3.4.3.2 Economics of Clay Resources at Yucca Mountain	3.11-63
3.11.3.4.4 Construction Aggregate	3.11-64
3.11.3.4.4.1 Construction Aggregate Occurrences at Yucca Mountain	3.11-64
3.11.3.4.4.2 Economics of Construction Aggregate at Yucca Mountain	3.11-64
3.11.3.4.5 Fluorite	3.11-65
3.11.3.4.5.1 Fluorite Occurrences and Resources at Yucca Mountain	3.11-65
3.11.3.4.5.2 Potential for Fluorite Resources at Yucca Mountain	3.11-65
3.11.3.4.6 Limestone	3.11-65
3.11.3.4.6.1 Limestone Occurrences at Yucca Mountain	3.11-65
3.11.3.4.6.2 Economics of Limestone Resources at Yucca Mountain	3.11-65
3.11.3.4.7 Pumice	3.11-66
3.11.3.4.7.1 Pumice Occurrences at Yucca Mountain .	3.11-66
3.11.3.4.7.2 Economics of Pumice Resources at Yucca Mountain	3.11-66
3.11.3.4.8 Silica	3.11-66
3.11.3.4.8.1 Silica Occurrences at Yucca Mountain ...	3.11-66
3.11.3.4.8.2 Economics of Silica Resources at Yucca Mountain	3.11-67

CONTENTS (Continued)

	Page
3.11.3.4.9 Vitrophyre/Perlite	3.11-67
3.11.3.4.9.1 Vitrophyre/Perlite Occurrences at Yucca Mountain	3.11-67
3.11.3.4.9.2 Economics of Perlite Resources at Yucca Mountain	3.11-68
3.11.3.4.10 Zeolites	3.11-68
3.11.3.4.10.1 Zeolite Occurrences at Yucca Mountain ..	3.11-68
3.11.3.4.10.2 Economic Resources of Zeolite at Yucca Mountain	3.11-69
3.11.3.5 Industrial Rocks and Minerals Resources Conclusions ...	3.11-70
3.11.4 Hydrocarbon Resources	3.11-70
3.11.4.1 Previous Studies of Hydrocarbon Resources	3.11-70
3.11.4.2 Hydrocarbon Genetic Models	3.11-71
3.11.4.3 Exploration History in the Great Basin-Chronology of Activity and Evolution of Concepts	3.11-72
3.11.4.3.1 The Railroad Valley Model	3.11-74
3.11.4.3.2 Exploration Results and Viability of Exploration Concepts	3.11-75
3.11.4.4 Source Rocks	3.11-76
3.11.4.4.1 Source Rocks of Great Basin Producing Areas	3.11-76
3.11.4.4.1.1 Proven Source Rocks, Great Basin	3.11-76
3.11.4.4.1.2 Potential Source Rocks, Great Basin	3.11-77
3.11.4.4.1.3 Chemical Analysis of Great Basin Source Rocks	3.11-77
3.11.4.4.2 Source Rocks of Southern Nevada	3.11-77
3.11.4.4.2.1 Eleana Formation	3.11-78
3.11.4.4.2.2 Chainman Shale	3.11-78
3.11.4.4.2.3 Joshua Hollow and Other Tertiary Strata ..	3.11-78
3.11.4.4.3 Source Rocks at Yucca Mountain	3.11-79
3.11.4.4.3.1 Paleozoic Strata	3.11-79
3.11.4.4.3.2 Tertiary Strata	3.11-79
3.11.4.5 Reservoir Rocks	3.11-79
3.11.4.5.1 Reservoir Rocks of the Great Basin Producing Areas	3.11-79
3.11.4.5.2 Reservoir Rocks in Southern Nevada	3.11-80
3.11.4.5.3 Reservoir Rocks of Yucca Mountain	3.11-80
3.11.4.6 Seals	3.11-82
3.11.4.6.1 Seals of Great Basin Producing Areas	3.11-82
3.11.4.6.1.1 Seal at Base of Valley Fill	3.11-83
3.11.4.6.1.2 Seal at Base of Tertiary Strata	3.11-83
3.11.4.6.1.3 Other Seals	3.11-84

CONTENTS (Continued)

	Page
3.11.4.6.1.4 Seals of Yucca Mountain Area	3.11-84
3.11.4.7 Traps in Great Basin Producing Areas	3.11-84
3.11.4.7.1 Description of Proven Great Basin Trap Types	3.11-84
3.11.4.7.2 Description of Unproven Great Basin Trap Types	3.11-85
3.11.4.7.3 Thrust-fold Traps of Mesozoic Age	3.11-85
3.11.4.7.4 Basin-Range Traps	3.11-86
3.11.4.8 Age of Petroleum-Influencing Structures in the Great Basin	3.11-88
3.11.4.8.1 Antler Structures	3.11-88
3.11.4.8.2 Late Paleozoic-Mesozoic Compression ...	3.11-88
3.11.4.8.3 Tertiary Extensional Structures	3.11-89
3.11.4.9 Structural Comparison of Railroad Valley/Pine Valley to Yucca Mountain Area	3.11-89
3.11.4.10 Timing and Generation (Maturity) in Southern Nevada ..	3.11-90
3.11.4.10.1 Distribution in Time	3.11-90
3.11.4.10.1.1 Pre-Neogene Episodes of Generation	3.11-90
3.11.4.10.1.2 Neogene Episode of Generation	3.11-90
3.11.4.10.2 Distribution in Space	3.11-91
3.11.4.10.2.1 Distribution of Generation Sites with Paleozoic Source Rocks	3.11-91
3.11.4.10.2.2 Distribution of Generation Sites with Tertiary Source Rocks	3.11-92
3.11.4.11 Summary Comparison of Yucca Mountain to Great Basin Producing Area	3.11-92
3.11.4.12 Description of Estimated Oil and Gas Resources	3.11-94
3.11.4.13 Tar Sands	3.11-95
3.11.4.13.1 Tar Sands Description and Models	3.11-95
3.11.4.13.2 Tar Sands in the Southern Great Basin ...	3.11-96
3.11.4.13.3 Tar Sands in Southern Nevada	3.11-96
3.11.4.14 Oil Shale	3.11-97
3.11.4.14.1 Oil Shale Description and Models	3.11-97
3.11.4.14.2 Oil Shale in the Southern Great Basin	3.11-98
3.11.4.14.3 Oil Shales in Southern Nevada	3.11-98
3.11.4.14.4 Oil Shale at Yucca Mountain	3.11-99
3.11.4.15 Coal	3.11-99
3.11.4.15.1 Coal Descriptions and Model	3.11-99
3.11.4.15.2 Coal in the Southern Great Basin	3.11-99
3.11.4.15.3 Coal in Southern Nevada	3.11-100
3.11.4.15.4 Coal at Yucca Mountain	3.11-101
3.11.4.16 Conclusions - Hydrocarbon Potential of the Yucca Mountain Area	3.11-102

CONTENTS (Continued)

	Page
3.11.4.17 Favorability for Tar Sands at Yucca Mountain	3.11-103
3.11.4.18 Favorability for Oil Shale at Yucca Mountain	3.11-104
3.11.4.19 Favorability for Coal at Yucca Mountain	3.11-104
3.11.5 Geothermal Resources	3.11-105
3.11.5.1 Geothermal Resource Definition, Classification, and Historical Development	3.11-105
3.11.5.1.1 Temperature	3.11-105
3.11.5.1.2 Geochemistry	3.11-105
3.11.5.1.2.1 Dissolved Constituents	3.11-105
3.11.5.1.2.2 Stable Isotopes	3.11-105
3.11.5.1.3 Depth, Volume, and Permeability	3.11-106
3.11.5.2 Methodology of Study	3.11-106
3.11.5.2.1 Assumptions	3.11-107
3.11.5.2.2 Methods of Analysis and Associated Uncertainties	3.11-107
3.11.5.2.2.1 Chemical Geothermometers	3.11-107
3.11.5.2.2.2 SiO ₂ versus Enthalpy Diagrams	3.11-108
3.11.5.2.2.3 Geophysics	3.11-109
3.11.5.3 Historical Developments	3.11-109
3.11.5.4 Conceptual Model of Geothermal Systems	3.11-110
3.11.5.5 Geothermal Resources of the Great Basin	3.11-111
3.11.5.5.1 Structure	3.11-112
3.11.5.5.2 Geothermal Models	3.11-112
3.11.5.6 Geothermal Potential at Yucca Mountain	3.11-112
3.11.5.6.1 Discussion on Lack of a Heat Source ...	3.11-112
3.11.5.6.2 Heat Flow at the Nevada Test Site	3.11-113
3.11.5.6.3 Hydrology and Heat Flow	3.11-113
3.11.5.6.4 Temperature Gradient Logs	3.11-114
3.11.5.6.5 Indirect Observations of Potential Geothermal Systems	3.11-114
3.11.5.6.5.1 Thermal Springs and Spring Deposits ...	3.11-114
3.11.5.6.5.2 Indications from Stable Isotope Geochemistry	3.11-115
3.11.5.6.5.3 Indications from Chemical Geothermometers	3.11-115
3.11.5.7 Gravity Data Indications	3.11-116
3.11.5.8 Economics of Geothermal Resources	3.11-116
3.12 REFERENCES	3.12-1
3.12.1 Documents Cited	3.12-1
3.12.2 Codes, Standards, and Regulations	3.12-132
3.12.3 Procedures	3.12-134

PREFACE

The *Yucca Mountain Site Description* (Site Description) presents our current understanding of the natural system at Yucca Mountain. The natural system is being characterized because of its key role in establishing the ability of the proposed repository at Yucca Mountain to demonstrate a safety case for the preclosure and postclosure periods. The natural system forms the environment for which engineered barriers must be designed. Working in concert, the natural and engineered systems must provide reasonable assurance that the health and safety of the public will be protected.

The safety strategy for the proposed repository relies on a number of key attributes of the natural and engineered systems at Yucca Mountain. These attributes are:

- The combined systems will limit water contacting the waste packages.
- The lifetime of the waste packages will be long.
- The rate of release of radionuclides from the waste form will be slow.
- The concentration of radionuclides will be reduced as they are transported through the engineered and natural barriers.

Site characterization activities have, in large part, addressed the scientific underpinnings of these attributes. They have focused on producing an adequate understanding of the natural system such that the performance of the proposed repository can be assessed. In addition, they also provide the framework for design of the proposed repository and the information needed to address requirements described in Part 60 of Title 10 of the Code of Federal Regulations.

The description of the site and surrounding region represents a snapshot in time. Results of characterization activities completed by the end of September 1997 are included. In some exceptional cases, additional work carried out during the early part of fiscal year 1998 is also discussed (e.g., results of a seismic hazard assessment). Because it represents a snapshot in time, and because it summarizes work carried out at different times, there are some inconsistencies within the document. As work to characterize the site reaches its completion and more complete integration of results is accomplished these inconsistencies will be resolved, and the technical information will be better integrated both between and within chapters.

The Site Description summarizes and synthesizes both work carried out in accordance with the *Quality Assurance Requirements and Description* (DOE/RW-0333P) and also work performed outside that quality assurance program. Because the Site Description is a summary and synthesis document, no data were generated in preparing it. In general, information on the quality status of data discussed in the Site Description is, therefore, found in the reports forming the basis for the summarized material and cited in the text. In some cases, however, information on the quality status of data is specifically addressed in the Site Description. For Section 3, the Q status of some references is indicated by a [Q] or [NON-Q] notation in the reference list. For references without a notation, the source document should be consulted. In Section 5.3, the Q status of many data sets is addressed in the subsections in which the data are discussed. Q status of data in Sections 6.1 and

6.4 is described at the end of Section 6.4. For data in Section 6.3, the Q status of data is listed in the introduction to the section. For all other sections, readers interested in the Q status of data should consult the source references cited in the text.

For some of the data discussed in the Site Description, a Data Tracking Number (DTN) is provided. These numbers indicate that the data are available in the Technical Data Management System. In other cases, the location of data is addressed in the cited references. Although for future revisions a data verification process will be implemented to ensure data are available in the Technical Data Management System and that the DTNs cited are correct, this version has not benefited from such a quality check. At the present time, therefore, cited data should be considered "to be verified (TBV)."

The Site Description will evolve over the next several years to support the Site Recommendation and, if the recommendation is favorable and approved, a license application. New results will be incorporated and integration of the various sections will be enhanced. Thus, while the findings presented in this document represent our understanding today, ongoing and future work may modify some of the conclusions.

The Site Description begins with a brief discussion of the geography and demography of the site. It then describes relevant facilities that are located at the site or in its vicinity. This is followed by a presentation of the current state of knowledge for the site's geology, climatology and meteorology, hydrology, and geochemistry. Finally, the effects of repository construction, including especially heat, are addressed as they affect the geomechanical, geohydrological, and geochemical aspects of the natural environment in the near-field and altered zone.

ACRONYMS

ADEM	Automated Digital Electron Microscope
AZ	Altered Zone
BLM	Bureau of Land Management
BREN	Bare Reactor Experiment Nevada
CHn	Calico Hills nonwelded
CNWRA	Center for Nuclear Waste Regulatory Analyses
CRWMS	Civilian Radioactive Waste Management System
DOE	U.S. Department of Energy
DOPA	Dihydroxyphenylalanine
DTN	Data Tracking Number
ESF	Exploratory Studies Facility
IARC	International Agency for Research on Cancer
INAA	Instrumental Neutron-activation Analysis
IRSR	Issue Resolution Status Report
LA	License Application
MAP	Mean Average Precipitation
MAT	Mean Average Temperature
M&O	Management and Operating Contractor
MSL	Mean Sea Level
NAFA	Nordic Aquatic Fulvic Acid
NFE	Near-Field Environment
NRC	U.S. Nuclear Regulatory Commission
OIS	Oxygen Isotope Stage
PET	Pentaerythritol
PTn	Paintbrush Tuff Nonwelded
R/EFPD	Radiological/Environmental Field Programs Department
RMR	Rock Mass Rating
RQD	Rock Quality Designation
SMOW	Standard Mean Ocean Water
SNL	Sandia National Laboratories
SZ	Saturated Zone

ACRONYMS (Continued)

TCw	Tiva Canyon Welded
TDIF	Technical Data Information Form
TSPA	Total System Performance Assessment
TSw	Topopah Spring welded
USAF	U.S. Air Force
USGS	U.S. Geological Survey
UZ	Unsaturated Zone
VA	Viability Assessment
YMP	Yucca Mountain Site Characterization Project
YMPB	USGS Yucca Mountain Project Branch

SYMBOLS/UNITS

Ag	silver
Al	aluminum
Am	americium
Ar	argon
As	arsenic
Au	gold
Ar	argon
B	boron
b.y.	billions of years
Ba	barium
Be	beryllium
C	carbon
°C	degree celsius
Ca	calcium
Ce	cerium
Cl	chlorine
Co	cobalt
Cr	chromium
Cs	cesium
DC	direct current
Eu	europium
F	fluorine
Fe	iron
Ga	giga-annum
Gd	gadolinium
H	hydrogen
Hf	hafnium
K	potassium
k.y.	thousands of years
ka	kilo-annum
La	lanthanum
Li	lithium
Lu	lutetium
m.y.	millions of years
Ma	mega-annum
md	millidarcy
Mg	magnesium
mL/g	milliliters per gram
Mn	manganese
MPa	megapascals
N	nitrogen
Na	sodium
Nb	niobium
Np	neptunium

SYMBOLS/UNITS (Continued)

O	oxygen
P	phosphorus
Pb	lead
pCi	picocurie
pmc	percent modern carbon
ppm	parts per million
ppmv	parts per million by volume
Pr	praseodymium
Pu	Plutonium
Rb	rubidium
S	sulfur
Sc	scandium
Si	silicon
Sm	samarium
Sr	strontium
Ta	tantalum
Tb	terbium
Tc	technetium
Th	thorium
Ti	titanium
U	Uranium
Y	yttrium
Yb	ytterbium
Zr	zirconium
‰	parts per mil

1. GEOGRAPHY AND DEMOGRAPHY

This section provides an overview of the general geography and demography of the region encompassing the potential repository at the Yucca Mountain Site. The discussion includes the general physiography and topography of the region and a more detailed description and identification of the Yucca Mountain Site, facilities, and conceptual boundaries. The section also identifies the three-county area which will receive most of the socioeconomic impacts of the repository. This section discusses the population distribution and density and provides a brief socioeconomic overview of the region, including a focus on the population within 84 km (52 mi) of the potential repository.

1.1 SITE LOCATION AND DESCRIPTION

The Yucca Mountain Site is located in Nye County in Southern Nevada, approximately 160 km (100 mi) northwest of Las Vegas (see Figures 1.1-1 and 1.1-2), on land controlled by three federal agencies: the U.S. Air Force (Nellis Air Force Range), the U.S. Department of Energy (DOE), Nevada Test Site, and the U.S. Bureau of Land Management (see Figure 1.1-3).

The Yucca Mountain Site and surrounding areas are in the southern part of the Great Basin, the northern-most subprovince of the Basin and Range Physiographic Province (Figure 1.1-4). The topography of the Yucca Mountain Site and surrounding region is typical of the Great Basin and the larger Basin and Range Province which are generally characterized by more or less regularly spaced, generally north-south trending mountain ranges and intervening alluvial basins that were formed by faulting. The Great Basin subprovince is an internally draining basin; i.e., precipitation that falls over the basin has no outlet to the Pacific Ocean (DOE 1996).

Elevation changes and variations in topographic relief are considerable within the area of the Yucca Mountain Site. On the Nevada Test Site, elevation varies from approximately 1,000 m (3,280 ft) above sea level in Frenchman Flat and Jackass Flat to about 2,339 m (7,675 ft) on Rainier Mesa and about 2,199 m (7,216 ft) on Pahute Mesa (DOE 1996). Within 50 miles south of the Yucca Mountain Site, Death Valley in California presents the lowest point in the Western Hemisphere, 282 feet below sea level at Badwater (NPS 1998).

Yucca Mountain is an irregularly shaped volcanic upland which reaches an elevation ranging from 1,500 to 1,930 m (4,922 to 6,332 ft) at the crest and has about 650 m (2,132 ft) of relief (DOE 1988, Vol. 1, Part A, p. A-2). The Yucca Mountain climate is arid and the mountain historically receives less than 25 cm (10 in) of rain per year.

There are no perennial streams in the general vicinity of the Yucca Mountain Site (DOE 1988, Vol. 1, Part A, p. A-2). Streams in the vicinity of the Yucca Mountain Site are ephemeral, fed by runoff from snowmelt and from precipitation during storms that are most common in winter, although they occur occasionally in spring and fall with localized thunderstorms during the summer. Surface water runoff in the Yucca Mountain area is through Fortymile Canyon and south through Fortymile Wash. Jackass Flats, east of the Yucca Mountain Site and one of the three primary valleys on the Nevada Test Site, is topographically open with drainage via the Fortymile Wash. The Fortymile drainage, in turn, intersects the Amargosa River in the Amargosa Desert about 32 km (20 mi) southwest of the Nevada Test Site. The Amargosa River

ends at Death Valley (DOE 1996). For more information on surface hydrology, see Section 5. Figure 5.1-1 shows the surface hydrology features of the Yucca Mountain region.

The Yucca Mountain Site exists in proximity to a number of natural hazards including faults/seismic activity and volcanic activity, and man-made hazards including weapons testing.

Faults have been identified and there has been historic seismic activity in the Southern Great Basin (DOE 1988, pp. 1-151). Subsection 3.10 describes the seismicity around Yucca Mountain. The Southern Great Basin has been the location of volcanic activity as recently as the Pleistocene; this activity and its proximity to the Yucca Mountain Site are described in Subsection 3.9. The Nevada Test Site has been the location of over 1,000 nuclear tests, and is currently used to test conventional weapons and to conduct toxic waste disposal and scientific experiments. Section 2, Nearby Industrial, Transportation, and Military Facilities, provides additional discussion of the Nevada Test Site and other activities in the vicinity of the potential repository. The Nevada Bureau of Mines and Geology has recently assessed this area and confirmed there has been no mining within 10 km of the potential repository subsurface area. (S.B. Castor et al., *Assessment of Metallic and Mined Energy Resources in the Yucca Mountain Conceptual Controlled Area, Nye County, Nevada*, Deliverable UNR2M or SPT7CM4 to U.S. Department of Energy, in review).

The YMP has identified, for administrative purposes, an area surrounding the potential repository known as the Conceptual Controlled Area (see Figures 1.1-5 and 1.1-6; the Conceptual Controlled Area is also shown but not specifically identified in Figures 1.1-1, 1.1-2, and 1.1-3). This area is approximately 5 km (3 mi) in radius and surrounds the repository block in an irregular pie shape. As the future administrative areas of the YMP have yet to be determined, the Conceptual Controlled Area is currently used as a boundary for determining infrastructure and activities that are "onsite" versus "offsite." As site characterization activities are completed, the YMP will identify the boundaries for the areas described in 10 CFR 60, *Disposal of High-Level Radioactive Wastes in Geologic Repositories*, Section 2, and listed below. The establishment of these regulatory-required boundaries that will replace the Conceptual Controlled Area will be coordinated with the identification and analysis of design basis events. The following definitions are from 10 CFR 60.2:

"Postclosure Controlled Area means a surface location, to be marked by suitable monuments, extending horizontally no more than 10 km in any direction from the outer boundary of the underground facility, and the underlying subsurface, which area has been committed to use as a geologic repository and from which incompatible activities would be restricted following permanent closure."

"Underground Facility means the underground structure, including openings and backfill materials, but excluding shafts, boreholes, and their seals."

"Preclosure Controlled Area means that surface area surrounding the geologic repository operations area for which the licensee exercises authority over its use, in accordance with the provisions of this part, until permanent closure has been completed."

"Geologic repository operations area means a high-level radioactive waste facility that is part of a geologic repository, including both surface and subsurface areas, where waste handling activities are conducted."

"Restricted Area means an area, access to which is controlled by the licensee for purposes of protection of individuals from undue risks from exposure to radiation and radioactive materials."

"Site means the location of the preclosure controlled area, or of the postclosure controlled area, or both."

"Unrestricted area means an area, access to which is neither limited nor controlled by the licensee."

In addition, in accordance with 10 CFR 60.121(b), "Additional Controls," DOE will need to establish appropriate jurisdiction and control outside the ultimate postclosure controlled area, to prevent adverse human actions that could significantly reduce the geologic repository's ability to achieve isolation. The rights of DOE may take the form of appropriate possessory interests, servitudes, or withdrawals from location or patent under the general mining laws. These additional controls will be discussed in the Working Draft License Application.

Public access to the Yucca Mountain Site and the Nevada Test Site is restricted¹ and guard stations are located at all entrances to the Nevada Test Site, as well as throughout the Nevada Test Site. Access to the Yucca Mountain Site is through the Nevada Test Site, which is accessed through four main, paved points. Other existing, unpaved roads can provide entrance or exit routes in case of emergency. The primary entrance to the Nevada Test Site is through Gate 100 on the Mercury Highway, which originates at U.S. Highway 95, 105 km (65 mi) northwest of Las Vegas. A second entrance, a turnoff from Highway 95 to Jackass Flats Road, is eight kilometers (5 mi) west of Mercury. This entrance is presently barricaded. A third entrance off Highway 95 is through Gate 510 at Lathrop Wells Road, approximately 32 km (20 mi) west of Mercury. These three entrances are shown in Figure 1.1-5. A fourth entrance to Nevada Test Site is via State Road 375 through Guard Station 700 in the northeast corner of Nevada Test Site (DOE 1996). Because this entrance is seldom used and due to its distance from the Yucca Mountain Site (approximately 50 km [31 mi]), it is not shown on any figure in this section. Transportation to the Yucca Mountain Site through the Nevada Test Site is primarily by Lathrop Wells Road, Jackass Flats Road, Cane Springs Road, and H-Road; and is further augmented by a network of graded gravel roads and jeep trails (DOE 1996).

If necessary, the site can be accessed by air at the Desert Rock Airport (Figure 1.1-5), located 5 km (3 mi) southwest of Mercury. The airport is unmanned but operational, its use controlled

¹ Because the Yucca Mountain Site is partially on U.S. Bureau of Land Management land (see Figure 1.1-3), access to the southwestern portions of the Conceptual Planning Area is possible by crossing public lands. Prior to construction of the potential repository, appropriate actions will be completed which will place the entire Preclosure Controlled Area of the potential repository under DOE control.

by DOE. The airport has a paved runway 2-km (6,560 ft) long and 30-m (100 ft) wide. No services are available at the airport; however, existing features include an administration/control building, a fireman-standby trailer, an aircraft unloading pad, aircraft parking tie-down spurs, two lighted windsocks, and radio-activated runway lights (DOE 1996).

Outside the Conceptual Controlled Area, the Field Operations Center and the Batch Plant are the only facilities operated by the YMP. These and other nearby Nevada Test Site facilities outside the Conceptual Controlled Area are shown in Figure 1.1-5, and the latitude/longitude and Universal Transverse Mercator coordinates and area occupied by each are found in Table 1.1-1. The other nearby facilities are operated by Nevada Test Site organizations and include:

- Test Cells A and C
- Engine Maintenance and Disassembly Building
- Reactor Maintenance and Disassembly Building
- Engine Test Stand 1
- Bare Reactor Experiment Nevada Tower
- Treatability Test Facility
- Gates 100 and 510
- Control Point 300
- Canyon Sub-Station, Mercury
- Desert Rock Airport

In addition, there is a short railroad, known as the Jackass Wells Railroad, which was used to connect and move heavy materials between Test Cells A and C, Engine Maintenance and Disassembly Building, Reactor Maintenance and Disassembly Building, and Engine Test Stand 1. This railroad was abandoned in place (DOE 1996). In 1997, Sandia National Laboratories began a series of rocket launches from Wahmonie in Area 26 (LVRJ 1997).

Possible repository surface facilities and infrastructure outside the site are to be determined.

There are several existing and proposed "key facilities" integral to the activities of the Yucca Mountain Site. Current surface facilities are those disturbed areas and structures used for exploratory studies activities. Proposed future surface facilities are those areas and structures that would be used for accepting and handling high-level waste at the site.

The existing surface infrastructure utilized by the YMP inside the Conceptual Controlled Area include the North and South Portal pads, Sub-docks 1 and 2, Muck Storage Area, Borrow Pit, Booster Station, Topsoil Storage and Extension Area, Rock Storage Area, and Water Storage Tank. These facilities and infrastructure are shown in Figure 1.1-6; and the latitude/longitude and Universal Transverse Mercator coordinates and area occupied by each facility are found in Table 1.1-2. In addition, there is a temporary trailer on the South Portal Pad, and a small number of temporary trailers, a change house, and a switchgear building on the North Portal Pad. As the trailers are temporary, and the change house and switchgear buildings are subject to major modification or removal if the potential repository becomes operational, they are not characterized here (*Repository Surface Design Engineering Files Report*, March 2, 1998, predecisional EIS document, B00000000-01717-5705-00009 REV 01, CRWMS M&O, Las Vegas, Nevada). In addition to existing facilities, potential repository surface facilities and

infrastructure will be located within the area currently designated as the Conceptual Controlled Area. At the North Portal Operations Area these facilities will be in the Radiologically Controlled Area, the Balance of Plant Area, or the Site Services Area. The North Portal Operations Area is shown in Figure 1.1-7. Other facilities that support the subsurface development of the repository will be located at the South Portal Development Operations Area. The size and location in latitude and longitude and Universal Transverse Mercator coordinates for all of these facilities are shown in Table 1.1-1 (*Repository Surface Design Engineering Files Report*, March 2, 1998, predecisional EIS document, B00000000-01717-5705-00009 REV 01, CRWMS M&O, Las Vegas, Nevada).

Facilities in the North Portal Radiologically Controlled Area include:

- Airlock Building
- Waste Handling Building
- Waste Treatment Building
- Carrier Preparation Building
- Transporter Maintenance Building
- Carrier Washdown Buildings
- Switchgear Building
- Change House

Should a railspur to the repository be built, rail lines and train parking will also be built (*Repository Surface Design Engineering Files Report*, March 2, 1998, predecisional EIS document, B00000000-01717-5705-00009 REV 01, CRWMS M&O, Las Vegas, Nevada).

The Balance of Plant facilities in the North Portal Operations area will include (*Repository Surface Design Engineering Files Report*, March 2, 1998, predecisional EIS document, B00000000-01717-5705-00009 REV 01, CRWMS M&O, Las Vegas, Nevada):

- Administration Building
- Medical Center
- Fire Station
- Central Warehouse
- Central Shops
- Motor Pool and Facility Service Station
- Mockup Building
- Utility Building
- Three security stations

The Site Services Area will include the Visitor Center and Cooling Tower. This area also includes general parking lots, but they are not shown in Figure 1.1-7 (*Repository Surface Design Engineering Files Report*, March 2, 1998, predecisional EIS document, B00000000-01717-5705-00009 REV 01, CRWMS M&O, Las Vegas, Nevada).

The facilities at the South Portal Development Operations Area include (*Engineering File-Subsurface Repository*, BCA000000-01717-5705-00005, REV 00, December 1997, predecisional EIS document, CRWMS M&O, Las Vegas, Nevada):

- Covered Laydown & Storage Area (warehouse)
- Locomotive and Railcar Repair Shop
- Air Compressor Building
- Change House
- Portal Site Offices
- Concrete Car Cleanout Shed
- Concrete Batch Plant
- Two Security Stations

These South Portal facilities are shown in Figure 1.1-8.

Part of the Conceptual Controlled Area includes a 4255.5 acre withdrawal (Figure 1.1-9) (BLM 1990) from the Mining and Mineral Leasing Law, precluding the staking of mining claims over the repository block. Prior to this withdrawal, there were 10 lode mining claims in this withdrawal area that were quit-claimed after negotiations with DOE.

In an area on BLM land south of the Conceptual Controlled Area, west of NTS, and just north of U.S. Route 95, there were 35 unpatented mining claims as of May 7, 1997 (the latest update of the Bureau of Land Management mining claims database). These are broken down as 11 lode claims and 24 placer claims (Figure 1.1-7) (*Land Use Environmental Baseline File*, January 14, 1998, predecisional EIS document, CRWMS M&O, Las Vegas, Nevada). Since 1991, when the government instituted an annual fee requirement for claims, the number of claims has been dropping rapidly, leaving only the serious miners. As the status of unpatented mining claims tends to change rapidly, it is too early to develop a strategy for dealing with claimants. However, it is reasonable to assume that any mining claims can be dealt with prior to repository closure (*Land Use Environmental Baseline File*, January 14, 1998, predecisional EIS document, CRWMS M&O, Las Vegas, Nevada). Also in this area just north of U.S. Route 95, there is a small privately-owned tract of land where the Cind-R-Lite Company is mining the cinder cone (Figure 1.1-7) for raw materials for concrete blocks. This location is well outside the areas required for preclosure control, and it is possible that by the time of repository closure, approximately 100 years in the future, that the resource might be consumed or supplanted by new technology. It is reasonable to assume that the property can be purchased prior to closure.

Additional discussion of facilities that could affect daily operations and performance of the proposed repository, or that could pose health or safety or radiological health and safety hazards, is provided in Section 2.

1.2 POPULATION DISTRIBUTION

The demographic study area surrounding the Yucca Mountain Site includes three counties: Clark, Lincoln, and Nye (see Figure 1.1-2), which cover approximately 95,000 sq km (37,000 sq mi) and have an estimated population of 1,223,920 persons (Nevada State Demographer 1998a).

Population and related economic activity in Southern Nevada are concentrated in Clark County in the incorporated cities and in the unincorporated areas of the Las Vegas Valley. The incorporated cities include Boulder City, Henderson, Las Vegas, Mesquite, and North Las Vegas, which contain 689,913 of Clark County's 1,192,200 persons (Nevada State Demographer 1998a). Most of the remainder of the Clark County population resides in the unincorporated areas near Las Vegas, including east Las Vegas (DOC 1998), Paradise, Spring Valley, and Sunrise Manor (Nevada State Demographer 1998b), which together total approximately 430,000 persons.

Lincoln County has a total population of only 4,110 persons, 2,620 (64 percent) of whom live in the incorporated town of Caliente or the unincorporated towns of Alamo, Panaca, or Pioche (Nevada State Demographer 1998a, 1998b). The overall population density of Lincoln County is only 0.15 persons per square kilometer.

Nye County, where the Yucca Mountain Site is located, has 27,460 persons, 0.59 persons per square kilometer. Of this population, 23,236 persons (84 percent) live in the incorporated town of Gabbs and the unincorporated towns of Amargosa, Beatty, Manhattan, Pahrump, Round Mountain, and Tonopah. The largest population concentration is in Pahrump, with 18,970 persons, fully 69 percent of the total county population (Nevada State Demographer 1998a, 1998b). Tables 1.2-1 and 1.2-2 present current population and areal data for the three counties of Clark, Lincoln, and Nye. Table 1.2-3 presents population projections for the three counties.

For the Viability Assessment, of greater importance to the Yucca Mountain Site than the population concentrations in the Las Vegas Valley is the population in the vicinity of the potential repository. Accordingly, an area of population analysis centered on the site (Easting 551135.7, Northing 4078351.6, Universal Transverse Mercator Grid Zone 11; Longitude 116°25'33.32" E and Latitude 36°51'11.61" N) has been established in accordance with Regulatory Guide 1.109 (NRC 1977). The area is 84 km (52 mi) in radius and is designated the Radiological Monitoring Grid. The circle at the center has a diameter of approximately 4 km (2.5 mi). Each succeeding circle has a radius 8 km (5 mi) greater than the previous circle. As is shown in Figure 1.1-2, much of the Grid is located in the southernmost portion of Nye County with smaller outer portions of the Grid in the Nevada counties of Clark, Lincoln, and Esmeralda, and in Inyo County in California. Figure 1.2-1 is the Radiological Monitoring Grid showing the 1997 population and density range for each sector.

The population concentrations within Nye County are of greatest importance for the Viability Assessment. In particular, there are no permanent residents within 20 km (12.5 mi) of the center of the Grid. The only residents in this area are transient populations at Mercury on temporary duty at the Nevada Test Site who are under the control of the Nevada Test Site and are subject to being moved as needed. The closest permanent population concentration is in Amargosa Valley,

a primarily agricultural-based community on the south edge of Nevada Test Site. The population densities in this region are between two and four persons per square kilometer in the inhabited sectors. Several of the sectors have zero populations. Similarly, in the Beatty area, population densities in the most populated sectors are approximately 6 and 11 persons per square kilometer. Populations by sector are provided in Table 1.2-4.

Pahrump is at the edge of the Radiological Monitoring Grid and has a population of approximately 19,000 (Nevada State Demographer 1998b) (it is partially within the Radiological Monitoring Grid and is the only town within the 84 km Radiological Monitoring Grid to have a population greater than 2,500). Rapid growth in Pahrump has been the result of increased immigration of retirees and increases in population of persons who live in Pahrump and commute to Las Vegas for employment.

Within the 84 km Grid, population concentrations are largely primarily a result of agricultural, mining, tourism, and service activities. Agricultural development is concentrated in Amargosa Valley and Pahrump. Mining operations, tourism, general services, and employment on the Nevada Test Site and the Nellis Air Force Range help support these two places and other towns located within the Radiological Monitoring Grid, including Mercury, Beatty, Johnnie, Furnace Creek Ranch, and Death Valley Junction. Current patterns showing the large percentage of federally owned land in the three counties are shown in Table 1.2-5.

Current land use patterns and economic drivers will drive future population changes within the 84 km area. In Figure 1.1-3 it can be seen that little of the area surrounding Yucca Mountain is privately owned, and there is very little built-up or urban land. Close to the Yucca Mountain Site it is likely that a large percentage of the land will remain federally owned and controlled. In addition, the Nevada Test Site is withdrawn from public use entirely. Considering the substantial disturbance of the environment on the Nevada Test Site, it is unlikely that it will be available for unrestricted public use or habitation in the near future. Consequently, it is assumed that there will be a lack of economic impetus and resulting infrastructure on the limited private land near the site sufficient to support large populations.

The disposal regulations identify a favorable condition related to population density. (10 CFR 60.122 (b)(6)). For a favorable condition to exist, a "low population density within the geologic setting and a postclosure controlled area that is remote from population centers, must be shown to be present." Highly populated areas are defined in 10 CFR 960, *General Guidelines for the Recommendation of Sites for Nuclear Waste Repositories*, as census designated "places" of 2,500 or more, "unless it can be demonstrated that such a place has a lower population density than the mean value for the continental United States." The Postclosure Controlled Area, although not finalized, is expected to extend "no more than 10 kilometers in any direction from the outer boundary of the underground facility" based on the current version of 10 CFR 60. Such an area currently contains no population and is remote from populated areas. Further, all census designated places in Nye County have lower population densities than the average for the continental United States, which is approximately 29.1 persons per square kilometer, based on a 1997 population of approximately 267,955,000 and a land area of 9,201,990 square kilometers (3,539,227 square miles) (DOC 1997). As such, the current state of population distribution within the Radiological Monitoring Grid fulfills the current 10 CFR 60.122 favorable conditions.

1.3 REFERENCES

1.3.1 Documents Cited

BLM (Bureau of Land Management) 1990. Public Land Order 6802. September 25. Bureau of Land Management, Department of Interior. TIC 221944.

CRWMS M&O (Civilian Radioactive Waste Management System Management and Operating Contractor) 1996. *Mined Geologic Disposal System Advanced Conceptual Design Report*. Volumes I through IV. B00000000-01717-5705-00027 REV 00. Las Vegas, Nevada: Author. TIC 233073.

DOC (U.S. Department of Commerce) 1996. *Land Area, Population and Density for States and Counties: 1990*. Summary Tape File 1C. March 12. Washington, D.C.: Bureau of the Census. TIC 239796

DOC 1997. "Population, by Country: 1980 to 2000." *Statistical Abstract of the United States 1997*. Table No. 1334. Washington, D.C. U.S. Government Printing Office. TIC 237816.

DOC 1998. *Population for Places: 1990*. Summary Tape File 3A. Washington, D.C.: Bureau of the Census. TIC 237813.

DOE (U.S. Department of Energy) 1988. *Site Characterization Plan, Yucca Mountain Site, Nevada Research and Development Area, Nevada*. DOE/RW-0199, Vol. 1, Part A, pp. A-2, 1-151, 1-340. Las Vegas, Nevada: U.S. Department of Energy, Yucca Mountain Site Characterization Office. TIC 223856 - 223864.

DOE 1996. *Final Environmental Impact Statement for the Nevada Test Site and Off-Site Locations in the State of Nevada*. DOE/EIS 0243, Vol. 1, Sect. 4. Las Vegas, Nevada: U.S. Department of Energy, Nevada Operations Office. TIC 226874.

Hunt, C.B. 1974. *Natural Regions of the United States and Canada*. San Francisco, California: W.H. Freeman and Co. TIC 208460.

LVRJ (Las Vegas Review Journal) 1997. *Fire in the Sky*, April 14, 1997. Las Vegas Review-Journal [Electronic newspaper article database] [Accessed September 18, 1998] Available: http://www.lvrj.com/lvrj_home/1997/APR-14-Mon-1997/news/5165508.html.

Nevada State Demographer 1998a. *Population of Nevada's Counties and Incorporated Cities*. Population Estimates - State, Counties, Incorporated Cities, and Unincorporated Towns. February 24. Reno, Nevada: Nevada Department of Taxation. TIC 237862.

Nevada State Demographer 1998b. *Population of Nevada's Unincorporated Towns*. Population Estimates - State, Counties, Incorporated Cities, and Unincorporated Towns. February 24. Reno, Nevada: Nevada Department of Taxation. TIC 237863.

Nevada State Demographer 1998c. *Population Estimates (1997) and Forecasts (1998-2018)*. March 16. Reno, Nevada: Nevada Department of Taxation. TIC 237864.

NPS (National Park Service) 1998. The National Park Service, Death Valley National Park (Home Page). [Accessed June 19, 1998; September 18, 1998]. Available: <http://www.nps.gov/deva>.

NRC (U.S. Nuclear Regulatory Commission) 1977. Calculation of Annual Doses to Man From Routine Releases of Reactor Effluents for the Purpose of Evaluating Compliance With 10 CFR Part 50, Appendix I. Regulatory Guide 1.109. Washington, D.C.: U.S. Nuclear Regulatory Commission. TIC 222641.

1.3.2 Regulations

10 CFR 60. Energy: Disposal of High-Level Radioactive Wastes in Geologic Repositories. TIC 238445.

10 CFR 960. Energy: General Guidelines for the Recommendation of Sites for Nuclear Waste Repositories. TIC 222164.

TABLES

	Page
1.1-1 Location and Characteristics of Facilities and infrastructure Near to the Conceptual Controlled Area (Figure 1.1-5)	T1.1-1
1.1-2 Location and Characteristics of Facilities and Infrastructure in the Conceptual Controlled Area (Figure 1.1-6)	T1.1-2
1.2-1 Population of Incorporated and Unincorporated Towns in Clark, Lincoln, and Nye Counties	T1.2-1
1.2-2 Population Density of Clark, Lincoln, and Nye Counties	T1.2-1
1.2-3 Clark, Lincoln, and Nye County Population Projections	T1.2-1
1.2-4 Population by Sector Within 84 Kilometers (52 miles) of the Yucca Mountain Site	T1.2-2
1.2-5 Federally Owned Land in Nevada by Entitlement Acreage and County, Fiscal Year 1995 (in Acres).....	T1.2-3

INTENTIONALLY LEFT BLANK

TABLES

	Page
1.1-1 Location and Characteristics of Facilities and infrastructure Near to the Conceptual Controlled Area (Figure 1.1-5)	T1.1-1
1.1-2 Location and Characteristics of Facilities and Infrastructure in the Conceptual Controlled Area (Figure 1.1-6)	T1.1-2
1.2-1 Population of Incorporated and Unincorporated Towns in Clark, Lincoln, and Nye Counties	T1.2-1
1.2-2 Population Density of Clark, Lincoln, and Nye Counties	T1.2-1
1.2-3 Clark, Lincoln, and Nye County Population Projections	T1.2-1
1.2-4 Population by Sector Within 84 Kilometers (52 miles) of the Yucca Mountain Site	T1.2-2
1.2-5 Federally Owned Land in Nevada by Entitlement Acreage and County, Fiscal Year 1995 (in Acres)	T1.2-3

Table 1.1-1. Location and Characteristics of Facilities and Infrastructure Near to the Conceptual Controlled Area (Figure 1.1-5)

Conceptual Administrative Areas	Facility Name	Long/Lat Coordinates		Universal Transverse Mercator Coordinates		Area (Sq Meters)	Perimeter (Meters)
		x-coord	y-coord	x-coord	y-coord		
		Preclosure Control Area	TBD	TBD	TBD		
Postclosure Control Area	TBD	TBD	TBD	TBD	TBD	TBD	
Restricted Area	TBD	TBD	TBD	TBD	TBD	TBD	
Existing Surface Facilities (Outside Conceptual Controlled Area)	Canyon Sub-Station	-116 20 33	36 49 26	558628	4075345	na	na
	Test Cell 'A'	na	na	na	na	na	na
	Test Cell 'C'	-116 16 43	36 49 49	564334	4076089	na	na
	Concrete Batch Plant	-116 23 20	36 48 38	554504	4073838	7,682	465
	Field Operations Center	-116 17 15	36 46 43	563591	4070337	na	na
	Engine Maintenance and Disassembly Building	-116 18 6	36 48 29	562293	4073589	na	na
	Reactor Maintenance and Disassembly Building	na	na	na	na	na	na
	Engine Test Stand 1	na	na	na	na	na	na
	Desert Rock Airport	na	na	na	na	na	na
	CP-300	-116 17 21	36 48 32	563398	4073713	na	na
	Mercury	-116 0 3	36 39 38	589283	4057485	na	na
	Gate100	-116 0 14	36 37 32	589046	4053606	na	na
	Gate 510	-116 24 14	36 40 15	553261	4058321	na	na
	Treatability Test Facility	-116 17 24	36 46 41	563350	4070278	TBD	TBD
	BREN Tower	-116 14 47	36 46 33	567262	4070072	TBD	TBD
	Sandia National Laboratories' Wahmonie Launch Site	na	na	na	na	na	na

TBD: To be determined; na: not currently available

Table 1.1-2. Location and Characteristics of Facilities and Infrastructure in the Conceptual Controlled Area (Figure 1.1-6)

	Facility Name	Long/Lat Coordinates		UTM Coordinates		Area (Sq Meters)	Perimeter (Meters)	
		x-coord	y-coord	x-coord	y-coord			
Existing Surface Facilities (Inside Conceptual Controlled Area)	Booster Station	-116 25 34	36 50 40	551173	4077563	799	117	
	Borrow Pit	-116 24 09	36 50 11	553269	4076680	322,114	2,321	
	Muck Storage Area (North Portal)	-116 25 12	36 50 48	551707	4077816	204,759	3,773	
	North Portal Pad	-116 25 36	36 51 09	551098	4078460	132,223	5,221	
	Rock Storage Area	-116 26 03	36 50 10	550432	4076638	4,552	266	
	South Portal Pad	-116 26 10	36 49 41	550276	4075733	36,546	776	
	Sub-Dock 1	-116 26 17	36 51 07	550097	4078400	65,337	1,758	
	Sub-Dock 2	-116 26 22	36 51 03	549963	4078254	25,087	733	
	Topsoil Storage Area	-116 25 58	36 50 08	550576	4076565	47,180	860	
	Topsoil Extension Area	-116 25 53	36 50 14	550682	4076751	50,033	910	
	Water Storage Tank	-116 25 45	36 50 55	550891	4078027	3,769.7	1,095.9	
Proposed Repository Surface Facilities (Inside Conceptual Controlled Area)		Long/Lat Coordinates		UTM Coordinates		Area (Sq Meters)	Perimeter (Meters)	
		x-coord	y-coord	x-coord	y-coord			
	North Portal Operations Area: Radiologically Controlled Area Facilities							
	Airlock Building	-116 55 48	36 51 00	551520	4078439	TBD	TBD	
	Waste Handling Building	-116 25 31	36 51 17	551228	4078703	21,248	656	
	Waste Treatment Building	-116 25 29	36 51 20	551288	4078790	4,930	300	
	Carrier Preparation Building	-116 25 04	36 51 34	551895	4079248	2,113	190	
	Transporter Maintenance Building	-116 25 30	36 51 04	551258	4078318	TBD	TBD	
	Carrier Washdown Building	-116 25 28	36 51 11	551320	4078530	TBD	TBD	
	Switchgear Building	-116 25 37	36 51 06	551090	4078369	TBD	TBD	
Change House (North Portal)	-116 25 37	36 51 15	551081	4078657	1,046	168		

T1.1-2

Table 1.1-2. Location and Characteristics of Facilities and Infrastructure in the Conceptual Controlled Area (Figure 1.1-6) (Continued)

Facility Name	Long/Lat Coordinates		UTM Coordinates		Area (Sq Meters)	Perimeter (Meters)
	x-coord	y-coord	x-coord	y-coord		
North Portal Operations Area: Balance Of Plant Areas						
Security Station 1 (Main BOP Portal)	-116 25 26	36 51 06	551373	4078365	TBD	TBD
Security Station 2 (RCA/BOP Portal)	na	na	na	na	na	na
Security Station 3 (RCA truck/rail Portal)	-116 24 47	36 51 41	552318	4079452	TBD	TBD
Administration Building	-116 24 49	36 51 44	552280	4079560	1,729	214
Medical Center	-116 25 25	36 51 00	551391	4078169	TBD	TBD
Fire Station	-116 25 26	36 51 00	551364	4078184	TBD	TBD
Central Warehouse	-116 25 17	36 51 04	551582	4078297	TBD	TBD
Central Shops	-116 25 20	36 50 59	551505	4078145	TBD	TBD
Motor Pool and Facility Service Station	-116 25 20	36 51 00	551505	4078203	TBD	TBD
Mockup Building	-116 25 21	36 51 06	551477	4078372	TBD	TBD
Utility Building	na	na	na	na	na	na
	Long/Lat Coordinates		UTM Coordinates		Area (Sq Meters)	Perimeter (Meters)
	x-coord	y-coord	x-coord	y-coord		
North Portal Operations Area: Site Services Areas						
General Parking (multiple locations)	TBD	TBD	TBD	TBD	TBD	TBD
Cooling Tower	-116 25 14	36 51 03	551664	4078272	TBD	TBD
Visitor Center	-116 25 26	36 50 53	551362	4077973	TBD	TBD

Proposed Repository Surface Facilities
 (Inside Conceptual Controlled Area)

T1.1-3

Table 1.1-2. Location and Characteristics of Facilities and Infrastructure in the Conceptual Controlled Area (Figure 1.1-6) (Continued)

	Long/Lat Coordinates		UTM Coordinates		Area (Sq Meters)	Perimeter (Meters)	
	x-coord	y-coord	x-coord	y-coord			
Proposed Repository Surface Facilities (Inside Conceptual Controlled Area)	South Portal Development Operations Area						
	Covered Laydown & Storage Area (warehouse)	-116 26 08	36 49 38	550346	4075648	TBD	TBD
	Locomotive and Railcar Repair Shop	-116 26 09	36 49 38	550300	4075663	TBD	TBD
	Air Compressor Building	-116 26 10	36 49 39	550285	4075685	TBD	TBD
	Change House	-116 26 12	36 49 37	550242	4075611	TBD	TBD
	Portal Site Offices	-116 26 12	36 49 38	550241	4075657	TBD	TBD
	Concrete Car Cleanout Shed	-116 26 07	36 49 40	550359	4075720	TBD	TBD
	Concrete Batch Plant	-116 26 07	36 49 40	550371	4075702	TBD	TBD
	Security Station – Main Gate	na	na	na	na	na	na
	Security Station – South Portal Entrance	na	na	na	na	na	na

TBD: To Be Determined; na: not currently available.

Table 1.2-1. Population of Incorporated and Unincorporated Towns in Clark, Lincoln, and Nye Counties

Place Name	Population	Place Name	Population
Clark County	1,192,200	Lincoln County	4,110
Incorporated		Incorporated	
Boulder City	14,493	Caliente	1,070
Henderson	147,870		
Las Vegas	425,270	Unincorporated	
Mesquite	9,270	Alamo	370
North Las Vegas	93,010	Panaca	410
		Pioche	770
Unincorporated			
Bunkersville	610	Nye County	27,610
East Las Vegas	11,087*	Incorporated	
Enterprise	11,120	Gabbs	400
Glendale	50		
Indian Springs	1,210	Unincorporated	
Laughlin	7,030	Amargosa	990
Moapa	720	Beatty	1,570
Moapa Valley	4,560	Manhattan	130
Mt. Charleston	1,110	Pahrump	18,970
Paradise	178,500	Round Mountain	900
Searchlight	810	Tonopah	2,760
Spring Valley	100,920		
Sunrise Valley	139,230		
Whitney	12,800		
Winchester	34,440		

Sources: Nevada State Demographer 1998a, 1998b; *DOC 1998

Table 1.2-2. Population Density of Clark, Lincoln, and Nye Counties

County	1997 Population	Area in Square Kilometers	Persons per Square kilometer
Clark	1,192,200	20,488	58.19
Lincoln	4,110	27,543	0.15
Nye	27,610	47,001	0.59

Sources: Nevada State Demographer 1998a; DOC 1996

Table 1.2-3. Clark, Lincoln, and Nye County Population Projections

County	2002	2007	2012	2017
Clark	1,501,436	1,815,842	2,158,383	2,541,796
Lincoln	3,818	3,472	3,103	2,730
Nye	34,204	36,479	34,080	32,898

Source: Nevada State Demographer 1998c

Table 1.2-4. Population by Sector Within 84 Kilometers (52 miles) of the Yucca Mountain Site

Distance (km) Direction	4	12	20	28	36	44	52	60	68	76	84
S	0	0	0	8	229	381	104	0	12	0	0
SSW	0	0	0	0	322	37	0	0	8	0	0
SW	0	0	0	0	0	0	0	649	0	0	0
WSW	0	0	0	0	0	0	0	0	0	27	0
W	0	0	0	0	659	0	0	0	0	0	0
WNW	0	0	0	0	1,109	0	0	0	0	0	68
NW	0	0	0	0	37	3	0	0	7	32	0
NNW	0	0	0	0	0	0	0	0	0	0	0
N	0	0	0	0	0	0	0	0	0	0	0
NNE	0	0	0	0	0	0	0	0	0	0	0
NE	0	0	0	0	0	0	0	0	0	0	0
ENE	0	0	0	0	0	0	0	0	0	0	0
E	0	0	0	0	0	0	0	0	0	0	0
ESE	0	0	0	0	0	0	0	0	0	1,471	0
SE	0	0	0	0	0	0	0	0	0	0	125
SSE	0	0	0	0	0	0	172	14	20	4,009	8,685
Total	0	0	0	0	2,356	421	2,76	663	47	5,539	8,878
										84 km	18,188

Source: Figure 1.2-1

Table 1.2-5. Federally Owned Land in Nevada by Entitlement Acreage and County, Fiscal Year 1995
 (in Acres)

County	Bureau of Land Mngt.	Forest Service	National Park Service	Corps of Engineers	Fish and Wildlife	Total	% of Federal Land/County
Clark	3,236,720	300,362	587,321	0	828,031	4,952,434	95.7%
Lincoln	5,633,723	30,672	0	671	761,490	6,426,556	94.3%
Nye	6,478,851	1,942,983	106,971	0	0	8,528,805	73.8%
Statewide	47,959,301	5,813,180	774,699	671	2,218,411	56,854,307	80.4%

NOTE: From EIS predecisional document: *Preliminary Draft Environmental Impact Statement: Renewal of the Nellis Air Force Range Land Withdrawal*, April 1998, Department of the Air Force, Las Vegas, Nevada.

INTENTIONALLY LEFT BLANK

FIGURES

	Page
1.1-1 Location of Nevada Test Site and Yucca Mountain Site, Nevada, USA	F1.1-1
1.1-2 Yucca Mountain Site in Proximity to Southern Nevada Counties	F1.1-2
1.1-3 Nevada Test Site Land Use and Private Land Holdings	F1.1-3
1.1-4 Boundaries and Larger Subprovinces of the Basin and Range Physiographic Province	F1.1-4
1.1-5 Location of Site Characterization Studies; Yucca Mountain Nevada	F1.1-5
1.1-6 Existing and Planned Infrastructure; Yucca Mountain, Nevada	F1.1-7
1.1-7 North Portal Operations Area	F1.1-9
1.1-8 South Portal Development Operations Area	F1.1-10
1.1-9 Nearby Mining Claims and Mining and Mineral Leasing Withdrawal	F1.1-11
1.2-1 Population Density and Study Area	F1.2-1

INTENTIONALLY LEFT BLANK

FIGURES

	Page
1.1-1 Location of Nevada Test Site and Yucca Mountain Site, Nevada, USA	F1.1-1
1.1-2 Yucca Mountain Site in Proximity to Southern Nevada Counties	F1.1-2
1.1-3 Nevada Test Site Land Use and Private Land Holdings	F1.1-3
1.1-4 Boundaries and Larger Subprovinces of the Basin and Range Physiographic Province	F1.1-4
1.1-5 Location of Site Characterization Studies; Yucca Mountain Nevada	F1.1-5
1.1-6 Existing and Planned Infrastructure; Yucca Mountain, Nevada	F1.1-7
1.1-7 North Portal Operations Area	F1.1-9
1.1-8 South Portal Development Operations Area	F1.1-10
1.1-9 Nearby Mining Claims and Mining and Mineral Leasing Withdrawal	F1.1-11
1.2-1 Population Density and Study Area	F1.2-1

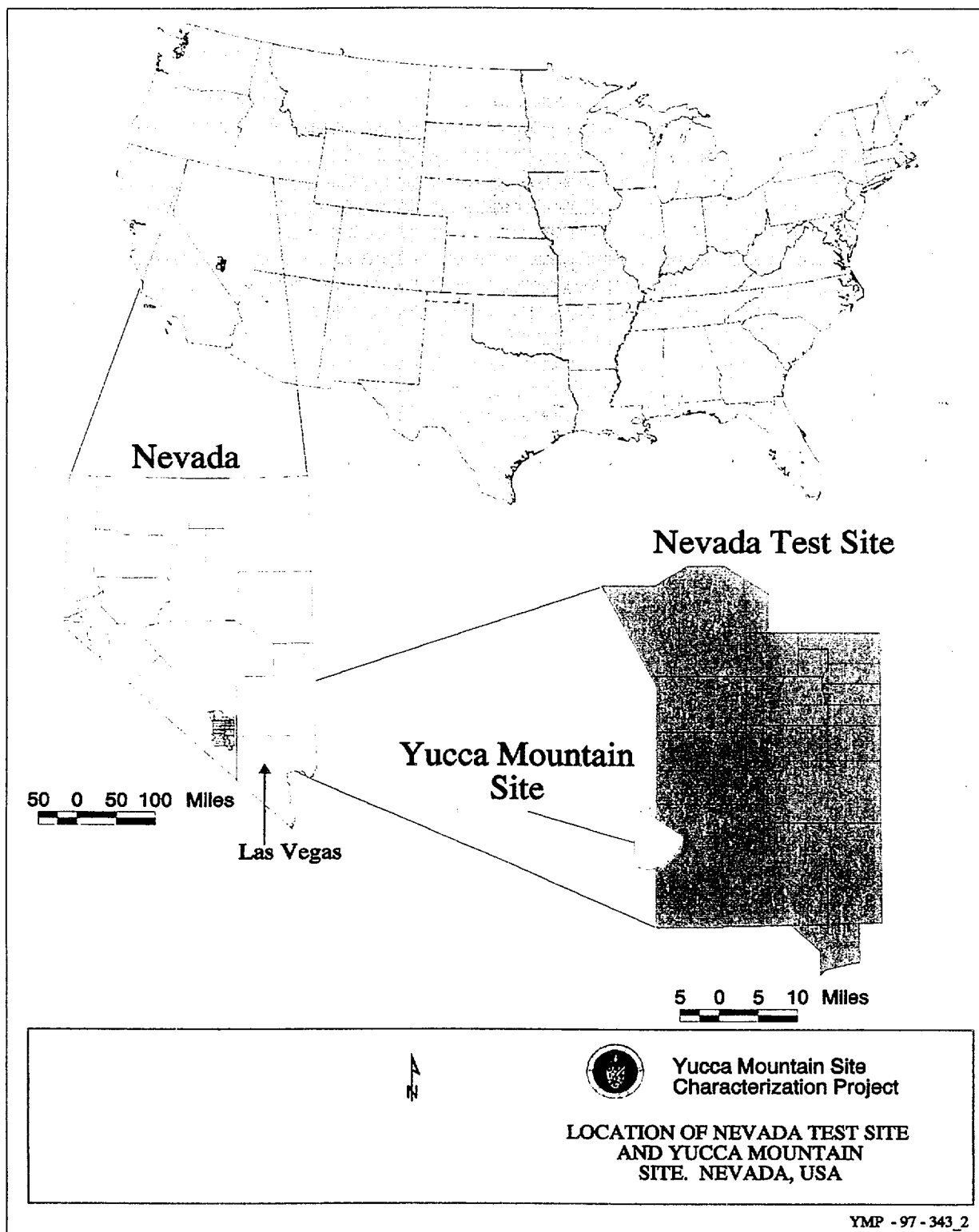


Figure 1.1-1. Location of Nevada Test Site and Yucca Mountain Site, Nevada, USA

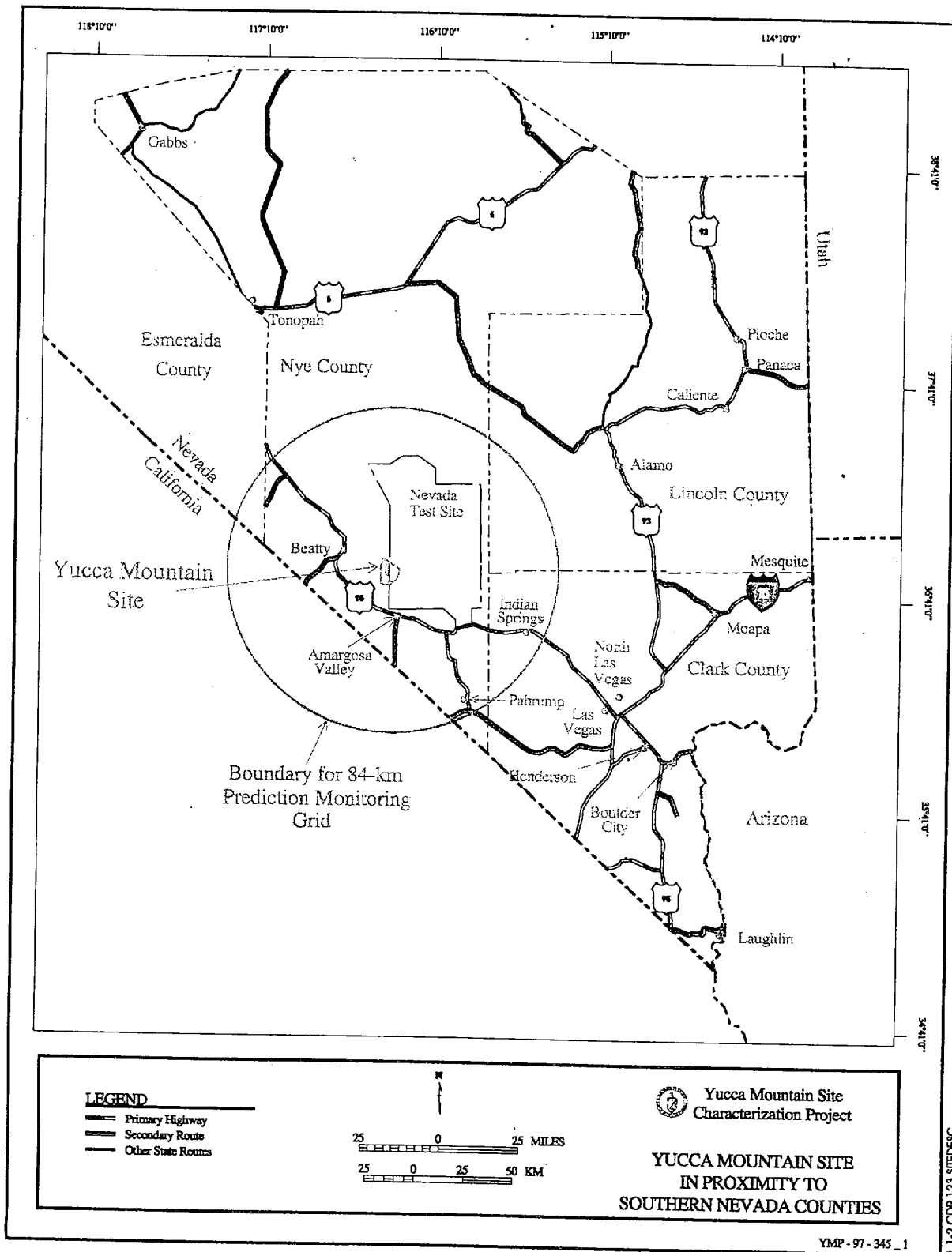


Figure 1.1-2. Yucca Mountain Site in Proximity to Southern Nevada Counties

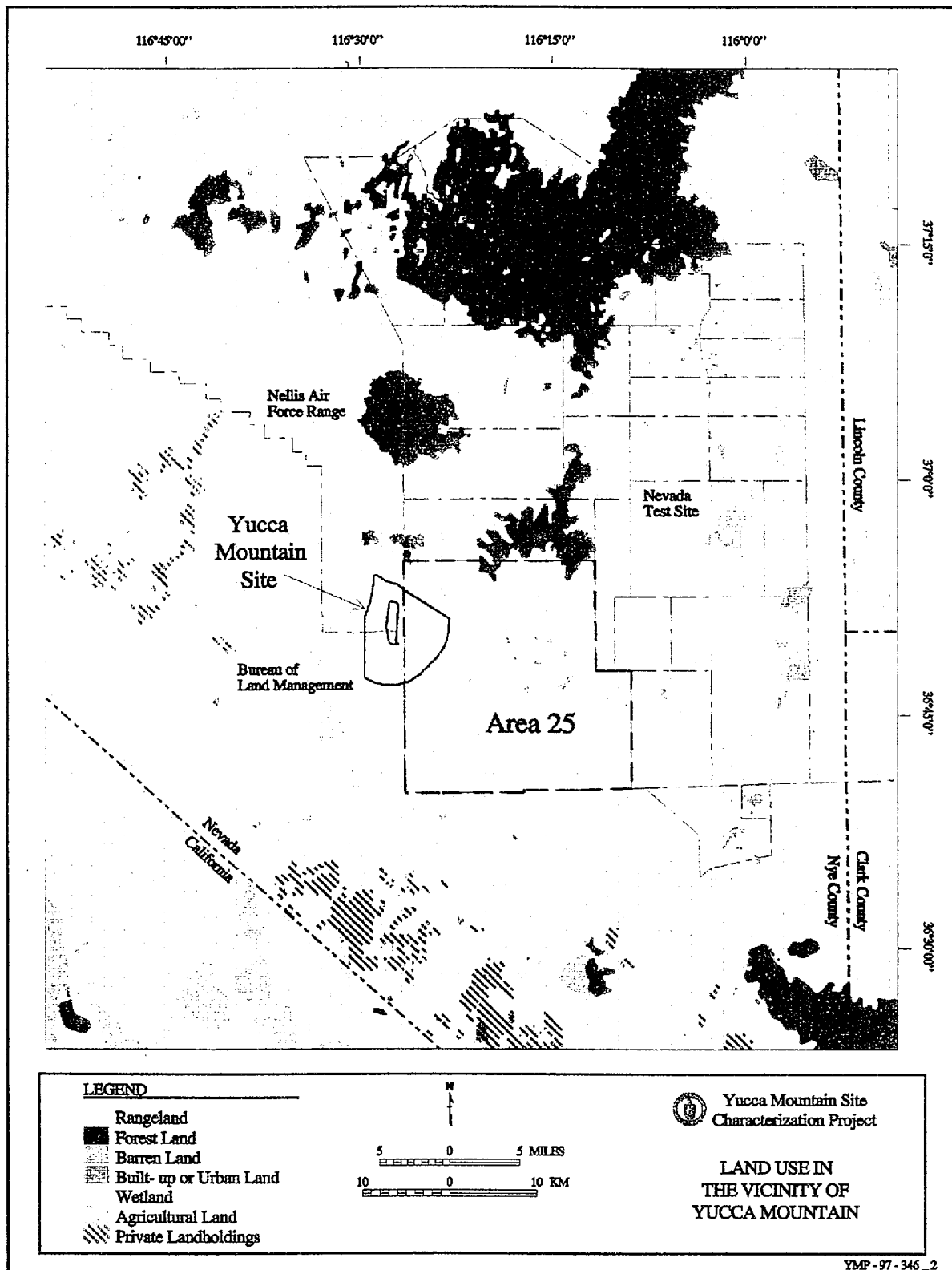


Figure 1.1-3. Nevada Test Site Land Use and Private Land Holdings

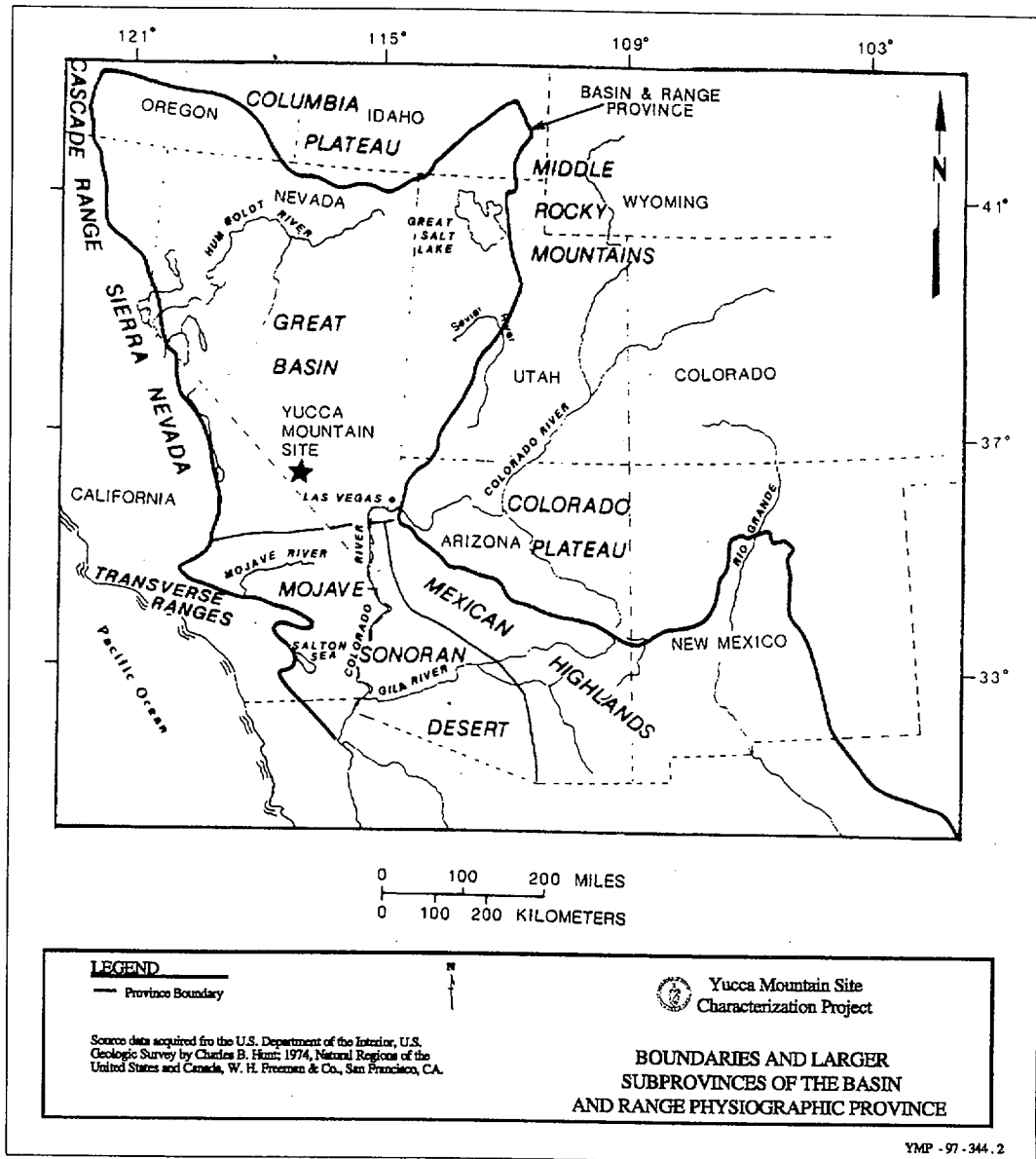
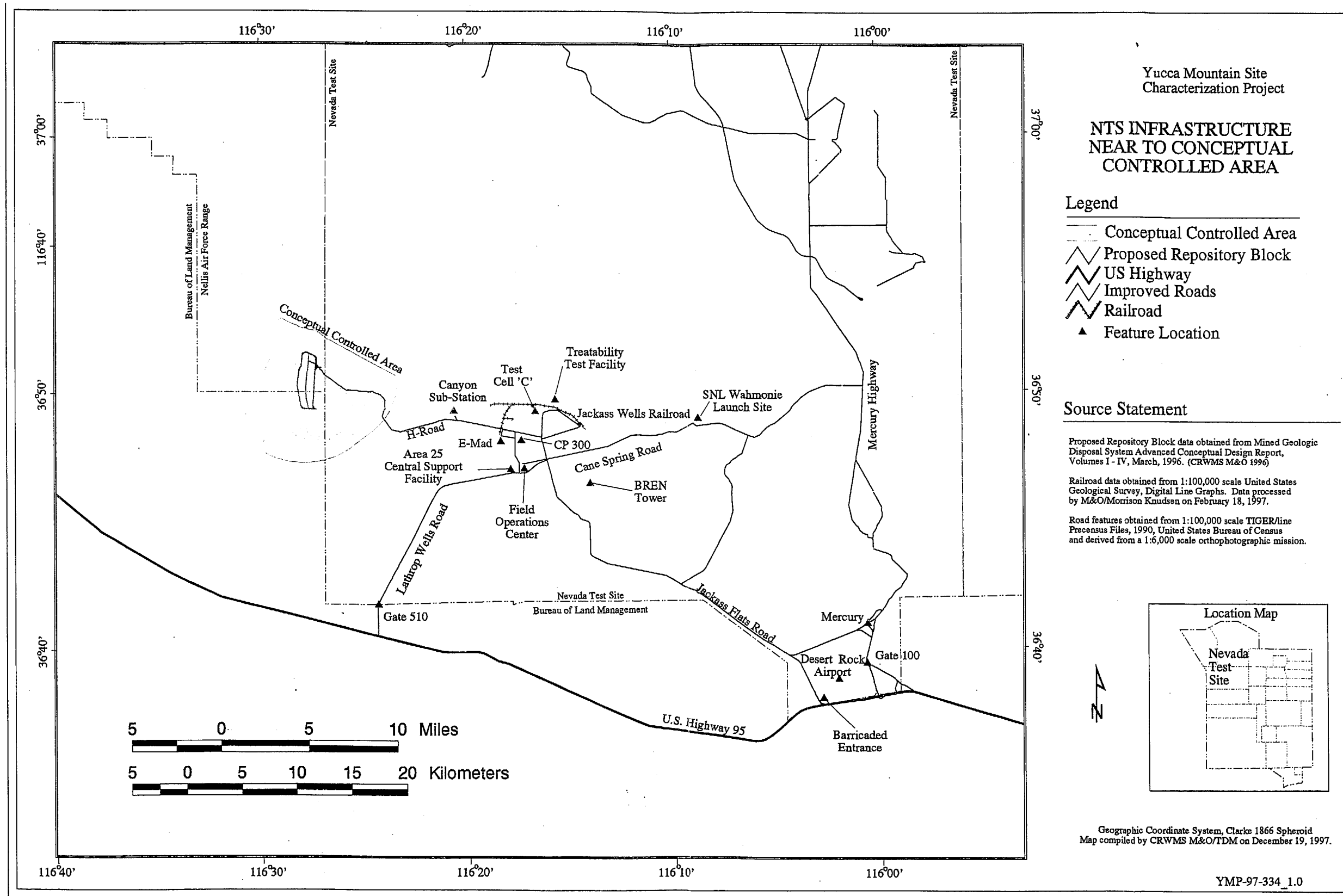


Figure 1.1-4. Boundaries and Larger Subprovinces of the Basin and Range Physiographic Province



APERTURE
 CARD

Also Available on
 Aperture Card

Figure 1.1-5. NTS Infrastructure Near to Conceptual Controlled Area

F1.1-5 **9902040045-01**

INTENTIONALLY LEFT BLANK

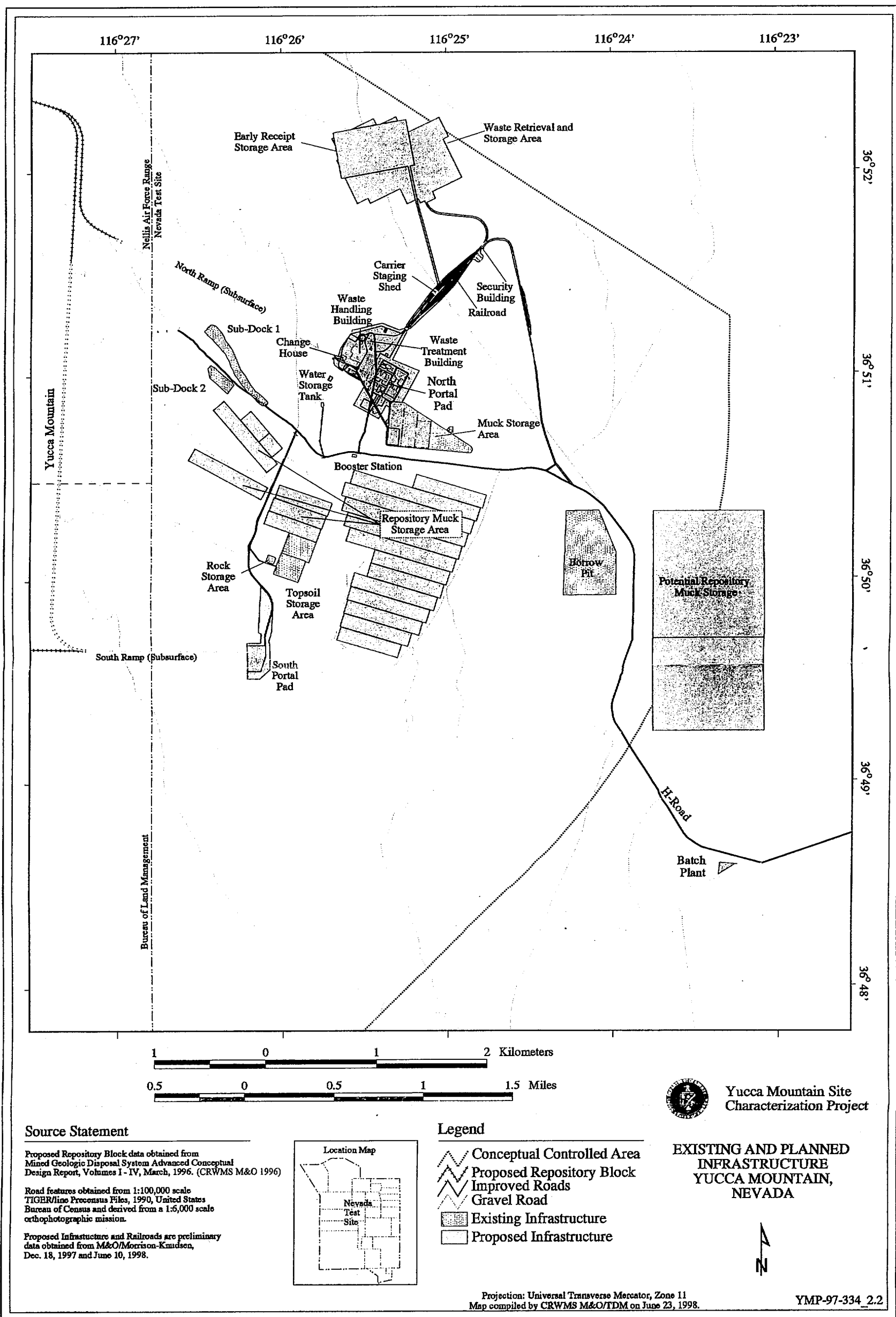


Figure 1.1-6. Existing and Planned Infrastructure;
 Yucca Mountain, Nevada
 FI.1-7

9902040045-02

Also Available on
 Aperture Card

CSCE/SI/ES/23.123.123.123

INTENTIONALLY LEFT BLANK

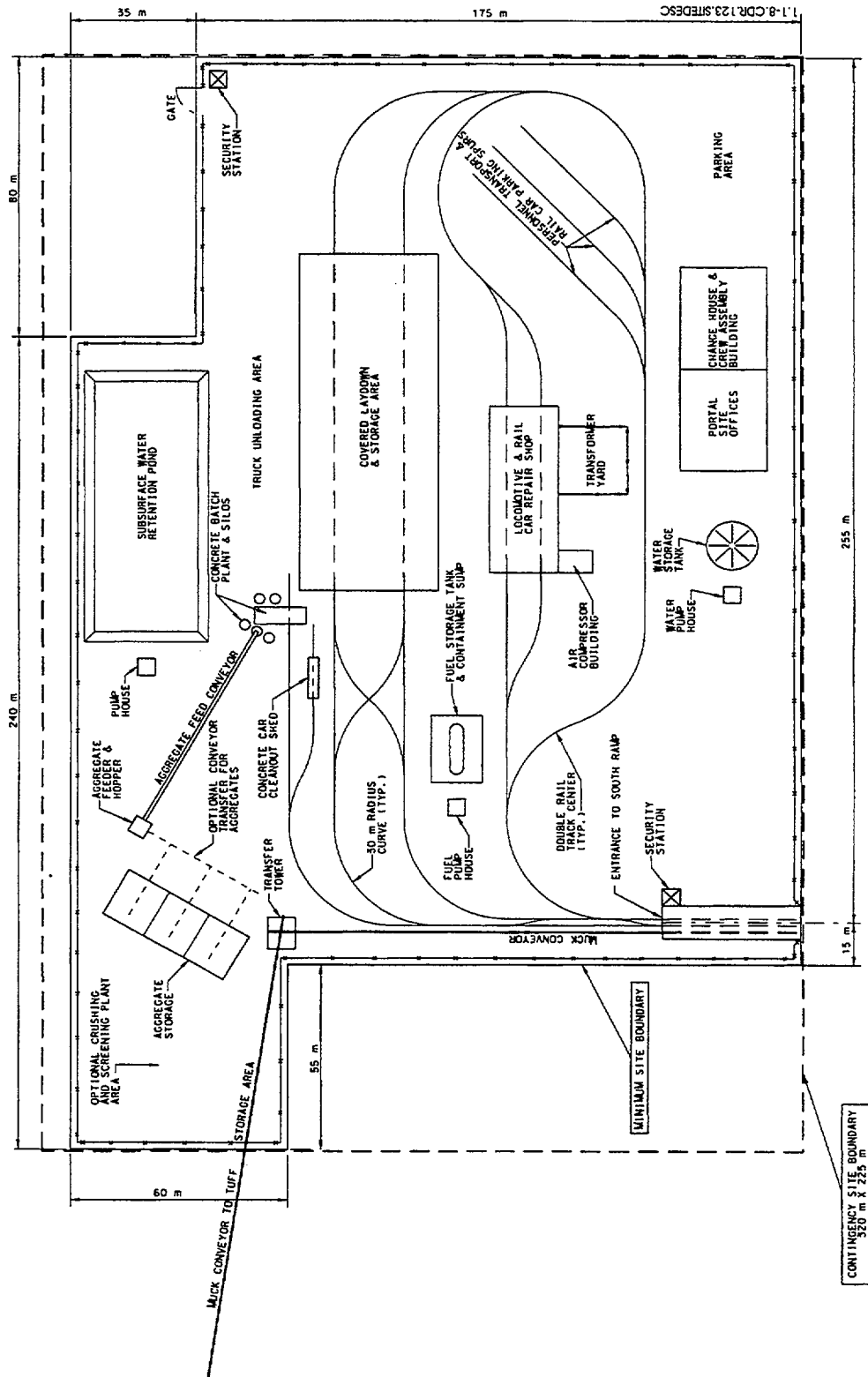
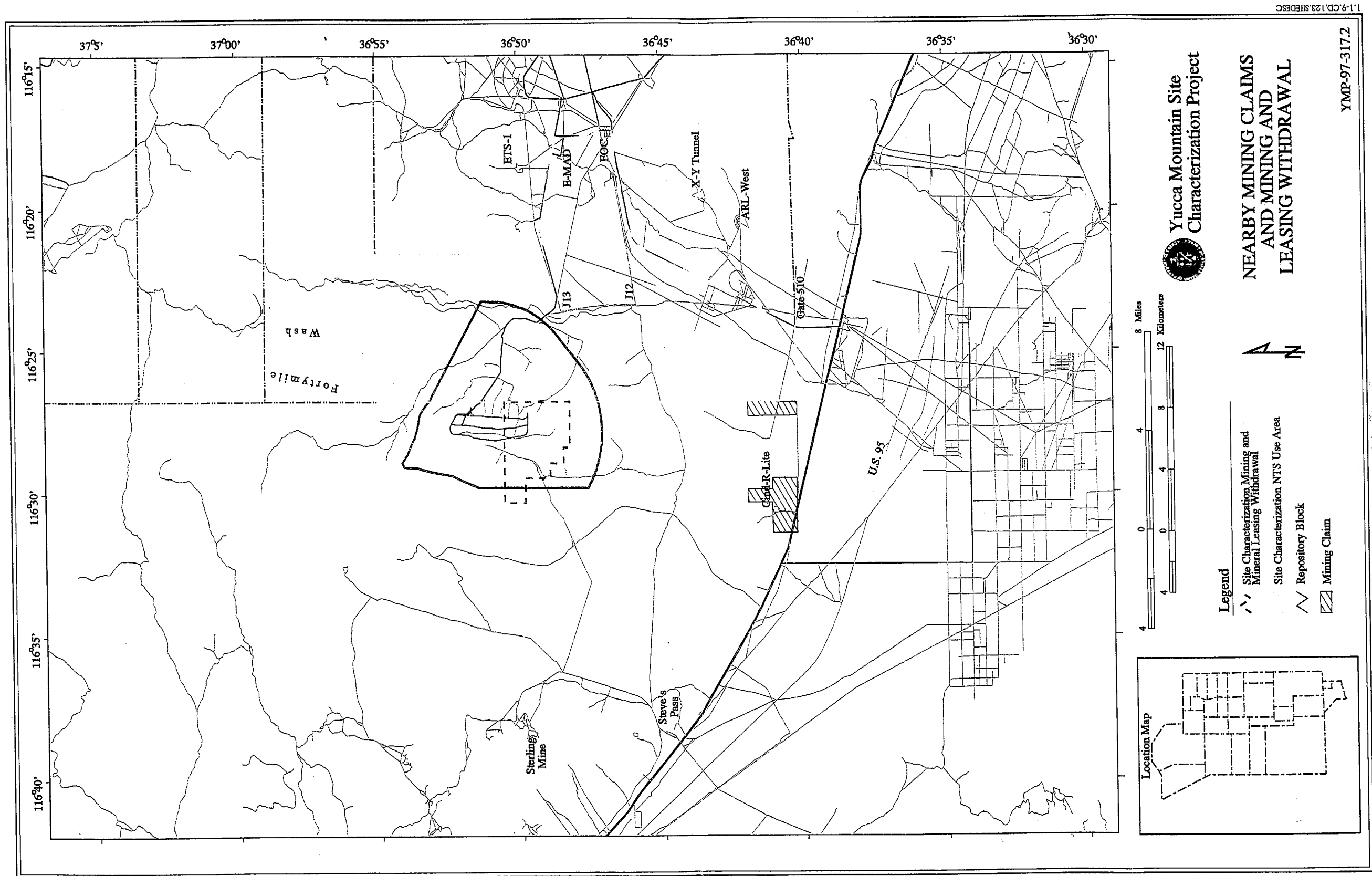
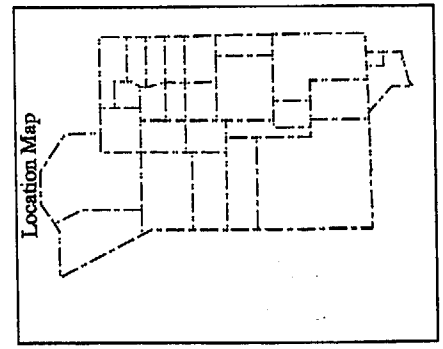


Figure 1.1-8. South Portal Development Operations Area



1:1-9-CD:123:MEDESC



- Legend**
- Site Characterization Mining and Mineral Leasing Withdrawal
 - Site Characterization NTS Use Area
 - ▨ Repository Block
 - ▤ Mining Claim



NEARBY MINING CLAIMS AND MINING AND MINERAL LEASING WITHDRAWAL

YMP-97-317.2

Also Available on Aperture Card

Figure 1.1-9. Nearby Mining Claims and Mining and Mineral Leasing Withdrawal

F1.1-11

9902040045 - 03

INTENTIONALLY LEFT BLANK

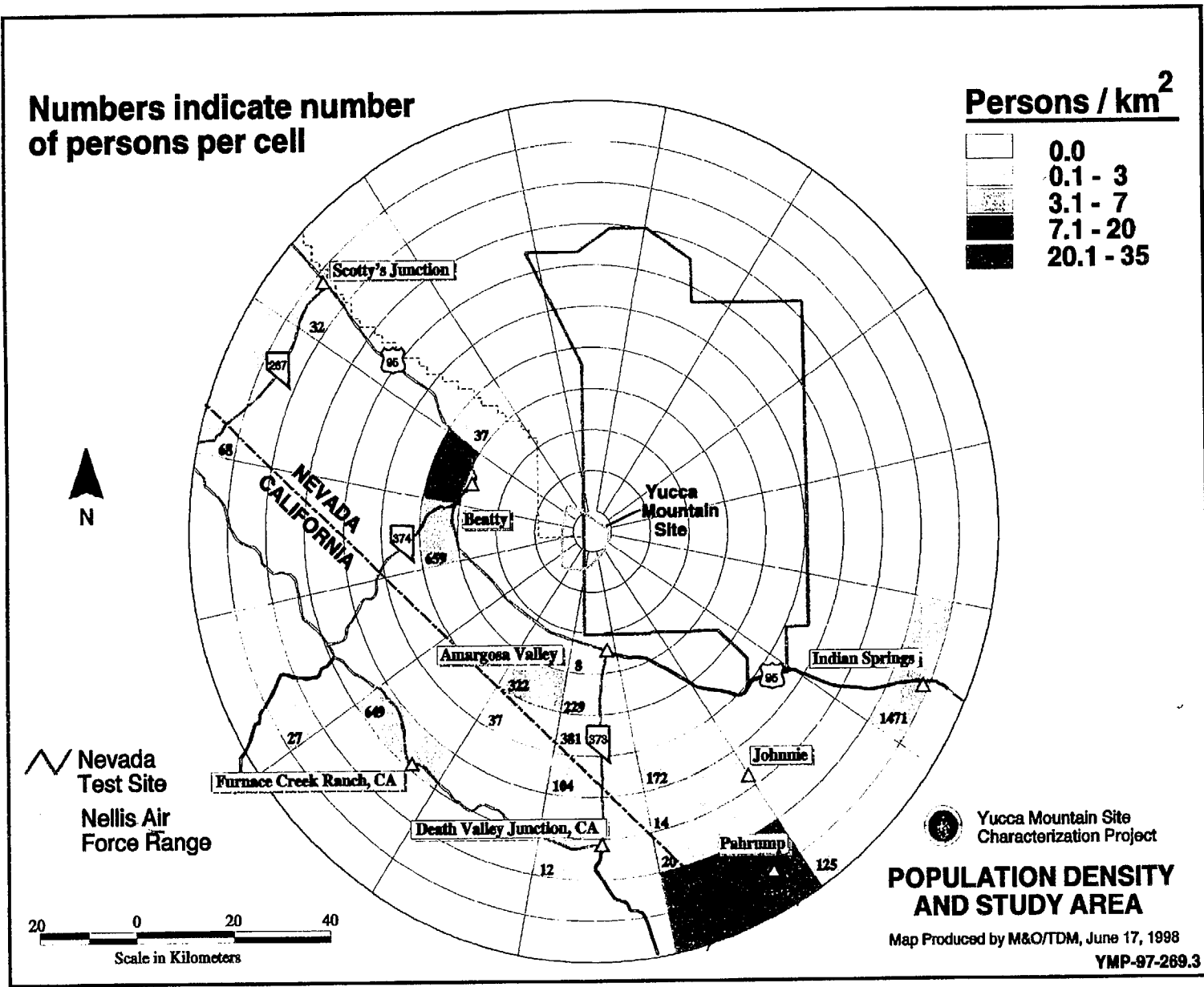


Figure 1.2-1. Population Density and Study Area

F1.2-1

1.2-1.COR.123.SITEDESC

INTENTIONALLY LEFT BLANK

2. NEARBY INDUSTRIAL, TRANSPORTATION, AND MILITARY FACILITIES

2.1 INTRODUCTION

This section identifies potential events associated with present and projected industrial, transportation, and military facilities and operations that occur in the vicinity of the Yucca Mountain Site and that need to be evaluated for their potential effect on daily operations and performance of the potential repository, or that could be used as design basis events to establish design parameters based on those potential events. Industrial operations includes commercial operations such as agriculture.

10 CFR 60, *Disposal of High-Level Radioactive Wastes in Geologic Repositories*, established the rules governing the licensing of the U.S. Department of Energy (DOE) to receive and possess source, special nuclear, and byproduct material at a geologic repository operated in accordance with the Nuclear Waste Policy Act of 1982. The License Application developed in accordance with those rules (or 10 CFR 63 when issued) will include a Safety Analysis Report that describes and assesses features of the Yucca Mountain Site that might affect the operations, design and performance of the potential repository.

At this time, regulatory guidance does not exist that defines a distance from the potential repository within which all facilities and operations must be identified and analyzed for potential impact on the potential repository. Therefore, this report uses as guidance U.S. Nuclear Regulatory Commission (NRC) requirements established for Nuclear Power Plants, specifically NUREG 0800 (NRC 1981) and Regulatory Guide 1.70 (NRC 1978) which direct the identification of all facilities and activities within 8 km (5 mi) of the plant. Both documents also direct that facilities and activities at greater distances should be analyzed if they have the potential for affecting safety-related features.

The term "plant" is interpreted for this section to represent the existing surface facilities at the Yucca Mountain Site and proposed surface facilities related to a repository (Table 1.1-2 and Figures 1.1-5 and 1.1-6), which will be active if the potential repository at Yucca Mountain is authorized for waste reception. The area within an 8 km radius of the potential repository includes parts of the Nellis Air Force Range, Area 25 of the Nevada Test Site, and public lands managed by the U.S. Bureau of Land Management (Figure 2.1-1). These 8-km buffers shown in Figures 2.1-1 and 2.1-2 are the combined outer boundaries of intersecting circles with radii of 8 km and centers at all facilities of the Exploratory Studies Facility.

INTENTIONALLY LEFT BLANK

2.2 NEARBY FACILITIES AND ACTIVITIES WITHIN 8 KILOMETERS (5 MILES)

Airspace—The area within 8 km of the potential repository is located beneath or adjacent to restricted airspace areas, control over which has been delegated to the U.S. Air Force and DOE by the Federal Aviation Administration. This restricted airspace was established because of the classified and/or hazardous nature of the activities conducted within these airspaces or in the areas beneath these airspaces. Restricted area R-4807 extends north of the potential repository site over Nellis Air Force Range withdrawn lands and overlies ground support facilities for military air-to-ground weapons training including convoys, simulated airfields, and electronic combat threat emitters. Electronic Combat South (Figure 2.1-2) is the closest subrange of R-4807 to the potential repository. Electronic Combat South is primarily used as an entry/exit corridor for the R-4807 subranges and contains manned electronic threat emitters (USAF 1996). No ordnance is used in this area. The potential repository underlies the western portion of R-4808 (R-4808W), a DOE-restricted area associated with Nevada Test Site activities. By agreement with the DOE, military aircraft may use flight routes within R-4808 for entering/exiting R-4807. Flight procedures generally keep aircraft east of the proposed repository at 16,000 feet above mean sea level while transiting this area (USAF 1996). Nellis aircraft using R-4808 to enter and exit the Nellis Air Force Range are randomly dispersed. There are currently no set entry and exit routes. There are ongoing discussions between DOE Nevada Operations Office and Nellis Air Force Base, which will result in a Memorandum of Understanding regarding use of R-4808 for entering and exiting the Nellis Air Force Range Complex.

Numerous military training routes that traverse the state are used by Air force and Navy aircraft for low level, high speed flight training. Most of these military training routes are located outside of the Nellis Air Force Range and may or may not be used in conjunction with other training taking place within the Nellis Air Force Range. One of these routes, VR-222, lies south and west of the potential repository and outside the Nellis Air Force Range (Figure 2.1-1). This military training route has a width of five nautical miles on either side of its centerline. The centerline is approximately 8 nautical miles from the proposed repository, therefore the military training route is 3 miles, at the closest, from the proposed repository (USAF 1997)

Nevada Test Site Area 25—Area 25, the largest area on the Nevada Test Site, occupies 223 square miles and is divided into four land use zones, the Yucca Mountain Site Characterization Zone; the Research, Test and Experiment Zone; the Reserved Zone; and the Solar Enterprise Zone (Figure 2.1-2). The Yucca Mountain Site Characterization Zone has been reserved by the DOE for Yucca Mountain Site characterization activities. The Research, Test, and Experiment Zone is used by the U.S. Army Ballistic Research Laboratory for depleted uranium testing and other activities. Reserved Zones at NTS are used to provide area and facilities that allow flexible support for diverse short-term testing and experimentation. The Reserved Zone in Area 25 is used for military land navigation and training exercises. Research sites within the Area 25 Reserved Zone include the Treatability Test Facility and Bare Reactor Experiment Nevada (BREN) Tower. The Treatability Test Facility was established for bench-scale testing of physical processes for separating plutonium and uranium from contaminated soils. The 465 m high BREN Tower has been used by a number of organizations to conduct sonic-boom research, meteorological studies, and free-fall/gravity drop tests. The Solar Enterprise Zone is designated for the development of a solar energy power-generation facility

and associated light industrial equipment and commercial manufacturing capability. In the 1980s, Area 25 was used for MX missile siting studies and canister ejection certification tests. (DOE 1996a). For point of reference, Figure 2.1-2 also shows facilities discussed in Section 1.1 and shown in Figure 1.1-5.

Bureau of Land Management Land—There are no known formal industrial/commercial land uses or infrastructure on Bureau of Land Management land (exclusive of dirt roads) within 8 km of the potential repository.

2.3 NEARBY FACILITIES AND ACTIVITIES GREATER THAN 8 KILOMETERS (5 MILES)

Outside of the 8 km radius from the potential repository, there are military, transportation, and industrial/commercial facilities and activities on the Nellis Air Force Range, the Nevada Test Site, and Bureau of Land Management land which could potentially affect daily operations and performance or be used as design basis events for the potential repository.

Nellis Air Force Range—The Nellis Air Force Range “north range” extends north of Electronic Combat South and is used extensively for weapons training and testing. Large amounts of live and inert ordnance are used on the northern portions of this range that are approved for ordnance use. There are substantial numbers of aircraft flights within the north range where training missions, exercises, and weapons testing take place daily. Although Yucca Mountain is not directly beneath any military routes or in close proximity to live ordnance use on the Nellis Air Force Range, the existence of a high density of flights in the Nellis Air Force Range and the possibility of an aircraft accident could present a potential threat to daily operations and performance of the potential repository. Such accidents could be considered design basis events.

Nevada Test Site—The Nevada Test Site was the primary location of United States continental nuclear weapons testing from 1945 to 1992, and during that period over 1,000 above and below ground nuclear weapons tests were performed. Underground nuclear tests were banned by treaty in 1992; however, the DOE is still directed by the Executive Office to maintain a state of preparedness to test nuclear weapons in the future. Potential areas for future tests include Pahute Mesa and Yucca Flat (DOE 1996a), both of which lie within approximately 60 kilometers of the potential repository (Figure 2.1-2). Nuclear weapons tests may affect seismicity in the region, which is described in Subsection 3.10. Also, administrative policies enforced during such weapons tests could affect the daily operations of the potential repository (DOE 1988). In addition to maintaining preparedness for possible nuclear weapons testing, Nevada Test Site operations include destroying damaged nuclear weapons and conducting dynamic experiments under the Stockpile Stewardship Program, including impact, passive, and chemical tests (DOE 1996a). Another activity includes rocket launches by Sandia National Laboratory from Wahmonie in Area 26 to the Tonopah Test Range, approximately 113 km (70 mi) to the northwest (LVRJ 1997). While these activities take place outside of the 8-km boundary, they could potentially pose a health and/or safety hazard and affect daily operations or performance of the potential repository. Other current and potential uses of the NTS are found in the NTS Environmental Impact Statement (DOE 1996a).

A part of the Nevada Test Site is under development for private use, and in 1997 a 10 year use permit was signed by Nevada Test Site Development Corporation and the DOE, enabling Kistler Aerospace Corporation to begin development of launch operations for a fully reusable orbital launch vehicle. Kistler Aerospace is expected to begin testing in Area 18 of the Nevada Test Site (Figure 2.1-2) in 1998. Kistler Aerospace activities are considered here because launch and re-entry activities could potentially pose a health and/or safety hazard to the potential repository and could be considered a design basis event if operations continue past 2010.

As work on the safety analyses goes forward and the Working Draft License Application is developed, this section in the Working Draft License Application may be expanded to identify

other nearby facilities and activities that may pose special public health and safety, or radiological health and safety hazards, to the development, operation, or closure of the potential repository. Potential Nevada Test Site activities are the development of new transportation corridors or the promotion of mineral resource exploration and development in Area 25. Should such Nevada Test Site activities be initiated, additional safety analyses will need to address such issues. This section will cross reference safety analysis and radiological monitoring information in the Working Draft License Application.

Other Areas—This report also considered commercial, industrial, and transportation operations more than 8 km from the Yucca Mountain Site that could pose a health or safety hazard or could affect daily operations at the potential repository. Three such operations were identified on land outside the Nevada Test Site and Nellis Air Force Range. The first is the Razorback Grazing Allotment, which borders the southwestern corner of the Nellis Air Force Range and is located just outside the 8-km buffer of the potential repository. The grazing allotment, covering 72,880 acres of public land, is scheduled to expire in 2005 (BLM 1997) and does not appear to pose a threat to preclosure activities at the potential repository.

The second activity is gold mining near Beatty and associated water usage from volcanic boreholes that support these mining activities. Currently, VH-2 is the only known volcanic borehole in the area that provides water for mining activities. Active mines, including the Bullfrog, New Discovery, and the Sterling gold mines, the Cind-R-Lite cinder mine, and volcanic boreholes near Yucca Mountain are shown in Figure 2.1-2. The area also contains numerous other boreholes that have been drilled as part of the site characterization activities. These are not shown in this section, but are available in the Site Atlas (CRWMS M&O 1997). These activities do not present a threat to the potential repository-related activities at Yucca Mountain.

The third activity is aircraft operations within commercial flight paths south of the Nevada Test Site and the Yucca Mountain Site. The centerlines of Federal Airway V 105, for air traffic below 18,000 ft mean sea level (DOC 1997), and overlying Jet Route J-92, for air traffic above 18,000 ft mean sea level (DOC 1992), are approximately 25-km (15 mi) southwest from the potential repository site. These routes travel from southeast to northwest and are primarily used by commercial air traffic between Reno and Las Vegas and other airports in the southwestern and northwestern U.S. (Figure 2.1-1). Most of this traffic consists of jet airliners operating at higher altitudes (24,000 to 30,000 ft) on Jet Route J-92. U.S. Highway 95 (Figure 2.1-1) is occasionally used as a visual reference by general aviation aircraft flying under visual flight rules through this area. The few aircraft flying under these conditions through this area are limited by Federal Aviation Regulations to altitudes below 18,000 ft mean sea level (DOC 1997). These activities do not present a threat to activities related to the potential repository at Yucca Mountain.

There are no other known commercial, industrial, or transportation operations outside of 8 km from Yucca Mountain which could pose a health or safety hazard to the potential repository.

2.4 NEARBY TRANSPORTATION ROUTES

Transportation routes of potential concern to health, safety, and normal operations at the potential repository are potential railroads or heavy haul truck routes that may be built or upgraded to transport high-level radioactive waste to the potential repository, highways in the vicinity of the Yucca Mountain Site, and commercial and military flight zones. There are no streams or rivers in the vicinity of the Yucca Mountain Site that are capable of supporting water-based forms of transportation.

Railroads and Heavy Haul Truck Routes—If the potential repository is built and operated, high-level radioactive waste may be transported to Nevada by railroad. When the high-level radioactive waste reaches Nevada, it will be transported from the national rail lines to the potential repository by either rail or heavy haul trucks. Because there are currently no rail lines to the potential repository at Yucca Mountain, if the rail implementing alternative is selected a line will have to be constructed. Similarly, if the heavy haul implementing alternative is selected, heavy haul routes will have to be either constructed or existing routes will have to be upgraded. There are currently five potential heavy-haul truck routes and five potential rail corridors in Nevada being considered for transportation of high-level radioactive waste to Yucca Mountain. These potential routes have been planned with consideration of necessary rights-of-way, land withdrawals, use restrictions and land-use conflicts, and are described in detail in the reference documents (CRWMS M&O 1996a; *Nevada Potential Repository Preliminary Assessment of the Caliente-Chalk Mountain Rail Corridor*, predecisional EIS document, 1997, B00000000-01717-4600-00077 REV 00, CRWMS M&O). There is only a small portion of each of these routes sufficiently close enough to the potential repository to potentially affect daily operations or performance. Scenarios for onsite high-level radioactive waste transportation hazards are being evaluated.

Flight Corridors and Highways—Military and commercial air transportation corridors and activities were described in Subsections 2.2 and 2.3. Aside from commercial aircraft traffic, U.S. Highway 95 is the only primary transportation route near the Yucca Mountain Site. U.S. Highway 95 lies in a northwest/southeast orientation and passes approximately 19 km (12 mi) to the southwest of the potential repository at Yucca Mountain. A traffic event on U.S. Highway 95 substantial enough to be pose a direct hazard to the plant, and that would be considered a design basis event, is not considered credible and need not be evaluated. However, U.S. Highway 95 is the primary land-based route to the potential repository at Yucca Mountain and is heavily relied upon for the transportation of workers and materials to the Nevada Test Site and the Yucca Mountain Site. A traffic event on U.S. Highway 95, particularly between Las Vegas and the entrances to the Nevada Test Site (Figure 1.1-5), could potentially disrupt the delivery of high-level radioactive waste, materials, and employees to the potential repository, and hence affect daily operations or performance, although such an event would likely be of short duration.

INTENTIONALLY LEFT BLANK

2.5 EVALUATION OF POTENTIAL ACCIDENTS

The preceding sections described the existing industrial, transportation, and military facilities/operations in the vicinity of the potential repository at Yucca Mountain. This section discusses the potential for accidents at these facilities and related operations.

A Preliminary Hazards List was developed using Preliminary Hazards Analysis methodology (described in the *System Safety Analysis Handbook* (SSS 1997)), which provides a systematic approach to identify preliminary hazards that may exist in any system design. These hazards have potential radiological consequences applicable to the proposed repository (as described in the *Mined Geologic Disposal System Advanced Conceptual Design Report* (CRWMS M&O 1996b)) during the preclosure period. The results of the Preliminary Hazards Analysis will undergo further screening and analysis based on the criteria that apply to the Design Basis Events analyses for the preclosure phase of the repository operations (CRWMS M&O 1996c).

The Preliminary Hazards Analysis addressed both internal and external hazards. This section addresses only external hazards, and focuses on man-induced hazards rather than natural hazards. Application of the generic checklist identified nine potential man-induced hazards for analysis. Of these, six have potential impact at the proposed repository during the preclosure period. They are:

- Aircraft Crash
- Industrial Activity Induced Accidents
- Military Activity Induced Accidents
- Loss of Off-Site/On-site Power
- Inadvertent Future Intrusions (man-made)
- Intentional Future Intrusions (man-made)

The intrusion hazards are security related and are addressed as requirements for site ownership and control (see Section 1) and in a Safeguards and Security Plan required to be developed by DOE in accordance with 10 CFR 60.21(b)(3), 10 CFR 60.21(b)(4), and 10 CFR 60.31(b). Loss of power is an issue that will be addressed in the design process to mitigate such events in accordance with Nuclear Regulatory Commission requirements (10 CFR 60.131) and will not be further discussed in this section.

General design criteria of 10 CFR 60.131 requires that the potential geologic repository provide protection against design basis events, "...which are sufficiently credible to warrant consideration, taking into account the potential for significant radiological impacts on public health and safety." The NRC has determined that (category 2) events with probabilities of occurrence lower than 1×10^{-6} per year can be screened from further repository risk analysis (61 FR 64259 (NRC 1996)).

Each of the three remaining events, Aircraft Crash and Industrial and Military Activities Induced Accidents, is being studied to determine if the anticipated frequency is greater than 1×10^{-6} . If so, an in-depth accident analysis will be developed and appropriate design basis requirements will be determined and the results will become part of the Safety Analysis Report. Events with

expected frequencies below a lower bound of 1×10^{-6} per year (less than once in a million years) need not be analyzed further and their effects need not be mitigated (NRC 1996).

Aircraft Crash—Initial, unpublished preliminary analyses of the frequency of aircraft accidents have been performed. These analyses are still under development and are awaiting revised Air Force data. The analyses will be completed during the Working Draft License Application phase as part of the Safety Analysis Report.

This initial, preliminary analysis has indicated that the frequency of a civilian aircraft crash on surface facilities at the potential repository is less than 1×10^{-6} per year and is not a credible event. This initial analysis of the potential for a military aircraft crashing onto a surface facility at the potential repository indicates that this event is near the lower bound frequency of 1×10^{-6} per year. Additional flight data are needed to better estimate the potential accident frequency. If comprehensive studies suggest that the potential frequency of this event is greater than 1×10^{-6} per year, it may be necessary to mitigate these findings by making changes to the air routes and reducing the potential frequency of accidents at the potential repository before it becomes operational. An evaluation of the effects of an aircraft crash accident has not been performed because it is anticipated that further analysis and implementation of appropriate adjustments in flight routes or procedures will result in a determination that this event is not credible. If an aircraft crash is still determined to be credible and therefore a design basis event, some of the surface facilities may need to be designed to minimize the adverse effects of such an event.

Industrial and Military Induced Accidents—Because there are no industrial or military activities (except possible overflights) within 8 km of the plant, no design basis events have been identified for this area. Industrial or military accidents beyond the 8 km area are being identified and evaluated. This analysis is ongoing because no accidents have yet been identified which would impact the operation of the repository facilities.

This section has provided an identification and description of facilities and activities that may impact health and safety or daily operations of the potential repository. As a description, this information does not appear to fall under the requirements for Qualified (Q)-data as defined in 10 CFR 60, Subpart G, Quality Assurance, and is not Q-data. However, the data collected and analyzed in other sections of the Viability Assessment and Working Draft License Application are collected, analyzed, and interpreted in accordance with the Quality Assurance program.

2.6 REFERENCES

NOTE: For each reference either a document accession number (NNA.19xxxxxx.xxxx) or a technical information center number (TIC xxxxxx) is provided. If a number is not currently available, it is noted by TBD (to be determined).

2.6.1 Documents Cited

BLM (Bureau of Land Management) 1997. *Grazing Lease NV: 065. Operator Number 276122.* U.S. Department of the Interior. Washington, D.C.: U.S. Government Printing Office. TIC 237117.

CRWMS M&O (Civilian Radioactive Waste Management System Management and Operating Contractor) 1996a. *Nevada Potential Repository Preliminary Transportation Strategy, Study 2.* B00000000-01717-4600-00050 REV 01. Las Vegas, Nevada: Author. MOL.19960724.0199; MOL.19960724.0200.

CRWMS M&O 1996b. *Mined Geologic Disposal System Advanced Conceptual Design Report, Volumes I through IV.* B00000000-01717-5705-00027 REV 00. Las Vegas, Nevada: Author. TIC 233073.

CRWMS M&O 1996c. *Preliminary MGDS Hazards Analysis.* B00000000-01717-0200-00130 REV 00. Las Vegas Nevada: Author. MOL.19961230.0011.

CRWMS M&O 1997. *Yucca Mountain Site Characterization Project Site Atlas, Part 1.* Las Vegas, Nevada: Author. TIC 236826.

DOC (U.S. Department of Commerce) 1992. *Instrument Flight Rules Enroute High Altitude Southwest Chart.* Washington, D.C.: U.S. Department of Commerce. TBD

DOC 1998. *Instrument Flight Rules Enroute Low Altitude—U.S. Chart L-5, August 13.* Washington, D.C.: U.S. Department of Commerce. TBD

DOE (U.S. Department of Energy) 1986. *Final Environmental Assessment: Yucca Mountain Site, Nevada Research and Development Area, Nevada.* 3 Volumes. DOE/RW-0073. May. Las Vegas, Nevada: U.S. Department of Energy, Office of Civilian Radioactive Waste Management. TIC 235716.

DOE 1988. *Site Characterization Plan for Yucca Mountain Site Research and Development Area Nevada.* DOE/RW-0199, pp. 1-209. Las Vegas, Nevada: U.S. Department of Energy, Yucca Mountain Site Characterization Office. TIC 223856-223864.

DOE 1996a. *Final Environmental Impact Statement for the Nevada Test Site and Off-Site Locations in the State of Nevada.* DOE/EIS 0243. Vol. 1. Las Vegas, Nevada: U.S. Department of Energy, Nevada Operations Office. TIC 226874.

DOE 1996b. *Record of Decision: Environmental Impact Statement for the Nevada Test Site and Off-Site Locations in the State of Nevada*. Federal Register, December 13, 1996. 61, n. 241, 65551-65563. Washington, D.C.: U.S. Government Printing Office. TIC 239429.

LVRJ (Las Vegas Review Journal) 1997. *Fire in the Sky*, April 14, 1997. Las Vegas Review-Journal [Electronic newspaper article database] [Accessed September 18, 1998] Available: http://www.lvrj.com/lvrj_home/1997/APR-14-Mon-1997/news/5165508.html.

NRC (U.S. Nuclear Regulatory Commission) 1978. *Standard Format and Content of Safety Analysis Reports for Nuclear Power Plants*. Regulatory Guide 1.70-2. Washington, D.C.: U.S. Nuclear Regulatory Commission. TIC 222636.

NRC 1981. *Identification of Potential Hazards in Site Vicinity*, Rev. 2. NUREG 0800: 2.2.1 – 2.2.2. Washington, D.C.: U.S. Nuclear Regulatory Commission. TIC 239428.

NRC 1996. *Disposal of High-Level Radioactive Wastes in Geologic Repositories; Design Basis Events*. RIN 3150-AD51. Federal Register 61 FR 64257-64270. Washington, D.C.: U.S. Nuclear Regulatory Commission. TIC 238559.

SSS (System Safety Society) 1997. *System Safety Analysis Handbook*. Albuquerque, New Mexico: System Safety Society. TIC 103284.

USAF (U.S. Air Force) 1996. *Space, Missile, Command and Control: Weapons Ranges*. AFI 13-212, Volume 1/ NAFB Supplement 1, May 21, 1996. St. Louis, Missouri: U.S. Air Force. TIC 236940.

USAF 1997. *Area Planning, Military Training Routes, North and South America*. DOD (U.S. Department of Defense) Flight Information Publication AP/1B. St. Louis, Missouri: National Imagery and Mapping Agency. TIC 239798.

2.6.2 Codes, Standards, and Regulations

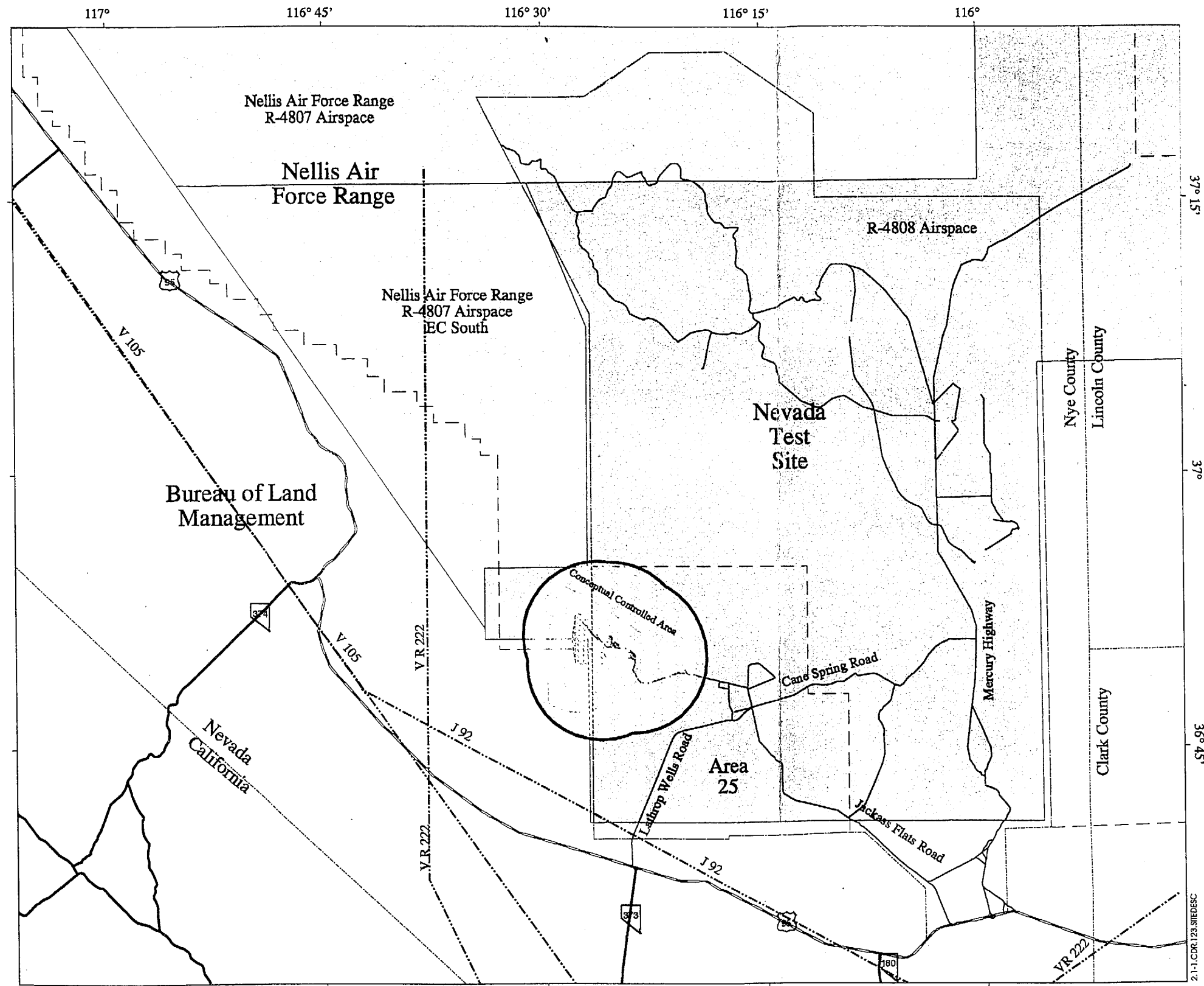
10 CFR 60. Energy: Disposal of High-Level Radioactive Wastes in Geologic Repositories. TIC 238445.

Nuclear Waste Policy Act of 1982. Public Law 97-425. 42 U.S.C. 10101-10226. Washington, D.C.: U.S. Government Printing Office. TIC 222165.

FIGURES

	Page
2.1-1 Transportation Facilities/Activities in Proximity to Yucca Mountain	F2.1-1
2.1-2 Industrial and Military Facilities in Proximity to Yucca Mountain	F2.1-3

INTENTIONALLY LEFT BLANK



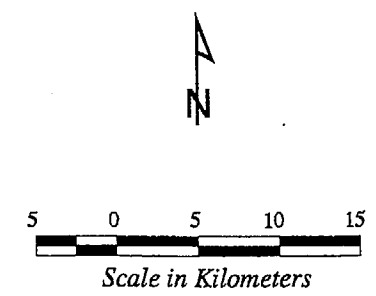
Yucca Mountain Site
 Characterization Project

Legend

- Repository Surface Facilities
- NUREG-0800 Defined 8K Area
- Proposed Repository Block
- R-4808 Airspace
- R-4807 Airspace
- Conceptual Controlled Area Boundary
- Federal Airways and Jet Routes
- NUREG-0800 Defined 8K Boundary

Sources

Proposed Repository Block data obtained from Mined Geologic Disposal System Advanced Conceptual Design Report, Volumes I - IV, March, 1996 (CRWMS/M&O 1996b).
 Area-25 Features Obtained From "NTS EIS Record Of Decision." USDOE 1996b.
 8K Plant Buffer Generated from NUREG-0800 Definition (NRC 1981).



Projection: Universal Transverse Mercator, Zone 11
 Map compiled by CRWMS M&O/TDM on September 2, 1998.

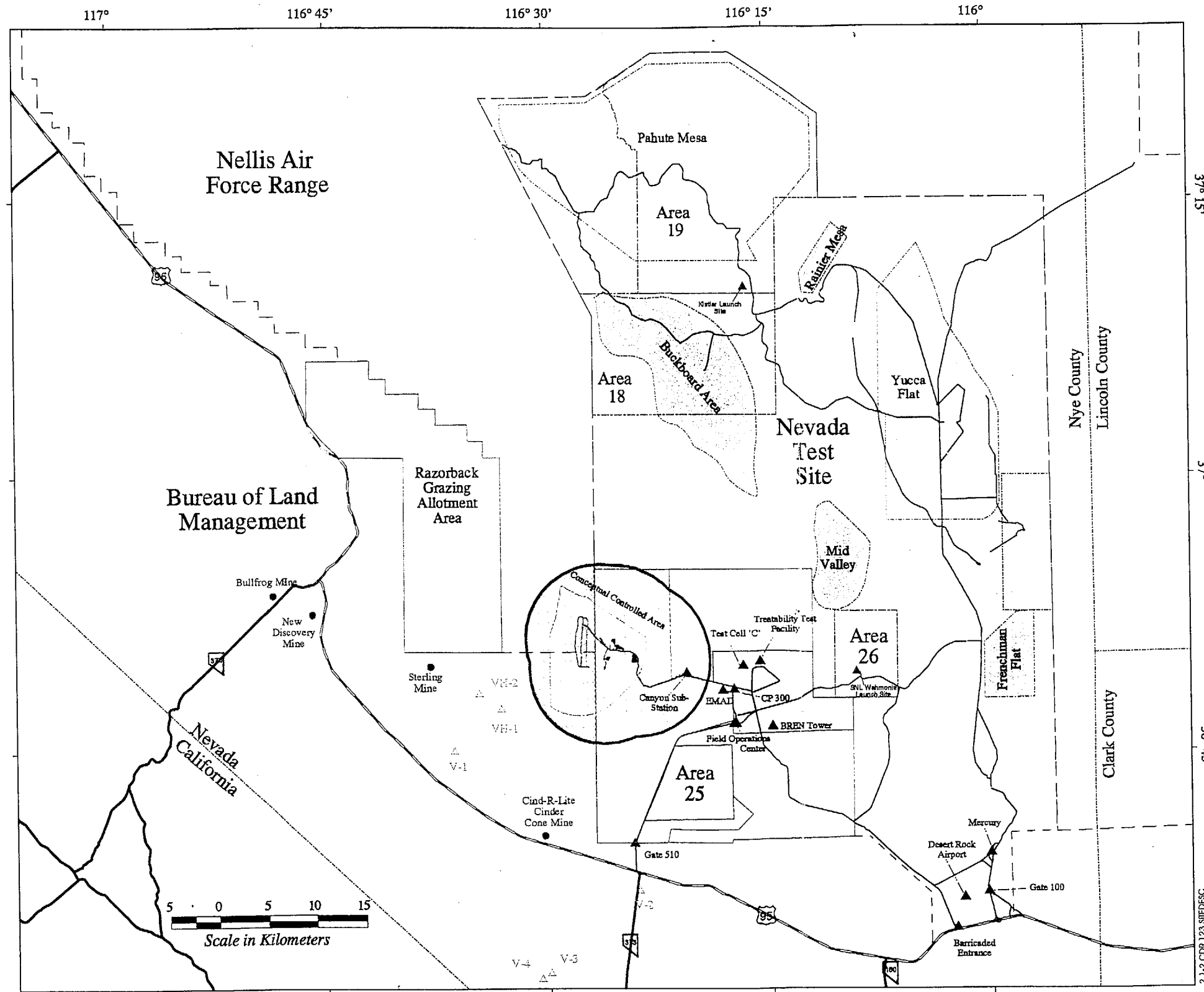
YMP-98-013-2.2

Figure 2.1-1. Transportation Facilities/Activities in Proximity to Yucca Mountain

F2.1-1 **9902040045-04**

APERTURE CARD
 ALSO AVAILABLE
 APERTURE CARD

INTENTIONALLY LEFT BLANK



Yucca Mountain Site
 Characterization Project

Legend

- Approximate Areas of Past and Potential Future Weapons Testing
- Approximate Areas of Past Weapons Testing
- Repository Surface Facilities
- NUREG-0800 Defined 8K Area
- Razorback Grazing Allotment Area
- Proposed Repository Block
- Research, Test and Experiment Zone
- Reserved Zone
- Solar Enterprise Zone
- Yucca Mountain Site Characterization Zone
- Volcanic Borehole Locations
- Active Mines
- Conceptual Controlled Area Boundary
- NUREG-0800 Defined 8K Boundary

Sources

Proposed Repository Block data obtained from Mined Geologic Disposal System Advanced Conceptual Design Report, Volumes I - IV, March, 1996 (CRWMS/M&O 1996b).

Weapons-Testing Areas Obtained "NTS EIS" (DOE 1996a).

Area-25 Features Obtained From "NTS EIS Record Of Decision" (DOE 1996b).

8K Plant Buffer Generated from NUREG-0800 Definition (NRC 1981).

Razorback Grazing Allotment Area Obtained from "Yucca Mountain Environmental Assessment" (DOE 1986).

Volcanic Borehole and Active Mine Locations obtained from Site Atlas (CRWMS/M&O 1997b).

Projection: Universal Transverse Mercator, Zone 11
 Map compiled by CRWMS M&O/TDM on September 2, 1998.

YMP-98-013-1.2

Figure 2.1-2. Industrial, Commercial, and Military Facilities/Activities in Proximity to Yucca Mountain

F2.1-3

9902040045-05

INTENTIONALLY LEFT BLANK

3. GEOLOGY

Section 3 provides a description of the geology of the Yucca Mountain Site and vicinity, as follows:

- An introduction that includes a discussion of methodologies employed
- A presentation of the regional stratigraphy and structure to provide the regional geologic framework
- A description and evaluation of Tectonic models
- A discussion of Quaternary stratigraphy and surficial processes with an emphasis on implications for erosion
- The immediate Yucca Mountain Site with discussions of the site stratigraphy, site structure, site geoenvironmental data, rock properties modeling, and the three-dimensional 3-D integrated site geologic model
- Discussions of volcanism and seismicity, including hazard assessments, as they pertain to the Yucca Mountain Site
- A description of natural resource assessments for the Yucca Mountain Site

3.1 INTRODUCTION

The geologic system at Yucca Mountain forms a fundamental framework for understanding the performance of the site as a potential geologic repository for high-level radioactive waste. The geologic system also provides key inputs for design of the repository; for example, the stratigraphy, structure, and rock material properties, as combined in the 3-D integrated site model, support the development of flow and transport process models. Results from geologic mapping, fracture analyses, and rock properties testing are used to design and analyze various repository structures, systems, and components. Studies of tectonics, igneous activity, earthquakes, and geomorphology provide information on how geologic processes might affect repository performance in the future. Assessments of potential natural resources at Yucca Mountain contribute to an evaluation of the likelihood of future human intrusion into a repository. Thus, the geologic system at Yucca Mountain represents a key element in assessing the overall performance of the repository with regard to protecting the health and safety of the public.

In addition to describing the geologic system at Yucca Mountain and its immediate vicinity, this section also places the site in the context of its regional geologic setting. For each component of the geologic system, such a discussion demonstrates the similarities and differences between Yucca Mountain and its surrounding region, and relates each component to the broader geologic history and processes that have operated in the region. In addition, the extent of the region that is pertinent to each component is described and justified.

Quality Assurance Controls Yucca Mountain Site Characterization Project (YMP) work summarized in this section comes under the control of the *Quality Assurance Requirements and Description* (DOE 1997). Much of the information presented and discussed, however, was developed outside of the YMP and has been included here through examination of the geological literature. Thus, the quality assurance status of the data in this section is determined by the activities and reports from which they were synthesized. As an aid in identifying the Q status of data discussed in this section, some references are notated with [Q] or [NON-Q] in the reference list. For those without such notation, the original reference should be consulted to determine the Q status of data.

3.1.1 Regulatory Framework

The regulatory framework for the work carried out at Yucca Mountain derives from various sources. Section 113(a) of the Nuclear Waste Policy Act as amended (1987) specified the requirement for carrying out appropriate site characterization activities at the Yucca Mountain Site. The U.S. Nuclear Regulatory Commission's (NRC) disposal regulations specified, in 10 CFR 60, *Disposal of High-Level Radioactive Wastes in Geologic Repositories*, Section 15(a), a program of site characterization to be conducted prior to submittal of an application for license. Finally, the U.S. Department of Energy (DOE) guidelines for siting a repository specified site characterization as the method to obtain information needed to support the site recommendation for repository development (10 CFR 960.3-1-4-4).

The description of the geologic system addresses requirements within 10 CFR 60. The information presented in this document provides a description and assessment of the geologic system of the site in accordance with 10 CFR 60.21(c)(1)(I) and 10 CFR 60.21(c)(1)(ii). Also provided is a basis for evaluating favorable and potentially adverse conditions (10 CFR 60.122) as required by 10 CFR 60.21(c)(1)(ii)(B), and natural resources as required by 10 CFR 60.21(c)(13). The description of the site further identifies the technical data and summarizes current analyses and interpretations needed to determine the suitability of the site and support the site recommendation.

An understanding of the geologic system of the site also contributes to addressing the NRC's key technical issues (NRC 1997a). Some of these issues involve the behavior of the natural systems at the site because the natural systems are a factor in the ability of the site to contain and isolate waste. For some key technical issues, information contained in this subsection provides most of the basis for addressing the issue (e.g., Igneous Activity, Structural Deformation and Seismicity). For others, results presented here are necessary but not sufficient to address the issue completely (e.g., Repository Design and Thermal-Mechanical Effects, Unsaturated And Saturated Flow Under Isothermal Conditions). For issues in the second category, results from more than one section need to be integrated to provide the needed evaluation.

3.1.2 Key Observations of the Geologic System

Investigations of the geologic system at Yucca Mountain have resulted in the following key observations and conclusions:

- The exposed stratigraphic sequence at Yucca Mountain is dominated by mid-Tertiary volcanic rocks, consisting mostly of pyroclastic flow and fallout tephra deposits with minor lava flows and reworked materials that were erupted from the southwestern Nevada volcanic field during the period 15.2 to 11.4 Ma (Section 3.5).
- Most lithostratigraphic units are laterally extensive within the site area and typically have a stratiform geometric shape (Section 3.5).
- The hierarchy of structures that affect the Miocene Paintbrush Group at Yucca Mountain comprises: north-striking block-bounding faults spaced one to 4 km apart, commonly with hundreds of meters of normal-sense Tertiary displacement; northwest-striking relay faults that transfer displacement between block-bounding faults; smaller intra-block faults (commonly with 1 to 20 m of displacement); and a network of joints and tectonic fractures that, where best-developed, divides the rock mass at the cubic-meter scale (Section 3.6).
- The most important controls on fracture attributes are primary, lithologic controls. The degree of welding, lithophysae development, vapor-phase alteration, and pumice content are all primary controls that affect fracture spacing, type, number of sets, continuity of individual fractures, and probably connectivity of the entire network. Structural controls on fracture distribution, such as proximity to faults, are secondary to primary lithologic controls (Section 3.6).
- The smallest structures are strongly controlled by local stratigraphy, whereas the largest structures reflect regional tectonic control. At the mesoscopic scale, the internal stratigraphy of the Paintbrush Group strongly controlled the development of early-formed networks of cooling joints that form the fundamental fabric element subsequently exploited by younger intra-block fault patterns. Among intra-block faults that are 0.5 km or greater in length, there is a transition from those whose geometry is fundamentally controlled by cooling joints and those whose geometry appears controlled by block-bounding fault displacements. The stratigraphic control so important to intra-block fault growth did not affect the propagation and geometry of block-bounding faults, which are purely a reflection of regional tectonic influences (Section 3.6).
- The relatively simple nature of Tertiary extensional deformation in the central and northern parts of Yucca Mountain (simple, 1 to 4 km wide fault-bounded panels with stratigraphic units dipping to the east) give way to more complex deformational patterns (with greater interaction between individual block-bounding faults) that characterize more highly extended terrain in southern Yucca Mountain, and in the area directly north of Yucca Mountain (Section 3.6).

- Long-term erosion rates on bedrock ridge crests (<0.1 to 0.3 cm/k.y.) and hillslopes (<0.2 cm/k.y.) of the Yucca Mountain area are very low and reflect the high erosional resistance of the Yucca Mountain bedrock (Section 3.4).
- The alluvial geology of Fortymile Wash records several cut and fill episodes during the last 500 k.y. in response to changing climatic conditions in the Middle to Late Quaternary (Section 3.4).
- The valleys that drain eastward down the flank of Yucca Mountain across the repository block were unable to completely excavate the alluvial fill within their valleys during the wetter climate of the last glacial episode. Thus, these valleys have a very low probability of removing the present alluvial fill and eroding any significant amount of bedrock, even if the climate becomes wetter during the next 10,000 years (Section 3.4).
- Yucca Mountain and Crater Flat Basin are located outside the zones of high strain rate observed in the central Nevada seismic zone, the eastern California shear zone, and a shear belt at 37°N latitude. Trilateration data for 1983 to 1993 from a network centered on Yucca Mountain showed no detectable strain accumulation, except possibly in the vicinity of the Little Skull Mountain earthquake (Section 3.3).
- The eruption rate for the past 5 Ma cycle of basaltic activity near Yucca Mountain is among the lowest of volcanic fields in the Western United States. Approximately 99.9 percent of the volume of the southwestern Nevada volcanic field, which encompasses the site, erupted by about 7.5 Ma. In terms of relative volumes, the southwestern Nevada volcanic field is considered to have virtually ceased activity since that time (Section 3.9).
- A probabilistic assessment of the likelihood that the potential geologic repository at Yucca Mountain will be intersected by volcanic processes indicates the annual frequency of intersection is 1.5×10^{-8} with a 90-percent confidence interval ranging from 5.4×10^{-10} to 4.9×10^{-8} (Section 3.9).
- Faults with demonstrated Quaternary activity exist in the vicinity of Yucca Mountain. Slip rates for these faults are low, ranging from 0.0002 mm/yr to 0.03 mm/yr. Average recurrence intervals for earthquakes producing surface displacement on a given fault range from about 13 k.y. to perhaps more than 100 k.y. Preferred values for single event displacements range from 3 to 170 cm (Section 3.10).
- A probabilistic analysis of ground motion at Yucca Mountain indicates that mean peak horizontal accelerations with a 10^{-3} and 10^{-4} annual frequency of being exceeded are 0.17 g and 0.53 g, respectively. These values correspond to a reference surface outcrop with rock properties found at a depth of 300 m at Yucca Mountain. They do not take into account the effect of the tuff overburden above the 300 m level (Section 3.10).
- A probabilistic analysis of fault displacement hazard at Yucca Mountain shows that, except for sites on block-bounding faults (e.g., Solitario Canyon, Bow Ridge), mean fault

displacement levels are less than or equal to 0.1 cm for annual frequencies of being exceeded of 10^{-4} and 10^{-5} (Section 3.10).

- The Yucca Mountain Conceptual Controlled Area contains no identified metallic mineral or uranium resources; no unique or economic deposits of industrial minerals; has low potential for energy resources, including oil and gas; and no potential for coal, tar sands, or oil shale; and no economically viable geothermal resources (Section 3.11).

3.1.3 Methods of Investigation

Studies to investigate the geologic system at Yucca Mountain and its surrounding region have relied primarily on standard geologic methods. In some cases, however, new methods were developed or existing methods were expanded to address site characterization needs. In this subsection standard methods are briefly described and innovative methods are discussed in more detail. To the extent that the details of a method are important to understanding the results obtained for a component of the geologic system, these methods are described more fully in the appropriate subsection. Details of the methods of investigation are also available in reports referenced in each subsection.

Determination of lithostratigraphic features, units, and relations relies on the standard tools used by field geologists. Most primary descriptions of lithostratigraphic features are at the macroscopic scale and are based on 5X to 15X hand-lens examination of field, core, or cuttings samples. For selected samples, 5X to 100X binocular stereo microscope examination facilitated the identification of minerals and textures. To carry out more detailed analysis of some rocks, covered or polished thin sections were studied. Some thin section samples were stained to aid in mineral identification and others were impregnated with blue-dye epoxy to enhance identification of pore space and geometry. Selected thin section samples also were analyzed with electron microprobe techniques to determine mineral chemistry.

For other samples, analyses employing X-ray fluorescence, to determine bulk-rock or mineral chemistry, and X-ray diffraction, to determine bulk-rock or mineral identity, were used. Elemental concentrations determined using the X-ray fluorescence method include potassium, calcium, titanium, rubidium, strontium, yttrium, zirconium, niobium, barium, lanthanum, and cerium. The general technique used is described by Jenkins and DeVries (1970) and in U.S. Geological Survey (USGS) Technical Procedure GCP-25. For the X-ray diffraction method, an extensive catalog of spectra allows not only mineral identification, but also determination of quantitative amounts of each mineral.

Analysis of surface and subsurface maps and of data from boreholes provide the basis to determine geometric relations and thicknesses of lithostratigraphic units. Determination of map and cross-section relations and examination of measured stratigraphic sections are the primary field-based approaches. For boreholes, macroscopic descriptions of lithostratigraphic units are based on available core and cuttings. For some boreholes, additional resources include 8 x 10 inch color photographs of core, video of core collected at the drilling site with pre- and post-sampling images (for many pre-1993 boreholes), video images of borehole walls, and acoustic televiewer logs for some pre-1993 boreholes. Photogrammetric and various point-counting techniques were locally

applied to surface and subsurface exposures and borehole data to collect quantitative and semi-quantitative estimates of features.

Identification of rock units and features also employs data on rock properties. These data include fundamental lithostratigraphic properties such as bulk density, porosity, material composition (e.g., glass; high-temperature crystallized minerals such as feldspar, quartz, and tridymite; and low-temperature minerals such as zeolite, clay, and opal), and fracture characteristics. Additional hydrogeologic properties that can be used in identifying lithostratigraphic units and features include water saturation and measurements of porosity and density taken after the samples are dried in either a 65°C oven under 60 percent relative humidity, or in a 105°C oven under ambient (low) relative humidity. Additional thermal-mechanical properties include compressive and tensile strength, P- and S-wave velocities, and thermal expansion. The spatial distribution of rock property data is variable.

Borehole geophysical logs also are used in identifying lithostratigraphic units and features. Geophysical logs exist for most boreholes. While the suite of logs that were run differs among the boreholes, a few common logs exist for most. Basic log types include caliper and density logs; video logs; logs using neutron or electrical techniques to infer or determine the amount of moisture in the rocks; and logs used to calculate element abundances such as potassium, uranium, and thorium. Selected boreholes, especially those drilled and logged in the early to middle 1980s, have P- and S-wave velocity and various magnetic logs. The borehole geophysical logs typically consist of data collected every 0.5 ft (0.15 m), while the borehole video logs display at 0.03 to 0.15 m (0.1 to 0.5 ft) increments.

The accuracy and precision to which lithologic units and features can be determined depends on the type of data being used and is scale dependent. Contact locations taken from 1:12,000 scale maps typically are uncertain to about 10 m. The accuracy of thickness determinations based on such maps are thus uncertain by a similar amount. Units with thicknesses on the order of millimeters can be identified from more detailed maps or from core. In thin sections, features can be measured to within micrometers.

The accuracy of lithostratigraphic contact depths determined from borehole core samples is generally 0.1 ft¹ or greater. In boreholes with 100 percent recovered core, accuracy of the recorded downhole depth is theoretically the same as the drilled downhole depth. Uncertainties related to borehole deviation from vertical depend on the amount of deviation and can be corrected for if the amount of deviation is known. For boreholes with variable amounts of non-recovered interval, which is the case for most Yucca Mountain boreholes, the accuracy of recorded core depth is proportional to the amount of non-recovered interval per drill run (typically 5 to 10 ft or 1.5 to 3.0 m). Thus, although depths in core are recorded to 0.1 ft, and geophysical and video logs can help to refine contacts to less than 0.5 ft, this recorded accuracy may not be real. Models and conclusions incorporating lithostratigraphic contact depths and thicknesses accommodate this uncertainty.

¹ Measurements of surface-based locations and borehole depths have historically been determined in feet. Metric equivalents are determined by calculation. In the underground excavations of the Exploratory Studies Facility, measurements, including drilling depths, are commonly recorded in metric units.

Geologic mapping to characterize the structure of the Yucca Mountain Site employed standard mapping techniques (e.g., USGS Technical Procedure GP-01). Early mapping of the area (Christiansen and Lipman 1965; Lipman and McKay 1965) was performed using a 1:24,000 scale USGS topographic base. The mapped stratigraphic contacts can be equated to the formational boundaries within the Miocene volcanic section as defined by Sawyer, Fleck et al. (1994). Scott, R.B. and Bonk (1984) also used a 1:24,000 scale USGS base, but compiled and published their map on an enlarged version of this base at 1:12,000 scale. They defined and mapped internal zones within the Tiva Canyon and Topopah Spring Tuffs based on geomorphic characteristics, lithophysal content, and glass content (vitric versus non-vitric). Spengler, Braun et al. (1993, 1994) employed the map-units defined by Scott, R.B. and Bonk (1984) and mapped a small part of Yucca Mountain, in the vicinity of the Ghost Dance fault, at a 1:240 scale using an enlarged version of the 1:6,000 scale Yucca Mountain Site Characterization Project (YMP) topographic base. Precise survey control was established with permanent survey markers on a 200 ft spacing, tied to the Nevada state coordinate system. Day, Potter et al. (1996a) and Potter, Dickerson et al. (1995) used the 1:6,000 scale YMP topographic base and map-units based on Buesch, Spengler et al. (1996a), including contacts separating zones and members within the Topopah Spring and Tiva Canyon Tuffs. In the case of Potter, Dickerson et al. (1995), the base map was enlarged to a 1:2,400 scale and the precise survey control established by Spengler, Braun et al. (1993, 1994) was used where available.

Data on the geometry and characteristics of the fracture network developed within Miocene volcanic rocks at Yucca Mountain come from surface investigations, data collected in the Exploratory Studies Facility, and from boreholes. Surface fracture investigations include detailed maps of cleared pavements and descriptive inventories of the fracture network at natural exposures. For pavement studies, fractures were mapped from air photographs or by hand surveying in an area from 300 to 1200 m². Studies of natural exposures include observations of the number of fracture sets, their relative termination (age) relationships, and average orientation of each set.

Types of fracture data collected within the Exploratory Studies Facility include geologic mapping, line surveys, and close-range photogrammetric mapping. Geologic mapping of the excavated walls of the Exploratory Studies Facility, including fractures, was carried out at a scale of 1:125. In addition, a line survey was performed in which the location and attributes of every discontinuity longer than 1 m (0.3 m through Exploratory Studies Facility Station 37+80) was measured along a datum line. Fracture location and attribute information also were determined for a limited area of the Exploratory Studies Facility using an analytical photogrammetric plotter and stereo photographs of the exposure.

Fracture data from boreholes include logging of recovered core and borehole televiewer logs. Fracture data from core provide information on fracture intensity (spacing), aperture, and mineral filling. Borehole televiewer data provide spacing and orientation data.

Determination of the geoen지니어ing properties of rocks at Yucca Mountain relies on field geologic studies, analyses, and laboratory testing of rock samples. Geologic logging of borehole core samples provides information on core recovery, rock quality designation, rock weathering and hardness, lithophysal content, and fracture characteristics. Key block analyses, based on the configuration of an excavation and the orientation of joint sets, examine the size of potential key blocks that might form and be kinematically capable of moving into an excavation.

Laboratory testing was conducted to characterize physical, mechanical, and thermal-mechanical properties of rocks. Bulk and physical property measurements were performed on specimens of tuff prepared from core samples. Properties evaluated include density, porosity, and mineralogy. Dry and saturated bulk densities, as well as average grain density, were measured for most laboratory test specimens following standard procedures. Porosity was computed from density measurements.

To relate thermal and mechanical properties to mineralogy and petrology, a suite of samples was examined as hand samples and also by laboratory analytical methods. Optical microscopy of thin sections provided modal point counts of identified constituents, and X-ray diffraction analysis of prepared powders was performed to identify finely crystalline minerals.

Laboratory testing of thermal properties, including thermal conductivity, thermal expansion, and heat capacity, was performed on core samples. Thermal conductivity is a measure of the ability of a material to transmit heat, and so relates to the ability of the host rock to conduct heat away from waste containers. Thermal expansion is the tendency of a material to undergo a nearly proportional degree of volume or length change as a result of change in temperature. Heat capacity is the amount of heat required to change the temperature of a substance by a given amount. In general, standard procedures were followed for thermal testing.

A comprehensive series of mechanical property measurements was conducted on specimens prepared from core samples to establish baseline properties and to study the vertical and lateral variability of mechanical properties at Yucca Mountain. Measurements included elastic constants, strength, and deformation characteristics for specimens from all thermal-mechanical units. Static Young's modulus and Poisson's ratio were computed from stress-strain data obtained from confined and unconfined compression tests. Confined compression tests were also performed at elevated temperatures. Dynamic elastic moduli were computed from compressional and shear wave velocities measured under ambient laboratory conditions. Brazil tests were performed to determine indirect tensile strength, and creep experiments were conducted to measure time-dependent strain accumulation. Fracture stiffness and fracture strength were measured for natural fractures to characterize the mechanical properties of fractures.

Rock mass quality indices and the parameters used to determine the indices were derived from direct observations of rock mass characteristics. Rock mass quality indices were determined and used to project ground support requirements as well as to empirically derive rock mass strengths and elastic moduli.

In situ stress at the Yucca Mountain Site was determined by hydraulic fracturing stress measurements and two-dimension modeling with assumed gravitational loading.

Geotechnical properties of surficial materials were investigated by means of data derived from geologic mapping, test pits, boreholes, and standard field and laboratory tests.

Geochronologic methods provide information supporting studies of igneous activity, Quaternary stratigraphy, surficial processes, and faulting. Techniques that contribute to understanding the basaltic volcanic activity in the vicinity of Yucca Mountain include $^{40}\text{Ar}/^{39}\text{Ar}$, K-Ar, U-Th disequilibrium, and ^3He cosmogenic exposure. The $^{40}\text{Ar}/^{39}\text{Ar}$ and K-Ar techniques are based on the

fact that ^{40}K decays to ^{40}Ar and ^{40}Ca with a half-life of approximately 1.25×10^9 years. By measuring the isotopes of Ar in a volcanic rock, its age can be calculated. Recently, $^{40}\text{Ar}/^{39}\text{Ar}$ has become the preferred technique over K-Ar because loss or gain of Ar from the system can be more reliably assessed and a more reliable age can usually be calculated. In general, the older a basalt is, the more reliably it can be dated because more time has elapsed for radiogenic Ar to accumulate in the rock. For this reason, basalts older than about 0.5 Ma in the Yucca Mountain region have been dated exclusively using either $^{40}\text{Ar}/^{39}\text{Ar}$ or K-Ar.

Basalts younger than about 0.5 Ma are generally harder to date using either $^{40}\text{Ar}/^{39}\text{Ar}$ or K-Ar because less radiogenic Ar is present. For this reason, multiple techniques have been used to date younger basalts as a cross-check to increase confidence that a true age has been obtained. For example, the youngest basalt of the region, at Lathrop Wells, has been dated using $^{40}\text{Ar}/^{39}\text{Ar}$, K-Ar, U-Th disequilibrium and ^3He and ^{36}Cl cosmogenic exposure. The U-Th disequilibrium method depends on U and Th fractionation during magmatic processes, leading to secular disequilibrium between the parent ^{238}U and the daughter ^{230}Th isotopes. Volcanic rocks as old as about 400,000 years (equal to 4 to 5 half-lives of ^{230}Th , at which point secular equilibrium is attained) can usually be dated with high precision using mass spectrometric measurements of U and Th isotopes.

Carbon-14 is formed in the atmosphere by a variety of nuclear reactions between cosmic-ray produced neutrons and nitrogen, oxygen, and carbon, but the majority is produced by reaction between slow neutrons and ^{14}N . The production rate for ^{14}C varies slightly as a function of latitude and has varied significantly as a function of time such that the activity of ^{14}C has not been constant; however, well constrained corrections for samples younger than 20,000 years can be made. During the last approximately 100 years, ^{14}C in the atmosphere has been diluted by the addition of nonradioactive carbon which has been produced by the combustion of fossil fuels. Ages are typically reported in radiocarbon years, which is years before 1950.

The above method assumes that living organisms maintain equilibrium with atmospheric ^{14}C and that after death of the organism ^{14}C decays with a half life of 5,730 years. The range of applicability for ^{14}C is about 300 to 50,000 years. For small samples and samples near the upper limit of the technique, accelerated mass spectrometry is used to measure the ^{14}C content. Younger samples, or samples with large amounts of ^{14}C , can be measured by decay-counting. More information can be found in Hill, D.P., Reasenberget al. (1993).

Carbon-14 is also used to obtain exposure ages in a manner similar to that described for ^{10}Be . In this case, inorganic carbon generated within solid surficial materials is analyzed.

Rock-varnish cation-ratio dating is a calibrated technique (Harrington and Whitney 1987; Whitney and Harrington 1993). It depends on developing a calibration curve that is based on measured chemical ratios ($[\text{Ca}+\text{K}]/[\text{Ti}, +\sim 1/3 \text{ Ba}]$) in varnish samples of known age from the same region as the samples to be dated. Ages are then calculated by measuring the same ratio in samples of unknown age and using the calibration curve to calculate an age. Cation-ratio measurements are made on rock-varnish samples by scanning electron microscope in combination with an energy dispersive X-ray analyzer. This ratio decreases with increasing age of the rock varnish. The technique is limited by regional calibration points to about 1.5 Ma in the Yucca Mountain area. The

method is strongly dependent on sampling methods that are described in a DOE Topical Report (YMP 1993a).

The in situ cosmogenic nuclide method is a means of determining rock surface exposure histories from measurements of rare nuclides produced in rocks by cosmic radiation reaching the surface of the earth. In situ cosmic-ray produced nuclides can be either stable (e.g., ^3He or ^{21}Ne) or radioactive (e.g., ^{10}Be , ^{14}C , ^{26}Al , ^{36}Cl , or ^{41}Ca). The types and rates of reactions that produce these nuclides vary. In situ ^{10}Be and ^{14}C are produced in quartz from spallation reactions of the oxygen atoms and, to a lesser extent, silicon (Nishiizumi et al. 1984; Jull et al. 1994). The abundance of a cosmogenic nuclide on a rock surface depends on the chemical composition of the exposed rock, the duration of exposure, the production rate of the nuclide in the target material, the rate of decay if the nuclide is radioactive, and the exposure history of the rock being sampled. The most appropriate nuclide (or ratio of nuclides) to measure depends on a variety of factors, most importantly the rock type, the age of the surface or event, and the particular problem being addressed (i.e., erosion rate or exposure age).

The abundance of a cosmogenic nuclide is the integral of its production rate (P) at the earth's surface, over the exposure duration (t). Cosmogenic nuclide production rates are not constant. Production rates vary as a function of time because the cosmic ray flux to earth's surface has fluctuated over time. Production rate increases with geomagnetic latitude due to poleward deflection of cosmic-rays by earth's geomagnetic dipole field. Production rate also changes with altitude and sample thickness because cosmic rays attenuate (and production rate decreases with depth) through mass they penetrate, in this case the atmosphere and rock (Lal 1991). For a young sample, altitude and geomagnetic latitude can be considered approximately invariant and sample thickness can be measured. However, the temporal change in production rate remains an important source of systematic uncertainty in applications of cosmogenic nuclide dating, particularly when comparing surfaces with significantly different ages. By measuring multiple nuclides in the same sample it is possible to obtain additional information about the erosion rate and exposure history of the rock surface, such as minimum burial duration or time-averaged erosion rates (Nishiizumi et al. 1991; Gosse, Grant et al. 1995).

The reliability of the calculations is controlled by the:

- Validity of the assumptions made (e.g., the effective production rate is known; the initial nuclide concentration was zero [i.e., no inherited concentration]; the rock or mineral behaved as a closed system that did not leak or gain a nuclide component except through known production or decay pathways; and for age calculations it is assumed that there was negligible erosion of the surface)
- Effectiveness of the sampling strategy to minimize factors that can influence the in situ production of the nuclide (e.g., complicated surface geometry, burial due to snow or ice cover (Gosse, Klein et al. 1995), and shielding of the cosmic rays by nearby structures)
- Precision of the analysis

Single date variances about a mean of dates for a landform can be as low as four percent, approaching the present total analytical reproducibility in the nuclide measurement (Gosse, Evenson et al. 1995).

Presently, the chief uncertainty in cosmogenic nuclide techniques is the difficulty of accurately knowing the cosmic-ray flux to a sample site over the exposure duration. However, it is also apparent that for exposure durations greater than 100 years (i.e., all samples analyzed from the Yucca Mountain area), the changes in cosmic-ray flux (with $\sim 10^4$ yr period) have less effect on the time-averaged production rate because the record is integrated over long time periods. The ± 25 percent 1 sigma uncertainty reported for all ages and erosion rates is assumed to be a reasonable consideration of all random and systematic errors (see Gosse, Reedy et al. 1996 for a summary of the state of knowledge of production rate variations).

The ^3He cosmogenic exposure method measures the amount of ^3He produced by surface exposure to cosmic ray irradiation. The age of the rock is proportional to the amount of cosmogenic ^3He measured in the rock, assuming that the ^3He production rate is known. This method can be used to date volcanic rocks from a few thousand years to several hundreds of thousands of years in age, assuming that a sample has been continuously near the surface and exposed to cosmic rays.

Information on the geochemical composition of basaltic rocks near Yucca Mountain is also used to understand their history and the likelihood of future occurrence. Standard geochemical measurement techniques, including X-ray fluorescence for major and trace elements, instrumental neutron activation analysis for trace elements and solid-source mass spectrometry for isotopic ratios, were used.

Isotopic compositions of lead and strontium have been used as natural tracers to look for evidence of ore-forming processes, to check correlations within geologic units, and to investigate petrogenetic processes. These isotopes are useful for these purposes because, unlike the light-stable isotopes, these heavier isotopes, as well as their parent isotopes, do not fractionate naturally. Strontium has four stable isotopes, but the amount of ^{87}Sr in any system increases as a function of time by the decay of ^{87}Rb . The amount of ^{87}Sr is not usually measured in absolute terms, but rather the ratio of ^{87}Sr to ^{86}Sr is reported. The rate of increase in this ratio is dependent on the ratio of rubidium to strontium and the half life of ^{87}Rb , which is 4.88×10^{10} years. Data are reported both as $^{87}\text{Sr}/^{86}\text{Sr}$ or as $\delta^{87}\text{Sr}$ which is defined as $((^{87}\text{Sr}/^{86}\text{Sr})/(^{87}\text{Sr}/^{86}\text{Sr})_{\text{std}} - 1) \times 1000$ where $(^{87}\text{Sr}/^{86}\text{Sr})_{\text{std}}$ is the ratio for a standard, which for this report is a modern coral for which the measured value of $^{87}\text{Sr}/^{86}\text{Sr}$ is 0.70920. There are four stable isotopes of lead, three of which are radiogenic daughters of uranium and thorium. ^{208}Pb is derived by the decay of ^{232}Th (half life = 14.01×10^9 yrs); ^{207}Pb is derived by the decay of ^{235}U (half life = 0.7038×10^9 yrs); and ^{206}Pb is derived by decay of ^{238}U (half life = 4.468×10^9 yrs). Each is reported relative to the abundance of ^{204}Pb . A general description of these techniques can be found in Peterman and Stuckless (1993b) and references therein, Peterman, Spengler et al. (1993), and Peterman, Widmann et al. (1994).

Quaternary stratigraphic units have been dated by thermoluminescence techniques and U-series disequilibrium. The thermoluminescence dating technique relies on metastable electron traps within crystal lattices of certain minerals (mainly feldspar and quartz) that can be filled with electrons excited by interaction with ionizing radiation (e.g., alpha, beta, gamma, or cosmic radiation). The number of trapped electrons is proportional to time and the rate of radiation. Trapped electrons are

released by heat or electromagnetic (e.g., ultraviolet light) energy sources. The technique assumes that sufficient energy is supplied to materials at the surface to empty all traps prior to burial, and that the thermoluminescence measured in the laboratory is a measure of time since burial. A full description of the technique can be found in Paces, Mahan et al. (1995).

The U-series disequilibrium technique utilizes the ^{230}Th - ^{234}U activity ratio, which evolves from an initial value to 1 in minerals that behave as a closed system. For minerals such as opal and calcite, which crystallize from water, the initial $^{230}\text{Th}/^{234}\text{U}$ can be assumed to be zero, but in a soil environment, entrained detrital materials may invalidate this assumption. Most of the results used for this study were obtained using mass-spectrometry, which has about 500 times greater measurement efficiency than alpha-spectrometry. Thus, analytical precision is much greater and sample sizes are much smaller than was true for earlier work. The half life of the ^{230}Th is 75,200 years and, therefore, the upper limit of ages determined by this technique is 300 to 500 thousand years. The half life of the ^{234}U is much longer (4.49×10^5 yrs) and, therefore, if the initial $^{234}\text{U}/^{238}\text{U}$ is known, U-series dating can be extended back to 1.5 Ma.

Although not a standard method for commercial mineral exploration, several studies of ore deposits in Tertiary igneous rocks have shown that the isotopic composition of oxygen (which is expressed as $\delta^{18}\text{O}$) is strongly perturbed in epithermal systems (Criss and Taylor 1986). In low water to rock systems, the isotopic effect of increased $\delta^{18}\text{O}$ will more easily be detected than mineralogic alteration (Taylor, H.P. 1974). Therefore, 159 samples were taken from the Tiva Canyon Tuff in the Yucca Mountain Conceptual Controlled Area and analyzed for oxygen isotopes to investigate any possible evidence for epithermal ore-forming processes at Yucca Mountain.

Three-dimensional geologic modeling is an integrative method that combines spatial and conceptual information on rock layers, faults, and rock properties beneath the Yucca Mountain Site. By requiring an interpretation at every point within the model volume, this method forces an objective rigor into the geologic interpretation process. The method also provides a set of visual and quantitative tools for analysis of information, and forms a framework for developing and interpreting other results (e.g., spatial models of rock properties).

The 3-D geologic model is developed by considering available spatial geologic information and applying standard geologic principles. Data from boreholes and surface mapping, along with geophysical results, are used to constrain the configuration of stratigraphic units. Thickness maps for modeled stratigraphic units were hand-drawn and then assembled electronically into a 3-D representation of rock layers. Faults were constructed from outcrop and geophysical data, and shaped at depth in accordance with structural styles and conceptual tectonic models. Final model assembly involves offset of rock layers along each fault. The final model honors the available data and represents a reasonable, although not unique, interpretation of the subsurface geology.

Seismic monitoring provides a record of the contemporary occurrence of earthquakes to complement the catalog of historical events and to provide data for analyses of earthquake source properties and seismic wave propagation in the vicinity of Yucca Mountain. The monitoring network initially employed analog telemetry with detected seismic events recorded at a central recording facility. The network has now been upgraded to digital telemetry of events detected at the field stations. In addition to the monitoring network, which currently detects all events with magnitude greater than

about -0.5 in the immediate vicinity of Yucca Mountain, strong motion recorders also have been deployed to record any significant future events.

Surface geophysical techniques make volumetric measurements that can be used to extrapolate and interpolate among point or surface data acquired by other methods. Techniques include seismic, gravity, magnetic, and magnetotelluric. The primary purpose of the geophysical methods is to investigate subsurface structure and lithology. The information is used to constrain geologic models and to extrapolate and interpolate information obtained from observations in boreholes and on the surface. Seismic methods use either compressional waves or shear waves energy to image the subsurface. Energy sources are placed on the surface or in boreholes and activated. Geophones placed at some distance from the seismic source receive the seismic energy after it has propagated through the intervening earth. Direct and reflected energy provide an image of the area between the source and the receiver. The most common use is when sources and receivers are placed in collinear arrays on the surface to detect reflection from a layered subsurface. The reflections are caused by differences in the acoustic and elastic properties in the rocks (i.e., density, bulk, and shear moduli).

The seismic reflection lines and vertical seismic profiling studies sampled a variety of geologic conditions and features of interest to the project. The target depth for the majority of the high resolution seismic lines was from 100 m to the depth of the potential repository and below, if possible. The lines in the repository area were designed to investigate structure, faulting, and lithology in or near the potential repository block, as well as to investigate lithology and structure that could provide insight into the apparent steep water table gradient at the north end of Yucca Mountain. Two regional seismic lines were designed to investigate deeper structure (1 to 24 km or deeper if possible) controlling regional tectonics and past volcanic activity.

Collection of seismic data in the vicinity of Yucca Mountain was complicated by the character of the rocks. Fracturing and different lithologies, in addition to the partial saturation, make it difficult to propagate seismic energy. The lithophysal zones and the varying degrees of welding further complicate the interpretation of the seismic data. Because of the various sizes of heterogeneities in the formations at Yucca Mountain, scattered waves play a prominent role in the interpretation process. Further complications arise because the shallow subsurface zone is known to be highly heterogeneous, including strong contrasts in material properties.

Gravity measurements are sensitive to the gross density changes in the subsurface. The measurement and interpretation of surface gravity can be quite useful in the interpretation of broad subsurface geologic structure. While gravity data alone are rarely sufficient to provide a unique interpretation of structure, when used in conjunction with other types of geophysical data, they can be quite decisive in choosing between various possible models of the subsurface. For this reason, gravity observations were collected along all of the seismic reflection lines at Yucca Mountain, as well as other lines.

Gravity observations are used in two different ways, to interpret the general regional structure and to complement other geophysical data in the interpretation of shallow local structure at Yucca Mountain. In using gravity data to arrive at a model of general regional structure, the primary objective was to identify variations in the depth to basement rocks beneath Yucca Mountain and the surrounding regions. Differences in density between the less dense sediments and tuffs of Cenozoic

age, and the more dense underlying basement rocks of Paleozoic age, were used to model variations in observed gravity in terms of variations in depth to basement. This interpretation process is non-unique. Lateral variations in density can be traded off with lateral variations in depth to basement. However, when used with other geophysical methods and geological data, gravity interpretation can help refine models of the crust. Contoured regional Bouguer gravity data for the Yucca Mountain vicinity are presented in Figure 3.1-1.

The magnetic method is another potential field method with magnetic susceptibility being the variable material property. The magnetization of a rock, which is dependent on its susceptibility, has both a magnitude and direction component. Thus, magnetic anomalies can result from variation in magnitude or variation in direction of magnetization. Additionally, the total magnetization of a rock mass is composed of induced and remanent magnetization. In the vicinity of Yucca Mountain, magnetic surveys are interpreted primarily for information on fault locations and volcanic features. Contoured regional aeromagnetic data for the Yucca mountain region are presented in Figure 3.1-2. A traditional use of the magnetic method, to investigate the depth to basement, is not viable at Yucca Mountain because the Paleozoic basement rocks are non-magnetic.

The magnetotellurics method was also investigated as a means to identify hidden faults and geological heterogeneities at Yucca Mountain. While the resistive nature of the tuffs make application of magnetotellurics difficult at Yucca Mountain, the use of a new approach, continuous profiling magnetotellurics, was tested. This approach is similar to seismic reflection in that a profile of stations at relatively close spacing (50 to 100 m) is acquired. Because of its expense, however, it was used sparingly at Yucca Mountain. In particular, it was used to investigate the Ghost Dance fault region.

In addition to magnetotellurics measurements, several other electrical methods were employed in the vicinity of Yucca Mountain. These methods were used to investigate near-surface (few hundred meters) structure for fault mapping and geotechnical purposes (Oliver et al. 1990, 1995). The studies employed DC resistivity and audio frequency electromagnetic methods. Limited areas were covered and not much information was derived on deeper structure or on properties of the potential repository volume. In general, the high near-surface resistivity (>100 ohm-meters) limited the value of these types of electrical studies.

3.2 REGIONAL GEOLOGIC SETTING

The regional geologic setting for Yucca Mountain consists of those tectonic, stratigraphic, and structural elements that contribute to the makeup and evolution of the site. The setting provides a context for understanding the processes currently acting at Yucca Mountain and for evaluation of its geology. Conclusions regarding the site geology need to be consistent with the regional framework. The regional geologic setting thus provides constraints on the descriptive models and process models that will be used to assess the ability of the natural system to play a role in the satisfactory performance of the site.

This discussion of the regional geologic setting contributes to meeting the requirements of 10 CFR 60.21(c)(1)(ii)(A) to describe and analyze the geology of the site. The discussion also addresses 10 CFR 60.21(13) which requires an identification and evaluation of the natural resources of the geologic setting, and 10 CFR 60.122 which provides siting criteria for a geologic repository that must be adequately investigated and evaluated. The regional geologic setting also provides the background for more detailed or specialized information that is described elsewhere in this document.

The information on the regional geologic setting differs from that for some subsequent sections that focus on the Yucca Mountain Site. Regional information is drawn mainly from the existing geologic literature. Such papers and reports were not prepared specifically for the YMP. Therefore, data were not collected and analyses were not carried out under the YMP quality assurance program. The papers and reports did, however, undergo peer review processes that applied to their particular publication. Differences in interpretations among scientists are to be expected and are reflected in the discussion of regional geology. These differences are especially apparent in some of the maps in this section.

Maps summarizing the surface distribution of rocks of different age groups are compiled from a number of sources. They do not show, however, where such rocks may be present below the surface. This would require interpretations based on projecting geologic structures into the subsurface, augmented by data from geophysical surveys and boreholes where available. The maps summarizing locations of thrust faults, folds, detachment faults and shear zones are also drawn from existing publications to show specific features discussed in the text. Thus they differ in details depending on the investigation and the subject emphasized.

The main value of a review of these regional studies is in making certain that structural interpretations and tectonic models of the Yucca Mountain site consider the implications of interpretations of the regional structure and tectonics obtained from investigations beyond the immediate area of Yucca Mountain.

3.2.1 Tectonic Setting

The current tectonic setting of Yucca Mountain results from extensional tectonism and magmatism caused by plate tectonic interactions at the western margin of the North American continent during the Middle and Late Cenozoic Era (e.g., Bohannon and Parsons 1995). Three regional tectonic domains characterize Yucca Mountain and its surrounding environs: the Walker Lane domain, which

includes the site; the Basin and Range domain, to the northeast; and the Inyo-Mono domain to the southwest (Figure 3.2-1). These domains are structurally bounded blocks of crust characterized by deformational features that differ from adjacent domains. Tectonic domains exist at different scales; this subsection addresses domains at a regional scale. At larger scales in the vicinity of Yucca Mountain, there is some mutual overlap or structural interference among the domains.

3.2.1.1 Walker Lane Domain

Yucca Mountain lies within the Walker Lane domain, an approximately 100 km-wide structural belt along the western side of the Basin and Range domain (Figure 3.2-1). The domain, also referred to as the Walker Lane belt (Stewart 1980) or simply the Walker Lane, extends northwestward from the vicinity of Las Vegas, subparallel to the Nevada-California border, into Northern California. The domain is characterized as an assemblage of crustal blocks separated by discontinuous northwest-striking right-lateral faults and northeast-striking left-lateral faults (Stewart 1988). Because of its structural heterogeneity, the Walker Lane is recognized as a tectonic terrane distinct from the Basin and Range only at regional scale. The local, northwest-striking faults give the domain its overall structural grain and they obscure basin and range (see below) structure to varying degrees. While there is no definitive eastern structural boundary to the Walker Lane as a whole, the Las Vegas Valley shear zone (Figure 3.2-1) can be interpreted as an eastern bounding structure for the domain's southern segment.

The Walker Lane domain is subdivided into sections, each of which is characterized by a distinct lithologic and structural pattern (Stewart 1988). With respect to the tectonic setting of Yucca Mountain, only three of these sections are of concern: the Goldfield section, which contains the Yucca Mountain site and is characterized by irregular, in places arcuate ranges, lack of major northwest-striking strike-slip faults, and a scarcity of major "basin-range" faults (Stewart 1988); the Spotted Range-Mine Mountain structural zone, which abuts the Goldfield section to the south and is a terrane dominated by northeast-striking left-lateral faults; and the Spring Mountains section, which is a terrane dominated by Paleozoic and Precambrian rocks that largely preserve pre-Basin and Range structural patterns (Figure 3.2-1).

3.2.1.2 Basin and Range Domain

The Basin and Range structural domain (Figure 3.2-1) is also a physiographic province, the physiography being virtually a direct expression of the bedrock structure (Stewart 1980). Structurally, the province is characterized by generally north-south aligned ranges separated by basins having thick deposits of alluvium derived from the adjacent ranges (Figure 3.2-2). The ranges are separated in the north-south direction by distances of roughly 25 to 30 km, but many ranges arc toward each other and merge along the strike. The general small-scale spatial pattern was aptly likened by G.K. Gilbert (1875) to an "army of caterpillars marching north out of Mexico." This pattern is the result of generally east-west-directed extension which began in Tertiary time and continues at present (e.g., Hamilton, W.B. 1988). Rocks of every age, from Precambrian to Pleistocene, are deformed by this extension; deformation is typically expressed as complex normal faulting that has facilitated the rotation of blocks to various dips around nearly horizontal axes. Thus, each range is fundamentally an assemblage of tilted fault blocks and is bounded by a major

range-front fault. Seismic reflection profiles show that this style of deformation extends beneath the intervening basins where it is buried by alluvium (Brocher, Carr et al. 1993; Hauge et al. 1987).

3.2.1.3 Inyo-Mono Domain

The Inyo-Mono domain includes all of the extended terrane west of the Furnace Creek-Death Valley fault zone, east of the Sierra Nevada front, and north of the Garlock fault (Figures 3.2-1 and 3.2-2). Its northern end is defined by the termination of the Fish Lake Valley fault and a major right step in the population of active northwest-striking faults along a "northeast-striking structural zone" (Carr, W.J. 1984). However, on the basis of gross structure and landform pattern, the domain could be projected northward to the northern terminus of the White Mountains (see Figure 3.2-2). It includes modern basins and ranges with great structural relief, including Death Valley basin and the Panamint Range. Because of its ongoing tectonic activity and exposure of originally deep-seated crustal rocks, the Inyo-Mono domain is an important part of the regional geologic setting of Yucca Mountain; it contains some of the more tectonically active structures in the Yucca Mountain region.

The Inyo-Mono domain is bounded to the west by the Sierra Nevada block and to the south, across the Garlock fault, by the Mojave terrane. Both the Sierra Nevada block and the Mojave terrane are tectonically isolated crustal elements that are not related to the evolution of Yucca Mountain.

Extension in the Inyo-Mono domain is dominated by dextral strike-slip and oblique transtension resulting in elevated crustal blocks and intervening deep, high-relief basins. Structural relief is very high (Blakely et al. 1995), in part because detachment faulting has unroofed some of the ranges, including the Funeral and Panamint Ranges. Distinctive as this domain is, it may partly be represented within the Walker Lane by less developed features including Amargosa Valley and Sarcobatus Flat, and perhaps even the Amargosa River rift of L.A. Wright (1989). These may be proto-basins initiated by the Inyo-Mono extension mechanism, but now largely or entirely abandoned. Further discussion with implications for Yucca Mountain is appropriate under evaluation of tectonic models (see Section 3.3).

Some consider the Inyo-Mojave domain to be a subdomain of the Walker Lane domain (Stewart 1980). For this discussion, however, it is treated as a separate domain based on its greater rate of recent deformation.

3.2.2 Regional Stratigraphy and Lithology

The stratigraphy and lithology of the regional geologic setting are relevant to the assessment of Yucca Mountain because these geological elements provide much of the history of deposition and deformation that has affected the site. The stratigraphy and lithology also constitute the framework for understanding other aspects of the Yucca Mountain site including its structural geology and tectonics, geoenvironmental properties, mineral resource potential, hydrology, and geochemistry. The following subsections describe rock stratigraphic units at a regional scale. Detailed descriptions of stratigraphic units occurring in the immediate vicinity of Yucca Mountain are given in Subsection 3.5 of this document.

Stratigraphic units are grouped below according to age from oldest to youngest. The units are defined in terms of group and formation names, but are described as lithosomes. Thus, bodies of rock are characterized in terms of gross lithology, thickness, and mineralogy, as well as lateral variations in these parameters, all of which reflect their genesis and depositional environments. Features associated with the history and distribution of these layered rocks are also discussed, including the character of regional unconformities, intrusive rocks, and alteration phenomena. Outcrop locations are generalized in terms of geographic area or physiographic features such as named ranges; the referenced studies are a source of detailed locations. Stratigraphic units are summarized in Tables 3.2-1 (Precambrian and Paleozoic), 3.2-2 (Mesozoic), and 3.2-3 (Tertiary and Quaternary).

3.2.2.1 Pre-Cenozoic Rocks

Pre-Cenozoic rocks in the Yucca Mountain region comprise chiefly Upper Precambrian (Proterozoic) through Paleozoic marine strata. The Precambrian section is dominated by siliciclastic strata; the Paleozoic section is dominated by limestones and dolomites. These rocks have undergone successive generations of faulting, fracturing, and broad to local folding about both vertical and subhorizontal axes (see Table 3.2-1). In the area of the southwestern Nevada volcanic field and within the Goldfield section of the Walker Lane, the pre-Cenozoic rocks are not well exposed. Hence their pre-Middle Miocene structural configuration is uncertain near Yucca Mountain. The pre-Cenozoic rocks are important, however, because they include the main regional aquifers and aquitards.

3.2.2.1.1 Precambrian Rocks

Precambrian rocks comprise two major assemblages: an older, metamorphosed basement assemblage (no basal contact is exposed), and a younger, metasedimentary assemblage the uppermost unit of which is partly of Cambrian age. The older assemblage consists chiefly of quartzofeldspathic gneisses and quartz-feldspar-mica schists of metasedimentary or metaigneous origin. The gneisses and schists are typically intruded by migmatitic veins or larger, deformed bodies of granite or pegmatite. The cumulative thickness of the exposed Precambrian section in the Yucca Mountain region ranges from 4.3 km to nearly 6 km (Wright, L. 1976; Stewart 1970).

These old metamorphic rocks are well-exposed in the Panamint Range (Figure 3.2-3) where they are mapped as the "World Beater Complex" (Lanphere et al. 1964), and have been radiometrically dated by Rb-Sr whole-rock and U-Pb zircon methods at about 1.7 Ga (Lanphere et al. 1964; Stern et al. 1966; Labotka, Albee et al. 1980). Rocks of this type crop out in Monarch Canyon in the Funeral Mountains (Hoisch and Simpson 1993; Wright, L.A. and Troxel 1993) at a railroad cut through the Bullfrog Hills (Cornwall and Kleinhampl 1964), and in the Trappman Hills (Ekren, Anderson et al. 1971) north of Yucca Mountain in the Goldfield section of the Walker Lane (Figure 3.2-3, except for Trappman Hills). Radiometric dates have not been obtained for the last site. East of Yucca Mountain, except in Eastern Clark and Lincoln counties (Stewart 1980), the deep metamorphic basement is not exposed in Basin and Range terrane.

The World Beater Complex is unconformably overlain by rocks of the Pahrump Group (Wright, L. 1976; Wright, L.A., Troxel et al. 1981; Troxel 1988; Labotka and Albee 1977) which includes three

formations: the basal Crystal Spring Formation, the Beck Spring Dolomite, and the overlying Kingston Peak Formation. In places (e.g., the Southern Death Valley region), however, Pahrump rocks are missing and the World Beater Complex is overlain directly by the Noonday Dolomite (see Table 3.2-1). Originally sandstones, siltstones, dolomite and conglomerate, the strata of the Pahrump Group are locally metamorphosed to facies ranging from greenschist to amphibolite similar to that of the high-grade rocks of the underlying World Beater Complex. High-grade metamorphism characterizes the Pahrump Group in the central Panamint Range and in the Northern Funeral Mountains (Labotka 1980; Labotka, Albee et al. 1980) where the Pahrump Group is most widely exposed (Figure 3.2-3).

The exact age of the Pahrump Group is unknown. The Crystal Spring Formation contains diabase sills radiometrically dated using the U-Pb method on baddeleyite at about 1.08 Ga (Heaman and Grotzinger 1992). The Kingston Peak Formation consists partly of conglomerates that are inferred to be of glacial origin (tillites) and, therefore, have been assigned an age of about 720 Ma on the basis of regional correlation (Miller, J. et al. 1981; Miller, J. 1985; Walker, J. et al. 1986).

The Pahrump Group is overlain at an erosional unconformity by Upper Proterozoic units, the Noonday Dolomite and the Johnnie Formation which, in turn, are capped by the Stirling Quartzite and the Wood Canyon Formation. The Wood Canyon Formation, a siltstone or locally calcareous silty sandstone, spans the Proterozoic-Cambrian boundary. The Upper Proterozoic formations are widely exposed in the Panamint Range of the Inyo-Mono structural domain (Labotka, Warasila et al. 1985), in the Spring Mountains section of the Walker Lane, in the Funeral Mountains, and at Bare Mountain, the Striped Hills and the Specter Range (Figure 3.2-3; exposures in the Striped Hills and the Specter Range are too small to show at the scale of the figure). The Stirling Quartzite and the Wood Canyon Formation are exposed locally east and north of Yucca Mountain (Ekren, Anderson et al. 1971). Metamorphic facies of the Upper Proterozoic strata is lower greenschist over wide areas of exposure, but in places, notably the northwestern corner of Bare Mountain, the section as high as the Wood Canyon Formation reaches garnet-amphibolite facies of metamorphism.

Regionally, the Upper Proterozoic units thicken and become increasingly calcareous across Nevada to the northwest (Stewart 1970; Diehl, P. 1976). They form the basal units of a miogeoclinal section and represent a marine depositional environment characterized by passive margin conditions and simple lithologies, chiefly siliciclastic rocks that grade upward into Paleozoic carbonate rocks. The Proterozoic rocks with their weakly to strongly metamorphosed fabrics form a regional aquitard or barrier to groundwater flow (Winograd and Thordarson 1975).

3.2.2.1.2 Paleozoic Rocks

Paleozoic rocks in the Yucca Mountain region comprise three lithosomes: a Lower, Cambrian through Devonian dominantly carbonate lithosome; a Middle, Mississippian fine-grained siliciclastic lithosome; and an upper, Pennsylvanian to Mid-Permian carbonate lithosome. The lower carbonate lithosome represents deposition in a deep to shallow marine passive continental margin (outer shelf to upper rise) setting (e.g., see Poole, Stewart et al. 1992). By Late Devonian time these conditions were interrupted by the Antler orogeny, the main result of which in the Yucca Mountain region was an influx of clay, silt, and sand into the depositional record (Trexler, J.H. et al. 1996). A carbonate platform (continental shelf) depositional environment was reestablished in Pennsylvanian time

across much of the region except in the area of the Inyo-Mono domain where a deeper trough or slope environment was formed (Stewart 1980; Dunne 1986).

The lower part of the lower carbonate lithosome is represented by a shallow water, mixed clastic to carbonate succession represented by the upper two-thirds of the Wood Canyon Formation, the Zabriskie Quartzite, and the Carrara Formation (Table 3.2-1). This succession is capped by a thick interval of monotonous dark-gray Cambro-Ordovician limestone, dolomite and minor shale: the Bonanza King and Nopah Formations and the Pogonip Group (Goodwin Limestone, Ninemile Formation and Antelope Valley Formation). The Cambro-Ordovician carbonates are well exposed in the central part of Bare Mountain, and in the Specter Range to the southeast (Figure 3.2-4). A portion of the sequence was penetrated in a well that was drilled in the Eastern Amargosa Basin (Felderhoff Federal No. 25-1; Grow et al. 1994; Carr, W.J., Grow et al. 1995). The Bonanza King Formation is widely exposed in the CP Hills and in the Halfpint Range (Figure 3.2-4); about 1,400 m of section is present in the Halfpint Range (Barnes, Christiansen et al. 1962, 1965). The Upper Cambrian Nopah Formation is similarly widespread, extending at least from the Halfpint Range southwest to the Nopah Range (Figure 3.2-4) as a variegated dolomite with subordinate silty-shaley and cherty intervals.

Although the Cambrian carbonates are strong and resistant to erosion, in many places they are characterized by stratally confined brecciation. At least two generations of breccia are present, the oldest of which may be of primary origin (submarine debris flows). One or more post-consolidation breccias, most likely of tectonic origin, are associated with interclastic voids in many parts of the calcareous section. This condition has enhanced cavernous dissolution, favoring the flow of groundwater. This feature, as well as the regional extent and uniformity, provide the conditions that make the lower carbonate lithosome a regional aquifer (the lower carbonate aquifer of Winograd and Thordarson 1975).

The character of the Cambro-Ordovician carbonate section described above contrasts with the Upper Ordovician Eureka Quartzite. The Eureka is typically a dense, white, sucrose quartzite that forms a unit as much as 150 m thick that is closely fractured. These characteristics promote the use of the Eureka Quartzite as a decorative building aggregate; they also enhance its properties as a fracture-flow aquifer. In many places the Eureka is stained red by hematite deposited in fractures by groundwater. The Eureka Quartzite is widely distributed and is a regional marker unit (Ekren, Anderson et al. 1971). The Eureka Quartzite is succeeded by the shallow water Ely Springs Dolomite, which marks a recurrence of the carbonate depositional regime. Ordovician strata grade up through the Ely Springs Formation, interrupted by minor erosional gaps, into dolomites that form the Siluro-Devonian section (Stewart 1980).

The Silurian system is thin and aerially restricted relative to the rest of the Paleozoic section in Southern Nevada (Stewart 1980); it is generally about 600 m thick in the Yucca Mountain region (Stewart 1980). The Silurian section in much of eastern Nevada consists of the Middle to Upper Silurian Laketown dolomite, a gray, thin-to-thick bedded to massive dolomite, presumably of shallow water origin (Stewart 1980). It is exposed in the Pintwater (Figure 3.2-5) Desert, Pahranaagat, and Pahroc Ranges, for example. To the west, this facies grades into a thin- to slabby-bedded to laminated, light to dark gray dolomite and lesser limestone that is locally sandy, cherty, or carbonaceous, and presumably of outer shelf origin (Stewart 1980). The two Silurian carbonate

facies are recognized at Bare Mountain (Figure 3.2-5) where the lower (deeper water), thin-bedded facies is assigned to the Roberts Mountains Formation, and the upper, massive (shallow water) dolomitic facies is assigned to the Lone Mountain Dolomite (Cornwall and Kleinhampl 1961b; Monsen et al. 1992). The Roberts Mountains Formation appears to be regionally unconformable on the Ely Springs Dolomite; in the Yucca Mountain area, the Roberts Mountains Formation crops out only in Northern Bare Mountain (Sawyer, Wahl et al. 1995). It ranges in age from late Early Silurian to probably latest Silurian (Monsen et al. 1992), and is about 190 m thick. The gradationally overlying Lone Mountain Dolomite is about 488 m thick; it is assigned a Silurian to perhaps Early Devonian age on the basis of lithology and stratigraphic position above the Roberts Mountains Formation (Cornwall and Kleinhampl 1961b; Monsen et al. 1992).

The Roberts Mountains and the Lone Mountain Dolomites are the only Paleozoic units penetrated by a borehole at Yucca Mountain (Carr, M.D., Waddell et al. 1986; Grow et al. 1994). Below a subsurface depth of 1,244 m, well UE-25 p#1 (see Figure 3.3.6-3) penetrated about 563 m of dolomite equivalent to the Roberts Mountains and Lone Mountain Dolomites exposed in Chuckawalla Canyon on the east flank of Bare Mountain (Carr, M.D., Waddell et al. 1986). At Chuckawalla Canyon the Roberts Mountains Dolomite crops out as a dark gray to black, finely crystalline cherty dolomite; the overlying Lone Mountain Dolomite is a light gray fine- to medium-grained crystalline dolomite. To the east, in the Spotted Range and Ranger Mountains, correlative Silurian strata are exposed in the lower part of the "dolomite of the Spotted Range" (Figure 3.2-5; Poole, Elston et al. 1965; Ekren, Anderson et al. 1971), but only the Lone Mountain Dolomite is lithologically similar to the chronostratigraphically correlative (Lower to Upper Silurian, chiefly Wenlockian) dolomite of the Spotted Range.

West of Bare Mountain the Silurian section is included in the lower part of the Hidden Valley Dolomite, a unit equivalent to the Laketown Dolomite. The Hidden Valley Dolomite ranges in thickness from about 350 m in the Inyo Mountains to about 415 m in the Death Valley area (Corbett, K. et al. 1988), and between 90 and 300 m in the Nopah Range and the Montgomery Mountains (Burchfiel, Hamill et al. 1983).

Devonian rocks in the Yucca Mountain region consist of a succession of limestone and dolomite that typically includes intervals of thick-bedded, gray, crystalline dolomite; fossiliferous, thin- or slabby-bedded or cherty limestone; and silty-sandy or quartzitic beds. The lithologic and stratigraphic variability, the fossil assemblage, and the presence of numerous erosional breaks indicate deposition in shallow (shelf to upper slope) water dominated at times by reef bank environments. Devonian strata tend to be siltier upsection and toward the northwest (Wright, L.A., Thompson et al. 1991), a lithostratigraphic distinction that becomes more pronounced in the overlying Mississippian section. Johnson, J.G. et al. (1989) and Sandberg et al. (1989) provide discussions of facies and depositional environments of Devonian rocks in the western United States, including lithofacies maps that show the complexity of regional stratigraphic relations across the Yucca Mountain region.

In the older literature the Devonian section in the vicinity of Yucca Mountain is grouped into three main units: the informal "Dolomite of the Spotted Range" (the upper part of which is Lower Devonian; Ekren, Anderson et al. 1971), the Nevada Formation (Lower and Middle Devonian; Merriam 1940), and the Devils Gate Limestone (Middle to Upper Devonian; Merriam 1940). This tripartite designation is widely applied in Southern Nevada, but the stratigraphic nomenclature for

Devonian units east of Yucca Mountain now more commonly adheres to unit designations defined by Nolan (1935): the Lower Devonian is represented by the upper part of the Sevy Dolomite, the Middle and Upper Devonian are represented by the Simonson Dolomite and by the Guilmette Formation, respectively (Table 3.2-1). Upper Devonian strata are also included in the lowermost part of the Eleana Formation, a unit defined at the Nevada Test Site (NTS) (Johnson, M.S. and Hibbard 1957; Poole, Hauser et al. 1961; Table 3.2-1).

The Devonian section is thick and extensive across Southern Nevada. Perhaps the thickest (1,844 m) and most complete Devonian section in the Yucca Mountain region is located in the Pahrangat Range (Tschanz and Pampeyan 1970; Figure 3.2-5). In the Nevada Test Site the Devonian section is estimated to have a total thickness of about 1,000 m (Robinson, G.D. 1985). The Sevy Dolomite or its correlative strata (Nolan 1935) extends over an area of about 260,000 square kilometers (Osmond 1957; Johnson, J.G. et al. 1989), from Western Utah to Eureka Nevada and south to the Inyo Range in California, as a homogeneous, microcrystalline, generally unfossiliferous, well-bedded gray dolomite capped in many places by a quartz sandstone (Tschanz and Pampeyan 1970). At the Nevada Test Site, the Sevy Dolomite is about 265-m thick (Poole, Hauser et al. 1961). The Simonson Dolomite is nearly as widespread, but is lithologically more variable and is fossiliferous. There is probably about 240 m of Simonson Dolomite at the Nevada Test Site (Tschanz and Pampeyan 1970). The Guilmette Formation is conspicuous for its massive reef breccia limestone facies and presence of sandy to silty limestones. Over 500 m of Guilmette Formation are present at the Nevada Test Site (Johnson, M.S. and Hibbard 1957).

The Simonson Dolomite and Guilmette Formation crop out at the southeastern corner of Shoshone Mountain, at Mine Mountain, and at the southernmost end of the Belted Range around the northern margin of Yucca Flat (Figure 3.2-5). These units are also well exposed at the southern end of the Spotted Range in and around Mercury Ridge, and in the southern part of the Ranger Mountains (Figure 3.2-5). The Sevy and Simonson Dolomites and the Guilmette Formation are widely exposed below (south of) the Specter Range thrust in the Specter Range; rocks of equivalent age and lithology crop out in the Calico Hills and form the westernmost outliers of the Striped Hills (Figure 3.2-5).

At Bare Mountain the Devonian section is represented by evenly-bedded dolomite and less abundant limestone and sandstone designated the Fluorspar Canyon Formation (see Figure 3.2-5, and Cornwall and Kleinhampl 1961b), a unit equivalent to the Nevada Formation (Table 3.2-1) and totaling about 520 m in thickness. However, thrust faulting has juxtaposed two different facies here; accordingly, Monsen et al. (1992) subdivided the Fluorspar Canyon Formation, retaining that name for well-bedded strata in the upper thrust plate, and designating more clastic, locally coralline strata below the thrust as "rocks of Tarantula Canyon." Both the Fluorspar Canyon Formation of Monsen et al. (1992) and the rocks of Tarantula Canyon are conformable with the underlying Silurian Lone Mountain Dolomite (equivalent to the lower part of the Sevy Dolomite) which is present on both sides of the thrust fault. However, the rocks of Tarantula Canyon are overlain by a silty-shaley unit designated Eleana Formation by Monsen et al. (1992) and Meiklejohn Formation by Cornwall and Kleinhampl (1961b). Monsen et al. (1992) interpreted a conformable contact at Tarantula Canyon and inferred that the lower part of the Eleana here may be Devonian, whereas Cornwall and Kleinhampl (1961b) interpreted the contact as a thrust and thereby designated the entire Meiklejohn Formation (i.e., Eleana Formation) as a displaced Mississippian section.

Farther west, Devonian rocks are exposed in the Nopah and Montgomery Mountains (Nevada Formation unconformable on Silurian strata; Burchfiel, Hamill et al. 1983; Figure 3.2-5). In the Southern Funeral Mountains and the Cottonwood Mountains of California, the Devonian section comprises the Lost Burro Formation, a carbonate unit about 750 m thick (McAllister 1974) and the top of the Hidden Valley Dolomite (Cemen et al. 1982) equivalent to the Sevy Dolomite (Figure 3.2-5). The Lost Burro Formation is a pale gray crystalline dolomite, locally cherty, with minor quartzite layers. It is equivalent to the Guilmette and most of the Simonson Dolomites (Tschanz and Pampeyan 1970). Devonian strata become increasingly argillaceous to the west (indicating a deep depositional trough), and pinch out in the Inyo Mountains (Snow 1992). The Hidden Valley Dolomite thins to the south and pinches out in the middle of the Panamint Range, the Nopah Range, and the Spring Mountains (Snow 1992, Figure 3.2-5), whereas Upper Devonian dolomite (the Lost Burro Formation) extends across a Middle Devonian unconformity on into Nevada (Poole, Sandberg et al. 1977).

Mississippian strata in the Yucca Mountain region are represented by sharply contrasting but locally intertonguing lithologies: a shale-siltstone section that thickens to more than 3,000 m toward its westward source (Stewart 1980), and a comparatively thinner and more uniform carbonate section that extends southeastward from the vicinity of Mercury and the Spotted Range, where it is about 300 m thick (Barnes, Ekren et al. 1982). Stevens et al. (1996) recognized three general, but contrasting, lithofacies belts of Mississippian age based on regional studies in Southern Nevada and East-Central California:

- A southeastern, predominantly limestone belt representing an extensive carbonate platform
- A central, mixed limestone and siliciclastic belt representing slope and base-of-slope environments
- A northwestern, dominantly siliciclastic belt deposited primarily in base-of-slope and basinal environment

The results of regional studies of Mississippian rocks across much of the western United States by Poole and Sandberg (1991) are presented in a series of paleogeographic maps showing the distribution of depositional environments during various segments of Mississippian time. In Southern Nevada, following the Late Devonian-Early Mississippian Antler orogeny, Poole and Sandberg (1991) show a north-trending emergent land mass flanked on the east by a predominantly carbonaceous mudstone facies that grades eastward into a carbonate facies during Early Mississippian time. In later Mississippian time, coarse to fine clastic sediments grading eastward into siltstone and mudstone accumulated east of the highlands in a prodelta depositional setting; the Chainman Shale (see below) is representative of the latter sequence.

Barnes, Ekren et al. (1982) mapped three Mississippian carbonate units in the Nevada Test Site: the Narrow Canyon Limestone (transitional with the underlying Devonian Devils Gate Limestone, or Guilmette Formation), the Mercury Limestone, and the informal limestone of Timpi Canyon (Table 3.2-1). Farther east, these Mississippian units are represented by the Rogers Spring and the Monte Cristo Limestones (Table 3.2-1). The Monte Cristo is now elevated to group status, with inclusion of an uppermost unit correlative with Mississippian clastic rocks of the Spotted Range

(Sawyer, D.A., Wahl et al. 1995). Along the west side of Yucca Flat (Figure 3.2-6), the Mississippian section is mostly the shaley, western facies, represented by the Eleana Formation (Table 3.2-1). The Eleana Formation is well exposed in its type locality, the Eleana Range (Poole, Hauser et al. 1961; Figure 3.2-6) where it is more than 700 m thick (Poole, Hauser et al. 1961; Cole, Wahl et al. 1989) and consists of thin-bedded turbidites, laminated siltstones, and limestone, chert, and/or quartz clast conglomerates that bottom as massive channel fills (Cole, Trexler et al. 1994). The upper part of the type Eleana Formation is chiefly calcareous turbidites, which is represented farther east and south by the Chainman Shale (Table 3.2-1), a monotonous siltstone or mudstone several hundred meters thick, interbedded with sparse quartz sandstone. The Chainman Shale crops out in the CP Hills and the core of the Calico Hills (Maldonado et al. 1979; Cole, Trexler et al. 1994; Sawyer, D.A., Wahl et al. 1995; exposures too small to display in Figure 3.2-6). Correlative strata crop out in the northeastern corner of Bare Mountain (Cornwall and Kleinhampl 1961b; Monsen et al. 1992).

About 770 m of Chainman Shale were penetrated by borehole UE-24 a-3 in the Calico Hills. The well bottomed in Silurian or Devonian dolomite (Maldonado et al. 1979). The borehole revealed low-grade thermal metamorphism of the shale, and this metamorphism provides one possible explanation for a magnetic anomaly that encompasses the Calico Hills. Alternatively, the anomaly could be explained by a depositionally thick section of Miocene tuff above the Paleozoic contact.

A section of Upper Devonian to Lower Mississippian strata above the Guilmette Formation at Shoshone Mountain (Figure 3.2-5) may be a transitional facies between the Eleana turbidite facies to the northwest and the carbonate-platform facies of the Spotted Range to the southeast. The lowest Mississippian strata consist of pale-green siltstone and shale, platy limestone, and black chert lenses, all of which may correlate with thin, Lower Mississippian limestone beds in the Spotted Range (Barnes, Ekren et al. 1982). The highest preserved intervals of the green quartz siltstone and calcareous shale at Shoshone Mountain probably correlate with the Chainman Shale (Cole, Trexler et al. 1994).

Mississippian rocks in the Funeral Mountains (exposures too small to show at the scale of Figure 3.2-6) are assigned to the Tin Mountain Limestone and the Perdido Formation (Monte Cristo Formation in the Nopah Range; Table 3.2-1). Rocks of Pennsylvanian to Permian age in the Yucca Mountain region are represented by the Tippipah Limestone (Table 3.2-1), a thick- to thin-bedded gray limestone, but locally silty and cherty (Frizzell and Shulters 1990). The Tippipah is exposed only at the east side of the Nevada Test Site, at the southern end of the Eleana Range (Syncline Ridge) and at the southern end of the CP Hills (Figure 3.2-6), where it is disconformable with the Chainman Shale (Cole, Trexler et al. 1994). The disconformity represents an erosional hiatus of as much as 10 m.y., which was followed by essentially synchronous regional carbonate shelf deposition (Cole, Trexler et al. 1994). The Pennsylvanian section is about 1,000 m thick in the Nevada Test Site (Frizzell and Shulters 1990) and about equally thick in the Spring Mountains (Figure 3.2-6) where it is designated the Bird Spring Formation (Table 3.2-1; Longwell and Dunbar 1936; Longwell et al. 1965; Rich 1961). With the exception of much of the Lower Pennsylvanian at the Nevada Test Site (Cole, Trexler et al. 1994), the section represents nearly continuous deposition during Pennsylvanian time and into Lower Wolfcampian time (Tschanz and Pampeyan 1970). Pennsylvanian strata have not been found at Bare Mountain, but the Bird Spring Formation is exposed farther south in the Nopah Range (Figure 3.2-6; Burchfiel, Hamill et al. 1983).

The Death Valley region approximates the location of a Carboniferous facies transition from a carbonate/quartzite lithology (shallow water platform environment) to the southeast to a siltstone/shale lithology (deep water environment) to the northwest (Snow 1992; Stevens 1986). The transition is marked by occurrence of the Rest Spring Shale (Table 3.2-1) in the Darwin Plateau area (Stone, Dunne et al. 1989; Snow 1992). The Rest Spring Shale is a variegated shale and siltstone with minor sandstone, equivalent to the Chainman Shale (Dunne 1986). In the Cottonwood Mountains the Pennsylvanian carbonate platform environment changes to a clastic rise section across a span of about 35 km (Snow 1992).

The stable carbonate platform began to collapse in mid-Wolfcampian time, as indicated by a stratigraphic interval more than 50 m thick consisting of turbidites, debrites, and argillaceous limestones (Snow 1992). By latest Wolfcampian, or earliest Leonardian time, the area shoaled and became the locus of shallow marine or alluvial deposits (Stone, Stevens et al. 1987), a situation that also prevailed throughout the Yucca Mountain region.

The Paleozoic section of the Inyo Mountains is only 2,760 m thick and it generally documents increasing water depth from Ordovician to Late Mississippian time (Stevens 1986). Thereafter the depositional environment is very complex, reflecting tectonic activity farther west. In the Darwin Plateau area, deep water environments in Late Pennsylvanian through Early Permian time are represented by massive, micritic limestone and turbidites; rapid shallowing occurred in Middle to Late Permian time, ultimately resulting in at least local subaerial exposure and deposition of coarse, terrigenous clastic rocks presently exposed in the Inyo Mountains (Dunne 1986; Snow 1992). A nearly unbroken Paleozoic section from Precambrian to Middle Pennsylvanian is exposed in and south of the Nopah Range (Figure 3.2-6), totaling more than 7,500 m (Burchfiel, Hamill et al. 1983). The only major unconformity in the section is at the base of the Devonian Nevada Formation, on the Silurian Hidden Valley Dolomite and on the Ordovician Ely Springs Dolomite (Burchfiel, Hamill et al. 1983). The total thickness of the pre-Tertiary section in the Nevada Test Site is estimated at about 11,500 m (Frizzell and Shulters 1990).

3.2.2.1.3 Mesozoic Rocks

Stratified Mesozoic rocks have not been found within the 100 km radius of Yucca Mountain; their closest occurrence to Yucca Mountain is at the periphery of this area, south and east of Charleston Peak in the Spring Mountains (Figure 3.2-7). There, a thick, well-exposed section of Mesozoic rock forms Wilson Cliffs at the latitude of Las Vegas (Longwell et al. 1965; Figure 3.2-7). Although Mesozoic strata are not a factor in the hydrologic or tectonic phenomena relevant to Yucca Mountain, a discussion is included here as an integral part of the geologic history of the Yucca Mountain region.

Carbonate deposition in the Yucca Mountain region continued into Late Permian time, but gradual uplift, accompanied by erosion, resulted in an unconformity. Deeper (and older) stratigraphic levels were exposed toward the west, whereas deposition of younger strata encroached from the east, progressively covering much of the eroded carbonate rock. Consequently, Lower Triassic strata unconformably overlie Middle to Lower Permian levels of the Bird Spring Formation in the western Spring Mountains. In the southeastern Spring Mountains the Permian section is more nearly complete and contains Permian red beds and the Toroweap and Kaibab Formations. Farther east,

in the Colorado Plateau, a virtually complete Permian through Triassic section is present. As the erosional hiatus across the unconformity diminishes toward the east, the younger Paleozoic strata below the unconformity reflect shallower, near-shore depositional environments, as do the Lower Triassic beds that lie above the unconformity.

The Lower Triassic strata are assigned to the Moenkopi Formation (Stewart 1980, Table 3.2-2). This unit includes interbedded silty limestone, reddish-brown siltstone to fine-grained sandstone, gypsum and local limestone pebble conglomerates, facies that indicate a shoaling marine to alluvial near-shore environment of deposition. Upper Triassic strata comprise the Chinle Formation and its basal member, the Shinarump Conglomerate (Table 3.2-2). The Shinarump consists of widespread chert-pebble conglomerate in sandstone matrix; the Chinle is chiefly weakly consolidated red shale, claystone, siltstone and fine sandstone. Unconformably above the Chinle are Lower Jurassic redbeds equivalent to the Moenave and Kayenta Formations of the Colorado Plateau. Conformably above these beds lies the Lower Jurassic Aztec Sandstone, the youngest Mesozoic deposit in the region (Table 3.2-2). The Aztec consists of conspicuously cross-bedded, pink to red, fine- to medium-grained quartzose sandstone as much as 750 m thick in the Wilson Cliffs (Figure 3.2-7). The top of the Aztec Sandstone is either eroded away or sliced off by an overthrust Paleozoic section (Longwell et al. 1965).

The Mesozoic section in the Spring Mountains (Figure 3.2-7) indicates that regional uplift continued and expanded eastward in Middle to Late Triassic time, exposing strata of the Moenkopi Formation to slight erosion and, during a later phase of uplift, exposing the Chinle Formation to erosion (Marzolf 1990). By Early Jurassic time the region evolved from an alluvial plain to a desert, and dune sands of the Aztec Sandstone were laid down (Marzolf 1990).

In California, Mesozoic strata are present in a band that stretches along the Inyo Mountains, the Darwin Plateau, and into the Argus Range (Figure 3.2-7; Stone and Stevens 1986). The section includes two Triassic lithosomes: a lower, marine to near-shore alluvial lithosome consisting of about 800 to 900 m of Lower Triassic micritic limestone and mudstone (Lewis et al. 1983; Dunne 1986), and an Upper Triassic (and perhaps even younger) continental volcanic and volcanoclastic lithosome as much as 3,000 m thick (Dunne 1986). Here, as in Nevada, the change in environment of deposition, from marine to continental, reflects regional uplift associated with tectonism. The Upper Triassic lithosome in California comprises an eastward prograding assemblage of fan deposits that were derived from the evolving Sierra Nevada plutonic/volcanic terrane to the west (now represented by the exposed Sierra Nevada batholith; Dunne 1986; Dunne et al. 1978). Most of the California Triassic sediments are metamorphosed as a result of igneous intrusion and concomitant crustal thickening (Dunne 1986). Igneous intrusion in this region occurred from about 186-147 Ma (Chen and Moore 1982; Dunne et al. 1978; Miller, C. 1978) and from 80-70 Ma (Labotka, Warasila et al. 1985).

Mesozoic rocks younger than Early Jurassic in the Yucca Mountain setting are intrusive, consisting of widely scattered granitic stocks and mafic dikes. Granitic stocks near Yucca Mountain (Figure 3.2-7) include the Climax and Gold Meadow stocks (101 Ma and 93.6 Ma, respectively; Naeser and Maldonado 1981) and a buried intrusive body near Yucca Flat (102 Ma; Cole, Harris et al. 1993), as well as numerous lamprophyre dikes (about 101 Ma; Cole, Trexler et al. 1994). In California a widely distributed population of mafic dikes that are aligned about N25°W (the Independence dike

swarm; Moore, J. and Hopson 1961; Chen and Moore 1979) is Late Jurassic (about 148 Ma: Chen and Moore 1979). The dikes represent an early phase of regional extension oriented N65°W (Chen and Moore 1979). The intrusion of granitic stocks represents a period of crustal thickening and heating that culminated probably in Late Jurassic to Early Cretaceous time. Metamorphism of the Proterozoic rocks in the Funeral Mountains has been attributed to intrusive activity in Mesozoic time. Many of the intrusive rocks are exposed at structural levels that indicate removal by erosion of several kilometers of rock since time of intrusion and crystallization.

3.2.2.2 Cenozoic Rocks

Cenozoic rocks of the Yucca Mountain geologic setting fall into three general groups: pre-Middle Miocene sedimentary rocks that predate creation of the southwestern Nevada volcanic field; the Middle to Late Miocene volcanic suite that constitutes the southwestern Nevada volcanic field; and the Plio-Pleistocene basalts and basin sediments. These lithostratigraphic groups are not well defined in terms of system boundaries (e.g., Tertiary, Quaternary) so systemic distinctions will not be emphasized in the following treatment.

At Yucca Mountain and in the surrounding area, Cenozoic rocks overlie complexly deformed Paleozoic and Precambrian rocks along a profound erosional unconformity. Thus, the distribution, geometry, and attitudes of these older rocks, and the extent to which these factors influenced the distribution and structure of the Cenozoic units, is indeterminable, given the present paucity of subsurface data. The age of the regional unconformity is also unknown, but erosional down-cutting, possibly associated with extension, most likely was underway in Late Cretaceous (post-Santonian) time, as the various Cretaceous stocks and dikes are all post-kinematic or indicate the influence of an extensional stress field during emplacement. The age of the basal Cenozoic deposits is unknown; the oldest such deposits within the 100 km radius of Yucca Mountain are at least Late Oligocene, but such deposits may include older basal colluvium or lag conglomerates.

The erosional surface shows evidence of considerable weathering suggestive of a warm, bi-seasonal savannah environment. The carbonates show a characteristic red (terra rosa) clay-rich weathering rind, local solution weathering (gnaggas) and rounded hill forms having relief of perhaps a hundred meters or less. Eocene climatic conditions were most likely conducive to such weathering. Cavernous weathering is only sparsely or weakly developed in the Paleozoic carbonates, and the character of the early Tertiary surface is in marked contrast to the sharply etched, high-relief, essentially unweathered surface formed in post-Miocene time. Also, much of the relief expressed in the exposed Paleozoic rocks owes its origin to Late Miocene extensional faulting. High structural relief is locally associated with the pre-Late Oligocene surface, but it is ordinarily affected by weathering. The relative contributions of erosion/weathering and tectonic displacement to the formation of paleo-relief are presently undetermined.

3.2.2.2.1 Tertiary Rocks

Pre-Middle Miocene sedimentary rocks are widely distributed throughout Nevada (Harris, H.D. 1959; Stewart 1980). The distribution and heterogeneous continental character of the deposits implies that they were laid down in restricted basins that may have been precursors to the present basins. The sediments typically comprise a basal conglomerate, lacustrine limestone, and tuffs. The

conglomerate is composed of locally derived clasts (Precambrian or Paleozoic provenance), commonly of cobble to boulder size, and is typically poorly sorted and set in an oxidized matrix. It ranges in textural characteristics from colluvial to fanglomeratic to stream channel gravel. The conglomerate typically intertongues with and is overlain by a characteristically pinkish-cream to buff or tan crystalline or clayey-silty lacustrine limestone. In outcrop, the limestone commonly shows soft-sediment deformation features, local slump folding, and algal mat structures. Upsection, the limestone is interbedded with and ultimately overlain by tuffaceous sandstone and distal airfall tuffs of uncertain provenance. In many places, these tuffs give $^{40}\text{Ar}/^{39}\text{Ar}$ radiometric ages of 30-27 Ma (Late Oligocene) (Saylor and Hodges 1994).

Strata of this age and lithologic assemblage are found in and near Rock Valley east of Yucca Mountain (Figure 3.2-8). These strata are designated informally the "rocks of Winapi Wash" (Table 3.2-3). Strata of similar age and lithology are exposed to the east in the Pahranaagat area; the coeval section includes up to 330 m of strata called the Hells Bells Canyon Formation (Dolgoff 1963). The thickest sections of this type and age (1,500 to 1,800 m) are present in the Spotted and Pintwater Ranges (Tschanz and Pampeyan 1970). To the west, along the east side of the Funeral and Grapevine Mountains and in small patches at the northeast corner of Bare Mountain, a section as much as 900 m thick forms the Titus Canyon Formation (Stock, C. and Bode 1935; Cornwall and Kleinhampl 1964). Tuff in the Titus Canyon Formation gives a radiometric age ($^{40}\text{Ar}/^{39}\text{Ar}$) as old as 30-27 Ma (Saylor and Hodges 1994). Tertiary sediment older than Miocene is very sparse west of the Funeral Mountains (Dunne 1986), but thick Lower Tertiary conglomerates are reported in the Cottonwood Mountains (Snow and White 1990).

Basin deposits of similar lithologies are found in the ranges east of Yucca Mountain (Guth et al. 1988), but ages have not been adequately determined to clearly discriminate the Oligocene "Winapi Wash" succession from a lithologically similar section that belongs to the Miocene Horse Spring Formation. The thickest sections of this lithologic assemblage are found in the Spotted and Pintwater Ranges, where as much as 1,500 m has been reported (Tschanz and Pampeyan 1970).

The presence of airfall tuffs high in the Oligocene section heralds a period of catastrophic explosive volcanism that began in Late Oligocene time and culminated in Middle-late to Early-late Miocene time with the creation of the southwestern Nevada volcanic field (Stewart et al. 1977; Carr, W.J. 1984) [Figure 3.2-9; see also Subsection 3.9.2]. The earliest of these great eruptions is represented by the Monotony Tuff, a unit dated 27.3 Ma and exposed mainly north of Yucca Mountain, in the Belted Range and the Rhyolite Hills (Figure 3.2-10) (Sawyer, D.A., Wahl et al. 1995). The Monotony Tuff has a maximum exposed thickness of about 300 m; it originated from a caldera located in the area of the present Pancake Range and Northern Reveille Range (Ekren, Anderson et al. 1971; Sawyer, D.A., Wahl et al. 1995) (see Figure 3.3.1-9; Pancake Range is north of the Reveille Range). The sequence of Upper Oligocene through Middle Miocene tuffs and associated sediments forms an important part of the Tertiary section in the setting north and east of Yucca Mountain; Ekren, Anderson et al. (1971) cite more than 6 km of such strata ranging in age from 27-7 Ma.

Deposition of the tuffs and establishment of the great caldera complexes interrupted and locally obliterated the established Tertiary depositional regime in the Yucca Mountain geologic setting. This regime continued elsewhere, however, with modifications imposed by tectonism, until nearly

the end of the Miocene when fundamental changes in climate and regionally active extensional faulting put an end to it throughout the Southern Great Basin.

In the vicinity of Yucca Mountain, the Oligocene rocks of Winapi Wash are succeeded by a complex assemblage of bouldery and poorly sorted stream gravel, volcanic arkose, shale and siltstone, freshwater limestone and marl, and a variety of tuffs. This assemblage, informally designated "rocks of Pavits Spring" (Table 3.2-3) (Hinrichs 1968), includes tuffs as old as 15 Ma. The fluvial-lacustrine environment inherited from the Oligocene persisted despite being swamped by volcanic sediment until the Ammonia Tanks Tuff was deposited at 11.4 Ma. Gravel (unit Tsd; Carr, W.J., Byers et al. 1986) possibly correlative with the rocks of Pavits Spring was penetrated by well UE-25 p#1 at Yucca Mountain, near the Paleozoic unconformity (see Figure 3.5-3). Old gravels deposited across the northeast corner of Bare Mountain contain, high in the section, tuffs approximately 8 Ma (C.J. Fridrich et al., *Cenozoic Basins of the Death Valley Region: Late Cenozoic Extension, Vertical-axis Rotation, and Volcanism in the Crater Flat Basin, Southwest Nevada*, Geological Society of America Special Paper, in press). These gravels have been described in print only from casual reconnaissance ("Gravel of Sober-up Ridge" of Monsen et al. 1992; Reheis 1988) but recently have been mapped in more detail by Fridrich (1998). Fridrich reports that the gravels previously lumped by others belong to two quite different units. The older unit, which was deposited concordantly on and deformed with the Ammonia Tanks Tuff, dips as steeply as 15°, and contains slide breccias of Paleozoic rocks and of rocks like those of the Lower Miocene Upper "Joshua Hollow Formation" but not of the Middle Miocene volcanic rocks. The younger unit overlies the older unit with angular unconformity, is deformed only by very gentle undulations and possibly by small faults, postdates all or most of the extension, and consists almost entirely of clasts of Paleozoic formations like those of nearby Bare Mountain.

Along the eastern flank of the Funeral Mountains, in the Bat Mountain area, a coarse, clastic succession called the Bat Mountain Formation (Figure 3.2-8; Table 3.2-3) overlies the latest Oligocene limestone and continues upsection to Middle Miocene (Cemen and Wright 1990). The Bat Mountain Formation consists largely of alluvial fan and basin strata similar to the rocks of Pavits Spring. A similar succession crops out in the Mt. Helen area (Sawyer, D.A., Wahl et al. 1995) and in the Weepah Hills and Silver Peak Range in the northwest corner of the Yucca Mountain region. The section in the Silver Peak Range that is comparable to the Miocene rocks of Pavits Spring is called the Esmeralda Formation (Table 3.2-3) (Turner 1900). The formation is unconformable on an Upper Oligocene or Lower Miocene tuff and ranges in age from about 16 Ma to about 6 Ma (Stewart 1980; Stewart and Diamond 1990). The total Tertiary thickness here may be as great as 5.4 km (Stewart and Diamond 1990).

The conditions under which the rocks of Winapi Wash were deposited apparently persisted in the area east of Las Vegas well into Miocene time, as indicated by the Horse Spring Formation. Lithologic similarities between the rocks of Winapi Wash and the Bitter Ridge Member of the Horse Spring Formation led Hinrichs (1968) to correlate the former unit in Rock Valley with the much younger Horse Spring Formation near Las Vegas. The Horse Spring Formation ranges in age from 20-12 Ma (Bohannon 1984). Cemen and Wright (1990) remark on the lithologic similarity of the Oligocene strata (25 Ma) at Bat Mountain with the type at Horse Spring Formation. Apart from their geographic isolation, these Oligocene through Miocene units could be considered different parts (older and younger) of a single lithosome.

The explosive volcanism that led up to and culminated in the formation of the southwestern Nevada volcanic field is the most significant depositional event of the Cenozoic era with respect to Yucca Mountain. It resulted in formation of six major calderas between about 15 and 7.5 Ma (Sawyer, D.A., Fleck et al. 1994), created Yucca Mountain, and brought to a close the regional deposition that spans domains of the Yucca Mountain geologic setting. The record of regional tuff deposition begins within the rocks of Pavits Spring. Tuff deposition is also documented in the eastern part of the Nevada Test Site where Redrock Valley Tuff (15.3 Ma; Sawyer, D.A., Wahl et al. 1995) and the tuff of Yucca Flat (15 Ma; Sawyer, D.A., Wahl et al. 1995) are significant components. The succession of tuff and lava units that form Yucca Mountain are listed in Table 3.2-3 and described in detail in Subsection 3.5. Several units that are widely distributed in the southwestern Nevada volcanic field include the Crater Flat Group (about 13.25 Ma), the Calico Hills Formation (12.9 Ma), the Paintbrush Group (12.8-12.7 Ma), and the Timber Mountain Group (11.6-11.4 Ma; Sawyer, D.A., Fleck et al. 1994). The lowest of the tuffs that form the foundation of Yucca Mountain is the Lithic Ridge Tuff (14 Ma; Sawyer, D.A., Fleck et al. 1994). Although pre-Lithic Ridge Tuffs are found in the rocks of Pavits Springs and beneath Yucca Mountain, little is known about their extent, age, and stratigraphic relations. In fact, caldera sources for all but the Tiva Canyon Tuff and the Timber Mountain Group Tuffs are uncertain (Sawyer, D.A., Fleck et al. 1994).

Lipman et al. (1966) first noted that the Topopah Spring Tuff and the Tiva Canyon Tuff of the Paintbrush Group represented eruptions from a zoned magma chamber. They attributed the zoning to fractional crystallization such that the upper portion of the chamber had evolved to a rhyolitic composition that was the first magma erupted and thus formed the base of each ashflow sheet. Eruption from successively deeper portions of the magma chamber had less siliceous compositions and a higher proportion of crystals which had settled into a deeper part of the magma chamber such that the top portions of the ashflow tuffs are crystal-rich quartz latites. Noble, D.C. and Hedge (1969) noted that strontium was more radiogenic in the first (older) erupted parts of the ashflows; and they concluded that the upper part of the magma chamber had assimilated crustal rocks. Working in a similar volcanic sequence, Stuckless and O'Neil (1973) used strontium and oxygen isotopes and bulk rock chemistry to show that fractional crystallization and wall-rock assimilation occurred simultaneously such that early-formed crystals were less radiogenic than their enclosing matrix. They proposed that the ashflow complexes were generated by partial melting in the lower crust, but neodymium isotope studies of several ashflow complexes, including those of the Timber Mountain area, suggest a large component of mantle-derived alkalic basalt (Perry, DePaolo et al. 1993).

In another interpretation, Broxton, Warren et al. (1989) proposed that the volcanic complex at Yucca Mountain erupted in a series of cycles from individual shallow plutons. The magma pools made their way well to within 3 km of the surface at which level cooling led to volatile saturation of the magma. As a direct result of this, the successive rhyolite reservoirs blew their tops virtually in continuous eruption for each formation of each major eruptive group. Broxton, Warren et al. (1989) infer that the differentiation/emplacement process was repeated for each major eruption sequence, or group. Peak volcanism in the southwestern Nevada volcanic field occurred during eruption of the Paintbrush and Timber Mountain Groups when more than 4,500 km³ of magma were erupted in two episodes separated by a span of about 750 k.y. (Sawyer, D.A., Fleck et al. 1994).

The Wahmonie Formation and the underlying Salyer Formation (Poole, Elston et al. 1965) form a sequence of andesite and dacite lava flows erupted from a source north of Skull Mountain and south of Shoshone Mountain. The Wahmonie Formation forms a distinctive marker between the Crater Flat Group Tuffs and the Calico Hills Formation east of Yucca Mountain (Figure 3.2-11). Rocks of the Wahmonie Formation are characteristically dark, iron-rich, massive or thick-bedded lava flows, autoclastic breccias, and agglomerates. The lower part of the Wahmonie Formation and the underlying Salyer Formation include interbedded volcanoclastic sediments - debris flows, lahars, and mudslides that indicate initial deposition in a relatively high relief setting transitional to the basinal environment of the rocks of Pavits Spring. The Wahmonie Formation was deeply eroded during the 1.5 m.y. period of subaerial exposure preceding eruption and deposition of the overlying unit, the Topopah Spring Tuff. In places, the Topopah Spring Tuff fills in gullies and depressions having as much as 100 m of relief cut in the Wahmonie Formation.

The Calico Hills Formation is named for exposures in the northwest part of the Calico Hills (Orkild and O'Connor 1970). It consists of rhyolite lavas, domes, and nonwelded ashflow tuffs. In the Yucca Mountain area it is 50 to 300 m-thick (Broxton, Chipera et al. 1993).

Other eruptive sequences and calderas associated with the southwestern Nevada volcanic field include the Ammonia Tanks Tuff (11.4 Ma), the Black Mountain caldera (9.4 Ma), and the Stonewall Mountain caldera and its associated Spearhead Tuff (7.5 Ma) (Figure 3.2-11) (Sawyer, D.A., Fleck et al. 1994). The various tuffs and lavas erupted in the post-11 Ma period form important volumes of rock in the Pahute Mesa-Sarcobatus Flat-Bullfrog Hills area northwest of Yucca Mountain. They are not, however, directly relevant to the history or makeup of Yucca Mountain. The youngest tuff that is found at Yucca Mountain is the Rainier Mesa Tuff of the Timber Mountain Group.

Physical properties of the tuff and lava units of the southwestern Nevada volcanic field contrast greatly across formational contacts but tend to be uniform laterally over wide areas. This characteristic results from:

- The conditions of deposition—large batches of homogenized material laid down quickly over large areas
- Differences in initial composition of each eruptive batch
- Post-depositional processes of welding, vapor phase crystallization, autolytic and pneumatolytic alteration, and gas dispersion

As a result, some of the tuff units are physically similar to ceramics or glass, whereas others are loose and porous, or vesicular and closely fractured or chemically altered. Understanding the spatial variation of these properties contributes to modeling the behavior of a potential repository under thermal loading and to modeling of hydrologic processes. The composition and physical properties of the units that represent the southwestern Nevada volcanic field at Yucca Mountain are treated in detail in Subsections 3.9 (Volcanic Hazards) and 3.5 (Site Stratigraphy). The spatial distribution of properties is presented in Subsection 3.8 (Integrated Site Model) and 3-D modeling of properties is discussed in Section 5 (Hydrology).

Miocene rocks west and south of Yucca Mountain, in the Inyo-Mono domain, that are chiefly of igneous origin are younger than about 16 Ma. These include the central Death Valley volcanic field (Wright, L.A., Troxel et al. 1981) and an irregular belt of volcanic rocks that extends from the Owshead Mountains and Southern Panamint Range eastward toward the Kingston Range, the Greenwater Range, the Black Mountains, and the Furnace Creek basin (Figure 3.2-9). Tuffs of the Artists Drive Formation, a unit comparable to the rocks of Pavits Spring near Yucca Mountain, date from about 12 Ma (Wright, L.A., Troxel et al. 1981). Above this lies the Furnace Creek Formation and the Funeral Formation, with a combined total thickness of about 3.6 km of pyroclastic sediments, basalt flows, intertonguing conglomerates, sandstones and mudstones. Basalts at the top of the Funeral Formation are dated at about 4 Ma (McAllister 1973). Wright, L.A., Thompson et al. (1991) note that this rock assemblage is most likely the direct result of Neogene local basin subsidence and extension.

The Central Death Valley volcanic field is underlain by the Willow Springs Pluton, a gabbro dated 11.6-9 Ma, exposed along the west side of the Black Mountains (Figure 3.2-9; Asmerom et al. 1990). The gabbro is intruded by small granite bodies. Basalt extrusion in the Resting Springs Range of about the same age (11.7 Ma) was followed by extensive silicic to mafic volcanism during the 10.5-5 Ma period. Volcanism culminated in the 8.5-6.5 Ma period with eruption of the Shoshone volcanic suite, chiefly dacites and rhyodacite tuffs (with associated sediments) exposed in the Eastern Black Mountains and southern part of the Greenwater Range (Figure 3.2-9). Silicic volcanism ceased in this area about 5-6 Ma with deposition of rhyolites of the Greenwater volcanic suite (Noble, L.F. 1941; Drewes 1963). Thereafter, diminishing basaltic volcanism continued into Late Pleistocene time as in the Goldfield section of the Walker Lane domain to the east.

The advent of basaltic volcanism at about 11 Ma signaled the end of crustal magmatism in the construction of Yucca Mountain. It indicates generation of small, discrete batches of basaltic magma at upper mantle depths (≥ 60 km) capable of making their way quickly to the surface in Crater Flat basin (Crowe, Perry et al. 1995). The history, evolution, and character of Plio-Pleistocene basaltic volcanism proximal to Yucca Mountain (within 25 km of the potential repository) is treated by Crowe, Perry et al. (1995) and by Fridrich (1998).

The oldest basalts in Crater Flat are dated at about 11.3 Ma, indicating that episodes of basaltic volcanism began very shortly following eruption of the Ammonia Tanks Tuff (11.46 Ma). However, no further basaltic volcanism occurred in Crater Flat until 3.7 Ma when a group of five northwest-aligned scoria cones and lava flows were emplaced in southeastern Crater Flat (Figure 3.2-12). This latter episode represents the largest volume basaltic emplacement in Crater Flat. The complex formed largely from Hawaiian type fissure eruptions and aa flows. Lava-filled fissures and feeder dikes are oriented north-south. The deposit was subsequently cut by faulting which produced dip-slip offsets of more than 1 m, west side down (Crowe, Perry et al. 1995).

3.2.2.2.2 Quaternary Rocks and Sediments

Quaternary deposits consist of alluvial sediments and infrequently erupted basalts. The basaltic eruptions represent a continuation of the activity during the Late Tertiary. Following the episode at 3.7 Ma, a subsequent basaltic eruption episode occurred between 1.7 to 0.7 Ma. It consists of four cinder cones (Little Cones, Red Cone, Black Cone, and Makani Cone) aligned north-northeast along

the axis of Crater Flat (Figure 3.2-12). Most of the volume from this episode is associated with Red and Black Cones. This episode spatially overlaps the area of eruption of the earliest (11.3 Ma) episode.

The most recent episode of basaltic volcanism created the Lathrop Wells Cone (Figure 3.2-12). The Lathrop Wells Cone complex comprises fissure eruptions, spatter and scoria cones, and aa flows. Satellitic spatter cones at the east base of the main cone have a northwest alignment. The Lathrop Wells Cone complex is probably about 75 ka. Uncertainty in the age determination and emplacement history of this eruptive complex is discussed by Crowe, Perry et al. (1995) and in Subsection 3.9.3.4.

Other basaltic groups in the Yucca Mountain vicinity include the 380 ka Sleeping Butte centers located 45-km northwest of Yucca Mountain, and the basalt of Amargosa Valley (Crowe, Wohletz et al. 1986) located about 3-km south of Amargosa Valley crossroads. The basalt here is buried but was sampled by drilling and gave an $^{39}\text{Ar}/^{40}\text{Ar}$ isochron age of 4.4 Ma (Turrin et al. 1991). The eruptive history of Quaternary basaltic volcanism in the Yucca Mountain region is discussed in more detail in Subsection 3.9.3.4.

Apart from sporadic and volumetrically minor basaltic volcanism, Quaternary deposition in the Yucca Mountain geologic setting is chiefly restricted to alluvial basin deposition. In many basins alluvial deposition is a continuation of sediment infilling that was well underway in Late Miocene time. For example, in Mid Valley (Figure 3.2-13), a continuous alluvial section 300- to 400-m thick includes a several meters thick interval of 7.5 Ma ashfall Spearhead Tuff (McArthur and Burkhard 1986). The tuff, penetrated by two boreholes, is overlain by about 360 m of fine to coarse sand and sandy gravel derived from the basin flanks.

Closed basins in the area received alluvial sediment hundreds of meters thick throughout the Plio-Pleistocene, in response to continuing faulting subsidence and range flank erosion. Basins such as Frenchman Flat and Yucca Flat basin, Mid Valley, Crater Flat basin, and especially the basins of the Inyo-Mono terrane (Figure 3.2-13) contain sediment that includes coarse alluvial clastic facies (debris flow deposits, colluvium, fan sheet gravel) and lakebed-playa deposits (siliceous clays, marls, evaporites). In some basins such as Crater Flat basin, aggradation has reached levels sufficient to have formed spillways so that alluvial deposition is graded to an adjacent valley (here Amargosa Valley; Figure 3.2-13) or basin.

Within the Yucca Mountain region broad valley or trough-like areas of subsidence are linked by graded fan assemblages and washes to form two separate drainage systems: the Las Vegas Valley watershed, and the Amargosa Valley watershed (Figure 3.2-13). Colluvium and scree commonly litter the range flanks. This sediment typically is brought to the basins as debris flows or mud flows during infrequent torrential rains that are characteristic of the present interpluvial climate.

An overall regional tilt to the south, established during the past 8 m.y. (Carr, W.J., Byers et al. 1984), seems to have driven regional drainage southward, resulting in a general ponding at the southern ends of major basins and development of spillways. Drainage through Amargosa Valley, for example, was ponded at a former Lake Tecopa, which was receiving sediment in Late Pliocene to

Early Pleistocene time. The lake was breached and the Tecopa Lake beds are presently being incised as drainage presently flows through the Sperry Hills, then west into Death Valley (Figure 3.2-13).

Although present deposition and erosion generally occur at very low rates and sporadically because of the arid climate, the Middle to Late Pleistocene depositional record (locally dated by distal ash layers such as the 750 ka Bishop Ash) indicates a highly variable and highly localized succession of sedimentary deposits, perhaps analogous to the Middle Miocene Rocks of Pavits Spring, but without the tuffaceous volcanic component. Sediment input is dominated by highly local sources that control lithologies of the coarse clastic components, lake or pond deposits are virtually the only datable record because of fine sediment and rare, but radiometrically datable volcanic ash beds. In places, large accumulations of eolian silts and sands are banked up against range flanks or as dune accumulations, notably Big Dune south of Bare Mountain (Figure 3.2-13). Further details on Pleistocene stratigraphy and depositional and erosional processes are found in Subsection 3.4.3.3 Quaternary Stratigraphy.

3.2.3 Regional Structure and Tectonic Deformation

3.2.3.1 Compressive Tectonics of the Yucca Mountain Region

The geologic setting of Yucca Mountain is characterized structurally by two distinctly different styles of tectonic deformation: an earlier shortening "mountain building" style of regional folding and overthrusting, and a later extensional "basin forming" style of regional normal and strike-slip faulting. The shortening style records orogenic events that occurred primarily during Paleozoic deposition, followed by a peak event that occurred in the Mesozoic and terminated marine deposition. Shortening deformation of Precambrian age also is recorded in Proterozoic and older rocks, but no orogenic pattern has been determined from the sparsely exposed rocks.

The earliest mountain building event (orogeny) that had an effect on Paleozoic rocks of the Yucca Mountain geologic setting is the Antler orogeny (Stewart 1980). Antler orogenic deformation is expressed chiefly by the Roberts Mountains overthrust belt, which is located well to the north of Yucca Mountain (Figure 3.2-14). The thrusting created a mountain range and a marine foredeep basin along its eastern margin into which coarse sediment, that eroded from the thrust belt, was deposited. The coarse, clastic sediment derived from the Antler highlands beginning in Middle-Devonian time and continuing into the Mississippian period, constitutes the Eleana Formation exposed at the Nevada Test Site (Trexler, J.H. et al. 1996). Farther to the east, a correlative section of shale (Chainman Shale) was deposited in an environment that has aspects of an inner shelf as well as a subsiding basin (Trexler, J.H. et al. 1996), and, east of that, a carbonate platform environment existed uninfluenced by the Antler orogeny (Figure 3.2-14). Similar depositional effects of the Antler orogeny are found in the Inyo-Mono domain, where the Upper Mississippian Rest Spring Shale and the shaley lower part of the Lower Mississippian Tin Mountain Limestone represent erosion of the Antler highlands (Dunne 1986) and, therefore, are part of the Eleana-Chainman lithosome.

The Antler orogeny is significant in the Yucca Mountain region for two reasons:

- The fine-grained, terrigenous lithology of the Eleana (and especially the Chainman Shale) lithosome forms a major Paleozoic aquitard north and east of Yucca Mountain, as well as a potential source rock for hydrocarbons.
- The subsequent juxtaposition of three distinct but coeval facies (Antler-derived clastic debris, black Chainman Shale, Mississippian and older carbonates) aids in recognizing the structural configurations that formed during the subsequent Sevier-Cordilleran orogeny.

Mountain building in the near vicinity of Yucca Mountain began with eastward-encroaching uplift in latest Permian to Triassic time and culminated during the Mesozoic with the Sevier orogeny (Stewart 1980; Fleck 1970; Burchfiel, Fleck et al. 1974). The Sevier orogeny resulted in a broadly north-to northeast-trending fold-thrust system (Figure 3.2-15). The thrust sheets are typically complicated by overturned or dismembered folds and local reverse or overthrust faults. The major thrusts are continuous along strike for distances of more than 100 km and exhibit stratigraphic juxtapositions that indicate translations of tens of kilometers. Nevertheless, the history of thrust faulting in the Yucca Mountain region, and the identity of each fault from place to place, is uncertain because of erosion, subsequent extension, and burial beneath Tertiary and Quaternary rocks and surficial deposits over wide areas. Therefore, only a general treatment, with an emphasis on geometric relations relevant to issues concerning Yucca Mountain, is presented below.

Two major thrusts are presently recognized in the vicinity of Yucca Mountain: The Belted Range thrust (Caskey and Schweickert 1992; Trexler, J.H. et al. 1996), and the CP thrust (Caskey and Schweickert 1992; Barnes and Poole 1968; Carr, W.J. 1974). The Belted Range thrust (Figure 3.2-15) is the structurally lower and older thrust. It is represented in outcrop at Bare Mountain (there referred to as the Meiklejohn Peak thrust), perhaps in the core of the Calico Hills (see discussion of Calico Hills below), and by small exposures at the southern end of the Belted Range west of Yucca Flat (Caskey and Schweickert 1992; Figure 3.2-15). Caskey and Schweickert (1992) estimated more than 25 km of stratigraphic displacement across the Belted Range thrust. Below the Belted Range thrust a stack of imbricate slices or "plates" place Middle Devonian strata and Eleana Formation over Chainman Shale along a previously unrecognized subhorizontal thrust in the Eleana Range (Trexler, J.H. et al. 1996; cf. Burchfiel, Pelton et al. 1970). The duplex stack extends about 7 km outboard (east) of the main Belted Range thrust; it includes structure at the Calico Hills ("Calico Hills plate"), Mine Mountain ("Mine Mountain plate"), the Eleana Range ("Castle plate, Dolomite Hills Plate, and Grouse Canyon plate"), and at Quartzite Ridge at the northern border of the Nevada Test Site (Trexler, J.H. et al. 1996; Figure 3.2-15). A component of the duplex stack in this northern area was identified as the Tippipah thrust by Robinson (1985). Thrusts that form the base of this duplex zone cut upsection into the Mississippian section, then form a décollement within the weak Chainman Shale (Trexler, J.H. et al. 1996). This interpretation implies that the magnetic gradient present beneath the volcanic deposits at the northern end of Yucca Mountain represents the duplex stack thrust against Silurian rocks penetrated by well UE-25 p#1.

The CP thrust lies to the east of and is a west-vergent back-thrust that is structurally above and younger than the Belted Range thrust (Caskey and Schweickert 1992; Figures 3.2-15 and 3.2-16). The CP thrust is a large, complex structure that extends for more than 180 km on strike and has

about 8.5 km of stratigraphic throw (Caskey and Schweickert 1992). It generally emplaces Precambrian through Cambro-Ordovician strata over Mississippian and Pennsylvanian strata. Rocks of the upper plate are imbricately faulted, highly folded, and locally overturned to the west. Large-scale, west-vergent, nearly recumbent folds occur in both the lower and upper plates of the CP thrust (Caskey and Schweickert 1992). The CP thrust was originally defined from a small patch of outcrop in the CP Hills which form the west flank of Yucca Flat (Figure 3.2-15 and Barnes and Poole 1968). Early work at the Nevada Test Site assigned all thrust structures in the area to the CP thrust (Barnes and Poole 1968; Carr, W.J. 1974; Wernicke, Axen et al. 1988; Wernicke, Snow et al. 1988; Snow 1992), but Caskey and Schweickert (1992) distinguished the CP thrust from the Belted Range thrust on the basis of lower plate folds that indicate westward thrusting of the CP thrust in opposition to eastward thrusting of the Belted Range thrust.

Caskey and Schweickert (1992) carried the CP thrust west through the Calico Hills and correlated it to the Panama thrust at the south end of Bare Mountain (Figure 3.2-15). This interpretation suggests that the CP thrust extends through the Paleozoic substrate beneath Yucca Mountain, possibly placing Silurian rocks above buried Eleana Formation or forming a north-vergent thrust south of and subparallel to the inferred Belted Range thrust duplex mentioned above. In other words, beneath Yucca Mountain there may exist two opposing thrusts, one correlative with the Meiklejohn Peak thrust and the other with the Panama thrust at Bare Mountain.

North of the CP Hills multiple structural interpretations have been presented: Caskey and Schweickert (1992) and Ekren, Anderson et al. (1971) infer that older over younger stratal juxtapositions at Mine Mountain are part of the CP thrust, in contrast to the interpretation of Trexler, J.H. et al. (1996) and Burchfiel, Pelton et al. (1970) who assign structure to east-vergent thrusting. In any case, the structural deformation at Mine Mountain is extensive and very complex. Barnes and Poole (1968) considered the structure at Mine Mountain to be a local assemblage of blocks (the Mine Mountain thrust) detached from the CP thrust but moved with it from the east. W.J. Carr (1974) and G.D. Robinson (1985) tentatively proposed that the older over younger block assemblage at Mine Mountain could be a dismembered gravity slide. This was substantially documented by Cole, Wahl et al. (1989). Cole, Wahl et al. (1989) considered that the structure at Mine Mountain, the CP Hills, and the Calico Hills could best be interpreted as low angle gravity sliding of Middle Miocene age; only the faults at Bare Mountain could be considered indisputable thrusts.

The structure exposed in the core of the Calico Hills could be assigned to either gravity sliding, the Belted Range thrust (Trexler, J.H. et al. 1996; Burchfiel, Pelton et al. 1970), or to the CP thrust (Caskey and Schweickert 1992). Uncertainty exists because of the difficulty in recognizing indisputable thrust-related deformation that expresses vergence, and because either thrust system could reasonably be projected through the Calico Hills. Simonds and Scott (1996) could not resolve the uncertainty, but tentatively advocated a thrust structure rather than a gravity slide structure. J.H. Trexler et al. (1996) made an interpretation based on juxtaposition of facies that suggests overthrusting of more than 6.5 km from the north.

Apart from the Calico Hills exposure, the east- and west-vergent thrust systems are separated by a span of rock that probably was never overthrust. Conodont alteration indices data indicate that the Chainman Shale at Syncline Ridge, located between the thrust systems (Figure 3.2-15), was never tectonically buried, hence neither thrust ever extended much beyond its present position (Trexler,

J.H. et al. 1996). Conodont alteration indices from the Silurian rocks penetrated by well UE-25 p#1 at Yucca Mountain indicate the rocks reached maximum temperatures of 140°-180°C. M.D. Carr, Waddell et al. (1986) concluded that these temperatures could have been achieved by normal burial depths for Silurian rocks in the Great Basin. This observation supports an interpretation that the Silurian rocks in UE-25 p#1 were not overthrust. The gap between the thrust fronts probably extends to Bare Mountain where the Meiklejohn Peak thrust (Belted Range thrust system) and the Panama thrust (CP thrust system) are presently separated by about 6.5 km. Small klippen of the Panama thrust near the center of the mountain (Monsen et al. 1992) indicate the gap, if it existed, was smaller.

The Spotted Range thrust and the Gass Peak thrust are present farther east (Figure 3.2-15). The Spotted Range thrust (named for its exposure in the Spotted Range; Barnes, Ekren et al. 1982) places Middle Cambrian strata over Upper Devonian and Mississippian strata which have tight to isoclinal folds overturned to the southeast, and has more than 25 km of offset (Caskey and Schweickert 1992; Longwell et al. 1965; Tschanz and Pampeyan 1970). Accordingly, the Spotted Range thrust cannot be correlated with the CP thrust (as proposed by Barnes and Poole 1968). Caskey and Schweickert (1992) observe that the lower plate of the Spotted Range thrust is structurally equivalent to the upper plate of the west-vergent CP thrust (Figure 3.2-16). Therefore, the Spotted Range thrust is an eroded, eastern outlier (klippe) of the Belted Range thrust.

The Gass Peak thrust is a large, east-vergent thrust that places Upper Precambrian and Cambrian rock over highly folded and locally overturned Pennsylvanian and Permian carbonate strata (Longwell et al. 1965; Guth 1981). It extends for at least 140 km along the east side of the northern part of the Sheep Range, through the Las Vegas Range (Longwell et al. 1965), and is traceable into the Spring Mountains (as the Wheeler Pass thrust) because of its consistent structural level (Figure 3.2-17; Guth 1990). Net horizontal displacement could exceed 30 km (Guth 1981). Because no major thrusts occur between the Gass Peak thrust and klippen of the Spotted Range thrust, the lower plate of the Spotted Range thrust is also equivalent to the upper plate of the Gass Peak thrust (Figure 3.2-16) (Caskey and Schweickert 1992). Therefore, the Gass Peak thrust and the CP thrust define the eastern and western structural boundaries of the same allochthon.

Late Paleozoic and Mesozoic thrust systems in the Inyo-Mono domain are more extensive and complex than any exposed east of the Funeral Mountains, but their structural relations are more clearly defined. The most extensive thrust system, the Last Chance thrust system (Figure 3.2-17), includes (from oldest to youngest) the Last Chance, the Talc City, the Race Track, the Marble Canyon, and the Lemoigne thrusts (Dunne et al. 1978). The system comprises imbricate, northeast-trending, generally east-vergent thrusts having at least 7 to 35 km of displacement in aggregate. The thrusts place rocks as old as Precambrian on rocks as young as Permian. Deformation typically involves locally recumbent and isoclinal folds in the overridden plates, but most folds are upright and open. Ductile deformation is common. The system was probably most extensively active from mid Triassic to Early Jurassic time (Dunne 1986), but thrusting could have begun as early as Permian time (Snow 1992). The Last Chance thrust system predates the 167-185 Ma Hunter Mountain batholith (Dunne et al. 1978), and it may predate intrusion of the 228 Ma White Top stock in the Cottonwood Mountains (Snow 1992). The Last Chance thrust system essentially comprises the Death Valley thrust belt (Snow 1992).

Numerous attempts have been made to correlate thrusts of the Death Valley thrust belt across the Furnace Creek-Death Valley fault into the Walker Lane and the Nevada Test Site area. Caskey and Schweickert (1992) argued that only three thrust plates exist at the Nevada Test Site, not five as in the Death Valley thrust belt (Snow 1992; Wernicke, Snow et al. 1993):

- Strata above the Belted Range thrust
- Strata below the Belted Range thrust and the CP thrust
- Strata above the CP thrust and the Gass Peak thrust

Accordingly, Caskey and Schweickert (1992) correlate only two thrusts, the Belted Range thrust with the Last Chance thrust. Caskey and Schweickert (1992) and Snow (1992) continue the Belted Range thrust west, connect it with the Grapevine thrust, and thereby correlate it with the Last Chance thrust system (Figure 3.2-17). Snow (1992) correlates the Meiklejohn Peak duplex zone (Calico Hills plate of Trexler, J.H. et al. 1996) with the Racetrack duplex zone beneath the Last Chance thrust. Snow (1992) also correlated the White Top thrust (or backfold) with the Panama thrust-CP thrust (Figure 3.2-17).

Attempts to trace thrusts across the Spring Mountains section of the Walker Lane domain into the Inyo-Mono domain are hampered because of dextral offset along the Stewart Valley fault and as much as 3.5 km normal offset along the Grapevine fault (Figure 3.2-17; Burchfiel, Hamill et al. 1983). The structurally lowest thrust in the Spring Mountains section, and in the entire Yucca Mountain geologic setting, is the Birdspring thrust, which places Bonanza King Formation on Lower Jurassic Aztec Sandstone; however, at its northern end the thrust loses throw and merely duplicates Permian redbeds (Burchfiel and Davis 1988). The Birdspring thrust is the base of a duplex sheet of imbricate faults and folds, all cut out by the overlying Keystone thrust (Figure 3.2-17) which puts Bonanza King over younger Cambrian and overturned Triassic strata.

In tracing thrusts west out of the Spring Mountains and into the Montgomery Mountains, Burchfiel, Hamill et al. (1983) tentatively concluded that the Wheeler Pass thrust is correlative with the Chicago Pass and Shaw Pass thrusts in the northern part of the Nopah Range (Figure 3.2-17). The Chicago Pass thrust and the closely related Shaw thrust have a net stratigraphic throw of about 5 km to the south. The thrust overrides a footwall syncline that infolds lowest Devonian to highest Carboniferous strata with a 300-m wavelength (Snow 1992; Burchfiel, Hamill et al. 1983). The Montgomery thrust places Stirling Quartzite over Ordovician rocks and Devonian Devils Gate limestone in a tight overturned syncline having a wavelength of about 1 km across a dip of about 30° to the northwest (Burchfiel, Hamill et al. 1983). Wernicke, Axen et al. (1988) and Wernicke, Snow et al. (1988) correlated thrusts as far west as the Slate Range in Eastern California with the Wheeler Pass-Gass Peak thrust system.

At present, the only aspects of the Mesozoic orogeny that are well known in the Yucca Mountain geologic setting are the geometry and the stratigraphic relations among the various thrust sheets. Questions regarding where the faults are rooted, how they climb section, and to what levels of the crust thrusting is involved, remain unresolved.

Many of the thrust systems in the Yucca Mountain region define regional folds. Robinson (1985) inferred that the major structure enfolding Yucca Mountain is a "synclinal basin" spanning the area between Bare Mountain and the Halfpint Range, a distance of more than 80 km (Figure 3.2-18).

In his interpretation, the basin is asymmetric, having steep to overturned limbs on the Bare Mountain side and along Rock Valley. The basin is bounded to the south by the Rock Valley fault zone and to the northeast by a "major northeast-trending thrust system," the Tippippah thrust zone (the Belted Range thrust of Caskey and Schweickert (1992) and Trexler, J.H. et al. (1996)). The principal deformation within the basin consists of broad, concentric folds 8 to 24 km apart that trend about N30°E and plunge northward (Figure 3.2-18). Robinson (1985) based his interpretations of fold structure on exposed dips, data from well UE-25 p#1, and aeromagnetic data. As a corollary to this tectonic interpretation, Robinson (1985) inferred that the Mine Mountain thrust and the CP thrust are minor structures; he suggested that they were local slides that resulted in response to regional folding.

Whether Robinson's assessment of fold geometry and the relative magnitudes of folding and thrusting is correct, there is little doubt that large amplitude, regional folds have accompanied thrust faulting in the region. An example of a large fold is the Panamint-Greenwater anticlinorium (Wright, L.A., Troxel et al. 1981), described by Dunne et al. (1978) as a "northwest-pointing tongue of Precambrian rock exposed in the Panamint, Black, and Greenwater Ranges." The fold is bounded by west-dipping strata of the East Sierra thrust system in the Argus Range, and by east-dipping strata in the Resting Spring and Nopah Ranges (Figure 3.2-19). Structural relief is probably in the range of about 7 km. The fold may be a large ramp anticline resulting from the generally eastward movement of a thrust stack of Proterozoic crystalline basement up and over a west-facing ramp (Dunne 1986).

Closer to Yucca Mountain, the CP and Gass Peak thrust plate is folded into large, north-trending open folds (Guth 1990) and more broadly cored by the Pintwater anticline (Longwell 1945) and the Spotted Range syncline (Barnes, Ekren et al. 1982), a regional fold pair traceable for about 100 km and having a combined width that spans four mountain ranges (Sheep, Desert, Pintwater, Spotted Ranges; see Figure 3.2-19). Structural relief is probably as great as 7 km (Caskey and Schweickert 1992). The west limb of the Pintwater anticline probably controls the ramp-like Pintwater thrust (Longwell et al. 1965), a steeply west-dipping thrust fault that extends about 25 km along the west side of the Pintwater Range (Figure 3.2-19) and has about 1 km of stratigraphic separation (Guth 1990).

Burchfiel, Hamill et al. (1983) argued that a large, recumbent east-trending anticline-syncline pair in the northwestern Spring Mountains correlates with the east-trending Pintwater anticline at the southern end of the Spotted Range. They felt that the fold pair cores a large anticlinorium having a structural relief of more than 6 km in the Wheeler Pass thrust sheet (Burchfiel 1965). The Montgomery thrust is inferred to pass through the northwestern part of the Spring Mountains, degenerating into a fold pair ultimately correlative with the Pintwater Range anticline (Figure 3.2-19).

The Belted Range thrust, as correlative to the Last Chance thrust, probably originated prior to latest Middle Triassic and ceased activity by 93 Ma, the age of the Climax stock (Longwell 1945) which intrudes complexly folded Ordovician strata north of Yucca Flat (Houser and Poole 1960). The age of the CP and the Gass Peak thrusts, which cut the Belted Range thrust (Figure 3.2-16), would be younger. The Keystone thrust was moving by Middle Jurassic (Burchfiel and Davis 1988), but it is unclear as to when overthrusting generally ceased in the Yucca Mountain region. The presence of

undeformed Late Cretaceous intrusives generally indicates that deformation did not continue through Cretaceous time in this region. Thus, the Sevier orogeny (Armstrong 1968; Fleck 1970) was a relatively short-lived compressional event in the Yucca Mountain region. Compressional tectonism in the Inyo-Mono terrane appears to have ceased completely in Paleogene time (Dunne 1986).

3.2.3.2 Extensional Tectonics of the Yucca Mountain Region

Extension in the Yucca Mountain region was active by Oligocene time (Smith, D.L. 1991; Axen et al. 1993; Dilles and Gans 1995; Hardyman and Oldow 1991; Ekren and Byers 1984; Dilles et al. 1993) and probably earlier (Constenius 1996; Seedorff 1991). This early phase of extension, sometimes referred to as "pre-basin and range extension" (Zoback et al. 1981), continued into Middle Miocene time. It is thought to have evolved by gravitational collapse of thrust-thickened crust following diminution of subduction-generated compression from the west (Stewart 1978; Wernicke, Christiansen et al. 1987; Hodges and Walker 1992). Extension during this Early Miocene phase is thought to have migrated from east-northeast to west-southwest and to have been unaffected by oblique shear (Zoback et al. 1981; Seedorff 1991). The result was a thinner, closely faulted crust and lithosphere heated and elevated by upper mantle convection (Atwater 1970; Stewart 1978; Davis 1979; Hamilton, W.B. 1989; Severinghaus and Atwater 1990; Bohannon and Parsons 1995). Although this phase of regional extension progressed under the influence of a west- to southwest-directed least principal stress (Zoback et al. 1981), northwest-directed oblique shear did influence the course of extension toward the west side of the widening province at an early date (Stewart 1993). By Early Miocene time (and likely by Middle-Late Oligocene), the characteristic features of the Walker Lane had been established, namely discontinuous north-northwest striking dextral faults and east-northeast striking sinistral faults (Ekren and Byers 1984; Hardyman and Oldow 1991). Deep-seated detachment may also have been a significant mechanism of Paleogene extension in this region. Geobarometry and fission-track age dates indicate that subhorizontal mylonites, presumably indicative of pre-detachment shear (Hamilton, W.B. 1988) were generated at depths of at least 15 km beneath the Funeral-Bare Mountains domain during this phase of deformation (Hoisch and Simpson 1993).

By about 15 Ma the main extensional features within the tectonic setting of Yucca Mountain were already established, namely a basin and range structural pattern defined chiefly by north-south oriented basins or troughs, and fault zones associated with the Walker Lane, namely the Rock Valley fault zone and the Las Vegas Valley shear zone and, perhaps, dextral faulting in the Funeral Mountains area. The Late Oligocene interval was punctuated by deposition of ashfall tuffs (the source of Late Oligocene ages: Axen et al. 1993) derived from eruptions east and north of Yucca Mountain. The advent of siliceous volcanism marks an important tectonic development in the early phase of extension; it signals a culmination of regional crustal heating, the so-called "ignimbrite flareup," during which large volumes of siliceous magma were emplaced in the middle to upper crust (Stewart and Carlson 1976; Axen et al. 1993).

Like the progress of early extension, magmatism proceeded from north to south through the Great Basin; in the south it seems to have generally lagged behind the extension. Thus, the Southwestern Nevada volcanic field may have been generated in an area of crust weakened by deep extensional basins and therefore conducive to volcanic venting (Seedorff 1991; Axen et al. 1993). An alternative interpretation by Sawyer, D.A., Fleck et al. (1994) suggests that basins proximal to Yucca Mountain

formed subsequent to the Oasis Valley-Timber Mountain caldera complex. However, a clastic succession (the "rocks of Pavits Spring"; Hinrichs 1968) may indicate deepening and integration of basins in the Yucca Mountain region occurred prior to formation of the Southwestern Nevada volcanic field.

The rocks of Pavits Spring record basin integration and increased structural and topographic relief by way of thick, torrential stream boulder gravels and volcanic arkoses. Increasingly proximal volcanic activity is indicated by increasing contributions of tuffs upsection including, ultimately, the major components of the Southwestern Nevada volcanic field beginning around 14 Ma with units of the Crater Flat Group.

The culminating tectonic event in the geologic evolution of the region and, coincidentally, the initiating event for structural formation of Yucca Mountain, was the creation of the Southwestern Nevada volcanic field. The Southwestern Nevada volcanic field was produced by a succession of at least 5 voluminous and numerous smaller eruptions that occurred over a period of 7.5 Ma, from about 15-7.5 Ma. The greatest of these eruptions created the volcanic pile (the Paintbrush and Timber Mountain Groups) of which Yucca Mountain is a part. Post-eruptive deflation likely created at least some of the present structural framework of Yucca Mountain, assuming that some post-Paintbrush Group subsidence of Crater Flat basin can be attributed to shrinkage of the underlying magma chamber. Local domainal extension, involving some strike slip displacements, clockwise rotation of crustal blocks, basin subsidence and range uplift, continued in the Walker Lane during the phase of siliceous volcanism (Sawyer, D.A., Fleck et al. 1994). Yucca Mountain was affected by this activity in the 12.7-9 Ma interval as evidenced by continued subsidence and extension across Crater Flat basin, and collapse of the Jackass Flats area and of volcanic terrane farther east.

The advent of basaltic volcanism at about 11 Ma signals the end of crustal level magmatism in the vicinity of Yucca Mountain. It indicates generation of small, discrete batches of basaltic magma at upper-mantle depths (≥ 60 km) capable of making their way quickly to the surface in Crater Flat basin (Crowe, Perry et al. 1995).

Tectonism of the post-11 Ma period in the Yucca Mountain region is dominated by three major tectonic developments: creation of left-lateral faulting of the Spotted Range-Mine Mountain structural zone east of Yucca Mountain; uplift of the Funeral and Bare Mountains and activity in the Inyo-Mono domain to the west; and localization of basaltic volcanism in Crater Flat and the westernmost fringes of Yucca Mountain. Following the 11 Ma basalt emplacement, but prior to 7 or 8 Ma, the style of tectonic deformation in the Yucca Mountain region became more clearly one of narrow basin subsidence, possibly accompanied by adjacent range uplift. This style of tectonism continues at present, most conspicuously at Frenchman Flat and Yucca Flat east of Yucca Mountain, and in Death Valley to the west. Some basins are quiescent or have not been active since mid Pleistocene, including Mid Valley, Jackass Flats, the westernmost side of Crater Flat, and Amargosa Valley. Nevertheless, historic seismicity and occasional large earthquakes accompanied by subsidence, such as the Cedar Mountain-Fairview Peak-Dixie Valley earthquakes, indicate that basin subsidence is sporadic. Presently, strike-slip faulting is active in Rock Valley (Coe, Yount et al. 1996) and in the Inyo-Mono terrane to the west (Keefer et al. 1996).

The post-11 Ma interval is notable also for reactivation of Basin and Range structures to the east, but under a west-northwest direction of extension (Minor 1995; Cole, Wahl et al. 1989). Large earthquakes on range-front faults during the past 100 years indicate that Basin and Range extension is still under way. The driving mechanism may be a mantle plume associated with generation of the Yellowstone hot spot (Saltus and Thompson 1995), or continued assimilation of the previously subducted East Pacific Rise (Severinghaus and Atwater 1990; Bohannon and Parsons 1995). A mantle plume may also be holding the Great Basin at relatively high elevations north of 37°N (Parsons et al. 1994). However, arguments have been presented against the hot spot/mantle plume interpretation (W.B. Hamilton, *Detachment Faulting and Tectonic Modeling in the Yucca Mountain Region*, report to U.S. Geological Survey Water-Resources Division, Yucca Mountain Project Branch, on work carried out under Memorandum of Agreement with the U.S. Geological Survey Geologic Division, Branch of Geophysics).

Funeral Mountains Detachment—A major detachment fault has denuded the core of the Funeral Mountains, revealing the broad, smooth profile of the exposed lower plate surface. Slickensides on the lower plate clearly indicate that the detached sheet rode north-northwestward, apparently upslope and over the crest. It seems clear that the lower plate (that is, the subjacent crust) rose up shortly following detachment to give the range its present crest and perhaps much of its overall relief. Fission track dating of apatite, sphene, and zircon from the lower plate rock indicates that cooling through the temperature interval 285°-120° (equivalent to about 5 km burial depth) took place between 11 and 6 Ma (Holm and Dokka 1991; Hoisch and Simpson 1993).

The elongate domiform or arch-like Funeral Mountain detachment and its lower plate of highly metamorphosed Upper Proterozoic rocks plunge gently northwestward beneath the almost unmetamorphosed upper plate of Upper Proterozoic to Miocene rocks of the Grapevine Mountains, which in most of the range dip gently. Restoration of Southern Grapevine rocks atop those of the Funerals indicates the former to have been transported about 35 km west-northwestward along the detachment surface (W.B. Hamilton, *Detachment Faulting and Tectonic Modeling in the Yucca Mountain Region*, report to U.S. Geological Survey Water-Resources Division, Yucca Mountain Project Branch, on work carried out under Memorandum of Agreement with the U.S. Geological Survey Geologic Division, Branch of Geophysics). The Boundary Canyon fault—or perhaps more correctly—the scarp face of the upper plate more or less rims the Funeral Mountains and is most accessible at Boundary Canyon (Figure 3.2-20), for which it is named.

Rocks comprising the upper plate of the Funeral Mountain detachment are well exposed along the eastern flank of the Funeral Mountains in the vicinity of the Bird Track Hills (Figure 3.2-20). The lower part of this rock sequence consists of chlorite-grade Stirling Quartzite and Wood Canyon Formation, which are complexly and irregularly faulted. This Precambrian section is overlain unconformably by the Titus Canyon Formation and tilted panels of Paintbrush Group Tuffs. The Titus Canyon Formation is composed of volcanoclastic strata and fluvial deposits derived from the Late Proterozoic rocks.

The base of the parautochthonous section shows no evidence of having undergone significant lateral transport of extension despite pronounced shearing along its base. The Titus Canyon Formation and a thick Lower Miocene lava flow and associated tuff are much faulted but can be seen on both remote sensor imagery and mapping to be generally continuous along the Grapevine Mountains for

at least 22 km and thus to preclude major deformation before eruption of the Middle Miocene ashflows. Most of the Cenozoic extension postdates 9 Ma but may predate 7.5 Ma. This accords with the Late Miocene cooling ages, determined by fission-track studies by Hoisch and Simpson (1993) and Holm and Dokka (1991), recording the tectonic denudation of the northwest end of the lower plate of the Funeral Mountains, which did not cool below $\sim 300^{\circ}$ - 200° C (sphene and zircon closure temperatures) until about 10 Ma, and below $\sim 120^{\circ}$ C (apatite closure temperature) until ~ 6 Ma. Tectonic denudation of these mid-crustal rocks and the rotation and detachment faulting of the Miocene supracrustal rocks were thus of about the same age and must have been linked kinematically.

Bullfrog Hills Detachment—The Bullfrog Hills consists of highly disrupted and structurally discordant, variably tilted blocks of tuffs of the Southwestern Nevada volcanic field. The assemblage is separated from Bare Mountain by the shallow, north-dipping, generally east-striking Fluorspar Canyon fault. This fault represents the near-headwall of the detachment as well as the accommodation plane for westward translation. The headwall (or breakaway) fault of the Bullfrog Hills is exposed along a north-trending line that defines at least one kilometer of stratigraphic offset (Fridrich 1998). This line or zone connects with the Fluorspar Canyon fault. The more evident high-angle faults farther west all project north out of the low-angle Fluorspar Canyon fault (Figure 3.2-21). After 11.7 Ma the breakaway zone occupied at least three successively more westward positions (Fridrich 1998).

Extension of the Bullfrog Hills began with northwest-side down faulting during the 11.7 to 12.7 Ma interval. The faulting produced translation and tilting that ranges from 45° at the head, to at least 60° in the hills just east of Beatty (Figure 3.2-21, Fridrich 1998). Numerous small wedge-shaped troughs formed between the translated and rotated blocks; they are filled with rock slide breccia and coarse alluvium (Fridrich 1998). This entire assemblage was then blanketed by Timber Mountain Group Tuff. Ammonia Tanks Tuff is tilted 20° to 55° eastward and 10.7 Ma basalt is much less tilted (Fridrich 1998). The faulting appears to have become inactive and the Bullfrog Hills stabilized when the western Amargosa Valley and Sarcobatus Flats basins (Figure 3.2-21) opened after 10 Ma (Weiss, Noble, Worthington et al. 1993).

The west-trending "grade discordance fault" of Hoisch (1995) (also known as the Gold Ace fault) converges with the Fluorspar Canyon fault at the northwest limit of outcrop at Bare Mountain (i.e., the Fluorspar Canyon fault truncates the Gold Ace fault (Figure 3.2-21)). However, Hoisch (1995) simply inferred that the two faults merge. Because the grade discordance fault separates rocks of contrasting metamorphic grade, as does the Boundary Canyon fault of the Funeral Mountains, Hoisch concluded that the Boundary Canyon fault is also a continuation of the Fluorspar Canyon fault. This interpretation is given some support by the existence west of Beatty of the Bullfrog fault, which apparently is a distal extension of the Fluorspar Canyon fault, or at least it is the basal fault plane on which the Bullfrog Hills fault blocks moved and presently rest. The Bullfrog fault separates Precambrian schist containing veins of foliated granite from overlying tilted blocks of Miocene tuff. Heating of the Precambrian section during the Miocene was apparently strong enough to reset the radiometric systems such that the rocks now yield Miocene ages.

In places, a selvage of highly fragmented nonmetamorphosed Paleozoic section lies above the Bullfrog fault and below the Miocene tuffs. This geometry prompted Maldonado and Hausback

(1990) to infer two stacked detachment faults west of Beatty. The lower one, the Bullfrog fault, is clearly the more consequential fault, it being the inferred link between the Boundary Canyon fault and the Fluorspar Canyon fault (Figure 3.2-20).

If this inferred fault continuity is correct, there are significant implications for the history of Bare Mountain. Hoisch (1995) infers that the present east dip of the north-trending grade discordance fault may be explained by horizontal axis rotation from an initial northwest dip, or the north-trending, east dipping grade discordance fault may be a remnant of a system of large mullions within the regional detachment. The mullion interpretation requires that Bare Mountain be rotated 30° counterclockwise to bring a mullion structure into proper northwest alignment with the Bullfrog detachment. Furthermore, the alignment would be enhanced by locating Bare Mountain 5 to 10 km to the west or southwest while maintaining the basement exposures in the Southern Bullfrog Hills at their present locations. Hoisch (1995) further speculates that translation and rotation were integral components of crustal extension in this region, perhaps leading to opening of the Amargosa Desert basin as well. Notions of wholesale block rotation and translation to accommodate structural alignments and juxtapositions in this region are also argued by Snow and Prave (1994); their arguments hinge on pre-Tertiary features and on regional strike-slip fault mechanisms. These mechanisms are discussed under evaluation of tectonic models (Subsection 3.3.2).

W.B. Hamilton (*Detachment Faulting and Tectonic Modeling in the Yucca Mountain Region*, report to U.S. Geological Survey Water-Resources Division, Yucca Mountain Project Branch, on work carried out under Memorandum of Agreement with the U.S. Geological Survey Geologic Division, Branch of Geophysics) interprets the structure in terms of regional detachment that began as deep-seated normal faulting. A normal fault dipped steeply west-northwestward beneath what became the upper plate of the grade discordance fault, reaching rocks that were then about 15 km deep (they had been ~25 km deep in Cretaceous time) in the vicinity of the Eastern Bullfrog Hills. The present length of the fault along the lower plate as defined is no more than 22 km if it dipped continuously down to the present exposures of the deep rocks, so, in order to descend 15 km, its initial dip would have been no gentler than 45°. This dip also accounts for the depth of formation of the garnet-staurolite rocks of northwesternmost Bare Mountain. W.B. Hamilton (*Detachment Faulting and Tectonic Modeling in the Yucca Mountain Region*, report to U.S. Geological Survey Water-Resources Division, Yucca Mountain Project Branch, on work carried out under Memorandum of Agreement with the U.S. Geological Survey Geologic Division, Branch of Geophysics) infers that the initial fault gave way at about the 15 km level to pure-shear flattening, which presumably accords with the detachment geometry and metamorphic petrology of the present day Funeral Mountains.

As slip proceeded on the initially steep fault, the footwall rose and flattened, stranding the thin Northeast Bare Mountain upper plate and progressively stranding panels of upper plate Middle Miocene rocks on the rising lower plate as a hinge migrated westward in the lower plate (W.B. Hamilton, *Detachment Faulting and Tectonic Modeling in the Yucca Mountain Region*, report to U.S. Geological Survey Water-Resources Division, Yucca Mountain Project Branch, on work carried out under Memorandum of Agreement with the U.S. Geological Survey Geologic Division, Branch of Geophysics). Faulting started ~12 Ma and by ~10 Ma was inactivated as far west as Northwest Bare Mountain. At 10 Ma, the active fault dipped steeply beneath the Bullfrog Hills region, where mid-crust rocks that were subhorizontal when faulting began were rising into the footwall of the

active fault. The shallow hinge of flattening and the deep hinge of pickup of mid-crustal rocks both migrated westward for another 2 m.y. or so, progressively stranding backtilted panels of Miocene rocks, and progressively bringing deep rocks to or near the surface. The tectonic lenses and breccias of Paleozoic rocks, now present between lower-plate metamorphic rocks and the panels of Miocene supracrustal rocks of the Bullfrog Hills, were scraped from the hanging wall of the retreating Grapevine megablock. Klippen of these lenses also lie on topographic crests on the metamorphic rocks south of Fluorspar Canyon. When the system was inactivated at 7 or 8 Ma, the final master fault dipped steeply beneath the Grapevine Mountains, which before 12 Ma lay close to the unmetamorphosed Paleozoic strata of Bare Mountain. The trace of the steep, active fault in these terms migrated ~35 km in 4 or 5 m.y. at a rate of ~7-9 mm/a.

The Las Vegas Valley Shear Zone—The Las Vegas Valley shear zone (Figure 3.2-1) represents the eastern boundary of the Walker Lane south of Rock Valley (Stewart 1988). The shear zone is generally thought to be a right-lateral strike-slip fault, chiefly on the evidence of displaced Mesozoic thrust faults on either side of the shear zone (Longwell 1974; Stewart 1988) and the clockwise curvature of the major ranges on the east side of the shear zone. The generally accepted displacement of about 50 km along the central part of the Las Vegas Valley shear zone (Burchfiel 1965; Longwell 1974) is thought to have occurred between 15-10 Ma (Bohannon 1984; Hudson, M.R. et al. 1994).

The Las Vegas Valley shear zone is important to the Yucca Mountain geologic setting because it forms a major domain boundary (Figure 3.2-1) and because it plays a role in some tectonic models applicable to Yucca Mountain. Unfortunately, little is known about the Las Vegas Valley shear zone. The structure is buried by Pleistocene fan deposits, exhibits little or no seismic activity, and is not characterized by available geophysical data. Consequently, the northern reach of the Las Vegas Valley shear zone is subject to widely disparate interpretation (Hinrichs 1968; Fox and Carr 1989; Caskey and Schweickert 1992).

Burchfiel (1965) considered the northwestern projection of the Las Vegas Valley shear zone to continue into the Specter Range thrust as shown in Figure 3.2-22. Burchfiel's interpretation requires an episode of substantial south-southeast-directed compression in Early Tertiary to effect 6,000 or more feet (1,830 m) of stratigraphic offset along the 50° to 60° northwest-dipping Specter Range thrust as well as approximately 35 km of right-lateral offset along the Las Vegas Valley shear zone as projected into Mercury Valley.

The Las Vegas Valley shear zone also has been interpreted as an accommodation zone (Hamilton, W.B. 1988; Duebendorfer and Black 1992) that marks the lateral margin of a large tract of detachment faults thought to include the Spotted Range and ranges farther southeast (Guth 1981). This interpretation avoids structural problems at the northern end of the Las Vegas Valley shear zone by inferring that lateral displacement decreases to zero somewhere northwest of Indian Springs, a consequence of detachment in this region (Guth 1981). The accommodation fault interpretation diminishes the significance of lateral displacement and accords with the estimate of 26 km of lateral displacement given by Caskey and Schweickert (1992). The accommodation model of Duebendorfer and Black (1992) requires 10 to 20 km of slip to be absorbed by oroclinal bending in the Specter Range, but evidence for such compression during the 14-13 Ma interval has not been recognized in or near Rock Valley. Therefore, arcing the Las Vegas Valley shear zone to the west

through Mercury Valley into alignment with the left-lateral Rock Valley fault zone is not a viable tectonic interpretation. Also, it is difficult to accept the hypothesis of a reverse fault arcing clockwise to a northwest-trending strike-slip fault in terrane where no other reverse faults are known to have such geometry.

Paleomagnetic studies indicate that the vertical axis, clockwise bending in ranges along the north side of the Las Vegas Valley shear zone, is not a consequence of simple fault drag (Sonder et al. 1994), but represents a broad zone of combined crushing and local rotations of blocks on the order of a few kilometers in lateral dimension (Nelson, M.R. and Jones 1987; Sonder et al. 1994). As much as 55 km of north-south crustal shortening in Late Middle Miocene is well-documented in the Northern Black Mountains along the Lake Mead fault zone (Anderson, R.E., Barnhard et al. 1994) and it is compatible with both right-lateral slip and domain-boundary compression along the Las Vegas Valley shear zone (Anderson, R.E., Barnhard et al. 1994).

Right-lateral transpression seems to have culminated in a Late Miocene event that involved crushing and bending of extended terrane north and east of the shear zone. Extension in the Sheep and Desert Ranges evidently continued late during deposition of strata tentatively correlated with the Miocene Horse Spring Formation (Guth 1981). In that case, right-lateral transpression that possibly had begun as early as 29 Ma must have peaked prior to about 14-13 Ma (Hudson, M.R. et al. 1994). If the deformed Tertiary strata are equivalent to the rocks of Winapi Wash, peak transpression may be considerably older, possibly pre 16-15 Ma.

Furnace Creek, Death Valley, Fish Lake Valley Fault—The combined Death Valley-Furnace Creek-Fish Lake Valley fault system forms the only major, throughgoing fault system in the Yucca Mountain region (Figure 3.2-23). The Death Valley-Furnace Creek-Fish Lake Valley fault system is a significant tectonic feature because it is a major domain boundary that separates a region of high strain rate and seismic activity (the Inyo-Mono domain) from one of relatively low strain rate and highly diverse structure and seismic activity (the Walker Lane). The Death Valley-Furnace Creek-Fish Lake Valley fault system varies in structural style along strike and links with associated lateral structures are uncertain. Therefore, its role in local fault development is open to speculation. It may represent the eastern border of a series of transtensional pull-aparts (Burchfiel and Stewart 1966; Blakely et al. 1995), or it may represent range front faults linked by strike-slip segments that are evolving into an increasingly coherent structure propagated northward along a strike distance of about 350 km.

The southern part of the fault system, the Death Valley fault segment, is primarily an oblique right-lateral range-front fault. It follows the salients and reentrants of the Black Mountains front, ranging in strike from north-south to N40°W. For the most part, the Death Valley fault dips steeply west, but toward its southern end, dips range from 35° to 65° east or northeast (Piety 1996). Fault length is uncertain because of disagreement on definition of its poorly exposed end points. A minimum length of 51 km is based on nearly continuously exposed west-facing scarps (Piety 1996).

The total offset of the Death Valley fault is unknown, but the dip-slip component, estimated from bedrock relief, is about 4,570 m. Hooke (1972) estimated a Holocene (about 10-11 ka) dip-slip displacement of about 63 m, based on elevation differences of coeval lake shore features on the east

and west sides of Death Valley. On this basis, Piety (1996) concluded that the main and most recent displacement is dip-slip. However, Fleck (1970) considered that most of the vertical displacement on the Death Valley fault is ancient, probably having its inception before deposition of the Furnace Creek Formation (about 6 Ma). Faulting is assumed to have begun in Middle Miocene time, based on ages of displaced volcanic rocks believed to be coeval with faulting (Brogan et al. 1991). Estimates of total lateral offset, based on offsets of Precambrian strata, range from 80 km (Stewart 1967) to about 8 km or less (Wright, L.A. and Troxel 1967; Piety 1996). Estimates of Late Tertiary and Quaternary offset range from 35 km (Butler 1984) to about 20 km (Brady 1984). Estimates of Pleistocene offset toward the southern end of the fault range from about 200 m to 15 m, with estimates of 1.5 to 3 m per event based on displaced drainage (Piety 1996). Toward the southern end of the Black Mountains, the Death Valley fault has mostly strike-slip displacement (Piety 1996). Holocene activity (within the last 2 k.y.: Hunt and Mabey 1966) is indicated by west-facing scarps 1.2 to 1.8 m in relief; folds, buckles, fissures in surficial sediment; and deflected drainage (Troxel and Butler 1986).

The Furnace Creek fault is chiefly a right lateral strike-slip fault that extends through alluvial fans along the central part of Death Valley. The continuous fault trace is well expressed in most remote sensor images, probably because of the well-developed Pleistocene to Holocene scarp that ranges in cumulative relief from 0.2 to 23 m (Piety 1996). Estimates of total lateral offset, based on displaced Precambrian units, are uncertain and range widely from 128 km to less than 8 km (Wright and Troxel 1967; Davis 1979; Piety 1996); however, most estimates of lateral offset are less than those for the Death Valley fault (Piety 1996). Estimates of Pleistocene lateral offset are 46 m, including single event offsets of 1.5 to 2.7 m (Piety 1996).

A link between the Death Valley fault and the Furnace Creek fault is not well established. The main trace of the Furnace Creek fault may veer southeastward along the southern end of the Funeral Mountains and into the Amargosa trough, and even link up with structures along the east side of Amargosa Valley (Wright and Troxel 1967). The Death Valley fault may intersect or merge with the Furnace Creek fault across the alluvial-filled valley between the Funeral and the Black Mountains, a 19 km long gap termed the "transition zone" by Klinger and Piety (1996). The structural nature of the inferred linkage is presently unclear, except that here fault traces and fold forms are relatively short, trend in various directions, and form a relatively wide zone (Klinger and Piety 1996).

Toward its northern end, between the Grapevine Mountains (Figure 3.2-23) and the Last Chance Range to the north, the Furnace Creek fault is distributed into a number of fault planes forming a zone that extends into Fish Lake Valley. The northernmost 80 km or more of this zone of strike-slip and primarily dip-slip range front faults is called the Fish Lake Valley fault. Estimates of maximum lateral displacement range from 25 km (Piety 1996) to 50 km (McKee 1968). Estimates of maximum vertical displacement range up to 750 m (Reheis and McKee 1991). In most places, the Pleistocene dip-slip component, which is as great as 64 m, exceeds the strike-slip component (Brogan et al. 1991). However, Pleistocene lateral displacement as great as 122 m (Sawyer, T.L. 1991) is recorded.

The Fish Lake Valley fault is thought to have propagated northward from the Furnace Creek fault sometime between 12 to 4 Ma (Reheis 1993). The fault dies out in a series of folds near the northern

end of Fish Lake Valley (Reheis 1993; Stewart 1967). Pleistocene activity along the fault has been high; vertical displacement of as much as 540 m may have accrued within the past 740 ka (Reheis and McKee 1991). However, modeling by Dixon et al. (1995), based on space geodesy, implies that activity along the Death Valley-Furnace Creek-Fish Lake Valley fault system has slowed during the past few million years as slip is increasingly taken up to the west, mainly along the Owens Valley fault zone. This transference of right-lateral slip activity to the west is reflected by the historical seismicity along the Eastern California shear zone (Dixon et al. 1995) and its convergence northward with the Fish Lake Valley fault.

Northeast Trending Strike-slip Fault Zones and the Spotted Range-Mine Mountain Structural Zone—The Spotted Range-Mine Mountain structural zone (Carr, W.J. 1984; Stewart 1988; Figure 3.2-1) is distinguished by prominent east-northeast trending left-lateral strike slip faults and fault zones: the Rock Valley fault zone, the Mine Mountain fault, the Wahmonie fault zone, and the Cane Spring fault (Figure 3.2-24). Because east-northeast-trending left-lateral faults that could represent extensions of the Rock Valley fault zone are unknown in the Spotted Range east of Yucca Flat, W.J. Carr (1984) inferred that the Rock Valley fault zone (and therefore the Spotted Range-Mine Mountain structural zone) is terminated to the east against a major north-northwest-trending right-lateral fault, the Yucca-Frenchman shear zone (Figure 3.2-25), thought by W.J. Carr (1984) to extend along the axis of Yucca Flat. Alternatively, the eastern end of the Rock Valley fault zone may arc to the north beneath Frenchman Flat and merge with more northerly faults that follow the axis of Yucca Flat and Frenchman Flat (Ander 1984), or that bound and/or obliquely transect the Spotted Range. A third possibility, supported by detailed aerial photograph examination, is that the Rock Valley fault zone (or at least part of it) curves southward and loses displacement between the Ranger Mountains and the south end of the Spotted Range where left-lateral shear strain is accommodated by complex crushing and a succession of parallel east-northeast left-lateral faults that slice the Paleozoic rocks east of Mercury and west of Indian Springs (Figure 3.2-25). The Yucca Flat-Frenchman Flat basin axis must represent a tectonic domain boundary, as indicated by Stewart (1988), such that the northeast trending strike-slip faults do not extend east of it.

The largest and most tectonically significant structural component of the Spotted Range-Mine Mountain structural zone is the Rock Valley fault zone (Whitney 1996). The Rock Valley fault zone is significant because it is an unusually well-exposed domain section boundary (against the Spring Mountains section of the Walker Lane: Stewart 1988; and Figure 3.9-1) having a history of activity dating back possibly to the Late Oligocene (Whitney, Taylor et al. 1996). It is also important because it is presently seismogenic and because it comprises a seismic source exceeded in size only by the Furnace Creek fault, which occurs at a greater distance from Yucca Mountain.

The Rock Valley fault zone coincides with a band of broad aeromagnetic lows bounded by a parallel gradient (-300 to -400 nT, Glen and Ponce 1991) along the south side of Little Skull Mountain and extending eastward to Frenchman Flat, a distance of about 40 km. The geophysical data, and local stratigraphy and structure indicate that the fault zone is part of a complex structural trough about 5 km wide. Three major fault sets comprise the Rock Valley fault zone:

- Long, dominantly strike-slip faults that strike N65° to 80°E
- Shorter normal, strike-slip and/or reverse bridging faults that strike N25° to 50°E

- Minor normal and strike-slip faults that strike N10° to 15°W

The zone is further complicated by N25°E striking faults that project into Rock Valley from the north. These faults are possibly related tectonically (but not specifically) to the Cane Spring fault and the Wahmonie fault zone that strikes through the gap between Skull and Little Skull Mountains (Figure 3.2-24).

Offsets along the fault planes are rarely demonstrable because cross-cutting features are uncommon. Estimates of total lateral offset of no more than 1.5-4 km are based on regional considerations (Barnes, Ekren et al. 1982) and geophysical data (Kane and Bracken 1983). A few observed lateral offsets are in the range of 30 to 40 m. However, they appear to be pre-Pleistocene, and a more precise age constraint is unlikely to become available. These large displacements may actually be the cumulative results of series of smaller events that were sufficiently closely spaced in time to have prevented erosional discrimination of smaller, component slips.

The N25°-50°E faults include bridging faults and splays off the main strike-slip strands. Faults of this group extend for lengths of one to 2 km between the more easterly trending traces. Typically, the bridging faults exhibit much more damage and more complex displacement phenomena than the controlling strike-slip faults, but they have weak or nondistinctive topographic expression. In many of these faults dip slip and strike slip, or slip at various steeply plunging angles, is recorded on different slip surfaces spaced a few centimeters or less apart. Some faults of this set show considerable brecciation and milling over widths of a few tens of centimeters or more.

North- to northwest-striking faults are not numerous, or at least are not as structurally conspicuous as the northeast-trending sets. They are typically brittle, gouge-filled or highly brecciated simple fractures that offset the east-northeast-striking strike-slip faults by several centimeters. Sense of displacement varies from place to place, but dextral offset is apparently common. These faults indicate that sinistral strike-slip on many east-northeast-striking fault strands was followed by imposition of a stress field that favored north-trending breaks having minor lateral offset.

A seismic reflection profile (Majer et al. 1996b) was shot across the Rock Valley fault zone about midway along its length. The southern end of the profile (EOL, Figure 3.2-26) is located north of a complex bounding fault or within a zone of complex fault-controlled structure that defines the southern margin of Rock Valley (and the inferred structural trough, the footwall of which is indicated by Paleozoic outcrop south of EOL). One of the major Rock Valley fault strands, fault RV3, appears to be the southernmost plane of a zone of faulting perhaps 100 m wide. Disruption in interval A and a general down-to-the-north flexure of Tertiary strata mark the location of the zone in the profile (Figure 3.2-26). Inferred offset of the Paleozoic contact is about 400 feet (122 m) down to the north. This is possibly the major structural expression of the southern fault strand of the Rock Valley fault zone. Fault strands RV4 and RV1 are not expressed at all in the seismic profile; the vertical offset component is probably less than acoustic resolution.

The seismic profile indicates that the Rock Valley fault zone is a series of slices or narrow blocks cut by faults that dip steeply north and do not change dip within the upper few thousand feet of section. The result is a subdued half-graben structure. While within the half-graben structure strata dip gently to the south (Figure 3.2-26), overall, in the general vicinity of the Rock Valley fault, the

Tertiary strata are horizontal or dip slightly to the north (generally about 20° or less). This indicates that dip-slip faulting is minor in the Rock Valley fault zone, and a significant amount of the faulting occurred during or preceding much of the deposition.

Historically, earthquakes have been relatively frequent toward the west end of Rock Valley, in the vicinity of Little Skull Mountain, the Striped Hills, and the Specter Range. Data summarized by Rogers, A.M., Harmsen et al. (1981) indicate that the earthquakes are mostly small magnitude events ($\leq M 4.0$) that occur from near surface to about 10 km depth on north- to northwest-striking faults that have strike-slip and oblique slip mechanisms. Most of the strike-slip mechanisms occur in the 4 to 9 km depth range. Fault-plane solutions for these pre-1993 earthquakes are in accord with the sense of slip of the mapped faults, but no individual seismogenic faults have been identified (Rogers, A.M., Harmsen et al. 1987).

The Cane Spring fault is expressed as a conspicuous rectilinear fault-line scarp lineament (Reheis and Noller 1991) that strikes N54°E along the north flank of Mt. Salyer (Figure 3.2-24). The Cane Spring fault itself is mapped for a total length of about 8 km. The fault evidently controls the location of Cane Spring, a large perched spring which gives the fault its name. Mapping by Ekren and Sargent (1965) provides little support for a southwest fault projection into Rock Valley, as faults mapped across the eastern flank of Skull Mountain are curvilinear normal faults of varied and minor displacement. These appear to be local faults unrelated to any inferred through-going strike-slip zone, and, in any event, they are old bedrock faults having no morphological expression. The south flank of Skull Mountain, in general, is broken by numerous steep normal faults that strike N40° to 65°E, and have displacements of a few to several meters. Some of these faults are intraformational slide faults of Pleistocene age. Some of the faults are penecontemporaneous with deposition, featuring soft-sediment deformation.

Outcrops show the Cane Spring fault to be a shear zone about 1.5-m wide, oriented N50°E, 90° to 80°S. The fault plane controls a discontinuous scarp that locally attains a relief as great as 3 m across the beds of a few down-slope gullies that cross the lineament west of Cane Spring. Local kinematic features imply left-lateral offset, but gross lithologic contacts indicate a dominantly normal, north side down movement. Poole, Elston et al. (1965) inferred three generations of alternating dip-slip ("yo-yo tectonics") in addition to strike-slip, but the basis for this inference is unclear. The contrast in landforms across the fault is pronounced, suggesting that the bulk of the offset has been dip slip. The southeast side of the fault (upthrown block) shows numerous lineaments diverging south from the fault trace at angles of 30° to 45°. These probably represent splay faults or fractures indicative of the sinistral mechanism. Total offset along the Cane Spring fault remains unknown. No indications of Late Pleistocene activity were observed; the most recent activity may have been 100 ka or older.

The fault is probably of Late Tertiary age; its exposure is a result of erosion, not post-Tertiary tectonic activity. Aerial photos show that the oldest and deepest stream courses on this slope cross the fault and are not offset by it. The fault plane lineament is discontinuous because of colluvial burial; this surficial cover is relatively old, as it is at least 2.5 m thick along cut banks that expose extensive caliche.

The Mine Mountain fault (Orkild 1968) extends along the south flank of Mine Mountain as two N35°E-striking subparallel faults that are separated by as much as 200 m. The faults interconnect and splay and apparently entrain slices tens of meters across. At Mine Mountain, the Tiva Canyon Tuff is offset for a distance of 1.2 km in a left lateral sense across the fault zone. No exposures of the fault have been found so the attitude of the fault plane(s) is unknown. The offset Tertiary units dip about 30°W, so given a steeply south-dipping fault (85° or more), purely normal displacement of about 500 to 600 m could produce the apparent left-lateral offset shown on the geologic map (Orkild 1968). Considering slip rakes on other faults in the region, an oblique slip seems most likely; Orkild (1968) interpreted the faults as oblique left-lateral, down to the south. No exposures of the fault were found during detailed reconnaissance of the mapped trace of the fault along the south flank of Mine Mountain. Numerous outcrops, chiefly Paleozoic limestone, indicate that the main fault occupies a zone of intense crushing and shear about 30 m wide along the axis of aligned swales. The fault along Mine Mountain is apparently very old and tight; there is no erosional nick or scarp or other declivity to mark it clearly. It is represented mainly by a color contact that goes up and down slopes formed by Pleistocene drainage that largely ignores the fault. The broad swale described above simply reflects erosional weakness of fault zone breccia.

The northern strand of the Mine Mountain fault zone was projected by Orkild (1968) southwest across Mid Valley along the southeast flank of Shoshone Mountain where it is depicted as a down-to-the-south range front fault. Maldonado (1985) retained Orkild's range-front fault projection but also projected the more southerly of the two Mine Mountain fault strands southwest across Mid Valley and out across Jackass Flats to a point due west of Little Skull Mountain (Figure 3.2-24). A range front fault certainly exists where Orkild has mapped it, but YMP field work did not reveal any evidence for the left-lateral fault trace projection of Maldonado (1985). Nevertheless, there is good evidence for strike slip faulting in bedrock exposures along the base of Shoshone Mountain and in a low bluff of Paintbrush Tuff (evidently an outlier of the Little Skull Mountain block) located just west of the Field Operations Center. It is likely that Maldonado's interpretation of the Mine Mountain fault is essentially correct.

Seismic profiles illustrated and interpreted by McArthur and Burkhard (1986) cross the projection of the Mine Mountain fault zone in Mid Valley. The profiles indicate disruption of reflections along the projection of the fault zone, but the nature of deformation is ambiguous. Simple large-scale block tilting is not in evidence. The garbled reflections suggest distributed shear rather than few individual fault planes. Because reflections cannot be traced north across the inferred fault plane profiles, lateral offset rather than normal displacement is indicated.

As no detailed Quaternary mapping has been done in the Mine Mountain quadrangle, the relation of faulting to Quaternary stratigraphy is essentially unknown. The surficial Skull Mountain quadrangle map to the south (Swadley and Huckins 1990) indicates that the fans underlain by the projected Mine Mountain fault zone are constructed of Late to Middle Pleistocene alluvium (Q2b and Q2c; Swadley and Huckins 1990). Reconnaissance along and across the southern alluvial flank of Shoshone Mountain, and examination of aerial photos of this area, revealed evidence of complex faulting, but no evidence of Late Quaternary displacements or any scarps in alluvium or any transcurrent fault trace in alluvium that extends southwest of Mine Mountain. Weakly etched short lineaments are found where the bedrock pediment is thinly covered; these features probably represent erosion focussed by shattered bedrock. No throughgoing fault plane was found among the variously

tilted and sheared pediment blocks, but a strong northeast oriented, shear-controlled fabric is evident in numerous bedrock exposures within fan gullies.

The total Late Tertiary normal displacement along the range front is difficult to judge because faulting is distributed across a zone more than a kilometer wide and because the volcanic units were deposited on a surface of high relief (as much as 100 m) eroded in faulted Paleozoic blocks and in the Wahmonie volcanic rocks that cover the Paleozoic rocks. Relief across the Shoshone Mountain front probably reflects both drape across an eroded surface that descends down to the basin, and subsequent faulting of that draped surface. Fault-related relief alone is less than 400 m. Where evident, the style of displacement is one of obverse dip away from the slope rather than toward it in the sense of a rotated slump block. This style, along with the sinistral shear component, suggests that Shoshone Mountain pulled away obliquely west-southwest from a subsiding basin and that faulting was preceded by formation of a down to basin monocline. An important feature of the early normal faulting is the involvement of hydrothermal alteration of the Rainier Mesa Tuff. The breccia is typically sliced by irregular, subplanar fractures having no slip indicators, that strike N20°-45°E, 85°S-90°.

No lineaments or other expressions of Quaternary faulting along the Mine Mountain fault trend have been recognized in the fan deposits graded to Yucca Valley to the east. A smooth 32 mgal gravity gradient that defines the structural west flank of Yucca Valley (Healey et al. 1987) permits no projection of the fault into Yucca Valley. To the southwest, the situation is more problematic. Outcrop evidence in the low hills of Topopah Spring Tuff, exposed west of the Field Operations Center, reveals the presence of left-lateral shear along Maldonado's projection, and the differentially tilted basalt capped blocks and adjacent tuff outliers indicate that complex block faulting cuts the Tertiary units just west of Little Skull Mountain, providing some structural relief. Exposures in the low butte of Topopah Spring Tuff at this locality show numerous minor shear planes that strike N20°-35°E, 75°E or W, and that tend to form zones of parallel or narrowly convergent brecciated slices, 20 to 30-m wide.

The 1:100,000 Bouguer gravity map of the test site (Healey et al. 1987) provides little indication of a significant crustal fault along the inferred projection of the Mine Mountain fault zone in Northern Jackass Flats. Here, the fault projection passes across an area in Jackass Flats of virtually no gradients or conspicuous anomalies. In Mid Valley the projection does pass along the northwest flank of a large minimum that represents the main depression of Mid Valley, and the fault could thus be considered as a bounding structure to the depression (Figure 3.2-24). West of Little Skull Mountain, the fault zone could possibly be projected south along the large north-south trending gradient that marks the trace of the "gravity fault" (Winograd and Thordarson 1975; Figure 3.3-1), but this connection (Figure 3.2-24) is not compelling (see also Figure 3.1-1).

The 1:100,000 aeromagnetic map of the Beatty quadrangle (Glen and Ponce 1991; see also Figure 3.1-2 this document) shows strongly aligned gradients and separation of distinct anomaly patterns along the projection of the Mine Mountain fault zone into Jackass Flats. The aeromagnetic gradients indicate that the fault zone projection is about 800 m wide along Shoshone Mountain and that it widens to about 1.5 km as it crosses Jackass Flats south of Calico Hills. This zone of aligned steep gradients, linear and positive anomalies extends into a crudely annular anomaly pattern of

short, steep highs rimmed with negative anomalies, about 8 km in diameter, centered west of the Field Operations Center.

The westward extent and the possible interaction of the convergent, westward extensions of the Rock Valley fault zone and the Mine Mountain fault are unknown. W.J. Carr (1984) projected the Spotted Range-Mine Mountain structural zone west into California to the Furnace Creek fault zone (Figure 3.2-25). However, no faults resembling the Rock Valley fault zone are known to transect the Funeral Mountains. The Rock Valley fault zone probably extends no farther west than a line drawn from the west side of Little Skull Mountain south to the west end of the Skeleton Hills (Figure 3.2-24). Laterally sheared Paleozoic rocks (and local Miocene volcanic rocks) exposed along this line imply the existence of a N 5° to 15° E-striking fault or shear zone. A fault along this trend is also indicated by gravity and aeromagnetic anomaly gradients (Winograd and Thordarson 1975) and seismic reflection data (Brocher, Carr et al. 1993), as well as sparse west-facing scarps in alluvial fans.

Attempts to find a segment of the Rock Valley fault zone west of the line described above (the "gravity fault") have been unsuccessful (Donovan 1991). Lineaments in the Amargosa Valley, however, suggest that a segment of the Rock Valley fault zone exists beneath the Amargosa Valley. On the other hand, the main strands of the Rock Valley fault zone veer to the south into the Specter Range east of the Striped Hills (Figure 3.2-24). Thus it is still unclear whether the zone extends all the way to the western end of Rock Valley.

INTENTIONALLY LEFT BLANK

3.3 REGIONAL TECTONIC MODELS

Tectonic models for Yucca Mountain and its vicinity attempt to explain current geologic structure in light of tectonic processes and the deformation events the site has experienced. They provide a means for integrating discrete data sets such as the histories of volcanism, deposition, and fault movement in the site vicinity. In addition, tectonic models, by their nature, include a representation of the structures that exist and the processes that operate at depth. Models also provide a basis for evaluating which tectonic processes and effects may occur in the future and potentially affect the ability of the site to maintain public health and safety during the preclosure and postclosure periods.

Development and evaluation of tectonic models also aid in addressing the requirements of 10 CFR 60.21 to describe and assess the site, including an analysis of the site geology. Models provide part of the basis for demonstrating whether the favorable and potentially adverse conditions listed in the disposal regulation siting criteria (10 CFR 60.122) are present and whether the present conditions have been adequately investigated and evaluated. Furthermore, tectonic models are an important element in addressing the NRC's key technical issues of Igneous Activity and Structural Deformation and Seismicity (NRC 1997a). For example, alternative tectonic models are a key input in assessing the likelihood and associated uncertainty of future volcanic eruptions and earthquakes at the site (see Subsection 3.9 and 3.10).

3.3.1 Elements and Constraints

The elements of a tectonic model for Yucca Mountain include:

- Physical extent—the space to which the model applies
- System geometry—the shape, orientation, and distribution of tectonic elements (e.g., fault and block geometry, volcanic vent distribution)
- Boundary conditions—external forces and processes at the boundary of the model, character and activity of bounding faults
- Driving forces—active processes (e.g., stresses, strain rates) thought to produce the observed features
- System response/dynamics—consequences of the driving forces and boundary conditions acting on the system geometry within the model's physical domain (e.g., fault activity: rates, interactions, rupture patterns, distribution of seismic potential; type of volcanism and rates; effects on groundwater flow and water table elevation; extension rate and distribution of effects)

Thus, a tectonic model integrates three components: geometry and spatial relations among structures; mechanisms by which structures interact and respond to regional stress; and the succession, duration, and evolution of deformation events (i.e., the history of strain).

In defining the elements of a tectonic model for Yucca Mountain, the known structures and deformation history provide input and constraints. Regional geologic structures are discussed in Subsection 3.2; Quaternary volcanism in the Yucca Mountain region is described in Subsection 3.9; information on the current state of stress, contemporary seismicity, and fault movement during the Quaternary are presented for the Yucca Mountain region in Subsection 3.10; site structures are described in Subsection 3.6. Information on key tectonic elements and deformational constraints is given below with an emphasis on its relevance to developing and evaluating tectonic models for the Yucca Mountain vicinity.

In general, the record of extensional tectonics over the past 13 m.y. resides in the present landscape that surrounds and includes Yucca Mountain. This post-13 m.y. landscape consists of tectonic landforms that represent the last major tectonic episode. This episode began with creation of the southwestern Nevada volcanic field, and has continued with diminished volcanic activity into Quaternary time.

Although other parts of the tectonic setting, such as Bare Mountain, the Bullfrog Hills, Frenchman and Yucca Flats, and Rock Valley, have undergone changes in form and structure within the last 10 m.y., Yucca Mountain seems relatively intact (Fridrich 1998). Uplift or depression has not altered its form or its original longitudinal profile, which is that of an effusive outfall apron that crests at the caldera rim. The faults that cut Yucca Mountain and that have facilitated extension are minor; the extension itself is moderate (Fridrich 1998). Yucca Mountain is not a discrete tectonic range, or at least has not functioned as one in post-Paleogene time.

The most conspicuous structural pattern at Yucca Mountain, and paradoxically the most uncommon in the overall geologic setting, is the succession of west-dipping normal faults that cut Yucca Mountain into a series of north-south elongated, east-tilted blocks. The structural and kinematic details of these faults and their histories are well described elsewhere in this document (Subsections 3.10 and 3.6). What remains uncertain are the structural boundaries to the enclave of normal faults at Yucca Mountain. Clearly, the Bare Mountain fault, an east-dipping range-front fault, defines the extreme western extent of the Yucca Mountain normal fault pattern. Likewise, the Timber Mountain caldera complex to the north forms a structural boundary, albeit a less pronounced one; but the boundary to the south is problematic. The Yucca Mountain faults appear to end abruptly, along with the elevated fault-bounded ridges, at an escarpment only a few hundred meters north of U.S. Highway 95. The structural nature of this boundary is hidden. The eastern boundary of the Yucca Mountain fault enclave is also uncertain; what is clear is that the boundary lies west of Little Skull Mountain, the Striped Hills, and the Rock Valley fault zone. No clearly defined bounding fault is expressed across the Calico Hills uplift or along Fortymile Canyon.

3.3.1.1 Yucca Mountain Faulting

Yucca Mountain is essentially a block-faulted drape of Miocene volcanic strata that partially fills Crater Flat Basin and partially rests on an old and completely unexposed outlier of Paleozoic rock that separates Crater Flat Basin from Jackass Flats Basin. The drape itself is probably not more than about 2 km thick, and the faults that cut it probably comprise two major populations: a fundamental set propagated up from the Paleozoic substructure, and a "superficial" set reflecting failure and

movement of the volcanic cover (Day, Potter et al. 1996b and Subsection 3.6 of this report). A third population, probably minor in cumulative displacement but nevertheless a complicating factor, comprises fractures and faults resulting from penecontemporaneous volumetric strain adjustments due to cooling, degassing, zeolitization, authigenesis, and revesiculation (Subsection 3.6 of this report).

The exposed rocks of Yucca Mountain were extended, in a west-northwestward direction, by a modest amount during Middle and Late Miocene time. Since that time there has been little further extension (Fridrich 1998). Most of the Yucca Mountain faulting and tilting occurred between the times of eruption of the Tiva Canyon Tuff (12.7 Ma) and the Rainier Mesa Tuff (11.6 Ma). Extension probably began prior to deposition of the Tiva Canyon Tuff (Carr, W.J. 1984; Scott, R.B. 1990), but peak extension was virtually coeval with its deposition. Paleomagnetic directions indicate that tilting of blocks within one imbricate zone occurred before magnetic remanence was locked in (Rosenbaum et al. 1991). Strikes of panels and faults swing from generally north-northeastward (azimuth $\sim 030^\circ$) in the south to northward (~ 000 to 010°) in the north. The southward-increasing dips and the southward oroclinal swing in strike are indicative of increasing relative local crustal extension in that direction.

Almost nothing is known about the fault population that exists in the Paleozoic/Precambrian substructure of Yucca Mountain. Nearby exposures of Paleozoic/Precambrian tracts (Bare Mountain, Specter Range, core of the Calico Hills) indicate that such faulting is very complex, dominated by close, normal faults many of which are near alignment with the faults exposed at the surface of Yucca Mountain. Complexity of seismic reflection data at this depth also supports a highly faulted substructure (Majer et al. 1996b).

The relation of faults in the volcanic supra structure to the Paleozoic/Precambrian substructure is in some cases uncertain. For the Solitario Canyon and Paintbrush Canyon faults (Figure 3.3-1), evidence suggests substructure faults penetrate through the supra structure to the surface. The evidence includes relatively high groundwater temperatures measured in wells close to these faults. The elevated temperatures suggest upward leakage of warm groundwater, presumably along deeply penetrating faults, from the deep carbonate aquifer (Sass, Lachenbruch, Dudley et al. 1988). Other evidence includes the traces of these faults expressed in aerial photos as conspicuously etched rectilinear lineaments that transect younger fault-controlled landform. These lineaments are unlike the more discontinuous, curvilinear traces of the younger surface-breaking faults that are more clearly expressed at larger scales. A further indication of deep crustal penetration of the Solitario Canyon fault is the presence of a basalt dike approximately 10 Ma (Carr, W.J. and Parrish 1985) located along part of the fault plane and exposed in trench 10 (see Figure 3.4-3) where it is offset by the fault. Aeromagnetic data suggest that the dike may be more extensive at depth (Bath and Jahren 1984). This dike is probably related to a swarm of en echelon dikes located along a northwest trend that may be an extension of the Drill Hole Wash fault (Scott, R.B. and Bonk 1984; Fridrich 1998).

The second population of faults, those that cut the volcanic carapace of Yucca Mountain and control the geometry of the tilted panels, has received much study (see Subsections 3.6 and 3.10). A

characteristic of these faults is the anastomosing, curvilinear trace pattern, generally concave toward the hanging wall (i.e., west-facing). This planimetric pattern suggests three things:

- The depth of the faults is comparable to the widths of the broken slabs.
- The faults join and/or terminate near the base of the Miocene volcanic pile.
- The fault pattern indicates a kind of detachment.

Two tectonic phenomena not directly related to lateral extension across Yucca Mountain but somehow genetically related to the faulting are vertical axis rotation of the southern part of Yucca Mountain, and basaltic intrusion proximal to the mountain. Both phenomena indicate the influence of a northwest-oriented structure, and both are late to postdepositional.

3.3.1.1.1 Vertical Axis Rotation

Paleomagnetic data (Rosenbaum et al. 1991; Hudson, M.R., Sawyer et al. 1994) show that the southern part of Yucca Mountain has been rotated clockwise 25° to 30° following deposition of the Tiva Canyon Tuff (12.7 Ma). Apparently most of the rotation occurred prior to deposition of the overlying Timber Mountain Group; rotation of the Ammonia Tanks Tuff amounts to only 6°±13° (Rosenbaum et al. 1991; Hudson, M.R., Sawyer et al. 1994). Hudson, M.R., Sawyer et al. (1994) surmise that the bulk of the angular rotation occurred during the period of faulting of the Tiva Canyon Tuff that marks the angular unconformity with the overlying Timber Mountain Group.

The clockwise rotation is limited to the southern part of Yucca Mountain; virtually no rotation has occurred at the north end of the mountain. Rosenbaum et al. (1991) stated that the declinations change gradually toward the south end of the mountain. Examination of aerial photos shows that individual fault blocks have rotated and that the noticeable change in strike to a more northeasterly orientation occurs to the south about halfway down the length of the mountain. This produces a hinge-like pattern rather than an arc. This transition coincides, in general, with a decrease in elevation and relief to the south, and with an increase in extension from 10 percent at the northern end of the mountain to at least 20 percent at the southern end, along with increased dip of the fault blocks. These characteristics suggest that rotation largely postdates faulting and extension and that torque was applied across a discrete zone that cut the southern half of the mountain.

The cause of the Late Miocene vertical axis rotation is unknown. Rosenbaum et al. (1991) inferred the influence of either a deep dextral shear zone that passed along the south end of Yucca Mountain (e.g., Sonder et al. 1994; Burchfiel 1965), or the influence of a strain gradient resulting from differential extension across a detachment inferred to be present south of Yucca Mountain (Wernicke, Axen et al. 1988; Hamilton, W.B. 1988; Carr, M.D. and Monsen 1988; Hagstrom and Gans 1989; Scott, R.B. 1990). Whatever the cause, it is of local extent because wider areal sampling of paleomagnetic data do not indicate a broad system of dextral rotation north of Yucca Mountain (Hudson, M.R., Sawyer et al. 1994). Hudson, M.R., Sawyer et al. (1994) infer that dextral shear originated in discrete shear zones along the southwest margin of the southwestern Nevada volcanic field, a consequence of obliquely extending crustal slabs undergoing vertical axis rotation across zones several kilometers wide, driven by post-12.7 Ma extension south of Yucca Mountain and west of the Spring Mountains (cf. Brocher, Carr et al. 1993).

Many of the north-striking, essentially normal faults that cut Yucca Mountain have a sinistral slip component that increases to the south and that is probably a consequence of the clockwise rotation. There is slight indication that northwest-trending dextral shear is widespread across the mountain; it is manifested by small jogs or right steps along north-oriented scarps or fault traces, and most notably by the conspicuous break along Yucca Wash. Although the "Yucca Wash fault" has been represented as a dextral fault (e.g., Carr, W.J. 1984), older strata are exposed on the north side and no lateral offset has been measured (see Subsection 3.6.2.3.2). The Yucca Wash fault and other similar oriented breaks to the south probably mark zones of shear, grinding, brecciation and very minor slip that locally accommodated the strain imposed by clockwise rotation across the brittle volcanic carapace to the south.

3.3.1.1.2 Basaltic Volcanism

The history, evolution, and character of Pliocene-Pleistocene basaltic volcanism proximal to Yucca Mountain (within 25 km of the potential repository) are exhaustively treated by Crowe, Perry et al. (1995) and summarized in Subsection 3.9 of this report. A brief description is provided here, with an emphasis on constraints for tectonic models.

The oldest eruptive basalts in Crater Flat are dated at about 10.5 to 11.3 Ma (Figure 3.2-12), which means episodes of spatially restricted volcanism began very shortly following eruption of the Ammonia Tanks Tuff (11.46 Ma). However, no further basaltic volcanism occurred in Crater Flat until 7.6 m.y. later, at about 3.7 Ma, when a group of five northwest-aligned scoria cones and lava flows were emplaced in southeastern Crater Flat. This episode represents the largest volume basaltic emplacement in Crater Flat (Figure 3.2-12). Lava-filled fissures and feeder dikes are oriented north-south. This group was subsequently cut by reactivated Yucca Mountain faulting which produced dip-slip offsets of more than 1 m, west side down (Crowe, Perry et al. 1995).

A subsequent basaltic eruption episode occurred about 1.0 Ma. It consists of four cinder cones (Little Cones, Red Cone, Black Cone, and "Makani" Cone) aligned north-northeast along the axis of Crater Flat (Figure 3.2-12). Most of the volume is in Red and Black Cones. Lava of this group overlaps the area of eruption of the earliest (10.5 to 11.3 Ma) episode (Figure 3.2-12).

The most recent episode of basaltic volcanism created the Lathrop Wells Cone, which lies along the trend defined by the older eruption groups (Figure 3.2-12). The Lathrop Wells Cone complex comprises fissure eruptions, spatter and scoria cones, and aa flows. Satellitic spatter cones at the east base of the main cone have a northwest alignment. The Lathrop Wells Cone complex is probably about 80 ka and possibly younger, although the age determination and emplacement history of this eruptive complex are subject to alternative interpretations (Crowe, Perry et al. 1995).

The episodic nature of basaltic eruptions (11.3 Ma, 3.7 Ma, 1.7 to 0.7 Ma, 80 ka), the aligned series of emplacements, and the generally consistent alkalic compositions of the basalts, indicate that emplacement depends on recurrent tectonic conditions that involve the entire thickness of the crust and part of the upper mantle. Deep, crust-penetrating faults must form the main conduits, as the basalt melts clearly originated and resided in the upper mantle (Crowe, Perry et al. 1995). The small volume of basalt erupted during each episode, the short and abrupt duration of emplacement, and the

evidence of high volatile content and rapid degassing (scoria, aa) indicate that the basaltic melt did not force its way through the crust by virtue of thermal energy and bulk buoyancy, but, rather ascended as a relatively low temperature, low viscosity, hydrous melt having virtually no crustal residence time.

Farmer et al. (1989) presented isotopic and trace-element data that suggest that basalts of the Southern Great Basin have been generated from lithospheric mantle during the last 10 m.y. Low mantle P_n velocities beneath much of the Basin and Range suggest that the upper mantle contains a small fraction of melt. Daley (1992) proposed that if this part of the upper mantle is hydrous it could generate basaltic magma at small rates of lithospheric extension by depressing the peridotite solidus. A hydrous mantle source for the basalts of Crater Flat is consistent with their low Rb contents, relative to other incompatible trace elements, which also suggest that breakdown of phlogopite may be the source of H_2O (Vaniman, Crowe et al. 1982; Crowe, Perry et al. 1995). For these small-volume, aqueous-rich magmas to ascend the crust and erupt at the surface without losing much volatile content en route, they must take advantage of dilatant pathways.

Measurements of spatial distributions and shapes of intrusive basalts and scoria cones support the inference that the subsurface rise of magma was guided by one or more northwest-trending structures (Crowe and Perry 1989). But an important feature of individual centers of volcanic eruption is the tendency for the clusters of cones or fissures to be aligned to the north-northeast (cf. Carr, W.J. 1990). The magmas probably followed a northwest structure at depth but at shallow depths followed the regional stress guide. The basalt dikes likely created their own fracture pathways near the surface because the locations of basaltic centers are largely independent of faults that cut the surface. In Crater Flat the transition in fracture pathways may occur at the contact between Paleozoic and Cenozoic units (Crowe, Perry et al. 1995).

The northwest alignment of basaltic eruptive centers, such as in Crater Flat, is emphasized by two other basaltic groups. The Sleeping Butte centers located 45 km northwest of Yucca Mountain are about 380 ka. The basalt of Amargosa Valley (Crowe, Wohletz et al. 1986) is located about 3 km south of Amargosa Valley crossroads. The basalt here is buried but was sampled by drilling and gave an $^{39}Ar/^{40}Ar$ isochron age of 4.4 Ma (Turrin et al. 1992).

The northwest alignment of the eruptive groups along with the north-northeast orientation of eruptive features suggests the recurrent influence of a dextral shear zone or perhaps merely a group of north-striking faults or fracture zones susceptible to dextral transtension along the trend of the eruptive centers. These dilate episodically and tap the upper mantle basaltic magma source. The occurrence of basaltic glass (tephra) in some of the fault fissure fills of Quaternary age along Yucca Mountain indicates that, in at least one episode, eruption essentially coincided with normal fault reactivation (Ramelli, Oswald et al. 1996 and Subsection 3.10 of this report).

3.3.1.2 Crater Flat Faulting

The faulted volcanic carapace of Yucca Mountain descends westward beneath the alluvium of Crater Flat. The westernmost of the Yucca Mountain faults observed at the surface are the Crater Flat fault (Figure 3.2-12) and, perhaps, an extension, the "west lava fault" of Ramelli, Bell et al. (1988). The

"west lava fault" has a scarp <1 m that cuts alluvium having an estimated age of 17 to 30 ka (Ramelli, Bell et al. 1991). Crater Flat itself is an alluvium-filled basin that drains to the south, via Windy Wash, into the Amargosa Valley. Two drillholes USW VH-1 (Carr, W.J. 1982) and USW VH-2 (Carr, W.J. and Parrish 1985) show that the alluvium is at least 350-m thick and consists of typical fan debris. The basin also contains about 3 km of tuff of the southwestern Nevada volcanic field. Total depth to Paleozoic/Precambrian basement is interpreted to be between 3 and 4 km (e.g., Brocher, Hart et al. 1996; Majer et al. 1996b).

The southern end of Crater Flat is defined by an east-southeast-trending eroded ridge that extends between Steve's Pass and the southern terminus of Yucca Mountain. Outcrops indicate that the Miocene tuffs are faulted down against Paleozoic rock to the west, but strata along the ridge dip about 10° north. Fridrich (1998) estimates the ridge formed post 10 Ma, and notes that it is the only major tilting effect which is not an expression of older extensional patterns. Outcrops south of the escarpment include Pleistocene siliceous spring deposits and an older, dense, buff-colored slabby limestone (probably Pleistocene spring sinter).

In general, Crater Flat Basin has the structure of a half-graben controlled by the Bare Mountain fault. Seismic and gravity data indicate that the Crater Flat Basin is deepest on the west side (Snyder and Carr 1984; Ackermann et al. 1988; Majer et al. 1996b; Brocher, Hart et al. 1996). This conclusion also is supported by the general stratigraphic thickening of exposed units along the southern and northern margins of the basin (Fridrich 1998). There is some evidence of a low longitudinal arch near the axis of the basin, a feature interpreted by Fridrich (1998) as a rollover consequent to Bare Mountain faulting.

Carr and Parrish (1985) inferred that Middle Miocene volcanic rocks beneath the alluvial cover of central Crater Flat have undergone almost no internal extension and define a broad, synclinal structure, faulted down on the west against a major, steep frontal fault at the east base of Bare Mountain. That such a major fault is lacking along central and Northern Bare Mountain and that most of the Crater Flat subsurface is broken into fault blocks is, however, indicated by magnetic and gravity data (McCafferty and Grauch 1997), as well as by the presence of exposed fault blocks, of Middle Miocene rocks, within the east part of the basin and projecting into the basin from both north and south. The 15 to 30° dips reported by Carr and Parrish for the Middle Miocene rocks in drillhole USW VH-2 probably record a tilted fault block, not the flank of a syncline as they assumed.

Gravity data, most informatively seen in the isostatic reduction (McCafferty and Grauch 1997; Oliver and Fox 1993; Ponce, Harris et al. 1988), show Crater Flat to have a markedly asymmetric gravity field, with gravity decreasing relatively steeply eastward from east of Bare Mountain and relatively gently westward from Yucca Mountain to an isostatic low that trends generally northward in the eastern part of the basin, where dense Paleozoic strata are likely about 3 or 4 km deep. The gravity field is well constrained by three traverses of close-spaced observations extending a few kilometers eastward from the foot of Bare Mountain. By far the steepest gradient is along the far southern part of Bare Mountain, where it is centered along the east base of Black Marble Hill and only about 1 km east of the topographic mountain front for a few kilometers north from there. The gradient continues

northward, becoming gentler although its total relief remains high, and its center lies 2 to 3 km east of the topographic front along center and Northern Bare Mountain.

3.3.1.3 Bare Mountain Fault—Western Structural Boundary of the Crater Flat Basin

The west side of the basin is defined by the Bare Mountain fault and the rugged 1 km high escarpment of Bare Mountain (Figure 3.3-1). The Bare Mountain fault extends from Steve's Pass, at the southern end of Crater Flat, north along Bare Mountain, and into and along a nonextended septum of Middle Miocene tuffs that make up Tram Ridge. Here the Bare Mountain fault bifurcates into the Tram Ridge fault and the Tate's Wash fault (Fridrich 1998). These faults decrease in throw and become part of a population of similar faults exposed along the caldera rim that flanks the north end of Crater Flat.

The presence of quartz latite dikes in the eastern part of Bare Mountain suggests that a discrete Bare Mountain fault did not exist prior to about 13.9 Ma. The dikes, which lie adjacent to Crater Flat and are roughly aligned with the basin axis, give a K/Ar age of about 13.9 Ma (Carr, W.J., Byers et al. 1986). The dikes indicate that a zone of deep, subparallel fractures or minor faults marked the west side of the basin rather than a single fault or a narrow zone of steep faults of large displacement. Subsequent to 13.9 Ma, Bare Mountain underwent rapid uplift during the peak and early declining phases of Yucca Mountain deformation (Hoisch 1995).

Although the east front of Bare Mountain was assumed to be due to a major young frontal fault by Fox and Carr (1989), Monsen et al. (1992), Reheis (1988), and others, no major post-Miocene faulting can be documented except in the far south. Reheis (1988) argued for recurrent "Late Pleistocene and Holocene" faulting but topographic profiles preclude significant Late Quaternary faulting (Klinger and Anderson 1994). Canyons at the east base of the range contain alluvial floors and have not been excavated by their streams to bedrock levels reached before the last major synglacial(?) pluvial period. A long, deep trench across one of Reheis' (1988; her locality 1) "active" faults does show a steep fault with a small, filled collapse moat, but its 1 m offset is of a very old, heavily calcified soil, and faulting was followed by much further deposition of caliche; the trench records a single event well back in the Pleistocene, not multiple latest Pleistocene and Holocene events.

The pediment that exists between the present range front and the buried fault trace is marked by a very low-relief magnetic pattern of east-trending anomalies that resembles that of Bare Mountain itself. The very low-relief, east-trending anomalies, produced by the Paleozoic and uppermost Proterozoic units of Eastern Bare Mountain, apparently continue east under Crater Flat alluvium. Paleozoic rocks possibly extend at shallow depth into this northwest part of Crater Flat Basin, broken at most by small step faults. Large masses of diversely magnetized Tertiary volcanic rocks cannot be present there in the subsurface. Hence, there may not be a single major fault along the east side of Northern Bare Mountain.

Snyder and Carr (1984) constructed a gravity model to fit the concept of a steep fault subcropping beneath alluvium some 5 km east of the foot of the range, with little or no faulting at the range front. This is more or less compatible with the aeromagnetic data also. W.J. Carr (1990) later suggested

that there is a major fault at the range front but that its gravity expression is masked by dense landslide breccias, derived from it, near the west edge of the Crater Flat Basin. This suggestion is precluded, however, by the continuity of east-trending, low-amplitude magnetic anomalies across both exposed and subsurface bedrock tracts. The most likely interpretations include a high-angle fault abutting dense slide debris on the hanging wall (cf. Carr, W.J. and Parrish 1985), or a series of normal faults that step down eastward toward the basin axis. Faults synthetic to the Bare Mountain fault predominate in the 0.5 km to 2 km outboard of the Bare Mountain fault in Crater Flat (Fridrich 1998). Present indications are that the Bare Mountain fault has been active in the Pleistocene (Anderson, L.W. and Klinger 1996) and has shown oblique dextral displacement, especially near the southernmost exposure of Bare Mountain where the Bare Mountain fault curves to a northwest strike (Fridrich 1998).

3.3.1.4 Eastern Structural Boundary of Crater Flat Basin

A feature identified by gravity surveys, and referred to as the "gravity fault" (Figure 3.3-1), trends northwest and north beneath surficial deposits along the northeast side of Ash Meadows, which lies south of Rock Valley (Winograd and Thordarson 1975). This feature is inferred to be a normal fault with down-to-the-west displacements ranging from 500 to several thousand feet. In recent studies (e.g., Fridrich 1998), the Gravity fault was extended northward across the western part of Jackass Flats (Figure 3.3-1) and interpreted to form the eastern boundary of the Crater Flat Basin (see additional discussion in Subsection 3.3.3).

Fox and Carr (1989) felt that the eastern limit of the pattern of normal faults that characterize Yucca Mountain is the Paintbrush Canyon fault. This is a good inference because the Paintbrush Canyon fault appears to be a deep-seated, infrastructural fault, and none farther east have been identified. Nevertheless, east of the Paintbrush Canyon fault, Busted Butte, Fran and Alice Ridges loom tall over the western edge of Jackass Flats, and they are also part of the structures related to the Crater Flat Basin.

3.3.1.4.1 Calico Hills

The Calico Hills, a local domiform uplift associated with late rhyolitic volcanism along the south flank of the caldera complex, provide little evidence for any boundary structure that might project northward out of Jackass Flats (i.e., the Gravity fault). The pattern of north-striking, down-to-the-west normal faulting seen at Yucca Mountain, or more precisely in the Chocolate Hills north of Yucca Wash, persists eastward across the west flank of the Calico Hills in the same tuff units that cap Yucca Mountain. In the Calico Hills, these faults are seen to cut the Miocene/Paleozoic contact (Simonds 1995). Most extension along the west flank of the Calico Hills occurred during the interval following deposition of the Tiva Canyon Tuff and prior to deposition of the Rainier Mesa Tuff, as happened at Yucca Mountain. Several of the north-trending down-to-the-west faults appear to merge with a major northeast-trending fault that defines the northwest edge of the Paleozoic core of the Calico Hills (Simonds 1995). This fault pattern is replaced by a radial pattern farther east (Simonds 1995).

3.3.1.4.2 Areas East and North of Calico Hills

Farther east and north of the Calico Hills, Shoshone Mountain and Rainier Mesa provide evidence of Paintbrush and Timber Mountain Group deposition along the caldera complex in the absence of extension or local uplift. The eroded south flank of Shoshone Mountain shows that the Middle Miocene volcanics of the Paintbrush Group and younger units were laid down on a rugged terrain of eroded 13 Ma volcanics of the Wahmonie Formation, and on block-faulted Paleozoic carbonates. The eroded surface was totally filled in and the Middle Miocene volcanics formed a plateau that completely masks underlying relief. Although the 13 Ma Wahmonie Formation is scarcely extended, the Paleozoic units show evidence of considerable block rotation and extension prior to deformation of the Wahmonie Formation.

3.3.1.5 Tectonic Implications of Eruptions in the Southwestern Nevada Volcanic Field

The southwestern Nevada volcanic field (Figure 3.2-9) is a fundamental element in the tectonic setting of Yucca Mountain, having created the volcanic succession that exhibits Middle Miocene and younger extension. An excellent summary of the origin and tectonic relevance of the southwestern Nevada volcanic field is provided by Sawyer, D.A., Fleck et al. (1994).

The association of normal faulting with magmatic activity in the southwestern Nevada volcanic field is poorly understood. It is clear that local extension was contemporaneous with peak caldera activity from 13 to 11 m.y. The caldera complex also seems to have punctuated earlier phases of normal faulting, or at least earlier structural patterns consequent to extension. However, there is not clear evidence that extension was actively underway in the region during the buildup to caldera formation (Axen et al. 1993; Sawyer, D.A., Fleck et al. 1994). D.A. Sawyer, Fleck et al. (1994) emphasize that cumulative Middle to Late Miocene extension in the central part of the southwestern Nevada volcanic field is small relative to surrounding parts of the Southern Great Basin, and that the surrounding areas underwent episodic nonuniform periods of extension at different times. Post-caldera extension (younger than the 11.45 Ma Ammonia Tanks Tuff) occurred only in these outlying areas (Sawyer, D.A., Fleck et al. 1994). Thus, D.A. Sawyer, Fleck et al. (1994) conclude that, although magmatism in the southwestern Nevada volcanic field and regional extension were broadly coeval, there is no apparent genetic link, or at least no correlation in relative extent or amount of activity.

There may be two reasons for this: one is that regional basin and range extension may have operated through the period of peak volcanism, but its effects may only have been imprinted in the southwestern Nevada volcanic field during periods of post-caldera magmatic deflation, when the upper crust presumably regained shear strength. Rainier Mesa Tuff is faulted across an east-west distance of 100 km from the Bullfrog Hills to the Halfpint Range, with no headwall breakaway zones or regions of uplifted lower plate rocks (W.B. Hamilton, *Detachment Faulting and Tectonic Modeling in the Yucca Mountain Region*, report to U.S. Geological Survey Water-Resources Division, Yucca Mountain Project Branch, on work carried out under Memorandum of Agreement with the U.S. Geological Survey Geologic Division, Branch of Geophysics). Extensional strain in and near the central southwestern Nevada volcanic field caldera cluster was relatively minor, however (Sawyer, D.A., Fleck et al. 1994). A second reason is that local domains may have been

influenced differently by magmatic activity resulting in different styles of extension, or no extension at all.

Typical Basin and Range structures are not developed within the caldera complex nor for another 15 or 20 km around it, and most of Yucca Mountain lies within this marginal ring zone. Beyond that outer limit, structural behavior remained typical of the Basin and Range Province. Some sort of crustal control of Yucca Mountain structures by magmatism or by products or thermal effects of magmatism thus must be considered.

The caldera complexes deformed differently during extension than did the sectors of outflow tuffs (Frizzell and Shulters 1990; Minor, Sawyer, Wahl et al. 1993). For example, the relatively simple pattern of small rotated blocks of ashflow tuffs of Yucca Mountain and the hills north of Crater Flat gives way northward, in part via accommodation faults and in part via zones of complex fault patterns, to much less regular and quite different deformation in the Timber Mountain-Claim Canyon caldera. Detailed relationships are in substantial part masked by the presence between internal caldera complexes and fault-block tracts of sheets of volcanic and sedimentary materials younger than most of the faulting.

Eruptive activity in the southwestern Nevada volcanic field must be considered to have had much greater tectonic significance than the creation of faulted tuff deposits. The relatively short periods of eruption (~150 k.y.) were preceded by lengthy (at least 750 k.y.) periods of buildup (Sawyer, D.A., Fleck et al. 1994) during which large amounts of heat and volatiles must have been transferred high into the crust (within at least 3 to 4 km of the surface at which level explosive volcanism due to volatile exsolution becomes possible). The abrupt collapse and strain release of this heated, pressurized crust immediately following eruption is the probable source of local extension in domains adjacent to the southwestern Nevada volcanic field. Evidence of high pore pressure effects related to extension associated with the southwestern Nevada volcanic field are widely seen in travertine dikes and abundant, extensive calcite or opaline breccia matrix in Paleozoic and younger units, and in hydrothermal alteration. Minor (1995) suggested that the superposition of caldera magmatic stresses upon the regional stress field resulted in several different types of temporary stress changes within a zone about 20 km wide surrounding the caldera complex.

Structural control by hot, weak crust must have occurred in important ways. Beneath the shallow magma chambers, the middle and deep crust must have been hot and ductile, with crystal mush perhaps widely present, during the period of extension. All but the uppermost crust in the caldera region likely had effectively zero strength when the surrounding region was undergoing Middle Miocene extension, and so was incapable of supporting the stresses which produced typical Basin-Range structural patterns. The anomalous style of deformation of Yucca Mountain and the rest of the area ringing the caldera complex may owe its character to the thermal, hence strength, configuration of the crust at the time.

Extension activity rapidly declined in the vicinity of the caldera complex after deposition of the 11.45 Ma Ammonia Tanks Tuff. This may be because the caldera complex substructure is basically a plug of intrusive rock that has not inherited pre-Miocene deformation; although it is highly faulted,

it has no imposed strain anisotropy, so it has resisted the styles of deformation that have occurred east and west of the Crater Flat Basin.

3.3.1.6 Pahute Mesa Faulting

W.J. Carr (1990) drew attention to the similar patterns of faulting at Yucca Mountain and in Pahute Mesa, north of the Timber Mountain caldera (Figure 3.3-2). Calico Hills Formation and tuffs of the Paintbrush Group thicken on the western, downthrown side of different faults at Pahute Mesa. The Rainier Mesa Tuff also thickens slightly over the same structures (Sawyer, D.A., Fleck et al. 1994). The pre-Timber Mountain Group volcanics are tilted northeastward 2 to 4° in the subsurface of Pahute Mesa (Warren, Byers et al. 1985). Slight normal faulting (offsets of >60 to 80 m on main faults) and <2° tilting cuts the 9.4 Ma Thirsty Canyon Group on the mesa (Orkild, Sargent et al. 1969). The Rainier Mesa Tuff is considerably thicker across down-to-the-west faults on the western side of Pahute Mesa than it is on the east side, indicating greater extension toward the west in the 12.7 to 11.7 Ma interval (Fridrich 1998). Fault offsets in the Rainier Mesa Tuff also increase from east to west across Pahute Mesa, similar to the pattern of increase to the west seen in the Crater Flat domain (Fridrich 1998). Also, the fault activity at Pahute Mesa shows a pattern of progressive decline after the 12.7 to 11.7 Ma volcanic pulse, as is true in Crater Flat (Fridrich 1998).

The similarities of fault style, attitude, and timing (Minor, Hudson et al. 1996) suggested a common genetic relationship which W.J. Carr (1990) attributed to extension localized within the Kawich-Greenwater rift (Figure 3.2-9). This spatial and temporal association implies that the rift may not only be a focus for this style of extension and for Miocene magma emplacement, it may also be a focus for whatever post caldera extension has occurred since the last 8 m.y., including the faulting within and tangential to the caldera. The moderate, north-striking, west-directed extension centered in the rift has not affected Shoshone Mountain to the east or the Bullfrog Hills-Oasis Valley terrain to the west.

3.3.1.7 Tectonic Stress and Strain in the Yucca Mountain Region

The state of stress and the character of strain in the Yucca Mountain region are important factors in assessing the tectonic evolution of Yucca Mountain and the path of future deformation at the mountain. Stress in the crust is conventionally resolved into three mutually perpendicular vectors of principal (compressive) stress, σ_1 , σ_2 , and σ_3 , such that $\sigma_1 > \sigma_2 > \sigma_3$. In an ideal normal fault regime σ_3 is perpendicular to the strike of normal faults. Typically, the state of stress is determined by three methods: direct measurement using strain gauges (piezometers) or induced rock failure; indirectly by analysis of earthquake focal mechanisms; and inferentially by analysis of fault populations and fault slip indicators. These techniques jointly indicate that in the Yucca Mountain region the least principal stress vector, σ_3 , is essentially horizontal and trends N50°-70°W (Carr, W.J. 1974; USGS 1984; Zoback and Zoback 1980; Minster and Jordan 1987; Wernicke, Axen et al. 1988; Zoback 1989).

Observations from boreholes at Yucca Mountain provide data on the state of stress within the upper 2,000 m of the mountain (USGS 1984; Stock and Healy 1988). Measured σ_3 values are low, near the margin of stability for normal faults that strike N25°-30°E and that have a coefficient of static

friction $\mu \geq 0.6$ (Figure 3.3-3). If pore pressure (hydrostatic stress) were elevated to equal or exceed values of σ_3 obtained at Yucca Mountain, such faults would slip (USGS 1984; Stock and Healy 1988). Although local in situ stress measurements at Yucca Mountain accord well with the history of normal faulting, local factors such as static stresses, composition, and fabric anisotropies influence the shallow stress field from place to place. Least principal stress directions measured at Rainier Mesa (Carr, W.J. 1974; Springer and Thorpe 1981) are oriented as much as 20° more northerly than the σ_3 measured at Yucca Mountain. Furthermore, near-surface stress ratios do not reflect conditions at seismogenic depths where strike-slip and oblique slip focal mechanisms are common (Rogers, A.M., Harmsen et al. 1987). Because strike slip and dip slip mechanisms occur throughout the uppermost 15 km of the crust (Rogers, A.M., Harmsen et al. 1987) the relative magnitudes of σ_1 and σ_2 at depth must be nearly equal. A.M. Rogers, Harmsen et al. (1987) describe the relation between σ_1 and σ_2 as "axially symmetric" (Figure 3.3-4).

It is clear that the stress field varies in space, both areally and with crustal depth. Stress distributions derived from fault orientation and displacement data indicate that large variations in the stress field have occurred over time as well. Analysis of faults near Yucca Flat and in the Basin and Range to the east indicate that the present stress regime originated around 9 Ma. Prior to that time σ_3 was oriented in a more westerly or southwesterly direction (Zoback et al. 1981; Minor 1995). Minor (1995) concluded that the stress field in the Yucca Mountain region rotated clockwise as much as 65° in the 11 to 8.5 Ma interval. The clockwise stress rotation is recognized elsewhere in the Great Basin (Carr, W.J. 1984; Angelier et al. 1985; Zoback et al. 1981; Michel-Noel et al. 1990), but estimates of its timing vary (Wernicke, Axen et al. 1988). Hardyman and Oldow (1991) envision a clockwise stress rotation of as much as 90° in the Northern Walker Lane that began in Late Oligocene and attained its present state in Late Miocene. Bellier and Zoback (1995) aver that the relative magnitudes of σ_2 and σ_1 attained their present ratios during Pliocene-Pleistocene time.

Rotation of the stress field figures greatly in the tectonic evolution of the Walker Lane and concomitant vertical axis rotation of Yucca Mountain (Minor, Hudson et al. 1997). A characteristic tectonic feature of the Walker Lane is the complex relationship of strike slip faulting and Basin and Range-style normal faulting. On this account, the Walker Lane can be considered a transition zone from the dominantly west-directed extension of the Basin and Range to the dominantly strike slip fault regime of Western California (Harmsen and Bufe 1992). Or, the Walker Lane can be considered to have an independent stress history as a broad band of distributed dextral shear, superimposed on earlier extension (Wernicke, Axen et al. 1988; Minor, Hudson et al. 1997).

The notion that the Walker Lane had an independent stress history in Neogene time is emphasized by Minor, Hudson et al. (1997). Based on paleostress studies (Scott and Hofland 1987; Throckmorton and Verbeek 1995) the boundary of the Walker Lane is placed across Yucca Mountain, oblique to the normal fault pattern (Figure 3.3-5). This is similar to the dextral shear zone inferred by Schweickert and Lahren (1997; and Figure 3.3-6 of this document). Minor (1995) concluded that Yucca Flat Basin opened under the influence of a regional normal-slip stress field characterized by a southwest to west-southwest σ_3 orientation. He further concluded the Yucca Flat Basin has not felt the clockwise stress rotation evinced in Crater Flat Basin since it is younger than Crater Flat Basin and outside the Walker Lane. In a similar fault slip analysis carried out in the Rock Valley fault zone, Frizzell and Zoback (1987) concluded from the close spatial association of fault

planes that showed either strike slip or dip slip displacement, that either rotations of the regional stress field had occurred during faulting, or local block rotations had occurred within the fault zone. The ambiguity highlights some of the problems of inferring regional stress history on the basis of local outcrop data.

Interpretation of regional stress data, and its application to tectonic activity, is uncertain. A number of factors complicate direct inferences of structural behavior that might be derived from stress analysis: large contrasts in mechanical properties characterize the rocks of the Yucca Mountain region; because stress measurements are point data, they reflect local anisotropies and widely variant boundary conditions. Therefore stress data are not good predictors of deformation. The crust has a long, poorly understood stress history that conditions bulk behavior in complex ways. Some stress measurements reflect conditions at failure, which is an instantaneous datum and a resultant force value. Consequently, we have a limited understanding of changes of stress with time, a point emphasized by Harmsen and Rogers (1986). Stress analysis provides information about fault shear strength at failure, but in an environment having a wide variety of faults of differing shear strengths, the theoretical bases of stress analysis are not met, so we know little about how or where the crust is accommodating strain.

A more meaningful assessment of deformation is provided by strain rates and patterns; strain investigation provides some idea of the 2-D deformation in the upper part of the crust and therefore alerts us to which faults are likely to slip in an order of priority based on attitude. In this respect, focal mechanisms indicate the regional tectonic strain tensor at shallow to mid-crustal depths (Harmsen and Bufe 1992; Savage, J.C. et al. 1995).

Strain measurements are obtained by trilateration networks, very long baseline interferometry observations, and satellite geodesy. Strain surveys show that the direction of extension in the Great Basin is toward the northwest, comparable to the direction of σ_3 , the least compressive stress (Minster and Jordan 1984, 1987; Gordon et al. 1993; Dixon et al. 1995; Savage, J.C. et al. 1995; Keefer et al. 1997). However, there are important spatial variations in the extensional strain rate. The Northern Basin and Range appears to be moving at 4.9 ± 1.3 mm/yr, $S82^\circ W$ with respect to the continental interior (Savage, J.C. et al. 1995), whereas the Southern Basin and Range has an extension rate of 3 mm/yr or less (Sauber 1989). The boundary between these two regions of differing extension is at about $37^\circ N$ latitude (Harmsen and Rogers 1986; Smith, R.B. and Arabasz 1991), a boundary that may represent a regional shear zone (Savage, J.C. et al. 1995) which contains local and perhaps transient zones of seismicity (Rogers, A.M., Harmsen et al. 1987).

The relatively high strain rate of the Northern Basin and Range is at least partly accommodated by the central Nevada seismic zone (Figure 3.2-1). The motion of the Sierra Nevada block relative to Ely, Nevada, is 9.1 ± 1.5 mm/yr at $N16^\circ \pm 8^\circ W$ (Savage, J.C. et al. 1995). Trilateration data show that at least 2.7 mm/yr of this extension is taken up by the central Nevada seismic zone, a rate calculation constrained by a 40-km wide network (Savage, J.C. et al. 1995). Dixon et al. (1995) note that northwest motion of the Sierra Nevada block is accomplished by a combination of east-west extension on north-striking normal faults, and by dextral motion on northwest-striking strike-slip faults of the Walker Lane and Eastern California shear zone (Figure 3.2-1). The dextral slip rate along the Eastern California shear zone (which includes most of the Inyo-Mono domain) may be as

high as 12 mm/yr (Sauber et al. 1994), but Dixon et al. (1995) report 8.8 mm/yr at $N9^{\circ}\pm 5^{\circ}W$. The component of west-directed extension across the Eastern California shear zone, reflected by normal faulting, ranges from 1.0 to 0.3 mm/yr (Savage, J.C. et al. 1995) to 0.2 to 0.1 mm/yr (Dixon et al. 1995). The integrated strain rate across the Eastern California shear zone is 12.1 ± 1.2 mm/yr at $N38^{\circ}\pm 5^{\circ}W$ (Dixon et al. 1995).

Crater Flat Basin and Yucca Mountain are located outside the zones of high strain rate (rapid rates of shear or extension or both) defined by the central Nevada seismic zone, the Eastern California shear zone, and the shear belt at $37^{\circ}N$ latitude. A 50 km aperture trilateration network centered on Yucca Mountain and operated from 1983 to 1993 showed no detectable strain accumulation (i.e., less than 2 mm/yr; Savage, J.C. et al. 1995). This low rate is compatible with strain rates in the Great Basin south of $37^{\circ}N$.

Strain data hold various tectonic implications for Yucca Mountain. Contemporary strain patterns are partitioned into zones of relatively high deformation that are not clearly correlated with structurally defined tectonic domains. The zones of high strain rate, such as the central Nevada seismic zone, may represent concentrations of active deformation among relatively stable blocks of crust (Savage, J.C. et al. 1995). The low strain rate (Savage, J.C. et al. 1994) and the low seismicity levels (Rogers, A.M., Harmsen et al. 1987 and Subsection 3.10.4 of this report) at Yucca Mountain and Crater Flat Basin therefore indicate that the site area is in a tectonic domain that may be isolated and uncoupled from zones of high strain to the west and north.

Geologic evidence suggests that the Eastern California shear zone has been a zone of high strain since Late Miocene time (10 to 6 Ma; Dixon et al. 1995). The kinematic boundary condition for Basin and Range deformation (the relative motions of the Pacific and North American plates) has been nearly constant for at least the past 3.4 Ma (Harbert and Cox 1989), which is within the time span for activity of the Inyo-Mono domain (Hodges et al. 1989). During this time, tectonic activity has gradually shifted westward, from the Death Valley-Furnace Creek fault to the Owens Valley fault (Dixon et al. 1995). Dixon et al. (1995) suggest that the Walker Lane accommodates significant dextral shear, at least in the vicinity of the Fish Lake Valley fault.

The central Nevada seismic zone trends obliquely across the older Walker Lane (Savage, J.C. et al. 1995). Therefore, it would seem that the westward migration of tectonism in the Inyo-Mono domain, the concentration of slip toward the Fish Lake Valley fault and across the Walker Lane, and the historical surface-rupturing earthquake activity along the central Nevada seismic zone, all represent a concentration of crustal strain of regional extent and significant longevity. This zone of strain appears to be shifting westward and perhaps northward (Dixon et al. 1995) away from any involvement with Yucca Mountain.

3.3.2 Evaluation of Tectonic Models

In this subsection, the various tectonic models that have been proposed for the Yucca Mountain vicinity or the surrounding region are described and evaluated. Although various hypotheses are characterized as "models" for the purposes of this discussion, in most cases they were not developed as rigorous models for which the model elements listed in Subsection 3.3.1 are provided. Thus, in

some cases, boundary conditions and driving forces are not addressed. Hence, each model is discussed primarily in terms of its structural elements and the processes hypothesized to be operating. The model's ability to explain the various data sets is documented and evaluated. Each of the models has shortcomings and thus far no single model has been described that satisfies all the data. The larger the area of a proposed model, the more likely it is that one will find local inconsistencies.

The NRC (1997b) also considered tectonic models for the Yucca Mountain region. They identify five models as viable:

- Deep detachment fault (12 to 15 km)
- Moderate detachment fault (6 to 8 km)
- Planar faults with internal block deformation
- Pull-apart basin
- Amargosa shear zone

These models are considered along with others in the discussion that follows, although they are categorized in a different manner. Volcanic and seismic hazard assessments for the Yucca Mountain site considered the range of viable tectonic models in deriving their results (see Subsections 3.9 and 3.10).

The first model to be discussed is the "Crater Flat-Prospector Pass caldera model" (Carr, W.J. 1988, 1990, 1992; Carr, W.J., Byers et al. 1986). Next, models falling into three generic classes defined on the basis of bulk mechanical behavior are described: simple shear models, pure shear models, and lateral shear models. Finally, in Subsection 3.3.3, the general features of a new tectonic model for the area immediately encompassing Yucca Mountain, Crater Flat, and vicinity are described.

3.3.2.1 Crater Flat-Prospector Pass Caldera Model

The Crater Flat-Prospector Pass caldera model was formulated by W.J. Carr (1982, 1984, 1988) to account for two major tectonic problems: the unknown source for the Crater Flat Tuff, and the form and structure of the Crater Flat Basin. Briefly, the model postulates that Crater Flat Basin reflects the structure of a subsided (now buried) caldera from which the Crater Flat Tuff was erupted.

Although recognizing the lack of direct supporting evidence, Carr's caldera concept was based primarily on the following general relationships:

- A thick sequence of welded Bullfrog Tuff was penetrated in drillhole USW-VH-1 (Figure 3.3-7), within the area of a broad positive aeromagnetic anomaly thought to indicate the presence of a thick circular body of volcanic rock that represented a resurgent dome (Figure 3.3-2).
- The negative gravity anomaly of Crater Flat is indicative of an underlying graben-like structure; the outline of the basin appears to conform to the shape of a caldera.

- The location of several structural and volcanic features (including the Bare Mountain fault and some Yucca Mountain faults, and the Lathrop Wells basalt cone) could be controlled by an inferred caldera rim.

Two other buried calderas were inferred to lie farther north, a "Tram caldera" (Carr, W.J., Byers et al. 1984), also referred to as the Prospector Pass Segment of the Crater Flat caldera, and an "older tuffs" caldera beneath Yucca Mountain (Figure 3.3-7). The Tram caldera was inferred on the basis of:

- Arcuate dikes in Bare Mountain that seem to correspond in age and composition to lava beneath the Tram Tuff; the lavas were thought to possibly represent early eruptions from the Tram caldera
- Thick Tram Tuff (457 m) in Beatty Wash (near the northern margin of Figure 3.3-7)
- Truncation of the Tram Tuff in Northern Crater Flat by a fault that "may be a caldera wall" (Carr, W.J. 1982, p.10)

The fact that the Tram and Lithic Ridge Tuffs are underlain by and contain dacites made it seem "likely" that the lavas formed an extensive pile beneath Crater Flat prior to eruption of the Crater Flat Group, and therefore were adduced as evidence for the caldera. Although W.J. Carr (1984) is equivocal about the "older tuff" caldera under Northern Yucca Mountain, he inferred that the Paintbrush Canyon fault may mark the eastern edge of such a caldera, or at least of a "large tectonic sag."

In presenting these points, W.J. Carr (1984) suggests that the basin has the shape of a caldera, and therefore the Crater Flat Basin had been formed by caldera collapse: "These interpretations together with much more suggestive evidence indicate a caldera lies immediately west of Yucca Mountain but its exact location and dimensions are not well known" (Carr, W.J. 1984, p. 71). W.J. Carr (1984) further states that there is "a good relationship between the location of fault segments active in the Quaternary and the proposed location of the caldera margins or ring fracture zones." But in W.J. Carr (1984; his Figure 28), a conspicuous exception to this relationship is shown by the northeast curvilinear alignment of 1.2 m.y. basalt cones that transect the site of the inferred caldera in Crater Flat. This post-caldera "rift" feature is also shown in Figure 3.3-7 (Carr, W.J. 1982).

Following publication of evidence that detachment faulting controlled Yucca Mountain tectonics, W.J. Carr (1990) abandoned the notion that caldera rim structure had a significant tectonic influence on fault patterns in Yucca Mountain. Instead, he emphasized the graben-like structure of Crater Flat and the "trapdoor" character of the caldera complex. He related the faults of Yucca Mountain with a coaxial zone of like faults in Pahute Mesa (Figure 3.3-2), and proposed that they all originated by "gravitational sliding toward the volcano-tectonic depression" represented by the Kawich-Greenwater rift (Figures 3.2-9, 3.2-11, and 3.3-1). The Bare Mountain fault now controlled subsidence of the caldera complex rather than being a local peripheral feature of the complex. More significantly, W.J. Carr (1990) reported that the faults at Yucca Mountain accord with a regional extensional stress axis oriented N50°W. The faults were thus associated with a regional strain

pattern and were no longer seen to be reactivated caldera rim features, except where they correlated with "properly oriented" segments of the inferred buried caldera.

R.B. Scott (1990) commented on the equivocal evidence for the caldera complex hypothesis, particularly referring to discrepancies in stratigraphic thickness and lithologic features cited by Carr, W.J. and Parrish (1985). The lack of demonstrable structural associations between a supposedly buried caldera and more recently acquired data further weaken the caldera complex model. For example:

- Paleomagnetic studies (Rosenbaum et al. 1991; Hudson, M.R., Sawyer et al. 1994) explain the curvature of faults at Yucca Mountain as a result of vertical axis rotation occurring about 12.7 Ma and later.
- Recent analysis of aeromagnetic data indicate that the prominent positive anomaly in Crater Flat originates within the Precambrian or Paleozoic section rather than from structures within the Tertiary section (Brocher, Hart et al. 1996; Langenheim and Ponce 1995b).
- Crater Flat seismic reflection profile (Brocher, Hart et al. 1996) gives no evidence for deformation in Crater Flat apart from block faulting of broadly warped, essentially conformable Tertiary strata.

An essential point about the caldera model is that it places peak tectonic activity in Crater Flat at about 14 Ma and requires that all subsequent deformation be guided by relict caldera rim structures. This hypothesis does not address the origins and mechanisms of Late Neogene and Quaternary strain effects, such as distributed and recurrent faulting at Yucca Mountain; the origins and impetus for basaltic extrusion in Crater Flat; the mechanisms for vertical axis rotation at the southern half of Yucca Mountain and the strike-slip component of faulting; the post-10 Ma uplift of Bare Mountain; the evidence for Quaternary faulting at Busted Butte; and the fact that styles of faulting similar to those at Yucca Mountain in Mid Valley, Yucca Flat, and on Pahute Mesa, have originated independent of any relict guiding caldera structures.

In summary, the Crater Flat-Prospector Pass caldera model is not a viable tectonic model because:

- Its inferred structural components are not demonstratable
- It fails to account for the origin and development of extensional faulting within the last 13 Ma
- It fails to provide a kinematic or dynamic link between Yucca Mountain and surrounding domains
- It fails to explain Late Pleistocene stress-strain relations in the region including basaltic volcanism

3.3.2.2 Simple Shear or Detachment Models

A variety of detachment fault models have been applied to Yucca Mountain. The models share one common factor: the mode of deformation is that of simple shear. In simple shear, one geometric axis of the deforming body rotates out of its original position. The hallmark of detachment faulting is creation of a succession of rotated fault blocks that rest cleanly on a low-angle shear plane (the "detachment fault") below which are older rocks that are not involved in the extensional faulting above. Extension is thus accomplished by multiple normal faults that jointly separate and rotate blocks of the upper crust (or "upper plate") in a common direction. Hence, it is convenient to group all detachment fault models under the common genetic heading of simple shear.

This style of extension implies several things about the nature of faulting and rock strength in the upper crust. First, it implies that the upper crust is sufficiently strong to undergo traction such that an "upper plate" can distribute extensional strain by responding to tensile stress through a variety of faulting mechanisms above a shallow angle ($\leq 30^\circ$) detachment fault that can extend for tens of kilometers across the crust. Second, it implies that structure (and active deformation) below the detachment is isolated from structure and deformation above. Third, it implies that extended tracts of rotated faults are bounded by a rigid headwall scarp and on the lateral margins by "accommodation zones" that behave partly like strike-slip faults and partly like ocean crust transform faults (Hamilton, W. and Myers 1966; Duebendorfer and Black 1992). The headwall scarp is ordinarily thought to have a sharply curved and even listric profile in order to promote initial fault block rotation (Wernicke, B. 1981).

Detachment faults behave somewhat like compound slump sheets, except that detachments are rooted in the crust. Consequently, detachment faulting requires certain assumptions about the properties and behavior of the failed crust. First, it assumes that the crust has high cohesive strength and that failure is simply a function of a laterally constant strain rate. Although this is true for undeformed sediments in the marine environment, for sandbox experiments, snowfields, and Quaternary deposits prone to slumping, it is not true for most rocks of the Southern Great Basin. Second, it assumes that narrow panels of rock and nearly flat, regional slip surfaces have coefficients of sliding friction that approach that of wet clay: master detachment faults either form on a ductile layer (in which case slip may actually be a late and relatively minor component of movement) or they require unusually high pore pressures or strong vertical gradients of physical properties. To induce this type of behavior requires either a hot, wet upper crust, or an initiating mechanism not reflected by the shallow-dipping detachment fault. The separate initiating mechanism is embodied in the "rolling hinge" concept (Spencer 1984; Buck 1988; Wernicke and Axen 1988; Hamilton, W.B. 1988; Hamilton, W.B. and Howard 1991).

Normal faulting in the brittle crust typically begins at high angles (~ 55 to 70°) and may extend with little or no curvature down to the depths of ductile deformation. Consequently, the rotation of upper crustal fault planes to angles shallower than 30° required either substantial shear along the basal contact (Gross, W.W. and Hillemeier 1982; the rotated domino or "bookshelf" deformation mechanism) or plastic deformation and uplift of the footwall (the rolling hinge mechanism). Each of these mechanisms requires behavior differences or different conditions of deformation from anything known in the present day extension regime. For example, Brun et al. (1994) were able to

develop a rolling hinge-type structure in sandbox experiments only by placing a discrete low-viscosity material where they wished footwall uplift to occur. Otherwise their models resulted in an entirely different structure. Likewise, McClay and Ellis (1987) were able to create a tilted domino fault succession, but only on a tilted table; the faults were initiated at the proper tilted attitudes but did not rotate into those attitudes from a previously steeper attitude. Furthermore, in dealing with the considerable problem of space gaps generated by rotated brittle blocks, McClay and Ellis (1987) noted the requirement of extreme and complex intra-block deformation and the tendency for listric faults to straighten by quasi-ductile deformation to overcome the space gaps.

For detachment faulting to work in the face of these constraints, it must involve very large areas and volumes of the crust to overcome the rheological limitations that ordinary brittle rock behavior imposes on the model. Although there is no doubt that detachment on this scale has occurred in the Middle to Late Miocene in areas of the Mojave and Southern Arizona (i.e., south of latitude 37°N), it is questionable whether appropriate conditions exist today in the crust of the Southern Great Basin to facilitate such extension. One point of discussion is the lack of any earthquakes that have the required focal mechanism for shallow detachment (Arabasz and Julander 1986; Jackson, J.A. 1987; Jackson, J.A. and White 1989; Wernicke 1995). Either detachment faulting does not operate at present, or it does so by aseismic creep, or detachment faults accumulate strain over periods of time and in ways not presently understood.

Detachment models have been applied to Yucca Mountain and its tectonic setting largely on the strength of four major arguments:

- Proximity—Late Miocene detachment faulting occurred west of Yucca Mountain at Bare Mountain, the Bullfrog Hills, and the Funeral Mountains.
- Exposed detachments typically are capped by steeply tilted fault blocks. Therefore, rotated fault blocks are necessarily underlain by a detachment—the rotated, quasi-parallel fault blocks of Yucca Mountain represent either a tilted domino or a listric fault set.
- Field observation—a detachment is exposed at the Tertiary/Paleozoic contact in places east and south of Yucca Mountain.
- Regional tectonic interpretation—a major deep detachment extends from near the Sheep Range west to Death Valley (Death Valley breakaway fault zone, Wernicke, Axen et al. 1988; Sheep Range detachment, Guth 1981).

Taking these four points into account, many geologists concluded in the late 1980s that at least one detachment fault passes under Yucca Mountain.

Two considerations make application of a detachment model to Yucca Mountain difficult:

- Detachment model applications cannot explain important qualifying or contradicting data (discussed below).

- Studies carried out by the site characterization program have produced new data that negate important elements of the four major arguments given above.

In the first case, each published model application is based on a single schematic east-west profile across Yucca Mountain, and each profile ignores huge variations in structural geometry and deformation history present several kilometers to the north or south of the profile. For example, the fact that just north of Yucca Mountain a huge volume of magma resided in the crust (Broxton, Warren et al. 1989) throughout the period of inferred maximum detachment activity was not addressed. The effects of large volumes of molten or near-molten rock on the inferred detachment mechanism were ignored. Detachment proponents simply assumed that detachment occurred within solid, uniform rock having no rheological perturbations or lateral boundary effects.

In the second case, detailed mapping now shows that:

- Any shallow detachment that occurred west of the Fluorspar Canyon fault after 14 Ma was isolated from any comparable deformation in Crater Flat east of Tram Ridge (C.J. Fridrich et al., *Cenozoic Basins of the Death Valley Region: Late Cenozoic Extension, Vertical-Axis Rotation, and Volcanism in the Crater Flat Basin, Southwest Nevada*, Geological Society of America Special Paper, in press).
- The pattern of faulting at Yucca Mountain does not reflect a systematic vergence to the west and the rate and progress of extension across Crater Flat is diachronous (Fridrich 1998; Brocher, Hart et al. 1996; Day, Potter et al. 1997; Simonds et al. 1995).
- All the Tertiary/Paleozoic contacts exposed east and south of Yucca Mountain are erosional contacts, not slip surfaces (Simonds et al. 1995).
- The deep detachment faults (or "systems") projected west of the Sheep Range by Guth (1981) and Wernicke, Axen et al. (1988) are not compatible with structures mapped at the Nevada Test Site (they ignore the significant strike-slip deformation of the Walker Lane), nor are they comparable with structure exposed in the Funeral Mountains, the Bullfrog Hills, or Bare Mountain.

In fact, chronologic and kinematic compatibilities among these latter structural assemblages are still unresolved. Interpretations of Miocene extensional structures east of Yucca Mountain are severely compromised by strike-slip faulting within the Spotted Range-Mine Mountain structural zone and by east-vergent extension east of the CP Hills.

W.B. Hamilton (1988) originally proposed a detachment at Yucca Mountain in the context of a regional "rolling hinge" model. Accordingly, Bare Mountain was seen as the uplifted lower part of the footwall; the smoothly east-sloping profile of Bare Mountain was interpreted to be the exhumed detachment plane. Hamilton did not ascribe significance to the Bare Mountain fault as a structure instrumental in the evolution of Yucca Mountain; the Bare Mountain profile was simply projected east under Crater Flat with no significant offset to become the surface of detachment under Yucca Mountain. The chronology of uplift at Bare Mountain meant that if detachment was occurring at

Yucca Mountain it would have ceased at about 10 Ma and produced no further slip at the mountain after that. By Late Miocene time, the upper plate had already been uplifted and stranded along the Grapevine Mountains. If faulting at Yucca Mountain represented headwall detachment, as proposed by R.B. Scott and Whitney (1987), it was a relatively minor and short lived event in a scheme of regional deformation that manifested itself most powerfully in the Funeral Mountains and the east flank of Death Valley.

R.B. Scott (1990) focused closely on the structural details of Yucca Mountain and called attention to the resemblance of the faults at Yucca Mountain to tilted dominos (Wernicke and Burchfiel 1982). This resemblance, along with the perceived detachment at the Tertiary/Paleozoic contact in the Calico Hills, Rock Valley, and Point of Rocks, led Scott to conclude that a detachment fault also occurred at the Tertiary/Paleozoic contact beneath Yucca Mountain at a depth of 1.5 to 2.5 km.

Evaluation of this interpretation reveals a number of structural problems. First, R.B. Scott (1990) claimed that the faults are listric on the basis of fault plane dips that become less steep with depth, and a rollover or local increase of hanging wall dip toward the footwalls. Although he drew a comparison to the listric faults exhibited in seismic reflection profiles from the Gulf of Mexico, his interpretive profiles of Yucca Mountain showed domino structures that required huge amounts of basal shearing and other deformation to achieve the basal geometry depicted (Figure 3.3-8). W.B. Hamilton (*Detachment Faulting and Tectonic Modeling in the Yucca Mountain Region*, report to U.S. Geological Survey Water-Resources Division, Yucca Mountain Project Branch, on work carried out under Memorandum of Agreement with the U.S. Geological Survey Geologic Division, Branch of Geophysics) rightly noted that R.B. Scott's (1990) profiles are non-retro deformable and that the displacements on the Yucca Mountain faults are so small as to require implausibly tight curvatures to be truly listric with the Paleozoic contact at about 2 km depth. The amount of structural deformation required to accommodate listric faulting (or domino tilt accommodation) low in the Miocene volcanic tuff section should be evident in core records, but the rock shows no evidence of such damage. Furthermore, if Hamilton's concept of a rolling hinge is correct, there can be no listric master fault for Yucca Mountain. The only major deformation found at depth at Yucca Mountain is the breccia in the Paleozoic limestone recovered from well UP-25 p#1 (Carr, W.J., Byers, et al. 1986). R.B. Scott (1990) refers this to a fault of "unknown attitude" although W.J. Carr, Byers et al. (1986) made a good case for deformation related to the steeply dipping Fran Ridge fault. The important point, however, is that the breccia is in the presumed lower plate, not in the upper plate where it should be, and it shows no shear fabric and no alignment parallel to the inferred detachment.

R.B. Scott (1990) acknowledged both the dependence of his interpretation on Wernicke, Axen et al. (1988) and the inferential content of his interpretation which "takes into account" the location of Yucca Mountain in a terrain "affected by low-angle extensional faulting." Embracing this concept, R.B. Scott (1990) considered that W.B. Hamilton's (1988) scheme was far too simplistic; Scott inferred the presence of two, possibly three detachment faults under Yucca Mountain, the deeper ones being more in accord with the regional concept of Wernicke, Axen et al. (1988) than with the local Yucca Mountain upper plate assemblage. Using a conceptual cross-section by McKee (1983) for illustration (Figure 3.3-9), R.B. Scott (1990) projected the Fluorspar Canyon fault over Bare Mountain and east, under Crater Flat, to meet the shallow Yucca Mountain detachment, and projected the Bullfrog Hills detachment east under Bare Mountain. He included all of the

deformation in Bare Mountain within this detachment envelope ("middle plate") and thereby related Yucca Mountain detachment to both shallow detachment west of Bare Mountain and to a deeper, through-going zone of deformation carried east to the breakaway fault zone at the west side of the Sheep Range (Guth 1981). Although R.B. Scott (1990) shows the Bare Mountain fault cutting the Yucca Mountain-Fluorspar Canyon detachment fault, he noted that extension (presumably related to detachment) continued at Yucca Mountain into the Pleistocene.

An interesting corollary of R.B. Scott's (1990) treatment of the detachment model is his assumption that vertical axis rotation at Yucca Mountain is an expression of an underlying dextral bend or shear zone. The inferred detachment represents a zone of partial decoupling across which narrowly confined shear is distributed into the tuff blocks according to the model of Hardyman (1978) and Hardyman and Oldow (1991). (Lateral shear models are discussed in detail in Subsection 3.3.2.4.)

As new information has been collected and analyzed the structural problems of shallow detachment have become more evident. W.B. Hamilton (*Detachment Faulting and Tectonic Modeling in the Yucca Mountain Region*, report to U.S. Geological Survey Water-Resources Division, Yucca Mountain Project Branch, on work carried out under Memorandum of Agreement with the U.S. Geological Survey Geologic Division, Branch of Geophysics) now recognizes that the Crater Flat domain represents a detachment separate from the Fluorspar Canyon-Bullfrog Hills detachment. W.B. Hamilton considers the Miocene rocks of Yucca Mountain to rest in depositional contact on a rotated Paleozoic hanging wall; the master detachment fault lies much deeper. Therefore, W.B. Hamilton (*Detachment Faulting and Tectonic Modeling in the Yucca Mountain Region*, report to U.S. Geological Survey Water-Resources Division, Yucca Mountain Project Branch, on work carried out under Memorandum of Agreement with the U.S. Geological Survey Geologic Division, Branch of Geophysics) infers that the faulting at Yucca Mountain is minor, largely post-detachment faulting formed after hinge line rotation had passed to the west. It is possible then, that some of the Yucca Mountain faults extend down through the Paleozoic substrate to merge with the still steep sector of the master west-dipping fault, possibly at around 9-km depth.

Fox and Carr (1989) treat detachment following the ideas of R.B. Scott (1986), but emphasize the significance of Crater Flat as a pull-apart that controlled fault activity at Yucca Mountain (Figure 3.3-10). They inferred that the postulated low-angle extensional fault at the base of the Tertiary section (they avoided calling it a detachment fault) was seen as a small fragment of a subregional Miocene detachment, a fragment locally reactivated in the Quaternary by sliding toward the extensional axis of Crater Flat. In this sense, their view of Yucca Mountain deformation is more akin to mass movement than to any of the detachment mechanisms. They also emphasized that extension in Crater Flat, hence Quaternary movement of Yucca Mountain faults, is related to the northwest-directed translation of the Inyo-Mono domain.

Fox and Carr (1989) inferred that local extension at Yucca Mountain was reactivated around 3.7 Ma in conjunction with basaltic volcanism in Crater Flat. They noted the presence of basaltic ash in Quaternary fault fissures at Yucca Mountain and suggested that the coincidence was related to a stress-strain cycle: minimum principal stress was signaled by faulting, fissuring and volcanism; subsequent calcrete precipitation within the fault crevices and fissures exerted a compressive stress that increased the least principal stress, but eventually this relatively weak strengthening effect was

overcome by the regional extensile strain and the cycle began anew. Fox and Carr (1989) cite a periodicity of about 75 ka based on a composite average recurrence rate on the Windy Wash fault (Figure 3.3-1) during the last 300 k.y.

W.J. Carr (1990) attempted to associate the Kawich-Greenwater rift (Figures 3.2-9 and 3.3-1), which is supported by structural data, with a detachment structure following the concepts of Wernicke (1981), Wernicke and Burchfiel (1982), Stewart (1983), Howard and John (1987), and Wright, L.A., Otten et al. (1974). In his treatment of the model, the east side of the rift (i.e., Yucca Mountain itself) constitutes the headwall for the big detachments to the west. The result is an array of fault contacts referred to a single schematic cross section (the "model," Figure 3.3-11) explained entirely in the context of structure of the Bullfrog Hills and Death Valley. In projecting the faults of Yucca Mountain to an undetermined depth into the Paleozoic section, W.J. Carr (1990) indicated no detachment at all. In doing this, W.J. Carr (1990) gave the term "headwall" a special meaning and stated that the faults of Yucca Mountain-Crater Flat are essentially planar and "need not be underlain by a regional detachment." Nevertheless, these faults were considered to be largely gravitational features of a "breakaway zone" within the Kawich-Greenwater rift (Figure 3.2-9).

Detachment faulting models for Yucca Mountain have been analyzed using geophysical data and simulation. For example, to demonstrate detachment Oliver and Fox (1993) used gravity data that Snyder and Carr (1982) had previously used to demonstrate a half-graben or structural trough beneath Crater Flat. Oliver and Fox (1993) used a computer to create a simulated gravity profile based on juxtaposition of slices of differing density and angular relations. The simulated gravity profile fit the Snyder and Carr (1982) profile when the slices were arranged to give the Bare Mountain fault a 27° dip and the Yucca Mountain "detachment" a dip of 12°.

Young et al. (1993) used a computer simulation technique to evaluate the common detachment hanging wall deformation mechanisms (flexural slip, slip line, domino, vertical shear) and found that the assumptions required to model detachment-style rollover at Yucca Mountain did not comply well with field data. Vertical shear provided the most acceptable mechanism for creating appropriate rollover. However, much of the vertical shear discussed and depicted by R.B. Scott (1990) to explain hanging wall rollover at Yucca Mountain is conceptual (Figure 3.3-8). The reality of such faults, which were "required by geometric constraints" (Scott, R.B. 1990), is doubted by W.B. Hamilton (*Detachment Faulting and Tectonic Modeling in the Yucca Mountain Region*, report to U.S. Geological Survey Water-Resources Division, Yucca Mountain Project Branch, on work carried out under Memorandum of Agreement with the U.S. Geological Survey Geologic Division, Branch of Geophysics).

Based on the current information base, a number of conclusions can be drawn concerning applicability of the detachment model to Yucca Mountain. First, shallow detachment at the Tertiary/Paleozoic contact can be eliminated as a credible interpretation. Numerous exposures throughout the area, as well as the Crater Flat seismic profile (Brocher and Hunter 1996), combine to show that the Paleozoic contact is an unconformity cut by high-angle faults; there never was a detachment at this level. This conclusion does not, however, rule out the possibility that the Paleozoic surface acts as a local stress guide due to rheological contrasts or material contrasts across the unconformity. W.J. Carr's (1990) conjectures on this topic may have some validity.

With respect to a "deep detachment" model, with slip surfaces located at depths from 6 to 15 km, if the big faults at Yucca Mountain are controlled by a deep detachment, they cannot behave like dominos. The domino model requires rigid behavior and completely distributed shear; there can be no rollover or opposed slip. The big blocks at Yucca Mountain do have some rollover, and there is local reversal of offset along strike on some of the big faults. Furthermore, domino rotation presumes tensile behavior at the base and uniform frictional slip across the entire width of the slip plane – unrealistic expectations to depths of 6 km at Yucca Mountain, even in the presence of extreme pore pressure.

Even though Quaternary faulting is well documented at Yucca Mountain, there is evidence that regional deep detachment has no role in the activity. Geophysical data indicate that none of the high-level intrusive bodies, particularly basalts, have been displaced west from lower crustal roots. The history of localized Late Neogene Basin deformation (Mid Valley, Yucca Flat Basin, Frenchman Flat, Sarcobatus Flat) with varied and opposed senses of flank collapse, indicates that a systematic west-directed sense of detachment faulting has not been a part of crustal evolution in Neogene time within the Walker Lane east of Bare Mountain. The structure of the Specter Range does indicate that regional detachment operated east of Bare Mountain, but this is pre-Late Oligocene deformation, possibly coeval with detachment-level shearing in the Funeral and Grapevine Mountains (Hamilton, W.B. 1988). Within the last several million years, extensive, deep detachment has not operated east of Bare Mountain. Brocher, Carr et al. (1993) pointed out that the apparent continuity of seismic reflections in basinal units south of the Specter Range indicated little or no faulting within the last 8.5 to 11 Ma; thus, detachment was not active here in Late Miocene time.

Any regional deep crustal detachment slip at or above the brittle-ductile transition was terminated along the Bare Mountain front by about 14 Ma. Beyond this time, dike intrusion and differential uplift along the Bare Mountain front isolated whatever deep crustal connection that detachment at Bare Mountain may have had with detachment farther east. By about 6 Ma, detachment faulting in the Funeral-Bare Mountains domain was also inactive (Hoisch and Simpson 1993). Any detachment mechanism operating in the Inyo-Mono domain west of the Furnace Creek fault does not influence Quaternary and present deformation at Yucca Mountain.

In considering the possibility that deep, regional detachment faults may have been dismembered by local basin formation, one should bear in mind L.A. Wright's (1989) surmise that detachments—as mass displacement phenomena in contrast to deep shearing phenomena—may be entirely local features associated with rapid uplift and tilting of individual crustal blocks (ranges). Despite W.B. Hamilton's (1988) objection to the process envisioned by Wright, the rolling hinge model more or less comes to the same end because each footwall uplift serves to terminate and isolate detachment in approximately 15 to 30 km increments. Once that happens, the block is then subject to any local through-the-crust deformation.

The most recent attempts to fit a detachment model to Yucca Mountain are provided by Ferrill et al. (1995) who describe two model variants based on syntheses of previous proposals. Model 1 assumes that the faults of Yucca Mountain developed as the headwall of the "Bullfrog Hills detachment system," which is thought to accommodate as much as 275 percent extension. According to this model Yucca Mountain faults were isolated from the Bullfrog Hills system by rise of the Bare

Mountain block along the Bare Mountain fault, which truncated the Yucca-Bullfrog detachment. Continued motion of the Bare Mountain fault led to formation of a deeper, east-directed detachment plane. According to this model the older, shallower, west-directed detachment accounts for the imbricate faulting at Yucca Mountain. The younger, deeper, east-directed detachment accounts for hanging wall collapse of the carapace into Crater Flat basin.

Model 2 accounts for hanging wall rollover and imbricate faulting at Yucca Mountain directly by assuming that the Bare Mountain fault is the driving listric (detachment) fault and that Yucca Mountain faults are simply antithetic to the deep, master, east-directed Bare Mountain detachment. However, in this version of the model, faults antithetic to the Bare Mountain listric fault are simultaneously listric faults synthetic to a breakaway fault located somewhere to the east in Jackass Flats. The result is a curious "bathtub" profile having listric faults at each end that merge at a common plane of detachment. It is not clear how slip is partitioned between the two apparently competing listric faults and along the common detachment surface.

Finite element modeling was applied by Ofoegbu and Ferrill (1995) to the problem of detachment-related fault slip. A five-layer linear elastic model was used, and the initial stress state included previous fault slip on simulated Yucca Mountain fault planes. In order for the model to work, it was necessary to treat each fault as a weakly cohesive or cohesionless layer having at least 150 m thickness and decoupled from confining rock. Slip was forced to occur on a selected fault by reducing its coefficient of static friction. Under reasonable confining stress, a friction angle of 0.93° is required. The model implies also that a significant proportion of fault displacement is taken up by deformation of the hanging wall and footwall. Ofoegbu and Ferrill (1995) found that slip rates in the detachment fault and in the steep, off-branching perturbed fault differed by six orders of magnitude. They concluded that a detachment fault is likely to slip aseismically in response to slip events that may occur at seismic rates on the off-branching steep faults. In reaching this conclusion, however, it seems that the modeled mechanism violates the concept of detachment faulting: steep fault perturbation is not supposed to generate strain in the detachment fault; rather, the detachment is the master slip plane and motion along it is supposed to generate slip along the faults of the upper plate and distribute strain among them by virtue of independent motion. In other words, the model did not demonstrate how detachment is supposed to control upper plate fault slip.

It is clear from the model, however, that detachment can only work along a weak layer that has an unusually low angle of friction and no cohesive strength. This is why detachments are so common as slump mechanisms in saturated sediments and in the marine environment (leaving apart the issue of low effective stress). It also explains why exposed detachments typically show evidence of ductile deformation in the lower plate.

3.3.2.3 Pure Shear Models

Pure shear models (horst and graben or tilted block models) were applied to the Basin and Range province because of the obvious, exposed horst-like or tilted block structure of the ranges. The term *pure shear* refers to a type of deformation wherein the orientation of geometric axes of a deforming body remains unchanged during deformation. In other words, a cube may become a stretched or flattened parallelepiped, but it does not undergo rotation or skewing from its original position.

Models that are grounded on a pure shear mechanism involve pure shear within the ductile or plastic lower crust, and segmentation and breakup of a passive, brittle upper crust that fails easily under tension. The result is a variety of rift-like or graben-like elongate basins in the upper crust having their long axes normal to the direction of extension. In contrast to the detachment mechanism, the intervening ranges may collapse or extend into the adjacent opening basins in any manner that reflects local rock strength, stress history, or other such constraint.

Pure shear models are in good accord with most exposed basin and range structure, and, unlike the simple shear models, they are compatible with the stress history of the upper crust. They are not, however, in accord with the fact that ranges typically are isostatically uncompensated. Also, the relatively steep observable faults are not geometrically compatible with many estimates of percentage of extension based on rates projected over time (Hamilton, W. and Myers 1966). Furthermore, the substructure of the horst and graben model is nowhere demonstrable in outcrop whereas detachment faults are well exposed in many parts of the Southern Great Basin, providing clear evidence that the detachment mechanism has operated in the past. On the other hand, present-day extension is manifested throughout most of the Southern Great Basin by normal fault displacement earthquakes that exhibit focal mechanisms with steeply-dipping faults at depths approaching 19 km (Doser and Smith 1989). Some form of pure shear extension seems to operate in the Southern Great Basin at present, and there is good evidence that pure shear mechanisms have operated throughout the Great Basin in the past.

Deep seismic reflection profiles (Hauge et al. 1987) and refraction profiles (Catchings and Mooney 1991) across central Nevada support the pure shear model. Seismic data reveal a layered crust, defined by both acoustic reflection and interval velocities, in which acoustic velocities of the upper crust vary about 0.3 km/s. Ranges cored by Mesozoic rocks have an acoustic velocity of 6.0 km/s and basins (or intervening ranges) underlain chiefly by Tertiary rock have an acoustic velocity of 5.7 km/s (Catchings 1992). Because most present-day seismicity is in basins rather than ranges, and occurs to depths of 12 km, Catchings (1992) infers that the lower velocity of 5.7 km/s probably indicates fracturing and faulting where extension is concentrated. The upper crustal depressions filled with rock having 5.7 km/s velocities are similar to the model of Dixie Valley by Okaya and Thompson (1985). Okaya (1985) concluded that Dixie Valley is underlain by highly broken rock to a depth of 20 km. Catchings (1992) noted that the seismic velocity structure implies the crust as a whole is extending laterally in "boudinage fashion," an image compatible with the pure shear model.

Sandbox models of laterally homogeneous layers subject to simulated gravity spreading produced a succession of tilted blocks upon a ductile layer that remained nearly planar during deformation, although the overlying blocks rotated and faults flattened (Brun et al. 1994). The larger unfaulted blocks showed some frictional bonding with the extending ductile layer and were separated from each other by collapsed, more intricately faulted basin segments. This style of extension is similar to that described from the seismic profiles by Catchings (1992).

The application of pure shear models to Yucca Mountain is complicated by the pervasive effects of lateral shear in upper crustal rocks of the Walker Lane. Many basins have opened in transtension as "pull-aparts" (Burchfiel and Stewart 1966) that are associated with strike-slip faulting. Basins that

may have formed by coaxial extension (pure shear) may have been modified later by application of lateral shear, or by a broadly distributed, transtensional torque inferred to characterize the Walker Lane (Carr, W.J. 1990). Some evidence suggests the former case. Paleomagnetic studies (Hudson, M.R., Sawyer et al. 1994) suggest that dextral shear that affected the region of the southwestern Nevada volcanic field occurred in discrete zones that were discontinuous in length and diachronous in age. According to M.R. Hudson, Sawyer et al. (1994), dextral shear in the Crater Flat domain is a local strain accommodation to post-12 Ma extension of the Inyo-Mono domain. Thus, Crater Flat Basin could have initially opened under nearly pure shear (as a half graben) and, within a million years of initial faulting, been subject to clockwise vertical axis shear (S.A. Minor [USGS, Denver], written communication to D. O'Leary [USGS, Denver], February 15, 1996, *Fault-Slip Analysis of the Northern Crater Flat Basin: Preliminary Results and Interpretations*).

The normal fault pattern and general north-south parallelism of a number of basin structures (Amargosa trough, Mid Valley, Yucca Flat) suggest coaxial strain leading to a graben-like form. On the other hand, similar structures in the Inyo-Mono domain are well explained as transtensional pull-aparts formed under the active influence of dextral faulting. Whether dextral shear is synkinematic or postkinematic, it is an important complication to models that invoke pure shear.

Yucca Mountain and the Crater Flat basin are interpreted as part of a large rift-like feature, the Amargosa trough (Figures 3.2-3 and 3.2-11) that can be modeled as a pure shear structure. The trough was identified primarily on the basis of geophysical evidence as the Kawich-Greenwater rift (Carr, W.J. 1988, 1990; Figure 3.2-11) and as the Amargosa Desert rift zone (Wright, L.A. 1989). W.J. Carr (1990) emphasized the volcanic affinities of the rift, mainly the fact that large volcanic centers partly define both its southern terminus and northern extent. W.J. Carr (1990) drew attention to the rift as being active generally from Late Miocene into the Quaternary on the basis of the Yucca Mountain style faulting of tuff in Pahute Mesa, the presence of Late Tertiary to Quaternary basalts, and Quaternary fault movement at Yucca Mountain and points farther south. Crater Flat Basin is an unusually deep and complicated segment of the overall rift. W.J. Carr (1990) attributed the rift structure at Yucca Mountain to several episodes of magmatic insurgence, doming, and caldera and sector graben collapse. The rift south of Yucca Mountain is not full of tuff, as indicated by the general absence of magnetic anomalies similar to those of Yucca Mountain and sparse data from the Felderhoff wells (Carr, W.J., Grow et al. 1995).

W.J. Carr (1990) noted that the west side of the rift is better defined than the east, giving it the form of an asymmetric graben. The lack of a distinct structural boundary in Jackass Flats, however, is a major problem for the rift model. Because gravity and aeromagnetic gradients do not guide a structural interpretation north of Little Skull Mountain, the question of an eastern border is open. Neither L.A. Wright (1989) nor W.J. Carr (1990) carried the eastern boundary farther north than the west side of Little Skull Mountain. Brocher, Hart et al. (1996), on the basis of seismic profile data, confirmed that the "gravity fault" of Winograd and Thordarson (1975) forms the structural boundary of the east side of the rift at about 36°35' N. From there they projected the border obliquely northwest across Jackass Flats and up Fortymile Canyon. Simonds and Scott (1996) infer that the eastern border of the trough trends roughly due north and is expressed by a set of down-to-the-west post-12.7 Ma faults along the west side of the Calico Hills.

Brocher, Hart et al. (1996) interpreted the "gravity fault" as being listric and presumably rooted to a reflector (K) at about 2 seconds (5.5 km) depth. Although Brocher, Hart et al. (1996) did not offer a preferred interpretation of reflector K, they did emphasize the role of ductile flow in the lower crust at a depth of about 6 seconds below the Amargosa trough. The "gravity fault" is not listric but probably extends to the zone of ductile flow and thus is controlled by pure shear deformation. Reflector K may then represent an abandoned pre-Late Oligocene detachment that controlled extension of the Specter Range.

Both L.A. Wright and W.J. Carr relate the Amargosa trough to a major right step in regional extension of the Walker Lane. L.A. Wright (1989) suggested that the trough does not terminate south at the Greenwater volcanic center (Carr, W.J. 1990), but forms a dynamic link with a series of narrow pull-apart basins associated with the Stewart Valley-Pahrump Valley fault zone (Burchfiel, Hamill et al. 1983). This interpretation provides a direct link to transtensional tectonics and latest Neogene subsidence associated with development of the Inyo-Mono domain. L.A. Wright (1989) therefore inferred that the Amargosa trough is tectonically linked to deformation in the Death Valley area. An important tectonic implication is that trough and range segmentation began at least as late as 13 Ma and probably as far back as 16 Ma, each trough and range having undergone a separate deformation history.

Fridrich (1998) presents a model for Yucca Mountain that involves pure shear. He notes that Crater Flat formed by a combination of east-west to southeast-northwest extension and northwest-directed dextral deformation. In terms of overall fault pattern, the Crater Flat Basin is a graben, but in Crater Flat the angular discordance between the Paintbrush and the Timber Mountain Group tuffs varies from as little as 10° at Northern Yucca Mountain to 25° to 40° at the south and southwest parts of the basin. The original pattern of extension in Crater Flat thus has a geometric pattern somewhat like a sphenochasm (a triangular pull-apart basin). It appears that the basin pivoted open with the northeast corner of the basin as the point of least extension. Although the spatial variation in the percentage of extension and in the degree of vertical axis rotation within the Crater Flat domain resembles that of some strike-slip (pull-apart) basins, detailed mapping has failed to uncover evidence for a major discrete strike-slip fault through the basin or at its boundaries. Fridrich notes that if the southwest corner also acted as a pivot point in the 12.7 to 11.7 Ma extension event, the overall geometry could be likened to a rhombochasm, an interpretation permitted by field data. Fridrich concludes that Crater Flat Basin is a hybrid feature that combines pure shear (graben extension) with dextral shear as well as the influence of Miocene magmatic evolution.

A pure shear mechanism is well suited to explaining the fundamental graben-like structure of the Crater Flat Basin, and because a pure shear mechanism can be directly tied to mid-crustal ductile deformation, it can adequately account for extension throughout Quaternary time, including basaltic volcanism.

3.3.2.4 Lateral Shear Models

Lateral shear, expressed as strike-slip faulting, is an important extensional mechanism throughout the Walker Lane and the Inyo-Mono domain to the west. The most significant of the lateral shear models are those that involve aspects of pure shear (pull-apart models, Burchfiel and Stewart 1966).

L.A. Wright (1989) applied this model to the terrane between Death Valley and the Amargosa Valley. The model treats the basins as obliquely extending rhombochasms (Wright, L.A. and Troxel 1973) connected by northwest-striking dextral faults. The intervening ranges are more or less structurally isolated and passive domains that can undergo separate deformational histories apart from the widening pull-apart basins. The lateral shear models are not predicated on systematic behavior of large tracts of crust but emphasize discrete tectonic development of basins and ranges depending on local structural conditions and local rock characteristics.

Lateral shear is also a component of "escape tectonics," a model applied by R.E. Anderson, Barnhard et al. (1994) to deformation along the Lake Mead fault zone. Escape tectonics brings into play an aspect of basin and range deformation ignored by the other models, namely contractional deformation normal to extension. Compression created by the collision of large crustal domains impinging on each other (raft tectonics) can lead to development of local arching, uplift and fold patterns described as meridional collapse folds by R.E. Anderson, Barnhard et al. (1994). Oblique compression drives the lateral escape of smaller blocks along strike-slip faults.

In emphasizing the varieties and relations of planimetric deformation, lateral shear models deal with a dimension not well treated by the other kinds of models, and they incorporate vertical axis rotation. Otherwise, lateral shear models can involve pure shear deformation of a ductile middle to lower crust, and a passive upper crust broken into blocks that move apart by normal faulting but that may be brought together by strike-slip faulting. The blocks continue to evolve structurally during extension by marginal collapse, uplift, or collision.

Strike-slip faulting oblique to the extension direction is an important extensional mechanism throughout the Walker Lane. Models that rely on this mechanism are often called "Walker Lane" models. These models have the benefit of demonstrable small-scale offset and the activity of present day strike-slip faulting for support. Among models of this type are those that infer large offset, the pattern and extent of which is determined by displaced foldbelts or terrane elements of Mesozoic or earlier origin (Caskey and Schweickert 1992; Snow and Prave 1994), those that align coeval features (Savage, J.C. et al. 1995; Schweickert and Lahren 1994, 1997), and those that associate detachment with buried strike-slip faults (Hardyman 1978; Hardyman and Oldow 1991).

Throughgoing strike-slip faults of the style of the Furnace Creek fault have not been recognized in or near Crater Flat. The model proposed by Hardyman (1978) for the central Walker Lane and presented by Hardyman and Oldow (1991) for the structure of the Gillis and Gabbs Valley Ranges implies that such a fault may be present but hidden beneath a shallow detachment. The model describes a "transtensional nappe" which actually requires that the detachment (listric fault tract) be bounded by a pair of strike-slip faults and that the detachment faults have a fixed geometry with respect to the strike-slip faults, visible or not. The strikes of the listric faults are the traces of the strike-slip faults. Hardyman and Oldow (1991) cite as the best examples of this style of faulting the faults in the Gabbs Valley where subdomains of listric normal faults of similar polarity exhibit dips of 60° to 20° and have displacements of several centimeters to several tens of meters or more. The listric fault pattern of the Gabbs Valley is distinctly different from that of Yucca Mountain and, in fact, none of the criteria or geometry required for Hardyman's model exist at Yucca Mountain. Hardyman and Oldow (1991) do cite high-angle normal faults in the central Walker Lane that cut

Tertiary strata, have dip-slip and oblique-slip, display straight-line map traces, and have variable strike orientations. They note that some of these faults presumably penetrate the crust, having guided the emplacement of Tertiary dikes. These faults, not subsumed by Hardyman's model, more closely resemble those that cut Yucca Mountain than do those of the Gillis and Gabbs Valley Ranges.

A different hypothesis regarding a hidden strike-slip fault beneath Crater Flat is presented by Caskey and Schweickert (1992), and Schweickert and Lahren (1994, 1997). The existence of a north-northwest-striking dextral strike-slip fault passing beneath Yucca Mountain is inferred from the interpreted displacement of a Mesozoic fold that originally aligned Bare Mountain and the Striped Hills, now offset by about 20 km (Caskey and Schweickert 1992) or by more than 30 km (Schweickert and Lahren 1994, 1997). The inferred fault was further defined as the Amargosa fault system by Schweickert and Lahren (1994, 1997), a system that comprises the Stewart Valley, Pahrump Valley, Stateline and (not shown) Ivanpah faults for a total length of about 250 km (Figure 3.3-6).

Schweickert and Lahren (1997) assert that evidence for the fault system includes gravity, seismic, structural, stratigraphic, and paleomagnetic data, the distribution of springs and basaltic volcanic centers, and patterns of Late Quaternary surface faulting. However, no throughgoing surface trace of the fault exists in the tuffs of the southwestern Nevada volcanic field. To explain the dearth of Miocene offset, Schweickert and Lahren appeal to the Hardyman model of surficial detachment. They attribute vertical axis rotations in ashflow tuffs to about 25 km of dextral displacement that may have occurred since about 11.5 Ma, consistent with dextral shear features near Yucca Mountain (normal faults, basalt cones). They point out that study of the exposed rotational normal faults of Yucca Mountain and Crater Flat will provide little information on the character of the strike-slip fault at depth. This statement concerning Yucca Mountain does not hold for the fault system farther south, where the Pahrump Valley fault zone consists of two prominent subparallel strands about 5 km apart that exhibit normal, west-side-down and dextral oblique offset (Hoffard 1991). The faulting here was active from Late Tertiary to Late Quaternary. Projection of the Pahrump Valley fault zone into the southern end of the Amargosa trough follows a N45°W trend, as indicated by various negative Bouguer gravity anomalies that probably reflect pull-aparts along the Amargosa River fault zone (Wright, L.A. 1989; Donovan 1991).

Some observations appear to be inconsistent with the existence of a large throughgoing dextral fault beneath Crater Flat. First, the inferred fault exhibits no throughgoing surface displacement in the Northern Amargosa Basin and in the vicinity of Crater Flat (Piety 1993). Second, inferred movement along the fault appears to have been intermittent with long periods of inactivity. The fault system seems to have been active into Late Oligocene time, then inactive until about 12.7 Ma, when it experienced activity during volcanism centered around this time, then another period of quiescence followed by resumed activity about 3.7 Ma. A 17 m.y. hiatus in extension-related movement along a 250 km long fault system in the Walker Lane is an unusual lapse of activity. Third, an alternative interpretation of the geology (Snow 1992; Snow and Prave 1994) projects the Striped Hills fold west to the Winter Peak anticline and an anticlinal axis in the Southern Funeral Mountains, and shows no offset in folds and south-vergent structures spanning the inferred trace of the Amargosa fault system. Fourth, observations of vertical axis rotation indicate it cannot always be interpreted as diagnostic of a discrete fault zone. For instance, in the Sleeping Butte-Tolicha Peak area near Black Mountain,

13.7 Ma Grouse Canyon Tuff is rotated 10° to 30° clockwise, whereas the unconformably overlying Rainier Mesa Tuff is unrotated; 10 km southwest, Rainier Mesa Tuff is rotated 30° clockwise, whereas Ammonia Tanks Tuff and 9.4 Ma Thirsty Canyon Tuffs are unrotated. This temporal and spatial variability is incompatible with a fixed throughgoing fault. Furthermore, the vertical axis rotation within the Crater Flat Basin does not accommodate 25 km of dextral offset, nor do any of the post-Miocene features between the Sleeping Butte basalts and Stewart Valley account for any significant dextral offset. Evidence of possible Quaternary faulting in Amargosa Valley closest to Yucca Mountain is provided by a group of N70°E-trending lineaments and subdued scarps that are inferred to represent the extension of the left-lateral Rock Valley fault zone (Donovan 1991).

Other interpretations of Quaternary and Late Tertiary strain phenomena suggest that Quaternary transcurrent features are more likely oriented oblique to the Walker Lane than along it. For example, Carr, W.J. (1984) relates all of the basaltic extrusion later cited by Schweickert and Lahren (1997) to the north-northeast trending Death Valley-Pancake Range belt (Crowe, Vaniman et al. 1983), a zone of concentrated Quaternary faulting (Carr, W.J. 1974), seismicity (Rogers, A.M., Harmsen et al. 1983), and basaltic activity that evolved largely in the last 6 to 8 m.y. (Crowe, Vaniman et al. 1983). J.C. Savage et al. (1995) document the central Nevada seismic zone, a "zone of weakness" that cuts across the Walker Lane from the northern end of the Eastern California shear zone. Moderate to large earthquakes that have occurred within the zone (e.g., Pleasant Valley, Dixie Valley, Fairview Peak, and Cedar Mountain earthquakes) appear to be responses of individual faults to stress within a broad N15°W shear zone rather than successive ruptures along a throughgoing fault. J.C. Savage et al. (1995) documented significant extensional strain across the central Nevada shear zone, but virtually no strain at all in the immediate vicinity of Yucca Mountain (Savage, J.C. et al. 1994). These observations indicate present extensional strain leading to active faulting is currently being concentrated along the Eastern California shear zone and the central Nevada shear zone rather than along a 250 km long fault system within and subparallel to the Walker Lane.

The closest potential example of an ancient dextral fault exhibiting clockwise vertical axis rotational features is the Las Vegas Valley shear zone. Sonder et al. (1994) however, concluded their paleomagnetic investigation of the Las Vegas Valley shear zone with the observation that clockwise rotation in the shear zone is likely controlled by the intrinsic rheology of the crust and the dimensions of the shear zone rather than by the location of preexisting faults or weakness in the upper crust.

Paleomagnetic data show that dextral shear that has deformed Yucca Mountain seems to be entirely confined to the Crater Flat domain. The idea that similar areas within the Walker Lane may be linked by a single transcurrent structure is an appealing one for many geologists, but there is no hint of such a structure. This is in contrast to structure west of the Funeral-Bare Mountains domain where long, continuous steep gravity gradients indicate the locations of such faults. The most that can be said for the Walker Lane as far as lateral shear is concerned is that the Walker Lane itself is the transcurrent structure.

3.3.3 A New Tectonic Model for Yucca Mountain

This section describes a new tectonic model for Yucca Mountain that combines aspects of some of the models discussed and evaluated in the previous sections. The model, which generally fits the structural and stratigraphic relations observed at Yucca Mountain, is that of a half graben filled by

a collapsed volcanic carapace (Figure 3.3-12). The structural asymmetry of the half graben, represented by Crater Flat Basin, is clearly shown by seismic reflection data (Brocher, Hart et al. 1996), with Bare Mountain forming the relatively uplifted footwall block to the west. Yucca Mountain is part of the faulted "slab" of volcanic rock that subsided into the half graben. Most of the block-bounding faults in and adjacent to the mountain dip westward and show a history of extension antithetic to the Bare Mountain fault.

The half graben model requires that the Bare Mountain fault be the master fault and that the strata to the east (the hanging wall, of which Yucca Mountain is a part) subside down it, like a falling trapdoor. This mechanical model encounters two problems:

- The cumulative Pleistocene dip slip on the Bare Mountain fault is less than that measured across Yucca Mountain.
- Some faults at Yucca Mountain and in Crater Flat have a down-to-the east offset (Faulds et al. 1994; Brocher and Hunter 1996).

The latter problem can be explained by local keystone faulting in the volcanic carapace, but the former problem is less readily solved. Nevertheless, the asymmetry of Crater Flat Basin, the great structural relief of Bare Mountain (several kilometers), the overall sense of slip on the main block-bounding faults of Yucca Mountain, the profound (about 30 mgal) gravity gradient along the Bare Mountain fault, and the evidence that the Bare Mountain front was the source of large slab slides into Crater Flat in Late Miocene time (Simonds 1995) indicate that the early history of the Bare Mountain fault was that of a master, range-front fault.

The pre-Pleistocene slip history of the Bare Mountain fault lies buried beneath the pediment cover in Crater Flat. The steep part of the gravity gradient, which lies a kilometer or more east of the present range front, indicates that the fault generally dips east at less than 50°. Rather than being a single fault, however, there is the possibility that the Bare Mountain fault consists of an imbricate zone of several more steeply dipping fault planes, variously banked at depth by colluvial wedges or mass movement deposits. The Pleistocene fault trace sampled by recent trenching (Subsection 3.10) may be the most recently active of several synthetic fault planes, and may have the least displacement (see Hancock and Revan 1987, Figure 10).

The form of Crater Flat Basin and its association with the caldera complex led W.J. Carr (1990) to interpret it as a sector graben (see Subsection 3.3.2.3), an area of subsidence caused by evacuation of a body of magma from the base of the crust during or shortly following eruption of the Topopah Spring Tuff. This interpretation accords well with the timing and magnitude of initial faulting of Yucca Mountain as well as the shape and position of the basin. Brun et al. (1994) effectively simulated the structure, in cross section, with a sandbox model that portrayed a low-density viscous mass at the base of the crust.

If the location and longitudinal axis of Crater Flat Basin indicate that it originated as a sector graben, they also imply that it is a flaw within the larger rift-like Amargosa trough (i.e., the Kawich-Greenwater rift of Carr, W.J. [1988, 1990] or the Amargosa Desert rift zone of Wright, L.A. [1989]); that is, it is a rift within a rift. As such, extension within Crater Flat Basin reflects the

structural orientation of the trough and perhaps is linked to basement faulting of greater extent. W.J. Carr (1990) noted the similarity between the faults at Yucca Mountain and a fault population in Pahute Mesa north of the caldera complex and on strike with Yucca Mountain (Figure 3.3-2) (Minor, Sawyer et al. 1993), and surmised that both fault sets reflect extension fundamentally tied to the evolution of the Amargosa trough. Accordingly, Crater Flat Basin can be understood as the southern part of an extended marginal flaw along the western flank of the Amargosa trough; or perhaps even a basin that projects south from the Basin and Range province deep into the Walker Lane. This rift-like aspect of the model downplays the notion of the Bare Mountain fault as a conventional range-front fault. It implies that Pleistocene extensional faulting at Yucca Mountain is not a function of antithetic slip controlled by the Bare Mountain fault, but is instead controlled by axial fractures within the deepest part of the Amargosa trough.

But casting Crater Flat Basin and Yucca Mountain in the context of a trough controlled (at least during its Middle Miocene phase) by dominantly east-west extension raises two questions relevant to faulting at Yucca Mountain:

- What becomes of the Bare Mountain fault at and beyond the south end of Yucca Mountain?
- What is the nature of the fault that bounds the east side of the Amargosa trough near Yucca Mountain?

The southward projection of the Bare Mountain fault is problematic. We infer that the fault is not traceable south of Steve's Pass (Figure 3.3-1) because there it loses its identity (including its expression as a pronounced gravity gradient) among a distributed set of small right-lateral fault segments within a shear zone that steps to the southeast for about 4 km across the dissected escarpment that marks the southern end of Crater Flat. The fault then reassembles, gains dip displacement, and strikes south as the boundary between the Funeral Mountains and the Amargosa trough.

The eastern margin of the Amargosa trough is bounded by the so-called "gravity fault" (Figure 3.3-1). The gravity fault was defined by Winograd and Thordarson (1975) on the basis of a gravity gradient that extends along the spring line in Ash Meadows north to Highway 95 and the west end of the Skeleton Hills. Down-to-the-west displacement is estimated to range from about 150 m at the north end to several hundred meters at the south end. Brocher, Carr et al. (1993), on the basis of seismic profile data, confirmed that the "gravity fault" forms the structural boundary of the east side of the trough at about 36°35'N.

A pronounced coincident gravity and aeromagnetic gradient shows that the "gravity fault" can be carried northward past the west end of Little Skull Mountain. The fault trace passes through the magnetic anomaly that marks the position of the 4.4 Ma buried volcano south of Highway 95. North of this point, a high magnetic anomaly along the gradient suggests that the hanging wall of the "gravity fault" contains considerable basalt or volcanoclastic sediment. There are sparse surface expressions of the "gravity fault." At the west end of the Striped Hills, bedrock exposures indicate strike-slip displacement, but the western flank of Little Skull Mountain is marked by Toreva blocks that indicate down-to-the-west collapse.

The "gravity fault" is an important domain boundary; it separates dominantly east-striking structures associated with the Rock Valley fault system to the east from the north-striking structures of the Amargosa trough-Crater Flat Basin to the west. North of Little Skull Mountain, the trace of the "gravity fault" and the eastern margin of the trough are obscure. The inference is made that the eastern border of the trough trends roughly due north, as expressed by a set of down-to-the west, post-12.7 Ma faults along the west side of the Calico Hills dome (Simonds and Scott 1996).

If the Bare Mountain fault and one or more crustal faults at Yucca Mountain are driven by a deep master fracture zone in the axis of Crater Flat Basin, they may be largely independent of each other in terms of slip budget. This modification of our basic model is based on a mechanism proposed by Okaya and Thompson (1985) and demonstrated by boundary element modeling done for Crater Flat Basin by King and Janssen (Chapter 8 of Whitney 1996). The concept is appealing because it also explains the localization of basaltic volcanism near the axis of the basin: extensional stress is focused along one or more axial fractures or fault intersections at the base of the seismogenic crust. Such intersections can focus dilational strain, even at depths of 15 to 20 km, and thereby facilitate the ascent of basaltic magma to higher crustal levels. The Bare Mountain fault and the Paintbrush Canyon-Stagecoach Road fault likely would be the primary intersecting faults at the deepest crustal level; interaction of these faults at a sufficient strain threshold could be accompanied by basaltic intrusion. It is assumed that such events would cause most faults at Yucca Mountain to slip, including those that might be antithetic to the Bare Mountain fault, and that some fault crevasses might receive basaltic ash fill. G. Thompson (Stanford University, written communication to Whitney, USGS, February 1995) proposed that basaltic dike intrusion would compensate for local extensional stress and significantly reduce deviatoric stress. If so, the strain threshold for post-intrusive faulting at Yucca Mountain would be reset to some higher level. However, as regional extensional stress continues to be applied to the mountain, small strain thresholds are exceeded and weaker faults slip from time to time. Ultimately, the maximum basinal strain threshold is exceeded, at which point the basin may experience widespread faulting associated with basaltic intrusion. This aspect of the model holds that not all faulting at Yucca Mountain is accompanied by volcanism, but that volcanism is always associated with faulting.

The alignment of basaltic cones and vents in Crater Flat follows a northeast trend, oblique to the axis of the basin. Volcanic rocks are clustered in the southwest quadrant of the basin, the area of most recent subsidence and deposition. These facts indicate a distinct tectonic asymmetry linked to processes active within the past 4 m.y. Tectonic asymmetry is also indicated by paleomagnetic evidence for clockwise vertical axis rotation of fault-bounded blocks across the south end of the mountain. The rotation, which is about 30 percent, most likely occurred following deposition of the Tiva Canyon Tuff at about 12.7 Ma (S.A. Minor [USGS Denver], written communication to D. O'Leary [USGS Denver] February 15, 1996). These data support an inference that Crater Flat Basin had evolved as a sphenochasm, opening at its southern end but fixed at its northern end.

This motion is compatible with a northwest-oriented zone of dextral shear at the southern end of the basin, and with a general N50°W-oriented transtensional stress throughout the Walker Lane. In terms of our model, the question is whether oblique dextral shear is confined to Crater Flat Basin (i.e., the basin itself is becoming distorted because of distributed, regional shear), or whether shear is imposed by a regional right-lateral fault that passes through Crater Flat Basin. The latter case has

been argued by Schweickert (1989) and modeled as a pull-apart basin in sandbox experiments by the Center for Nuclear Waste Regulatory Analyses (NRC 1997a, and Section 3.3.2.1 this document).

Nonsystematic distributions of vertical axis rotations in time and space within the southwestern Nevada volcanic field, as reported by Hudson, M.R., Sawyer et al. (1994), imply that individual basins have responded uniquely to distributed northwest-oriented dextral shear typical of the Walker Lane setting. This observation, plus the lack of evidence for transcurrent dextral fault offset of Pleistocene age though Crater Flat Basin, supports the notion that dextral shear is restricted to the basin itself. The only hint of a discrete dextral shear feature within the basin is a N25°W-striking alignment known informally as the hinge line (Figure 3.3-1). The hinge line separates paleomagnetic rotations of 10° or less to the north from rotations of 20° or more to the south. The boundary is more strongly indicated by the divergence of aeromagnetic gradient alignments across the mountain, and by landform terminations along the trace of the hinge line. The hinge line plausibly defines a structural boundary that concentrates dextral shear between it and the southern end of the mountain.

Despite painstaking investigation, researchers have identified no expression of any feature comparable to the hinge line along its projection northwest of Crater Flat. However, a strong structural alignment does exist to the southeast of Crater Flat. This structural alignment extends along Stewart Valley and along the trace of the Pahrump-Stewart Valley fault zone.

The structural alignment, which includes the Yucca Mountain hinge line, is regarded as a likely projection of the Pahrump-Stewart Valley fault zone into, but not through, Crater Flat Basin. The basin may act as a hole that distributes dextral shear, thus accounting for clockwise vertical axis rotation at Yucca Mountain, northeast alignment of basaltic volcanic centers in Crater Flat, dextral shear at the south end of Crater Flat Basin, and a dextral slip component toward the southern end of Bare Mountain fault. Additionally, shear stress concentrated at the edge of the basin may have contributed to uplift of Bare Mountain and Calico Hills within the past 9 m.y.

Yucca Mountain is the morphological expression of a faulted layer about 2.5 km thick of volcanic rock (the carapace) that rests unconformably on a thicker crustal layer (15- to 20-km thick) of Paleozoic and Precambrian marine sedimentary and metasedimentary rocks. This configuration is important because the layers differ greatly in bulk material properties and the underlying layer has a stress history that includes the period of time before the overlying volcanic rocks were deposited. The sub-carapace structure is revealed at Bare Mountain, the Specter Range, and the core of the Calico Hills.

While the major block-bounding faults that have produced large earthquakes during the Quaternary (see Subsections 3.6 and 3.10) must extend deep into the Paleozoic and Precambrian substrate in some fashion, secondary intrablock faults may be confined to the carapace. A speculative model that treats the secondary faults in this way is presented in the following paragraphs.

Much of the fault pattern at Yucca Mountain has the structural characteristics of an arrested slab slide. The abundance of Toreva blocks and graben-like splays; the presence of footwall slices that are only a kilometer or two wide and that pinch out and change elevation along strike; and faults that die out or fray out along strike, that are better described as breccia zones than faults (such as the

Ghost Dance fault) all constitute a pattern of local tearing, spreading, and extensile damage within which it is difficult to discern the traces of deep-seated faults that span the length of the mountain (the trace of the Solitario Canyon fault being an exception). Some of these faults may represent postseismic strain adjustments in the carapace or reflect strain originating within or at its base.

The closest structural analog to Yucca Mountain is the faulted volcanic carapace exposed along the south and west flanks of Mid Valley, about 22 km to the northeast. There, the faulted blocks of Timber Mountain Group and Paintbrush Group Tuffs closely resemble those at Yucca Mountain, except the individual blocks are about half the size. The carapace rests unconformably on an eroded substrate of well-exposed 13 Ma Wahmonie dacite flows that does not reflect the structural attitude of the overlying tilted slices. The Wahmonie volcanic substrate is analogous to the Paleozoic carbonate substrate beneath Yucca Mountain. Two features are important here:

- The Mid Valley carapace has subsided and partly extended into Mid Valley Basin.
- Deep stream erosion has isolated the blocks, facilitating some local faulting and tilting.

These features suggest that the fault pattern in the carapace is a local, slope-controlled phenomenon rather than one controlled by a system of deep-seated faults.

Could such an effect explain some of the fault characteristics at Yucca Mountain? It could work only by way of a weak layer beneath the carapace. Outcrop data indicate that a Miocene sedimentary section is present below the volcanic carapace and above the underlying Paleozoic rocks (c.f. Subsection 3.2.2.2.1). Strata beneath the volcanic carapace in Crater Flat Basin are equivalent to Rocks of Pavits Spring, a pre-14 Ma unit well exposed near Pavits Spring in Rock Valley (Hinrichs 1968). The Rocks of Pavits Spring include weakly consolidated volcanoclastic silts and fine-grained sands. In a saturated state (normal hydrostatic stress), such sediment could be susceptible to undrained failure or abrupt loss of shear strength. For example, soft-sediment faults are exposed below the volcanic section at the base of the south flank of Skull Mountain. Extensive failure of this type may have facilitated the collapse of the south flank of Skull Mountain into Rock Valley. Deformation of this type is well documented in the extensively collapsed Eocene lower Absaroka Volcanic Supergroup, Wyoming (Decker 1991). Additional failure of this type may have been facilitated by weak layers within the carapace (e.g., the nonwelded and bedded tuffs).

In Crater Flat, the extent of a weak layer is unknown. The model assumes that the sediments form a continuous deposit that thins and perhaps pinches out against the Paleozoic rock that forms the relatively elevated eastern rim of Crater Flat Basin. This distribution implies that the eastern margin of Yucca Mountain (east of the Paintbrush Canyon-Stagecoach Road fault) is anchored directly on the Paleozoic substrate (cf. well UE-25p #1; Carr, W.J., Byers et al. 1986), leaving the carapace to the west susceptible to deformation involving a weak layer.

The bulk movement to be expected from weak layer failure is chiefly translational. Such motion could explain the relatively minor offset accompanied by extensive damage along some of the faults. For example, the Drill Hole Wash fault, as projected into the Exploratory Studies Facility, is a breccia zone about 2-m wide that contains rotated blocks as much as a meter in diameter. The characteristic breccia that defines the Ghost Dance fault could also be of oblique extensional origin.

At an early stage of failure and collapse, the entire volcanic carapace may have pulled away from the caldera rim as Crater Flat Basin widened and deepened to the southwest (cf. Fossen and Gabrielsen 1996). Such motion could explain Yucca Wash as a minor extensional structure, as well as account for the odd down-to-the-east offsets along the west side of the mountain. Extension of the carapace to the west is limited by the footwall of the Bare Mountain fault. In situ stress measurements by Stock, J.M. et al. (1985) reveal that the least compressive stress at Yucca Mountain is at the limit of normal fault slip, implying that the carapace may be held together by the strength of the strata on which it rests.

The carapace effect does not explain the long, throughgoing, nearly rectilinear trace of the Solitario Canyon fault, nor the major block-bounding aspect of fault segments such as the Windy Wash fault. Accordingly, the large block-bounding faults (e.g., the Paintbrush Canyon-Stagecoach Road fault, the Solitario Canyon, and Windy Wash faults) must be through-the-crust seismogenic faults, many intra-block faults such as the Ghost Dance fault, may be confined to the carapace.

In summary, the favored tectonic model for Yucca Mountain is that of a half graben that includes the Bare Mountain fault and faults of Yucca Mountain antithetic to the Bare Mountain fault. This model posits the block-bounding faults of Yucca Mountain and the Bare Mountain fault as discrete, single plane faults that descend into the seismogenic crust. It also provides a mechanism for one or more of the block bounding faults to interact with the Bare Mountain fault at the deepest seismogenic level where basaltic magma intrusion may be facilitated by fault displacement or dilation, thus providing a mechanism for coupled volcano-seismic events. Faults of Yucca Mountain antithetic to the Bare Mountain fault mitigates seismic hazard and also partly obviates a fault slip budget tied to activity of the Bare Mountain fault. This fundamental model provides for individual fault scenarios as well as linked and distributed fault scenarios.

Two modifications to the basic model that could account for hidden faults, are entertained: the collapsed carapace effect and a dextral strike-slip fault external to Crater Flat that projects from the southeast into Crater Flat beneath the carapace. These modifications are not exclusive; they are permitted by some data, but require further study to be more than speculative.

3.4 QUATERNARY STRATIGRAPHY AND SURFICIAL PROCESSES

An understanding of the Quaternary stratigraphy in the Yucca Mountain vicinity, and the surficial processes that are largely responsible for its development, are important for assessing a number of issues related to the design and performance of a repository at the site. The Quaternary stratigraphy provides information that can be used to evaluate the recency of fault movement, determine the interval between large earthquakes on major faults, assess recent tectonic activity, determine the characteristics of recent volcanism, assess past climates, and estimate erosion rates. The landforms created by surficial processes are also a factor underlying current land use in the vicinity of Yucca Mountain, which is a consideration in developing a biosphere model for performance assessment. An understanding of surficial processes also has proved valuable in evaluating the genesis of some deposits found near the surface. The results of these studies, when integrated with other project findings, contribute to addressing some of the NRC's key technical issues.

3.4.1 Regional Physiographic Setting

3.4.1.1 Structural Setting

The Yucca Mountain region lies in the north-central part of the Basin and Range physiographic province, within the northernmost subprovince commonly referred to as the Great Basin that encompasses nearly all of Nevada as well as adjacent parts of Utah, Idaho, Oregon, and California. The regions surrounding Yucca Mountain can be further subdivided into several well-defined physiographic areas that reflect regional variations in their geologic characteristics (see also Subsection 3.2). These areas include:

- The large elongate north-northeast-trending basins and ranges of the Central Great Basin.
- The somewhat smaller, more arcuate, and more closely spaced basins and ranges of the Southeast Great Basin.
- The massive ranges and deep basins of the Southwest Great Basin (Inyo-Mono subsection of W.J. Carr 1984).
- The highly variable terrane of the Walker Lane belt, which trends northwest between the southeastern and southwestern segments of the Great Basin toward the south, and between the Central Great Basin and the Sierra Nevada toward the north (Figure 3.4-1). The southern margin of the Great Basin subprovince is considered to be the Garlock fault and its northeast projection. South of this feature lies the northeastern part of the Mojave Desert, characterized by relatively small, irregularly shaped basins and ranges.

The mountain ranges of the Great Basin, mostly tilted fault-bounded blocks, may extend for more than 80 km (50 miles), are generally 8 to 24 km (5 to 15 miles) wide, rise 300 to 1,500 m (1,000 to 5,000 feet) above the floors of the intervening basins, and occupy approximately 40 to 50 percent of the total land area. The deep structural depressions forming the basins contain sedimentary fills of late Tertiary and Quaternary ages ranging in thickness from a few hundred m to more than 3 km. The floors of closed basins are nearly level to gently sloping, and are commonly covered in part by

playas. Open basins are generally moderately to deeply dissected with axial drainage ways. Within this landscape, erosion and erosional processes are concentrated in the high, steep, and relatively wet uplands, whereas deposition and depositional processes are generally concentrated in the low, relatively arid lowlands.

The Yucca Mountain area is located within the Walker Lane belt, which is a major structural lineament considered to be a zone of transition between: the central and southeastern parts of the Great Basin, characterized by dip-slip normal faulting and typical basin-and-range topography; and the southwestern Great Basin, characterized by both dip-slip and right-lateral strike-slip faulting and by irregular topography (Carr, W.J. 1984; Figure 3.4-1). Yucca Mountain itself is situated on the south flank of the southwestern Nevada volcanic field, which consists of a series of volcanic centers from which large volumes of pyroclastic flow and fallout tephra deposits were erupted from about 14.0 to 11.4 Ma (Sawyer, D.A. et al. 1994; Byers, Carr, Orkild et al. 1976; see also Subsections 3.2 and 3.9). Accordingly, the mountain and many of the adjacent landforms carry the imprint of the area's extensive volcanic history as well as its deformational history. The geologic relations suggest that many (and perhaps most) of these landscape features took on their basic topographic form during the period 12.7 to 11.7 Ma.

Yucca Mountain lies near the center of the upper Amargosa River drainage basin, which originates in the Pahute Mesa–Timber Mountain area to the north and includes the main tributary systems of Beatty Wash and Fortymile Wash (Figure 3.4-2). The basic drainage pattern of the area was established soon after caldera collapse and resurgent dome formation that followed the Late Cenozoic eruptions in the southwestern Nevada volcanic field, and the gross pattern has changed little since then (Huber 1988).

3.4.1.2 Climatic Setting

Climatic conditions in the Yucca Mountain region, and over Nevada and much of the southwestern United States, are described in several publications that address this general subject (e.g., Spaulding 1985; Houghton et al. 1975). In general, the climate of South-Central Nevada can be characterized as arid to semiarid, with average annual precipitation ranging from 100 to 200 mm (4 to 8 in) in most lowland areas, 200 to 400 mm (8 to 16 in) over parts of the uplands, and more than 400 mm (16 in) along some mountain crests. This climate exists because the Sierra Nevada Mountains (Figure 3.4-1) are a major barrier to moist air moving in from the west. Precipitation from Pacific air masses that do reach the potential repository area accounts for about 50 percent of the total amount, and occurs during the months of November through April. Precipitation in the form of snow is infrequent.

Summer is generally the driest time of year, but the limited summer precipitation commonly occurs as localized thunderstorms rather than from large-scale frontal activity. These storms have a much greater flood potential than the frontal precipitation that occurs during the winter months because of their release of significant amounts of rainfall in relatively short periods of time. Thunderstorm activity produces a secondary precipitation peak during July and August.

A detailed discussion of the climate at and near Yucca Mountain can be found in Section 4.

3.4.2 Physiographic Setting of Yucca Mountain and Vicinity

3.4.2.1 Description of Major Landform Elements Around Yucca Mountain

The area surrounding Yucca Mountain can be subdivided into eight clearly defined physiographic elements that combine to produce a variable and diverse terrane typical of the Walker Lane (Figure 3.4-2). These are summarized as follows.

Amargosa Desert—The Amargosa Desert occupies a broad northwest-trending basin approximately 80 km long and as much as 30 km wide. The basin is one of the largest in the Southern Great Basin. Its floor slopes gently southeastward from elevations of about 975 m at the north end, near Beatty, to about 600 m toward the south end. The channel of the Amargosa River, into which the streams draining the Yucca Mountain area empty, extends southeastward along the basin axis, then swings westward and northwestward and terminates in the internal drainage system of Death Valley.

Bare Mountain—Bare Mountain is an upfaulted block, consisting of complexly deformed sedimentary and metasedimentary rocks of Paleozoic and Precambrian age, that bounds the west side of Crater Flat. The range, roughly triangular in plan view, is about 20 km long and from less than 2 km to about 10 km wide. Adjacent piedmont surfaces, sloping southwestward into the Amargosa Desert basin and eastward into Crater Flat, respectively, are generally steep and slightly to moderately dissected proximal to the range flanks, but flatten and are largely undissected toward the basin centers. The piedmont-range junction on the east side of Bare Mountain rises gradually from about 915 m at the south end to almost 1,200 m at the north end. Elevations along the range crest vary between 1,460 and 1,925 m. The southwestern flank of the range is embayed by steep, flat-floored valleys. The eastern flank is sharply defined and only slightly embayed, being structurally controlled by the bounding high-angle, east-dipping Bare Mountain normal fault that was active into Quaternary time.

Crater Flat—Crater Flat, flanked by Bare Mountain on the west and Yucca Mountain on the east, is a structural basin approximately 24 km long and 6 to 11 km wide. The basin has the overall form of a graben, its west side having been down-dropped several kilometers along the east-dipping Bare Mountain fault and its east side down-dropped a few hundred m along a series of west-dipping normal faults next to the western slope of Yucca Mountain (Carr, W.J. 1984; Simonds et al. 1995; Fridrich 1998). The axial part of the basin floor, covered by alluvial deposits that overlie a thick (as much as 3 km) sequence of Late Cenozoic volcanic rocks, rises gradually from altitudes of about 840 m at the south end to as much as 1,280 m at the foot of Yucca Mountain to the north. Four basaltic vents and their associated lava flows form prominent cones that attain heights ranging from 27 to 140 m above the alluviated surface of the central basin area. These are described in more detail in Subsection 3.9

Yucca Mountain—Yucca Mountain is an irregularly shaped upland, 6 to 10 km wide and about 40 km long. The crest of the mountain reaches elevations of 1,500 to 1,930 m, about 650 m higher than the floors of adjacent washes in Crater and Jackass Flats. The dominantly north-trending en echelon pattern of ridges and valleys that characterizes this prominent upland is controlled by high-angle faults (Scott and Bonk 1984; Day et al. 1996b) with displacements of several hundred m in places. The fault blocks, composed of fine-grained volcanic rocks, are tilted eastward, so that the

fault-bounded west-facing slopes are generally high, steep, and straight in contrast to the more gentle and commonly deeply dissected east-facing slopes. With the exception of the caprock-protected dip slopes that characterize some of the crest areas, the ridge crests are mostly angular and rugged. The valleys are generally narrow and V-shaped along their upper and middle reaches, but locally contain flat, alluviated floors in their lower reaches. Valley morphology ranges from shallow, straight, steeply sloping gullies and ravines to relatively deep, bifurcating, gently sloping valleys and canyons. The hillslopes between ridge crests and valley floors typically include at least three general forms: narrow upper convexities, extensive straight segments, and broad lower concavities. Drainage from the west flank of the mountain flows southward down narrow fault-controlled canyons and out into Crater Flat. Drainage from the east flank flows southeastward down Yucca, Drill Hole, and Dune Washes into Fortymile Wash.

Fortymile Wash—Fortymile Wash drains an area of approximately 620 km² east and northeast of Yucca Mountain. From its northern headwaters, it flows southward through Fortymile Canyon, a steep-sided drainage course some 300 m deep along the east side of Pinnacles Ridge, and continues down the south-sloping piedmont that forms the west end of Jackass Flat. Along this latter reach, the wash has cut a nearly linear trench, 150 to 600 m wide and as much as 25 m deep, into the Quaternary alluvial deposits of the piedmont. This entrenchment gradually decreases downslope until the wash merges with the general level of the piedmont near the northeastern margin of the Amargosa Desert basin.

Jackass Flats—Jackass Flats is an asymmetric alluviated basin, 8 to 10 km wide and nearly 20 km long, that lies east of Yucca Mountain and Fortymile Wash. It is formed principally by piedmonts that slope away from bounding highlands to the north, east, and south, merge in the central basin area, and descend gradually westward and southwestward toward Fortymile Wash. Toward the highlands, the piedmont areas are moderately dissected, with shallow (5 to 10 m deep) arroyos and rounded interfluves; elsewhere, the basin floor is largely undissected. Topopah Wash is the main axial drainage.

Pinnacles Ridge—Pinnacles Ridge is a roughly triangular upland, about 11 km long and 6 km wide, that is bounded by Beatty Wash on the north, Fortymile Wash on the east, and Yucca Mountain on the southwest. The ridge is contiguous with and extends southeastward from the northeastern flank of Yucca Mountain. Its south flank is structurally and lithologically similar to Yucca Mountain, and its crest is the eroded southern margin of the Timber Mountain caldera (Carr, W.J. 1984), one of the main centers of eruption in the southwestern Nevada volcanic field (see Subsections 3.2 and 3.9). The ridge crest rises 250 to 670 m above the prominent washes that surround it, and tributaries to these washes have cut deep, linear valleys into its flanks.

Beatty Wash—Beatty Wash, one of the larger tributaries of the upper Amargosa River, drains an irregularly shaped area of about 250 km² north of Yucca Mountain and Pinnacles Ridge. The basin topography is generally steep and irregular, with valley depths ranging from about 200 to 790 m. Total relief from the mouth of the basin to the crest of Timber Mountain to the north exceeds 1,200 m.

3.4.2.2 Influences on Geomorphology

3.4.2.2.1 Tectonics/Faulting

As described above, Yucca Mountain is one of a series of en echelon fault blocks formed by a series of parallel, north-striking, primarily dip-slip faults that have sliced up a broad apron of Miocene ashflow tuffs. The faults have been active during the Quaternary, as shown by detailed mapping (Simonds et al. 1995) and by trenching studies on each fault (Whitney and Taylor 1996). The details of Quaternary paleoseismic behavior at Yucca Mountain are summarized in Subsection 3.10.6.

Quaternary offset along block-bounding faults have influenced depositional patterns on hillslopes and on adjacent valley or basin floors. Average rates of offset from the middle Quaternary to the present range from 0.002 mm/yr to 0.04 mm/yr for all faults and the average for all faults is about 0.01 mm/year, or about one meter of offset every 100,000 years. These are very low rates of offset, and the paleoseismic studies on each fault indicate that surface-faulting earthquakes have long return times of about 20,000 to 100,000 years. This low rate of faulting has resulted in subtle landforms, and has been a contributing factor to the preservation of Early and Middle Pleistocene deposits on Yucca Mountain hillslopes (Whitney and Harrington 1993). A striking feature of Yucca Mountain hillslopes is the lack of well-defined, rounded alluvial fans at the base of the slopes. On the west side of Yucca Mountain, hillslopes are of nearly uniform gradients, decreasing gradually from 32° near ridge tops to about 15° near the base, because of the homogeneous nature of the underlying volcanic tuff at the ridge crest, and because the low rates of uplift have not caused over-steepened slopes or high relief. The lower slopes of the Yucca Mountain appear more like pediments than alluvial fans. This pedimentation of lower hillslopes is evident in fault trenches (Figure 3.4-3) on Bow Ridge (trench 14-d) and the main Yucca Mountain western hillslope (trench SCF-T1), where Early and Middle Pleistocene deposits are truncated and overlain by a thin veneer (less than one meter thick) of Late Pleistocene-Holocene alluvium.

Fault scarps are commonly visible along the block-bounding faults. The scarps are generally located between the bedrock footwall and colluvium on the hanging wall. The bedrock scarps appear sharp with fault dips of 55° to 75° because the volcanic bedrock weathers very slowly (see bedrock weathering rates below). The exposed fault scarps along the Solitario Canyon and Northern Windy Wash faults were exposure-dated by cosmogenic ¹⁴C in order to determine whether the scarps may have been formed by Holocene surface ruptures (Harrington, Whitney et al. 1994). Analyses of the in situ cosmogenic radiocarbon from both scarps indicate both scarps have been exposed for greater than 20,000 years. A pattern of enhanced erosion at the base of the scarps near channels and rills indicates that the scarps have been significantly enhanced by hillslope erosion. The Stagecoach Road fault also exhibits a prominent scarp where eolian sand has washed away from a scarp formed in a well-cemented, reworked tuff. Thus, most prominent scarps at Yucca Mountain appear to be fault-line scarps, tectonic in origin but significantly enhanced by erosion.

3.4.2.2.2 Volcanology

Although Yucca Mountain is comprised entirely of volcanic rocks, none of the original morphology is preserved except for the eastward dip-slope formed by tilting of the block by movement along the block-bounding faults. The volcanic morphology of the Timber Mountain caldera is fairly well

preserved such that the topographically high resurgent dome in the center of the caldera and the surrounding moat are readily visible in either aerial photographs or topographic maps. The morphology of younger volcanic features in the immediate vicinity of the mountain vary from poorly to extremely well preserved. Details on igneous activity in the Yucca Mountain area are found in Subsection 3.9.

The volcanic topography associated with the 3.7 Ma basaltic centers in Central Crater Flat (Figure 3.4-2, see also Figure 3.2-12) has been strongly modified by erosion. The original volcanic cones are deeply eroded, exposing dikes that formed along fissures from which the lava was extruded into these centers. The limited area of flow surfaces exposed along the Windy Wash fault possess no original topography and are everywhere formed on the non vesicular basalts of the flow interior.

Four middle Quaternary cinder cones (ca. 1 Ma) are fairly well preserved. Several near-surface features such as pressure ridges and bombs with original morphology are preserved at these eruptive centers.

The youngest volcanic center is the Lathrop Wells crater. Cosmogenic ^3He and ^{36}Cl dating of the flow surfaces of the Lathrop Wells center demonstrate there has been no apparent topographic modification (pristine flow structure is still present), although the surfaces have been exposed to the climatic conditions of the last ca. 80 ky. The Lathrop Wells Cone itself shows little sign of degradation, which initially prompted speculation that it might be as young as 10,000 years old (Wells et al. 1990b).

3.4.3 Surficial Geology

3.4.3.1 Surficial Geologic Mapping in the Yucca Mountain Area

Surficial mapping of Quaternary deposits in the Yucca Mountain Site Area has been progressively refined over the years, and Table 3.4-1 compares various units designated by different studies within the region. Early work in the Nevada Test Site region differentiated three major late Cenozoic stratigraphic units using correlation characteristics (Hoover, D.L. and Morrison 1980; Hoover, D.L. et al. 1981; Swadley et al. 1984; Hoover, D.L. 1989). This original work was patterned after work done in the Vidal Junction area in the Mojave Desert of Southern California (Ku et al. 1979; Bull and Ku 1975; Bull 1991). The concept of "correlation characteristics" utilizes physical and morphologic characteristics of landscape elements, including landform, drainage network, soils (the presence or absence of the Av horizon), topographic position, desert pavement, desert varnish, depositional environment, and lithology. According to these original studies, the oldest surficial unit, QTa, is Quaternary (early Pleistocene) or Tertiary in age or both. Units Q2 and Q1 represent middle-to-late Pleistocene and Holocene deposits, respectively. Each major geologic unit of Hoover, D.L. et al. (1981) is divided yielding a total of 10 subunits. According to Hoover, D.L. et al. (1981, p.8) "three additional subunits of uncertain age may belong in unit Q2" in the Nevada Test Site region. Swadley (1983; Swadley and Carr 1987; Swadley and Parrish 1988; Swadley and Huckins 1989, 1990) mapped the major late Cenozoic stratigraphic units on the east and west sides of Yucca Mountain, but no detailed surficial geologic mapping subdividing these units was published for Midway Valley until E.M. Taylor (1986) mapped the fluvial terrace sequence along Yucca and Fortymile Washes.

E.M. Taylor (1986) mapped six Tertiary to Quaternary geologic units along Yucca and Fortymile Washes. Geologic units were distinguished, and pedogenic soil profiles were described from these units to assess the influence of time and climate on soil development, and to quantify the variability in past Quaternary climates by modeling the degree of development of the calcic horizon. The ages of map units were assigned based on an inferred correlation with the stratigraphy and numerical dates of Hoover, D.L. et al. (1981); Szabo et al. (1981); and Hoover (1989). E.M. Taylor (1986) demonstrated that age correlates with soil morphology and the progressive accumulation of secondary carbonate, clay, and silica. Calcium carbonate, calcium-magnesium carbonate, and other carbonate species in soils were not distinguished; the term "carbonate" was used to refer to all pedogenic carbonate species. The term "silica" was used to refer to pedogenic silica species, which was shown to be predominately opal-CT (Vaniman, Bish, and Chipera 1988). Taylor's work clearly demonstrated the usefulness of soils for stratigraphic correlations and the estimation of the age of surficial units within the Yucca Mountain area.

Six major allostratigraphic units were mapped by Peterson, F.F (1988), Faulds et al. (1994), and Peterson, F.F. et al. (1995) in the Crater Flat area, located less than 5 km west of Midway Valley. The primary purpose of their soils-geomorphic study was to evaluate the ages and correlations of the Quaternary surficial deposits stratigraphy (QTa, Q2, and Q1) of Hoover 1989. Two allostratigraphic units were delineated within areas previously mapped as QTa, two allostratigraphic units were delineated in areas previously mapped as Q2bc (undifferentiated Q2b and Q2c), and the use (in earlier studies) of the Av horizon as a major criterion for distinguishing Pleistocene from Holocene surfaces was questioned by Peterson, F.F. (1988). Additionally, numerical ages of allostratigraphic units are younger than numerical age estimates of surficial deposit units of earlier studies by factors of about 2 to 10. However, the numerical age estimates for both the earlier and more recent studies are uncertain because of the experimental nature of radiocarbon dating of rock varnish, varnish cation-ratio dating, thermoluminescence dating of coarse alluvial deposits, and uranium-series dating of pedogenic carbonate and silica, and the lack of reliability of uranium-trend dating (Rosholt 1980; Szabo et al. 1981; Rosholt et al. 1985; Szabo and O'Malley 1985; Harrington and Whitney 1987; Dorn 1988; Harrington et al. 1990; Krier et al. 1990; Bierman and Gillespie 1990, 1991, 1994; Reneau and Raymond 1991; Reneau et al. 1992; Reneau 1993).

Wesling et al. (1992) mapped the surficial geology of Midway Valley at a scale of 1:6,000, and Lundstrom et al. S.C. Lundstrom and E.M. Taylor, *Preliminary Surficial Deposits Map of the Southern Half of the Topopah Spring NW 7.5-minute Quadrangle*, USGS-OFR-95-132, in press, GS940108315142.005, MOL.19960403.0218; S.C. Lundstrom et al., *Preliminary Surficial Deposits Map of the Northwest Quarter of the Busted Butte 7.5-minute Quadrangle*, U.S. Geological Survey, Open File Report, in press, GS940708315142.008; S.C. Lundstrom et al., *Preliminary Surficial Deposits Map of the Northeast Quarter of the Busted Butte 7.5' Quadrangle, Nye County, Nevada*, U.S. Geological Survey, Open File Report, in press, GS940108315142.004 mapped the surficial geology of Eastern and Southern Yucca Mountain area at a scale of 1:12,000. These studies delineate alluvial geomorphic surfaces (as defined by Bull and Ku 1975; Bull 1991) that represent informal allostratigraphic units that consist of deposits separated by bounding unconformities such as geomorphic surfaces. Eight alluvial geomorphic surfaces (Q0 through Q7) ranging in age from Plio-Pleistocene to Holocene, as well as colluvium and eolian deposits, are identified on these maps and are described in a later section.

3.4.3.2 Geochronology

The development of geomorphology in the Yucca Mountain region is dependent upon several geologic variables such as tectonics, climate and time. Quantitative dating of Quaternary units is difficult owing to the paucity of chronometers well-suited to the last 1 m.y. and the lack of material that meets ideal geochronologic criteria such as closed system behavior for isotopic systems and a short period of formation relative to the age of the system. Soils, for example, may form over periods of thousands of years and be only a few thousand to tens of thousands of years old. Several different methods on a variety of materials have been used in an attempt to quantify timing and rates of surficial processes in the Yucca Mountain vicinity. A compilation of all age determinations for Quaternary materials in the Yucca Mountain region is given in Table 3.4-2. Figure 3.4-3 shows the locations of fault trenches in the immediate vicinity of Yucca Mountain from which many of the samples were obtained.

The age estimates in Table 3.4-2 exhibit variability with respect to their inferred Quaternary stratigraphic unit. This scatter is due to several causes. Some of the data were collected during the early stages of the program when geochronologic techniques were just under development. Each technique includes explicit assumptions that may not be met by each sample. Table 3.4-2 is comprehensive; in using age estimates to support interpretations, scientific judgment is used to select reliable data.

The dating techniques include methods that provide:

- Estimates of ages of surfaces, which can be done using ^{14}C or cation-ratio dating of rock varnish and in situ, cosmogenic nuclide dating such as ^{36}Cl or ^{14}C . These methods assume that the material sampled has been on the surface for the entire history of the surface, and as such they represent minimum ages. Uncertainties include the possibility that sampled material has a history prior to its inclusion on the surface being dated.
- Estimates of deposit ages by included material, which can be done on the basis of archaeology, ^{14}C on charcoal, or tephrochronology. These assume that the material did not have a pre-history or in the case of charcoal, that the sample has not gained or lost carbon since burial.
- Soil age estimates, which can be done using thermoluminescence on the fine-grained component of soil or uranium-series on the secondary carbonate. The secondary carbonate yields a minimum age because the soil had to exist prior to build up of carbonate. Thermoluminescence based age estimates assume that samples collected below the modern surface do not contain secondary eolian additions and that the sample was not exposed to sunlight at some point during its history.

Each technique provides an age estimate with consequent geologic interpretations. Ideally, more than one dating technique should be used at each site to estimate the time of a tectonic event or the age of a stratigraphic unit. This occurs, however, infrequently in the study area owing to the lack of suitable materials.

Carbon-14 and cation-ratio dating on rock varnish—Rock varnish dates have been determined for samples from surfaces in the Crater Flat area. These dates provide the age of surface samples and thus give a minimum age for the underlying deposit. The range of applicability for ^{14}C is about 300 to 60,000 years; the cation-ratio technique is limited by regional calibration points to about 1.5 Ma in the Yucca Mountain area.

In situ cosmogenic nuclide method—The in situ cosmogenic nuclide method determines a rock surface exposure history from measurements of rare nuclides produced in rocks by cosmic radiation. The method records the time a rock has been exposed on the Earth's surface. The chief uncertainty associated with this method relates to temporal variation in the cosmic ray flux. The main method used was the measurement of ^{10}Be .

Archaeology—One artifact has been recognized in soil about 50 cm below the surface in a trench excavated on the east side of Bare Mountain. An artifact produced during a distinct time interval by early habitants of the region, collected from within a deposit, can provide an estimate of the maximum age of the deposit. In Southern Nevada, the maximum age range of artifacts is about 10,000 years. Although bioturbation of the soil may incorporate a younger artifact into an older deposit, no evidence for reworking was noted at the sample site.

Carbon-14 on charcoal—Charcoal from a few sites near Beatty has been dated. Although ^{14}C is a well accepted dating technique, its use in the Yucca Mountain region is severely limited by the paucity of datable material. If one assumes that the datable material was deposited with the alluvium, shortly after it formed, dates obtained provide a maximum age estimate for the deposit.

Tephrochronology—Ash has been collected from sand ramps, trenches, and spring deposits. The presence of an airfall ash, which is geochemically distinct or otherwise recognizable, provides an age estimate based on a known age for the ash. Ash samples should not be reworked because a reworked ash will record the age of the airfall event and not the younger age of deposition. The presence of airfall ash in a deposit provides a maximum age estimate for the deposit.

Thermoluminescence—Material collected in the Yucca Mountain area has included soil vesicular A horizons (buried and at the surface), colluvium with reworked eolian sand (sand ramps), buried alluvial fine-grained overbank deposits, eolian-rich tectonic wedges, silica-cemented Bt horizons, and fine-grained groundwater discharge deposits. Several of these applications differ significantly from materials for which the technique was developed. For example, translocation of fine-grained material to depth within a deposit can result in ages that are too young. The thermoluminescence technique provides an age when the material dated was last exposed to sunlight, and as such, provides a minimum age for a deposit.

Uranium-series—Uranium-series dating has been used on pedogenic calcium carbonate and silica. The early dating (pre-1993) used alpha spectrometry to measure isotopic concentrations, whereas the more recent dating has utilized the more accurate mass spectrometric technique. Uranium-series dating assumes that carbonate or opal, once precipitated, is in a closed system. The technique produces a minimum age of the soil in which the dated minerals formed.

Uranium-trend analyses—Uranium-trend ages were based upon an assumed open system following the model proposed by Rosholt (1980). Recent work has shown that these ages are usually unreliable and that there is no a priori way to determine which ages are in error. Thus, uranium-trend ages are not included in Table 3.4-2.

3.4.3.3 Quaternary Stratigraphy

The symbols for Quaternary and Tertiary stratigraphy used in this subsection are as follows. Uppercase Q or T indicate age of the unit as Quaternary or Tertiary, respectively or that the unit could be either or both when both letters are used. If the uppercase letter is followed by a lowercase letter, that letter indicates the type of deposit: a = alluvium, c = colluvium, e = eolian, sd = spring deposits, and no letter = undifferentiated as to type of deposit. Qu is undifferentiated, with respect to age or stratigraphic position, Quaternary deposits. Numbers in the symbol indicate relative stratigraphic position with 0 being the oldest. Letters after a number represent subdivisions of a unit. General characteristics of surfaces and soils developed on surficial deposits and geomorphic surfaces are given in Table 3.4-3.

3.4.3.3.1 Quaternary Deposits, Soils, and Geomorphic Surfaces

An alluvial geomorphic surface is the same as the top of an allostratigraphic unit. Such a unit is defined as a mappable stratiform body that is defined and delineated based on its bounding discontinuities (North American Commission on Stratigraphic Nomenclature 1983). Primary characteristics used to assess the relative stratigraphic ages of the map units include relative stratigraphic and geomorphic position, lithologic characteristics, degree of desert pavement development, amount and degree of desert varnish accumulation, degree of preservation of original bar-and-swale topography, and degree of soil profile development.

Surficial deposits in the Yucca Mountain area include alluvium that underlies alluvial fan and fluvial terrace surfaces and is deposited along active washes, colluvium and debris-flow deposits that occur along the base and mantle the lower parts of the hillslopes, areas of mixed bedrock and thin colluvium, and eolian deposits.

The informal allostratigraphic units have age-dependent surface properties that reflect interactions and feedback mechanisms among soil development, eolian deposition, clast weathering, desert varnish accumulation, biological activity, and progressive erosional instability. Young units (Qa5-Qa7) exhibit relatively unaltered original surface characteristics, including incipient to weak soil development, no to nascent desert varnish accumulation, little to no desert pavement development, relatively unaltered bar-and-swale relief, and minimal eolian accumulations in the upper horizons of soil profiles. Older units (Qa2-Qa4) have more strongly developed desert pavement, more continuously and darkly varnished clasts, greatly reduced bar-and-swale relief, strongly developed soils, and relatively thick accumulations of silt and fine sand in the upper parts of soil profiles. The oldest units (QT0 and Qa1) have degraded surface characteristics and soil profiles reflecting erosional modification of geomorphic surfaces.

The relative ages of the deposits, soils, and geomorphic surfaces around Yucca Mountain are well established, but there is only limited direct numerical age control. Most numerical ages are derived from colluvium in trenches dug to evaluate fault activity on the major faults.

Available numerical age control (Table 3.4-1), relative-age data, and regional soil-stratigraphic correlations (Table 3.4-1) were used to assign ages to map units. Establishing exact numerical ages of surficial units in arid environments is difficult because of the time-transgressive nature of fluvial deposition and geomorphic surface development, the paucity of suitable materials for dating, and the imprecise nature of dating complex geomorphic and pedogenic systems using available dating methodologies (uranium-series dating of pedogenic carbonate and thermoluminescence dating of the silt-size fraction of eolian and fluvial sediments). The presence of the 0.76 million years old (Ma) Bishop tephra and several minor late Pleistocene basaltic ashes in Quaternary sediments of the Yucca Mountain region potentially can contribute significantly to numerical dating studies. However, the usefulness of the basaltic ashes may be limited because of extensive reworking of the tephras at some localities, the apparent inability to differentiate geochemically among different tephras, and large age uncertainties that result from indirect dating of the tephras. Correlations to other desert soil chronosequences based on soil-stratigraphic studies is another important technique for estimating the ages of surficial units, but quantitative soil chemistry and particle size data are unavailable to rigorously assess ages. Based on these considerations, a multiple-parameter dating approach was used to estimate the ages of surficial units. Ages of the principal alluvial units, based on thermoluminescence dates, tephrochronology, U-series dates, and correlations of soils to other desert chronosequences, are as follows:

- Qa7 latest Holocene to historic
- Qa6 middle-to-late Holocene to historic
- Qa5 late Pleistocene to middle Holocene
- Qa4 late Pleistocene
- Qa3 middle-to-late Pleistocene
- Qa2 middle Pleistocene
- Qa1 early-to-middle Pleistocene
- QTa0 Pliocene to early Pleistocene (?)

The approximate numerical ages for the above subdivisions of the Tertiary and Quaternary Epochs are shown in Table 3.4-4.

3.4.3.3.1.1 Alluvial Deposits and Geomorphic Surfaces

Alluvial geomorphic surfaces compose the bulk of boundaries for surficial units in the Yucca Mountain Site Area. Deposits associated with these surfaces include alluvium, and minor eolian and debris-flow sediments. Sedimentologic properties of the various alluvial units are very similar. In general, fluvial deposits are predominately sandy gravel with interbedded gravelly sand and sand. Fluvial facies present in these deposits include relatively coarse-grained channel bars and intervening finer-grained swales. The grain size of the bars and swales is dependent on their position within the landscape (proximal or distal fan region) and the sediment source. In the proximal alluvial fan regions, grain size is greater where larger material is available for transport and where stream flow is concentrated. In the distal reaches of the fans sediment is finer grained, although coarser-grained

facies are present locally. Gravel size ranges from pebble to boulder, and clasts generally are subangular to subrounded. In soil-pit and stream-cut exposures of Qa5, Qa6, and Qa7 the cross-sectional bar-and-swale characteristics are so well preserved that the changes in facies between the bars and swales is readily observed. The deposits associated with depositional bars include non-indurated, cobble-boulder gravel and a finer-grained sand and gravel deposit. The deposits associated with swales include a finer-grained, silt-rich, sandy gravel and gravelly sand. The boulder gravel associated with the bars typically is about 0.5 m thick. Unweathered deposits are light grey (10YR 7/2 d), poorly to moderately sorted, massive to well bedded, and clast supported to matrix supported (Notation refers to Munsell Soil Color Chart [Munsell Color Company 1988] d=dry, m=moist). Rodent burrows are ubiquitous on Qa5 and Qa6, most likely reflecting the ease of excavation. Qa5 and younger deposits are relatively loose and do not hold a well-formed free face when excavated. In soil pits and stream-cut exposures buried soils are commonly observed in intervals less than 2 to 3 m thick. These buried soils may be older stratigraphic mapping units that have been buried, or they may represent a hiatus in the aggradational sequence of a single depositional unit. In cases where the buried soils represent a hiatus in a single depositional sequence, the surface soil characteristics reflect these variations in the amount of time they have been exposed. These variabilities are expressed in the range of soils developed on a single mapping unit.

Debris-flow deposits were observed locally in natural outcrops, soil pits, and trenches. These deposits are matrix supported and have pebbly to cobbly, silty, fine to medium sand texture. The gravel fraction composes approximately 15 to 30 percent of the deposit. Debris-flow deposits are nonbedded and massive and have a relatively hard consistency.

Given the similarities in sedimentologic properties of deposits among the various map units, distinctive surface properties and soil profile characteristics were the primary features used to delineate and correlate map units. These features, along with available numerical-age information, serve as a basis for assigning ages to units and for correlating with sections in local and regional soil-stratigraphic studies. The characteristics of eight identified alluvial geomorphic surfaces, their associated soil profiles, and the available numerical age control, and correlations with local and regional studies are described below for each major mapped unit.

Pliocene to Early Pleistocene Alluvium (QT0)—QT0 consists of a single terrace remnant on the upthrown block of the Paintbrush Canyon fault at the north end of Alice Ridge, although this unit is also found and mapped outside the Yucca Mountain area in Mercury Valley. The surface forms a pronounced topographic bench (elevation 1,168 m) that is 25 m higher than Qa1 and 46 m above the active channel of Yucca Wash. Deposits associated with QT0 consist of lag gravel on a bedrock surface eroded into the Tiva Canyon Tuff. Clast lithologies that include the rhyolites of Fortymile Wash are sufficiently abundant and distinct to indicate that they are exotic to Alice Ridge. Because of its limited areal extent and the extensive post-depositional erosion of the surface, no detailed soils data were collected for the QT0 surface. One unique characteristic of the deposit is that the cemented matrix is commonly more resistant to erosion than the clasts. The thickness of the unit is unknown but is probably less than a few meters.

The age of QT0 is probably early Quaternary to Tertiary based on its stratigraphic position relative to Qa1, its highly dissected and eroded nature, and it has a rounded landform morphology. Lundstrom et al. (S.C. Lundstrom et al., *Preliminary Surficial Deposits Map of the Northeast*

Quarter of the Busted Butte 7.5' Quadrangle, Nye County, Nevada, U.S. Geological Survey, Open File Report, in press, GS940108315142.004) speculate that probable Tertiary deposits (their unit Tgp) along Fortymile Wash may be correlative to QT0 because of their similar heights above the modern washes and their rounded landform morphology. Although no soil was observed on QT0 (eroded), the partially preserved soil on Tgp has a strongly developed K horizon about twice as thick as the K horizon of the Qa1 soil. If these units are correlative, QT0 is probably Tertiary in age.

Early to Middle Pleistocene Alluvium (Qa1)—Qa1 is preserved at the surface on the Yucca Wash alluvial fan north of Sever Wash in Midway Valley; the fan surface has been dissected by younger drainages and is preserved as somewhat rounded interfluves. Qa1 also is found on the west flank of Yucca Mountain and in Northeastern Crater Flat. Locally, the desert pavement associated with the Qa1 surface is very well developed, but in most areas it has been extensively degraded (Table 3.4-3). Several characteristics, including freshly exposed rock surfaces on clasts, fragments of secondary carbonate and silica platelets, and surface or near-surface calcic horizons, collectively impart a lighter tonal quality to the unit when viewed in the field or on aerial photographs. Although darkly varnished clasts are present in some areas, surface clasts typically are not darkly varnished. No original depositional bar-and-swale morphology is preserved on the surface, and larger clasts appear to be distributed randomly rather than being concentrated in areas that define depositional bars. Angular unvarnished rock fragments are common on the surface owing to spallation of larger varnished clasts and exposure of fresh rock surfaces. Many clasts are fractured and strongly weathered. The total thickness of Qa1 cannot be determined from available exposures. A buried soil was observed beneath Qa1 at a depth of 2.5 m in one soil pit, but no buried soils were encountered to depths of more than 3.3 m in other soil pits on Qa1.

The strongly developed Qa1 soil is greater than 1.5 to 2.0 m thick and has a laminar petrocalcic horizon (Kqm) with stage IV carbonate morphology (cf. Gile et al. 1966) at or near the surface (Table 3.4-3). The petrocalcic horizon may be overlain by as much as 30 cm of eolian fine sand and silt. Soil development on the eolian deposits is characterized by brownish to reddish (10-7.5YR hues) Btk and Btkq horizons that have strong, medium subangular blocky structure and continuous, moderately thick clay films. The soil developed in the overlying eolian sand and silts appear to be much younger than the underlying petrocalcic horizon formed in alluvial sediments.

Age control for Qa1 indicates that the unit is probably early-to-middle Pleistocene. Swadley et al. (1984) mapped Qa1 as QTa in Northern Midway Valley where Qa1 is present, and Hoover (1989) notes that the best developed soils and landforms that are representative of QTa occur in Northern Midway Valley. These workers assign a Pliocene to early Pleistocene age to QTa, but Hoover (1989) notes that the unit is probably only Pleistocene in age. In other parts of the Yucca Mountain area, deposits mapped as QTa overlie alluvial sediments of the ancestral Rock Valley Wash that contain a 2.1 Ma ash. Swadley and Hoover (1989a, 1989b) and Hoover (1989) note that eolian (Q2e) and alluvial (Q2c) sediments younger than QTa contain the Bishop tephra (~740 ka, Sarna-Wojcicki and Pringle 1992; van-den-Bogaard and Schirnack 1995) at several locations within the Yucca Mountain area. However, Peterson, F.F. et al. (1995) report Bishop tephra within alluvial deposits that were mapped as QTa by Swadley et al. (1984) in Northeastern Crater Flat. Peterson, F.F. (1988) and Peterson, F.F. et al. (1995) map this unit in Crater Flat as their Solitario geomorphic surface and assign a numerical age between about 430 ka to 740 ka based on the varnish cation-ratio

ages and the reported presence of the Bishop tephra. The evaluation of stratigraphic position and geochemical identification of these tephras are in progress.

An early-to-middle Pleistocene age for Qa1 is supported by regional soil-stratigraphic correlations. The somewhat rounded, eroded morphology of Qa1 surfaces and the strongly developed soil on Qa1 are similar to those on early-to-middle Pleistocene units in Nevada and California (Table 3.4-1) (Taylor, E.M. 1986; Wells et al. 1990b; Harden et al. 1991a, 1991b; Slate 1991; Reheis et al. 1992; McDonald and McFadden 1994).

Middle Pleistocene Alluvium (Qa2)—Qa2 is recognized at the surface primarily as thin elongated patches of alluvium in Midway Valley, where it is inset into Qa1. On color aerial photographs, Qa2 surfaces have a darker, more reddish hue than the other units. This darker color and reddish hue reflect more compact and continuous desert pavement, better developed desert varnish, and the presence of reddish Bt horizons near the surface. Qa2 has a well-developed desert pavement that contains darkly varnished clasts (Table 3.4-3). Some clasts are split and fractured, and varnish has also developed on some fractured surfaces of clasts. The original bar-and-swale morphology has been reduced to the height of the larger clasts above the surface. The upper part of the unit typically has a cap of eolian silt and fine sand ranging from 30 to 50 cm thick. The total thickness of Qa2 varies from 2.5 to more than 3.5 m as observed in soil pits.

The strongly developed Qa2 soil has a 40 to 70 cm thick, reddish (7.5-5YR hues) argillic horizon (Btkq) and a zone of carbonate and silica accumulation having stage II to III+ carbonate morphology (Table 3.4-3). The upper solum (Av and Btkq horizons) of the Qa2 soil is cumulate and has formed in the eolian sediments that have accumulated on the surface (Table 3.4-3). The upper part of the Btkq horizon lacks significant carbonate but contains a silica-cemented zone that is reddish brown to yellowish red (5YR 5/4-6 d) in color and is laminar in appearance. Therefore, the morphology of the upper part of the soil is controlled by silica accumulation, whereas the morphology of the lower part of the soil is controlled by both carbonate and silica accumulation. This gives the Qa2 soil an appearance of overall stage IV morphology.

A middle Pleistocene age for Qa2 is supported by its stratigraphic position between the early-to-middle Pleistocene Qa1 and the middle-to-late Pleistocene Qa3, and the degree of soil profile development. The degree of soil profile development on the Qa2 alluvial geomorphic surface appears to be similar to that on Q2c or QTa of E.M. Taylor (1986) and Harden et al. (1991b, 1991c). Based on correlations with local and regional soil chronosequence studies (Taylor, E.M. 1986; Wells et al. 1990b; Harden et al. 1991a, 1991b; Slate 1991; Reheis et al. 1992; McDonald and McFadden 1994), Qa2 is probably middle Pleistocene in age.

Middle to Late Pleistocene Alluvium (Qa3)—Qa3 occurs as large remnant alluvial fan surfaces and as fluvial terraces. It is one of the dominant map units in the Yucca Mountain area and underlies the main Fortymile Wash terrace. A well-developed desert pavement that contains darkly varnished clasts characterizes the Qa3 surface that has a dark brown or black tone on color aerial photographs (Table 3.4-3). Larger clasts, some more than 30 cm in diameter, are distributed on the surface in diffuse, poorly defined bars. (Clast size as given in this report is maximum intermediate diameter unless otherwise stated.) The original depositional bar-and-swale morphology has been reduced to

the height of individual clasts above the surface. The thickness of Qa3 averages approximately 2 to 2.5 m and may exceed 3.3 m locally as observed in soil pits.

The strongly developed Qa3 soil has a 20 to 75 cm thick argillic (Bt and Btkq) horizon overlying a 100 to 130 cm thick horizon of secondary carbonate and silica accumulation (Table 3.4-3). Clay films, reddening (7.5YR hue), and strong blocky structure are characteristic of the argillic horizon that also commonly has accumulations of secondary carbonate and silica. A Bkq or weakly developed Kq horizon having Stage II to III carbonate morphology typically underlies the Btkq horizon.

The middle-to-late Pleistocene age for Qa3 is supported by stratigraphic relations, numerical dating, and correlations with local and regional soil-stratigraphic studies. Areas mapped as Qa3 (Wesling et al. 1992) within Midway Valley have been mapped as Q2 by Swadley et al. (1984) and Q2c by E.M. Taylor (1986) and Harden et al. (1991b, 1991c), who originally considered the unit to be 270 to 440 ka on the basis of uranium-trend dating of deposits exposed in fault trenches (Hoover et al. 1981; Szabo et al. 1981; Swadley et al. 1984).

Menges et al. (1994) correlate colluvial deposits in trench 14D with Qa3 on the basis of a similar degree of soil profile development on these units. Uranium-series dating of pedogenic carbonate associated with these colluvial deposits in the trench yielded an age estimate of 234 +47/-35 ka, and a thermoluminescence age of 132 ±23 ka on a mixed eolian-colluvial unit that composes the middle part of the sequence correlated with Qa3 (Menges et al. 1994). Four uranium-series ages of about 100 to 140 ka also were obtained on pedogenic carbonate in the uppermost part of the Q3 sequence in trench 14D.

Apparent similarities in soil profile development may indicate that Qa3 correlates with the Early Black Cone surface in Crater Flat (Peterson, F.F. 1988; Peterson, F.F. et al. 1995). However, the correlation of these units based on soil profile data is uncertain because of the extremely shallow nature of soil pits that were dug on the Early Black Cone surface. The middle Pleistocene age of greater than 159 to 200 ka was assigned to the Early Black Cone surface based on varnish cation-ratio dates (Dorn 1988; Peterson, F.F. 1988; Peterson, F.F. et al. 1995).

The degree of soil development on Qa3 is similar to that on middle-to-late Pleistocene soils in other parts of the Western United States (Taylor, E.M. 1986; Wells et al. 1990b; Harden et al. 1991a, 1991b, 1991c; Slate 1991; Reheis et al. 1992; McDonald and McFadden 1994). Table 3.4-1 shows the correlation of Qa3 with regional chronosequence studies that indicate Stage III carbonate morphology generally occurs in middle-to-late Pleistocene soils.

Late Pleistocene Alluvium (Qa4)—Qa4 consists of small, inset fluvial terrace and alluvial fan remnants on the east side of Yucca Mountain and of thin alluvial deposits overlying older basin deposits in Crater Flat. The desert pavement of the Qa4 surface ranges from loosely to tightly interlocking and is noticeably less well developed than pavements formed on the older fluvial surfaces. Although desert varnish is discernible on surface clasts of the Qa4 pavement, it occurs at a much lower percentage than on surface clasts of older units (Table 3.4-3). Indistinct depositional bars are preserved as diffuse accumulations of larger clasts; bar and swale relief on Qa4 has been

mostly reduced to clast height above the surface. The thickness of Qa4 averages about 1 m and does not exceed 2 m where observed in soil pits and trench exposures.

The strongly developed Qa4 soil is characterized by a reddened (7.5YR hues) argillic horizon and accumulations of carbonate and silica (Table 3.4-3). The upper part of the soil has silica accumulation, stage I to II carbonate morphology, and a strongly developed Btkq horizon with a sandy or silty clay loam texture. Continuous, thin to moderately thick clay films coat pedologic faces of the Btkq. An Av horizon overlies the Btkq horizon.

Qa4 is estimated to be late Pleistocene in age on the basis of its stratigraphic position, thermoluminescence ages from fault trenches, and the degree of soil profile development. A thermoluminescence age of 25.7 ± 8 ka was obtained for an Avb horizon of Qc4 in trench MWV-T5. The Avb represents post-depositional eolian accumulation on Qc4; therefore, the age represents a minimum estimate for the depositional age of Qc4. Eolian/colluvial sediments that have similar soil profile development as Qa4 yielded thermoluminescence ages of 38 ± 6 ka and 73 ± 9 ka in Trench MWV-T4. Paces, Menges et al. (1994) report a preliminary thermoluminescence age of 48 ± 20 ka for the upper part of a unit with a strongly developed Btkq horizon, which Menges et al. (1994) correlate with Qa4.

Additionally, a late Pleistocene age for Qa4 appears to be reasonable based on comparison of soil morphology data with that of regional chronosequences (Table 3.4-1). These comparisons suggest that Qa4 soil has morphologic characteristics similar to soils formed on units that were deposited about 20 to 80 ka (Taylor, E.M. 1986; Wells et al. 1984; Harden et al. 1991a, 1991b; Slate 1991; Reheis et al. 1992; Peterson, F.F. et al. 1995).

Latest Pleistocene to Holocene Alluvium (Qa5)—Qa5 covers large areas of alluvial fans and occurs as inset terraces along drainages. The desert pavement is loosely packed and poorly formed, and surface clasts have minor accumulations of rock varnish (Table 3.4-3). Qa5 surfaces display well-developed bar and swale morphology. The amount of bar-and-swale relief is related to landscape position and sediment sources; coarsest-grained bars lie in the proximal fan regions. Smaller, lower, partly buried bars lie on distal fans, where the intervening swales are partly filled by fine-grained eolian silts and sands. Surface clasts are relatively unweathered. In soil pit and trench exposures the average thickness of Qa5 is approximately 1 m, and the maximum observed thickness is about 2.5 m.

Weakly developed soils are formed on Qa5 (Table 3.4-3). Soil development is stronger in the swales where a silt-rich zone occurs in the upper 30 to 40 cm of the unit; soils are more weakly developed on bars. The Qa5 soil typically has a Bwk or incipient Btjk horizon with 10YR hues, weak subangular blocky structure, and colloidal stains on grains. Carbonate is disseminated in the matrix, and below about 30 cm depth in the Bk horizon, the bottoms of clasts have powdery coats of carbonate (stage I carbonate morphology). Where Qa5 is sufficiently thick, the carbonate content decreases below the Bk to form a transitional horizon (BC or CB) or a Ck; where Qa5 is relatively thin and underlain by a buried soil, the Bk persists to the base of the unit.

Qa5 is assigned a latest Pleistocene to early Holocene age based on numerical ages from the Yucca Mountain region and correlations to regional soil-stratigraphic studies. This age assignment is

consistent with a maximum age determined for Qc5/Qa5 based on thermoluminescence ages of 25.7 ± 8 ka and 27 ± 5 ka on the Av horizon of a buried Qc4/Qa4 soil that lies directly beneath Qc5 in trench MWV-T5 and Qa5 in soil pit MWV-P10, respectively. These dates suggest that the age of Qc5/Qa5 is latest Pleistocene or younger. Qa5 in soil pits MWV-P10 and MWV-P14 yielded thermoluminescence ages of 6.9 ± 1.2 ka and 4.0 ± 0.7 , respectively. The presence of extensive burrowing in Qa5/Qc5 and translocation of fine material by soil-forming processes may account for the somewhat younger-than-expected thermoluminescence ages for deposits in these soil pits. In Stagecoach Road trench SCR-T1, sandy colluvium capped by a weak calcic soil that exhibits similar profile development as the Qa5 soil has yielded thermoluminescence ages of 8.9 ± 1.2 ka and 12 ± 6 ka (Menges et al. 1994). Carbonized wood obtained from alluvial unit Q1c of Swadley et al. (1984) near Beatty, Nevada, yielded a radiocarbon age of 8.3 ± 0.075 ka; reconnaissance investigation of that site during this study indicates that Q1c has a soil profile similar to that of Qa5. Based on radiocarbon dating of rock varnish in Crater Flat, minimum ages of 6 to 11 ka were obtained for the Little Cones unit, which has a profile similar to the Qa5 soil (Peterson, F.F. et al. 1995).

The weakly developed Qa5 soil appears to have similar profile characteristics as latest Pleistocene to Holocene units described in nearby and regional soil-stratigraphic studies (Table 3.4-1; Taylor, E.M. 1986; Wells et al. 1984; Harden et al. 1991a, 1991b; Slate 1991; Reheis et al. 1992). The cambic B horizon that is characteristic of most Qa5 soil profiles indicates that the unit may be as young as early-to-middle Holocene in age (Dohrenwend et al. 1991).

Middle to Late Holocene Alluvium (Qa6)—Qa6 occurs along the active washes as low flood plains less than 1 m above the active channels and as vegetated bars. No desert pavement has developed (Table 3.4-3), and surface clasts are unvarnished and unweathered. Relief on the Qa6 surface is primarily the result of preservation of original bar and swale morphology. Locally, an eolian cap as much as 5 to 10 cm thick may bury all but the largest surface clasts. Natural outcrops and man-made exposures indicate that the total thickness of Qa6 does not exceed 2 m.

Qa6 soils lack a significant eolian cap that is common to the older surfaces (Av horizon), and soil development is limited to minimal oxidation of the deposit (Cox formation) and sparse accumulation of carbonate (Table 3.4-3). Carbonate is more concentrated toward the upper 10 cm of the deposit, although the matrix typically contains widely disseminated carbonate. Clasts in the upper 30 cm have little visible carbonate, but samples effervesce when hydrochloric acid is applied. Carbonate varies from isolated patches on the undersides of clasts to thin, relatively continuous coatings. Evidence that many clasts within the deposit have been reworked from older deposits includes randomly oriented carbonate coatings on clasts and percussion marks where the coatings are chipped from the clasts.

Qa6 is assigned a middle Holocene to historic age because of its very weak to weak soil development and its inset nature within Qa5. There is no color or structural B-horizon development and carbonate morphology varies from incipient to stage I. Historic is given as a minimum age, because Qa6 receives sediments during overbank runoff events. As shown in Table 3.4-1, several middle-to-late Holocene alluvial units are recognized in the region (Wells et al. 1990b; Bull 1991; Harden et al. 1991a; Slate 1991).

Late Holocene to Modern Alluvium (Qa7)—Qa7 consists of the deposits along active channels and the adjacent flood plains. No desert pavement has formed on the Qa7 surface (Table 3.4-3). No desert varnish occurs on clasts, except where it is apparently inherited thick, dark desert varnish is present in small protected areas (small fractures and exposed voids) of some surface and subsurface clasts. However, varnish is too well developed to be actively accreting in modern channels and apparently has been reworked from older surfaces. Clasts are unweathered, and the original depositional bar and swale relief is unaltered. The total exposed thickness of Qa7 does not exceed 2 m.

No in situ pedogenic alterations were observed for Qa7 deposits (Table 3.4-3). The overall color of the deposit is pale brown to brown (10YR 5-6/3 d). The matrix of the deposit contains reworked, disseminated carbonate. Reworking of older surficial units is indicated by numerous clasts that have thick accumulations of carbonate. These clasts appear to be distributed randomly throughout Qa7. The coatings, which originally formed on the bottoms of the clasts, have no preferred orientation in the reworked deposits. Carbonate is generally not apparent on the undersides of clasts, but noticeable effervescence occurs when hydrochloric acid is applied. This unit includes modern deposition in channels (Qa7) and on hillslopes (Qc7).

3.4.3.3.1.2 Colluvial Deposits (Qcu)

Colluvial deposits (Qcu) are undifferentiated because of their limited areal extent and the limited exposure of all but the youngest deposits. However, sequences of colluvial deposits are exposed in fault trenches around Yucca Mountain and in soil pits at the prospective surface facilities site on the east side of Exile Hill. The colluvial stratigraphy of Midway Valley, as described below, is primarily based on trench and soil-pit exposures.

Middle Pleistocene to Holocene Undifferentiated Colluvium (Qu)—This unit occurs as colluvial and debris-flow deposits, and in situ weathered bedrock mantling hillslopes and, locally, includes areas mantled by eolian and reworked eolian deposits. The colluvial deposits consist of gravelly silty sands and silty fine to medium gravel with pebble to small cobble clasts. The color of the colluvial deposits is very pale brown (10YR 7/4 d) to reddish yellow (7.5YR 6/6 d) with white (10YR 8/1 d) for the older carbonate-cemented units. The colluvial deposits and debris flows are poorly sorted and nonbedded to very crudely bedded. They are predominantly matrix-supported and are locally clast-supported with as much as 90 percent gravel. The gravels are predominantly medium to very coarse, subangular to angular pebbles with lesser abundances of cobbles to 20 cm diameter and small boulders to 30 cm diameter. The thickness of individual colluvial units is generally less than 2 to 3 m based on trench and soil-pit exposures.

The younger colluvial deposits, possibly equivalent to Qa5, have thin, weakly developed soils with an AB horizon over a weakly developed Bwk horizon. Colluvial deposits of probable Qa4 age display well-developed Btkq textural B horizons 40 to 50 cm thick. Colluviums of possibly equivalent to Qa3 and Qa2 have multiple superimposed soils consisting of Bkq and Btkq horizons that have stage II to III carbonate morphology. The oldest exposed colluviums have strongly developed Kqm horizons (Whitney and Harrington 1993).

At the surface, most of the hillslope areas mapped as undifferentiated colluvium (Qu) have surface characteristics of Qa5 and Qa6. Colluvium having surface characteristics similar to Qa4 surfaces commonly occur near the toe of the hillslope. Relict Q1 to Q3 colluvial deposits are generally found elevated 1 to 2 m above the modern slope and coated with dark desert varnish. The oldest dated Quaternary deposit on Yucca Mountain is the colluvium on the lower western slope of Yucca Mountain. Stage IV carbonate soil on this deposit, dated by U-series, is about 1 Ma.

Eolian Deposits (Qe)—Three types of eolian deposits are observed in the Yucca Mountain area:

- Reworked eolian deposits within sand ramps surrounding Busted Butte, against the west slope of Fran Ridge, and along the flanks of the southern ridges of Yucca Mountain
- Thin accumulations of silt and fine sand in most surface soils and buried soils, and small coppice dunes on desert pavements
- Lenses of eolian sand in predominantly alluvial sequences

Middle Pleistocene to Holocene Eolian-Colluvial Deposits (Qeu)—Sand ramps at Busted Butte and in southeastern Midway Valley are composed of a stacked sequence of eolian-colluvial units that have textures of pebbly, silty, fine to medium sand interbedded with some sandy, pebble to cobble gravel. Minor, alluvial sandy pebble gravel deposits are present locally within the sand ramp deposits. Sand ramp deposits vary from very pale brown to light gray (10YR 7/2-4 d), are poorly to moderately sorted, and are moderately bedded to massive. This type of unit is predominantly matrix supported although the alluvial gravel and parts of some colluviums are locally clast supported. Gravel clasts are angular to subangular and commonly less than 5 cm in diameter, although some clasts are as large as 50 cm diameter. The maximum thickness of the sand ramp deposits exceeds 15 m. A weakly to moderately interlocking desert pavement occurs over most of the surface. Soil development in near-surface deposits consists of a well-developed reddish yellow (7.5YR 6/6 d) Btkq horizon with a sandy clay loam texture that appears to be similar to the soil formed on Qa4. Typically, one or more buried soils occur within the sand ramp deposits in Midway Valley. The buried soil observed within trench MWV-T4 has a Kq horizon with stage IV carbonate morphology. Additionally, multiple buried soils have been observed within Busted Butte sand ramp deposits south of Midway Valley (Whitney, Swadley et al. 1985; Whitney and Muhs 1991; Menges et al. 1994).

The presence of Bishop tephra in lower sand ramp deposits at Busted Butte (Whitney, Swadley et al. 1985; Menges et al. 1994) and at other localities near Yucca Mountain (Hoover 1989) indicate that these landforms began forming within the region sometime shortly before 740 ka. Multiple buried soils above the Bishop tephra suggest that accumulation of the sand ramps is episodic and punctuated by surface stabilization and soil formation. At Busted Butte, some of these buried soils have been dated as middle-to-late Pleistocene using uranium-series disequilibrium methods (Menges et al. 1994). Thermoluminescence dates from the upper 3 m of sand ramp deposits in Southern Midway Valley, 38 ± 6 and 73 ± 9 ka (Table 3.4-1), and Busted Butte, 36 ± 10 ka, indicate that the two most recent major depositional episodes on sand ramps occurred about 35 to 40 ka and about 60 to 80 ka. A thermoluminescence age of 6.2 ± 1.3 ka on the surface A horizon of a sand ramp in Southern Midway Valley indicates that small-scale eolian additions have occurred in the Holocene.

3.4.3.3.1.3 Eolian Accumulations on Geomorphic Surfaces

A few centimeters to several tens of centimeters of eolian silt and fine sand have accumulated on most alluvial geomorphic surfaces and have been incorporated into soil profiles formed on those surfaces. These eolian accumulations are not mapped separately in spite of their broad areal distribution because of their relatively thin and discontinuous nature. Models of desert pavement and soil formation recognize the importance of eolian accumulations as a source for the fine earth fraction, carbonate, and other soluble salts that occur in otherwise clean sandy gravel deposits in arid regions (McFadden 1982; Birkeland 1984; McFadden et al. 1987; McFadden and Weldon 1987; McDonald and McFadden 1994; Wells et al. 1992). With time, surface weathering, soil formation, and eolian additions result in incremental modifications to geomorphic surfaces. These modifications include reduction of original surface topographic relief (bar-and-swale relief), formation of Av horizons, desert pavement development, the accumulation of desert varnish on surface clasts, and weathering of surface clasts. In Midway Valley, these modifications have produced a distinctive surface morphology for a unit of a given age, and the surface morphology is used as a basis for mapping alluvial geomorphic surfaces. Relative to younger surfaces, older surfaces generally have a more subdued surface topography, stronger desert pavement development, darker and thicker desert varnish on surface clasts, and stronger soil development. The relative thickness of eolian accumulations generally is greater on older units. Eolian additions to Qa6 and Qa7 are minimal at best, whereas eolian sediments plug the upper part of Qa5 deposits and partially fill paleo-swales to form a muted bar-and-swale topography. The surfaces of units Qa2, Qa3, and Qa4 are plugged with eolian sediments that form a continuous surface sheet and result in a nearly flat topography. The original eolian mantle on Qa1 has been stripped and replaced by a younger eolian mantle.

3.4.3.3.1.4 Spring Deposits (late? to middle Pleistocene)

Spring deposits are discussed in detail in Subsection 5.2.6, which gives the age distribution of this type of deposit. These deposits are formed in an environment where groundwater has intersected the surface. Parts of deposits are uniformly fine-grained silt deposits, pale-yellowish brown, and unconsolidated. They may be massive to very poorly bedded. Locally, they are weakly cemented by calcium carbonate and weather into popcorn-shaped nodules covering the modern surface. Also locally, they contain white diatomite beds up to 75 cm thick. The diatomite deposit locally bears minor reworked ash and small pumice lapilli of the 740 ka Bishop Tuff.

3.4.3.4 Origin of Secondary Carbonate

Pedogenic carbonate, occurring both as slope parallel deposits and as remobilized fracture fillings, has raised a controversy as to the existence of a possible adverse condition. Szymanski (1987; 1989) postulated that these deposits were formed by groundwater rising to the surface and, therefore, through the potential repository horizon. This subsection summarizes the work done to resolve this issue, and the project's conclusion that there are no paleogroundwater discharge deposits in the immediate vicinity of Yucca Mountain. In fact, the closest such deposit is approximately 15 km to the southwest (see Subsection 5.3.7, Site Paleohydrology).

3.4.3.4.1 History of the Issue of the Existence of a Potentially Adverse Condition

The concerns began in 1982 with shallow excavation on the west side of Exile Hill for examination of the Bow Ridge fault as part of the investigation of Quaternary faulting in the vicinity of Yucca Mountain (Swadley et al. 1984). The 2 m deep excavation, designated as Trench 14 (Figure 3.4-3), exposed a vein-like deposit of calcium carbonate and subordinate opaline silica (Figure 3.4-4) as well as breccia deposits in the bedrock that contain drusy quartz. The trench was deepened in 1984 to 4 m to elucidate further the origin of the deposits. Two workshops on the Trench 14 deposits were held in Las Vegas, Nevada, in early 1986. The first addressed the present state of knowledge (Voegele 1986a). The second proposed methods of investigation (Voegele 1986b). Both were open to the public and were attended by representatives of the U.S. Nuclear Regulatory Commission and the State of Nevada.

Following these workshops, the DOE established a five member peer review panel to examine the issue. This review panel summarized four main categories of depositional models and suggested ways to investigate and evaluate the origin of the deposits. The depositional models proposed were:

- Pedogenic, which includes any origin involving the interaction of meteoric waters and surficial materials with subsequent deposition of calcium carbonate and silica within soil profiles and/or fractures
- Hydrothermal springs, which involves movement of hot or warm water ($T > 30^{\circ}\text{C}$) up along faults with deposition of minerals
- Cold springs, which involves movement of regional or perched groundwater along normal hydrological gradients with deposition of minerals
- Seismic pumping, which involves the movement of hot or cold water up along faults in direct response to pressures generated by tectonism

All but the first of these models imply that groundwater could have risen to the surface through the repository horizon, thereby creating a potentially adverse condition. The recommendations of this panel (Hanson et al. 1987) were factored into the development of the Quaternary Regional Hydrology study plan from Site Characterization Plan Section 8.3.1.5.2.1. This study plan was reviewed by more than twenty Project scientists and consultants, and was reviewed by the NRC and the State of Nevada.

Concurrent with these project activities, Jerry Szymanski, a DOE physical scientist, proposed an hypothesis of catastrophic upwelling of groundwater, similar to the seismic pumping model, for the origin of the deposits. DOE requested that he draft a report to DOE management (Szymanski 1987). The Project Office performed an internal review of his report (DOE 1989) and found it to be in need of extensive revision. Szymanski produced a revised report (Szymanski 1989). In 1990, DOE convened a five-member review panel, external to the DOE or its project contractors. The panel completed its review in 1991 and provided its findings in two reports due to an inability to reach a consensus (Powers et al. 1991; Archambeau and Price 1991). A seventeen-member panel of the National Academy of Sciences/National Research Council was also asked by the DOE in 1990 to

"evaluate (1) if the water table had risen in the geologically recent past to the level of the proposed Mined Geologic Disposal System, and (2) if it is likely that it would happen in the manner described in the DOE staff geologist's final report within the 10,000-year period covered by the regulations." The panel completed its review and provided its findings in a final report (National Research Council 1992).

3.4.3.4.2 Calcite Deposits along Faults, Fractures, and at the Surface

3.4.3.4.2.1 Field Data

Comparison of the physical and chemical characteristics of the calcite-silica deposits exposed at Trench 14, with those of pedogenic and spring deposits, favors a pedogenic origin for the deposits exposed in Trench 14 (Taylor, E.M. and Huckins 1986). Trench 14 exposes slope-parallel calcium carbonate-enriched zones (Figure 3.4-4) that are laterally extensive for thousands of square m (Taylor, E.M. and Huckins 1995), unlike springs which form discrete mounds. The slope-parallel deposits are physically typical of carbonate-enriched pedogenic deposits that occur throughout the southwestern United States and other semi-arid regions of the world (Bachman and Machette 1977). The carbonate-enriched horizons exposed in Trench 14 can be traced upslope and over the fault and fracture fillings. Locally, the near-vertical veins and the carbonate horizons merge. In addition, the deepened portion of Trench 14, in the area of the near-vertical veins, exposes the veins pinching out and becoming discontinuous with depth (Taylor, E.M. et al. 1995). At depth, where the Bow Ridge fault is intersected by the Exploratory Studies Facility, deposits are restricted to the footwall of the fault. In contrast to these observations, feeders for spring mounds typically maintain subparallel walls over depths of tens to hundreds of meters.

The calcite-silica veins contain a black ash that must have washed into open fractures. It is difficult to explain the presence of the ash in an environment where water is issuing from an open fissure. Other physical features for distinguishing between pedogenic and nonpedogenic carbonate deposits are summarized by Taylor, E.M. and Huckins (1995).

3.4.3.4.2.2 Mineralogic and Textural Data

Earlier studies of the vein deposits in Trench 14 and similar deposits around Yucca Mountain emphasized the similarity of calcite-opal-sepiolite mineralogy to that of the widely distributed slope calcretes (Vaniman, Bish and Levy 1984; Vaniman, Downey et al. 1985). This similarity suggests that one depositional mechanism accounts for both slope and vein calcretes. On a centimeter scale, distinctions between slope and vein calcretes based on orientation become meaningless. Laminae within the calcretes often reveal multiple episodes of fracturing and cross-cutting deposition. These structural complications are particularly prominent in the blocky rubble near faults.

The vein material in Trench 14 is poorly indurated and fine grained. This contrasts sharply with the typical discharge feeder veins which are well indurated and coarse grained. The centimeter-scale banding at Trench 14 consists of:

- Laminae with abundant root casts
- Laminae with abundant ooids and pellets

- Denser laminae which show evidence of shearing
- Thin (<5 mm) laminae of opal
- Rare sepiolite rich laminae

The ooids are generally <0.5 mm in diameter and have concentric coatings (mainly calcite or opal). Pellets are larger round or ellipsoidal calcite-opal bodies that generally include several detrital fragments and may include earlier-formed ooids.

Because ooids and pellets contain one or more detrital fragments, laminae with an abundance of ooids and pellets contain the most detritus. The detritus consists of tuffaceous volcanic rocks and minerals from the immediate vicinity of Trench 14, plus a small amount of exotic rock fragments. The dense, sheared laminae generally contain less tuff detritus than those laminae with abundant preserved root fossils or ooids. Some of the dense laminae consist of closely intergrown calcite and opal with essentially no detritus, but to date the only pure mineral separates from the calcretes have been of opal, either from the opaline laminae or calcite from large root fossils (Vaniman, Bish, and Chipera 1988). Calcite crystals are small; most (>95 percent) are <5 μ m and calcite is closely intergrown with opal or more rarely, sepiolite. All attempts to obtain pure calcite separates by crushing and density separation have failed because of intimate intergrowth with other minerals. These intimate intergrowths and the existence of ooids and pellets are atypical of any type of spring deposits (Vaniman, Bish and Chipera 1988; Stuckless, Peterman et al. 1992), but are common in soils (Brewer 1964).

Calcite and opal are not typically intergrown in spring deposits because of the general, long-term stability of the chemistry or their depositional environment. Cool and warm springs, from deep or perched sources, have higher water flow that lead to distinct pH regimes in which either calcite or silica is precipitated (White et al. 1956; Viles and Goudie 1990). In contrast, evaporative processes within arid soils of siliceous igneous terranes can cause a rise in pH from only slightly alkaline to >9 (Vaniman, Ebinger et al. 1992; Chadwick et al. 1989), passing from regimes of calcite dissolution and silica precipitation into those of calcite precipitation and silica dissolution (Watts 1980). Numerous pedogenic wetting and drying cycles can lead to the complex calcite and opal intergrowths seen in the calcretes of Trench 14. The closest analogous spring deposits would be evaporative seeps (Vaniman, Bish and Chipera 1988); however, deposits in such environments have distinct differences attributable to more abundant water. Evaporative seeps lack concentric ooidal accumulations of calcite and opal around detrital nuclei and have simpler and often single-stage calcite-to-silica transitions, in which opal-CT forms thin (~10-20 μ m) "isopach" coatings over calcite along fractures and authigenic quartz may occur as late veins. These features reflect the longer time scales for evaporation of seep deposits, tied to deep-seated flow rates, in contrast with the constant seasonal cycling of pedogenic environments.

Also present in evaporated seeps is biogenic evidence of their past higher water content: ostracode fossils, casts of phreatophyte plants, and algal or diatomaceous deposits of opal-A. Fossil remains found in pedogenic calcretes consist of root casts with very delicate filaments. Superficially similar calcareous filaments occur as algal products in active spring deposits (Viles and Goudie 1990), but these delicate features are not preserved in the fossil deposits where the high water/rock ratio of the spring environment leads to their dissolution. Moreover, algal filaments in springs are not restricted

to associations with fossil roots of vascular plants, as are the calcified filaments in the Trench 14 calcretes.

Quantitative X-ray powder diffraction provides a direct measurement of calcite, clay, and detrital mineral abundances in the calcretes. Although both opal-A and opal-CT are recognized in the X-ray diffraction data, opal-A abundance must be determined by difference from 100 percent, using internal standard methods. Petrographic, electron microprobe, and scanning electron microscope studies confirm the widespread distribution of opal in the calcretes. Sepiolite is locally abundant (~50 percent) in only a few laminae; the overall abundance of sepiolite and amorphous Fe, Mn, Ti-oxides is less than 1 percent. The X-ray analysis shows a total lack of dolomite, which is inconsistent with any involvement of the carbonate aquifer (Vaniman, Ebinger et al. 1992). The overlying soils differ from the calcretes in their very low abundance of calcite. This is the expected relationship where calcrete forms pedogenically by accumulation of calcite leached from overlying soils (Machette 1985). In contrast, carbonate-free soils are not likely to form in place above calcite-rich spring deposits.

3.4.3.4.2.3 Major- and Trace-Element Data

Chemical composition of the overlying soil can be an important factor in evaluating calcrete origin. If the calcrete is pedogenic, the detritus incorporated into it is likely to carry with it the effects of surface exposure and soil-zone processing. Nonpedogenic calcretes may also incorporate soil detritus, but if they originate from upwelling waters, the veins should show more evidence of interaction with their wall rock than with the surface soil. This will particularly be the case for vein deposits as seen in Trench 14, where proposals of deep origin postulates explosive injection and wall-rock brecciation by the vein-forming fluids (Archambeau and Price 1991; Szymanski 1989). Chemical data for the calcretes and the overlying soils have similar lanthanide-element signatures even where X-ray diffraction data detect no detritus. A similar effect is seen in the Fe and Sc data where the Fe/Sc ratio of both the calcretes and the overlying soils are very similar (YMP 1993b; Vaniman, Chipera et al. 1994). Examination of abundances as well as ratios indicates that many of the individual laminae in the calcretes have high Fe and Sc contents, even though the laminae contain no more than 25 percent detritus. The enrichments in Fe and Sc result from weathering of detritus (Vaniman, Chipera et al. 1994). This suggests that the detritus in the calcretes must be derived from surface soils with the same Fe/Sc ratio but higher Fe and Sc content than the tuff. Few of the volcanic rocks at Yucca Mountain have sufficiently high Sc; those that do differ from the detritus in the calcretes by having very different La/Yb or other chemical ratios, and by lacking key minerals, such as sphene, that characterize the detritus in the calcretes.

Archambeau and Price (1991) have suggested that there is too much calcite and opal in Trench 14 to be accounted for by pedogenic accumulation. This is not the case. The subsurface accumulation of calcite and opal is greatest within the fault (2.25 m maximum width calcrete vein near the surface and wedging down to a few centimeters width at 4.75 m depth). Approximately six-tenths of the material in this wedge is laminated calcrete; the remainder consists of blocks of the wall-rock tuffs. Average bulk density of the calcretes is 1.6 g/cm³. The average calcite weight fraction of the calcretes is 53 percent, leading to an estimated calcite abundance of 5.1x10⁵ g per m² of surface overlying this wedge of vein calcrete. Estimates of eolian carbonate accumulation rates for the southwestern United States range from 0.3 to 5 g/m²/yr (Machette 1985; Reheis 1992). At these

rates, the amount of calcite within the excavated veins at Trench 14 could accumulate over a time span between 4,000,000 and 240,000 years. This represents a maximum estimate because the extensive area of impermeable bedrock up slope where dust could accumulate and be washed to the fault is not considered. Furthermore, carbon and oxygen isotope data suggest that most of the calcite in Trench 14 was deposited during colder and wetter climates (Quade and Cerling 1990; Whelan and Stuckless 1990), when carbonate accumulation rates were relatively rapid. The data suggest that the carbonate portion of the calcretes in Trench 14 could easily have been deposited pedogenically during the Pleistocene. Similar calculations show that even less time is needed to accumulate the observed silica (YMP 1993b).

3.4.3.4.2.4 Stable Isotope Data

Carbon and oxygen isotopes in the vein carbonates at Trench 14 match those in pedogenic carbonate (Cerling et al. 1989; Quade, Cerling et al. 1989) collected over a wide area of Southern Nevada (Figure 3.4-5). In detail, the isotopic compositions suggest pedogenic deposition of the Trench 14 calcites under conditions of a cooler climate with a mean temperature of about 15°C (Quade and Cerling 1990). Samples of soil carbonates and vein infilling from both Trench 14 and Busted Butte show that the isotopic compositions of oxygen and carbon of most samples are virtually identical for the two locations and for the two types of deposits, soils and veins (Whelan and Stuckless 1990). A few of the Busted Butte soil carbonates are slightly enriched in ¹³C and ¹⁸O (Figure 3.4-6), but the variability in the data is small enough such that all of the soil and vein carbonate can be explained by pedogenesis.

The calculated carbon and oxygen isotopic compositions of hypothetical calcites formed in equilibrium with groundwaters of the Yucca Mountain area are very different from those measured for the vein calcites (Figure 3.4-7). This difference shows that the veins could not have formed directly from groundwaters like those present in the region today. Most of the available groundwater data are for the Cenozoic aquifer for which the water table is at a depth of 460 to 700 m in the vicinity of Yucca Mountain (Waddell et al. 1984). Calculations based on lower temperatures for calcite precipitation would produce better agreement with the observed oxygen compositions of the vein calcites, but some of the waters would have to be cooled to impossibly low temperatures (0°C and lower) to precipitate calcite with the appropriate isotopic composition (Figure 3.4-7). The isotopic compositions of Trench 14 calcites could be derived through deposition from water similar to modern precipitation at reasonable temperatures (5° to 22°C).

Carbon isotopes do not fractionate significantly between dissolved carbonate and calcite at the temperatures in question. About half of the groundwater samples, including the one sample analyzed from the Paleozoic aquifer, are either too enriched or too depleted in ¹³C to be possible sources for the vein carbonates. Based on the similarity of carbon isotopic data in soils and the Trench 14 deposits, the most likely source for carbon in the Trench 14 calcites is biogenic.

The preceding discussion assumes that the isotopic composition of groundwater beneath Yucca Mountain is representative of groundwater that might have formed the Trench 14 veins. However, groundwaters beneath Yucca Mountain have apparent ¹⁴C ages of less than 20,000 years in the Tertiary aquifer and about 30,000 years in the Paleozoic aquifer (Benson and McKinley 1985),

whereas the deposits in Trench 14 are much older with ages greater than 400,000 years (Szabo and O'Malley 1985), and as young as 92 ± 5 ka (YMP 1993b).

The isotopic composition of ancient groundwaters in the Yucca Mountain region cannot be determined. However, the Ash Meadows flow system, which is located east of the groundwater flow-system that underlies Yucca Mountain (Winograd and Thordarson 1975), has left a long-term record near its discharge site. Uranium series ages have been obtained for individual laminae within a vein of continuously deposited calcite at Devils Hole (Winograd et al. 1988; Ludwig et al. 1992), and oxygen isotope analyses of these laminae (Figure 3.4-8) show a variation that is generally less than ± 1 per mil about the present-day value during the last 560 ka (Winograd et al. 1988; Winograd, Coplen et al. 1992). A similar variation for waters beneath Yucca Mountain would be reasonable because the isotopic composition of both flow systems should be governed by the same climatic conditions. Even if a similar per mil increase (at currently observed temperatures) did occur for groundwater beneath Yucca Mountain, precipitated calcites would not have the isotopic compositions of those observed at Trench 14.

3.4.3.4.2.5 Radiogenic Tracer Isotope Data

Studies of strontium isotopes in calcite from the Yucca Mountain area support a pedogenic origin for the veins exposed in Trench 14 and argue against a groundwater origin (Marshall et al. 1990; Marshall et al. 1991; Stuckless et al. 1991). Strontium isotopes do not fractionate in nature, and therefore, the isotopic composition of strontium in calcite provides a record of the isotopic composition of water from which it precipitated (Peterman and Stuckless 1993b). There is almost no overlap between the isotopic compositions of strontium for the Trench 14 vein carbonates (4.54 ± 0.32 , Marshall et al. 1991) and that of groundwater within the Tertiary aquifer near Yucca Mountain ($1.74 \pm .90$, Figure 3.4-9). Samples with the lowest values were taken from the saturated zone in the presumed upflow direction of Trench 14 (Figure 3.4-9). A bailed sample from the Paleozoic aquifer ($3.60 \pm .13$ for UE-25 p#1) is also significantly different from the Trench 14 veins. Thus, none of the saturated-zone waters sampled to date in the Yucca Mountain area can be related genetically to the calcite deposits in Trench 14.

Data from Devils Hole can again be used to evaluate the likely compositional changes in ancient groundwater beneath Yucca Mountain. $\delta^{87}\text{Sr}/^{86}\text{Sr}$ values for water presently issuing from Devils Hole and for six samples of calcite deposits ranging in age from approximately 100 to 600,000 years (Figure 3.4-10) differ by only 0.71 per mil (Marshall et al. 1990). $^{87}\text{Sr}/^{86}\text{Sr}$ values of water within the Cenozoic aquifer in the Yucca Mountain area probably behaved in a similar fashion because the recharge area and host aquifer have most probably not changed during the Quaternary, as suggested by the general geomorphic and tectonic stability of the landscape noted earlier in this subsection. Furthermore, the isotopic composition of strontium is more variable in the Paleozoic aquifer (Peterman, Stuckless et al. 1992) than in the Cenozoic aquifer (Peterman and Stuckless 1993b), and therefore, potentially susceptible to larger fluctuation at its discharge region as a function of time. Thus, it is highly unlikely that water beneath Yucca Mountain ever had high enough $^{87}\text{Sr}/^{86}\text{Sr}$ values to have been a source for the strontium in the Trench 14 deposits.

The isotopic compositions of strontium in calcite in the near-vertical vein and sub-horizontal deposits at Trench 14 show a fairly close correspondence, but the vein materials, on average, have

a somewhat higher value (Marshall et al. 1990). Over a broader region around the Nevada Test Site, the correspondence between vein (0.71238 ± 0.00026 , $N=39$) and pedogenic calcite (0.71233 ± 0.00028 , $N=37$) is much stronger (Marshall et al. 1991).

The isotopic composition of the vein carbonate at Trench 14 and Busted Butte may have been influenced in part by reaction of depositing fluids with entrained solid material, and the isotopic composition may also be affected by reaction with the host wall rock as well (Marshall et al. 1990). However, most of the strontium in the subhorizontal deposits (and, by geochemical analogy, calcium as well) seems to come from a well homogenized source such as wind-blown dust. Limited data for eolian carbonate do not provide an exact match to isotopic compositions of pedogenic carbonate causing Marshall and Mahan (1994) to conclude that "an additional source or past variation of strontium composition is required to model the pedogenic carbonate system."

The remarkable homogeneity of strontium isotopic composition in pedogenic deposits over a broad geographic region argues against deposition from groundwater because the isotopic composition of groundwater is very inhomogeneous in the vicinity of the Nevada Test Site (Peterman, Stuckless et al. 1992; Peterman and Stuckless 1993b). Water emerging at the surface would impart this inhomogeneous characteristic to deposited calcite.

Lead isotopic data yield the same general conclusions as strontium (Zartman and Kwak 1993a, 1993b). A direct comparison between the isotopic compositions of water and the carbonate deposits has not been attempted because of the very low lead concentrations of water (<1 ppb) and the high probability of contamination during sampling. The problems of contamination are severe even when sampling slightly enriched (1 to 5 ppb) groundwaters (Gulson 1986), and at Yucca Mountain, water is several hundreds of meters below the surface. There is no adequate way to evaluate the potential contamination problems that may have developed from the drilling equipment and fluids, or the sampling equipment. Even carefully cleaned tubing hundreds of m in length could contain more lead than the sampled water.

The lead in the calcite silica deposits has two isotopically distinguishable fractions (Zartman and Kwak 1993a, 1993b). The carbonate fraction of lead can be leached from the sample with dilute (0.8 N) acetic acid. This lead is much more radiogenic than that in the wall rock that hosts the carbonate vein deposits, and consequently more radiogenic than that expected for water within the Cenozoic rocks. The silicate lead, which remains after removal of the carbonate lead, is very similar isotopically to that in the Miocene volcanic rocks. The carbonate lead in pedogenic samples is also distinctly radiogenic, thereby suggesting a genetic relation between the vein and pedogenic carbonates. The ultimate source of this radiogenic component is not known; two samples of eolian dust lack this radiogenic component. Locally, unmetamorphosed limestones and dolomites contain radiogenic lead (Zartman and Kwak 1993b) as would the Precambrian crystalline rocks to the west. Thus, as with the strontium isotopic data, a change in the eolian component of the pedogenic carbonates as a function of time is required in order to match the observed data.

Groundwater in Southern Nevada is typically anomalous with $^{234}\text{U}/^{238}\text{U}$ greater than 2.0 for most samples from both the Paleozoic and the Tertiary/Quaternary aquifers (Osmond and Cowart 1982; Ludwig et al. 1993), but vein and soil calcites at Trench 14 and Busted Butte were largely deposited by waters with a $^{234}\text{U}/^{238}\text{U}$ less than 1.5 (Figure 3.4-11). The difference between water and initial

vein compositions is even more pronounced in the vicinity of Yucca Mountain where three samples from the Tertiary/Quaternary aquifer have values greater than 5.0, and one sample from the Paleozoic aquifer is 2.71 ± 0.09 . The two analyzed vein samples have initial $^{234}\text{U}/^{238}\text{U}$ less than 1.4 (Stuckless et al. 1991). Thus the veins and groundwaters cannot be genetically related. In contrast, the initial $^{234}\text{U}/^{238}\text{U}$ for soils of the Yucca Mountain area is generally less than 1.40 with only one value as high as 2.0 (Rosholt et al. 1985). These values agree well with those observed for the Trench 14 carbonate veins and, therefore, support a pedogenic origin for the fault infillings.

The record from Devils Hole can again be used to evaluate the variability of the $^{234}\text{U}/^{238}\text{U}$ during the past 300,000 years. The ratio in Devils Hole calcites has ranged from 2.53 to 2.85 (Figure 3.4-12). If a similar variability has occurred in waters beneath Yucca Mountain, the veins at Busted Butte and Trench 14 cannot have been precipitated from either of the regional aquifers.

3.4.3.4.2.6 Paleontological Data

Taylor, E.M. and Huckins (1995) note that the calcareous deposit at Trench 14 is devoid of fossil ostracodes or other aquatic life forms. Eight samples of soil and vein carbonate were taken from the Trench 14 area to determine if calcareous microfossils were present. No ostracodes or other aquatic animals such as mollusks were found. The absence of such fossils implies that the carbonate veins were not deposited in an environment that was saturated with water for periods longer than about one month, which is roughly the time needed for the animals' life cycle. Ostracodes are common in saturated environments of Southern Nevada today including lacustrine settings, perched springs, and discharge points for the regional aquifers, with a range of temperatures of 0 to 55°C (Forester 1991). Quade et al. (1995) report abundant fossils at paleodischarge sites in the Southern Great Basin.

Vaniman, Chipera et al. (1994) note that pedogenic calcretes lack aquatic assemblages of fossils but typically contain delicate filaments which are not preserved in fossil spring deposits. These are remains of bacteria and fungus which are flushed out by water fluxes typical of seeps or springs, and would certainly not be preserved in the high energy environment proposed by Szymanski (1987, 1989) for Trench 14 veins. Extremely fine needle-fiber calcites and filaments are common at Trench 14 in oldest through youngest material, suggesting that the entire deposit is pedogenic.

Eleven soil and vein samples were collected from the Trench 14 area to look for chrysophyte cysts (the resting stage of certain forms of fresh-water algae). Rare cysts were found in two vein samples. In the modern environment, cysts are far more common in places where dilute surface waters are entering the hydrologic system (recharge areas) than in places where relatively concentrated groundwater is emerging (discharge areas). In fact, modern chrysophyte cysts have been found in modern mud at the bottom of Trench 1 on Yucca Crest. Taken together, the two types of paleontological data argue against any type of spring environment for deposition of the Trench 14 calcite and opaline silica veins; and, therefore, the data are consistent with a pedogenic mode of deposition for the veins.

3.4.3.4.2.7 Possibility of Perched Water

The isotopic data are not particularly useful in evaluating a possible perched spring origin for the deposits exposed in Trench 14, because isotopic data are not available for perched waters. However,

geologic and paleontologic data suggest that a perched origin is highly unlikely. Perched water occurs above aquitards such as air fall tuffs (Winograd and Thordarson 1975) or nonwelded and unfractured tuffs (Waddell et al. 1984). Such aquitards are more than 100 m deep in the vicinity of Exile Hill, and the veins pinch out along the fault contact with the welded tuff at Trench 14 which is highly fractured and very permeable. Perched springs today support ostracodes and other biologic forms that should leave a fossil record, and as noted above, no such fossils have been found. These facts and the relatively small catchment area upgradient from Trench 14, argue against a perched spring origin for the vein deposits at Trench 14.

3.4.3.4.2.8 Data Pertaining to a Hypogene Origin

C.A. Hill et al. (1995) have recently asserted that much of the data available for the calcite/opal deposits can be explained by the upwelling of warm, CO₂ rich water along faults. Once these waters reach the surface, they are postulated to flow down hill, acquiring a pedogenic character and depositing the slope parallel deposits. In a critique of this hypothesis, Stuckless et al. (1997) conclude that "the paper contains several misstatements of fact, some important omissions of pertinent and readily available information, and some misleading generalizations that together bias the reader toward the erroneous conclusion that the hypogene model remains viable." There are no recent results that suggest that the fracture-filling and slope-parallel deposits are other than pedogenic in origin.

3.4.3.4.2.9 National Academy of Sciences' National Research Council Findings

The National Academy of Sciences and National Research Council was requested by the DOE to evaluate: if the water table had been raised in the geologically recent past to the level of the proposed repository, and if a water table rise was likely to occur over the proposed life of the repository in the manner proposed by Szymanski (1989). A panel, established by the National Academy of Sciences/National Research Council for this purpose, reviewed the pertinent literature and available data, consulted with scientists involved in field and laboratory studies, and spent several days in the field visiting the sites of calcite-silica deposits. The panel's overall conclusion (National Research Council 1992, p. 3) was that none of the evidence cited as proof of groundwater upwelling in and around Yucca Mountain could reasonably be attributed to that process. Further, the panel stated that "The preponderance of features ascribed to ascending water clearly were related to the much older (13-10 Ma) volcanic eruptive processes that produced the rocks (ashflow tuffs) in which the features appear, contained contradictions or inconsistencies that made an upwelling groundwater origin geologically impossible or unreasonable, or were classic examples of arid soil characteristics recognized world wide." (p. 130) Based on physical and textural evidence from the veins in the trenches, the panel concluded that a sedimentary, low-temperature origin from descending meteoric water was supported rather than an origin involving upwelling of thermal water from deep within the crust. The panel concluded "that the carbonate rich fracture fillings exposed in trenches in the region are composed of wind blown dust cemented by material deposited from evaporating water that had infiltrated unsaturated rock along open fractures." (p. 60) The panel also concluded "that to date the preponderance of evidence supports the view that the calcretes and other secondary carbonates in veins of the area formed from meteoric water and surface processes." (p. 56)

The panel added their own field observations to the database. They observed that at Busted Butte, slope-parallel deposits are thinner downslope from the vertical fracture fillings than the slope-parallel deposits above the fracture and that delicately calcified roots of plants are found wrapped around cobbles of volcanic rocks. Both of these observations are deemed inconsistent with formation by upwelling water. Formation of these slope-parallel deposits by upwelling water from the vertical fracture would thus require that the water flow upslope in greater quantity than downslope. Upwelling water would also be expected to flow over the land surface and form deposits at the land surface rather than specifically in the root zone. Both of these observations are consistent with the soil and vein carbonates forming from normal arid climate soil-forming processes.

Occurrence of mosaic breccias at Yucca Mountain and Busted Butte has been suggested as support for upwelling of pressurized groundwater. These breccias consist of angular fragments of local bedrock encased in a matrix of calcite and opaline silica. These rocks have been interpreted as forming as either a result of large and fast buildups and releases of fluid pressure or rapid downslope sliding of bedrock with simultaneous infilling of spaces between the fragments by minerals precipitated from upwelling deep-seated fluid. The National Academy of Sciences panel disagreed with both of these interpretations based upon the field evidence. Three types of breccia were noted: talus breccia, fault breccia, and small pipe-like structures with breccia cemented in them. The panel concluded that the carbonate cementing the talus breccia was deposited by evaporating rain water, progressively and simultaneously with accumulation of the talus deposit. The carbonate cementing the fault breccia was concluded to be of pedogenic or surface origin, based on grain size, structural characteristics, and the presence of older detrital zircons. The most likely origin of the small irregular breccia-filled pipes in the Topopah Spring Tuff was thought to be channeling of steam and of the volatiles degassing during the cooling of the ash flow tuff. As a final note, the panel concluded that there was no good evidence in support of upwelling deep hot water to account for the brecciation or the silica-carbonate cementation.

The panel also evaluated the theoretical basis for the model of upwelling water. They considered the experience of historic earthquakes and the results of different types of modeling of earthquake responses. Credible assumptions and various types of modeling indicate that the seismic pumping mechanism is inadequate to raise the water table more than tens of m and that significant water table excursions to the design level of the repository are unlikely. With regard to a heat source to drive upwelling water, the panel noted that the geologic record indicates that during the lifetime of the repository, a low volume basaltic intrusion is the only likely style of intrusion in the Yucca Mountain area. The panel concluded that the elastic effect of dike intrusion would result in raising the water table no more than a few tens of meters.

3.4.3.5 Comparison of Regional Quaternary Stratigraphies

The Quaternary stratigraphy at Yucca Mountain is similar to that seen regionally, much of which has good age control (Table 3.4-1). The section at Silver Lake, California provides a sequence of Quaternary stratigraphic units with ages based on radiocarbon dating of shell material and tufa from shoreline features (Reheis et al. 1989; Wells et al. 1990b). This stratigraphy includes 10 units, with age control in the Holocene. The Kyle Canyon Fan in Southern Nevada provides a comparable stratigraphy based on uranium-series age estimates on secondary carbonate rinds formed in limestone gravel. Fish Lake Valley, north of Death Valley (Slate 1991; Reheis and Sawyer 1997) and the

Providence Mountains in the Eastern Mojave Desert (McDonald and McFadden 1994; Wang et al. 1996) also provide stratigraphies that suggest similar age ranges for timing of deposition and soil formation.

All areas, except Kyle Canyon, preserve at least three Holocene depositional units represented by the modern wash, a slightly elevated terrace in the range of 1,000 years, and the dominant Late Pleistocene-Early Holocene unit primarily deposited during the onset of a drier and hotter regional climate, following the last major glaciation. The late Pleistocene unit in these regional studies has an estimated age range of 30 to 100 ka with a preferred age on the order of 50 ka. This unit represents a major period of soil formation. The timing of deposition of this late Pleistocene unit is coincident with regional climatic records of transition from a wetter to drier climate (Winograd, Coplen et al. 1992), similar to that noted for the late Pleistocene-early Holocene (see Table 3.4-13 and Subsection 4.2.3). A middle Pleistocene stratigraphic unit, apparently formed during another period of transitional climate, is common to the Yucca Mountain and Providence Mountain regions, however, no similar-aged unit is mapped in Fish Lake Valley. Age constraints for this time period are poor in the Providence Mountains for unit (Q3f), however, the reported preferred age of 150 ka falls within the Middle Pleistocene Q3 unit age of the Yucca Mountain region for which the estimated age is 100 to 250 ka. Middle Pleistocene deposits are preserved in all the regional study areas, and the presence of buried Bishop Ash at or near the base of several of these deposits constrains their maximum ages.

The problem with using age estimates from trenches exposed to look for tectonic offset of depositional units is that the trenches are not in locations typical of the local and region Quaternary geology. These trenches are located at and adjacent to active mountain fronts where erosion, deposition, and eolian processes are different than on stable alluvial surfaces which dominate the broad flat valleys. Once the ages were determined from samples collected in the fault trenches, the Quaternary mapping unit exposed in the trench was determined (Table 3.4-3). Many investigators, familiar with the local and regional Quaternary geology, were present when these unit assignments were made. Uncertainties associated with any geologic mapping are inherent in the assignment of stratigraphic units.

3.4.3.6 Distribution of Quaternary Deposits in the Yucca Mountain Area

The Quaternary landscape in the Yucca Mountain area has been dominated by physical weathering, colluvial, eolian, and alluvial processes that have responded to varying climates, climatic changes, as well as to the topography of the mountain and adjacent basins that has been formed by extensional tectonic processes over the past 14 Ma. Patterns of Quaternary deposits reflect both the tectonic environment and climatic history in the area.

One noteworthy map pattern at Yucca Mountain is the preservation of early and middle Quaternary colluvial deposits on many hillslopes. These deposits have been dated by cosmogenic isotopes, volcanic ashes, cation-ratio dating, and uranium series dating on colluvial soils. The preservation of older Quaternary deposits indicates that hillslope erosion processes have been ineffective in eroding colluvial deposits that were weathered from bedrock during the colder, pluvial climatic episodes (Whitney and Harrington 1993). The slow removal of hillslope colluvium is also reflected in the lack of either large or steep alluvial fans at the base of the slopes at Yucca Mountain. The lack

of fans along the base of tilted fault blocks is a strong indication of very low rates of tectonic activity. As discussed in Subsection 3.10 Quaternary uplift rates are generally 0.01 mm/year or less for the faults in the Site Area.

Another interpretation can be made from the preservation of older Quaternary deposits at Yucca Mountain: the amount of climatic time that erosional processes dominate the landscape is less than the time during which hillslopes are mostly stable. Recent studies by Paces, Mahan et al. (1995) on the paleo-discharge deposits south of Yucca Mountain suggest that this scenario may be true. Climatic conditions appear to have been wetter and cooler than the present about 75 percent of the time during the last 100,000 years.

Southern and eastern hillslopes around Yucca Mountain are mantled by a relatively unique deposit called a sand ramp. These deposits are dominated by eolian sand that has blown against hillslopes and has been washed back down the slope, usually with an added component of coarse debris. The primary origin of the sand is the vast alluvial fan and terraces of Fortymile Wash and other washes that deposit fine-grained sediment in the Amargosa Valley. Sand ramps are as much as 30 m thick around Busted Butte, part of Fran Ridge, and slopes of the unnamed flanks of Southern Yucca Mountain. These sandy deposits are products of a very dry and windy climate that took place during some part of the interglacial component of the climatic cycle. Up to six buried soils have been found in some sand ramps that demonstrate the cyclic nature of dry, arid conditions at Yucca Mountain. The presence of Bishop ash near the base of several sand ramps indicates that eolian sand deposition goes back at least 760,000 years. The preservation of essentially unconsolidated sand on Yucca Mountain hillslopes underscores again the ineffective hillslope erosional processes during the last half of the Quaternary.

The distribution of Quaternary deposits of different ages in Crater Flat appear to reflect the ongoing opening, or extension, of the basin. Deposits of Q1 to Q3 age are concentrated on the eastern side of the basin near or adjacent to Yucca Mountain. Deposits of Q5 and Q6 age are concentrated along the southwest and southern margin of the basin, the area of maximum subsidence defined on the regional seismic reflection line (Brocher, Hart et al. 1996; Majer et al. 1996b; see also Subsection 3.3). A strong contrast in runoff patterns can be seen between the east flowing alluvial fans from Bare Mountain and the southerly slope of the drainage of Central Crater Flat. This drainage contrast probably reflects the presence of a buried fault in Central Crater Flat, and possibly a buried splay of the Bare Mountain fault near the base of the Bare Mountain fans. The fans of Bare Mountain are not rounded in typical fan shape, but terminate against a sharp, north-trending lineament defined only by a change in drainage patterns. Fault controlled sedimentation has occurred along the Windy Wash and Fatigue Wash faults. Uplifted early-to-middle Quaternary alluvium is juxtaposed to late Quaternary alluvium and colluvium.

On the east side of Yucca Mountain sedimentation patterns do not appear to reflect active tectonism, except where colluvial wedges have deposited locally against fault scarps. The northerly trend of Fortymile Wash, which is parallel to but not coincident with the Paintbrush Canyon fault, has raised questions about whether its origin is in part tectonically influenced. Several geophysical studies, summarized in the geophysical synthesis report, suggest that a very shallow graben may exist beneath the central alluvial portion of the wash (south of the canyon); however, the regional seismic reflection line does not show any significant offset of the Tertiary-Paleozoic contact beneath the

wash. No evidence of Quaternary tectonic activity has been associated with the wash. The southerly depositional pattern of the wash is controlled by the base level of the huge Amargosa valley.

Midway Valley is underlain largely by Q1 and Q2 deposits, because of a stream capture of Yucca Wash that appears to have taken place during the Middle Quaternary (Taylor, E.M. 1986). During Q1 time Yucca Wash flowed southeastward into Fortymile Wash through the gap between Alice and Fran ridges. After Q2 time Yucca Wash flowed eastward into Fortymile Wash north of Alice ridge.

In general, hillslopes are dominated by colluvial deposits that are produced during pluvial climates. The erosion and redistribution of these deposits takes place during drier climates, when hillslopes are no longer stabilized by vegetation. Hence most of the alluvial map units in the basins and valleys, which dominate the landscape at Yucca Mountain, were deposited during interpluvial episodes. Eolian deposits record exceptionally dry and windy conditions that occur in the climatic cycle; whereas paleo-discharge deposits from springs were deposited during the wetter and cooler conditions of the pluvial part of the cycle (see Subsection 5.2.7 for a complete description of paleo-discharge deposits and history). These patterns of deposition on Yucca Mountain are supported by multiple dating and descriptions of soils, surfaces and deposits.

3.4.4 Paleoenvironmental History of Yucca Mountain

The eight map units identified on and around Yucca Mountain represent nearly a million years of paleoenvironmental history. The landscape has experienced many cycles of Quaternary climatic change while tectonic activity has continued at a slow, almost imperceptible, rate. The surficial deposits at Yucca Mountain have left a fragmented record of climate history by recording sedimentary deposits, soils, and erosional unconformities that relate to the predominant geomorphic processes associated with past climatic episodes. The geologic record becomes more fragmented and indistinct with older map units because of poor exposure, burial by younger units, and because they generally cover greater periods of time. Still, many of the trends that can be interpreted in younger deposits with better age control can be assigned to older units on the basis of sedimentological characteristics and soil type.

Fortunately, a nearly continuous climatic record exists near Yucca Mountain at Devils Hole. The length and intensity of cool-wet to warm-dry climatic cycles for the Southern Great Basin is well defined for about 417,000 years (Winograd, Coplen et al 1992; Szabo et al. 1994). Long climatic records with some erosional breaks are also available from the studies of lacustrine cores from Owens Lake (Smith, G.I. et al. 1997) and especially from Death Valley (Li et al. 1996), which receives waters from the Amargosa drainage basin. These records, as well as Amargosa paleo-discharge records, pack-rat midden studies, and other Great Basin climatic records are discussed in detail in Section 4. These more continuous climatic histories are used here to help evaluate the climatic conditions that existed at Yucca Mountain when each of the identified map units was deposited, soils were formed, and erosional intervals dominated the landscape.

As discussed earlier, the Quaternary stratigraphy of Yucca Mountain is dominated by coarse colluvium and alluvium, and by eolian deposits. However, a small area of fine-grained spring discharge/marsh deposits is located at the south end of Crater Flat and at the north edge of the Amargosa desert. Paces, Neymark et al. (1996) have concluded that these deposits are analogous

to spring discharge deposits along the Spring Mountains formed by regional groundwaters that discharged at the surface during pluvial episodes (Quade, Mifflin et al. 1995). In the vicinity of Yucca Mountain, pluvial recharge may have raised the water table around 100 m (Quade, Mifflin et al. 1995).

A summary of age ranges for Yucca Mountain stratigraphic units and interpreted erosional intervals is shown in Figure 3.4-13. Also shown are time lines and paleoclimate records from SPECMAP (based on deep sea cores), Devils Hole, Death Valley, and Owens Valley to compare with Yucca Mountain stratigraphy. The strongest correlation is between the dry, warm Holocene climate and the deposition of units Q5 to Q7 around Yucca Mountain. These deposits record the most recent (and ongoing) erosion-dominated environment at Yucca Mountain. Following the disappearance of pluvial conditions about 17-15 ka, springs dried up and the dense vegetation that stabilized Yucca Mountain hillslopes gave way to more xeric and sparse vegetation. Summer storms result in localized debris flows that strip small areas on hillslopes and deposit debris nearby in local channels or at the base of a slope (Coe, Glancy et al. 1997).

Stratigraphic unit Q4 in Crater Flat appears to have been deposited during similar climatic conditions to Q5 and Q6. The unit contains abundant reworked basaltic ash that originated from the nearby Lathrop Wells volcanic center at about 75 ± 5 ka and soil carbonate which yields a similar age. These ages indicate that deposition of Q4 began sometime during the last major interglacial, known as Oxygen Isotope stage 5. Upper sand ramp deposits were also deposited during this interglacial. Younger soil ages of 38 to 40 ka are common on Q4, which indicates no deposition took place on this surface for about 30,000 years while soil development progressed. This time interval roughly correlates with Oxygen Isotope stage 4, a pluvial episode believed to be weaker than the last pluvial 22-18 ka; however, springs were discharging in Crater Flat and Fortymile Wash incised its most recent valley during this pluvial (Lundstrom, Wesling et al. 1996).

There was a pause in the downcutting of Fortymile Wash, represented by small, mostly strath terraces mapped as Q4f. The soil on this terrace is 25 to 35 ka, which indicates that this terrace probably formed during the short, drier climate of Oxygen Isotope stage 3. If this interpretation is correct, then Q4 in Crater Flat and Q4f on the east side of Yucca Mountain are not correlative in time. This difference in geomorphic response of processes on the landscape is probably due to the difference in the size of the Fortymile Wash drainage relative to the small, local watersheds on the western flanks of Yucca Mountain.

The next oldest map unit, Q3, exhibits similar age and soil development in Crater Flat and in Midway Valley on the east side of Yucca Mountain. Soils range in age from 128 to 150 ka on this deposit, which suggests that deposition mostly took place during Isotope Stage 7 followed by soil development during Stage 6. Fortymile Wash deposit Q3f has recently been shown to be about 74 to 102 ka, which suggests that it may depositively correlate in time with unit Q4 in Crater Flat. Q3, where exposed in trenches, includes one or more buried soils that suggests that this unit is time transgressive and includes more than one Middle Pleistocene climatic cycle. Also, at least two episodes of eolian activity occurred during the interpluvial climates of Q3 time. A buried soil below Q3f on Fortymile Wash was dated at 150 to 170 ka, which suggests the terrace alluvium below the soil was deposited during Q3, or Isotope stage 7 time, and soil formation subsequently took place during Isotope stage 6. During Isotope stage 6, former Lake Tecopa filled to overflowing (Morrison

1991b) and the last deep lake (Lake Manley) existed in Death Valley. During this wet pluvial Fortymile Wash probably incised a larger valley than now exists. The valley subsequently filled in Q4 (or oxygen isotope stage 5) time and buried former terraces on the west side of the wash with 2 to 3 m of coarse alluvium.

Detailed U-series dating using mass spectrometry shows that surface soils on older deposits at Yucca Mountain are time transgressive. A Q1 soil rind on a boulder yielded multiple age determinations that ranged from 35 ka to about 400 ka. The older ages are probably closer to the age of a deposit. U-series dates on Q1 ranged back to over 900 ka on Solitario Canyon hillslope deposits. This unit probably covers over 500 ka of alluvial history and covers several climatic cycles of time, but dating and correlations of the unit from place to place are not precise enough to interpret the Isotope stages during which alluvial deposition was active.

Given the inherent difficulty of dating coarse, arid-region deposits primarily by the time-transgressive soils that formed on them, a good to very good correlation exists between cyclic climate change and erosion and deposition at Yucca Mountain. Dated stratigraphic units at Yucca Mountain for approximately the last 150 ka show a strong correlation of spring deposition and stream incision during pluvial episodes (Isotope stages 2, 4, and 6), and hillslope erosion accompanied by valley and basin alluvial deposition during interglacial climates (Isotope stages 1, 3, 5, and 7), and times of rapid climatic change. The correlation of Quaternary units at Yucca Mountain with similar-age units in nearby areas, discussed above, strengthens the interpretation that episodes of erosion and deposition have been climatically controlled. A model of landscape response to climatic change in the Southern Great Basin is discussed below in greater detail.

Model of Landscape Response to Climate Change at Yucca Mountain—The model of landscape response proposed for the Yucca Mountain region is an area specific modification of, and builds upon, the general semiarid landscape model of Bull (1991). Parts of the Yucca Mountain landscape response model are similar to models proposed for Fish Lake Valley, Nevada-California (Reheis et al. 1996) and to the model for the Providence Mountains Piedmont, California (McDonald and McFadden 1994). The Yucca Mountain landscape response model, however, emphasizes hillslope processes response to climate change.

The Yucca Mountain landscape model is primarily driven by climate change and emphasizes the different depositional and erosional processes that are active, especially on hillslopes, during different phases of the Quaternary climatic cycle. Several factors help determine the texture and volume of sediments derived during a specific climatic phase. These include:

- Amplitude and duration of climate change in terms of both differences in temperature and precipitation
- The type and distribution of both summer and winter precipitation
- The sensitivity of the bedrock (Bull 1991, Table 3.5) to effects of these climatic changes

Rock types that have a high climatic (e.g., coarse-grained granites) sensitivity respond to a wetter climate by rapidly weathering. Such lithologies produce large quantities of fine grain material that

results in high volumes of hillslope sediment delivered to adjacent basins and relatively thick, fine grained basin depositional units. Conversely, rock types that are insensitive to climate change (e.g., welded tuffs) respond very slowly to a change to a wetter climate and may show little effect to either a short-term or small-amplitude climate change. During long wetter phases, such rock types may produce only small quantities of fairly coarse grained sediments that result in thin, coarser grained alluvial basin deposits.

In the landscape response model for the Yucca Mountain region, major geomorphic work (i.e., erosion and deposition) occurs primarily during climatic transitions, with times of more constant climate being times of relative landscape stability. The greater the magnitude in temperature and precipitation fluctuations during these transitions, the greater is the landscape response. Thus, the times of climate transition, from pluvial to interpluvial conditions (i.e., from wetter and colder to drier and warmer), as well as from interpluvial to pluvial conditions, are the times during which more rapid modification of the landscape occurs.

The climate model for landscape response in the Yucca Mountain region has four phases with primary characteristics as follows:

- A. Pluvial (full glacial) conditions: characterized by much wetter and colder than modern. Bedrock weathering occurs by both block extraction, due to freeze and thaw processes (Whitney and Harrington 1993), and by other physical weathering that results in reduction of initial block size. Freeze and thaw processes break out large blocks from bedrock outcrops and physical weathering reduces the size of rock clasts; chemical weathering processes are relatively ineffective and may produce minor granular disintegration and small amounts of fine grained material. The quantity of large blocks and smaller clasts produced depends upon the duration of the colder and wetter conditions. Aggradation on mid to lower hillslopes occurs during the coldest intervals; the dominant hillslope process that moves material downslope is rock and soil creep. Creep is slow movement under the force of gravity and aided by both moisture concentration and by freeze and thaw processes. Deposition of bouldery colluvium, produced during cold pluvials, protects parts of the lower hill slope from subsequent debris flow stripping (Whitney and Harrington 1993). If large quantities of boulders are produced during this climatic phase, talus may mantle entire hillslopes; if not abundant enough to mantle the entire hillslope, boulders tend to fill drainage channels, forming boulder streams. Colluvial aprons that cover the lower hillslope form during these climatic episodes and, if conditions persist long enough, grow headward up the hillslope, until they reach the hillslope summit.

Hillslope surface stability is enhanced by vegetation, which results in low sediment yield into stream valley drainages. On the east side of Yucca Mountain, runoff discharges into Fortymile Wash, but the discharge carries relatively little sediment. Streams may incise through alluvium; either through valley fill or through fan alluvium, and form stream terrace levels. Wetter periods are times of accelerated soil formation as eolian deposited carbonate is moved by water from near the surface to depth within the soil, resulting in formation of carbonate (k) horizons within the soil. These wetter periods are times during which soil B₁ horizons are formed. Pluvial conditions result in the "chemical weathering" of material in this soil zone to produce a fine grained (silt and clay) reddish horizon.

- B. Pluvial to interpluvial climatic transition: characterized by progressively warmer and drier conditions that result in lower vegetation density, especially on hillslopes. Hillslopes are progressively destabilized due to increased vegetation loss. Sediment yields from the hillslopes increase and are transported to the basin floor. Erosion on the hillslopes occurs primarily through debris-flow transport of previously weathered material. Physical erosion of bedrock on the hillslope is not an efficient process, as evidenced by a lack of incised bedrock channels on the hillslope; instead, broad, shallow channels are only minimally cut into the hillslope bedrock.

A change in precipitation regimens occurs, from relatively equally distributed seasonal precipitation of the pluvials, to drier summers with infrequent thunderstorms. Debris-flow stripping of hillslopes occurs through mobilization of hillslope sediments during infrequent, high intensity, short-duration thunderstorms, with attendant increase in sediment deposition in basins. The deposition of sediment results in both alluvial fan building, valley aggradation, and the formation of alluvial fill terraces. Eolian activity increases and sand ramp aggradation occurs.

- C. Interpluvial (interglacial) conditions: characterized by much warmer and drier conditions. Low and infrequent, although probably high intensity, precipitation and runoff occurs during this climate phase, resulting in low vegetation density with little-to-no grassland present. Infrequent hillslope stripping results in local aggradation and fan building. Main valleys aggrade slowly or remain essentially stable, while smaller washes aggrade. Eolian deposition of silt dominates surfaces and enhances carbonate buildup in near-surface soils. Eolian silt builds up on surfaces forming Av soil horizons beneath desert pavements. Eolian fine-grained material is also deposited on hillslopes, forming the matrices of boulder deposits which can effectively trap eolian fine sand and silt. A large, but infrequent, sediment yield from hillslopes continues until most colluvium has been removed; then hillslopes stabilize as a result of lack of sediment on the hillslopes that can be moved toward the basins.
- D. Interpluvial to pluvial transition: characterized by progressively greater and more seasonally equal precipitation (wetter) and cooler temperatures. Increasing precipitation results in increased vegetation density, greater hillslope stability, and lower hillslope sediment yields. Alluvial deposition in main channels changes to valley incision as increased vegetation leads to greater hillslope stability. Hillslope deposition begins as greater vegetation density retards removal of hillslope colluvium and enhances trapping of eolian material on the hillslopes. Eolian deposition decreases as vegetation density increases.

There appears to be a general correlation of basin sediment thickness and coarseness with the duration of the previous optimum weathering period (including both temperature and precipitation) on the adjacent hillslopes. Deposits that have a high ratio of coarse to fine grained material suggests that the hillslopes provided dominantly physically weathered material, suggesting that weathering occurred when temperatures were cold enough to promote frost wedging of bedrock outcrops. Basin deposits that contain high percentages of fine grained material, consist of both reworked eolian material transported to the basin

floor by debris-flows, and rock material that was continually downsized during long-term physical weathering. In like manner, deposits that are thick, when measured between sequential erosional surfaces or buried soils, indicate longer weathering duration than thin deposits that indicate weathering episodes of relatively short duration.

3.4.5 Erosion at Yucca Mountain and Vicinity

3.4.5.1 Erosion and Deposition in the Present Climate

Little data on modern geomorphic processes have been collected in the Yucca Mountain area. The primary reason for the paucity of data and studies is because of the infrequent runoff events that have occurred since the early 1980s when characterization studies of Yucca Mountain began.

Modern dust deposition in Southern Nevada has been studied by annual collection of dust samples from 1984 to 1989 from 55 sites in Southern Nevada and Southern California (Reheis and Kihl 1995; Reheis, Goodmacher et al. 1995). The average silt and clay flux (rate of deposition) ranges from 4.3 to 15.7 grams/m²/year. Annual dust flux increases with mean annual temperature and appears to be more strongly effected by decreases in annual precipitation than increases in temperature. Playa and alluvial sources produce about the same amount of dust per unit area; however, the total volume of dust produced is much larger from alluvial sources. The mineralogic and major oxide composition of dust samples indicates that sand and some silt is locally derived and deposited, whereas clay and some silt can be derived from distant sources. Eolian dust constitutes much of the pedogenic material in the Pleistocene and Holocene soils in desert regions. Modern and Holocene dust has been accumulating primarily as vesicular Av horizons below desert pavements on alluvial and colluvial surfaces in the Yucca Mountain region.

Hillslope processes and stream runoff at Yucca Mountain are related to large, but infrequent, storms that pass across the Southern Great Basin. One such runoff event at Yucca Mountain took place on March 11, 1995. It is important because it represents the first documented case during site characterization studies in which Fortymile Wash and Amargosa River flowed simultaneously throughout their entire reaches in Nevada (Beck and Glancy 1995). U.S. Geological Survey and Nevada Test Site rain gauges showed that cumulative precipitation ranged from 2 to 6 inches during March 9 to 11, with the larger amounts falling at higher altitude sites. In addition to the rainfall, high-altitude snowmelt also probably contributed to the 10- to 12-hour runoff event in Fortymile Wash. State highway 95 which is located on the alluvial fan of Fortymile Wash was closed for almost 10 hours due to flooding and sedimentation across the road. The last time both rivers were reported to have flowed extensively was in February 1969.

Short-duration flow in Fortymile Wash was first documented during site characterization studies in March 1983, and again during the summer of 1984, when the wash flowed briefly on three separate occasions in response to severe, but localized, convective storms.

The storm that occurred on July 21 or 22, 1984 also triggered debris flows on the south hillslope of Jake Ridge, located about 6 km east of the Yucca Mountain crest. Nearby rain gauges recorded 65 mm and 69 mm on July 21 and 20 mm and 17 mm on July 22. Rainfall intensities ranged up to 73 mm/hour on the 21st and 15 mm/hour on the 22nd. Using digital elevation models from pre-

storm and post-storm aerial photographs, a map was made to show the hillslope erosion and downslope redistribution of debris (Coe, Glancy et al. 1997). Volumetric calculations indicate that about 7,040 cubic m of debris was redistributed during the two-day storm. About 65 percent of the eroded sediment was deposited at the base of the slope and on a Fortymile Wash stream terrace, and the remaining 35 percent was deposited in a short tributary of Fortymile Wash, and in the wash itself. The maximum and mean depths of erosion were about 1.8 m and 5 cm, respectively. Precipitation intensity/duration relations developed from data recorded at a nearby precipitation gauge show that this storm was more intense than the hypothetical 500-year storm. Furthermore, field observations of the amount and stability of the remaining hillslope sediment, indicate this erosional event is related to a storm interval significantly greater than 500 years because even a frequency of occurrence of 500 years would have stripped most of the colluvium from Jakes Ridge. This conclusion is further strengthened by the paucity of modern erosional scars in the general region of the Nevada Test Site. The 1984 debris flow at Jake Ridge is a characteristic of the present erosional environment related to the dry, semiarid climate at Yucca Mountain.

3.4.5.2 Quaternary Erosion on Volcanic Land Forms

Surface exposure dating and ages of basaltic flows and cones show that erosion of topographic highs in the vicinity of Yucca Mountain has proceeded very slowly. Erosional modification of flows was evaluated at the Black Cone center where the flows were erupted ca. 1 Ma. Rock samples for cosmogenic ^{10}Be analysis were collected from an outcrop of degraded pressure-ridge as near as possible to the site where the K-Ar age of 1.0 ± 0.1 Ma was obtained (Crowe, Perry et al. 1995). The samples collected were from bedrock outcrops that were extensively coated with rock varnish. Cosmogenic ^{10}Be surface exposure dates, adjusted for existing shielding conditions and assuming no recent erosion of the rock surface because of the presence of thick continuous coatings of rock varnish, are 860, 470, 480, and 290 ky (± 25 percent). The minimum exposure age of the lava is taken to be the ~ 860 ky (± 25 percent) date because all geologic factors affecting the exposure history of the flow surfaces (erosion, burial, uncompensated shielding) will result in exposure ages that are younger than the true age. The measured ^{10}Be in these samples could have originated only from cosmic-ray bombardment of the lava surface after the flow cooled. This exposure age is similar to and consistent with a K/Ar age of 1.0 ± 0.1 Ma (Crowe, Perry et al. 1995) for the time of flow deposition and overlaps each of three other K-Ar ages reported by Crowe, Perry et al. (1995). Therefore, no statistical difference exists in the ^{10}Be exposure age and the K-Ar ages.

A maximum erosional lowering of the flow surface was calculated for the sample possessing the greatest exposure age in order to constrain the amount of erosion that has occurred on this bedrock outcrop since deposition of the flow. The maximum erosion rate at this site is 0.02 cm/ky. This calculation assumes constant, gradual erosion of the site. Using this erosion rate, the total eroded material from the flow surface, at this site, since the time of deposition, is ~ 17 cm and for the other sites with younger exposure ages is still less than one meter. This low quantity of erosional lowering of the crest of a pressure ridge on the Black Cone flows indicates that erosion of such volcanic features occurs very slowly in this area and that volcanic rocks are relatively insensitive to the range of climatic conditions that have existed in the Yucca Mountain area since the mid Quaternary.

The low erosional rates for the Crater Flat basalts can be explained by a model that includes armoring by desert varnish. The evolution of stable surfaces on lava flows starts with minor

erosional degradation of the primary surfaces of the flow soon after deposition. Rock varnish accumulation then begins on these semi-stable surfaces. The erosional stability of the rock surfaces would be enhanced by continuing deposition of rock varnish until the rock surface is completely covered by a fairly thick and continuous coating of varnish. The continuation of varnish accumulation would ultimately result in the long term stability of these rock surfaces. This hypothesis is supported by field evidence from boulder deposit clasts that commonly possess little to no weathering rind on the rocks beneath the rock varnish coating, indicating that formation of an impermeable rock varnish coating begins soon after deposition of the boulder.

As noted earlier, both the approximately 1 Ma cinder cones and the younger approximately 80 ka cinder cone of Lathrop Wells have retained much of their original morphology. In the case of the latter, Wells et al. (1990a) have concluded that the cone slope is virtually unmodified by erosion such that the morphology is similar to the 15 to 20 ka cones of the Cima volcanic field.

3.4.5.3 Erosion Rates at Yucca Mountain

Studies of past erosion on Yucca Mountain were carried out to address the regulatory concern as to the possibility of erosional breaching of the repository horizon during the regulatory period. Also emphasized by these studies is an analysis of the possibility of extreme erosion having occurred during the Quaternary Period at Yucca Mountain.

Two styles of erosion were examined in the Yucca Mountain area: erosion rates on hillslopes by removal of colluvial materials, and erosion rates on bedrock outcrops on ridge crests.

On the ridge crests of Yucca Mountain, erosion on exposed bedrock outcrops proceeds by the processes of exfoliation (detachment of thin rock sheets) and grusification (the grain by grain weathering of a rock). A unique advantage of cosmogenic nuclide techniques over other dating methods is their utility in directly determining, for a sampled outcrop, the maximum possible rate of bedrock erosion, assuming that erosion proceeded at a gradual and constant rate over the exposure duration. Such an erosion rate (the vertical bedrock erosion rate) can be calculated from the measurement of a single nuclide (^{10}Be) in multiple surface samples. The concentration of a cosmogenic nuclide is controlled by the production rate of that isotope and by the erosion of the surface. If the exposure time is considered infinite, the maximum erosion rate that could permit the measured concentration can be calculated.

Rock samples, taken from bedrock outcrops along an east-west ridge crest profile on two ridge spurs (Antler Ridge and Whaleback Ridge) on the eastern flank of Yucca Mountain, were analyzed for ^{10}Be in quartz separates from the tuff bedrock (Table 3.4-5). Because these tuffs are relatively quartz deficient (~2 percent) only small quantities of fine grained quartz was obtainable, even after very lengthy lab processing times. The concentrations of ^{10}Be in these seven rock samples results in the calculated maximum possible erosion rate for these bedrock outcrops of 0.04 to 0.27 cm/ky (Table 3.4-6). Thus, the vertical erosion rates on bedrock on the summit of Yucca Mountain range from <.10 to .30 cm/ky. This maximum possible erosion rate integrates all erosion occurring on the summit of Yucca Mountain under all climatic conditions that have existed in the area during a significant part, if not the entire Quaternary. The ^{10}Be data from the summit bedrock outcrops records a remarkable erosional stability for this landscape.

The rate of vertical erosion on bedrock (0.1 to 0.3 cm/ky) compares remarkably well to the long term average erosion rate in hillslope colluvium on the mid to lower hillslopes at Yucca Mountain (YMP 1993a) which was recalculated (0.22 cm/ky) using the recalibrated, rock varnish cation-ratio curve for Yucca Mountain (see Figure 3.4-14) with the uncertainties derived by applying the 95 percent confidence limits for the regression line of the curve.

The bedrock erosion values for Yucca Mountain also are very similar to erosion rates calculated for Australian granitic landforms (Bierman and Caffee 1996) where bedrock erosion rates of <0.5 cm/ky were determined for landforms in an arid part of Australia and a rate of 1 to 3 cm/ky was derived for a less arid Northern Australian area.

3.4.5.3.1 Hillslope Erosion Rates from Dated Colluvial Boulder Deposits

Relict boulder deposits on Yucca Mountain and nearby hillslopes were dated using the rock varnish cation ratio and the in situ cosmogenic nuclide dating methods (Whitney and Harrington 1993; Gosse, Reedy et al. 1996) to calculate the long-term rate of removal of unconsolidated material on the middle and lower hillslopes of Yucca Mountain. Boulder deposits range from wide continuous mantles to isolated narrow bands that are often bounded by gullies. The boulders in these deposits range in size from 0.3 to 2 m diameter. Eleven boulder deposits were sampled for cation-ratio dating: 6 on the flanks of Yucca Mountain, 3 on the southwest hillslope of Skull Mountain, one on the northeast slope of Little Skull Mountain, and one on the east slope of Buckboard Mesa (Whitney and Harrington 1993). The sampling and analysis process is described in Whitney and Harrington (1993).

Additionally, the average depth of erosion on the hillslope adjacent to the boulder deposits was measured perpendicular to the hillslope. The paleotopographic hillslope surface was assumed to be represented by the top of the boulder deposit on the hillslope. Because of the low relief across the middle hillslope today (on the order of 2 m of maximum relief across the hillslope), and inasmuch as stripping of hillslopes by debris flows is the dominant process at present moving material down these hillslopes, the modern relief on these hillslopes is probably a maximum for much of the Late Quaternary.

3.4.5.3.1.1 Cation-Ratio Dating of Hillslope Boulder Deposits

Cation-ratio dating of these boulder deposits was done to ascertain the deposit ages. Subsequently, in situ cosmogenic nuclide dating was done for four of the previously dated deposits to evaluate the cation-ratio dating results.

The cation-ratio data were first plotted on the original rock varnish cation-ratio curve calibrated for the Yucca Mountain area (Figure 3.4-14 and Harrington and Whitney 1987); calibrating the cation ratios to ages of surfaces independently dated by K-Ar and U-trend methods. K-Ar dating was used for sites on basalt rocks of more than 0.5 Ma and U-trend dating for sites on younger tuff surfaces (Harrington and Whitney 1987). The cation-ratio ages of the boulder deposits, calculated from the 1987 curve, ranged from 170 ka (130 to 220 ka) to ca. 1.4 Ma (1,030 to 1,890 ka), (Table 3.4-7, Column 3 and Whitney and Harrington 1993).

Following a re-evaluation of the calibration sites used for the original cation-ratio dating curve, new younger ages were used to recalibrate the cation-ratio curve, based on U-series, Thermoluminescence, and cosmogenic surface exposure ages (Figure 3.4-15). The cation-ratio ages for the boulder deposits were recalculated using the recalibrated curve. The recalculated rock varnish cation-ratio ages of the twelve dated boulder deposits range in estimated age from 100 (80 to 140 ka) to 1020 ka (730 to 1,430 ka) (Table 3.4-7, Column 4).

3.4.5.3.1.2 In Situ Cosmogenic Nuclide Dating of Hillslope Boulder Deposits

The boulder deposits dated by the cosmogenic nuclide method and their rock varnish age estimates (Table 3.4-7, Column 3) are:

- Buckboard Mesa deposit 1,030 to 1,890 ka
- Little Skull Mountain deposit 720 to 1,270 ka
- West side, lower hillslope Yucca Mountain deposit (YMW-3) 540 to 920 ka
- East side, upper hillslope Yucca Mountain deposit (YME-1) 490-830 ka (Figure 3.4-15)

These deposits were selected because they had the older cation-ratio ages and their substrate lithology included either basalt or ashflow tuff. The older deposits were selected for cosmogenic dating so that differences in the two dating techniques would be amplified by the longer time period being utilized.

The cosmogenic dating of the boulder deposits was carried out to evaluate whether the rock varnish cation-ratio age estimates earlier obtained for the hillslope colluvial boulder deposits were in reasonable agreement with the new cosmogenic nuclide exposure ages of the deposits, and to determine whether the differences in the two dating techniques would result in a large discrepancy in the calculated age, such that the calculated hillslope erosion rate might increase by more than an order of magnitude.

Each potential cosmogenic sample was examined to obtain those which possessed:

- The most complete rock varnish coating for the deposit
- No rock varnish on the underside of the rock sample, but instead a rubification (reddish hue) on the bottom surface
- Clasts with no appreciable weathering rind beneath the rock varnish coating on the rock sample.

Such precautions were taken to increase the likelihood that the rock sample was derived from the interior part of the source outcrop and minimize (although not preclude) the possibility of an inherited cosmogenic concentration in the hillslope boulder deposit sample.

In addition, most samples were collected from boulders with top surfaces that were flat and horizontal; a geometry correction was needed for only one sample.

It is generally impossible to determine the inherited cosmogenic nuclide concentration that may have been present in the boulders at the time of deposition (the deposit from the crest on the eastern flank, YME-1 is an exception, see below). Thus, the sampling strategy was selected to minimize the probability of an inherited cosmogenic nuclide component being present. If the sampled boulders do, however, contain some inherited concentration (i.e., C_{To} is not 0) the apparent exposure age calculated will be older than the true age of the boulder deposit.

The in situ cosmogenic ^{10}Be exposure ages (the assigned uncertainty for all cosmogenic dates is 25 percent, see discussion on uncertainties in Appendix 3.3-A, Methods of Investigation) for the four dated boulder deposits (Table 3.4-5) are somewhat younger than the cation-ratio ages for the same deposit. With the exception of the Buckboard Mesa deposit, however, the cosmogenic age uncertainty bounds overlap with the cation-ratio age bounds (Table 3.4-8).

The boulder deposit on the upper eastern flank of Yucca Mountain (YME-1) is unique among all the boulder deposits dated because it appears to have formed in situ; that is the clasts were not transported downslope after formation. In addition, there is no indication of drainage channels that incise the margins of the deposit, but instead, the deposit lies close to the crest of the hillslope in the zone of little to no erosion. Thus the entire concentration of cosmogenic isotopes in the boulders was acquired while they were at their present location (as either outcrop or boulders). Therefore, the maximum cosmogenic date (460 ky) must represent the time the boulders in this deposit have been at the surface (Table 3.4-5). The cosmogenic age range for this deposit clearly overlaps the lower uncertainty range for the rock varnish (320-590 ky) and demonstrates basic agreement of the results from the two dating techniques for this deposit.

The cosmogenic ^{10}Be analyses for the two basalt samples from the Buckboard Mesa deposit (Table 3.4-5), which were collected at some distance apart, yield almost identical exposure ages (510 and 550 ky). Unless these samples had acquired a significant and similar inherited cosmogenic concentration due to exposure in the outcrop prior to being dislodged as a boulder or during transport down the hillslope, there should be a low probability that these two boulders would have the same calculated exposure age. Additionally, this boulder deposit was dated using the in situ ^{36}Cl cosmogenic method. These data are reported in Whitney and Harrington (1993) and are only summarized here. Three samples from the Buckboard Mesa boulder deposit yielded ^{36}Cl ages of 310, 420, and 600 ka. Such ages are not inconsistent with the ^{10}Be age of approximately 530 ka. Therefore, a high probability exists, that the exposure age of the Buckboard Mesa deposit is approximately 530 ka.

The basalt boulder deposit in Skull Mountain Pass yields fairly different exposure ages for each of the three basalt samples collected for cosmogenic dating; 360 ka, 710 ka, and 1,010 ka (Table 3.4-5). The boulders of this deposit were derived from the flow that once covered the part of little Skull Mountain that lies directly uphill from the boulder deposit. Except for a couple of small outcrop areas, almost all of the flow has been removed by the downhill movement of basalt blocks. Therefore, an inherited concentration of cosmogenic nuclide is probable for some of the boulders within this deposit. The exposure age of this deposit is taken as the mean of the cosmogenic ages (697 ka).

The hourglass shaped boulder deposit (YMW-3) on the mid to lower hillslope on the western flank of Yucca Mountain also provided very different exposure ages for the three samples of ashflow tuff boulder analyzed for in situ cosmogenic ^{10}Be : 300 ka, 940 ka, and 2,700 ka (Table 3.4-5). Because an inherited cosmogenic component may have been acquired while in the source outcrop, and certainly that is true for the 2,700 ka date, the cosmogenic age for this deposit is taken as the mean of the younger two samples (620 ka).

The cosmogenic ^{10}Be exposure ages for the four boulder deposits appear to result in the same relative age chronology as the cation-ratio ages, except for the Buckboard Mesa deposit. The small number of cosmogenic samples, however, do not permit a statistically-based conclusion to the question of similar relative chronologies. In like manner there is not a large enough data set to conclude if the lithologic substrates influence the agreement between the cation ratio and the ^{10}Be exposure ages for these deposits.

The erosion rate (rate of stripping of unconsolidated material from the hillslopes) calculated using the cation-ratio dating curve of Harrington and Whitney (1987) averages ~ 0.2 cm/ky (.02 to .60 cm/ky) for the Yucca Mountain hillslopes. When the ages of the boulder deposits are either calculated using the recalibrated cation-ratio dating curve or calculated using the cosmogenic nuclide exposure ages, the long term average erosion rates for Yucca Mountain hillslopes is still less than 0.5 cm/ky.

3.4.5.4 Hillslope Stripping (Erosion) During the Q5 Interval

The record in Fortymile Wash and Midway Valley documents that in any of the climatic cycles recorded within the valley alluvium, the record is one of general landscape stability, punctuated by short pulses of either hillslope stripping or valley incision. Evidence that periods of hillslope stripping did not remove all colluvial material from the hillslopes is the presence of relic boulder deposits that cover parts of most hillsides.

The time interval during which the Q5³ alluvial unit (Lundstrom, McDaniel et al. 1995) was deposited in Midway Valley and Fortymile Wash can be used to derive quantitative boundary values for the amount of erosion occurring on the hillslopes of Yucca Mountain during this time interval (17 ka to 2 ka; see correlation chart). This 15 ky period covers the last pluvial to interpluvial transition (time during which the last climate transition from wet and cool to warm and dry) occurred. This period, as is true today, was a time of maximum late Quaternary dryness so the maximum erosional stripping of hillslope sediment probably occurred during this time interval (15 ky). An estimate of the material removed from these hillslopes (Lundstrom, McDaniel et al. 1995) has a mean depth of 27 cm of unconsolidated hillslope material. If this mean depth of material is assumed to have been deposited during the Q5 interval (15 ky of maximum hillslope stripping) a bounding rate of 1.8 cm/ky for erosion of unconsolidated hillslope material is derived. This rate does not incorporate either the eolian sediment addition to the hillslopes nor the sediment that moved through Midway Valley and into Fortymile Wash. If this alluvial unit were assumed to have been entirely derived from hillslope bedrock outcrops (which would be about 1/3 denser) the bedrock eroded would decrease to 18 cm and the rate of bedrock erosion to 1.2 cm/ky for the Q5 interval. This rate, calculated for a time interval of maximum hillslope stripping during the late Quaternary is larger by almost a factor of ten, than the erosion rate calculated for the middle and late Quaternary, on the

hillslopes (0.22 cm/ky) and bedrock ridges (0.1 to 0.3 cm/ky) of Yucca Mountain. Additionally, this erosion rate for a period of maximum hillslope stripping provides a bounding maximum erosion rate from which to calculate possible future erosion.

Note, however, that in the 10 ky prior to Q5 deposition, incision was occurring in both Midway Valley and Fortymile Wash, and little material was being removed from the surrounding hillslopes. Thus, the erosion rate for the complete climatic cycle for the Yucca Mountain hillslopes is 1.1 cm/ky for unconsolidated material and 0.7 cm/ky for hillslope bedrock, during the period from 27 ka to 2 ka.

3.4.5.5 Evolution of Fortymile Wash

Fortymile Wash drains the upper eastern part of the Amargosa River Basin, a drainage basin that is centered primarily on the Timber Mountain caldera that drains southward across the Amargosa Desert and empties into Southern Death Valley. Modern Fortymile Wash drains Eastern Pahute Mesa and Timber Mountain, the east flanks of Yucca Mountain, and Western Jackass Flats. Near the south end of Yucca Mountain the wash spreads across its own alluvial fan deposited in the Amargosa Desert. This fan has pushed the main Amargosa River southward against the alluvial fans of the Funeral Mountains.

Upper Fortymile Wash is characterized by the 25 km long Fortymile Canyon that is up to 500 m deep. Below the canyon the wash continues southward about another 20 km along the east edge of the Yucca Mountain complex of fault blocks before entering the Amargosa Desert. Between the canyon and the Amargosa Desert, Fortymile Wash has entrenched its own alluvial fill up to 25 m. The incision tapers off within 6 km where the channel becomes the head of a long fan that crosses the Amargosa Desert. The alluvial and incision history of Fortymile Wash is important to an understanding of how the wash will behave during the projected 10,000 years of regulatory concern for the potential HLNW site at Yucca Mountain.

By an analysis of the sedimentary provenance and altitude distribution of volcanic rocks in Fortymile Canyon, Lundstrom and Warren (1994) established that Fortymile Canyon was formed during the late Miocene or Pliocene, some time before 3 Ma. A relict gravel deposit exposed in Fortymile Wash contains a different lithology than the Quaternary gravel fills, which suggests that the present drainage captured a formerly northward-flowing drainage along the moat of the Timber Mountain caldera sometime after 9 Ma and before 3 Ma.

The Quaternary stratigraphy and incision of the wash are shown on two cross-sections, located a few hundred m north and south of the road that crosses the wash (Figure 3.4-16). These cross-sections are based on recent Quaternary mapping of Yucca Mountain by Lundstrom et al. (S.C. Lundstrom et al., *Preliminary Surficial Deposits Map of the Northwest Quarter of the Busted Butte 7.5-minute Quadrangle*, USGS-OFR-95-133, scale 1:12,000, in press) and recent dating of soils along Fortymile Wash Paces et al. 1995. The recognition and dating of buried soils and deposits along Fortymile Wash indicates that the alluvial history of the wash is more complex than originally believed (Taylor and Huckins 1986; Huber 1988; DOE 1995). Extensive dating of alluvial deposits around Yucca Mountain over the past seven years (Table 3.4-1), primarily by U-series, thermoluminescence dating, and volcanic ashes has shown that the experimental U-trend dates originally used to characterize the

age of Quaternary units around Yucca Mountain are generally too old. A revised dating of Quaternary units has shown that Late Pleistocene alluvium is present in Fortymile Wash and in Crater Flat (Faulds et al. 1994; Peterson, F.F. et al. 1995; Paces, Menges et al. 1994; Paces, Neymark et al. 1995; S.C. Lundstrom et al., *Preliminary Surficial Deposits Map of the Northwest Quarter of the Busted Butte 7.5-minute Quadrangle*, USGS-OFR-95-133, scale 1:12,000, in press).

The stratigraphy in the Fortymile Wash cross-sections shows a complex history of aggradation and incision. At the Fortymile Wash crossing (Figure 3.4-16) four coarse gravelly alluvial fills are exposed on the west wall of Fortymile Wash. A soil developed over each gravel deposit. These soils represent times when the deposit at this location was stable and not aggrading. Because vegetation density is high during pluvial episodes, little debris is eroded off hillslopes and deposited in stream valleys. Because pluvial episodes represent times of greatest precipitation, runoff, and little sediment yield, stream incision is possible during this part of the climatic cycle.

Evidence for multiple episodes of downcutting in Fortymile Wash can be seen by comparing the different stratigraphies on the east and west walls of both cross-sections. At Fortymile Wash Road crossing the buried soils on the west wall are missing from the east wall, which suggests the alluvial fill on the east of the wash wall is older than the 50 to 100 ka soils at the top of the fill, but younger than the 300 ka buried soil exposed in the west wall. Farther north at the Fortymile Wash-Calico fan site, the highest buried soil is about 170 ka on the west side, but is missing on the east wall. Exposed in gullies in the east wall are late Tertiary gravels and Middle Pleistocene eolian deposits that are overlain by Q3f alluvium. These angular unconformities are evidence of at least two episodes of downcutting that predate the deposition of Q3f. If the 170 ka date on the buried soil in the west wall is correct, then a major incision and erosion of older alluvium took place during the climatic time of isotope stage 6 of the global climate record (derived from marine cores), the wettest climatic episode at the end of the Middle Pleistocene. This is the same time that Lake Tecopa filled to overflowing (Morrison 1991b) and the last deep lake existed in Death Valley (Forester et al. 1996).

The alluvium of Q3f that underlies the main Fortymile Wash stream terrace was subsequently deposited during the interglacial oxygen isotope stage 5e-5a, and has developed a soil in it that is primarily of oxygen isotope stage 4 age.

The most recent incision of Fortymile Wash (Lundstrom, Mahan et al. 1996) probably took place during the penultimate pluvial episode, isotope stage 4, which is dated by Szabo et al. (1994) from about 116 ka to 60 ka. Within 2 m of the present channel of Fortymile Wash are remnants of a strath terrace with a thin alluvial deposit mapped as Q4f. This terrace most likely represents a pause in the downcutting of Fortymile Wash during the last, relatively short interglacial climate represented by isotope stage 3. The last 2 to 4 m of incision probably occurred during the last pluvial climate at Yucca Mountain 22-18 ka. Aggradation has taken place in the channel and on the lower Fortymile Wash fan, represented by Q5 deposits, during the Pleistocene-Holocene transition, and continuing through the Holocene up to the present. The history of Fortymile Wash, then, supports the climatic-geomorphic process response model described above.

The potential use of the incision history in terms of rates of incision must be evaluated in the light of three factors: the cyclical nature of cutting and filling that has taken place over at least several

Quaternary climatic cycles; relating incision rates to episodes of wetter time periods within a pluvial; and examining the base level for downcutting represented by the floor of the Amargosa Desert.

3.4.5.6 Incision in Valleys that Directly Overlie the Repository

Most of the valleys that drain eastward down the dip slope of Yucca Mountain and directly over the potential repository, merge in Midway Valley, then discharge into Fortymile Wash. The true base level for these valleys is Fortymile Wash, but the effective, present and likely future base level, is the floor of Midway Valley. Midway Valley is presently undergoing aggradation, because the present climate is warm and dry, resulting in infrequent but intense thunderstorms. Since at least the beginning of the Holocene, these storms activate debris-flow stripping of the hillslopes around Midway Valley and the sediment is carried onto the valley floor, resulting in a rising base level in Midway Valley. If a period of incision were to ensue, as a result of a change in climate to one of greater effective moisture, the main wash in Midway Valley would ultimately start to incise its valley floor. If the washes of Midway Valley were to proceed to incise their channels, such erosion might, over time, work its way headward, initiating a period of incision in the valleys over the repository. As part of such incision, the existing fill in the valleys would begin to be removed, and if this climatic condition were to continue for a long enough time, all the sediment in these valleys might be moved to the basin floor. An examination of the fill in Coyote Wash demonstrates that such a complete emptying of the alluvium in these valleys did not occur during the last glacial cycle. Not all the fill covering the present floors of these valleys has been deposited there in the Holocene; some dates back into the late Pleistocene. This relict fill, documents the incomplete stripping of the valley alluvium during the last two climatic cycles; the climate change (ca. 28 ka) to one favoring sediment removal from the valleys did not last sufficiently long enough (until sometime between 17 ka and 10 ka) to allow complete removal of sediments from these valleys. Since ca. 17 ka these valleys have been in an aggradational mode, with the climate becoming dry enough to produce high intensity thunderstorms, that produce debris flow stripping on the adjacent hillslopes. The most recent, well documented climate change in Fortymile Wash and Midway Valley, that resulted in a change from aggradation to incision, occurred following the deposition of Q4f by ca. 25 ka and before the beginning of deposition of Q5 at ca. 17 ka (see correlation chart). In valleys that overlie the repository, this period of incision resulted in incomplete removal of Q4 alluvium, so all incision was into unconsolidated alluvium, not the bedrock floors. During this same erosional phase, Q4 alluvium in Fortymile Wash was incised less than 2 m. It seems probable, therefore, that 10 ky would be a minimum estimate of the time necessary for a change in climates to that favoring incision in these valleys and for removal of the alluvium now covering the bedrock floor in these valleys. Based on our best documented period of erosion in the valleys that overlie the repository, it would require substantially more than 10 ky to effectively remove the alluvium and begin to actively erode the bedrock floor of these valleys.

INTENTIONALLY LEFT BLANK

3.5 SITE STRATIGRAPHY

3.5.1 Introduction

The exposed stratigraphic sequence at Yucca Mountain is dominated by mid-Tertiary volcanic rocks, consisting mostly of pyroclastic flow and fallout tephra deposits with minor lava flows and reworked materials (Figure 3.5-1), that were erupted from the Southwestern Nevada volcanic field during the period 15.2 to 11.4 Ma (Sawyer, D.A., Fleck et al. 1994; see Subsection 3.2, Regional Geologic Setting). Figure 3.5-2 shows the location of Yucca Mountain with respect to the southern part of the nested caldera complex that comprises the eruptive source of this extensive volcanic field, and the general distribution of the principal stratigraphic units. Regionally, the thick series of volcanic rocks (and older Tertiary rocks, where present) that form Yucca Mountain overlies Paleozoic sedimentary strata along a pronounced unconformity. The Paleozoic strata found in the region are discussed in Subsection 3.2. The volcanic rocks, in turn, are covered in many areas by a variety of late Tertiary and Quaternary surficial deposits (see Subsection 3.4, Quaternary Stratigraphy and Surficial Processes). Detailed descriptions of the Precambrian, Paleozoic, Mesozoic, Cenozoic, Tertiary, and Quaternary stratigraphy have been compiled into the *Yucca Mountain Project Stratigraphic Compendium* (CRWMS M&O 1996e). The compendium also includes information on each borehole in the area, regional and site geologic mapping, borehole geologic logs, available geochronology, and has various figures, charts, and graphs related to the stratigraphy in the Yucca Mountain area.

Because of their importance in contributing to a fuller and more comprehensive understanding of the geologic systems that could affect the suitability of the potential site at Yucca Mountain to safely dispose of high-level radioactive wastes, the volcanic rocks have been, and continue to be, a major focus of stratigraphic studies being conducted as part of the site characterization program. Summaries of geologic studies in the Yucca Mountain area have been published periodically (e.g., Eckel 1968; USGS 1984; Carr, W.J. Byers, and Orkild 1986; Carr, M.D. and Yount 1988; DOE 1988a; Buesch, Nelson et al. 1996), and reports describing the results of specific stratigraphic studies are numerous. In particular, much basic data on the thickness, lateral extent, correlation, and lithologic characteristics of the rocks in both surface and subsurface settings were obtained during detailed studies of cores from boreholes at key localities (e.g., Spengler, Byers et al. 1981; Carr, M.D., Waddell et al. 1986; Spengler and Chornack 1984; Scott, R.B. and Castellanos 1984), as well as the 1:12,000-scale geologic mapping by R.B. Scott and Bonk (1984). These studies revealed the lateral continuity of the major formations along approximately west-to-east and south-to-north profiles (Figures 3.5-3 and 3.5-4). In recent years, a large number of boreholes and cores from these boreholes were examined (or re-examined) and analyzed, and several surface sections of the volcanic units were measured and described (Figure 3.5-5) to collect new lithostratigraphic data that substantially supplement and refine the stratigraphic framework that had been developed during the earlier geological investigations. Some of the results of these more recent studies have been published by Geslin and Moyer (1995); Geslin et al. (1995); Moyer and Geslin (1995); Moyer, Geslin, Buesch (1995); Buesch, Spengler et al. (1996a); Rautman and Engstrom (1996a, 1996b); and D.C. Buesch and R.W. Spengler ("Stratigraphic Framework of the North Ramp Area of the Exploratory Studies Facility, Yucca Mountain, Nevada," in *Hydrogeology of the Unsaturated Zone, North Ramp Area of the Exploratory Studies Facility, Yucca Mountain, Nevada*: USGS Water-Resources Investigations Report 98-4050, in press). Much of this work was accomplished within

what is referred to as the "central block of Yucca Mountain," an area that is bounded on the west by the Solitario Canyon fault, on the east by the Bow Ridge fault, on the north by Yucca Wash, and on the south by Abandoned Wash (see Day et al. 1998a, for detailed geologic map of central block area).

Many investigations during the site characterization program of the Yucca Mountain area have focused on lithostratigraphic, hydrogeologic, and thermal-mechanical properties, and each has developed a stratigraphic system (Scott, R.B. and Bonk 1984; Spengler and Fox 1989; Moyer and Geslin 1995; Moyer, Geslin, Buesch 1995; Buesch, Spengler et al. 1996a; Day et al. 1997, 1998; Montazer and Wilson 1984; Flint, L.E. 1998b; Ortiz et al. 1985; Tables 3.5-1 and 3.5-2 show how these different stratigraphic systems correlate to each other). Each of these types of investigations has obtained a wide variety of data that is unique to each discipline, but all have a common foundation in the use of rock properties such as density and porosity, and therefore the systems are only semi-independent with lithostratigraphy often serving as the common framework.

Based on variations of geologic features in the rocks, formations within the Paintbrush Group have been divided into members, and the members into zones, zones into subzones, and subzones into intervals, and other formations have also been divided into these principal units (Buesch, Spengler et al. 1996a; Moyer and Geslin 1995; Moyer et al. 1996; Sawyer, D.A., Fleck et al. 1994). Separating the sequence into several hierarchical units and subunits has enabled other types of studies that depend upon stratigraphic data to be conducted at various scales as necessary to achieve their objectives. Examples of these various scales include:

- Geologic mapping at relatively small scales (1:6,000 or 1:24,000; see Subsection 3.6) in the site area or at much larger scales (1:2,400 or larger) along some fault zones, on cleared exposures for fracture studies, on walls of excavated trenches, and in the Exploratory Studies Facility
- Defining and correlating hydrogeologic and thermal-mechanical units
- 3-D modeling of rock properties

Thus, the system of lithostratigraphic unit identification and nomenclature that has been developed provides a consistent stratigraphic framework that can be applied in many other studies in the site characterization program.

Six principal results culminate from these lithostratigraphic studies and provide the context for subsequent investigations and chapters:

- Nineteen formations and interstratified bedded tuffs have been described in detail.
- Identification of lithostratigraphic units is based on changes in depositional features, development of zones of welding and devitrification, and in some rocks the development of alteration, such as the formation clay and zeolite minerals.

- The nomenclature and symbols of lithostratigraphic units consist of a systematic and hierarchical structure that enables identification and mapping of units at very detailed to generalized scales.
- The detailed lithostratigraphic system provides a framework within which the vertical and lateral continuity or variation of units can be evaluated, and although some units only occur locally, most are laterally extensive within the site area; therefore, lithostratigraphic units typically have a stratiform geometric shape.
- Rock properties, including density and porosity, are used in identification of lithostratigraphic units, and some of these properties are important in determining hydrogeologic and thermal-mechanical units.
- Lateral correlation of lithostratigraphic units that comprise the hydrogeologic and thermal-mechanical units, especially those units within the Topopah Spring Tuff that form the host rock of the potential repository (lower part of the Tptpul down to the base of the Tptpln, see Tables 3.5-2 and 3.7-1), indicates that the geometric volume and continuity of the rocks are conducive for continued evaluation for a potential repository at Yucca Mountain.

3.5.2 Criteria for Differentiating Volcanic Rock Units

The volcanic sequence at Yucca Mountain is composed primarily of pyroclastic flow deposits (also referred to as ignimbrites or ashflows) with volumetrically small amounts of bedded tephra deposits and localized lava flows and redeposited material. Most formations, which are shown in Figure 3.5-1 and identified with the three-lettered symbols, have some part that is at least partially welded, and typically some part of the section that has devitrified during cooling of the deposit. Additionally, the vitric (glassy) parts of many formations have been partly altered to clay and zeolite minerals, and all rocks have developed various amounts of fractures resulting from cooling or tectonic activity. Therefore, an understanding of the sequential development and overprinting of processes that formed the deposits (referred herein as primary processes), subsequently welded, devitrified, and fractured the deposits (referred herein as secondary processes), and ultimately altered and tectonically fractured the rocks (referred herein as tertiary processes) are critical in documenting and interpreting the lithostratigraphic sequence (Table 3.5-3). This tripartite division of processes represents distinctive segments of the geologic history that occur up to the time of deposition (primary), within the first 10 to several hundred years after deposition (secondary), and subsequently hundreds to millions of years after deposition (tertiary). These increments of time result from general limitations deduced from stratigraphic relations for rocks at Yucca Mountain and constrained by age determinations (Figure 3.5-1); studies of other areas including historical eruptions such as Katmai and Valley of Ten Thousand Smokes, Alaska (Fenner 1920); and numerical modeling of welding and cooling in pyroclastic flow deposits (Riehle et al. 1995). This division into primary, secondary, and tertiary is not entirely exclusive, and some processes such as faulting can occur during or shortly after deposition, or local alteration to clays and zeolites can occur during the cooling of a pyroclastic flow deposit (Levy and O'Neil 1989). General features of ashflow tuffs or pyroclastic deposits have been described by Ross and Smith (1961) and R.L. Smith (1960a, 1990b).

3.5.2.1 Lithology, Mineralogy, Geophysical Logs, and Rock Properties

Individual formations in the volcanic sequence that underlies Yucca Mountain represent either volumetrically significant eruptive units or a series of products interpreted to have formed from compositionally distinct magma batches. Many of the interstratified bedded tuffs and the locally occurring lava flows are distinct from the superjacent and subjacent formations and probably represent small volume eruptions. Separation of formations into subunits is based on macroscopic features (degree of welding, glass or devitrified, etc.) of the rocks as they appear in core and outcrop (Buesch, Spengler et al. 1996a), and their identification is augmented by quantitative mineralogy (Bish and Chipera 1986; Bish, Carey et al. 1996; Chipera, Vaniman et al. 1995, 1996; Chipera, Carter-Krogh et al. 1997), borehole geophysics (Muller and Kibler 1984; Nelson, P.H. et al. 1991; Nelson, P.H. 1996; Buesch, Nelson et al. 1996; CRWMS M&O 1997d, 1996b), and rock properties such as density and porosity (e.g., Moyer et al. 1996; Flint, L.E. 1998b).

Division of formations into lithostratigraphic units and their associated symbols was initially proposed by Warren, Sawyer et al. (1989) for rocks in the Yucca Mountain area that are a part of the Southwestern Nevada volcanic field (e.g., Lipman et al. 1966). This terminology was extended in greater detail in the Yucca Mountain area by Buesch, Spengler et al. (1996a). Several formations in the Southwestern Nevada volcanic field have an upper crystal-rich (> 10 percent phenocrysts) member and a more voluminous lower crystal-poor (< 5 percent phenocrysts) member, with a relatively thin transition in phenocryst abundance between members (Lipman et al. 1966; Broxton, Warren et al. 1989; Ferguson et al. 1994). In the vicinity of Yucca Mountain, the Tiva Canyon and Topopah Spring Tuffs of the Paintbrush Group, which are the most widespread bedrock units in the potential site area, are classic examples of this compositional zonation (Lipman et al. 1966). This transition in phenocryst abundance is typically 5- to 10-m thick and is included as a crystal-transition zone at the base of the crystal-rich member (Buesch, Spengler et al. 1996a).

Zones, subzones, and intervals are identified on the basis of textures, structures, and lithic fragments associated with pyroclastic flow and bedded deposits (depositional processes), zones of welding and crystallization (post-depositional processes), and geometry and surface roughness of fractures (mechanical properties of the rock) (Buesch, Spengler et al. 1996a). Zones are defined by:

- Vitric versus devitrified pyroclasts
- Occurrence of lithophysae and related light gray rims and spots and amount of pale red-purple groundmass versus the pale brown to light gray groundmass that is typical of nonlithophysal rocks
- Planar versus irregular geometry and smooth versus rough surfaces of fractures

Subzones and intervals are defined by:

- Surface roughness
- Abundance of pumice clasts
- Amount of welding

- Type of crystallization or alteration of pumice clasts
- Interstratification of thin units with characteristics of adjacent zones or subzones

Bedded tuff units within the Paintbrush Group (Tpbt1 to Tpbt4) that are not identified with any established formation are arbitrarily placed with the next overlying tuff sequence (i.e., the pre-Tiva Canyon Tuff bedded tuff underlies the Tiva Canyon Tuff; Table 3.5-2), and this terminology is consistent with previous usage (Spengler and Rosenbaum 1980; Diehl, S.F. and Chornack 1990). This nomenclature has been extended to the bedded tuffs that underlay the Calico Hills Formation and Prow Pass Tuff (Moyer and Geslin 1995). The post-Tiva Canyon Tuff bedded tuff (Tpbt5), which is an exception to this arbitrary assignment, is identified only where rocks associated with the rhyolite of Comb Peak (the youngest of the Paintbrush Group) can be identified. Many of the bedded tuffs consist of tuffaceous rocks not correlated with known eruptive units based on detailed tephrostratigraphic studies, and they commonly are capped by paleosols which separate them from the superjacent rocks.

Distribution of physical properties such as bulk density, porosity, and pore size are controlled largely by variations in the grain size and sorting, the abundance of volcanic glass, degree of welding, types and abundance of crystallization, amount and type of alteration to clay or zeolite, and fracture characteristics. Thickness, geometry, and internal heterogeneity of these lithologic components are influenced by the primary processes of eruption and deposition, the secondary processes of cooling and crystallization of lava flows or welding and crystallization of some pyroclastic flow deposits, and by the tertiary processes of alteration of glass to clay and zeolites by reaction with aqueous solutions and fracturing or faulting from tectonism (Table 3.5-3). Numerous papers describe the relation of physical properties to hydrologic and hydrogeologic properties (Scott, R.B., Spengler et al. 1983; Montazer and Wilson 1984; Flint, A.L. and Flint 1990; Rautman and Flint 1992; Istok et al. 1994; Moyer et al. 1996; Rautman et al. 1995; Flint, L.E., Flint, Rautman et al. 1996a; Flint, L.E. 1998b). To varying degrees, several of these papers discussed the influence of the primary, secondary, and tertiary processes on hydrogeologic properties, although various authors did not always use this tripartite division or consistent terminology of processes during these discussions. Several papers describe the relation of physical properties, primarily porosity, to mechanical properties (Price, R.H., Martin et al. 1993; Brechtel et al. 1995), but the correlation of thermal properties to porosity has only been evaluated informally. Therefore, knowledge of these rock-forming processes provides important tools for estimating and predicting the lateral continuity and heterogeneity of key properties of the stratigraphic, mineralogic, hydrologic, and thermal-mechanical frameworks.

Different types of eruption (effusive versus explosive) and the mechanisms of transport and deposition all combine to produce deposits with a range of depositional features (Table 3.5-3). For example, depositional features result from the variations in the amounts of components (glass shards, phenocrysts, and clasts of pumice and lithic fragments), size and shape of these components, and the degree of sorting of grain sizes. Many depositional features can change very sharply; such as contacts between bedded tephra beds and pyroclastic flow deposits. Contacts of this sort can be identified within millimeters. Other contacts such as changes in abundance of lithic or pumice clasts within a pyroclastic flow or fallout tephra deposit can be gradational across decimeters to many meters. Some contacts, including the amount of phenocrysts in the crystal-rich and crystal-poor members of the Tiva Canyon and Topopah Spring Tuffs, can have transition zones that are 5- to 10-

m thick and the contact is identified by a threshold value such as the decrease down-section to 5 percent (or less) phenocrysts at the top of the crystal-poor member.

Welding occurs in pyroclastic flows and (more rarely) bedded tephra deposits where glass shards and pumice clasts plastically deform as a result of combined deposit thickness (i.e., lithostatic load) and glass viscosity (a function of geochemical composition and temperature) (Smith, R.L. 1960a, 1960b; Ross and Smith 1961). However, depositional processes and the ability for interstitial gas to diffuse out of the deposit at low lithostatic pressure can enhance welding in some deposits (Buesch and Valentine 1989). Welding is the process whereby glass particles deform, porosity is reduced, and the geometry and connectivity of pore space are restricted. The concomitant increase in bulk rock density with increased welding results from the reduction in pore space with no change in density of the nonporous glass. Matrix density of vitric high-silica rhyolite and quartz latite (or trachyte), which are the two most common compositions in the rocks at Yucca Mountain, is typically 2.35 and 2.40 g/cm³, respectively. These densities have been measured optically by determining the refractive index of glasses that are compositionally similar to non-Yucca Mountain samples, and with helium and water pycnometry of crushed samples from Yucca Mountain (Scott, R.B., Spengler et al. 1983; Anderson, L.A. 1981, 1984, 1991; Flint, L.E. 1998b). These densities of nonporous glass provide a composition-based end member for evaluating the degree of welding determined from bulk rock measurements of core or from geophysical logs. Most rocks at Yucca Mountain contain some phenocrysts and lithic clasts, and most have devitrified during cooling, or exhibit some alteration to clay or zeolite minerals. All of these nonglass constituents have different densities. Most of the nonglass constituents are higher in density than glass with the exception of most clay and zeolite minerals that have lower densities. Therefore, these constituents will influence the bulk density, porosity, and particle density that are measured or calculated from bulk rock samples.

In their classic papers on the zones of welding, R.L. Smith, (1960b) and Ross and Smith (1961) divided tuffs into zones of no welding, partial welding, and dense welding, but provided no quantified measures of the amount of welding. An attempt to quantify this tripartite division of degree of welding has been based on bulk density and porosity (Sheridan and Ragan 1977) and with measurements of the aspect ratios of pumice clasts (Peterson, D.W. 1979). Vitric rocks have been divided into nonwelded rocks with porosity greater than 45 percent of the total volume, partially welded rocks with 45 to 10 percent porosity, and densely welded rocks are less than 10 percent porosity (Sheridan and Ragan 1977). Based on macroscopic and microscopic textures, rocks at Yucca Mountain are divided into the zones of nonwelded, partially welded, moderately welded, and densely welded (Spengler, Byers et al. 1981; Maldonado and Koether 1983; Scott, R.B. and Castellanos 1984; Spengler and Chornack 1984; Moyer and Geslin 1995; Buesch, Spengler et al. 1996a; Moyer et al. 1996; Figure 3.5-6). Based on the comparison of macroscopic features and measured porosity in core, these zones of welding have approximate ranges of 65 to 45 percent porosity for nonwelded rocks, 45 to 25 percent porosity for partially welded rocks, 25 to 10 percent porosity for moderately welded rocks, and less than 10 percent porosity for densely welded rocks. These ranges, especially the boundaries of partially to moderately welded and nonwelded to partially welded, should not be held as absolute thresholds between the zones because the values can vary from 22 to 30 and 40 to 50 percent for these zone boundaries. Processes such as incipient crystallization, vapor-phase corrosion and mineralization, and alteration can result in modification of these general thresholds and ranges. As described by R.L. Smith (1960b), these zones are vertically distributed in a simple cooling unit with nonwelded rocks at the top and bottom and

increasingly welded rocks toward the center of the deposit. Thick deposits can have the complete range in welding, both laterally and vertically, but thin deposits can lack the more welded central parts.

The five zones of crystallization include the vitric, high-temperature devitrification, vapor-phase corrosion and crystallization, lithophysal, and fumarolic alteration and crystallization zones (Smith, R.L. 1960b). Vitric zones occur where the original glassy components remained as glass after the period of high-temperature crystallization and final cooling of the deposit had ended. The clastic texture is typically well defined, except where completely fused in some densely welded rocks. Material less than about 2 mm is referred to as matrix to the larger clasts (which include pumice, lithic fragments, and phenocrysts). High-temperature devitrification forms rocks composed mostly of feldspar and silica minerals (quartz, cristobalite, or tridymite) with a variety of minor amounts of other minerals, and these minerals texturally form the groundmass that crystallized within the glass particles. Grain sizes and shapes are typically small (less than to much less than 1 mm), intricately intergrown, and referred to as microgranophyric. As defined by R.L. Smith (1960b), a granophyric zone has grain sizes that are macroscopically identifiable, but this zone typically occurs only where deposits are very thick, such as inter-caldera fill and, therefore, has not been an important zone in the outflow facies that form most of the rocks at Yucca Mountain. Locally, groundmass minerals can have distinctive morphologic forms that are referred to as spherulitic and axiolic.

R.L. Smith (1960b) defined the vapor-phase zone where crystals grow in pore spaces, but detailed work at Yucca Mountain has shown that this zone can be divided into vapor-phase corrosion and vapor-phase mineralization (D.C. Buesch and R.W. Spengler, "Stratigraphic Framework of the North Ramp Area of the Exploratory Studies Facility, Yucca Mountain, Nevada," in *Hydrogeology of the Unsaturated Zone, North Ramp Area of the Exploratory Studies Facility, Yucca Mountain, Nevada: USGS Water-Resources Investigations Report 98-4050*, in press). During initial periods of high temperature, the vapor phase is capable of corroding glass to form a secondary porosity. For example, initially solid glass shards can be corroded to form pores that mimic the shapes of the shards (Figure 3.5-7). Vapor-phase corrosion enhances porosity by corroding pumice, shards, and interstitial dust, and, therefore, changes the pore-size geometry and distribution. Vapor-phase mineralization occurs as the temperature cools and precipitates minerals such as tridymite or cristobalite, sanidine, and minor amounts of other minerals (Vaniman, Bish, Broxton et al. 1984; Buesch, Spengler et al. 1996a). Vapor-phase mineralization also reduces pore-size geometry and distribution. The balance between vapor-phase corrosion and mineralization results from the activity of the vapor-phase gases, and locally, either of these two processes can dominate the system. Both do not always occur at the same location. The importance of these processes and results of vapor-phase corrosion and mineralization have only recently been recognized (D.C. Buesch and R.W. Spengler, "Stratigraphic Framework of the North Ramp Area of the Exploratory Studies Facility, Yucca Mountain, Nevada," in *Hydrogeology of the Unsaturated Zone, North Ramp Area of the Exploratory Studies Facility, Yucca Mountain, Nevada: USGS Water-Resources Investigations Report 98-4050*, in press), and are currently only in the state of documentation with a preliminary ability to model the distribution. Pore-size geometry and distribution has an important effect on hydrogeologic and thermal-mechanical properties, but at this stage of understanding the interplay of corrosion and mineralization processes cannot predict a priori the results of these processes.

Lithophysal zones occur where vapor concentrates in the densely welded part of ignimbrites to form lithophysal cavities (Ross and Smith 1961), although lithophysae can also form in lava flows. Lithophysae consist of a cavity, which is commonly coated with vapor-phase minerals on the inner wall of the cavity. This is surrounded by a fine-grained zone, which, in turn, is surrounded by a thin, very fine-grained border (Figure 3.5-8). In the Tiva Canyon and Topopah Spring Tuffs, lithophysae typically range in size from 1 to 50 cm in diameter. Surface exposures, borehole videos, and exposures in the Exploratory Studies Facility locally contain lithophysae with diameters as much as 1 m; thus, regions of poor core recovery might indicate large lithophysae. Locally, lithophysae can be relatively uniform in size and shape, either all centimeters or decimeters in diameter, but lithophysae can also locally occur in a wide range of sizes and shapes within a lithophysal zone. Lithophysae can be nearly spherical with aspect ratios (length divided by height) approximately 1 to 2 or highly oblate with aspect ratios greater than 10 or 20. Some lithophysae are extremely oblate with cavities only 1- to 2-mm thick and 20- to 40-cm long, which results in an aspect ratio of as much as 400. These lithophysae appear to merge with larger features that have no macroscopic aperture, such as stringers and vapor-phase partings observed in the Exploratory Studies Facility. Rims of lithophysae are as much as 3 cm wide. Associated with the lithophysae are light-gray to grayish-orange pink spots 1 to 5 cm in diameter. Some spots may represent the cross sections of rims on lithophysae, whereas others have a crystal or lithic clast in the core that could have acted as a nucleation site.

Lithophysal zones in the Tiva Canyon and Topopah Spring Tuffs are identified by a combined occurrence of lithophysae, spots, and fracture characteristics (Figure 3.5-8). The shape of lithophysae and spots and width of the rims on the lithophysae can be diagnostic of specific lithophysal zones. Lithophysal zones have fewer fractures compared to nonlithophysal zones, and the fractures are typically irregular in profile and have rough surfaces with few high-angle, planar, and smooth fractures. Near the contacts of lithophysal zones and subzones, a localization of vapor-phase activity is indicated by an increase of veinlets and streaks in boreholes and core, and in the Exploratory Studies Facility there are larger features such as stringers and vapor-phase partings. Within the site area, the Yucca Mountain and Pah Canyon Tuffs do not contain lithophysae, but lithophysal zones are well developed in adjacent areas where these formations are thickest.

Lithophysae form in rocks that are densely welded, and possibly moderately welded, where the vapor phase accumulated at superlithostatic pressure to inflate a cavity that resulted in deformation of the matrix. This deformation must have occurred early in the post-depositional history while the matrix was viscous glass and prior to crystallization of the groundmass. Some lithophysae appear to have formed in pumice clasts, and might have utilized the slight structural discontinuity of the pumice clast compared to the matrix as an initial point of weakness. There is no direct evidence for the minerals that form rims and spots to have crystallized from the vapor phase (i.e., the morphology appears completely different from the cavity and fracture coating minerals that are typically interpreted as vapor-phase precipitates), but these minerals appear to have crystallized in the presence of vapor that probably diffused into the matrix surrounding the lithophysal cavity or along fractures.

There are few specific matrix-property data on the rims of lithophysae or on spots, but these features are very porous and have a lower density than the surrounding groundmass. Partial inclusion of these features in a sample of core or as part of the borehole probably creates some of the high

variability of properties measured in the lithophysal zones. During the 1980s, the core was commonly coated with water to enhance contrast of features and colors during the photographic sessions. Within minutes, the rims and spots were visibly dried, probably from adsorption into the rim or spot, whereas the adjacent groundmass remained wet for a much longer period of time.

Fumarolic alteration locally produces argillic and possibly zeolitic alteration mineralization that replaces glass or is deposited interstitially in pore space, sillar textures (nonwelded, incipiently crystallized with possible lithification by vapor-phase mineralization), and oxidation of iron in glass to form variegated red and orange colors. The most commonly recognized and documented type of fumarolic alteration occurs at localized points or along fractures where the vapor phase is released from the top of a cooling ignimbrite (Fenner 1920; Smith, R.L. 1960b; Ross and Smith 1961). This geometry of fumarolic alteration differs from that of the vapor-phase zones of corrosion and mineralization, or the vapor-phase zone described by Smith, R.L. (1960b), in that vapor-phase zones are much more laterally extensive and pervasive, although there can be localized variations in the amount to which it is developed. There is also a difference in source of the vapor phase between the vapor-phase zones and fumaroles. In vapor-phase zones, the vapor phase is derived from escape of gas that was interstitial to the grains of pyroclasts and lithic clasts in addition to vapor released during crystallization of the glass. In fumaroles, the vapor phase can be released from the interior parts of the deposit, or it results from the formation of steam as meteoric water percolates downward and encounters the hot, but cooling, parts of the deposit. Zones of fumarolic alteration and crystallization are not common in most of the rocks at Yucca Mountain, but occur locally in the crystal-rich, vitric, nonwelded subzone of the Topopah Spring Tuff and the pre-Pah Canyon Tuff bedded tuff (Levy, Norman et al. 1996; Barr et al. 1996; Peterman, Spengler, Singer et al. 1996a; Buesch, Spengler et al. 1996a; D.C. Buesch and R.W. Spengler, "Stratigraphic Framework of the North Ramp Area of the Exploratory Studies Facility, Yucca Mountain, Nevada," in *Hydrogeology of the Unsaturated Zone, North Ramp Area of the Exploratory Studies Facility, Yucca Mountain, Nevada*: USGS Water-Resources Investigations Report 98-4050, in press; see Table 3.5-2 for rock description and units). D.C. Buesch and R.W. Spengler, ("Stratigraphic Framework of the North Ramp Area of the Exploratory Studies Facility, Yucca Mountain, Nevada," in *Hydrogeology of the Unsaturated Zone, North Ramp Area of the Exploratory Studies Facility, Yucca Mountain, Nevada*: USGS Water-Resources Investigations Report 98-4050, in press) proposed that during the cooling of the Topopah Spring Tuff there was a diffuse, but widespread, type of fumarolic activity near the paleogeomorphic surface during the cooling phase of the Topopah Spring Tuff. This interpretation is based on the widespread occurrence of an argillically altered layer labeled unit c by Moyer et al. (1996) within the pre-Pah Canyon Tuff bedded tuff observed in borehole cores and at exposures in Solitario Canyon, in Harper Valley in the south-central part of Yucca Mountain (Levy 1993), and in the Exploratory Studies Facility (Barr et al. 1996; Levy, Norman et al. 1996; Peterman et al. 1996a). One critical aspect of this fumarolic activity is that it can be very tightly constrained based on lithostratigraphic relations whereby deposits in the uppermost part of the pre-Pah Canyon Tuff bedded tuff (unit D of Moyer et al. 1996) and superjacent deposits of the Pah Canyon and pre-Yucca Mountain Tuff bedded tuffs are not altered.

Analyses of samples from the unsaturated zone of Yucca Mountain indicate that smectite, clinoptilolite, and mordenite are the dominant low-temperature alteration products (Bish and Chipera 1989; Table 3.5-3). The low-temperature alteration potential of any lithologic unit is dependent on rock composition, rock texture, proximity to structure, and water-rock interaction (D.C. Buesch and

R.W. Spengler, "Stratigraphic Framework of the North Ramp Area of the Exploratory Studies Facility, Yucca Mountain, Nevada," in *Hydrogeology of the Unsaturated Zone, North Ramp Area of the Exploratory Studies Facility, Yucca Mountain, Nevada*: USGS Water-Resources Investigations Report 98-4050, in press). Volcanic glass that crystallized at high temperature is not susceptible to alteration except under high-temperature hydrothermal conditions. However, high porosity and permeability, whether inherited from the process of deposition or induced by fracturing, typically promote alteration of glass because of the high surface area of the particles. As a result of zeolitization, glass shards can be partially or completely replaced, and the porosity can be reduced by the in-filling with zeolite (Figure 3.5-9). Moderately to densely welded glassy rocks, including the crystal-poor vitrophyre of the Topopah Spring Tuff or obsidian in lava flows, have relatively low porosity and permeability and do not readily alter except along fractures as observed in some boreholes (see below).

Alteration to clays and zeolites occurs in three fundamentally different lithostratigraphic, structural, and hydrologic settings (Broxton, Bish et al. 1987): one within the saturated zone and two in the unsaturated zone. Alteration within the unsaturated zone is suspected to be associated with faults and through-going fracture systems and perched water horizons or horizons of lateral flow. One example of the importance of alteration along fractures is illustrated in numerous boreholes where borehole video shows the crystal-poor vitric densely welded subzone of the Topopah Spring Tuff has been significantly altered along high-angle fractures (Levy 1984a, 1984b; R.W. Spengler, USGS, written communication to R. Craig, December 13, 1996). Another source of clay minerals not described by Broxton, Bish et al. (1987) are the several paleosols and beds of redeposited materials where clays probably result from pedogenic processes. Rocks beneath ancient or present saturated zones can be pervasively altered (Broxton, Bish et al. 1987). The contact between vitric to pervasively zeolitized rock in nonwelded tuffaceous rocks occurs at or within a single bed in a few boreholes; whereas in several boreholes, the transition can be as much as 100 ft thick and the gradational alteration is dependent on grain size (R.W. Spengler, USGS, written communication to R. Craig, December 13, 1996).

In most of the formations, contacts between vitric and devitrified boundaries (including zones of vapor-phase corrosion and mineralization) are commonly marked by intervals of several millimeters to several meters that contain clay and/or zeolite alteration minerals (R.W. Spengler USGS, written communication to R. Craig, December 13, 1996). In some of the deeper formations vitric rocks near this vitric-devitrified contact are pervasively altered to zeolite, but there typically appears to be two stages in the alteration. The contact of the nonlithophysal zone and vitrophyre of the vitric densely welded subzone in the crystal-poor Topopah Spring Tuff, represents a relatively abrupt contact between high temperature devitrified rock and underlying glassy rock, but commonly a thin transition interval consists of well developed argillic or zeolitic alteration (Levy 1984a, 1984b; Levy and O'Neil 1989; Chipera, Vaniman et al. 1995; Buesch et al. 1996; D.C. Buesch and R.W. Spengler, "Stratigraphic Framework of the North Ramp Area of the Exploratory Studies Facility, Yucca Mountain, Nevada," in *Hydrogeology of the Unsaturated Zone, North Ramp Area of the Exploratory Studies Facility, Yucca Mountain, Nevada*: USGS Water-Resources Investigations Report 98-4050, in press; R.W. Spengler, USGS, written communication to R. Craig, December 13, 1996). Based on re-examination of core, cuttings, borehole video, and borehole geophysical logs, this interval of alteration occurs in most boreholes in the site area, and locally is as much as several meters thick. Levy and O'Neil (1989) determined that the alteration to clays and zeolites near this contact occurred

at moderate temperature, approximately 40 to 100 degrees centigrade, and proposed that this alteration occurred during the cooling phase of the Topopah Spring Tuff. With the recognition of argillic and zeolitic alteration near the crystallization front in many formations, this moderate temperature alteration might be a more common phenomenon than previously recognized (Table 3.5-3). The significance of this moderate temperature alteration has not been evaluated for hydrogeologic and thermal-mechanical modeling. Two possible additional locations of this type of alteration in rocks of the Paintbrush Group include the argillic alteration that is common near the vitric-devitrified contact in the crystal-poor Tiva Canyon Tuff, and the zeolitic alteration that occurs near the vitric-devitrified contact in the crystal-rich Topopah Spring Tuff (quantitative mineralogic data in UZ#16 from Chipera, Vaniman et al. 1995).

At Yucca Mountain, the overlap of depositional and zonal features typically results in an internal stratigraphy that is stratiform on regional and subregional scales, but locally, complex detailed lithostratigraphic relations may exist (Moyer and Geslin 1995; Buesch, Spengler et al. 1996a; Moyer et al. 1996). Zones of welding and crystallization are variously developed in the Rainier Mesa, Tiva Canyon, Yucca Mountain, Pah Canyon, Topopah Spring, Prow Pass, Bullfrog, and Tram Tuffs. Figure 3.5-10 conceptually illustrates how development of depositional features of a simple flow unit and the zones of welding and crystallization can result in a complex lithostratigraphic sequence. In this illustration, depositional features include changes in phenocryst content and abundance of pumice clasts. The zones of welding are nonwelded and partially, moderately, and densely welded. Zones of crystallization include vitric, devitrified, vapor-phase mineralization, and lithophysal zones. Although this illustration is to conceptually show the sequential overprinting of depositional features by the zones of welding and crystallization, it also represents a simplified rendition of the zones in the Tiva Canyon Tuff.

Based on the vertical succession of formations and interstratified deposits, development of the zones of welding and crystallization, and subsequent alteration and fracturing, there are myriad lithostratigraphic units, but there are actually only 23 rock types that comprise Yucca Mountain (Figure 3.5-11). Sixteen rock types are extensive and characteristic of large volumes of rock. Seven rock types are not common but possibly have local importance to hydrogeologic or thermal-mechanical process modeling. Six rock types occur only locally and do not (at this time) appear to be volumetrically or spatially important to hydrogeologic or thermal-mechanical process modeling.

3.5.2.2 Geochemical Criteria

In addition to the stratigraphic variations of rock properties and mineralogy discussed above, the volcanic rocks at Yucca Mountain show systematic variations in their chemical compositions. These variations, even within individual ignimbrite sheets, can occasionally assist in stratigraphic correlation and in the identification of altered zones.

Chemical and isotopic variations between different ignimbrite sheets are caused by variations in the erupted magmas, reflecting differences in magma sources and differentiation histories. Chemical and isotopic variations within individual ignimbrites sheets are due to igneous differentiation and assimilation processes in the magma chamber leading to vertical zonations in the chamber and inverse zonations in the ash-flow sheet as the volcanic eruption proceeds to tap increasingly deeper portions of the magma chamber (Lipman et al. 1966). Crystallization and vapor-phase activity during

cooling of the ignimbrite sheets may cause redistribution of some elements. Also, percolation of surface water into the volcanic rock section can deposit secondary minerals that locally modify the original igneous chemistry.

Many published reports are based primarily on geochemical analyses of the volcanic rocks. Peterman, Spengler, Futa et al. (1991) discussed the Topopah Spring Tuff as sampled in borehole a #1 (borehole locations shown in Figure 3.5-3). The crystal-rich member (Tptr, Table 3.5-2) is clearly distinguishable from the crystal-poor member (Tptp) on the basis of trace element concentrations. In this borehole, rocks in the vitric zone of the Topopah Spring Tuff (Tptpv) have been altered, and this alteration is marked by an increase in strontium concentrations with a corresponding change in strontium isotopic ratios. Spengler and Peterman (1991) discuss the trace element geochemistry of core samples from boreholes G-1 and G-3/GU-3 with emphasis on the volcanic units beneath the Topopah Spring Tuff. Detailed variations of trace elements within the crystal-rich member (Tpcr) of the Tiva Canyon Tuff provide a rather precise indication of stratigraphic position; Singer et al. (1994) provide an example of this application of geochemical stratigraphy. Peterman and Futa (1996) summarize the detailed geochemical stratigraphy of the Tiva Canyon Tuff from borehole NRG#3 and compare it to three outcrop sections. Lateral variation in the Tiva Canyon Tuff is evident and a possible fault in borehole NRG#3 was identified (Peterman and Futa 1996) based on a missing portion of the geochemical stratigraphic section. Also, geochemical stratigraphy was used to document separation on several strands of the Ghost Dance fault (see Taylor, E.M., Menges et al. 1996). To compare outcrop samples of the deeper volcanic section with the core samples, Peterman, Spengler, Singer et al. (1993, 1996b) provide geochemical and strontium isotope stratigraphy for a large suite of samples from Raven Canyon and Paintbrush Canyon (see Figures 3.5-2 and 3.6-1 for location). These analyses show that the drill core, although sampled below the water table, has comparable geochemical characteristics to the surface samples. In a study designed to evaluate the potential for a large-scale meteoric-hydrothermal system, Marshall et al. (1995) analyzed a large suite of surface samples of the Tiva Canyon Tuff. These samples were analyzed for a larger array of trace elements in order to identify anomalous metal contents and to evaluate the relative mobility of different elements during cooling of the ignimbrite sheet.

Borehole G-1 provides core samples extending from within the Topopah Spring Tuff down through the older Tertiary volcanic section to a total depth of 1806 m. As an example of the distribution of relatively immobile trace elements, zirconium and titanium concentrations are shown in Figure 3.5-12. Large variations both between formations and within formations are evident; these variations are primarily due to original magmatic compositional variation. Another deep borehole, a #1, shows similar variations in these elements (Figure 3.5-13), confirming the general lateral continuity of the Tertiary volcanic rocks. In this borehole, which extends to younger rocks in the stratigraphic sequence than were penetrated in borehole G-1, the break between the crystal-poor and crystal-rich members of the Topopah Spring Tuff is easily distinguished as the point at which the zirconium and titanium abundances begin to increase upsection.

Knowledge of the normal, igneous variations in the geochemistry allows identification of altered zones based on trace element abundances. Unlike zirconium and titanium, strontium is more easily mobilized by post-depositional fluid movements and transport of carbonate by infiltrating water. Even outcrop samples are susceptible to strontium and calcium additions due to the abundant soil

carbonate at Yucca Mountain. Zeolitization and clay alteration are evident in the crystal-poor, vitric, densely welded rocks of the Topopah Spring Tuff in borehole a #1. Strontium concentrations increase dramatically due to addition of strontium to the rock during alteration (Figure 3.5-14). Peterman, Spengler, Futa et al. (1991) calculate water/rock ratios of at least 100 during alteration, assuming that groundwater is the altering fluid.

Both the Topopah Spring Tuff and the Tiva Canyon Tuff show similar internal stratigraphy (Buesch, Spengler et al. 1996a). In particular, both formations contain a crystal-poor member overlain by a crystal-rich member. Trace element concentrations within the crystal-rich members vary systematically with stratigraphic position. As an example, zirconium, barium, and titanium increase upsection in the crystal-rich member of the Tiva Canyon Tuff in borehole NRG#3 (Figure 3.5-15) whereas niobium and rubidium decrease in the same interval (Figure 3.5-16). A striking feature of most of the geochemical profiles is the constancy in concentrations within the crystal-poor members of both the Topopah Spring Tuff and the Tiva Canyon Tuff. A comparison of the geochemistry of the crystal-rich member of the Tiva Canyon Tuff with that of the crystal-poor member of the Tiva Canyon Tuff in borehole NRG#3 (Figure 3.5-17) shows the general enrichments of compatible elements in the crystal-rich member, consistent with igneous crystal fractionation in the source magma chamber prior to eruption.

Strontium isotopic variations have also been documented in borehole NRG#3 (Figure 3.5-18). Not only have the crystal-rich and crystal-poor members of the Tiva Canyon Tuff evolved to very different isotopic compositions over their 12.7 million-year history, but calculated initial ratios also vary, indicating that the source magma chamber varied in isotopic composition due to melting processes in the crust. These strontium isotope variations provide another stratigraphic criterion that is useful for inferring small amounts of alteration and addition of strontium from infiltrating fluids.

In summary, the geochemical stratigraphy supports and augments the stratigraphy derived from detailed petrography and field characteristics. In some cases, the geochemistry helps to refine stratigraphic picks and can be used to verify small-scale fault offsets. In unaltered samples, the geochemical analyses provide background information that can be used to assess post-depositional alteration processes.

3.5.2.3 Borehole Geophysical Log Characteristics

A suite of borehole geophysical logs has been collected in 57 boreholes that are concentrated in the central block of Yucca Mountain, with several located near the bounding edges of the site area (Nelson, P.H. 1996; CRWMS M&O 1997d). In most boreholes, the suite commonly includes caliper, gamma ray, density, induction, resistivity, and neutron logs. In a few boreholes, there are magnetic, p- and s-velocity logs, and borehole gravimeter logs. With the aid of geophysical logs, many lithologic features can be correlated across the potential repository site (Nelson, P.H. et al. 1991; Buesch, Spengler et al. 1996b; CRWMS M&O 1996b). Welding and devitrification or alteration are important geologic controls on log response (Nelson, P.H. et al. 1991), and locally the grain size, sorting, and lithic clast content also can affect log response (Buesch, Spengler et al. 1996b). Increased welding causes matrix density to increase and porosity to decrease. Devitrification increases density, but porosity can remain unchanged, or it can increase or decrease depending on the amount of vapor-phase corrosion or mineralization. Mineral alteration (clays and

zeolites) causes a decrease in resistivity and an increase in neutron absorption, resulting in a high apparent neutron porosity. The magnetic susceptibility and remanence differs between formations depending on the chemistry of the rock and earth's magnetic field at the time of eruption and deposition. Additionally, volcanic glass can retain some magnetic properties, but devitrification (because it is at high temperature and occurrence shortly after deposition) forms highly magnetic minerals that typically increase the magnetic field of the rocks. Alteration typically reduces the intensity of many magnetic properties.

Boreholes GU-3/G3 and UZ#16 were continuously cored and, therefore, provide a coherent context for correlating geophysical logs with lithostratigraphic features (Figures 3.5-19 and 3.5-20). Many boreholes, including WT-2, were drilled with techniques that produced only cuttings and no core, but the geophysical logs have signatures indicative of various lithostratigraphic features (Figure 3.5-21). Based on core measurements and a study of geophysical logs from forty boreholes scattered across the Yucca Mountain area, P.H. Nelson et al. (1991) observed the following general relationships between lithologic features and gamma-ray, density, resistivity, and magnetic log responses. These relations have been reinforced and expanded upon with the addition of calculated porosity values derived from geophysical logs (Nelson, P.H. 1994, 1996), and inclusion of observations from geophysical logs from recently drilled boreholes (Buesch, Spengler et al. 1996b; R.W. Spengler, USGS, written communication to R. Craig, December 13, 1996; Rautman and Engstrom 1996a, 1996b; Engstrom and Rautman 1996; CRWMS M&O 1997d, 1996b).

- Tiva Canyon Tuff exhibits relatively uniform high density logs alternating with lower and more erratic density log responses; a uniform, high-intensity, gamma-ray log; high resistivity; and a low-amplitude, reverse-remnant magnetic field.
- The contacts of bedded tuffs interstratified between the Tiva Canyon and Topopah Spring Tuffs (units Tpbt4, 3, and 2, Table 3.5-2) typically show sharp, moderate to large changes in density, resistivity, neutron response, and computed porosity that mimic the bedded characteristics of these units. The pre-Pah Canyon Tuff (unit Tpbt2) characteristically has a broad, relatively smooth decrease in density and increase in resistivity and porosity that is bounded at the top and bottom by slightly more dense, lower resistivity, higher neutron, and lower porosity log responses.
- Yucca Mountain and Pah Canyon Tuffs, which are interstratified with bedded tuffs Tpbt4, -3, and -2 in the central and northern parts of Yucca Mountain, are almost indistinguishable on geophysical logs from the bedded tuffs in the southern part of their extent where they are thin, vitric, nonwelded ignimbrites (Figures 3.5-20, 3.5-21, and Figure 3.5-31). In the northern part of the site area, these two tuffs display characteristic welding profiles, are increasingly welded, devitrified, and vapor-phase corroded and therefore, are distinctive in relation to the bedded tuffs (Nelson, P.H. et al. 1991; Nelson, P.H. 1996; Buesch, Spengler et al. 1996b).
- The Topopah Spring Tuff is characterized by relatively uniform high density log values alternating with lower and more highly variable density log values; a highly uniform, high-intensity, gamma-ray log; high resistivity; and a low-amplitude, normal-remnant magnetic field.

- Tuffaceous rocks of the Calico Hills formation produce a low amplitude gamma-ray log, low density and resistivity logs, and a nonperturbed magnetic field. The formation is typically altered to clays and zeolites, except where it is vitric in the southwestern part of the central block and at Busted Butte. Compared to vitric rocks, altered rocks have a slightly higher density and lower resistivity. Effective porosity, which can be about the same as in the vitric rocks, is commonly slightly lower.
- The upper part of the Prow Pass Tuff is characterized by high resistivity and enhanced gamma-ray activity; a normal-remnant magnetic-field anomaly at the top serves as an excellent marker.
- The Bullfrog Tuff appears as a zone of high-amplitude gamma radiation, erratically higher density and resistivity, and a large-amplitude, normal remnant magnetic field. A decrease in welding at the top and bottom of the formation helps to define it on the logs.
- Tram Tuff has two different geophysical log signatures. The upper unit of the Tram Tuff is easily recognized by its very high amplitude, reverse remnant magnetic-field log and by high values of gamma radiation, density, and resistivity. The lower unit of the Tram, which is typically lithic rich, shows only low-level magnetic-field perturbations and moderate values for gamma radiation, density, and resistivity.

Geophysical logs respond to changes in rock properties, and hence lithostratigraphic features, that range from zones that can be 10 to 60 m thick and are defined by relatively consistent attributes, to distinctive intervals or beds that are less than 1 m thick. Lithophysal and nonlithophysal zones can be identified from bulk density logs and calculated porosity and water saturation values (Nelson, P.H. 1994, 1996; CRWMS M&O 1996b), as can many of the nonlithophysal vapor-phase corroded rocks such as those near the top and bottom of the Tiva Canyon Tuff and in the upper parts of the Topopah Spring and Prow Pass Tuffs (Buesch, Spengler et al. 1996b). Buesch, Spengler et al. (1996b) and R.W. Spengler (USGS, written communication to R. Craig, December 13, 1996) summarized the following correlations of lithostratigraphic features with geophysical logs. Calculated porosity and water saturation values can be used to identify, but cannot distinguish between, argillic and zeolitized rocks, especially near the devitrified-vitric boundary near the base of the Tiva Canyon Tuff (between units Tpcpln and Tpcpv2, Table 3.5-2), near the top of the pumiceous tephra deposited on top of the Topopah Spring Tuff (unit Tpbt2), and at the devitrified-vitric tuff contact in the lower part of the Topopah Spring Tuff (unit Tptpv3a at the Tptpln-pv3 contact). In many boreholes, the bulk density and calculated porosity and water saturation values respond to depositional changes in texture and composition including fallout tephra deposits interbedded with pyroclastic flow deposits, fine versus coarse-grained bedded tephra, and increases in the amount and size of lithic clasts. Although characteristic mineralogic variations between formations are not detected in the standard geophysical log suite, many eruptive sequences are capped by redeposited material or paleosols that commonly can be recognized on bulk density, calculated porosity and water saturation, epithermal neutron, induction, or resistivity logs.

For many lithostratigraphic features and units there is a good correlation of borehole geophysical logs (especially density, epithermal neutron, resistivity, and calculated porosity values) with matrix properties such as density and porosity, mineralogy, and borehole video observations. Figure 3.5-20

shows the relations between lithostratigraphic units (Geslin et al. 1995), porosity calculated from borehole geophysics (CRWMS M&O 1996d), matrix porosity measured at 105°C and relative humidity conditions (Flint, L.E. 1998b), quantitative mineralogy (Chiperá, Vaniman, Bish 1996), and the location of minor water seeps observed in borehole video. Intervals where the differential porosity (calculated by subtracting the relative humidity porosity from 105 porosity) is greater than 5 percent (Flint, L.E. 1998b) are also plotted. Calculated total porosity in UE-25 UZ16 utilized the calculations of P.H. Nelson (1996) and Thompson (CRWMS M&O 1996d). Five basic relations are depicted in Figure 3.5-20 (note that formations have three-letter symbols and the zones or units have shortened symbols):

- Devitrified, moderately to densely welded rocks of the Tiva Canyon, Topopah Spring, and Prow Pass Tuffs have porosities less than 25 percent and differential porosities less than 5 percent, are primarily "high temperature" mineral assemblages with mostly quartz+feldspar and moderate amounts of cristobalite or tridymite, and have very minor amounts of "low temperature" minerals such as clay (smectite+mica), zeolites (clinoptilolite+mordenite), and opal-CT. Lithophysal zones of the Topopah Spring Tuff and vapor-phase corroded zones of the Topopah Spring and Prow Pass Tuffs have calculated porosities as much as 45 percent and matrix porosity from core measurements as much as 30 percent.
- Vitric, nonwelded to partially welded rocks near the base of the Tiva Canyon Tuff, nonwelded bedded tuffs (Tpbt4, -3, and -2) and Yucca Mountain Tuff, and the nonwelded to partially welded rocks near the top of the Topopah Spring Tuff have porosities greater than 30 percent, locally have differential porosities greater than 5 percent, and are mostly glass with minor amounts of quartz+feldspar and minor amounts of clay.
- Vitric, densely welded rocks of the Topopah Spring Tuff typically have porosities less than 10 percent, differential porosities less than 5 percent, and are mostly glass. Rocks near the top of the crystal-poor, vitric, densely welded subzone of the Topopah Spring Tuff are pervasively altered to zeolite, form the altered interval (Tptpv3a), and have porosity greater than 10 percent with differential porosity greater than 5 percent.
- Rocks of the moderately welded to nonwelded subzones of the Topopah Spring Tuff (Tptpv2 and Tptpv1), the nonwelded pyroclastic flow deposits and bedded tuffs of the Calico Hills Formation (Tac4, 3, 2, 1, and Tacbt), and the nonwelded rocks of units 4 and 2 in the Prow Pass Tuff (Tcp4 and Tcp2) are pervasively zeolitic, have calculated and 105 porosity typically between 20 and 35 percent and differential porosities greater than 5 percent.
- Two minor water seeps are associated with a 6 cm-thick bedded tuff at the base of unit 4 and at the top of the bedded tuff near the base of the Calico Hills Formation. Both seeps occur where there is a textural change in the rocks (fallout tephra deposits overlain by pyroclastic flow deposits) and an increased amount of lithic clasts in the bedded tuff compared to the pyroclastic flow deposits. These textural and compositional changes are represented in the calculated porosity log and quantitative mineralogy.

In borehole WT-2, similar relations occur for lithostratigraphic units, calculated total and water-filled porosity (Nelson, P.H. 1996), and quantitative mineralogy for cuttings samples (Bish and Chipera 1989) (Figure 3.5-21). In comparison with the same lithostratigraphic units as in borehole UZ16, the:

- Calculated total porosity appears slightly greater
- Calculated water-filled porosity has similar values to the relative humidity porosity
- Separation in total and water-filled porosity in the lithophysal zones and vapor-phase corroded zones of the Topopah Spring Tuff is similar to the difference between calculated total porosity and the matrix porosity
- Crystal-poor, vitric, densely welded, altered interval in the Topopah Spring Tuff (Ttpv3a) can be identified on the porosity logs at depth of approximately 1,190 ft

There are two significant differences in lithostratigraphic features and geophysical logs between these two boreholes. First, the vitric-zeolitic boundary (where rocks above the boundary are mostly, if not completely, vitric and those below are pervasively altered to zeolite and indicated by the symbol CHnv-z) occurs very near the base of the vitric, densely welded subzone of the Topopah Spring Tuff in UZ16, and in WT-2 this boundary is very near the base of unit 3 in the Calico Hills Formation (Tac3). Identification of the vitric-zeolitic boundary is based on examination of cuttings (R.W. Spengler, USGS, written communication to R. Craig, December 13, 1996) and where the water-filled porosity is greater than total porosity (Nelson, P.H. 1994, 1996). P.H. Nelson (1994, 1996) describes the rationale for the interpretation that the rocks have more water than can be accommodated in pores; some of the water is in the mineral phase (this is also referred to as structural or bound water). Second, the upper part of unit 3 in the Prow Pass Tuff (Tcp3) shows a large separation in total and water-filled porosities and this corresponds to the vapor-phase corroded part of the unit. There are almost no clays and zeolites in this part of the section; therefore comparison of this unit in these two boreholes might indicate lateral variation in the development of the secondary porosity and pore geometry.

Geophysical logs have been invaluable in correlating lithostratigraphic features and units across Yucca Mountain, and can be used to calculate porosity and saturation curves (Nelson, P.H. 1993, 1994, 1996; CRWMS M&O 1996d) that serve as primary input for porosity and property models (Rautman 1996; also see discussions in CRWMS M&O 1996g, 1997d, and in Subsection 3.8, Integrated Site Model, CRWMS M&O 1997e).

Regardless of the utility of geophysical logs, great care must be taken to properly correlate and interpret these data. One example of an apparent spurious result from geophysical logs that occurs in several boreholes involves the localized alteration of the crystal-poor, vitric, densely welded subzone of the Topopah Spring Tuff (Buesch and Spengler 1998). This pervasively altered material, which is referred to as the altered interval of the vitric, densely welded subzone (Unit Ttpv3a, Table 3.5-2), is associated with the vitric zone because glass can alter to clays and zeolites whereas minerals resulting from devitrification processes typically do not under most temperature and geochemical conditions at Yucca Mountain (Bish and Aronson 1993; R.W. Spengler, USGS, written communication to R. Craig, December 13, 1996). Figure 3.5-22, which is a conceptual composite

from several logs, illustrates the general relations of devitrified, vitric, and altered rock near the contact between the lower nonlithophysal and crystal-poor vitric zones of the Topopah Spring Tuff. Lithostratigraphic relations, which have been observed in several boreholes, include vitric pumice clasts near the base of the lower nonlithophysal zone (Ttptln1), spherulites in the upper part of the vitric densely welded subzone, and alteration along the contact and along high-angle fractures (Ttptv3a). Based on measured and calculated techniques, the typical grain density for densely welded devitrified rock is 2.55 g/cm^3 , densely welded vitric rock is 2.35 g/cm^3 , and alteration (clay and zeolite) minerals are 2.10 g/cm^3 . Ideally, crystal-poor, densely welded tuff with no lithic clasts that devitrified with porosity less than 10 percent will vary in bulk density from 2.24 to 2.55 g/cm^3 , whereas vitric rocks with porosity less than 10 percent will vary from 2.12 to 2.35 g/cm^3 .

Figure 3.5-22a illustrates typical variations across a nonaltered contact where vitric rocks result in a decrease in the density log. Figure 3.5-22b illustrates the pronounced decrease in the density log of narrow width where the contact is altered, and a pronounced but sustained decrease in the density log where the contact is altered and the borehole traverses a near vertical fracture, whereas the host rock is the vitric densely welded subzone. Thus, using geophysical logs one can often identify localized alteration of the upper contact of the crystal-poor, vitric, densely welded subzone of the Topopah Spring Tuff (R.W. Spengler, USGS, written communication to R. Craig, December 13, 1996).

3.5.3 Stratigraphic Descriptions

During the course of stratigraphic investigations at Yucca Mountain, formations within the Paintbrush Group were divided into members, and the members into zones, zones into subzones, and subzones into intervals (Buesch, Spengler et al. 1996a). The underlying Calico Hills Formation and the Prow Pass Tuff of the Crater Flat Group were likewise systematically studied and each subdivided into several lithostratigraphic units (Moyer and Geslin 1995). However, volcanic rocks older than the Prow Pass Tuff and younger than the Paintbrush Group (Timber Mountain Group), which are known primarily from the logging of cores and drill cuttings from a few boreholes and from observations of very limited outcrops, were not subjected to the same degree of separation into individual units as were the Prow Pass Tuff, Calico Hills Formation and formations within the Paintbrush Group.

Lithologic descriptions are given in two tables: Table 3.5-1, which includes generalized descriptions of the pre-Prow Pass Tuff volcanic rocks that were not subjected to a large degree of subdivision; and Table 3.5-2, which includes detailed descriptions of all the members, zones, subzones, and intervals that were defined within the Prow Pass Tuff (of the Crater Flat Group), Calico Hills Formation, and formations of the Paintbrush Group, as well as generalized descriptions of the next overlying units of the Timber Mountain Group. Only summary discussions of the larger stratigraphic units (formations and members, or other principal subdivisions) will be given below. Thicknesses of formations are given in both metric and English units, but those for subunits are given only in metric units for the most part. In general, stated borehole thicknesses are apparent, depending on the geometry of the borehole and the dip of the stratigraphic units. Locations of measured surface sections and boreholes are shown in Figure 3.5-5.

3.5.3.1 Pre-Cenozoic Rocks

Pre-Cenozoic rocks, believed to consist primarily of upper Precambrian and Paleozoic strata, underlie the Tertiary volcanic rocks at Yucca Mountain, but little detailed information is available on their thickness and overall lithology. The only direct evidence of their presence is in borehole p#1, located about 2 km east of Yucca Mountain, which penetrated Paleozoic carbonate rocks in the depth interval 1,244 to 1,805 m (Figure 3.5-3). These rocks, almost entirely dolomites, have been correlated with the Lone Mountain Dolomite and Roberts Mountains Formation on the basis of exposures of these formations at Bare Mountain to the west, and on the presence of conodonts of Silurian age (Carr, Byers and Orkild 1986). Descriptions of pre-Cenozoic rocks in the region surrounding Yucca Mountain are given in Subsection 3.2 (Regional Geologic Setting) and further details have been compiled in the Yucca Mountain Project Stratigraphic Compendium (CRWMS M&O 1996e).

3.5.3.2 Pre-Lithic Ridge Volcanic Rocks

The oldest known volcanic rocks in the Yucca Mountain area were deposited approximately 14 Ma and underlie the Lithic Ridge Tuff. Because these pre-Lithic Ridge Tuff rocks are not exposed at Yucca Mountain, little is known about their extent and stratigraphic relations except locally where they have been penetrated in boreholes. In boreholes G-1, G-2, and G-3 (Figure 3.5-4), the pre-Lithic Ridge Tuff sequence consists of bedded tuffaceous deposits, pyroclastic flow deposits, and quartz-latic to rhyolitic lavas and flow breccia (Broxton, Byers et al. 1989); penetrated thicknesses vary from approximately 45 m (148 ft) in G-3, to approximately 350 m (1,148 ft) in G-2. In borehole p#1, 180 m (590 ft) of older, altered tuff occurs between the Lithic Ridge Tuff and Paleozoic strata (Muller and Kibler 1984). The pre-Lithic Ridge rocks contain alteration products, such as clays, calcite, and chlorite (Spengler, Byers et al. 1981; Bish and Vaniman 1985) that have been used to compile an alteration history of these older rocks (Bish and Aronson 1993; Chipera, Carter-Krogh et al. 1997). Details of the stratigraphy of these pre-Lithic Ridge rocks have been compiled in the Yucca Mountain Project Stratigraphic Compendium (CRWMS M&O 1996e).

3.5.3.3 Lithic Ridge Tuff

The Lithic Ridge Tuff is a thick, massive pyroclastic flow deposit (Carr, Byers, and Orkild 1986) with thicknesses ranging from 185 m (607 ft) at borehole G-2, north of the potential repository, to 304 m (997 ft) in borehole G3/GU3, at the south end of the repository (Figure 3.5-4). The formation is nonwelded to moderately welded and has been extensively altered to clays and zeolites. Many slight variations in the degree of welding, phenocryst ratios, and lithic-fragment content suggest that several eruptive surges are represented, which is in part supported in borehole geophysical logs. The formation is separated from the overlying dacitic lava and flow breccia (where present) by a bedded tuff unit composed mainly of fallout tephra (Table 3.5-1), and is distinguished from the Tram Tuff by a lower quartz content, by the presence of sphene, and by a differing content of lithic fragments (Broxton, Byers et al. 1989).

3.5.3.4 Dacitic Lava and Flow Breccia

Dacitic lava and flow breccia overlie the Lithic Ridge Tuff in deep drillholes in the northern and western parts of Yucca Mountain, but are absent elsewhere. The thickness of the unit is 112 m (367 ft) in borehole H-1 and 249 m (817 ft) in borehole H-6. In borehole G-1, most of the unit is flow-breccia made up of angular to subangular fragments of dacite, commonly from 2 to 10 cm long, which is intercalated with a few lava flows ranging from 1 to more than 17 m thick (Spengler, Byers et al. 1981). The breccia is autoclastic, suggesting that its formation is largely due to fragmentation of semisolid and solid lava during relatively slow movement of the lava flow. The flow breccia is underlain by about 8 m of reworked pyroclastic fallout and bedded tuff deposits in borehole G-1 (Spengler, Byers et al. 1981). Similar mineral constituents suggest a genetic link between these tuffs and the overlying flow breccia, and most of the upper part of the bedded interval has a volcanic texture suggesting postemplacement fusion.

3.5.3.5 Crater Flat Group

The Crater Flat Group consists of three formations of rhyolitic, moderate to large volume, pyroclastic flow deposits and interstratified bedded tuffs that are distinguished by their stratigraphic relations and petrologic and geochemical characteristics. In ascending order, these formations are the Tram, Bullfrog, and Prow Pass Tuffs (Sawyer, D.A., Fleck et al. 1994; see Carr, Byers and Orkild 1986, and Byers, Carr, Orkild et al. 1976, for original descriptions). The Bullfrog Tuff is associated with the Silent Canyon caldera complex, but sources of the Tram and Prow Pass Tuffs are less certain (Sawyer, D.A., Fleck et al. 1994). The Crater Flat Group is distinguished from other pyroclastic units in the vicinity of Yucca Mountain by the relative abundance of quartz and biotite phenocrysts. In addition, the Prow Pass Tuff and, to a lesser degree, some parts of the Bullfrog Tuff contain distinctive lithic clasts of reddish-brown mudstone. At Yucca Mountain, the Crater Flat Group overlies dacitic lavas and flow breccias in the northern part of Yucca Mountain, and the Lithic Ridge Tuff in the southern part (Broxton, Byers et al. 1989; Figures 3.5-4 and 3.5-5). Generalized descriptions of the Tram Tuff and Bullfrog Tuff are given in Table 3.5-1 and detailed descriptions of subunits within the Prow Pass Tuff are included in Table 3.5-2.

3.5.3.5.1 Tram Tuff

There has not been a recent systematic lithostratigraphic study of the Tram Tuff that includes all boreholes at Yucca Mountain. However, numerous depositional units have been distinguished by observed changes in the abundance and types of pumice and lithic clasts in pyroclastic flow deposits and rare bedded tuff interbeds. The most easily recognized stratigraphic divisions are the lower lithic-rich unit, which in itself can be locally divided into a lower lithic-poor and an upper lithic-rich set of subunits, and an upper lithic-poor unit (Table 3.5-1), first described by Maldonado and Koether (1983). Both lithic-rich and lithic-poor units have been identified and described in several boreholes including p#1, G-1, b#1, G-3 and H-1 (Spengler, Byers et al. 1981; Maldonado and Koether 1983; Scott, R.B. and Castellanos 1984), whereas in borehole G-2 the upper lithic-poor unit is absent and the lithic-rich unit is well developed (Maldonado and Koether 1983). Welding is variable throughout the Tram Tuff (Scott, R.B. and Castellanos 1984), and, locally, the large concentration of lithic clasts such as in borehole G-2 apparently reduced the degree of welding. In general, the lithic-poor unit is more densely welded than the underlying lithic-rich unit (as can be

inferred from the correlated change in geophysical logs (gamma, density, porosity) above and below the 980-m depth in borehole G-3/GU-3, Figure 3.5-19); however, the stratigraphic position of the zone of maximum welding within the upper unit is not the same everywhere. Argillic and zeolitic alteration occurs in both units of the Tram Tuff. In the lithic-poor unit, the alteration appears to occur in two zones separated by the zone of maximum welding that typically is devitrified. Thicknesses of the Tram Tuff across Yucca Mountain range from about 60 m to as much as 396 m (200 to 1,300ft; Figure 3.8-14). A regional isopach map by Carr, W.J., Byers, and Orkild (1986) shows the thickness of the formation to be in excess of 400 m (1,310 ft) in the northern part of Crater Flat to the west.

The lithic-rich unit is underlain by a complex sequence of altered and weathered pyroclastic fallout deposits and minor pyroclastic flow deposits (e.g., see Diehl, S.F. and Chornack 1990). These pre-Tram Tuff bedded tuffs range in thickness from 50 m (164 ft) in borehole G-2 to only about 8 m (26 ft) in borehole G-3 (Figure 3.5-4; Maldonado and Koether 1983; Scott, R.B. and Castellanos 1984).

3.5.3.5.2 Bullfrog Tuff

The Bullfrog Tuff, which is partially exposed only in limited outcrops near Prow Pass in the northwest corner of the Yucca Mountain site area, was penetrated wholly or partially in approximately twenty boreholes. In general, the Bullfrog Tuff consists of welded to partially welded, zeolitic upper and lower parts separated by a central zone of moderately to densely welded tuff (Carr, W.J., Byers, and Orkild 1986), and includes a unit of reworked and weathered tuffaceous deposits (termed pre-Bullfrog Tuff bedded tuffs, Table 3.5-1) at the base. Thicknesses are from 76 to 275 m (250 to 900 ft; Figure 3.8-13). Regionally, Carr, W.J., Byers, and Orkild (1986) show the Bullfrog Tuff to be as much as 400 m thick (1,310 ft) in a region of maximum deposition in the southern part of Crater Flat.

The pre-Bullfrog Tuff bedded tuffs consist largely of weathered pyroclastic flow deposits interbedded with thin zones of fallout tephra. Diehl, S.F. and Chornack (1990) correlated five marker horizons through the sequence between boreholes G-1, G-2, G3/GU-3, G-4, and b#1, and reported thicknesses ranging from 8 to 23 m (26 to 75 ft). The pre-Bullfrog Tuff unit in borehole SD-7 consists of medium-grained sandstone containing 10 to 15 percent small pumice grains (average size 5 mm), 15 to 20 percent quartz and feldspar grains, and 3 to 5 percent small devitrified volcanic and red siltstone lithic fragments in a fine-grained matrix (Rautman and Engstrom 1996b).

There has not been a systematic study of the Bullfrog Tuff that includes examination of all boreholes in the Yucca Mountain site area. Lithologic descriptions of the formation included in Table 3.5-1 are based primarily on studies of core from boreholes G-1 and G-4 (Spengler, Byers et al. 1981; Spengler and Chornack 1984). The formation in these two wells is composed of two pyroclastic flow deposits separated by an interval of pumiceous fallout. Both of the upper and lower deposits are simple cooling units that are moderately welded in their central portions. The middle pumiceous fallout deposit, partly to moderately welded, varies in thickness from about 20 cm to 1.5 m. Rautman and Engstrom (1996b) recognized four pyroclastic flow units within the Bullfrog Tuff in a study of cores from borehole SD-7. The basal part of each of these flow deposits includes some reworked tuffaceous materials. Except for a partially to moderately welded unit next to the top of

the formation, the pyroclastic flow deposits are generally nonwelded and zeolitically altered. Pumice clasts vary from 5 to 15 percent in most units, but increase to as much as 35 to 60 percent in some zones. The phenocryst assemblage generally includes 20 to 25 percent quartz and feldspar and 5 to 10 percent biotite, hornblende, and pyroxene. Lithic-clast content ranges from 1 to 5 percent.

Development of the zones of devitrification within the Bullfrog Tuff resulted in a devitrified, vapor-phase mineralized interior bounded by upper and lower zones that were initially vitric but have undergone zeolitic/argillic alteration. The upper zeolitic zone varies in thickness from 4 m (borehole G-4) to as much as 45 m (borehole G-1), and the zeolitic alteration continues into the overlying bedded tuffs at the base of the Prow Pass Tuff. Vapor-phase crystallization is generally well developed in the middle and upper portions of the central devitrified zone. Pumice clasts are typically replaced by vapor-phase crystals, although some have spherulitic and axiolitic texture. Biotite crystals are partially oxidized in vapor-phase altered zones, and siltstone lithic clasts are locally enclosed in light-gray margins. Near the base of the formation, the devitrified zone overlies a thin interval of argillic alteration, which, in turn, overlies a zone dominated by zeolite mineralization that continues into the underlying pre-Bullfrog Tuff bedded tuffs.

In addition to an intervening bedded tuff unit (T_{cpbt}, Table 3.5-2), the Bullfrog Tuff can be differentiated from the overlying Prow Pass Tuff on the basis of phenocryst assemblage and bulk chemistry (Moyer and Geslin 1995). Units of the Prow Pass Tuff contain altered orthopyroxene and generally subequal amounts of biotite. In contrast, the Bullfrog Tuff lacks pyroxene and contains abundant biotite.

3.5.3.5.3 Prow Pass Tuff

The Prow Pass Tuff is a sequence of variably welded pyroclastic deposits formed by eruptions from an unidentified source between 13.0 and 13.2 Ma (Sawyer, D.A., Fleck et al. 1994). Descriptions given below are summarized from Moyer and Geslin (1995), based primarily on studies of core samples from boreholes G-1, G-2, GU-3, G-4, UZ-14, a#1, c#1, (and nearby c#2 and c#3), and UZ#16, and from observations of exposures at Prow Pass, Busted Butte, and Raven Canyon (Figure 3.5-2).

Four pyroclastic units and an underlying interval of bedded tuff, the combined thicknesses of which range from 60 to 228 m (200 to 750 ft) compose the Prow Pass Tuff in the Yucca Mountain area (Table 3.5-2; Figure 3.8-12). The basal bedded tuffs, less than 1 m to as much as 11 m thick, consist of welded and zeolitically altered tuffaceous deposits that include a laminated ash deposit underlain by a highly variable sequence of pumiceous fallout and pyroclastic flow deposits. A thin (≈ 0.5 m) basal breccia containing angular clasts of the underlying Bullfrog Tuff and, locally, other volcanic lithologies, occurs in several places.

The lowermost pyroclastic flow deposit of the Prow Pass Tuff (unit T_{cp1}, Table 3.5-2), with an aggregate thickness of 25 to 70 m, consists of three subunits separated on the basis of their lithic clast content. The subunits are generally similar, with zeolitically altered matrices; the upper and lower subunits may not be differentiated where the middle subunit is absent. The next overlying unit (T_{cp2}) is a sequence of pyroclastic flow deposits that have not been subdivided because distinguishing characteristics are lacking. However, locally preserved ash horizons and abrupt

changes in the amounts and sizes of pumice and lithic clasts indicate that at least three flow deposits can be observed in most of the boreholes studied. The aggregate thickness ranges from about 3 m to 34 m. Unit Tcp3 consists of six subunits defined by changes in the degree of welding or the intensity of vapor-phase alteration. Locally preserved, interbedded ashfall horizons and abrupt variations in the amounts and sizes of pumice and lithic clasts mark flow boundaries. Thickness of unit Tcp3 ranges from 40 m to nearly 80 m. The top unit of the Prow Pass Tuff (Tcp4), which ranges from 4 m to as much as 20.5 m thick in cored boreholes, can be divided into three irregularly distributed subunits differentiated by changes in the average diameter and percentage of pumice clasts that decrease stratigraphically upward. The contact between crystallized rocks (including vapor-phase corroded and mineralized) and vitric (or subsequently zeolitized) rocks is typically marked by a thin horizon of argillically altered pumice clasts and the largest matrix grain. This mineralogic contact occurs at the contact of units 3 and 4, and near the contact of units 2 and 3, although the mineralogic change is locally at the contact of the moderately welded and partially welded rocks in unit 3 or in the upper part of unit 2. Rocks in units 1, 2, and 4 are typically altered to zeolite and lesser amounts of clay throughout most of Yucca Mountain. Units 2 and 4 are vitric in the southwestern part of the central block with vitric rocks in unit 4 occurring as far north as borehole H-5 (R.W. Spengler, USGS, written communication to R. Craig, December 13, 1996).

A variety of criteria are used to distinguish the lithostratigraphic units of the Prow Pass Tuff from those of the next younger Calico Hills Formation, the most prominent being the ubiquitous siltstone clasts and altered orthopyroxene of the Prow Pass Tuff (Moyer and Geslin 1995). The two formations also have different amounts of phenocrysts, proportions of quartz in the phenocryst assemblage, and chemical compositions. The basal bedded tuff and sandstone units of the Calico Hills Formation serve as consistent stratigraphic marker beds in several of the boreholes studied (Diehl, S.F. and Chornack 1990).

3.5.3.6 Calico Hills Formation

The Calico Hills Formation is a series of rhyolite tuffs and lavas that resulted from an episode of volcanism at approximately 12.9 Ma (Sawyer, D.A., Fleck et al. 1994). Five pyroclastic units, overlying a bedded tuff unit and a locally occurring basal sandstone unit, have been distinguished in the Yucca Mountain area by Moyer and Geslin (1995). The formation thins southward across the potential repository site area, from composite thicknesses of as much as 460 m (1,500 ft) to only about 15 m (50 ft) (Figure 3.8-11). The following descriptions are summarized from Moyer and Geslin (1995), whose studies are based on examinations of cores and observations of outcrops in the same boreholes and surface localities as listed above for the Prow Pass Tuff.

The basal volcanoclastic sandstone unit of the Calico Hills Formation (unit Tacbs, Table 3.5-2) is interbedded with rare reworked pyroclastic flow deposits; thicknesses of the unit range from 0 to 5.5 m. The overlying bedded tuff (unit Tacbt), 9 to 39 m thick, is composed primarily of pyroclastic fall deposits with subordinate, primary, and reworked pyroclastic-flow deposits. Each of the five pyroclastic units forming the bulk of the Calico Hills Formation (units Tac1-Tac5) consists of one or more pyroclastic flow deposits with similar macroscopic characteristics. The flow deposits are separated by locally preserved fall horizons; these pumice- and lithic-fall deposits are grouped arbitrarily with the superjacent pyroclastic unit.

X-ray diffraction of samples from drill core by Caporuscio et al. (1982; Vaniman, Downey et al. (1985); Bish and Vaniman (1985); and Bish and Chipera (1986) and of outcrop samples by Broxton, Chipera et al. (1993) show an abundance of authigenic zeolites in all units of the Calico Hills Formation. Exceptions occur in the southwest part of the central block of Yucca Mountain (boreholes H-3 and GU-3) where the entire formation is vitric, and in borehole H-5 where the bedded tuff at the base is zeolitized but the remainder is not.

The Calico Hills Formation is overlain by a bedded tuff unit (Tpbt1, Table 3.5-2) that marks the base of the Topopah Spring Tuff. The Calico Hills Formation can also be distinguished from the Topopah Spring Tuff by differences in mineralogy and chemical composition—lithostratigraphic units of the former have phenocryst assemblages with a higher proportion of quartz and higher calcium and barium contents than units in the latter.

3.5.3.7 Paintbrush Group

The Paintbrush Group consists of four formations, each of which is primarily composed of pyroclastic flow deposits that are interstratified with small-volume pyroclastic flow and fallout tephra deposits, and, locally, lava flows and secondary volcanoclastic deposits from eolian and fluvial processes (Buesch, Spengler et al. 1996a). In ascending order, the formations include the Topopah Spring, Pah Canyon, Yucca Mountain and Tiva Canyon Tuffs. This group is one of the most widespread and voluminous caldera-related assemblages in the Southwestern Nevada volcanic field (Sawyer, D.A., Fleck et al. 1994). The Topopah Spring Tuff forms the host rock for the potential radioactive waste repository and therefore is one of the most intensely studied formations at Yucca Mountain. Locations of eruptive centers for the Topopah Spring and Pah Canyon Tuffs are uncertain, but the Claim Canyon caldera (Figure 3.5-2) is identified as the source of the Tiva Canyon Tuff and possibly the Yucca Mountain Tuff (Byers, Carr, Orkild et al. 1976; Sawyer, D.A., Fleck et al. 1994).

Descriptions of the formations within the Paintbrush Group are generalized from detailed studies of outcrops and borehole cores by Buesch, Spengler et al. (1996a) and supplemented by core descriptions obtained from Geslin et al. (1995), Geslin and Moyer (1995), and Moyer, Geslin and Buesch (1995). During the course of investigation, Buesch, Spengler et al. (1996a) divided the Tiva Canyon and Topopah Spring Tuffs into several zones and subzones, many of which can be correlated across Yucca Mountain (Table 3.5-2). Divisions of these formations from members to the most detailed of intervals indicate that both are simple cooling units within the site area and can be used as analogs for one another. The interplay between depositional, welding, crystallization, and fracturing processes produces unit contacts that can be sharp where one of the attributes changes abruptly, or are gradational where an attribute changes gradually (Buesch, Spengler et al. 1996a). Depositional contacts such as the base of pyroclastic flow and fallout deposits and redeposited material are examples of sharp contacts. Tops of these deposits are typically sharp, but can be gradational where there is evidence of reworking or pedogenesis. The transition from nonwelded to densely welded tuff is typically gradational, such as near the base of the Topopah Spring Tuff in boreholes GU-3 and W.T.-2. Contacts of several lithostratigraphic units correspond with boundaries of hydrogeologic and thermal-mechanical units throughout Yucca Mountain and have been used in the development of 3-D geologic and hydrogeologic models (Table 3.5-2).

3.5.3.7.1 Topopah Spring Tuff

The Topopah Spring Tuff has a maximum thickness of about 380 m (1,250 ft) in the vicinity of Yucca Mountain (Figure 3.8-9). The formation is divided into two members—a lower crystal-poor member and an upper crystal-rich member—each of which is divided into numerous zones, subzones, and intervals based on variations in depositional features such as crystal content and assemblage, size and abundance of pumice and lithic clasts, distribution of welding and crystallization zones, and fracture characteristics (Buesch, Spengler et al. 1996a). The Topopah Spring Tuff is compositionally zoned with an upward chemical change from high-silica rhyolite in the crystal-poor member to quartz latite (also referred to as quartz trachyte) in the crystal-rich member (Lipman et al. 1966; Sawyer, D.A., Fleck et al. 1994). As discussed in Subsection 3.5.2.2, these two members are also clearly distinguishable on the basis of mineralogy and trace-element concentrations.

The crystal-poor member (unit Tptp, Table 3.5-2), which is characterized by less than 3 percent phenocrysts, is divided into vitric rocks of the vitric zone near the base (unit Tptpv) and devitrified rocks of the upper lithophysal (unit Tptpul), middle nonlithophysal (unit Tptpmn), lower lithophysal (unit Tptpll), and lower nonlithophysal (unit Tptpln) zones. The vitric zone is divided primarily on the degrees of welding that range upward from a nonwelded subzone at the base, which includes partially welded rocks near the top, through a moderately welded subzone, to a densely welded subzone that caps the sequence. The vitric densely welded subzone (unit Tptpv3), commonly referred to as the "vitrophyre" in many previous reports, is identified as an important thermal-mechanical unit (unit TSw3, Table 3.5-2).

The crystal-rich member (unit Tptr, Table 3.5-2) is characterized by greater than 10 percent phenocrysts with a crystal-transition subzone at the base where the percentage of phenocrysts increases upward from 5 to 10 percent. The member is divided into lithophysal (unit Tptrl), nonlithophysal (unit Tptrn), and vitric (unit Tptrv) zones. Rocks in both the lithophysal and nonlithophysal zones are devitrified, and the division is based on the presence or absence of lithophysae. The vitric zone, which caps the member (unit Tptrv), is distinguished by the preservation of the volcanic glass to form rocks with a vitreous luster that typically grade upward from densely welded to nonwelded.

A sequence of bedded tuffaceous rocks (unit Tpbt2) occurs between the Topopah Spring Tuff and the Pah Canyon Tuff. The lower part of this unit, 5- to 15 m thick, consists of moderately well sorted pumiceous tephra with a thin (2 cm) lithic-rich fallout tephra overlying a thin (2 cm) very fine-grained ash bed at the base. This thin basal bedset occurs across Yucca Mountain in core from boreholes and in surface exposures from the southwestern flank of the mountain along Solitario Canyon to north of Yucca Wash near Fortymile Wash (Figure 3.5-2).

3.5.3.7.2 Pah Canyon Tuff

The Pah Canyon Tuff is a simple cooling unit (Christiansen 1979) composed of multiple flow units. The formation reaches its maximum thickness of about 70 m (225 ft) in the northern part of Yucca Mountain (Figure 3.8-7), and thins southward to zero in the vicinity of borehole UZ-16 (Moyer et al. 1996). The Pah Canyon varies from nonwelded to moderately welded, and, throughout much of

the area, vitric pumice clasts are preserved in a nondeformed matrix that is sintered or lithified by vapor-phase mineralization. Large pumice clasts contain distinctive clusters of phenocrysts. Phenocrysts in the matrix and in most pumice clasts comprise 5 to 10 percent of the rock, with a high ratio of feldspars to mafic (biotite and clinopyroxene) phenocrysts. Lithic clasts (up to 5 percent of the rock) of devitrified rhyolite are common, and clasts of porphyritic obsidian occur in some horizons. Shards occur either as poorly preserved clear glass or as devitrified material.

A bedded tuff unit (Tpbt3, Table 3.5-2) intervenes between the Pah Canyon Tuff and the overlying Yucca Mountain Tuff where these two formations are present in the Yucca Mountain site area (Diehl, S.F. and Chornack 1990). Several units, consisting of rhyolite lava flows and fallout tephra deposits, also occur in this general stratigraphic interval (e.g., rhyolite of Black Glass Canyon, Table 3.5-2; locality shown in Figure 3.6-1) in areas mostly to the northeast of Yucca Mountain, but are not present at Yucca Mountain.

3.5.3.7.3 Yucca Mountain Tuff

The Yucca Mountain Tuff is a simple cooling unit (Christiansen 1979) that is nonwelded throughout much of the Yucca Mountain area, but is partially to densely welded where it thickens in the northern and western parts of Yucca Mountain. Although typically vitric in most locations in the central part, the tuff is increasingly devitrified where it is thick. The Yucca Mountain Tuff, which varies in thickness from 0 to 45 m (0 to 150 ft; Figure 3.8-6), locally includes a thin (few centimeters) ground layer at the base of the pyroclastic flow deposit that was originally interpreted as a pumiceous fallout tephra bed. The formation is nonlithophysal throughout Yucca Mountain but contains lithophysae where densely welded in Northern Crater Flat.

A bedded tuff sequence (unit Tpbt4) overlies the Yucca Mountain Tuff. In borehole GU-3, this sequence is about 15 m thick and characterized by thin beds of pyroclastic fallout tephra deposits interbedded with thin oxidized, weathered zones (Diehl, S.F. and Chornack 1990).

3.5.3.7.4 Tiva Canyon Tuff

The Tiva Canyon Tuff is a large-volume, regionally extensive, compositionally zoned (from rhyolite to quartz latite) tuff sequence that forms most of the rocks exposed at the surface of Yucca Mountain (Christiansen and Lipman 1965; Lipman and McKay 1965; Lipman et al. 1966; Scott, R.B. and Bonk 1984). Thicknesses of those portions of the formation penetrated in boreholes or observed in outcrops range from less than 50 m to as much as 175 m (165 to 575 ft). Separation of the formation into a lower crystal-poor member and an upper crystal-rich member, and into zones within each of these members, is based on similar criteria as discussed above for the Topopah Spring Tuff.

The crystal-poor member (unit Tpcp) in the lower part of the Tiva Canyon Tuff is divided into five zones: vitric (unit Tpcpv), lower nonlithophysal (unit Tpcpln), lower lithophysal (unit Tpcpll), middle nonlithophysal (unit Tpcpmn), and upper lithophysal (unit Tpcpul) zones. Divisions into subzones is based on vitric versus devitrified rocks, degree of welding, differences in pumice clasts, presence or absence of lithophysae, and fracture morphology. The crystal-poor member and overlying crystal-rich member are separated by a thin transitional subzone in which there is an upward increase in crystal content and an increase in the ratio of mafic to felsic phenocrysts.

The crystal-rich member (unit Tpcr) in the upper part of the Tiva Canyon Tuff consists primarily of devitrified nonlithophysal material, which locally contains lithophysae near the base, and is capped by a thin (less than 1 m) vitric zone that is only locally preserved and typically has been eroded from most of Yucca Mountain. The crystal-rich nonlithophysal zone (unit Tprn) is divided into four subzones based upon depositional features such as abundance of phenocrysts and pumice, but much of this zone has undergone corrosion and alteration that has significantly increased porosity compared to the overlying and underlying rocks. As discussed in Subsection 3.5.2.2, detailed variations of trace element concentrations within the crystal-rich member provide rather precise indications of the stratigraphic positions of various units.

3.5.3.8 Post Tiva Canyon-Pre-Rainier Mesa Tuffs

A sequence of pyroclastic flow and fallout tephra deposits occurs between the top of the Tiva Canyon Tuff and the base of the Rainier Mesa Tuff of the Timber Mountain Group in the vicinity of Yucca Mountain (unit Tpbt5). Rocks in this stratigraphic position occur in the subsurface beneath alluvial deposits in Midway Valley, on the east flank of Yucca Mountain (Figure 3.5-2; Carr, W.J. 1992; Geslin and Moyer 1995; Geslin et al. 1995). The sequence ranges in thickness from 0 to 61 m (0 to 200 ft) and is intermediate in composition between the Tiva Canyon and Rainier Mesa Tuffs. Some of these units have been placed in the Timber Mountain Group (Sawyer, D.A., Fleck et al. 1994) and others in the Paintbrush Group (Buesch, Spengler et al. 1996a); they are described by Buesch, Spengler et al. (1996a) as consisting of tuffaceous rocks correlated with known eruptive units based on detailed tephrostratigraphic studies, as well as other tuffaceous deposits that have not been correlated with known eruptive units. Included are units in the Timber Mountain Group that have been referred to as rhyolite of the Loop (Sawyer, D.A., Fleck et al. 1994) and Windy Wash lavas and tuffs (Fridrich 1998), and units in the Paintbrush Group such as the rhyolites of Comb Peak and Vent Pass (Buesch, Spengler et al. 1996a). A lithic-rich unit, which was informally referred to as tuff unit "x" by Carr, W.J. (1992), occurs in these bedded tuffs and has been correlated with the rhyolite of Comb Peak (Buesch, Spengler et al. 1996a).

3.5.3.9 Timber Mountain Group

The Timber Mountain Group includes all of the quartz-bearing pyroclastic flow and fallout tephra deposits that were erupted from the Timber Mountain caldera complex (Figure 3.5-2) about 11.5 Ma (Byers, Carr, Orkild et al. 1976; Sawyer, D.A., Fleck et al. 1994). The complex consists of two overlapping, resurgent calderas: an older caldera formed by the eruption of the Rainier Mesa Tuff, and a younger, nested caldera formed by eruption of the Ammonia Tanks Tuff (Minor, Sawyer et al. 1993; Sawyer, D.A., Fleck et al. 1994).

3.5.3.9.1 Rainier Mesa Tuff

Byers, Carr, Orkild et al. (1976) describe the Rainier Mesa Tuff as a compositionally zoned compound cooling unit consisting of high-silica rhyolite tuff overlain with a partial cooling break by a considerably thinner quartz latite tuff that is restricted to the vicinity of the Timber Mountain caldera (Figure 3.5-2). The formation does not occur across much of Yucca Mountain, but is locally exposed on the downthrown blocks of large faults in valleys on either side of the mountain (Scott, R.B. and Bonk 1984; Gibson et al. 1992; Figure 3.5-2) and has been penetrated in a few

boreholes on the east side. Based on examination of cores from boreholes NRG#2, #2B, #2C, and #2D (located between boreholes NRG#1 and NRG#3 in Figure 3.5-5), the Rainier Mesa Tuff consists of a nonlithified to lithified and partially welded pyroclastic flow deposit (Geslin and Moyer 1995; Geslin et al. 1995). In localities near Yucca Mountain, a maximum thickness of 240 m (787 ft) for the Rainier Mesa Tuff was observed in the southwestern part of Crater Flat. Thicknesses reported from studies of boreholes on the east side of Yucca Mountain are generally less than 30 m (Geslin and Moyer 1995; Geslin et al. 1995).

A nonlithified fallout-tephra deposit initially interpreted to form the basal part of the Rainier Mesa Tuff (Geslin and Moyer 1995; Geslin et al. 1995) is now considered to be part of an older bedded tuff sequence that also contains nonlithified pyroclastic (?) flow deposits. This sequence, referred to as the pre-Rainier Mesa Tuff bedded tuff, occupies intervals of about 17 m in boreholes NRG#2C and NRG#2D and is characterized by moderately well-sorted white pumice lapilli and volcanic lithic clasts.

3.5.3.9.2 Ammonia Tanks Tuff

The Ammonia Tanks Tuff is not present across Yucca Mountain, but is exposed in the southern part of Crater Flat and has been penetrated by one borehole in the Crater Flat area. The formation consists of welded to nonwelded rhyolite tuff, with highly variable thicknesses ranging up to about 215 m (705 ft).

3.5.3.10 Younger Basalt

The youngest volcanic rocks at and near Yucca Mountain are the basalts in Crater Flat basin, and the basalt dikes on the west side of Yucca Mountain along the Solitario Canyon fault near the head of Solitario Canyon (Figure 3.5-2) just south of the Drill Hole Wash fault (Scott, R.B. and Bonk 1984; Crowe, Perry et al. 1995). The basalts in Crater Flat basin, in the form of scoria cones and thin lava flows and flow breccias, were erupted during four major episodes dated as 11 Ma, 3.7 Ma, 1 Ma, and approximately 0.08 Ma, respectively (Crowe, Perry et al. 1995; Fridrich, Dudley et al. 1994). The thin dikes that were intruded along the Solitario Canyon fault consist of fine-grained, olivine-bearing basalt, locally with scoria and altered volcanic glass (Scott, R.B. and Bonk 1984); they are dated as 11 Ma. A detailed discussion of basaltic volcanism in the Yucca Mountain area is given in Subsection 3.9 (Volcanic Hazards).

3.5.3.11 Surficial Deposits

Surficial deposits of late Tertiary and Quaternary ages are widespread in the Yucca Mountain area (Figure 3.5-2). Included is a large variety of alluvial deposits and soils that blanket the floors of all the major washes and colluvial deposits that mantle many hillslopes. The results of the detailed mapping and stratigraphic and geochronological studies of these materials that were conducted as part of the site characterization program are discussed in Subsection 3.4 (Quaternary Stratigraphy and Surficial Processes).

3.5.4 Correlation of Lithostratigraphic, Hydrogeologic, and Thermal-Mechanical Units

During site characterization at Yucca Mountain, three primary stratigraphic systems have developed to investigate the distribution of lithostratigraphic, hydrogeologic, and thermal-mechanical units. Common to all these systems are the properties of bulk rock density, grain density, and porosity. Where there are changes in these rock properties, it is reasonably expected that there are commensurate changes in many of the associated hydrogeologic and thermal-mechanical properties. Thus, it has been suggested that lithostratigraphic, hydrogeologic, and thermal-mechanical units share some common boundaries (Buesch, Spengler et al. 1996a; Moyer et al. 1996). Although it is acknowledged that there are differences in many of the boundaries, these differences result in large part from how individual boundaries (time-stratigraphic, hydrogeologic, or thermal-mechanical) are defined. Most of the material presented below focuses on the properties common to the three types of units; more detailed discussions of the hydrogeologic properties in the unsaturated zone and thermal-mechanical properties are presented elsewhere (see Subsection 3.7, Site Geoengineering Properties, and Subsection 5.3, Site Hydrology).

Lithostratigraphic units have been grouped into five major hydrogeologic units in the Yucca Mountain area, the different units based principally on major variations in the degree of welding and fracture characteristics (Montazer and Wilson 1984). These include the undifferentiated overburden unit (surficial deposits down through the upper part of the crystal-rich member of the Tiva Canyon Tuff), TCw, PTn, TSw, and the CHn (Table 3.5-2). The distribution and characteristics of these units are discussed by D.C. Buesch and R.W. Spengler ("Stratigraphic Framework of the North Ramp Area of the Exploratory Studies Facility, Yucca Mountain, Nevada," in *Hydrogeology of the Unsaturated Zone, North Ramp Area of the Exploratory Studies Facility, Yucca Mountain, Nevada*: USGS Water-Resources Investigations Report 98-4050, in press). Thirty detailed hydrogeologic units applicable to hydrologic studies in the unsaturated zone at Yucca Mountain have been identified by L.E. Flint (1998b) and are the source data for many of the properties and relations described below. The boundaries of these detailed hydrogeologic units also correspond for the most part to lithostratigraphic subzones (typically within 2 m). Correlation of lithostratigraphic features and contacts to the detailed hydrogeologic units are outlined in D.C. Buesch and R.W. Spengler, ("Stratigraphic Framework of the North Ramp Area of the Exploratory Studies Facility, Yucca Mountain, Nevada," in *Hydrogeology of the Unsaturated Zone, North Ramp Area of the Exploratory Studies Facility, Yucca Mountain, Nevada*: USGS Water-Resources Investigations Report 98-4050, in press).

The TCw hydrogeologic unit consists of devitrified, moderately to densely welded tuff (Montazer and Wilson 1984; Buesch, Spengler et al. 1996a). The unit is widely exposed, thus it is important to infiltration studies at Yucca Mountain (Flint, A.L. and Flint 1994). Four detailed hydrogeologic units have been identified (Flint, L.E. 1998b, Table 3.5-2). The main divisions of the detailed hydrogeologic units are closely approximated by the changes in the amount of vapor-phase corrosion in nonlithophysal zones such as between units CCR and CUC, or the amount of lithophysae such as between units CUC, CUL, and CW (Table 3.5-2). The lower part of the Tiva Canyon Tuff contains the first significant change in hydrologic properties below the present topographic surface in the potential repository site area (Moyer et al. 1996). L.E. Flint, Flint, Rautman et al. (1996b) report average porosity of 6 to 9 percent and average bulk density of 2.25 to 2.34 g/cm³ for samples collected from younger densely welded units in the Tiva Canyon Tuff. The downward decrease in

welding near the base of the pyroclastic flow deposits (between Tpcplnc, or Tpcpv3c where present, and Tpcpv2; Table 3.5-2) is manifested by increasing porosity and decreasing bulk density. Hydrologic-property measurements obtained from core samples from 13 boreholes show that, across the dense to moderate welding contact, mean porosity increases from 12.5 to 22.8 percent and average bulk density decreases from 2.16 to 1.88 g/cm³ (Moyer et al. 1996). Because this contact is gradational, porosity and bulk density values for densely welded samples immediately above the contact differ from those higher in the section.

There are two fundamentally different types of contacts that form the base of the TCw hydrogeologic unit and the detailed hydrogeologic unit CW. In most locations, where devitrified rocks contact rocks of the vitric moderately welded subzone, the interaction of downward decrease in welding and advancement of the crystallization front during cooling greatly affects the properties of the rock, primarily from the process of vapor-phase corrosion. Grain density increases as the rock crystallizes whereas the secondary porosity formed by vapor-phase corrosion can be almost double the porosity of a noncorroded rock. The resulting rock is highly porous, in which many pores are larger than 5 to 10 mm, and altered to minimal amounts of clay or zeolite. Where these highly porous devitrified rocks occur, the base of hydrogeologic units TCw or CW can be several meters above the contact between the columnar (Tpcplnc) and vitric moderately welded (Tpcpv2) subzones. In the southwestern part of the central block where rocks of the vitric densely welded subzone (Tpcpv3) are preserved, a different type of change in properties occurs, and, although there are few measured data of core, the lithostratigraphic features and some borehole geophysics indicate that these changes can occur within approximately 1 m of the contact. In these locations, vapor-phase corrosion appears to have been minimized and localized in the lower part of the devitrified columnar subzone, probably because these rocks became densely welded with very little porosity prior to encroachment of the devitrification and vapor-phase fronts. There is a slight, but relatively sharp, decrease in density with negligible change (if not a slight decrease) in porosity at the devitrified-vitric contact (Tpcplnc-Tpcpv3). Vapor-phase corrosion and mineralization has been minimal in the vitric densely and moderately welded rocks; therefore, the gradational downward increase in density and porosity is dominated by the welding profile.

The PTn is characterized by rocks with low density and high porosity that are interstratified with rocks with high density and low porosity (Montazer and Wilson 1984; Buesch, Spengler et al. 1996a; Moyer et al. 1996). Almost all of the lithostratigraphic units included within the PTn are thickest in the northern part of the central block of Yucca Mountain and thin southward. An isopach map shows the greatest change in total thickness occurs in the area near borehole NRG-7a (58 m/km to the north, 20 m/km to the south) (D.C. Buesch and R.W. Spengler, "Stratigraphic Framework of the North Ramp Area of the Exploratory Studies Facility, Yucca Mountain, Nevada," in *Hydrogeology of the Unsaturated Zone, North Ramp Area of the Exploratory Studies Facility, Yucca Mountain, Nevada*: USGS Water-Resources Investigations Report 98-4050, in press). Most of this southward thinning results from changes in thickness of the Yucca Mountain and Pah Canyon Tuffs, and an unnamed pyroclastic flow deposit in the pre-Yucca Mountain Tuff bedded tuff (Moyer et al. 1996). Many individual units within the PTn, even those that are only centimeters thick, can be correlated across the northern and central block of Yucca Mountain in numerous boreholes, as well as in the North Ramp of the Exploratory Studies Facility (D.C. Buesch and R.W. Spengler, "Stratigraphic Framework of the North Ramp Area of the Exploratory Studies Facility, Yucca Mountain, Nevada," in *Hydrogeology of the Unsaturated Zone, North Ramp Area of the Exploratory Studies Facility,*

Yucca Mountain, Nevada: USGS Water-Resources Investigations Report 98-4050, in press; Barr et al. 1996).

The PTn contains more variability in properties than the other major hydrogeologic units, but most of this variability results from the different lithostratigraphic units that form the vertical stratification and the lateral changes in some of these units. Figure 3.5-23 shows the values for bulk densities and porosities obtained from cores of the various PTn zones, subzones, or bedded tuffs penetrated in four boreholes at Yucca Mountain (Moyer et al. 1996), and some of the general relations are as follows:

- The gradational decrease in density and increase in porosity in the upper part of the PTn, or the detailed hydrogeologic units CMW and CNW, reflects the transitional characteristics between densely welded and moderately to nonwelded tuffs (Tpcpv2 to Tpcpv1).
- Hydrogeologic unit BT4 consists of the pre-Tiva Canyon Tuff welded tuff (Tpbt4). In each profile, there is a sharp decrease in density and increase in porosity associated with the moderately well sorted fallout tephra. Typically, this bedded tuff is capped by a paleosol that is only locally sampled for analysis of matrix properties, but from the macroscopic features such as an increased amount of fine-grained material and poor sorting along with a few analyzed samples, the paleosol has a slightly higher density and lower porosity than the underlying fallout tephra or the basal part of the vitric nonwelded subzone of the Tiva Canyon Tuff.
- The TPY hydrogeologic unit consists of the Yucca Mountain Tuff where it is partially to moderately welded in the northern boreholes, including UZ-N33 and UZ-14, and has variable amounts and types of vapor-phase corrosion and mineralization that affect the density and porosity. In the southern extent of the Yucca Mountain Tuff, including borehole UZ#16, it is completely vitric and nonwelded and has properties similar to the BT4 and BT3 hydrogeologic units; therefore the TPY hydrogeologic unit is not explicitly identified in these southern areas (Moyer et al. 1996).
- Hydrogeologic unit BT3 corresponds to the pre-Yucca Mountain Tuff bedded tuff and consists of as many as seven different beds or bedded sequences that represent a series of separate eruptions; therefore, there can be numerous changes in the density and porosity in these beds.
- Hydrogeologic unit TPP consists of the Pah Canyon Tuff, and typically has uniformly low density (between 1.0 to 1.3 g/cm³) and high porosity (between 0.4 and 0.55 cm³/cm³). These density and porosity values are among the lowest and highest, respectively, of all the lithostratigraphic and hydrogeologic units. Except for relatively thin (typically less than a few meters) nonwelded vitric top and bottom, which can have slightly higher or lower values, most of this minimal variation in density and porosity results from the nonwelded to partially welded and highly vapor-phase corroded and mineralized characteristics of the tuff.
- Hydrogeologic unit BT2 includes the pre-Pah Canyon Tuff bedded tuff and the vitric nonwelded moderately welded subzones of the Topopah Spring Tuff. These rocks form a

characteristic profile of low density and high porosity throughout most of the unit, but the top and bottom have higher density and lower porosity than the middle part of the unit. The higher density values near the top of the pre-Pah Canyon Tuff bedded tuff result from a nonwelded, poorly sorted, bed or bed sets referred to as unit D (Tpbt2D), and the uppermost (typically argillically altered) part of the fallout tephra deposits in unit C (TPbt2C) (Moyer et al. 1996). D.C. Buesch and R.W. Spengler ("Stratigraphic Framework of the North Ramp Area of the Exploratory Studies Facility, Yucca Mountain, Nevada," in *Hydrogeology of the Unsaturated Zone, North Ramp Area of the Exploratory Studies Facility, Yucca Mountain, Nevada*: USGS Water-Resources Investigations Report 98-4050, in press) interpreted this argillically altered material near the top of unit C, which is typically 0.5 to 2 m thick, as a form of widely distributed fumarolic alteration during the cooling phase of the Topopah Spring Tuff, and it is this same horizon that can be traced to and merges with the top of the fumarole exposed in the Exploratory Studies Facility near station 10+30. The potential hydrogeologic importance of the density and porosity contrasts between unit D with the argillically altered material in unit C compared to the lower density and higher porosity rocks above and below has not been determined. Near the base of hydrogeologic unit BT2 the properties change sharply, and most of this results from: the relatively thin, vitric, moderately welded subzone (Ttpv2); the local vapor-phase corrosion and mineralization of rocks in the nonwelded and moderately welded subzone that might relate to localized fumarolic activity; and the local formation of zeolitized rocks that was identified by Chipera, Vaniman, Carlos et al. (1995) in borehole UZ#16 (Figure 3.5-24).

The TSw hydrogeologic unit consists of devitrified, moderately to densely welded tuff (Montazer and Wilson 1984; Buesch, Spengler et al. 1996a) and is divided into six detailed hydrogeologic units (Flint, L.E. 1998b; Table 3.5-2). Although most lithostratigraphic zones and subzones of the Topopah Spring Tuff and corresponding detailed hydrogeologic units within TSw can be traced across the central block of Yucca Mountain, thicknesses of individual units vary considerably, but typically not sharply across short distances. Like the TCw discussed earlier, the TSw exhibits significantly lower mean porosities and higher bulk densities than the overlying PTn. Some of the changes in matrix properties that span the PTn-TSw contact include the differences in matrix density and porosity measured on core samples, total and water-filled porosity calculated from borehole geophysical logs, and mineralogy (Figures 3.5-23 and 3.5-24 in which Figure 3.5-24 is a detail of Figures 3.5-20 and 3.5-21 with the addition of epithermal neutron and resistivity logs in USW WT-2). The vitric, densely welded subzone at the top of TSw, is very thin in places and locally does not occur because of extensive devitrification of the densely welded rocks, but it has highly contrasting hydrogeologic properties when compared to the overlying rocks. Overall, porosities within TSw range from about 20 percent to less than 9 percent. However, individual units typically have slightly different mean porosities and smaller ranges (Flint, L.E. 1998).

Hydrogeologic properties, including porosity profiles, within the Calico Hills nonwelded (CHn) hydrogeologic unit (basal part of the Topopah Spring Tuff, the Calico Hills Formation, and the Prow Pass and Bullfrog Tuffs, Tables 3.5-1 and 3.5-2), are related to welding features or lack thereof. Most of these rocks are nonwelded with relatively high porosities, their hydrogeologic properties primarily defined by alteration of vitric minerals to zeolites, the distribution of the vitric-zeolite boundaries, and the extent of the alteration (Flint, L.E. 1998). Flint, L.E. (1998) has proposed use of the differential porosity as an indicator of the amount of alteration in otherwise vitric tuffs, and

this technique does not always indicate alteration in rocks that have been vapor-phase corroded and mineralized. The contact between TSw and CHn is marked by a sharp shift in porosities from 10 percent or less to porosities that are 30 percent or greater (Flint, L.E. 1998b).

Stratigraphic units with distinct thermal and mechanical properties within the volcanic rock sequence at Yucca Mountain have been identified by Ortiz et al. (1985). As with the hydrogeologic units, correlations of the boundaries of thermal-mechanical units with lithostratigraphic zones and subzones (Tables 3.5-1 and 3.5-2) are based on changes in macroscopic features that define lithostratigraphic units, and the preliminary correlation of lithostratigraphic units with preliminary laboratory measurements (Buesch, Spengler et al. 1996a). Most of the thermal-mechanical unit boundaries roughly correspond to lithostratigraphic contacts that mark the transition from vitric moderately welded rocks to densely welded subzones, or the contact between the vitric moderately welded rocks and high temperature devitrified rocks; additional criteria are based on the percentage of lithophysae (Table 3.5-2; Figure 3.5-25). Figure 3.5-25 illustrates the variations in porosity, density, p- and s-wave velocity, Young's modulus, and ultimate strength plotted versus depth and lithostratigraphic zone (labeled) and subzones (not labeled). Several of the lithostratigraphic zones have distinctive values and ranges, but some of the minor variations within these properties are correlated to some of the subzones. Figure 3.5-25 shows a fairly typical distribution of thermal-mechanical property data and this points out the fact that compared to the closely spaced hydrogeologic data (Flint, L.E. 1998), the thermal-mechanical data can be used to determine general properties of the units, but it is typically difficult to identify a unique contact between the units. Detailed discussions of the thermal and mechanical properties of the various thermal-mechanical units are given in Subsection 3.7.

INTENTIONALLY LEFT BLANK

3.6 SITE STRUCTURAL GEOLOGY

3.6.1 Introduction

Several structural features of the site are critical to a safety assessment of a potential repository. A description of all structural features at the site (in the Yucca Mountain Conceptual Controlled Area) is required by 10 CFR 60.21(c)(1). In response to the specific information needs called for in this regulation, the following subsection will provide data on the orientation, distribution, and origin of faults, fractures, discontinuities, and heterogeneities. The data will provide a basis for addressing the favorable condition of free drainage (10 CFR 60.122 [b][8][iv]) and the potentially adverse condition of movement of gaseous radionuclides in the unsaturated zone (10 CFR 60.122 [c][24]). Likewise, the data will help in evaluation of the favorable condition of groundwater travel time (10 CFR 60.122 [b][7]) as well as elements of the waste containment and isolation strategy. The data presented here will be used to address some of the NRC's key technical issues. Knowledge of the structural features is necessary input for design and analysis of surface- and subsurface-engineered facilities important to safety.

The spatial and temporal patterns of faulting and other fracturing of the volcanic bedrock are the fundamental elements of the structural geology of the potential underground repository for high-level radioactive wastes at Yucca Mountain. To document and discuss these patterns, it is necessary to summarize two types of studies: geologic mapping, and fractured rock mass studies, which together encompass a wide range of scales of observation. As discussed in the following subsections, fundamental structural studies of both types had been completed before the establishment of the *Site Characterization Plan* (DOE 1988b). The detailed geologic mapping and systematic fracture studies that were initiated in the early 1990s in response to the *Site Characterization Plan* were built on the foundation provided by these earlier studies to provide a better understanding of the structural geology in and adjacent to the potential site area.

The geologic mapping studies were conducted at scales of 1:2,400 to 1:24,000, using either USGS or YMP topographic base maps. Bedrock map units correspond to formational boundaries of Sawyer, D.A., Fleck et al. (1994) for 1:24,000 mapping and to zonal contacts of Buesch, Spengler et al. (1996a) or R.B. Scott and Bonk (1984) for more detailed mapping. Faults with five or more meters of offset were recorded on the 1:24,000 mapping, whereas faults with 1 m or more of displacement were mapped in the more detailed studies.

Fractured rock mass studies included detailed studies of the distribution of fractures in natural exposures, cleared pavements, and underground excavations. Fractures were mapped at scales of 1:240 and greater (typically 1:120 and 1:125) in these studies. The largest volume of fractured rock mass data comes from the detailed mapping of the Exploratory Studies Facility, an 8 km long, 7.6 m diameter tunnel completed in 1997 through part of the potential repository area.

Figure 3.6-1 encompasses the area that is informally referred to as the Yucca Mountain site area, mapped at 1:24,000 scale by Day et al. (1997). For the purpose of this report, the term "site area" corresponds to this 12 km x 14 km area, extending from the Prow on the north to Busted Butte on the south, and from Windy Wash on the west to Fortymile Wash on the east. As shown in Figure 3.6-2, the pie-shaped "Conceptual Controlled Area boundary," the "site" as defined by 10 CFR 60.2,

lies within the site area. The outline of the Central Block Geologic Map (Day et al. 1998a), and the map boundaries of R.B. Scott and Bonk (1984) are shown in Figure 3.6-2. In general, the detailed geology of the potential repository is addressed by geologic mapping and fractured rock mass studies within the central block, whereas the subregional context for the geology of the potential repository is found in the site area.

Definitions—Several key structural terms with specific meanings relative to the Yucca Mountain Site are defined here:

Block-bounding faults—A series of north-striking normal faults (rotated to northeast-striking south of the site area) that are spaced 1 to 4 km apart. They commonly have experienced hundreds of meters of Tertiary displacement of Miocene Paintbrush Group Tuffs, with subordinate amounts of strike-slip motion. In some places, Quaternary offset has been documented on these faults (see Subsection 3.10, Seismic Hazards).

Cooling joints—Smooth, gently curved to planar discontinuities that are inferred to have formed early in the history of the volcanic rock mass, in response to contraction during cooling. Cooling joints are most easily identified where tubular structures are present on the joint surface (Barton, C.C., Howard et al. 1984). A combination of other criteria may be used to recognize cooling joints where tubular structures are absent (Throckmorton and Verbeek 1995), including: low surface roughness; smooth, continuous traces; great length relative to other fractures; parallelism with proven cooling joints nearby; presence of demonstrated early age as shown through abutting relations with fractures of other sets; and the presence of bleached margins composed of minerals that formed at high temperatures (Levy 1993).

Faults—Planar or curvilinear discontinuities along which displacement of bedrock has occurred. Because this subsection addresses bedrock structural geology, our use of the term “fault” is confined to structures that produced displacements of units within the bedrock; only in rare cases are these structures associated with displacements of Quaternary units. Because the numerous geologic mapping and fractured rock mass studies were subject to widely varying scales of observation, percentage of bedrock exposure, and precision of stratigraphic control, the lower limit on fault-displacement magnitudes portrayed in each study also varies widely.

Fault system—A complex, commonly anastomosing array of faults that are geometrically and kinematically linked. At Yucca Mountain, “fault system” is generally reserved for fault arrays that have trace lengths of several kilometers (such as “block-bounding fault systems”) although it has also been applied to smaller fault zones in some cases.

Fracture intensity—A general term used to describe spatial changes in the spacing or density of fractures. Intensity may be computed based on the distance between neighboring fractures and thus reported as either spacing (the distance between fractures) or frequency (number of fractures per linear distance). Areal fracture intensity may be computed in terms of fracture density, for example the number of fractures per square meter, or meters of fracture trace length per square meter.

Intra-block faults—Relatively minor faults that lie entirely within the structural blocks defined by the block-bounding faults. In the central block, intra-block faults have 1 to 30 m of displacement,

and typical mapped lengths of less than 1 km, up to a maximum mapped length of 7 km (this maximum length represents the combined length of the Ghost Dance and Abandoned Wash faults).

Joint set—A population of joints that are subparallel in an area.

Structural domains—Used in this subsection to describe portions of the site area that are characterized by a particular structural style distinct from that of adjacent areas. These site area structural domains are defined at the 1:24,000 map scale and are distinct from the tectonic domains presented in Subsection 3.2. All of the site area domains defined in this subsection lie within the more regional Crater Flat tectonic domain as defined in Subsection 3.2 (Regional Geologic Setting).

Tectonic fractures—Discontinuities across which less than 10 cm of displacement, or simple opening (face separation), has occurred in response to regional tectonic stresses or local stresses; in some cases these structures have reactivated pre-existing cooling joints.

3.6.2 Geologic Mapping: Structural Framework

3.6.2.1 History

Regional structural studies of Yucca Mountain began with the systematic 1:24,000 scale geologic mapping of quadrangles in and near the Nevada Test Site, by the USGS in the 1950s and 1960s. In the immediate vicinity of Yucca Mountain, the relevant maps from these studies are Christiansen and Lipman (1965) and Lipman and McKay (1965). These maps, although primarily reconnaissance in nature, portrayed the block-bounding faults and some intra-block faults that affected the principle Miocene ashflow tuffs and the underlying Paleozoic rocks.

Anticipating the need for larger scale geologic mapping in the early stages of site suitability studies, renewed field investigations in the central and northern portions of Yucca Mountain resulted in the publication of a 1:12,000 scale map by R.B. Scott and Bonk (1984) (Figure 3.6-2). Their mapping shows geologic structure in considerably greater detail than the earlier quadrangle maps. R.B. Scott and Bonk (1984) defined numerous map units (zones) within each of the Tiva Canyon and Topopah Spring Tuffs (the principle bedrock formations at Yucca Mountain; see Subsection 3.5, Site Stratigraphy), which led to the delineation of numerous minor faults not previously recognized. Although considered to also be the result of reconnaissance mapping, R.B. Scott and Bonk's (1984) 1:12,000 scale map served as the primary source of bedrock geologic data at Yucca Mountain for nearly a decade, and a valuable guide to help define the most favorable areas in which to concentrate further potential repository site studies. A preliminary 1:12,000 scale geologic map of the southern part of Yucca Mountain (Scott, R.B. 1992) was also completed.

Regional compilations at smaller scales (Frizzell and Shulters 1990; Maldonado 1985) summarize the results of the quadrangle mapping and place Yucca Mountain geology in a regional context.

Simonds et al. (1995) compiled a 1:24,000 scale fault map for Yucca Mountain, integrating new data on Quaternary to recent fault activity (neotectonic studies of fault scarps, etc.); the compilation was based in part on bedrock faults mapped by R.B. Scott and Bonk (1984) and R.B. Scott (1992).

In the 1990s, renewed geologic mapping as part of the YMP was conducted primarily at scales of 1:6,000 and 1:24,000, within the central block area and the site area, respectively (Figures 3.6-2, 3.6-3, and 3.6-4). Maps at these two scales are the principle products resulting from recent field investigations (Day et al. 1998a; Day et al. 1997). These maps (Day et al. 1998a; Day et al. 1997) include significant modifications of structural details, relative to the earlier reconnaissance efforts.

Geologic mapping at scales larger than 1:6,000 was conducted in selected areas to show essential fault relations not well portrayed at the smaller scales. The Ghost Dance and Sundance fault zones, for example, were mapped at scales ranging from 1:240 to 1:2,400 (Braun et al. 1996; Spengler, Braun et al. 1993; Spengler, Braun et al. 1994 ; Potter, Dickerson et al. 1995). Geologic mapping of the Exploratory Studies Facility, an 8-km-long, 7.6-m-diameter tunnel through the potential repository block beneath the east flank of Yucca Mountain (Figure 3.6-4), was carried out between 1993 and 1997 at a scale of 1:125. Results of these larger scale (1:125 to 1:240) mapping efforts are included here to the extent that they provide additional information on structures that are included on the smaller scale maps.

3.6.2.2 Approach

All of the geologic mapping investigations employed standard geologic mapping techniques, summarized in USGS-Yucca Mountain Project Technical Procedure GP-01. Early mapping of the area (Christiansen and Lipman 1965; Lipman and McKay 1965) was done using a 1:24,000 scale USGS topographic base, and the mapped stratigraphic contacts correspond to formational boundaries that were subsequently defined within the Miocene volcanic section by Sawyer, D.A., Fleck et al. (1994). R.B. Scott and Bonk (1984) also used a 1:24,000 scale USGS topographic base, but compiled and published their map on an enlarged version of this base, at 1:12,000 scale. R.B. Scott and Bonk (1984) established and mapped internal zones that they defined within the Tiva Canyon and Topopah Spring Tuffs, based on geomorphic characteristics, lithophysal content, and glass content (vitric versus nonvitric). Braun et al. (1996) employed the map units defined by R.B. Scott and Bonk (1984), and mapped a small part of Yucca Mountain (in the vicinity of the Ghost Dance fault) at a 1:240 scale using precise survey control that they established with permanent survey markers on a 200-foot spacing, tied to the Nevada State coordinate system. Their map was plotted on an enlarged version of the 1:6,000 scale YMP topographic base. Day et al. (1998a) and Potter, Dickerson et al. (1995) used the 1:6,000 scale Yucca Mountain Project topographic base, and map units based on Buesch, Spengler et al. (1996a) including contacts separating zones and members within the Topopah Spring and Tiva Canyon Tuffs (Table 3.5-2; Subsection 3.5). In the case of Potter, Dickerson et al. (1995) the base map was enlarged to a 1:2,400 scale, and the precise survey control established by Braun et al. (1996) was used where available.

3.6.2.3 Site Area Structure

3.6.2.3.1 Hierarchy of Faulting

The structural geology of Yucca Mountain is controlled by block-bounding faults (defined above), spaced 1 to 4 km apart. In the site area (Figure 3.6-3) these faults include (from west to east) the Windy Wash, Fatigue Wash, Solitario Canyon, Dune Wash, Bow Ridge, Midway Valley, Paintbrush Canyon faults, Busted Butte faults, and several unnamed faults in the southernmost part of the site

area. Fault scarps commonly dip 50° to 80° to the west, with scattered dips in the 40° to 50° and 80° to 90° ranges. A subordinate component of left-lateral displacement is commonly associated with these faults as determined from slickenside orientations (Scott, R.B. and Bonk 1984; Simonds et al. 1995; Day et al. 1998a). The orientation, amount of offset, and nature of the associated deformation varies from north to south (and to some degree from west to east) within the site area (Figure 3.6-3). The nature of these variations is discussed in this subsection.

Map patterns demonstrate that tectonic mixing of various Paintbrush Group lithologies has occurred within the most intensely deformed parts of block-bounding fault systems. This is most apparent in the Solitario Canyon fault system (Scott, R.B. and Bonk 1984; Day et al. 1998a). In this system, which is up to 400 m wide, there are domains in which lenses from stratigraphically diverse parts of the Tiva Canyon Tuff are juxtaposed, similar zones in which slices of Topopah Spring Tuff are mixed, and several areas where lenses from more than one Paintbrush Group formation are tectonically mixed (Day et al. 1998a). Tectonic mixing is also apparent along the Windy Wash fault system west of Prow Pass, along the Bow Ridge fault system in the saddle between Bow Ridge and Boundary Ridge, and in the Paintbrush Canyon fault system, along the west flank of Fran Ridge (Scott, R.B. and Bonk 1984; Day et al. 1998a). Individual fault strands within these tectonically mixed zones are highly brecciated, and in some cases the fault-bounded lenses have a high degree of internal brecciation.

Displacement is transferred between block-bounding faults along relay faults, which intersect block-bounding faults at oblique angles, providing an intra-block kinematic link between the bounding structures. As such, the relay faults (and related structures that comprise relay fault zones) are significant components of the block-bounding fault systems, particularly (but not exclusively) in the southern half of Yucca Mountain. Most of these relay faults are actually complex zones of faulting. Through most of the site area (Figure 3.6-3), block-bounding faults strike to the north and relay faults strike to the northwest, whereas south of the site area block-bounding faults strike to the northeast and relay faults strike to the north.

Within structural blocks, small amounts of strain are accommodated along intra-block faults (defined above). In many cases, intra-block faults appear to represent local structural adjustments in response to displacements on the block-bounding faults. In some cases, intra-block faults are expressions of hanging wall or footwall deformation that affects the block within a few hundred meters of the block-bounding faults. Other intra-block faults, such as the northwest-trending, narrow grabens in the southeast part of the central block geologic map (Day et al. 1998a), accommodate strains in narrow zones between overlapping tips of block-bounding faults. Such intra-block faults may have evolved into relay faults at the higher magnitudes of horizontal extension that are present in the southern part of Yucca Mountain.

3.6.2.3.2 Structural Domains

Ten structural domains within the site area are defined here (Figure 3.6-5), each characterized by a distinctive structural style; one other domain in the northwest corner of the site area extends farther to the west and is not discussed further. These structural domains all lie within the more regional Crater Flat tectonic domain as defined in Subsection 3.3 (Regional Tectonic Models). The term "structural domain" is used to denote an area characterized by a particular structural pattern that is

distinct from that of adjacent areas. The distinctive structural patterns that characterize individual domains may include the nature and intensity of faulting as well as magnitude and direction of stratal dips. These domains record an integrated structural response through time, and are not defined on the basis of timing of deformation or response to a particular tectonic episode. The concept of structural domains can be applied at any scale; for the purposes of this report, the structural domains are defined at the 1:24,000 map scale, corresponding to the scale of the site area geologic map produced by Day et al. (1997). The site area structural domains are briefly described below, as a summary of the overall structural geology of the site area.

The largest and structurally simplest domain is the Central Yucca Mountain domain, which comprises three east-tilted blocks bounded by west-dipping block-bounding faults. From west to east, these blocks include: the West Ridge block, bounded on the west by the Windy Wash fault and on the east by the Fatigue Wash fault; the Jet Ridge block, bounded on the west by the Fatigue Wash fault and on the east by the Solitario Canyon fault; and the central block which includes a large part of the "central block area of Yucca Mountain" defined by Day et al. (1998a) as being bounded by the Solitario Canyon fault, Bow Ridge fault, and Abandoned Wash on the west, east, and south sides respectively (see Figures 3.6-2 and 3.6-5), as well as a narrow segment that continues to the south where it is bounded by the Iron Ridge fault on the west and the East Ridge fault and an unnamed normal fault on the east. At the latitude of the proposed repository, the West Ridge block is about 1 km wide, the Jet Ridge block is about 2 km wide, and the central block is about 3.5 to 4.0 km wide. In each of these blocks, dip values for the Paintbrush Group ashflow tuffs are typically 5° to 10°, and along the eastern edges of the blocks in the hanging walls of block-bounding faults, dips are locally as high as 15° to 20° (Scott, R.B. and Bonk 1984; Day et al. 1998a). Intra-block faults, such as the north-striking Ghost Dance and Abandoned Wash faults in the central block and the Boomerang Point fault in the Jet Ridge block, are locally prominent. These prominent intra-block faults have locally undergone tens of meters of west-side-down displacement and tend to be associated with a simple, narrow zone of deformation, in contrast to the hundreds of meters of displacement and broad complex deformation zones commonly associated with block-bounding faults. The central block and, to a much lesser extent, the Jet Ridge block, contain complex zones of intra-block faulting along their eastern edges (Scott, R.B. and Bonk 1984; Day et al. 1998a). This block-margin faulting, accompanied by steepening of stratal dips, reflects the internal deformation produced in the hanging wall of a complex block-bounding fault zone (Scott, R.B. 1990; Day et al. 1998a). R.B. Scott (1990) used the term "imbricate zone" to describe this intense block-margin faulting, and proposed that it records deformation above a listric block-bounding fault above a shallow detachment. Details of block-margin faulting in the central block are discussed later.

The Central Yucca Mountain domain has undergone about 10 percent of post-12.7 Ma east-west extension, corresponding to the minimum extension values calculated by C.J. Fridrich et al. (*Cenozoic Basins of the Death Valley Region: Late Cenozoic Extension, Vertical-Axis Rotation, and Volcanism in the Crater Flat Basin, Southwest Nevada*, Geological Society of America Special Paper, in press). In Subsection 3.6.2.3.5 there is a discussion of slight overestimation of stratal dips by Fridrich et al. (*Cenozoic Basins of the Death Valley Region: Late Cenozoic Extension, Vertical-Axis Rotation, and Volcanism in the Crater Flat Basin, Southwest Nevada*, Geological Society of America Special Paper, in press), which produces somewhat exaggerated numbers for horizontal extension; the minimum values for extension calculated by Fridrich et al. (*Cenozoic Basins of the Death Valley Region: Late Cenozoic Extension, Vertical-Axis Rotation, and Volcanism in the Crater*

Flat Basin, Southwest Nevada, Geological Society of America Special Paper, in press) appear to be the most reasonable. Within block-bounding fault zones and in areas of intense block-margin deformation, extension values are locally higher.

The fault systems that bound the three blocks of the Central Yucca Mountain domain are internally complex, in contrast to the geologically simple east-tilted blocks. In the Solitario Canyon fault system, in addition to the tectonic mixing summarized above, there are domains where coherent panels of Tiva Canyon Tuff, up to 250 m wide, dip to the west, opposite to the prevailing easterly dips of the major structural blocks (Scott, R.B. and Bonk 1984; Day et al. 1998a). Locally, anticlines with axes subparallel to the fault zone are apparent in map patterns within individual fault slices and in the immediate footwall of the Solitario Canyon fault (Day et al. 1998a); these apparent folds are likely produced by contractional faults that have rotated volcanic strata. Mapped fold hinges may in fact be small-offset, brittle fault zones at these very shallow structural levels. Thrust faults are mapped within the Solitario Canyon fault system and in the hanging wall of the Bow Ridge fault near the south portal of the Exploratory Studies Facility (Day et al. 1998a). The anastomosing pattern of fault strands that characterizes these fault systems also produced individual fault splays that cut into both the hanging wall and footwall (e.g., splays mapped on the west-facing slope of Solitario Canyon in the footwall of the Solitario Canyon fault; Scott, R.B. and Bonk 1984; Day et al. 1998a). In areas south of the Central Yucca Mountain domain (discussed below), relay faults commonly transfer displacements between block-bounding faults. However, within the Central Yucca Mountain domain, this phenomenon was observed only on West Ridge, where a complex northwest-trending relay fault zone crosses the ridge and links the displacement of the Northern Windy Wash fault to that of the Fatigue Wash fault (Scott, R.B. and Bonk 1984; Day et al. 1997).

The northern parts of the West Ridge and Jet Ridge blocks are more highly deformed than the main parts of these blocks to the south. This is particularly obvious near The Prow (Figures 3.6-1, 3.6-3), where the frequency and intensity of intra-block faulting increases. Along the northwest-trending edge of Yucca Mountain between The Prow and Castellated Ridge, northeast facing southeast-dipping Paintbrush Group strata are cut by a series of north- to north-northwest-striking normal faults that range in offset from 2 m to 70 m; east-side-down and west-side-down displacements are about equally divided (Day et al. 1997; Scott, R.B. and Bonk 1984; Christiansen and Lipman 1965). Through the northwestern corner of the site area and to the north of the site area, the Windy Wash fault maintains its character as a complex, west-side down block-bounding fault. The Fatigue Wash fault continues through the Prow area as a west-side-down block-bounding fault.

In contrast to the gradual northerly increase in deformation in the West Ridge and Jet Ridge blocks, the transition from the northern margin of the central block to the Azreal Ridge domain (Figure 3.6-5) is marked by a decrease in the magnitude of east-west extension, manifested in a fundamental change in the nature of the two block-bounding faults. West-side-down displacements along the Solitario Canyon fault and the Bow Ridge fault diminish to zero at hinge points within northern Yucca Mountain. North of these hinge points, east-side down displacements are mapped or inferred from drillhole data along these faults (Figure 3.6-3). For the Solitario Canyon fault, the hinge point is in Teacup Wash (Day et al. 1998a), and for the Bow Ridge fault, the hinge point lies beneath Quaternary alluvium east of Isolation Ridge (Dickerson and Drake 1998b). The Azreal Ridge domain occupies the little-extended area bounded by the segments of these two faults that have undergone minimal displacements near the hinge points. The magnitude of post-12.7 Ma

extension in the Azreal Ridge domain was about 0 to 7 percent (using the minimum value of 7 percent calculated by Fridrich et al. (*Cenozoic Basins of the Death Valley Region: Late Cenozoic Extension, Vertical-Axis Rotation, and Volcanism in the Crater Flat Basin, Southwest Nevada*, Geological Society of America Special Paper, in press), and acknowledging the presence of a "null zone" of zero displacement on two block-bounding faults).

In addition to the decreased magnitude of extension, the Azreal Ridge domain is characterized by a change in the direction of stratal dips and a change in intra-block faulting style. In contrast to the easterly dips that are predominant in the Central Yucca Mountain domain, the Azreal Ridge domain consists of southeast-dipping Paintbrush Group strata. Because the main ridges and washes at Yucca Mountain have generally developed parallel to the dip of the Paintbrush Group welded tuffs, this southeast dip is geomorphically expressed as a strong northwest-trending topographic grain. The southeasterly dipping strata in the Azreal Ridge domain actually comprise one limb of a broad southeast-plunging syncline, and the other limb is defined by the east-dipping strata of the central block. The axis of this syncline lies beneath Drill Hole Wash.

The long northwest-trending washes are underlain by faults that show evidence for dextral strike-slip motion in addition to a southwest-side-down dip-slip component (Scott, R.B., Bath et al. 1984). Evidence for dextral slip on the northwest-trending faults includes subhorizontal slickensides and mullion structures on the nearly vertical Sever Wash fault, and Reidel shears on the Pagany Wash fault (Scott, R.B., Bath et al. 1984; Day et al. 1998a). The Drill Hole Wash fault was mapped as a dextral strike-slip fault by R.B. Scott and Bonk (1984). One key piece of evidence for this included the dextral offset of a north-striking fault by the (presumably younger) northwest-trending Drill Hole Wash fault near the southeast end of Tonsil Ridge. Day et al. (1998a) found that the intersecting fault pattern mapped by R.B. Scott and Bonk (1984) is not present. According to Day et al. (1998a) the Drill Hole Wash fault, along which the Tiva Canyon Tuff is displaced 15 m down-to-the-southeast on Tonsil Ridge, is a discontinuous structure along which the amount of stratigraphic throw decreases abruptly in both directions from the point where the fault crosses Tonsil Ridge. Where the Drill Hole Wash fault zone crosses the Exploratory Studies Facility 400 m to the southeast, the stratigraphic throw may be as little as 1.2 m. Subhorizontal slickensides that indicate a dextral sense of offset are apparent on one strand of the Drill Hole Wash fault in the Exploratory Studies Facility (Day et al. 1998a). In the lower part of Drill Hole Wash, southeast of the Exploratory Studies Facility alignment, Spengler and Rosenbaum (1980) used logs of oriented drill core to infer the presence of two fault strands, buried beneath surficial deposits along the northwest and southeast margins of Drill Hole Wash. The drill core showed evidence of shearing and rotation of foliation and remanent magnetization vectors in these locations, and Spengler and Rosenbaum (1980) interpreted the buried fault strands as sinistral strike-slip, or oblique-slip faults.

North of the Azreal Ridge domain, the Yucca Wash domain records a northward increase in the magnitude of east-west extension, accommodated by displacements along north- to northwest-striking intra-block faults. These include several prominent splays of the Sever Wash fault, along which the amount of stratigraphic displacement increases markedly to the north, just south of Yucca Wash. This structural style is similar to that in the adjacent part of the Central Yucca Mountain domain near The Prow, as discussed above, and it continues on the north side of Yucca Wash within the Yucca Wash domain (Figure 3.6-5).

Geologic and geophysical evidence in the Yucca Wash domain argue strongly against the existence of the Yucca Wash fault, proposed by R.B. Scott and Bonk (1984) as a significant buried strike-slip fault. The base of the Pah Canyon Tuff projects across Yucca Wash with no apparent displacement, whereas the presence of a significant strike-slip fault, oriented approximately parallel to the dip of the strata, would produce significant stratigraphic throw (Dickerson 1996). Langenheim, Ponce et al. (1993) acquired ground-based gravity and magnetic data from four traverses across Yucca Wash and three parallel traverses along the length of Yucca Wash. These data reveal a distinct high magnetic anomaly trending across Yucca Wash near borehole UE-25 WT#6. This magnetic anomaly is not offset along any northwest-striking structure, nor is a distinct magnetic plateau southeast of this anomaly offset to the northwest or southeast. These ground-based geophysical data define several north-striking anomalies, interpreted as normal faults, that can be traced beneath the wash to bedrock exposures of normal faults on both sides of Yucca Wash. Aeromagnetic data by McCafferty and Grauch (1997) show northwest-trending gradients between magnetic highs and lows that are parallel to the northwest-striking faults in Drill Hole Wash, Pagany Wash, and Sever Wash. Conversely, the aeromagnetic anomalies and gradients between them are oriented along north-south trends in the Yucca Wash area, as are a number of mapped normal faults. These data indicate that the structural grain beneath Yucca Wash is dominated by north-striking normal faults that are not disrupted by a significant northwest-trending structure. The Yucca Wash fault was not recognized by either Christiansen and Lipman (1965) or Day et al. (1998a; 1998b).

The Paintbrush Canyon domain is characterized by closely spaced faults that divide this domain into a series of long, narrow, north-trending and east-dipping blocks ranging in width from 0.6 to 1 km. The domain is bounded on its east and west sides by the Paintbrush Canyon and Bow Ridge faults, respectively, and it includes prominent north-striking faults such as the Black Glass Canyon fault, the Midway Valley fault, and the Exile Hill fault. In the northern part of the domain, fault blocks are juxtaposed along down-to-the-west normal faults that have extensive deformation in their hanging walls (Dickerson and Drake 1998a). This hanging-wall deformation includes graben development, numerous splays, pull-apart structures, and wide, internally sheared, massively brecciated, multi-plane main fault zones. Geophysical interpretations strongly suggest that fault blocks buried beneath surficial deposits in Midway Valley define a horst-and-graben pattern (Ponce and Oliver 1996). Exile Hill, for example, represents a horst and another buried horst occurs to the east beneath the center of Midway Valley; these horsts are 0.3 to 0.7 km in width (Ponce 1996; Dickerson and Drake 1998b).

The continuity of north-trending faults from north of Yucca Wash southward through Midway Valley is one of the unifying characteristics of the Paintbrush Canyon domain. Geophysical and geologic data indicate that the main faults exposed north of Yucca Wash continue southward beneath Quaternary deposits to the southern part of Midway Valley (Dickerson 1996; Dickerson and Drake 1998b). This observation argues strongly against the presence of the Yucca Wash fault as a major structure.

Along the eastern edge of the Paintbrush Canyon domain, the magnitude and complexity of the Paintbrush Canyon fault increase toward the south. There are over 200 m of displacement along this fault in upper Paintbrush Canyon (Dickerson and Drake 1998a), and over 300 m of displacement near Fran Ridge. Beneath the southeastern part of Midway Valley, buried northeast-striking splays are inferred to have propagated from the main trace of the Paintbrush Canyon fault (Ponce 1996;

Dickerson and Drake 1998b). The horst-and-graben pattern that characterizes most of Midway Valley is cut off by (or merges into) these splays (Ponce 1996; Dickerson and Drake 1998b). At the southern end of the Paintbrush Canyon domain, the Paintbrush Canyon fault becomes a major fault system, as it merges with the Dune Wash and Bow Ridge faults (Figures 3.6-3, 3.6-5). The Paintbrush Canyon fault system collects the aggregate displacement of all of these faults. Unfortunately, the area of intersection(s) of these faults, surely one of the most deformed and structurally complex areas of Yucca Mountain, is concealed beneath surficial deposits northwest of Busted Butte. Considered in the context of relay faults, the northwest-striking segments of the Dune Wash and Bow Ridge faults transfer displacement between their north-striking segments (to the north) and the north-striking Paintbrush fault system (to the south).

East of the Paintbrush Canyon domain, the Fran Ridge domain is a north-south trending, largely intact block between the Paintbrush Canyon fault and Fortymile Wash. It includes (from north to south): Comb Peak and the bedrock tract to its south, Alice Ridge, Fran Ridge, and Busted Butte (Figure 3.6-1). The Fran Ridge domain is characterized by less internal deformation than that found in the Paintbrush Canyon domain. Smaller faults splay eastward off the Paintbrush Canyon fault at Joey Ridge, Alice Ridge, and Fran Ridge, and indicate a greater amount of footwall deformation for the Paintbrush Canyon fault than is demonstrated for faults in the Paintbrush Canyon domain. Although the internal deformation in most of the Fran Ridge domain is minor, there are a few intra-block faults with significant amounts of offset, such as the Busted Butte fault (75 m) and the fault south of Comb Peak (130 m). Additionally, the Fran Ridge domain is both stratigraphically and structurally higher than the adjacent Paintbrush Canyon and Fortymile Wash domains. Gaps between the topographic highs within the Fran Ridge domain are occupied by buried down-to-the-north faults that lie between Busted Butte and Fran Ridge, and between Fran Ridge and Alice Ridge. These buried faults are probably northwest-striking splays within the footwall of the Paintbrush Canyon fault, and are identified by stratigraphic mismatches between outcrops on the topographic highs.

Geologic relations within the Fortymile Wash domain are poorly understood because the bedrock geology of this domain is largely concealed by the Quaternary (and possibly older) surficial deposits of Jackass Flats. However, data from borehole UE-25 J#13 indicate that this area has been faulted down along a major fault east of Fran Ridge. Furthermore, the prevailing easterly dip of the Paintbrush Group strata in the Fran Ridge domain strongly suggests that a major west-side-down normal fault lies beneath the western part of Jackass Flats (east of the down-to-the-east fault shown east of Fran Ridge in Figure 3.6-3), possibly the "gravity fault" shown in Figure 3.3-1. The northern part of the Fortymile Wash domain consists of the extensively faulted rocks east of Fortymile Wash. There is no preferred orientation for faults in this area, as faults strike east-west, north-south, northeast-southwest, and southeast-northwest. It is not known to what extent this random fault pattern characterizes other parts of the Fortymile Wash domain where bedrock is not exposed.

In domains south of the Central Yucca Mountain domain there is a dramatic increase in the magnitude of extension accompanied by significantly different structural styles (Scott, R.B. and Bonk 1984; Day et al. 1997). The transition from the less-extended northern part of Yucca Mountain to the more-extended southern part of the mountain is generally expressed on geologic maps by the presence of numerous fault splays that fan out to the south from block-bounding faults that cross this transition from the north. In intra-block areas, the transition is expressed by the appearance of

numerous closely spaced minor faults that coalesce and gain displacement to the south. These patterns are apparent in the northern part of Dune Wash and particularly near the mouth of Abandoned Wash (Scott, R.B. and Bonk 1984; Day et al. 1998a) (Figure 3.6-4). In domains south of the Central Yucca Mountain domain, increased east-west extension is accompanied by the southward splaying of the Solitario Canyon fault, the development of a broad, complexly faulted graben between Dune Wash and the unnamed ridge between Dune Wash and Abandoned Wash, and the convergence of several block-bounding faults along the west side of Busted Butte.

In the southern part of the site area (south of N 750,500), the amount of extension, intensity of deformation and the amount of vertical-axis rotation all increase (Scott, R.B. 1990, 1992; Day et al. 1998b; Rosenbaum et al. 1991). R.B. Scott (1990) expressed the southward increase in deformation as an increase in the area underlain by "imbricate fault zones," characterized by steeper eastward dips of strata and "an imbricate pattern of closely spaced, steep, west-dipping faults with minor, down-to-the-west offsets of a few meters or less." Clockwise vertical-axis rotations of Paintbrush Group strata increase from north to south, from 5° to 10° in the central block of the Central Yucca Mountain domain, to 30° at the extreme south end of Yucca Mountain, south of the site area (Rosenbaum et al. 1991). Northwest to north-northwest-striking splays are common components of the north-striking block-bounding fault systems. In some places, these northwest striking splays have developed into major relay faults that transfer displacement between block-bounding faults. In the extreme southern part of Yucca Mountain (south of the site area), the strike of the Southern Windy Wash and Stagecoach Road block-bounding faults are rotated to northeasterly orientations, and the subsidiary splays are north-trending (Simonds et al. 1995).

In the Southwest domain, which lies between Iron Ridge and Crater Flat, north-trending, block-bounding faults are linked together kinematically by northwest-trending relay faults and associated structures, which act to disperse the regional tectonic strain across several of the faults (Day et al. 1997). An excellent example is the complex northwest-striking relay zone between the Solitario Canyon and Iron Ridge faults, near the north end of the Southwest domain (Scott, R.B. and Bonk 1984; Day et al. 1997). There are commonly northwest-striking narrow grabens associated with relay faults, here and elsewhere in the southern part of Yucca Mountain. Day et al. (1997) show that block-bounding fault systems in this domain are west-dipping, upward widening arrays, with west dips ranging from relatively shallow (45° to 50°) to steep (75° to 85°). As the upward widening fault zones attain shallower dips, the amount of secondary faulting preserved in the footwall of the block-bounding fault system increases dramatically. In addition, fracturing of the footwall increases near the major relay faults.

The Dune Wash domain (Figure 3.6-5) is defined by a northwest-trending complex graben, bounded on the east side by the down-to-the-west block-bounding Dune Wash fault. Its western margin is bounded by a down-to-the-east block-bounding fault zone with at least 120 m of down-to-the-east displacement, which is equal to or greater than that of the more widely known Dune Wash fault. This down-to-the-east fault zone is approximately 100 m wide, contains tectonically brecciated and juxtaposed units of the Topopah Spring Tuff, and, in places, exhibits higher degrees of oxidation, silicification and alteration relative to other block-bounding faults. This fault zone splays to the south into several faults with down-to-the-east displacement southwest of bore hole UE-25 WT#17. The splays each have over 30 m of displacement (Day et al. 1997). Within the interior of the graben are numerous smaller horst-and-graben structural blocks whose strata dip dominantly to the east.

The structure of the interior of the graben is highly complex with numerous discontinuous steeply dipping faults. The Dune Wash domain is one of the areas depicted by R.B. Scott (1990, Figure 6) as a broad imbricate fault zone. Although it is intensely faulted, it is not characterized by consistent west-side-down offset along the array of faults, as R.B. Scott (1990) implies by his definition and use of the term "imbricate fault zone."

In the northern end of the Dune Wash graben (southwest of borehole USW WT-1), the western bounding fault on the graben steps about 200 m to the west and displacement decreases. This fault places the crystal-rich member of the Tiva Canyon Tuff down against the pre-Tiva Canyon, post-Topopah Spring nonwelded tuffs (see Table 3.5-2 for criteria defining stratigraphic units). The displacement on individual faults within the graben decreases to the north, but the overall horst-and-graben pattern is maintained. At the northern end of the graben, just south of the mouth of Abandoned Wash, the faulting resembles the closely-spaced faulting that characterizes block-margin deformation in the central block to the north. The southern end of the Dune Wash domain, which is buried beneath Quaternary deposits southwest of Busted Butte, seems to terminate against the down-to-the-west Paintbrush Canyon fault.

The East Ridge domain lies to the west of Dune Wash. It is bound on the west by the unnamed block-bounding fault west of borehole WT-12 and the down-to-the-east block-bounding faults just east of East Ridge on the western edge of the Dune Wash graben. This domain differs from the adjacent Central Yucca Mountain domain in that the amount of intra-block faulting is more intense, recording a greater amount of extensional deformation. The strata strike north-northeast and dip generally 15° to 20° to the east, which is steeper than is observed in the Central Yucca Mountain domain. This domain also has numerous east-side-down faults, which splay off the western margin of the Dune Wash graben.

The Plug Hill domain includes low lying hills of Tiva Canyon Tuff at the western edge of the map area as well as the Rainier Mesa Tuff exposed on Plug Hill itself. The northern margin of the domain is delineated by the relay structures on the southern tip of Jet Ridge; the eastern and southern margins by the Solitario Canyon fault, which curves from a north strike to a more northeasterly strike. Although the bedrock is poorly exposed, where present it is made up of highly faulted, eastward-dipping blocks of units of the Paintbrush Group downdropped along the normal faults that rim the domain. Plug Hill is made up of Tiva Canyon Tuff that is overlain by nonwelded and welded units of the Rainier Mesa Tuff. The amount of faulting within the Rainier Mesa Tuff is hard to detect because it is poorly exposed. Day et al. (1998a) mapped faults in the underlying Paintbrush Group rocks as being overlain by unfaulted Rainier Mesa Tuff, suggesting that deposition of the Rainier Mesa Tuff postdated some of the post-Paintbrush Group movement on the hanging wall of the Solitario Canyon fault. Here, as is true elsewhere, the Rainier Mesa Tuff is preserved only on the hanging wall of the block-bounding faults.

3.6.2.3.3 Timing of Deformation

Six different lines of investigation have been used to evaluate the specific timing of Neogene deformation in the Yucca Mountain site area:

- Evaluation of geologic map patterns along faults and lithologic logs of boreholes in the vicinity of faults to discern stratigraphic evidence for growth relations or episodic fault motion
- Evaluation of systematic contrasts in stratal dip across unconformities
- Paleomagnetic studies of spatial and temporal variations in vertical axis rotations
- Fault slip directions derived from detailed field measurements of fault planes and slickensides, temporally constrained by stratigraphic control where available
- Evaluation of the sequence of development of tectonic fractures in outcrops, cleared pavements and excavations
- Neotectonic studies of Quaternary to recent faulting in surficial materials

Of these, the first five are summarized below, and the sixth (neotectonic studies) is summarized in Subsection 3.10.

3.6.2.3.3.1 Stratigraphic Relations Across Faults

Among block-bounding faults, geologic map patterns contain clear evidence for episodic Miocene movement along the Solitario Canyon and Fatigue Wash faults during deposition of formations within the Paintbrush Group. For example, on the east side of Solitario Canyon, across a prominent footwall splay of the Solitario Canyon fault, the pre-Pah Canyon bedded tuffs (Tpbt2, which directly overlies the Topopah Spring Tuff; Table 3.5-2) and the overlying Pah Canyon Tuff undergo 7 m and 2 m, respectively, of stratigraphic thinning from the hanging wall to the footwall (Day et al. 1998a). The top of the Topopah Spring Tuff is offset by 13 m, whereas bases of the Yucca Mountain Tuff and Tiva Canyon Tuff are offset by about 3 m along this fault. These relations indicate that this splay of the Solitario Canyon fault was active during deposition of map unit Tpbt2 and the Pah Canyon Tuff (12.8 to 12.7 Ma), and underwent lesser movement after deposition of the 12.7 Ma Tiva Canyon Tuff.

There is further evidence for episodic fault displacement to the north along the Solitario Canyon fault on the north side of Teacup Wash. The lower nonlithophysal zone of the Tiva Canyon Tuff thickens near and across the fault by about 10 m from the footwall to the hanging wall (Day et al. 1998a). (Here the Solitario Canyon fault is an east-dipping normal fault.) This thickening in the lower part of the Tiva Canyon Tuff suggests that there was fault-controlled relief of about 10 m across this fault, immediately before deposition of the Tiva Canyon Tuff. Thus, there may have been at least 10 m of pre-Tiva Canyon Tuff displacement, and the displacement of markers near the top of the Tiva Canyon Tuff demonstrates about 12 m of post-Tiva Canyon Tuff displacement (Day et al. 1998a).

Just southeast of the Prow, along the steep northeast-facing slope of Yucca Wash, an abrupt thickness change in the pre-Yucca Mountain Tuff bedded tuffs (Tpbt3) across the Fatigue Wash fault indicates that this fault was active during or just prior to deposition of this unit (12.8 to 12.7 Ma). There was an additional 50 m of post-Tiva Canyon Tuff (post-12.7 Ma) displacement, evidenced by 50 m of offset of the base of this formation. One hundred fifty meters to the west, a parallel fault

with no mapped connection to the Fatigue Wash fault has a 45-m-thick rhyolite flow (map unit Tpz: Table 3.5-2) stratigraphically between the Pah Canyon Tuff and the pre-Yucca Mountain Tuff bedded tuffs (Tpbt3). This flow is not present on the footwall, implying that at least 45 m of post-Pah Canyon Tuff, pre-Tpbt3 fault displacement occurred in order to accommodate this flow. There is also about 16 m of growth in the thickness of the Yucca Mountain Tuff across this fault, as well as 20 m of post-Tiva Canyon Tuff (post-12.7 Ma) displacement, evidenced by fault displacement of the base of the Tiva Canyon Tuff (Day et al. 1997).

Some intra-block faults also appear to have moved episodically. In the central block, borehole USW UZ-7a penetrates the Ghost Dance fault, and lithologic logs indicate a structural thinning of the upper lithophysal zone of the Topopah Spring Tuff (Tptpul) by 30 m. Thus there appears to be at least 30 m (98 ft) of fault displacement of the Topopah Spring Tuff here, whereas geologic mapping (Day et al. 1998a) demonstrates about 15 m (49 ft) of displacement at the surface, within the Tiva Canyon Tuff. Thus there was about 15 m of post-Topopah Spring, pre-Tiva Canyon Tuff (12.8-12.7 Ma) displacement along the Ghost Dance fault, and about 15 m of post-Tiva Canyon Tuff fault displacement at this locality. On cross-section B-B' in Day et al. (1998a) (generalized in Figure 3.6-6), this difference in fault displacement is accommodated by an assumption of growth faulting (represented by stratigraphic thinning across the fault) during deposition of the crystal-rich member of the Topopah Spring Tuff and during deposition of the bedded tuffs that lie stratigraphically between the Topopah Spring Tuff and the Tiva Canyon Tuff (Table 3.5-2). This cross-section also assumes a small amount of fault-related topography immediately prior to deposition of the Tiva Canyon Tuff.

Numerous minor faults on the west side of Fran Ridge and the north end of Busted Butte (splays of the Busted Butte fault) offset the top of the Topopah Spring Tuff and the superjacent pre-Pah Canyon Tuff bedded tuffs (Tpbt2) by 1 to 10 m, but do not offset the younger pre-Tiva Canyon Tuff bedded tuffs (Tpbt4) or the base of the Tiva Canyon Tuff. Thus these faults were active during the 100,000 year interval between the eruption of the 12.8 Ma Topopah Spring Tuff and the deposition of the 12.7 Ma Tiva Canyon Tuff, but not in post-Tiva Canyon Tuff time.

In and near the upper part of Paintbrush Canyon in the northern part of the site area (north of Yucca Wash), several minor faults show evidence for episodic or continuous fault movement throughout deposition of the Paintbrush Group (Dickerson and Drake 1998b). Along several faults, there is decreasing offset of successively younger units throughout the Paintbrush Group.

In summary, stratigraphic relations across faults in the site area, including both block-bounding and intra-block faults, show evidence for fault movements throughout the deposition of the Paintbrush Group. Evidence for these movements includes apparent growth relations (stratigraphic thickening across faults) within various post-Topopah Spring, pre-Tiva Canyon units, and fault related paleotopography at the base of the Tiva Canyon Tuff. Notably, post-Topopah Spring, pre-Tiva Canyon fault movements do not produce discernible angular discordances between successive units. This may indicate that faults of this age produced vertical displacement but not extension, or it may just be a function of the minor nature of most of these faults. Isolation of the characteristics of the pre-Tiva Canyon phase of faulting is difficult because the post-Tiva Canyon Tuff displacement on nearly all of these faults greatly exceeds the pre-Tiva Canyon Tuff displacement. The scattered and limited nature of exposures of the Rainier Mesa Tuff makes evaluation of the amount of post-Rainier

Mesa faulting difficult, although all exposures of the Rainier Mesa Tuff in the site area are cut by faults. As summarized below, there is evidence in the site area that the Rainier Mesa Tuff experienced fault displacement and tilting nearly equivalent to the faulting and tilting that affected the Tiva Canyon Tuff.

3.6.2.3.3.2 Angular Discordance Across Unconformities

Fridrich (1998) and C.J. Fridrich et al. (*Cenozoic Basins of the Death Valley Region: Late Cenozoic Extension, Vertical-Axis Rotation, and Volcanism in the Crater Flat Basin, Southwest Nevada*, Geological Society of America Special Paper, in press) have systematically evaluated the progressive Miocene deformation of Yucca Mountain and Crater Flat through analysis of contrasts in stratal dip across unconformities. Specifically, C.J. Fridrich et al. (*Cenozoic Basins of the Death Valley Region: Late Cenozoic Extension, Vertical-Axis Rotation, and Volcanism in the Crater Flat Basin, Southwest Nevada*, Geological Society of America Special Paper, in press) compiled maps that portray the amount of angular discordance between the 12.8-12.7 Ma Paintbrush Group and the 11.7 to 11.45 Ma Timber Mountain Group; and between the Timber Mountain Group and 10.5 Ma basalts and sedimentary breccia sheets. Because stratified 10.5 Ma units are not exposed in the site area, and because the majority of post-11.6 Ma deformation is confined to the part of Crater Flat west of the site area, only the Paintbrush-Timber Mountain unconformity is significant with respect to the timing and magnitude of extensional deformation at Yucca Mountain.

C.J. Fridrich et al. (*Cenozoic Basins of the Death Valley Region: Late Cenozoic Extension, Vertical-Axis Rotation, and Volcanism in the Crater Flat Basin, Southwest Nevada*, Geological Society of America Special Paper, in press) indicate that in the Yucca Mountain site area, the 12.7 Ma Tiva Canyon Tuff was tilted by 10° to 20° to the east and southeast prior to deposition of the 11.6 Ma Rainier Mesa Tuff. Their summary maps indicate that less than 5° of eastward tilting occurred in the site area between 11.6 and 10.5 Ma, and that less than 5° of eastward tilting occurred after 10.5 Ma (C.J. Fridrich et al., *Cenozoic Basins of the Death Valley Region: Late Cenozoic Extension, Vertical-Axis Rotation, and Volcanism in the Crater Flat Basin, Southwest Nevada*, Geological Society of America Special Paper, in press). These angular relations are not well constrained in most of the site area, because units younger than the Tiva Canyon Tuff are sparsely exposed there. C.J. Fridrich et al. (*Cenozoic Basins of the Death Valley Region: Late Cenozoic Extension, Vertical-Axis Rotation, and Volcanism in the Crater Flat Basin, Southwest Nevada*, Geological Society of America Special Paper, in press) relied on extrapolation from northern Crater Flat, as well as a few scattered exposures in the site area (southern Boundary Ridge, Plug Hill) to establish the reported contrasts in dip between the Tiva Canyon and Rainier Mesa Tuffs. R.B. Scott (1990), using compaction foliations, suggested that there is over 10° of discordance between the Rainier Mesa Tuff and the Tiva Canyon Tuff west and northwest of Busted Butte (including the southern Boundary Ridge area). No 10.5 Ma stratified rocks are present in the site area, so angular relations involving this unit, reported by C.J. Fridrich et al. (*Cenozoic Basins of the Death Valley Region: Late Cenozoic Extension, Vertical-Axis Rotation, and Volcanism in the Crater Flat Basin, Southwest Nevada*, Geological Society of America Special Paper, in press) are complete extrapolations from the western part of Crater Flat.

In contrast to the angular relations suggested by C.J. Fridrich et al. (*Cenozoic Basins of the Death Valley Region: Late Cenozoic Extension, Vertical-Axis Rotation, and Volcanism in the Crater Flat*

Basin, Southwest Nevada, Geological Society of America Special Paper, in press) and by R.B. Scott (1990), subsequent mapping by Day et al. (1997) indicates minimal angular discordance between the Paintbrush and Timber Mountain Groups over most of the site area. For example, west of Busted Butte the basal bedded layers in the Rainier Mesa Tuff are parallel to strata in the underlying post-Tiva Canyon Tuff bedded tuff (Tpbt5), and to flattened pumice attitudes in the Tiva Canyon Tuff. Thus the Tiva Canyon, post-Tiva Canyon, and Rainier Mesa Tuffs are separated by disconformities, not by angular unconformities, west of Busted Butte. Other localities where Day et al. (1997) have mapped little or no (5° or less) angular discordance between the Tiva Canyon Tuff and the Rainier Mesa Tuff include southern Boundary Ridge (east of Dune Wash) and Plug Hill.

Mapping in the north ramp of the Exploratory Studies Facility, just west of the Bow Ridge fault (Beason et al. 1996), provides additional constraints on the amount of post-Paintbrush Group, pre-Timber Mountain Group tilting in the site area. There, depositional contacts in the uppermost part of the Tiva Canyon Tuff dip 15° to 19° E, and depositional contacts in the lowermost tuffs of the Rainier Mesa Tuff dip 10° to 18° . (There is significant overlap in the values for these two units; the 10° dip appears to be measured in an anomalous segment.) The Comb Peak Rhyolite, which is the uppermost formation in the Paintbrush Group, intervenes between the Tiva Canyon Tuff and the base of the Timber Mountain Group in the Exploratory Studies Facility, and has similar dips, but there are no clear depositional markers mapped in the Comb Peak. The steep dips on these strata, relative to the strata to the west in the central block and the Azreal Ridge domain, are typical of block-margin deformation in the immediate hanging wall of the Bow Ridge fault. The angular discordance between the Paintbrush and Timber Mountain Groups is minimal at this location.

The amount of angular discordance beneath the Timber Mountain Group appears greater in the extreme northwest part of the site area. In northern Windy Wash, Day et al. (1997) report 8° of angular discordance between post-Tiva Canyon Tuff bedded tuffs (Tpbt5) and the nonwelded base of the Rainier Mesa Tuff. R.B. Scott (1990) found only 0° to 4° of angular discordance between the Rainier Mesa Tuff and the Tiva Canyon Tuff in northwest Yucca Mountain. The results of Day et al. (1997) suggest that the amount of post-Paintbrush Group, pre-Timber Mountain Group tilting increased to the west within the northwestern-most part of the site area (west of the Northern Windy Wash fault), and the synthesis of C.J. Fridrich et al. (*Cenozoic Basins of the Death Valley Region: Late Cenozoic Extension, Vertical-Axis Rotation, and Volcanism in the Crater Flat Basin, Southwest Nevada*, Geological Society of America Special Paper, in press) indicates that the amount of tilting in this time period increased to the northwest of Yucca Mountain, toward northern Crater Flat where these stratigraphic relations are better constrained.

C.J. Fridrich et al. (*Cenozoic Basins of the Death Valley Region: Late Cenozoic Extension, Vertical-Axis Rotation, and Volcanism in the Crater Flat Basin, Southwest Nevada*, Geological Society of America Special Paper, in press) calculate an upper bound on the amount of horizontal extension in Crater Flat and Yucca Mountain using a simple mathematical formula (Nur et al. 1989) that assumes a tilting-domino style of extension and is a function of fault dip and stratal dips. Reconstruction of cross-sections resulted in lower amounts of horizontal extension, which C.J. Fridrich et al. (*Cenozoic Basins of the Death Valley Region: Late Cenozoic Extension, Vertical-Axis Rotation, and Volcanism in the Crater Flat Basin, Southwest Nevada*, Geological Society of America Special Paper, in press) took to be minimum values. For the site area, their calculations of cumulative horizontal extension from 12.7 Ma to the present yield maximum values of 15 to 30 percent (greater in the south than in

the north) and minimum values of 7 to 15 percent. They proposed that most of this extension took place between 12.7 and 11.6 Ma, based on their assumptions on the dip contrasts discussed above (C.J. Fridrich et al., *Cenozoic Basins of the Death Valley Region: Late Cenozoic Extension, Vertical-Axis Rotation, and Volcanism in the Crater Flat Basin, Southwest Nevada*, Geological Society of America Special Paper, in press).

The geologic mapping of Day et al. (1998a) and R.B. Scott and Bonk (1984) yields lower dips and consequently lower extension magnitudes than those reported by C.J. Fridrich et al. (*Cenozoic Basins of the Death Valley Region: Late Cenozoic Extension, Vertical-Axis Rotation, and Volcanism in the Crater Flat Basin, Southwest Nevada*, Geological Society of America Special Paper, in press). In the Azreal Ridge and Yucca Wash domains, and near the Prow in the Central Yucca Mountain domain, dips determined using three point calculations on depositional contacts in the crystal-rich member of the Tiva Canyon Tuff (away from block-bounding faults) range from 1° to 8°SE and are typically about 5°SE (Day et al. 1998a). To the south in the Central and Jet Ridge blocks of the Central Yucca Mountain domain, these same contacts dip 5° to 11°E, with a typical value of about 7° (Day et al. 1998a). In contrast, C.J. Fridrich et al. (*Cenozoic Basins of the Death Valley Region: Late Cenozoic Extension, Vertical-Axis Rotation, and Volcanism in the Crater Flat Basin, Southwest Nevada*, Geological Society of America Special Paper, in press) report that the Tiva Canyon Tuff in these domains was tilted 10° to 15° prior to deposition of the Rainier Mesa Tuff, and that it was tilted by several more degrees post-11.6 Ma. The reported pre-11.6 Ma tilts for the Tiva Canyon Tuff (C.J. Fridrich et al., *Cenozoic Basins of the Death Valley Region: Late Cenozoic Extension, Vertical-Axis Rotation, and Volcanism in the Crater Flat Basin, Southwest Nevada*, Geological Society of America Special Paper, in press) exceed the present-day dip of this formation. Only in the hanging walls of block-bounding faults (as discussed above in the north ramp of the Exploratory Studies Facility), do stratal dips approach those reported by C.J. Fridrich et al. (*Cenozoic Basins of the Death Valley Region: Late Cenozoic Extension, Vertical-Axis Rotation, and Volcanism in the Crater Flat Basin, Southwest Nevada*, Geological Society of America Special Paper, in press). Part of the discrepancy may stem from the reliance of C.J. Fridrich et al. (*Cenozoic Basins of the Death Valley Region: Late Cenozoic Extension, Vertical-Axis Rotation, and Volcanism in the Crater Flat Basin, Southwest Nevada*, Geological Society of America Special Paper, in press) on attitudes of flattening foliations, defined by flattened pumice and lithophysae. Flattening foliations in the same crystal-rich zones of the Tiva Canyon Tuff are 5° to 14° in the Azreal Ridge Domain and 8° to 20° in the Central and Jet Ridge blocks of the Central Yucca Mountain domain (Scott, R.B. and Bonk 1984; Day et al. 1998a). Day et al. (1998a) demonstrated that the dips of flattening foliations commonly exceed true stratal dips (determined by three-point calculations on depositional contacts) by 5°. Truly representative stratal dip values for the site area, used in the tilting-domino-extension calculation of Nur et al. (1989), yield cumulative (post-12.7 Ma) extension values that are very close to the minimum extension values of 7° to 15° reported by C.J. Fridrich et al. (*Cenozoic Basins of the Death Valley Region: Late Cenozoic Extension, Vertical-Axis Rotation, and Volcanism in the Crater Flat Basin, Southwest Nevada*, Geological Society of America Special Paper, in press).

Thus, the marked angular unconformity mapped by Fridrich (1998) in northern Crater Flat cannot be extended with confidence through the site area, and the total amounts of tilting and extension, particularly in the northern and central parts of the site area, are significantly less than reported by C.J. Fridrich et al. (*Cenozoic Basins of the Death Valley Region: Late Cenozoic Extension, Vertical-Axis Rotation, and Volcanism in the Crater Flat Basin, Southwest Nevada*, Geological Society of

America Special Paper, in press). Unlike the western part of Crater Flat, most of the extension in the site area apparently postdated the eruption of the Rainier Mesa Tuff.

3.6.2.3.3 Vertical-axis Rotations

Rosenbaum et al. (1991) summarize paleomagnetic data from the Tiva Canyon Tuff that demonstrate a progressive north-to-south increase in post 12.7 Ma vertical-axis rotations from 0° (no rotation) at the Prow to about 30° at the south end of the mountain (10 km south of the south edge of Figure 3.6-1). Within the site map area (Figures 3.6-1 and 3.6-3), the vertical-axis rotation varies from 0° at the Prow to about 5° at the latitude of Busted Butte (south edge of the map). These results are placed in geographic and stratigraphic context through the comprehensive paleomagnetic summaries of M.R. Hudson, Sawyer et al. (1994) and M.R. Hudson, Minor et al. (1996), who used paleomagnetic techniques to temporally and spatially constrain regional vertical axis rotations in the southwestern Nevada volcanic field. C.J. Fridrich et al. (*Cenozoic Basins of the Death Valley Region: Late Cenozoic Extension, Vertical-Axis Rotation, and Volcanism in the Crater Flat Basin, Southwest Nevada*, Geological Society of America Special Paper, in press) present these results for the Crater Flat tectonic domain, which comprises Crater Flat and Yucca Mountain. They show that the apparent north-to-south increase in vertical-axis rotations at Yucca Mountain is really part of a subregional trend of northeast-to-southwest-increasing vertical-axis rotations of Miocene volcanic units. The main pulse of vertical-axis rotation apparently occurred during the interval 11.6 to 11.45 Ma. This is based on the statistically identical amounts of rotation for the 13.25 Ma Bullfrog Tuff and the 12.7 Ma Tiva Canyon Tuff, a slight decrease in the amount of rotation for the 11.6 Ma Rainier Mesa Tuff, and the significant decrease in the amount of rotation of the 11.45 Ma Ammonia Tanks Tuff. M.R. Hudson, Minor et al. (1996) and C.J. Fridrich et al. (*Cenozoic Basins of the Death Valley Region: Late Cenozoic Extension, Vertical-Axis Rotation, and Volcanism in the Crater Flat Basin, Southwest Nevada*, Geological Society of America Special Paper, in press) argued that this main pulse of vertical-axis rotation postdates the major pulse of extension by about 1 m.y., because of the conclusion of C.J. Fridrich et al. (*Cenozoic Basins of the Death Valley Region: Late Cenozoic Extension, Vertical-Axis Rotation, and Volcanism in the Crater Flat Basin, Southwest Nevada*, Geological Society of America Special Paper, in press) that most of the extension predated the Rainier Mesa Tuff. As stated above, the majority of tilting and extension in the site area may be post-Rainier Mesa Tuff, so extension and vertical-axis rotation in the site area were likely synchronous, accompanying oblique displacement on block-bounding faults. The curved map patterns of faults south of the site area, in the more highly extended and rotated southern part of the mountain, indicate that clockwise vertical axis rotation outlasted major east-west extension there (C.J. Fridrich et al., *Cenozoic Basins of the Death Valley Region: Late Cenozoic Extension, Vertical-Axis Rotation, and Volcanism in the Crater Flat Basin, Southwest Nevada*, Geological Society of America Special Paper, in press).

3.6.2.3.4 Fault Slip Analyses

In the site area, post-12.7 Ma oblique displacement (i.e., post-Tiva Canyon Tuff faulting) included a sinistral component observed consistently on north-striking block-bounding faults (Scott, R.B. and Bonk 1984; Day et al. 1998a; Day et al. 1997) and a dextral component on some northwest-striking faults, particularly those in the Azreal Ridge domain. R.B. Scott (1990) reported that striations on northwest-striking fault planes are consistent with dextral components of motion, that striations on

northeast-striking faults are consistent with sinistral components, and that faults with northerly strikes show a mix of dextral and sinistral motion. However, major north-striking block-bounding faults in the site area, such as the Solitario Canyon and Paintbrush Canyon faults, have indicators of a sinistral component of slip (Scott, R.B. and Bonk 1984; Dickerson and Spengler 1994; Day et al. 1998a).

R.B. Scott (1990) used fault slip data on normal and strike-slip faults preserved in bedrock at Yucca Mountain to infer that the minimum horizontal stress direction was nearly east-west at the time that the bedrock fault scarps and striae were formed. This direction is consistent with the range of Middle Miocene minimum stress directions determined by Zoback et al. (1981) for this part of the Basin and Range, and is distinct from present day west-northwesterly minimum stress directions reported by Stock et al. (1985). This confirms that fault striae preserved in bedrock at Yucca Mountain record dominantly Miocene fault displacements.

Fault slip analyses by Minor, Hudson et al. (1996) across the northern flank of Crater Flat are relevant to an understanding of kinematic evolution of the site area. The excellent stratigraphic control in northern Crater Flat allowed Minor, Hudson et al. (1996) to separate a 12.7 to 11.6 Ma pulse of normal fault slip, from an 11.6 Ma and younger period of oblique slip. The oblique slip in northern Crater Flat was characterized by sinistral slip components on northeast-striking faults and dextral slip components on north-striking faults (Minor, Hudson et al. 1996). A north-northeast shortening direction is kinematically compatible with these fault motions in northern Crater Flat, whereas the post-12.7 Ma fault motions in the Yucca Mountain site area correspond to a north-northwest shortening direction. These shortening directions are radial to the center of the Timber Mountain caldera complex to the north, implying that eruptive processes in the caldera influenced the subregional stress field and strain patterns throughout Crater Flat and Yucca Mountain. East of the caldera complex, the maximum horizontal extension direction is radial to the caldera margin (Minor 1995) and extensional faults strike northerly; thus, regional strain effects related to the caldera complex are clearly second-order effects, superimposed on (pre-existing?) tracts of north-striking faulting.

3.6.2.3.3.5 Sequential Joint Formation and Relation to Site Scale Structural Evolution

Patterns of tectonic extension joints (joints that originate as tensional openings, rather than shear fractures) in the site area yield information on the relative age of structures with diverse orientations. Systematic sets of tectonic extension joints reflect components of the stress field in which they formed. Each tectonic joint set is interpreted to represent a distinct episode of jointing and an associated stress field. The observable sequential development of joint sets is thus interpreted to relate to systematic changes in the local or regional stress field. For each joint set, two components of the stress field at the time of fracture can be defined: the minimum compressive stress, s_3 , perpendicular to the median fracture plane; and the maximum horizontal compressive stress, s_{hmax} , parallel to fracture strike. The maximum compression in the horizontal plane (s_{hmax}) is not necessarily equivalent to either of the principle compressive stresses s_1 or s_2 . Thus, vertical to subvertical joints may have been generated in a "normal" stress field (s_1 roughly vertical) or in a "strike-slip" stress field (s_1 roughly horizontal).

Throckmorton and Verbeek (1995) identified four joint sets of tectonic origin, which they labeled T1, T2, T3 and T4. The median orientation of tectonic fracture sets are: T1, N05°W to N05°E/86° to 89°W; T2, N35°W to N25°W/85°SW; T3, N25°E to N45° E/88°NW; and T4, N75°E to N85°E/88°SW. Throckmorton and Verbeek (1995) interpreted the subvertical north-striking, northwest-striking, and northeast-striking joint sets at Yucca Mountain to have developed sequentially as products of noncoaxial regional extension during basin-range faulting. In their model, each of the fracture sets represents a distinct phase of regional extension, requiring the regional direction of maximum horizontal compressive stress to first have rotated counterclockwise, from s_{hmax} about north-south to about N30°W, during the time interval between the formation of the north-striking and northwest-striking joints; then clockwise, from about N 30° W through north again and thence to about N40°E, during the time interval between the formation of the northwest-striking and northeast-striking events.

Throckmorton and Verbeek (1995) interpreted the north-striking joints to be the earliest-formed tectonic fracture set, because they are the longest tectonic fractures, have the largest percentage of fracture ends that terminate in unfractured rock, and are only truncated by pre-existing cooling joints. In certain places, the northwest-striking fracture set appears to postdate the north-striking set (Throckmorton and Verbeek 1995). At some localities the northwest-striking fracture set has consistent termination relations against the north-striking set (Throckmorton and Verbeek 1995; Sweetkind, Verbeek et al. 1995b). There are rare examples of north-south striking fractures that appear to have renewed growth at their tips in the northwest-striking direction, yielding a bent or even sigmoidal overall fracture shape (Throckmorton and Verbeek 1995).

In many of the locations studied by Throckmorton and Verbeek (1995) and at more recently mapped exposures, the age relationship between the north-striking and northwest-striking sets is not clearly defined. The two sets often have ambiguous or contradictory termination relationships, and, in some instances, the northwest-striking set appears to be the older (Sweetkind and Williams-Stroud 1996). In contrast to the fracturing sequence reported by Throckmorton and Verbeek (1995), there is no clear evidence that the northwest-striking set is consistently later than the north-striking set. In general, the two fracture sets appear to be roughly coeval. Northeast-striking tectonic joints consistently terminate against cooling joints and the two sets of tectonic fractures described above (Throckmorton and Verbeek 1995; Sweetkind, Verbeek et al. 1995b; Sweetkind, Verbeek et al. 1995a). Thus, the northeast-striking tectonic joints formed relatively late in the sequence.

Geologic evidence throughout the Yucca Mountain region indicates dominantly east-west extension during the deposition of the Paintbrush Group, with little evidence for a separate phase of northeast-southwest extension. Faulting on north-striking, block-bounding faults, which had extension directions compatible with the opening of north-striking fractures, began prior to eruption of the Paintbrush Group, and continued during and after the deposition of the Paintbrush Group (Scott, R.B. 1990). Fault-slip analyses in nearby areas to the north record continuous east-west directed extension until around 8.5 Ma (Minor 1995). Because joints form at very low resolved stress, north-striking fractures probably formed throughout and after the time represented by the deposition of the Paintbrush Group, in response to east-west directed extension.

Evidence for continuous east-west directed extension and lack of consistent evidence of the relative age of the north-striking and northwest-striking tectonic fracture sets suggests that the regional

direction of maximum horizontal compressive stress probably did not rotate counterclockwise, from s_{hmax} about north-south to about N30°W, between the time of formation of the two fracture sets, as suggested by Throckmorton and Verbeek (1995). A more likely explanation is that the northwest-striking fractures formed during the same period of time as the north-striking fractures. Formation of northwest-striking fractures could be the result of locally rotated s_3 directions within a regime of regional east-west directed extension. For example, initiation of sinistral slip on major, block-bounding faults (Scott, R.B. 1990; Simonds et al. 1995) could favor the formation of northwest striking extension fractures within the fault-bounded blocks (Dyer 1988).

The geometric and timing relationships observed between north- and northwest-striking joints are mirrored by similar map scale relations of faults at Yucca Mountain. Day et al. (1998a) pointed out that the north- and northwest-striking faults formed coevally and were kinematically related. Recent work on concurrently active normal and strike-slip faults in the southern Great Basin indicate that adjacent faults having disparate slip vectors need not require temporal changes in the stress field (Wesnousky and Jones 1994; Morris et al. 1996). The work suggests that given relative magnitudes of the principle stresses where $s_1=s_2 \gg s_3$, a complex record of normal, oblique, and strike-slip events might arise from a relatively simple stress history. Alternatively, roughly concurrent motion along normal and strike-slip faults could result from the interplay between active Basin and Range extension and initiation of strike-slip motion along the Walker Lane zone (Bellier and Zoback 1995). Variability in the relative importance of these two stress regimes could explain the perplexing and often ambiguous relative timing relationships between the north-striking and northwest-striking fractures.

Northeast-striking tectonic joints are a consistently late joint set, based on termination relationships with all other cooling joints and tectonic joints at Yucca Mountain (Throckmorton and Verbeek 1995; Sweetkind, Verbeek, et al. 1995b; Sweetkind, Verbeek, et al. 1995a). Northeast-striking extension joints are consistent with the present-day direction of s_{hmin} (equivalent to s_3 for subvertical fractures), as determined from hydrofracture tests and orientations of borehole breakouts (Haimson et al. 1974; Springer et al. 1984; Stock, J.M., Healy et al. 1985; Stock, J.M. and Healy 1988) and from earthquake fault plane solutions and inversion of slip vectors on active faults in the region (Rogers, A.M., Harmsen, Carr et al. 1983; Bellier and Zoback 1995). Fault-slip analysis in nearby areas to the north record dominantly east west directed extension until 8.5 to 9 Ma (Minor 1995), after which time, the extension direction shifted toward the present-day orientation. Fault-slip analyses in nearby areas to the north (Minor 1995) confirm a regional shift from dominantly east-west directed extension prior to 8.5 to 9 Ma, to northwest-oriented extension after that time.

3.6.2.3.4 Summary of Timing of Deformation

Stratigraphic relations across faults and angular relations across unconformities demonstrate that block-bounding faults were active at Yucca Mountain during eruption of the 12.8 to 12.7 Ma Paintbrush Group, and significant motion on these faults continued until after the 11.6 Ma Rainier Mesa Tuff was deposited. Most of the stratal tilting in the site area occurred after 11.6 Ma, probably synchronous with the main pulse of vertical-axis rotation, which occurred during the interval 11.6 to 11.45 Ma. Fault slip analyses support a mid-Miocene age as the main period of motion of Yucca Mountain faults, and suggest that the fault patterns at Yucca Mountain, dominated by north-striking faults, are consistent with regional strain patterns, with an overprint of caldera-related deformation

in northernmost Yucca Mountain. Studies of sequential formation of tectonic extension joints, in the context of regional paleostress studies, indicate that north- and northwest-striking joint sets formed during a regional east-west extension in Paintbrush Group time, and that a prominent northeast-striking joint set was consistently later, probably post-9 Ma.

3.6.2.4 Central Block Structural Framework

Because the site of the potential repository lies in the central block of the Central Yucca Mountain domain (Figure 3.6-5), the structural framework of the central block is discussed here in greater detail. This subsection is a discussion of intra-block geology; the block-bounding faults are treated only to the extent that they affect the intra-block structure. The discussion is based primarily on geologic mapping, and also incorporates results from site area geophysical studies, underground geologic mapping, and borehole investigations.

The central block is bounded on the west by the Solitario Canyon fault, on the east by the Bow Ridge fault, and on the north by the northwest-striking Drill Hole Wash fault. The southern boundary of the central block is marked by a transition to structural styles that accompany greater magnitudes of extension. Although its eastern and western boundaries are block-bounding faults, its northern and southern boundaries are structural domain boundaries that do not coincide with block-bounding faults.

Surface geologic mapping (Scott, R.B. and Bonk 1984; Day et al. 1998a) as well as ongoing underground geologic mapping of the Exploratory Studies Facility confirm the fundamental structural style of the central block. Much of it is little-deformed (Yucca Crest sub-block, Figure 3.6-4), cut only by widely spaced intra-block faults that commonly have 1 to 10 m of displacement, and in only rare cases have greater than 10 m of displacement. The eastern and southern edge of the central block are cut by numerous faults. This more highly faulted area is termed the Boundary Ridge sub-block (Figure 3.6-4) and is the site of block margin deformation, defined above.

The cross-section through the central block shown in Figure 3.6-6 illustrates some of the fundamental differences among the different types of faults that affect the central block. This cross-section includes the two block-bounding faults (Solitario Canyon and Bow Ridge faults), the discontinuous minor faults as well as the Ghost Dance fault in the Yucca Crest sub-block, and the more intensely faulted Boundary Ridge sub-block. There is an obvious fundamental contrast in dip between the block-bounding faults, which dip 60° to 70° to the west, and the intra-block faults (in both the Yucca Crest and Boundary Ridge sub-blocks) whose map traces indicate they are nearly vertical. This contrast is related to the fact that the block-bounding Bow Ridge and Solitario Canyon faults are major extensional faults that root at mid-crustal levels, whereas the intra-block faults accommodate small strains within the block, commonly exploiting pre-existing steep cooling joints. There is also a fundamental contrast between the discontinuous nature of the intra-block faults in the Yucca Crest sub-block and the more continuous nature of the block-margin faults in the Boundary Ridge domain. This is because the block-margin faults are inferred to be an integral part of the Bow Ridge fault hanging-wall deformation, and, as such, are projected to intersect with the Bow Ridge fault at depth. Figure 3.6-6 and other cross-sections of the central block (Scott, R.B. and Bonk 1984; Day et al. 1998a) imply that the intra-block faulting must postdate most of the stratal tilting. This

inference is based on the observation that, if one removes the easterly dip on the central block, and assumes that the steep intra-block faults in both the Yucca Crest and Boundary Ridge sub-blocks predated tilting, most (or all) of them would have had a reverse sense of displacement. This seems highly unlikely, in light of the transtensional tectonic regime that characterized this area. It is much more likely that the easterly dips were achieved very early, in response to initial movement on the block-bounding faults, and the subsequent development of intra-block faults effected a pre-tilted section. During the early tilting, cooling joints were rotated from initial subvertical dips into steeply west-dipping orientations prior to tectonic activation of many of these joints by intra-block faults. Movement on the intra-block fault accompanied the continued movement on the block-bounding faults. An assessment of the likelihood of fault displacement on intra-block faults in response to future movement on block-bounding faults is described in Subsections 3.10.9.4 and 3.10.9.5.

3.6.2.4.1 Prominent Intra-block Faults in the Central Block—Distribution and Geometry

3.6.2.4.1.1 Ghost Dance Fault

The Ghost Dance fault (Figures 3.6-3, -4) is the main throughgoing structure within the central part of the Central Yucca Mountain domain (Scott, R.B. and Bonk 1984; Day et al. 1998a) with a trace length of 3.7 km between Abandoned Wash (in the south) and Wren Wash (in the north). In general, the Ghost Dance fault is a north-striking normal fault zone, steeply west-dipping (75° to 85°) with down-to-the-west displacement. The displacement, amount of brecciation, and number of associated splays vary considerably along its trace (Spengler, Braun, Linden et al. 1993).

The Ghost Dance fault zone can be divided into three segments based on the amount of offset and brecciation. The amount of offset in meters is shown in boxes in Figure 3.6-7. Along the northern segment, north of Split Wash, the fault is a relatively narrow zone (2 to 4 m wide) with as much as 6 m of down-to-the-west displacement. The central segment of the Ghost Dance fault zone has greater west-side-down displacement than the northern segment, and extends from Split Wash to Broken Limb Ridge. On Antler Ridge within this central segment, there are 13 to 20 m of cumulative displacement across several splays of the Ghost Dance that are distributed over a map width of approximately 100 to 150 m (Day et al. 1998a). Individual splays are characterized by a 1- to 2-m- wide breccia zone. To the south on Whale Back Ridge, the fault zone is about 55 m wide and has about 30 m down-to-the-west offset. There, the zone is bounded by two north-striking faults. The eastern fault is the main trace of the Ghost Dance. Locally, the immediate hanging wall of the principle splay of the Ghost Dance fault is highly fractured.

Within the central segment of the Ghost Dance fault zone, on the north-facing slope of Antler Ridge, the main trace of the Ghost Dance forms two overlapping strands in map view, defining a right-stepping pattern (Figure 3.6-8). Spengler, Braun, Martin et al. (1994) suggested that the two strands were offset along a younger northwest-striking fault. However, subsequent mapping by Potter, Dickerson et al. (1995) does not support the existence of a younger strike-slip fault; they suggested that the two Ghost Dance strands, which are separated by about 50 m on the surface, merge into one fault at depth, and that the abundant breccia between the two fault tips may be indicative of a local accommodation zone between the two individual fault tips that are exposed. Alternatively, the Ghost Dance fault may have “stepped over” along a pre-existing discontinuity such as a set of closely spaced northwest-striking cooling joints (Potter, Dickerson et al. 1995). Neither hypothesis requires

a separate tectonic event to explain the discontinuous nature of the Ghost Dance fault at this location. (A similar example of overlapping Ghost Dance fault tips is found on Live Yucca Ridge in the northern segment of the Ghost Dance fault; Potter, Dickerson et al. 1995; Day et al. 1998a). The southern segment of the Ghost Dance fault extends southward from Broken Limb Ridge where it bifurcates, one strand striking southwest into the Abandoned Wash fault of R.B. Scott and Bonk (1984) and the other to the southeast toward, but not into, the Dune Wash fault (Day et al. 1998a). Although there are two principle fault splays here, the fault zone in detail is made up of numerous fault splays that both parallel the main north-striking trace of the zone and branch off the main fault laterally and vertically. Vertical "horse-tailing" is present both on the south side of Whale Back Ridge and on the north-facing slope of Broken Limb Ridge.

The amounts of displacement and brecciation along the southwestern projection of the Ghost Dance fault across Highway Ridge are considerably less than those preserved along the central segment. On the south-facing slope of Broken Limb Ridge the offset is less than 6 m and intense fracturing in the hanging wall (in map unit Tcpmn; Table 3.5-2) extends about 15 m to the west. In the Ghost Dance Wash area (near the southern bend in the Exploratory Studies Facility) displacement on the fault is less than 3 m, both on the surface and in the Exploratory Studies Facility. Deformation is also considerably less, in that the zone of intense fracturing and brecciation is relatively narrow (2 m). Offset on the fault increases to the southwest from Ghost Dance Wash, becoming about 16 m down-to-the-west in Abandoned Wash on the eastern splay of the Abandoned Wash fault (Day et al. 1998a). In the southern part of the central block, the Ghost Dance fault merges with the Abandoned Wash fault. The combined trace length of these two structures is at least 7.4 km (Day et al. 1997).

Mapping in the Exploratory Studies Facility has shown that the Ghost Dance fault has a consistent dip of 80° to 90° (depending on the position along strike) from the surface to the depth of the potential repository, based on two crossings of the fault in alcoves (S. Beason, U.S. Bureau of Reclamation, written communication to W.C. Day, U.S. Geological Survey, 1997) and one in the main drift (Albin et al. 1997). This is true for both the low-offset and high-offset parts of the fault.

3.6.2.4.1.2 Sundance Fault

The Sundance fault has been the subject of differing interpretations ever since it was first identified by Spengler, Braun, Martin et al. (1994), and mapped as a 1.5 km long zone of nearly vertical, N30° to 40° west-striking faults extending from Antler Ridge northwest across Split Wash to Live Yucca Ridge. Many of the faults, considered by Spengler, Braun, Martin et al. (1994) to occupy a zone at least 274 m wide, were shown to have minor amounts of down-to-the-northeast displacements and possible components of dextral strike-slip movement. Spengler, Braun, Martin et al. (1994) also suggested that the fault may continue both to the southeast and to the northwest for a total distance of at least 3 km, based on observations of structural lineaments, concentrations of brecciated rock, and other northwest-trending faults, and the Ghost Dance fault was offset in a dextral sense along the Sundance fault system by about 50 m.

R.B. Scott and Bonk (1984) did not map the Sundance fault, but, based on air photo interpretations, they inferred that several northwest-trending fractures define a 750m-long zone across Live Yucca and Dead Yucca ridges, just west of the Ghost Dance fault. On the basis of geologic reconnaissance, C.A. Braun and L.G. Martin (Science Applications International Corporation, written

communication to R.W. Spengler, 1995) reported that the Sundance fault could be traced for at least 4.5 km, from Antler Ridge northwest across Little Prow at the crest of Yucca Mountain, and into a northwest-striking fault mapped by R.B. Scott and Bonk (1984) between the Little Prow and the Prow of Yucca Mountain.

The only systematic and comprehensive investigation of the Sundance fault was by Potter, Dickerson et al. (1995), who mapped a 460 m wide northwest-trending "strip" (Antler Ridge to Ammo Ridge) at 1:2,400 scale and found that the northwest-striking Sundance fault zone can be traced for about 750 m in the northern part of the Yucca Crest sub-block, from Dead Yucca Ridge to Live Yucca Ridge (Figure 3.6-4). Potter, Dickerson et al. (1995) concluded that the Sundance fault zone has a significantly smaller along-strike extent than the 4.5 km (or greater) extent suggested by previous workers. At its northwest end, the Sundance fault zone appears to terminate abruptly north of Dead Yucca Ridge. The faults in this zone are almost exclusively characterized by northeast-side-down displacement. The maximum width of the Sundance fault zone is about 75 m and the cumulative northeast-side-down vertical displacement across the fault zone does not exceed 11 m (Potter, Dickerson et al. 1995). Even though some horizontal slickensides have been observed, significant strike-slip displacement along the Sundance fault zone is not suggested by the field relations (Potter, Dickerson et al. 1995).

Southeast of the mapped extent of the Sundance fault zone, the Ghost Dance fault can be projected along an essentially straight trend beneath the Quaternary cover in Split Wash with no apparent offset along the Sundance trend (Potter, Dickerson et al. 1995; Day et al. 1998a). This contradicts the suggestion of Spengler, Braun, Martin et al. (1994) that the Ghost Dance fault is offset in a right-lateral sense across the Sundance fault beneath Split Wash. On the south slope of Antler Ridge near the projected trend of the Sundance fault zone, several northwest striking faults occur over a 170 m wide area, but they can be mapped only locally in the crystal-poor member of the Tiva and do not appear to be throughgoing structures (Potter, Dickerson et al. 1995). These discontinuous faults lie west of the location where Braun et al. (1996) mapped a "Sundance fault" on the south slope of Antler Ridge, northeast of borehole USW H-4. Although Braun et al. (1996) mapped 6 m of northeast-side-down stratigraphic throw on this proposed structure, the subsequent mapping of Potter, Dickerson et al. (1995) demonstrated no fault at this locality.

Individual faults in the Sundance fault zone and elsewhere at Yucca Mountain are vertically and laterally discontinuous; one or more mechanisms of strain accommodation must operate in the Tiva Canyon Tuff to accommodate displacements in the rock volume between the discontinuous discrete fault segments. Two probable mechanisms are distributed brittle deformation, associated with diffuse breccia bodies, and minor offsets along numerous pre-existing cooling joints (Potter, Dickerson et al. 1995).

The Exploratory Studies Facility passes beneath the southeastern end of the Sundance fault zone as mapped by Potter, Dickerson et al. (1995), where displacement is minimal on the south flank of Live Yucca Ridge. In the Exploratory Studies Facility, the Sundance fault is identified within a broad zone of discontinuous minor northwest-striking faults and joints in the middle nonlithophysal zone of the Topopah Springs Tuff (map unit Ttpmn), similar in character to the fault zone mapped at the surface near its southeastern termination on the south-facing slope of Live Yucca Ridge (Potter, Dickerson et al. 1995; Day et al. 1998a). The single northwest-striking fault identified as the

Sundance fault in the Exploratory Studies Facility is located near Station 36+00 (Albin et al. 1997). This fault has orientation of N25°W with a dip of 84° to the west, the amount and sense of offset along this fault is unknown, and there are subhorizontal mullion structures and slickenlines developed on the polished fault surface. It is unlikely that this specific fault is directly correlative with the principle strand of the Sundance fault as mapped at the surface because the fault observed in the Exploratory Studies Facility occurs approximately 50 m north of where the main trace of the Sundance fault would project to the Exploratory Studies Facility, and the fault observed in the Exploratory Studies Facility dips to the west.

3.6.2.4.1.3 Diabolus Ridge Fault

The Diabolus Ridge fault is a locally prominent intra-block fault that produces about 7 m of west-side-down displacement of the base of the crystal-rich member of the Tiva Canyon Tuff at the crest of Diabolus Ridge (Figure 3.6-4), and has been mapped by Lipman and McKay (1965), R.B. Scott and Bonk (1984), and Day et al. (1998a). These maps each portray a somewhat different map pattern for this fault. On the 1:6,000 scale map of Day et al. (1998a), the fault is a north-northwest-striking thrust fault. This is considered to be the most reliable of the three map patterns, because it is based on the largest scale mapping and incorporates the greatest degree of stratigraphic detail.

The Diabolus Ridge fault is present on the south-facing slope of Diabolus Ridge, about 450 m west of the northern termination of the Ghost Dance fault; and the southern termination of the Diabolus Ridge fault occurs in the Wren Wash drainage, 150m south of Diabolus Ridge (Scott, R.B. and Bonk 1984; Potter, Dickerson et al. 1995; Day et al. 1998a). Lipman and McKay (1965) portray an east-northeasterly strike for this fault, contouring along the south-facing slope of Diabolus Ridge, but this is not borne out by subsequent mapping.

On the northeast side of Diabolus Ridge, R.B. Scott and Bonk (1984) continued the Diabolus Ridge fault to the base of the slope and projected it beneath surficial deposits in Drill Hole Wash and onto the southwest-facing slope of Tonsil Ridge. Day et al. (1998a) demonstrated that the fault does not continue down the northeast-facing slope of Diabolus Ridge (based on the lack of displacement of the top of map unit cpll on that slope), and, like Lipman and McKay (1965), found that the trace of this fault hooks to the east-southeast high on the northeast-facing slope of Diabolus Ridge. This east-southeasterly hook, mapped by R.B. Scott and Bonk (1984) as a slump, is defined by displacement of a zonal contact in the crystal-rich member of the Tiva Canyon Tuff (base of map unit Tcr2; Day et al. 1998a).

On a cross-section constructed by D.S. Sweetkind (Levy, Sweetkind et al. 1997) the Diabolus Ridge fault has a 30° dip to the southeast. This gentle fault dip is based on: three point calculations from the mapped trace of the fault as it crosses Wren Wash; the attitude of breccia zones observed along the fault; and the intersection of this fault by borehole USW SD-9 (Engstrom and Rautman 1996). The dip may be even shallower where the trace of the fault hooks to the east-southeast on the northeast slope of Diabolus Ridge. Because the hanging wall has been translated upward relative to the footwall along the entire mapped trace, the Diabolus Ridge fault is a thrust fault.

3.6.2.4.2 Structural Geology of the Yucca Crest Sub-block

The Yucca Crest sub-block comprises a relatively undeformed east-dipping panel cut by relatively sparse minor faults. The Tiva Canyon Tuff, exposed at the surface over most of this block, typically dips 4° to 8° to the east. The three faults described above are the most prominent faults in the Yucca Crest sub-block (Figure 3.6-4). Aside from these prominent faults, which have trace lengths of 0.5 km to 7.5 km, the faults in the Yucca Crest sub-block have maximum trace lengths of about 200 m, and commonly much less. These minor intra-block faults are marked by breccia zones that are commonly 0.1 to 1.0 m in width, and are both laterally and vertically discontinuous (Scott, R.B. and Bonk 1984; Potter, Dickerson et al. 1995; Braun et al. 1996; Day et al. 1998a). Many of the intra-block faults are parallel to the dominant orientations of cooling joints in the Tiva Canyon Tuff, of which the two most prominent sets of joints have orthogonal northeasterly and northwesterly strikes. These faults have likely reactivated pre-existing cooling joints, a conclusion that is supported by the presence of thin (1 cm thickness) tabular tectonic breccia bodies along cooling joints. Strictly speaking, such breccia-lined cooling joints are faults of unknown but probably very small offset.

Figure 3.6-9 is a representative part of the Yucca Crest sub-block, from the central block geologic map of Day et al. (1998a). It is reproduced here at 1:9,000 scale, rather than the 1:6,000 scale of Day et al. (1998a). The Ghost Dance fault runs along the east edge of Figure 3.6-9 and the Sundance fault crosses Purgatory Ridge near the northeast corner of Figure 3.6-9. It is apparent from this figure that, between the Ghost Dance fault and the west-facing slope of Solitario Canyon (at the west edge of Figure 3.6-9), all of the mapped faults are short and discontinuous.

The greatest concentration of minor intra-block faults is mapped on the south slope of Antler Ridge for 400 m east of the Ghost Dance fault, where numerous northwest-striking faults and several north- and northeast-striking faults offset contacts within the crystal-poor member of the Tiva Canyon Tuff, but do not continue up into the crystal-rich member (Potter, Dickerson et al. 1995; Day et al. 1998a). (A detailed map illustrating faulting style in a small part of this 400 m stretch is shown in Figure 3.6-10). Breccia occurs along many of the faults, and there are also pods of breccia distributed across the slope with no apparent relation to faults. On this slope, only one small fault in addition to the Ghost Dance cuts the base of the crystal-rich member. However, the base of the crystal-rich member is poorly exposed along most of this slope, so there are possibly additional minor concealed offsets (with 1 m or less of displacement) of this contact. Stratigraphic throw across the mapped minor faults ranges from 0.3 m to 6 m, with most displacements in the 1 to 3 m range. Almost all of these faults have a mapped length of less than 50 m, and none of them has a mapped length in excess of 100 m. In nearly every case, the limited extent of fault strands are constrained by unfaulted contacts that cross the projected location of known faults that are mapped either upslope or downslope (Potter, Dickerson et al. 1995).

The discontinuous nature of faulting requires that fault displacements be balanced by distributed deformation within the rock mass between the mapped discrete faults. Potter, Dickerson et al. (1995) inferred that much of the breccia on this slope (most of which is seen only in blocks of colluvium rather than in outcrops) developed as part of a distributed brittle deformation that operated in concert with the discontinuous discrete faults to accommodate strain in these strata. This deformational style is illustrated in detail in Figure 3.6-10. This figure shows a small graben

bounded by northeast-striking and northwest-striking faults along which the base of map unit Tc_{pmn3} is offset by 5 m and 7 m, respectively. Downslope (to the south), the northwest-trending breccia zone appears to truncate the northeast-trending breccia zone (or the northeast-trending zone merges into the northwest-trending zone). Neither the northeast- nor the northwest-trending fault can be traced an appreciable distance upslope. The breccia zone that marks the northeast-trending fault cannot be traced above the base of Tc_{pmn3} (in the footwall), and the top of Tc_{pmn3} is not offset along the projected trace of this fault. Instead, a northeast-trending fault located 20 m to the west offsets this contact by 5 m. Pods of breccia occupy the middle nonlithophysal unit between the two noncontinuous northeast-striking faults; this appears to be a zone of distributed brittle deformation accommodating the displacement on the two northeast-trending faults. The northwest-trending fault that bounds the west side of the small graben cannot be traced upslope as a single discrete fault, but appears to branch into several smaller northwest-trending splays that offset the top of the middle nonlithophysal zone. Thus, one of the faults bounding this small graben steps to the northwest as it moves upsection via an accommodation zone that exhibits distributed brittle deformation, and the other branches into at least three splays upsection. The result is a complex zone of deformation that constitutes an instructive case example of common styles of deformation in the Tiva Canyon Tuff at Yucca Mountain (Figure 3.6-10).

Other examples of discontinuous faulting in the Yucca Crest sub-block are provided by detailed geologic relations within the Sundance fault zone. On Purgatory Ridge and Dead Yucca Ridge (Figures 3.6-1, 3.6-4, 3.6-9), several strands of the Sundance fault comprise a 25 to 70 m wide zone at the top of the middle nonlithophysal zone of the Tiva Canyon Tuff (Tc_{pmn}), low on the south-facing slopes (Potter, Dickerson et al. 1995). On both ridges, only one fault strand continues up into the crystal-rich member at the top of the ridge, but the displacement accomplished by this single strand (13 m) is somewhat less than the cumulative displacement across the broader fault zone that cuts the top of the middle nonlithophysal zone.

These map patterns in the Sundance fault zone exemplify a stratigraphically-controlled faulting style. A zone of discrete, discontinuous faults affects a broader area in the crystal-poor member than in the overlying crystal-rich member of the Tiva Canyon Tuff. This stratigraphic control of faulting reflects a fundamental contrast in material properties between the crystal-rich and crystal-poor members of the Tiva Canyon Tuff. Such a contrast may be related to inherent physical properties, as measured in experimental deformation of unjointed samples, or it may be related to mesoscopic characteristics, such as the number and distribution of cooling joints, which were produced before significant tectonism affected the welded tuff. The available experimental data suggest that the sampled zones of the crystal-poor member (Tc_{pll}, Tc_{pmn}, Tc_{pul}) and the crystal-transition subzone (Tc_{r1}) at the base of the crystal rich member have significantly greater tensile and ultimate strengths than the overlying subzones (Tc_{r2}, Tc_{r3}) of the crystal rich member (Boyd, Price et al. 1996a; also see Subsection 3.7.3.3 and Tables 3.7-21, 3.7-22, and 3.7-23). There is also a greater abundance of cooling joints (which have preferential northwest and northeast-striking orientations) in the middle nonlithophysal zone (Tc_{pmn}) than in the upper lithophysal zone or in the overlying crystal-rich member (Sweetkind, Barr et al. 1997). Thus the broad distributed deformation in the Tc_{pmn}, and the upward narrowing of the fault zone through the Tc_{pul} and into the crystal rich member may be attributed to either the more brittle character of the Tc_{pmn} or the availability of pre-existing cooling joints in the Tc_{pmn} for exploitation by the Sundance fault zone. Conversely, the narrower, more restricted deformation in the crystal-rich member may be attributed to the less brittle nature of the

unit or to the lower frequency of cooling joints there. In fact, the contrast in the frequency of cooling joints between the units may also reflect their differing material properties providing a consistent explanation for the observed features.

The lack of vertical continuity for individual fault strands through the different stratigraphic levels requires a mechanism for lateral accommodation of strain in the Tiva Canyon Tuff. The accommodation probably occurred in a distributed fashion along locally exposed, gently-dipping breccia zones that acted as zones of decoupling, and through incremental slip on a large population of cooling joints. As such, the faulted crystal-poor member exhibits numerous irregular small blocks that have slipped and/or rotated along pre-existing joints and synkinematic breccia zones. In contrast, the relative paucity of cooling joints in the overlying crystal-rich member has confined the offset to a fewer number of discrete faults between larger, undeformed blocks.

Boundary Ridge Sub-block. The Boundary Ridge sub-block comprises the eastern and southern margins of the central block and is characterized by an increased density of intra-block faulting (Figure 3.6-11). The block-margin deformation along the eastern margin of the central block records complex deformation in the hanging wall of the Bow Ridge fault, whereas the block-margin deformation along the southern edge of the central block records an along-strike transition to structural styles that accompany greater magnitudes of extension to the south.

The block-margin deformation along the eastern edge of the central block occupies a zone about 650 to 900 m wide, and is characterized by steep north- and northwest-striking faults that have normal displacement both down-to-the-west and down-to-the east (Day et al. 1998a). There is as much as 70 to 80 m of cumulative down-to-the-west offset at the north end of Boundary Ridge. Stratal dips in the Tiva Canyon Tuff steepen to 10° to 20° in the Boundary Ridge sub-block, compared with the 4° to 8° dips that typify the Yucca Crest sub-block.

There are many more faults with long trace lengths in the Boundary Ridge sub-block, relative to the Yucca Crest sub-block. The largest faults involved in the block-margin deformation, particularly in the hanging wall of the Bow Ridge fault, have trace lengths of several kilometers (Figure 3.6-11). These faults are inferred to intersect the Bow Ridge fault at depth.

R.B. Scott (1990) employed the term “imbricate fault zone” to describe this series of closely spaced, steeply dipping faults associated with hanging-wall deformation on the Bow Ridge fault (Figure 3.6-4) and similar zones that are more widespread in the southern part of Yucca Mountain. He defined them as an “imbricate pattern of closely spaced, steep, west-dipping faults with minor down-to-the-west offsets of a few meters or less.” Spengler and Fox (1989) pointed out that the term is unclear, and Day et al. (1998a) abandoned the term because the style of block-margin deformation does not correspond to a conventional definition of the term “imbricate fault zone.”

The eastern-most faults exposed in the Boundary Ridge sub-block (and in the Azreal Ridge domain to the north) are a series of east-dipping, down-to-the-east normal faults that crop out on Bleach Bone, Azreal, Live Yucca, Antler, and Boundary Ridges (Day et al. 1998a). These faults comprise the western boundary of a hanging-wall graben or series of grabens that is bounded on the east by the Bow Ridge fault; most of the graben (or series of grabens) is buried beneath alluvial cover. Within the graben, flattening foliations in the crystal-rich member of the Tiva Canyon Tuff dip

steeply to the east (20° to 30°). Note, however, the limitations on using flattening foliation discussed in Subsection 3.6.2.3.5.

Locally, contractional faulting is present in the hanging wall of the Bow Ridge fault. Near the south portal of the Exploratory Studies Facility on the eastern flank of Boundary Ridge, an east-dipping reverse fault is exposed at the surface and dips toward the Bow Ridge fault, recording local shortening in the Bow Ridge hanging wall (Figure 3.6-11; Day et al. 1998a). Just a few meters below the surface, where intersected by the South Ramp of the Exploratory Studies Facility, this fault steepens to a near-vertical dip. This shortening and similar thrust-fault-related shortening in the Bow Ridge footwall on Bow Ridge (actually part of the Paintbrush Canyon domain) are likely produced by a subtle restraining bend with respect to oblique displacement on the Bow Ridge fault (Day et al. 1998a).

There are several intra-block northwest-striking en echelon grabens in the southeastern part of the central block near Boundary Ridge (Figure 3.6-11; Day et al. 1998a; Scott, R.B. and Bonk 1984). These narrow (100 m wide), long (as much as 750 m long), steep-walled, "canoe-shaped" grabens, termed "synthetic grabens" by R.B. Scott (1990), have significant internal displacement, and their bounding faults locally exceed 30 m of displacement, although there is minimal relative offset between the strata on either side of each graben. On Boundary Ridge, the en echelon grabens occur between the Bow Ridge fault and the northern termination of the Dune Wash fault, and merge with the north trending zone of block-margin hanging-wall deformation. The grabens appear to be analogous to tension gashes in shear zones, kinematically compatible with a sinistral component of displacement on the Dune Wash and/or Bow Ridge block-bounding faults. Comparison of surface mapping (Day et al. 1998a) with geologic mapping in the Exploratory Studies Facility shows that in their present orientation these grabens are bounded by faults that dip toward the center of the graben; i.e., the entire structure has not been tilted to the east (so that steep faults would dip to the west), as suggested by R.B. Scott (1990). This relation is key, because it indicates that the formation of the grabens postdates the tilting (or most of the tilting) of the Tiva Canyon Tuff.

Mutually crosscutting relations between the north-striking and northwest-striking faults in the Boundary Ridge sub-block support a coeval development of the north- and northwest-trending structures. The development of the north- and northwest-striking structural features was apparently coeval and kinematically linked.

3.6.2.5 Site Scale Geophysical Investigations of Yucca Mountain Structure

A variety of geophysical methods was used to characterize the structure within the potential repository volume (Feighner et al. 1996; Majer et al. 1996b). Seismic reflection, gravity, and magnetic studies were employed to investigate subsurface structural geometry. One magnetotelluric line and several vertical seismic profiles were also carried out to provide supplementary information (Figure 3.6-12).

The seismic reflection lines were designed to investigate structure, faulting, and lithology in or near the repository block as well as to investigate lithology and structure that could provide insight into the large hydraulic gradient (Robison 1984) at the north end of Yucca Mountain (see Subsections 5.2.2.2 and 5.3.5.1.4). The target depth for the majority of the high resolution seismic reflection

lines in the central block was from 100 m to repository depth and below, if possible. Before the seismic reflection work began at Yucca Mountain, the terrain was known to be a difficult area for seismic imaging because fracturing, lithologic heterogeneities in volcanic rocks (e.g., lithophysal zones, varying degrees of welding), and partial saturation all conspire against efficient propagation of seismic energy. Because of the various scales of heterogeneity in the stratigraphy at Yucca Mountain, scattered waves play a prominent role in the interpretation process. Local contrasts in material properties exist throughout the survey area, further complicating geophysical interpretation of the shallow subsurface (Feighner et al. 1996).

Gravity data were collected along all of the seismic reflection lines at Yucca Mountain, and along other geophysical survey lines. Ground-based gravity data measure density contrasts. As such, the hanging wall of a fault may be characterized by a local gravity low, particularly where alluvium has filled in against a fault scarp. These gravity surveys were initially designed as a constraint on the interpretation of the seismic reflection data. However, because the high-resolution seismic reflection lines did not achieve sufficient depth of penetration to image basement structure, it became necessary to place more dependence upon the gravity data as a means of arriving at a model of the basement structure in the vicinity of Yucca Mountain. Thus, the gravity observations were used in two different ways: first, to interpret general regional structure; and second, to supplement other geophysical data in the interpretation of shallow structure at Yucca Mountain, such as the location and displacement on faults. However, in some cases (e.g., the Ghost Dance fault) the contrast in density of the different tuff layers is not large enough for small offsets to be detectable.

Ground magnetic surveys are mainly used at Yucca Mountain to infer fault locations and offset. The Topopah Spring Tuff is the most strongly magnetic Tertiary volcanic formation and contrasts in magnetic anomalies across faults are typically interpreted to result from the offset of this formation (Bath and Jahren 1984). Although the magnetic anomaly generated by a fault can be more complex than a gravity anomaly because of variations in magnetic direction and remanent magnetism, simple models can be used to create an interpretation which can be constrained by other geophysical and geologic evidence. The aeromagnetic data respond to deeper and stronger magnetic sources than the ground-based magnetic data, so interpretations of the aeromagnetic data bear more directly on regional to subregional geologic patterns, rather than site scale geologic patterns.

Hidden faults and geological heterogeneities at Yucca Mountain can be a concern for the long-term performance of the potential repository. An attempt was made to detect and characterize these features using the magnetotelluric method. The utility of the magnetotelluric method can be greatly enhanced if the method is coupled with other geophysical techniques, such as gravity and magnetic surveys, and, in particular, the seismic method for structural constraints.

A primary question to be addressed is the amount, style, depth, and continuity of faulting in the potential repository volume. In order to illustrate how the geophysical data were used, the geophysical signatures of two characteristic faults at Yucca Mountain are systematically summarized below. These include a block-bounding fault (Bow Ridge fault) and a prominent intra-block fault (Ghost Dance fault). Ground-based gravity and magnetic surveys (Ponce, Langenheim et al. 1993; Ponce and Langenheim 1995), high-resolution seismic reflection surveys (Majer et al. 1996b), and an aeromagnetic survey (McCafferty and Grauch 1997) were examined. In addition to the systematic characterization of these two faults, the locations of faults mapped within the central block by Day

et al. (1998a) were compared to locations of possible faults inferred from careful examination of the high-resolution seismic reflection, ground-based gravity and magnetic surveys in the central block.

In terms of geophysical studies at Yucca Mountain, the most closely examined area was in the vicinity of the Ghost Dance fault. Vertical seismic profiling, surface seismic-reflection at four different scales, (REG 2, HR-2, YMP 13 and 14, and Line 1/YMP-3), gravity, ground magnetic, and magnetotelluric methods were all applied in this area (Figure 3.6-12). Figure 3.6-13 summarizes the geophysical data along a profile across the Ghost Dance fault (Line YMP-3). The ground-based magnetic and magnetotelluric data worked well for detecting the Ghost Dance fault, whereas the ground-based gravity data and the seismic reflection data did not have significant anomalies. No profiles of ground-based gravity data that crossed the Ghost Dance fault yielded useful information about this fault. There are very small gravity lows on the hanging wall of this fault on the Antler Ridge and Live Yucca Ridge traverses, but no associated anomaly exists on the WT-2 Wash traverse. Four profiles of ground-based magnetic data were acquired across the Ghost Dance fault; these indicate a characteristic magnetic low on the footwall of the Ghost Dance fault. This magnetic low is typically about 100 m wide. The magnitude of this low decreases northward, as does the amount of vertical offset. The Ghost Dance fault does not have an aeromagnetic signature. In fact, the aeromagnetic anomalies and gradients (not shown) are oriented at a high angle to the trend of this intra-block fault, apparently in response to a regional trend. The magnetotelluric data show a clear change in resistivity for the Ghost Dance fault.

The Ghost Dance fault is not apparent on standard high resolution seismic reflection lines (those with 6 to 12 m station spacings). Without prior knowledge of the existence or location of this fault, its presence would not likely be detected based on these seismic reflection data. The fundamental problem is the lack of continuity for any individual reflections on these profiles (Feighner et al. 1996). Attempts to associate aseismic reflection signature with the Ghost Dance fault have identified an attenuation of individual reflectors in the upper 0.1 to 0.2 seconds (65 m to 130 m) of both the stacked and migrated seismic reflection profiles (Feighner et al. 1996). However, on the very high resolution seismic reflection lines, where the spacing was on the order of 1 to 2 m, the Ghost Dance fault did show up as a reflection anomaly. Individual splays of the Ghost Dance can be mapped on these data in WT-2 Wash. These very high-resolution lines are interpreted to show steeply dipping extensional faulting with complex intersecting structures (Feighner et al. 1996). There is abundant geophysical evidence of multiple subparallel fracture zones or faults associated with mapped faults, most definitively for the Ghost Dance fault. There is also evidence for the presence of shallow, low velocity material in the fault zones, presumably due to intense fracturing and rubble zones, as indicated by seismic refraction studies. It is difficult, however, to trace the faulting from one geophysical line to another.

In the case of the Bow Ridge fault, only the ground-based gravity data and the aeromagnetic data are reliable in detecting the fault. The ground-based gravity data show a distinct gravity low on the hanging wall of the Bow Ridge fault. This gravity low is very pronounced south of Exile Hill to north of Exile Hill, then attenuates to zero southeast of Isolation Ridge. The Bow Ridge fault is characterized by a noticeable aeromagnetic high on the footwall and an aeromagnetic low on the hanging wall. This characteristic is present from the area east of Isolation Ridge southward to southern Dune Wash. The magnitude of the contrast across the Bow Ridge fault is greater for the area east of Pagany Wash and Sever Wash than it is for the area of Exile Hill. However, this contrast

reverses from an apparent down-to-the-west signature southward from Exile Hill to a down-to-the-east signature from Yucca Wash northward, in agreement with the geologic understanding of displacement on the Bow Ridge fault (Day et al. 1997; Dickerson and Drake 1998b). Using ground-based magnetic data, the Bow Ridge fault seems to be characterized by a distinct magnetic high from Exile Hill southward. North of Exile Hill the magnetic signature of the Bow Ridge fault becomes indistinct; however, east of Isolation Ridge the Bow Ridge fault is again a zone of anomalously high magnetization. The ground-based magnetic anomaly cannot be correlated to either the hanging wall or the footwall because the Bow Ridge fault is imprecisely located where it is covered with surficial deposits. The seismic reflection data demonstrate mixed results in locating the Bow Ridge fault. Seismic reflection profiles YMP-4 (which had poor resolution due to low stacking fold where it crossed the Bow Ridge fault) and YMP-7 show an attenuation of certain reflections on either side of the approximate location of the fault on stacked profiles, but profile YMP-12 shows nothing at all of the Bow Ridge fault. Regional seismic reflection line REG-3 also crossed the Bow Ridge fault, but had poor resolution at a shallow depth (Brocher, Hart et al. 1996).

The comparisons discussed above provide some useful criteria for evaluating the geophysical signatures of characteristic faults at Yucca Mountain. In general, there are fairly consistent geophysical signatures associated with the Bow Ridge fault so that it can be consistently mapped beneath Quaternary deposits with a variety of geophysical techniques, particularly when they are used in concert. Seismic reflection is the notable exception. The Ghost Dance fault, however, lacks a consistent geophysical expression, and the high resolution seismic reflection lines are particularly nondiagnostic with respect to the Ghost Dance fault. Very high resolution seismic reflection data, with a station spacing of 1 to 2 m, were successful in imaging details of the Ghost Dance fault zone. This is the only technique capable of reliably imaging intra-block faults smaller than the Ghost Dance, but deployment of the very high resolution seismic reflection surveys over large areas of Yucca Mountain would not be logistically feasible. Based on the results with the Ghost Dance fault, no other geophysical techniques, or set of geophysical techniques, are successful in imaging faults smaller than the Ghost Dance fault at Yucca Mountain. Given the clear geophysical signature of the Bow Ridge fault, any hypothetical concealed faults of this magnitude would have been identified with the standard geophysical techniques that were used in Yucca Mountain site investigations. In fact, Ponce (1996) used potential field data to infer the presence of several smaller, intermediate offset faults beneath surficial deposits in Midway Valley, including the Midway Valley fault which correlates to a fault mapped on southern Bow Ridge by R.B. Scott and Bonk (1984) and by Day et al. (1997). Thus the standard geophysical techniques employed at Yucca Mountain are best suited for detection of faults with at least tens of meters of offset.

3.6.3 Fractured Rock Mass Studies

Fracture data have been collected at Yucca Mountain over the past 15 years as part of the geologic and hydrologic site characterization. Data on the geometry of the fracture network developed within the Miocene volcanic rocks at Yucca Mountain are obtained from: mapping and observation of natural and cleared surface exposures; examination of borehole cores, television logs, and interpretation of borehole geophysical logs; and full periphery geologic mapping and scanline surveys within the Exploratory Studies Facility, a 7.6-m-diameter tunnel excavated at the site (Figure 3.6-14). These diverse field data have been collected at Yucca Mountain to fill various project needs. Applications include characterization of the fracture network for hydrologic flow,

including development of surface infiltration models (Flint, A.L. and Flint 1994); numerical simulations of discrete fracture networks (Anna and Wallman 1997); and calculations of bulk rock permeability for use in equivalent continuum models of the unsaturated zone (Schenker et al. 1995; Arnold et al. 1995). Fracture data at Yucca Mountain are also used to characterize the fracture network for mechanical stability of the potential repository, and to better understand the paleostress history of Yucca Mountain. Results of fracture studies to date are summarized in large part from Sweetkind and Williams-Stroud (1996) and Sweetkind, Barr et al. (1997). Use of lithostratigraphic unit names and symbols is based on descriptions given in Tables 3.5-1 and 3.5-2 in Subsection 3.5.

3.6.3.1 Types of Fracture Studies

3.6.3.1.1 Fracture Data from Surface Exposures

Surface fracture studies at Yucca Mountain can be subdivided into two broad types: studies in which all fractures above a certain length within a prescribed area or along a prescribed scan line are measured, termed a “global inventory” by Throckmorton and Verbeek (1995); and studies where fracture attributes are collected from members of particular fracture sets, termed a “selective inventory” by Throckmorton and Verbeek (1995). Surface fracture studies that have employed the global inventory approach include mapping, detailed line survey, and photogrammetry studies (Sweetkind and Williams-Stroud 1996). The selective inventory approach has been employed primarily in observations of natural outcrops (Figure 3.6-14). Fracture data have been collected from the Tiva Canyon Tuff, the rock units included in the PTn hydrogeologic unit, the Topopah Spring Tuff, the Calico Hills Formation, and the Bullfrog Tuff (Crater Flat Group) using both the global inventory and selective inventory approaches. Much of the data collected from surface exposures have been summarized by Sweetkind and Williams-Stroud (1996).

There are 13 surface sites at Yucca Mountain where a map of the fracture network has been produced (Sweetkind and Williams-Stroud 1996). Nine sites are exposures, called pavements, that have been physically cleared by excavation or hydraulic clearing (three of these pavements are described in Barton, C.C. et al. 1993); four sites are natural exposures. Mapped pavements at Yucca Mountain range in area from 300 to 1,200 m². Fractures have been mapped from air photos or by manual surveying; the number of fractures measured at each pavement ranges from 100 to 1,200 (Sweetkind and Williams-Stroud 1996). At each pavement, all fractures that exceed a specific length cutoff, typically from 0.3 to 1.5 m, were mapped. C.C. Barton et al. (1993) summarized the methodologies used during the mid-1980s for mapping fracture-trace networks at cleared pavements and for measuring or describing fracture parameters, including trace length, orientation, connectivity, aperture, roughness, shear offset, trace-length density and mineralization. Pavement maps also provide critical information on the termination (relative age) relations and connectivity of fracture sets. Fracture data from pavements at Yucca Mountain are dominantly from the uppermost portions of the Paintbrush Group. Eight of the 13 mapped exposures are in the Tiva Canyon Tuff; six of which are in the crystal-poor upper lithophysal zone (Tpcpul). Three large natural exposures of the rock units included in the PTn hydrogeologic unit were mapped as pavements (Sweetkind, Verbeek et al. 1995a), and two pavements have been cleared in the middle non-lithophysal zone of the Topopah Spring Tuff (Ttpmn) (Sweetkind, Verbeek et al. 1995b).

Data collected at natural outcrops using the selective inventory approach provide a descriptive inventory of the fracture network in the area being studied (Throckmorton and Verbeek 1995), but individual fractures are not mapped. Fracture sets are identified by inspection, primarily by subdividing fractures on the basis of orientation and relative age, and average attributes for each fracture set are measured (Throckmorton and Verbeek 1995). Information obtained includes: number of fracture sets and their relative visual prominence at the outcrop, termination (age) relationships, average orientation of each set (a representative number of fractures of each set are measured), ranges of trace length and trace height, and mineral filling (Throckmorton and Verbeek 1995).

There are 54 outcrop stations in the general vicinity of the potential repository (Figure 3.6-14) that are located on various units of the Paintbrush Group (Throckmorton and Verbeek 1995; Sweetkind, Verbeek et al. 1995a). Additional outcrop data have also been collected from the basal vitrophyre of the crystal-poor member of the Topopah Spring Tuff at Busted Butte (unit Ttpv), from zeolitized pyroclastic flow units of the Calico Hills Formation (see descriptions in Table 3.5-2) at Prow Pass, and from moderately welded Bullfrog Tuff (Crater Flat Group) at Raven Canyon and Little Skull Mountain. Fracture data were also collected during large scale geologic mapping of an area straddling the Ghost Dance fault (Spengler, Braun et al. 1993). Within the area mapped near the Ghost Dance fault, all observed fractures greater than 2 m in length were mapped and a limited suite of fracture attributes was collected (Braun et al. 1996).

3.6.3.1.2 Fracture Data from Subsurface Exposures in the Exploratory Studies Facility

The detailed line survey is the primary method of collecting fracture data in the Exploratory Studies Facility. The detailed line survey method provides a statistical sampling of the fracture network and is a relatively rapid method for obtaining directional fracture data along a traverse (La Pointe, P.R. and Hudson 1985). In the Exploratory Studies Facility, the location of a discontinuity is measured along a horizontal datum line and fracture attributes including orientation, infillings, terminations, fracture length, roughness, and aperture, are recorded (see Barr et al. 1996, for a complete discussion of detailed line survey methodology as used in the Exploratory Studies Facility). The detailed line survey method was also used to obtain fracture data at a number of surface exposures, including the ARP-1 pavement, the USW NRG-1 drill pad (McKeown 1992), various cleared areas around the Exploratory Studies Facility North Portal, the Prow Pass vicinity, and Busted Butte.

Full-periphery maps of the excavated tunnel walls provide the geologic context for interpreting the fracture data collected in the Exploratory Studies Facility. As tunneling progresses, the excavated walls of the Exploratory Studies Facility are mapped at a scale of 1:125. Lithologic contacts, fault orientations and characteristics, shear zones and fractures greater than 1 m in length are mapped across the full periphery of the tunnel exposure. Rock mass quality ratings are routinely reported during tunnel excavation; these data generally correlate with fracture intensity. Geologic data from full-periphery geologic mapping and detailed line survey of the first 6.5 km of the Exploratory Studies Facility (halfway between Sta. 60+00 and 70+00 in Figure 3.6-14) are incorporated in this report.

Fracture data collected using the detailed line survey method are available for more than 16,000 fractures in the first 6.5 km of tunnel. The data are tied to lithology and location, and the

nature of the exposure allows detailed identification of fault and shear offsets. Although the detailed line survey method is a one-dimensional sample of fracture attributes, it provides data comparable to 2-D data sets because trace lengths and termination relationships are recorded. Fracture data collected using the detailed line survey method are biased against recording fractures that are subparallel to the trace line. The North Ramp of the Exploratory Studies Facility has an orientation of 299° (a trend of N61°W), thus resulting in a bias against the recording of steeply dipping, northwest-striking fractures. The Main Drift of the Exploratory Studies Facility has an orientation of 183° (a trend of N3°E), thus resulting in a bias against the recording of steeply dipping, north-striking fractures. In all portions of the Exploratory Studies Facility, the use of a subhorizontal trace line results in a bias against recording gently dipping fractures.

A map of the fracture network in a portion of the Exploratory Studies Facility has also been produced using close-range photogrammetric techniques along a 65-m-long exposure (Sta. 3+60 to 4+25) of the Tiva Canyon Tuff exposed in the North Ramp of the Exploratory Studies Facility (Coe 1996a). Fracture attributes similar to those measured at surface pavements were obtained for each of the 1,171 fractures mapped at this locality, except that aperture, roughness, and mineral fillings were not obtained.

3.6.3.1.3 Fracture Data from Boreholes

A large number of subvertical boreholes have been drilled at Yucca Mountain. Data from many of the early boreholes drilled at Yucca Mountain were collected and interpreted by the USGS (Spengler, Byers et al. 1981; Scott, R.B. and Castellanos 1984; Spengler and Chornack 1984). In recent years, Agapito Associates, Inc., under contract to Sandia National Laboratory, has collected fracture data from additional boreholes (Engstrom and Rautman 1996; Rautman and Engstrom 1996a, 1996b).

For each drillhole, coring-induced fractures were eliminated and the total number of natural fractures and fractures of indeterminate origin were tabulated from core logs over 10-ft depth intervals. Core recovery for each 10-ft interval was tabulated from the core logs. Methods for accounting for unrecovered core and rubble zones are discussed in recent Sandia National Laboratories reports on drillholes USW SD-7 (Rautman and Engstrom 1996a), USW SD-9 (Engstrom and Rautman 1996), and USW SD-12 (Rautman and Engstrom 1996b). The number of observed fractures was adjusted for unrecovered core by assuming that fracture density in the unrecovered core and rubble zones was the same as in the recovered core. The total number of fractures adjusted for core recovery was thus calculated by dividing the sum of the natural and indeterminate fractures by the percentage of core recovered for each ten-foot interval (length of core run minus length of unrecovered core plus rubble zones).

Fracture frequency (number of fractures per unit length) is obtained from unoriented core, downhole television logs or geophysical techniques such as sonic logs. Boreholes also provide important information about variations in fracture intensity with depth and lithology. However, there are a number of difficulties in comparing borehole fracture data to data collected at the surface and in the Exploratory Studies Facility: much of the recorded borehole fracture data is based on unoriented core, and thus cannot be compared statistically to true fracture orientations measured in outcrops or in the Exploratory Studies Facility; borehole data do not directly provide information on fracture lengths or termination relationships; assessing in situ fracture characteristics from boreholes requires

the understanding and correction of orientation and length bias inherent in borehole sampling of a fracture network; and the air or air/foam mixture used to minimize hydrologic perturbations during drilling adversely affect core recovery and diminish the quality of downhole television logs.

3.6.3.2 Comparison of Data Collection Methods

The various fracture studies at Yucca Mountain have resulted in a diverse and not entirely compatible collection of data sets. Even where the same fracture attribute was measured (for example, trace-length), different collection methods may use different measurement criteria (for example, different lower-limit trace-length cutoffs) that make data difficult to compare. A further difficulty in integrating the data sets lies in comparing 1-D (detailed line survey) and 2-D (pavement maps, outcrop observations, and full-periphery maps in the Exploratory Studies Facility) sampling approaches and integrating them into an accurate representation of the fracture network.

Sweetkind and Williams-Stroud (1996); Sweetkind, Williams-Stroud et al. (1997); and Sweetkind, Barr et al. (1997) have discussed various approaches and strategies for the comparison and integration of diverse fracture data. Fracture studies at the surface and the Exploratory Studies Facility were found to yield generally consistent orientation distributions, trace length distributions, and fracture spacing (both true spacing of individual fracture sets and average apparent spacing) (Sweetkind, Barr et al. 1997). Borehole fracture data, however, have severe length and orientation bias. The orientation bias is the result of sampling subvertical fractures with a subvertical borehole. The length bias results from the general inability to evaluate the fracture trace length distribution of the fracture population being sampled. Sweetkind, Barr et al. (1997) concluded that the amount of information needed for a complete integration of borehole data with 2-D data from outcrops and the Exploratory Studies Facility is generally not available; consequently, no attempt was made to explicitly correct borehole fracture data for severe length and orientation bias.

3.6.3.3 Fracture Attributes of Lithostratigraphic Units

Yucca Mountain is composed of numerous lithostratigraphic zones, defined by differences in degree of welding, lithophysae development, and pumice content (see Table 3.5-2). There are a number of primary controls on fracture characteristics within the Paintbrush Group that are related to stratigraphy, upon which any later tectonic signature is superimposed. Fracture characteristics in the pyroclastic flows are primarily controlled by variations in the degree of welding; lithophysal development, alteration, and pumice content are secondary controls important in specific stratigraphic intervals. These primary lithostratigraphic controls affect fracture spacing, type, number of sets, continuity of individual fractures within each lithostratigraphic zone and also affect the fracture connectivity of the network as a whole (Sweetkind and Williams-Stroud 1996; Sweetkind, Barr et al. 1997).

3.6.3.3.1 Tiva Canyon Tuff

The fracture network in many of the lithostratigraphic units within the welded, devitrified portion of the Tiva Canyon Tuff is dominated by steeply dipping fractures with northwest, north, or northeast strikes (Table 3.6-1) (Sweetkind and Williams-Stroud 1996). Fractures within the crystal-rich

member are dominantly cooling joints with lengths of at least 2.5 m, and spacing of 1 to 2 m (Sweetkind and Williams-Stroud 1996).

The underlying upper lithophysal zone of the crystal-poor member (unit Tpcpul) is characterized by consistently well developed cooling joints that generally occur as two sets of steeply dipping fractures forming a prominent rectangular pattern observable at most of the cleared pavements in this unit (Barton, C.C., Larsen et al. 1993), and at nine outcrop localities studied by Throckmorton and Verbeek (1995). These joints range in length from 2 to 10 m. Spacing ranges from 0.5 to 3 m but is variable, with a tendency for the cooling joints to occur as local zones of closely spaced (0.5 to 1 m) joints separated by areas of more widely spaced joints (2 to 3 m). A number of tectonic joint sets, often 1 to 2 m in length, are common in this unit as well (Throckmorton and Verbeek 1995). The tectonic joints commonly abut the earlier cooling joints. A study of fractures in outcrops in the vicinity of Live Yucca and Dead Yucca Ridges highlighted the dominance of cooling joints over tectonic joints in the upper lithophysal zone of the crystal-poor member (unit Tpcpul) of the Tiva Canyon Tuff (Morgan 1984; summarized by Barton, C.C., Page et al. 1989).

The middle nonlithophysal zone of the crystal-poor member of the Tiva Canyon Tuff (unit Tpcpmn) is characterized by abundant short (1 to 2 m or less), curving fractures of diverse orientation (Sweetkind and Williams-Stroud 1996). This zone commonly exhibits closely spaced, foliation parallel, incipient cooling joints, informally called vapor-phase partings in the Exploratory Studies Facility (Barr et al. 1996). These partings impart a "stair-step" appearance to exposures at the surface where the unit corresponds to the "rounded step" map unit of R.B. Scott and Bonk (1984). These vapor-phase partings decrease significantly in abundance in the underlying lower lithophysal zone of the crystal-poor member of the Tiva Canyon Tuff (unit Tpcpll).

Northwest-striking cooling joint sets become more prominent and easy to identify in the underlying lower lithophysal zone of the crystal-poor member of the Tiva Canyon Tuff (unit Tpcpll). Cooling joints range in length from 1 to 4 m, and have spacing of 0.1 to 3 m. Tectonic joints are, in this unit, shorter (0.5 to 1 m) with variable spacing (Throckmorton and Verbeek 1995). Throughout most of the underlying lower nonlithophysal zone (unit Tpcpln), cooling joints are difficult to identify because tubular structures are all but absent and roughness is not definitive. A network of very short, curved, anastomosing fractures that break the rock mass into 2 to 4 cm fragments (hackly subzone, unit Tpcplnh) is locally developed in this zone; and in the lower part of the lower lithophysal zone. The base of the lower nonlithophysal zone is characterized by a hexagonal network of cooling joints that divide the rock into abundant, crude, vertical columns 2 to 5 m high (unit Tpcplnc, the columnar zone of Scott, R.B. and Bonk 1984; Throckmorton and Verbeek 1995). Column diameters of 0.2 to 1 m are common. Cooling joints that bound the columns extend upward only short distances into the lower nonlithophysal zone and downward into the underlying crystal-poor vitric zone (unit Tpcpv) (Sweetkind, Verbeek et al. 1995a).

3.6.3.3.2 Lithostratigraphic Units Equivalent to the PTn Hydrogeologic Unit

The stratigraphic interval within the Paintbrush Group at Yucca Mountain that extends from the base of the densely welded and devitrified portion of the Tiva Canyon Tuff downward to the top of the densely welded portion of the Topopah Spring Tuff includes various interstratified pyroclastic flow and fall deposits with a minor amount of reworked pyroclastic material (Moyer et al. 1996). This

interval includes parts or all of four formations (the basal part of the Tiva Canyon Tuff, Yucca Mountain Tuff, Pah Canyon Tuff, and the uppermost part of the Topopah Spring Tuff) and three informally designated intervening bedded tuff units (Moyer et al. 1996; see Table 3.5-2).

Fracture characteristics of the pyroclastic flows within this stratigraphic interval are closely tied to degree of welding (Sweetkind, Verbeek et al. 1995a). Fracture intensity increases with the degree of welding within the pyroclastic flows. Even partly to moderately welded tuffs have much higher fracture intensity and network connectivity than interstratified nonwelded and bedded units (Sweetkind, Verbeek et al. 1995a; Sweetkind and Williams-Stroud 1996). Throughout most of the central portion of Yucca Mountain, the Yucca Mountain and Pah Canyon Tuffs are nonwelded (Moyer et al. 1996) and fracture intensity is low (Sweetkind, Verbeek et al. 1995a). North of Drill Hole Wash, the Yucca Mountain and Pah Canyon Tuffs become welded and devitrified (Moyer et al. 1996). In this area, cooling joints are present in both units and fracture intensity is much greater than in the distal, nonwelded portions of these pyroclastic flows (Sweetkind, Verbeek et al. 1995a).

The crystal-poor vitric zone at the base of the Tiva Canyon Tuff (unit Tpcpv) has transitional fracture characteristics and physical properties that are related to the rapid vertical variation in degree of welding (Moyer et al. 1996; Sweetkind, Verbeek et al. 1995a). Cooling joints of the columnar subzone of the lower nonlithophysal zone of the Tiva Canyon Tuff (unit Tpclnc) are observed in surface exposures to terminate downward into a network of small, irregular cooling joints in the densely welded upper part of the crystal-poor vitric zone of the Tiva Canyon Tuff (unit Tpcpv3) (Sweetkind, Verbeek et al. 1995a). Cooling joints are abundant and commonly outnumber tectonic joints in the moderately welded tuff part of the zone (unit Tpcpv2). Both types of joints have a limited vertical extent and terminate downward into poorly welded tuff (unit Tpcpv1) that has significantly greater matrix porosity and permeability (Moyer et al. 1996; Sweetkind, Verbeek et al. 1995a; Barr et al. 1996).

The fracture characteristics of nonwelded pyroclastic flows and interstratified pyroclastic fall deposits within the Paintbrush Group are controlled primarily by variations in lithology across depositional boundaries (Sweetkind, Verbeek et al. 1995a). Higher pumice content and clast size are correlated to lower fracture density. Among the nonwelded units, recognizable sets of fractures are most common in the basal, nonwelded portion of the crystal-poor vitric zone of the Tiva Canyon Tuff (unit Tpcpv1) and in nonwelded units of the Yucca Mountain Tuff, both of which generally contain 15 percent or less of pumice clasts (Moyer et al. 1996). Nonwelded units with 30 to 70 percent pumice clasts, which include most of the bedded tuffs and nonwelded flows between the base of the Yucca Mountain Tuff and the top of the Topopah Spring Tuff, are much more sparsely fractured, and definable joint sets are lacking at many localities and joint spacing is irregular (Table 3.6-2) (Sweetkind, Verbeek et al. 1995a). Many of the fractures terminate at compositional boundaries, such as the contacts with pumice-rich fall deposits. Pumiceous tephra deposits containing 80 percent or more of pumice clasts generally are not fractured except for sparse weathering joints (Sweetkind, Verbeek et al. 1995a).

The effect of clast size is difficult to separate from other important controls on fracture network development. Nevertheless, increasing clast size appears to inhibit the development of fractures (Sweetkind, Verbeek et al. 1995a). Comparison of the three pumiceous fallout tephra within the Paintbrush Group (informal subunits Tpbt3a, Tpbt3d, and Tpbt4, of Moyer et al. 1996), reveals that

the finest-grained of the three (unit Tpb4) consistently contains the most fractures. Similar relationships between joint development and grain size are known in sedimentary rocks, particularly sandstone and conglomerates (Price, N. 1966).

3.6.3.3 Topopah Spring Tuff

The population of fractures within the crystal-rich member of the Topopah Spring Tuff is dominated by steeply dipping cooling joints of various orientations (Table 3.6-3) (Sweetkind, Barr et al. 1997). Exposed lengths of cooling joints in surface exposures range from 1 m to 4 m; tectonic joints are mostly less than 1 m, although some are as long as 4 m (Throckmorton and Verbeek 1995). Many of the fractures within the densely welded crystal-rich vitrophyre of the Topopah Spring Tuff (unit Tptprv1) terminate upward within the overlying poorly welded pumiceous material (Barr et al. 1996). The crystal-rich vitrophyre of the Topopah Spring Tuff is underlain by a thin (2 to 3 m) interval of devitrified tuff that contains argillically altered pumice clasts (unit Tptrn3). Below this zone, pumice clasts are replaced with coarsely crystalline vapor-phase minerals (Buesch, Spengler et al. 1996a). Within the Exploratory Studies Facility, vapor-phase crystallization is intense in the upper portions of the crystal-rich member of the Topopah Spring Tuff (unit Tptrn2) between Exploratory Studies Facility stations 12+75 to 13+36, where pumice fragments are corroded and the rock matrix contains pockets of vapor-phase minerals. The fracture intensity in this vapor-phase-altered interval is high. Below this interval (at Exploratory Studies Facility Station 13+37 and beyond) fracture frequency decreases and interfracture distance increases. This change corresponds to a vapor-phase alteration boundary within the crystal-rich member of the Topopah Spring Tuff, and most likely indicates a change in the "brittleness" of the units (Barr et al. 1996).

In the Exploratory Studies Facility, fracture density in the crystal-rich member of the Topopah Spring Tuff decreases at the contact with the upper lithophysal zone of the crystal-poor member of the Topopah Spring Tuff (unit Tptpul), where fracturing is infrequent and discontinuous (Barr et al. 1996). In contrast to the crystal-rich member, steeply dipping cooling joints are rare in the upper lithophysal zone (unit Tptpul). The predominant fractures are north- and northwest-striking tectonic joints that have spacings that typically range from 0.5 to 3 m (Table 3.6-3). Tectonic fractures in the highly lithophysal rock are short and most cannot be followed as continuous surfaces for more than 3 m. Joint surfaces are rough and pockmarked by abundant lithophysal cavities, and their traces are irregular. In many cases, the fractures appear to link lithophysae. All of these properties reflect the difficulty of propagating a smoothly continuous fracture through a rock containing numerous large voids, resulting in a network of relatively short, widely spaced, discontinuous tectonic fractures with a high proportion of blind fracture terminations (Sweetkind, Verbeek et al. 1995b).

A network of long, relatively closely spaced joints generally characterizes the middle nonlithophysal zone of the crystal-poor member of the Topopah Spring Tuff (unit Tptpmn). At least five joint sets are interpreted to be present in this unit in the Exploratory Studies Facility, including three subvertical sets, having northwest, northeast, and east strike directions, a northwest striking set with moderate dips, and a subhorizontal set (Albin et al. 1997; Sweetkind, Barr et al. 1997). Northwest-striking joints are the most prevalent set throughout the unit, followed in abundance by northeast-striking joints (Albin et al. 1997). From approximately Station 42+00 to 51+50 there is an intensely fractured zone where the overall fracture frequency is more than double the frequency observed in other areas. Within this intensely fractured zone, a northwest-striking set, oriented N 67° W to

N 34° W, dominates all other joint sets. These joints are smooth, with manganese-oxide coatings and some vapor-phase mineralization (Albin et al. 1997). The origin of the intensely fractured zone is currently unresolved. A northwest-striking joint set with moderate dips was found to occur only at the north end of the Exploratory Studies Facility Main Drift; joints with intermediate dips are uncommon south of, approximately, Station 37+00. Subhorizontal joints are observed throughout the middle nonlithophysal zone, except within the intensely fractured zone (Albin et al. 1997). Within the Exploratory Studies Facility, fracture intensity in the middle nonlithophysal zone is high, with an average apparent fracture spacing of 0.36 m for fractures 1 m long and longer. This value includes the effect of the intensely fractured zone between Exploratory Studies Facility Stations 42+00 to 51+50. Average apparent spacing in this unit north of the intensely fractured zone is 0.52 m, and to the south the average is 0.40 m. Average apparent fracture spacing within the intensely fractured zone itself is 0.23 m (see Figure 3.6-15).

The fracture network within the middle nonlithophysal zone of the crystal-poor member of the Topopah Spring Tuff has been mapped at pavements 1000 and P2001, both located on the east flank of Fran Ridge, 3 km to the east of the crest of Yucca Mountain (Sweetkind and Williams-Stroud 1996). Pavement P2001 exposes three mutually orthogonal cooling joint sets: two subvertical sets, striking northwest and northeast, and one subhorizontal set (Sweetkind, Verbeek et al. 1995b). Four subsequent sets of tectonic fractures are all steeply dipping; the earliest tectonic fractures are oriented north-south, followed by northwest-striking, northeast-striking, and east-west sets. The orientations of northwest and northeast striking joints at P2001 are similar to those observed in the Exploratory Studies Facility (Albin et al. 1997; Sweetkind, Barr et al. 1997). However, north-striking joints observed at P2001 and prominent at P1000 (Sweetkind and Williams-Stroud 1996) are not well-expressed in the Exploratory Studies Facility (Table 3.6-3). Detailed line survey scanlines in the Main Drift of the Exploratory Studies Facility have orientations of 183° (a trend of N3°E), thus resulting in a bias against the recording of steeply dipping, north-striking fractures. North-striking joints are locally observed within the northern Exploratory Studies Facility turn from the North Ramp to the Main Drift and in the east-trending alcoves (Sweetkind, Barr et al. 1997). It is possible that orientation bias alone cannot account for the small number of north-striking joints in the Exploratory Studies Facility. The presence of north-striking joints at Fran Ridge may represent real spatial variability in joint orientations in this lithostratigraphic unit. North-striking joints may also be related to proximity to the Paintbrush Canyon fault (Sweetkind, Verbeek et al. 1995b).

Fracture intensity drops sharply and fracture character changes markedly at the contact between the middle nonlithophysal and lower lithophysal zones of the Topopah Spring Tuff (units Tptpmn and Tptpll, respectively). Fractures within the middle nonlithophysal zone tend to be planar or arcuate with low surface roughness; fractures within the lower lithophysal zone are subplanar but extremely rough. On average, fractures in the middle nonlithophysal zone are significantly longer than fractures in the lower lithophysal zone. The numerous large fractures that characterize the middle nonlithophysal zone typically terminate abruptly at the contact with the lower lithophysal zone of the crystal-poor member of the Topopah Spring Tuff (unit Tptpll). Below this contact, fractures are infrequent with an average apparent spacing of 3.3 m (Table 3.6-3) (Albin et al. 1997).

No fracture data from the surface or the Exploratory Studies Facility are available for the lower nonlithophysal zone of the crystal-poor member of the Topopah Spring Tuff (unit Tptpln). Fracture frequency from borehole core measurements for this unit typically range from 19.4 to 23.7 fractures

per ten-foot interval (Sweetkind, Barr et al. 1997). These fracture frequencies are high relative to the lithophysal-bearing units in the crystal-poor member of the Topopah Spring Tuff, but are subequal to fracture frequencies obtained from the middle nonlithophysal zone (Figure 3.6-15).

Three sets of steeply dipping cooling joints form an incipient columnar network of joints within the crystal-poor vitrophyre of the Topopah Spring Tuff (unit Tptpv) (Sweetkind, Barr et al. 1997). Also present are large, subhorizontal discontinuities that separate intervals of columns. Mean fracture spacing is 0.5 m, which is more closely spaced than that observed in most of the welded, devitrified units within the Exploratory Studies Facility.

3.6.3.3.4 Calico Hills Formation

Fracture data were collected from surface exposures of zeolitically altered Calico Hills Formation in the vicinity of Prow Pass. In general, two steeply dipping fracture sets are present within the pyroclastic flow units, a prominent northwest-striking set and a slightly less well developed northeast-striking set (Sweetkind, Barr et al. 1997). Between individual pyroclastic flow units, there are slight differences in the orientation of the two principle sets, but average fracture spacing and trace length are similar, regardless of orientation. The true spacing interval between discontinuities of an individual set ranges from 0.4 to 4 m; average apparent spacing for the unit as a whole is 1 to 2 m (Table 3.6-4). At Prow Pass, northwest-striking joints tend to occur as a series of widely spaced northwest-trending zones. Each zone consists of a number of northwest-striking joints that are typically long (5 to 10 m) and closely spaced (0.5 to 1 m). These northwest-trending zones are spaced 50 to more than 100 m apart; between the zones the spacing of the northwest-striking joints is 2 to 4 m or more (Sweetkind, Barr et al. 1997).

3.6.3.3.5 Bullfrog Tuff

Fracture data from the welded, devitrified middle portion of the Bullfrog Tuff have been collected from surface exposures at Raven Canyon and Little Skull Mountain, 15 and 20 km, respectively, from central Yucca Mountain (Sweetkind, Barr et al. 1997). The majority of fractures measured at both localities are steeply dipping. At Raven Canyon, cooling joints form two sets: a northeast-striking set with high dispersion of orientation, and a north- to northwest-striking set. Tectonic fractures have dominantly northwest strikes; there are a subordinate number of northeast strikes. Average apparent spacing is 0.3 m at Raven Canyon, and 0.4 m at Little Skull Mountain (Table 3.6-4). Fractures from Little Skull Mountain may be subdivided into six sets of steeply dipping cooling and tectonic joints (Sweetkind, Barr et al. 1997). Sets of cooling joints have median strike directions of N52°E, N4°E, and N60°W, respectively. The predominant tectonic joint set has a median strike direction of N34°E, with less well-expressed tectonic sets oriented at N17°E and N14°W.

3.6.3.4 Fracture Intensity

Fracture data from boreholes at Yucca Mountain indicate that welded flow units in the Tiva Canyon and Topopah Spring Tuffs have consistently higher fracture frequencies than the surrounding nonwelded units of the PTn and the Calico Hills Formation (Spengler and Chornack 1984; Scott, R.B. and Castellanos 1984; Engstrom and Rautman 1996; Rautman and Engstrom 1996b). Surface

mapping also shows that the density of fractures within nonwelded and poorly welded units is much lower than in the surrounding welded units (Table 3.6-5). The intensity of fracturing increases with degree of welding within the welded pyroclastic flows due to the presence of cooling joints and because increasing brittleness of the rock favors an increase in the number of tectonic joints.

Fracture intensity for the various lithostratigraphic units described above is summarized by Sweetkind, Barr et al. (1997) and shown in Figure 3.6-15. Surface fracture data and Exploratory Studies Facility data are reported in terms of spacing, the distance in meters between fractures (upper axis of Figure 3.6-15). Apparent fracture spacing from surface data is shown as bars that indicate a range of values resulting from various surface studies (Figure 3.6-15). In contrast to the surface data, the apparent fracture spacing from Exploratory Studies Facility data are shown as a single point. Average apparent Exploratory Studies Facility fracture spacing is calculated as the number of fractures observed in a particular lithostratigraphic unit divided by the distance in the tunnel that rocks of that unit are exposed (Sweetkind, Barr et al. 1997). Borehole fracture density for lithostratigraphic units is reported as the number of fractures per 10-ft interval, adjusted for unrecovered core (Figure 3.6-15) (Brechtel et al. 1995; Sweetkind, Barr et al. 1997). These data are not corrected for either orientation or trace length bias. Although they cannot be directly compared to the surface and Exploratory Studies Facility data, the borehole data mirror the trends in fracture intensity seen in the surface and Exploratory Studies Facility data (Sweetkind, Barr et al. 1997). Values for borehole fracture frequency appear along the bottom axis of Figure 3.6-15, and the scale has been reversed so that fracture intensity increases to the left and decreases to the right in both the upper and lower axes.

Different lower-limit trace-length cutoffs make statistical comparisons of fracture data collected by different methods difficult. The shapes of fracture trace length distributions at Yucca Mountain are generally consistent with a power-law or exponential model to these distributions. Therefore, use of a smaller lower-limit trace-length cutoff results in the measurement of increasing numbers of fractures in a given area. Borehole fracture lengths have no lower truncation, so bias in favor of measuring short fractures is extreme. One benefit of reporting borehole fracture frequency separately from the surface and Exploratory Studies Facility data (Figure 3.6-15) is that a measure of fracture density is available from two general size classes of fractures. The surface and Exploratory Studies Facility data yield apparent fracture spacing (reported as distance between fractures) for fractures 1 m and greater. In contrast, borehole data yield fracture density (reported as number of fractures per unit distance, equivalent to $1/\text{spacing}$) for all fractures larger than the diameter of the core.

3.6.3.5 Fracture Connectivity

Fluid flow through a fracture network depends in part on the degree to which the fractures are interconnected. Fracture connectivity, in turn, is dependent upon fracture size and orientation distributions, fracture density, and the fracture system geometry, particularly the distribution of intersection types, which can be measured or described through field observations and geometric analysis of the resulting pavement maps.

One method of estimating fracture connectivity is through a graphical comparison of fracture termination relationships (Barton, C.C., Larsen et al. 1993). Fractures may terminate in the rock matrix as a blind or dead end, may cross each other as an intersection or X termination, or may abut

each other at a T or Y termination. The relative proportions of these termination types in an exposure may be expressed as ratios using the terms of termination probability and termination percentage. Termination probability, the likelihood that a fracture will abut an earlier formed fracture, is calculated as the number of abutting intersections divided by the total number of fracture intersections (abutting and crossing). Termination percentage, the likelihood that a fracture will intersect another fracture rather than end blindly, is calculated as the number of abutting and crossing terminations divided by the total number of fracture endpoints (Table 3.6-5; Figure 3.6-16).

Fracture connectivity must be integrated with fracture intensity in an evaluation of the potential flow properties of a fracture network; well-connected fractures may still yield very few continuous pathways given low fracture densities. One such combination of connectivity and intensity is intersection intensity. Intersection intensity is calculated as the number of fracture intersections per area ($\#/m^2$) for the pavement map data. For scanline data from the detailed line survey, intersection intensity is reported in terms of number of fracture intersections per unit fracture trace length (Table 3.6-5; Figure 3.6-16). The calculation of intersection intensity is dependent on both fracture intensity and on network geometry. For example, a network consisting of many subparallel fractures would yield a low intensity by this measure. In general, however, this method of measuring intensity yields values that are quite consistent for both 1-D and 2-D fracture measures (Table 3.6-5; Figure 3.6-16).

Fracture termination percentage and intersection density is highest in the densely welded interiors of pyroclastic flows, and lowest in the surrounding nonwelded rock (Table 3.6-5; Figure 3.6-16). The complex fracture networks in the densely welded interiors of pyroclastic flows are well connected because the development through time of multiple fracture sets promotes fracture interaction. Abundant cooling joints and early tectonic joints limited the amount of available area for subsequent fractures to propagate, thus many late fractures simply connect pre-existing fractures. Poorly welded pyroclastic flows and nonwelded bedded units are characterized by poorly connected networks and an abundance of blind fracture terminations in rock (Table 3.6-5; Figure 3.6-16).

Fracture connectivity within the welded portions of the pyroclastic flows of the Paintbrush Group is dependent on the degree of communication between fracture networks within individual zones. High effective permeabilities resulting from overall high fracture connectivity within the welded units at Yucca Mountain may be inferred from airflow in wells as a result of barometric and topographic effects (Weeks, E.P. 1987), transient pneumatic pressure disturbances caused by the excavation of the Exploratory Studies Facility (Rousseau et al. 1998), and pathways analysis of a simulated fracture network in the Tiva Canyon Tuff (Anna and Wallman 1997; and Subsection 5.3.3.1.2.1 this document).

3.6.3.6 Structural Controls on Fracture Network Properties

3.6.3.6.1 Fracture Intensity Near Fault Zones

Hydrologic models require that the width and hydraulic properties of fault zones be defined in order to evaluate the influence of faults on flow pathways (Wittwer et al. 1993). The total width of the fault zone may include an area around the fault plane, here called a zone of influence, in which fracture

intensity is higher, or some other parameter, such as orientation, changes in response to the presence of the fault.

In the Exploratory Studies Facility, overall variability in the frequency of fractures 1 m long or longer is primarily a function of lithology, not proximity to faults (Sweetkind and Williams-Stroud 1996; Sweetkind, Barr et al. 1997) (Figure 3.6-17). Fracture intensity correlates to lithologic differences, being lowest in lithophysal units and nonwelded to partially welded tuffs, and highest in densely welded, non-lithophysal rock. At the fine-scale used for mapping in the Exploratory Studies Facility there are no sharp increases in the number of fractures larger than 1 m in close proximity to faults (Figure 3.6-17). The relationship of fractures smaller than 1 m in length to faults was evaluated by visual examination of every fault in the Exploratory Studies Facility (Sweetkind, Barr et al. 1997) that could be correlated with a fault mapped at the surface (Day et al. 1998a) (Table 3.6-6). Principle conclusions based on observations in the Exploratory Studies Facility are as follows (Sweetkind, Barr et al. 1997):

- The width of the zone of influence on fracture frequency in the immediate vicinity of a fault is, in general, quite narrow, ranging from less than 1 m to about 7 m from the fault (Table 3.6-6).
- The width of the zone of influence in the immediate vicinity of a fault correlates in a general way with the amount of fault offset. Intra-block faults with very small amounts of offset (1 to 5 m) have zones of influence that are 1 to 2 m in width. Block-margin faults with tens of meters of offset (faults at Exploratory Studies Facility Stations 11+20 and 70+58; Table 3.6-6) have zones of influence that range up to 6 to 7 m wide. The limited available data from block-bounding faults are not definitive regarding the nature of attendant fracturing. The Dune Wash fault is exposed in the Exploratory Studies Facility near Station 67+88. Offset on the Dune Wash fault is 65 m at this latitude (Sweetkind, Barr et al. 1997), relatively minor for a block-bounding fault. The zone of increased fracture frequency in the vicinity of the fault is 6- to 7 m wide. The Bow Ridge fault has very little attendant fracturing despite the 100 m offset and being exposed very near the surface (approximately 35 m of overburden). Lack of deformation around the fault zone probably results from the presence of nonwelded pre-Rainier Mesa Tuff in the hanging wall of the fault.
- The width of the zone of influence around a fault does not appear to be related to depth, at least within the Exploratory Studies Facility. The width of the zones of influence is similar for small faults observed along the North Ramp of the Exploratory Studies Facility where overburden is 50 to 60 m thick, as it is for small faults observed elsewhere in the Exploratory Studies Facility where overburden thickness is two to three times as great. However, upward splaying faults can result in apparent broad zones of influence at the surface as the fractured zones surrounding individual fault splays overlap.
- The amount of deformation associated with the faults appears, in part, dependent upon which lithologic unit is involved in the faulting. Faults within non- to partly-welded portions of the crystal-poor vitric zone of the Tiva Canyon Tuff (unit Tpcpv) are generally sharp, discrete breaks with minimal fault gouge or secondary shear surfaces (Table 3.6-6, faults at Stations 8+45 and 10+44). Individual pumice clasts along some faults can be traced to

the fault surface without visible sign of breakage, and wall rocks show little evidence of deformation. In comparison to brittle, welded rocks, nonwelded units apparently can accommodate a greater amount of extensional strain before failing by fracture.

Broad, fault-related zones of influence on the fracture network are evident at two cleared surface exposures that cross the Ghost Dance fault. One of the localities is the vertical cut at the USW UZ-7a drill pad, and the other is the ARP-1 pavement on the south-facing slope of Antler Ridge (Figure 3.6-1). In general, the Ghost Dance fault is a north-striking normal fault zone, steeply west dipping (85° to 90°) with down-to-the-west displacement. The displacement, amount of brecciation, and number of associated splays vary considerably along its trace (Spengler, Braun et al. 1993; Day et al. 1996b). Both of the cleared exposures intersect the Ghost Dance fault in the segment of the fault with the greatest displacement (13 to 30 m) and greatest number of associated fault splays.

The vertical cut at the USW UZ-7A drill pad (Figure 3.6-1) exposes the middle nonlithophysal zone of the Tiva Canyon (unit Tpcpmn) in the hanging wall of the Ghost Dance fault. At the surface, the Ghost Dance fault dips steeply (85° to 87°) to the west and has approximately 15 m of down-to-the-west displacement (Day et al. 1998a). A secondary, east-dipping fault with 3 to 4 m offset occurs 42 m west of the trace of the Ghost Dance fault. The intervening rock is intensely broken and consists of a complex network of short fractures that bound blocks as small as 10 cm (Sweetkind and Williams-Stroud 1996). True fracture intensity (measured with no trace length cutoff) is extremely high, nearly 12 m of fracture trace length per square meter of exposure (12 m/m^2), and fracture connectivity is also high. Rocks of the lowermost part of the lower lithophysal zone of the Tiva Canyon Tuff (unit Tpcpll) are exposed in the footwall of the Ghost Dance fault at the UZ-7A exposure, but these footwall rocks do not display the intense breakage that is exhibited in the hanging wall.

The ARP-1 pavement is located on the south flank of Antler Ridge (Figure 3.6-1), and exposes the upper lithophysal, middle nonlithophysal, and lower lithophysal zones of the Tiva Canyon Tuff (Tpcpul, Tpcpmn, Tpcpll, respectively). On Antler Ridge, there are 13 to 20 m of cumulative west-side-down displacement across several splays of the Ghost Dance that are distributed over a map width of approximately 100 to 150 m (Day et al. 1998a). Individual splays are characterized by a 1- to 2-m-wide breccia zone. The 100-m-wide pavement straddles the main trace of the Ghost Dance fault and two small associated faults. The fracture network at ARP-1 is dominated by closely-spaced, steeply dipping fractures striking $N5^{\circ}W$ to $N25^{\circ}W$ (C.A. Braun, Science Applications International Corporation, written communication to L.R. Hayes, U.S. Geological Survey, 1995). There is abundant tectonic breccia present at ARP-1 and many fractures show minor amounts of offset. The closely-spaced fractures and abundant brecciation at ARP-1 may be interpreted to be the result of proximity to the Ghost Dance fault. However, it may be equally likely that the pavement exposes distributed faulting that is unrelated to the Ghost Dance fault, similar to structures mapped by Potter, Dickerson et al. (1995) to the east of ARP-1 on the south slope of Antler Ridge (Figure 3.6-10).

3.6.3.6.2 Links Between Discontinuous Faults and the Fracture Network

The fracture network acts as a significant pre-existing weakness in the rock mass that can accommodate extensional strain through distributed slip along many reactivated joints. Evidence for reactivation of joints includes the presence of thin breccia zones along cooling joints and

observable slip lineations along joint surfaces (Sweetkind, Potter, Verbeek 1996). Cooling joints originally formed as tensional openings, having only face separation, not shear. However, thin selvages of tectonic breccia are often present along the trace of a cooling joint, indicating later slip.

Each lithostratigraphic zone at Yucca Mountain has characteristic fracture attributes including preferred orientations, spacing, trace length, and joint type (Sweetkind, Barr et al. 1997), so each is unique in its ability to deform by distributed slip. The result is stratigraphic control of structural geometry; what may be a discrete break in one lithostratigraphic unit may be a broad zone of distributed deformation in another.

Many of the intra-block faults within the Yucca Crest sub-block are short, discontinuous, have minor displacement (1 to 10 m), and represent the localization of slip along pervasive pre-existing weaknesses in the rock mass (Potter, Day et al. 1996a, 1996b). The northwest-striking Sundance fault zone has as much as 12 m of dip-slip separation where it offsets the crystal-rich member of the Tiva Canyon Tuff (Potter, Dickerson et al. 1995). However, within the crystal-poor member of the Tiva Canyon Tuff, the fault zone reaches a maximum width of about 70 m and total displacement is the summation of numerous 1 to 2 m contact offsets along small, discontinuous, discrete fault segments (Potter, Dickerson et al. 1995). The trend of each fault segment corresponds to one of the dominant orientations of cooling joints exposed on this portion of the mountain (Morgan 1984; Barton, C.C., Larsen et al. 1993; Barton, C.C., Page et al. 1989), implying that these discontinuous faults are themselves likely to be reactivated cooling joints (Potter, Day et al. 1996b; Sweetkind, Potter, Verbeek 1996). Stratigraphic offset associated with small, discontinuous faults may die out as displacements are distributed over a wide zone within the fracture network (Sweetkind, Potter, Verbeek 1996). Elsewhere at Yucca Mountain, mapped offsets of lithostratigraphic contacts are accompanied by the presence of numerous irregular small blocks showing evidence for minor slip and/or rotation and by pervasive brecciation along fracture sets and as isolated breccia bodies (Potter, Dickerson et al. 1995; Potter, Day et al. 1996b). Stratigraphic offset in these areas is accomplished through distributed slip over a broad zone, rather than by movement along a single plane.

3.6.3.7 Spatial Variability of Fracture Properties

Throckmorton and Verbeek (1995) summarized dominant joint set orientations over a broad area of northern and central Yucca Mountain extending from the Solitario Canyon fault on the west to the Bow Ridge fault on the east (Figure 3.6-3). Strike directions for cooling joints identified at 15 outcrop locations and four pavements within the Tiva Canyon Tuff were interpreted to belong to two sets: one striking N20° to 70°W and the other N34° to 71°E (Throckmorton and Verbeek 1995). Cooling joints form a rectilinear network of two joint sets with overall median strike directions for the two sets of N45°W and N50°E. Within the Tiva Canyon and Topopah Spring Tuffs, a third cooling joint set is developed at least locally. This set is subparallel to the flattening foliation and roughly orthogonal to the other two cooling joint sets (Sweetkind and Williams-Stroud 1996). Cooling joints certainly vary in their relative importance in particular stratigraphic intervals but, where identified, they seem to have consistent orientations throughout the northern and central portions of Yucca Mountain (Throckmorton and Verbeek 1995).

Over the same broad area, Throckmorton and Verbeek (1995) also identified four subsequently formed joint sets of tectonic origin, which they labeled T1, T2, T3 and T4. The median orientation

of tectonic fracture sets are: T1, N05°W to N05°E/86° to 89°W; T2, N35°W to N25° W/85°SW; T3, N25°E to N45°E/88°NW; and T4, N75°E to N85°E/88°SW. In addition, there is a set of subhorizontal tectonic joints that have variable strikes and dips less than 10 degrees (Throckmorton and Verbeek 1995). These joint sets are observable in various combinations in all of the surface outcrop data (Throckmorton and Verbeek 1995).

Sweetkind and Williams-Stroud (1996) attempted an evaluation of spatial variability of fracture orientation by combining the above data from Throckmorton and Verbeek (1995) with pavement and outcrop fracture data from rock units that are equivalent to the PTn hydrogeologic unit (Sweetkind, Verbeek et al. 1995a) and a limited amount of Exploratory Studies Facility data (Coe 1996a). Rose diagrams of strike distributions (Figure 3.6-18) from these studies were subdivided into the following lithostratigraphic categories (see Table 3.5-2):

- Crystal-rich member of the Tiva Canyon Tuff
- Upper lithophysal zone of the crystal-poor member of the Tiva Canyon Tuff
- Middle nonlithophysal zone, crystal-poor member of the Tiva Canyon Tuff
- Lower lithophysal and nonlithophysal zones of the crystal-poor member of the Tiva Canyon Tuff
- Lithostratigraphic units that are equivalent to the PTn hydrologic unit, including the crystal-poor vitric zone of the Tiva Canyon Tuff, the Yucca Mountain Tuff, the Pah Canyon Tuff, and interstratified bedded tuffs
- The Topopah Spring Tuff

Sweetkind and Williams-Stroud (1996) reported that much of the variability seen in joint orientations across Yucca Mountain (Figure 3.6-18) might be attributed to the variable expression of cooling joints. Cooling joints appear as a system of joint sets in all of the welded units with considerable variability of their orientations. The tectonic joints described by Throckmorton and Verbeek (1995) were evident across the entire central portion of Yucca Mountain, especially where cooling joints were not present, such as lithostratigraphic units that are equivalent to the PTn hydrologic unit.

In contrast to the general consistency of fracture orientations across the central and northern portions of Yucca Mountain (Throckmorton and Verbeek 1995; Sweetkind and Williams-Stroud 1996), there is important local variability in fracture character within individual lithostratigraphic units. One obvious example is the presence of the intensely fractured zone that is exposed within the middle nonlithophysal zone of the Topopah Spring Tuff (unit Ttpmn) from Exploratory Studies Facility Stations 42+00 to 51+50. In addition, the strike of the predominate joint set within this fracture zone gradually swings through 30 degrees of arc (Albin et al. 1997). Another example of variability in fracture character within individual lithostratigraphic units is the distribution of gently-dipping cooling joints that are an important component of the fracture network in the middle portion of the Tiva Canyon Tuff in northern Yucca Mountain (the "rounded step" unit of Scott, R.B. and

Bonk 1984), but become much less pronounced in the central portion of Yucca Mountain (Scott, R.B. and Bonk 1984; Day et al. 1998a). Spatial variability in fracture characteristics is also linked to welding variations in the pyroclastic flows. North of Drill Hole Wash, the Yucca Mountain and Pah Canyon Tuffs become welded and devitrified (Moyer et al. 1996) and have distinctly different fracture characteristics than the distal, nonwelded portions of these pyroclastic flows exposed in the vicinity of the potential repository (Sweetkind, Verbeek et al. 1995a).

3.6.3.8 Correlation of Small Scale Structures from the Surface to the Subsurface

Concurrent geologic mapping activities in the central block at the surface and within the Exploratory Studies Facility have defined a number of areas where there is good correlation of structural features between the surface and the subsurface. Correlation is best for faults with a meter or more of apparent vertical separation, particularly within the Tiva Canyon Tuff, where uncertainties in surface-to-Exploratory Studies Facility projections are minimal (Sweetkind, Beason et al. 1996a). Along the North Ramp of the Exploratory Studies Facility, the numerous faults that cut Azreal Ridge have virtually the same expression in the surface and subsurface; the same number of faults are observed, with virtually the same amount of offset (Barr et al. 1996). The southern extension of the Ghost Dance fault is observed to be a single, simple fault plane that dips steeply to the west with minor offset (1 to 2 m) both at the surface (Day et al. 1998a), and where it is exposed near the southern end of the Main Drift of the Exploratory Studies Facility, 250 m below the surface (Albin et al. 1997).

In certain instances, the correlation of structural features between the surface and the subsurface is problematic. One example involves the southern splay of the Drill Hole Wash fault system, which is exposed in bedrock northwest of borehole USW H-1. Here the fault strikes N30°W, dips steeply 80° to 85° to the southwest, has a cumulative offset of approximately 15 m, and is downthrown to the southwest (Day et al. 1998a). Projection of this fault into the subsurface suggests that the fault intersects the Exploratory Studies Facility at Station 22+65, directly beneath the center of Drill Hole Wash (Day et al. 1998a). As exposed in the Exploratory Studies Facility, the fault has an average strike of N10°W and dips 80° to the southwest. On the west side of the Exploratory Studies Facility drift the fault strikes between N1°W and N30°W and dips to the southwest. On the east side of the drift the fault strikes N0° to 15°W, and dips to the southwest. Apparent offset across the zone is at least 1.2 m down-to-the-southwest (Barr et al. 1996). The variability in relative vertical offset (15 m at the surface versus 1.2 m in the Exploratory Studies Facility) along the fault trace in the 400 m distance between its outcrop exposure and the Exploratory Studies Facility and variability in orientation (N30°W versus N10°W, respectively) is similar to strike variability observed for other intra-block faults at Yucca Mountain (Day et al. 1998a).

In rare cases, structural features observed in the subsurface have no correlative surface expression. The most prominent example is the intensely fractured zone, exposed within the middle nonlithophysal zone of the Topopah Spring Tuff in the Exploratory Studies Facility but not in the overlying rocks at the ground surface. Joints within this zone have some attributes typical of cooling joints, including great length, smooth, curving traces, low surface roughness, and local evidence of vapor-phase mineralization (Albin et al. 1997). Cooling joints are specific to individual pyroclastic flows and cannot be correlated with joints in surrounding units. A cooling joint origin for the joints in the intensely fractured zone would explain their absence in overlying units (Albin et al. 1997).

Correlation of structures between surface and subsurface must take into account possible changes in fault geometry at depth and along strike. Structures may be correlative even though they have differing amounts of offset, number of splays, width of breccia. Controls on the variability of fault geometry between surface and subsurface (or along strike) include:

- The effect of the margins and free surface of the structural block on fault geometry. Upward splaying faults are a common, but not universal, geometry at Yucca Mountain, resulting in disparate surface and subsurface geometries (Day et al. 1998a). The proximity to the earth's surface plays a role in the upward-splaying nature of the faults, largely because confining stresses are nearly zero. Structural blocks are bounded on all sides by major faults, and proximity to these faults can affect the character of the minor faults, which often increase in displacement at the block margins.
- The effect of pre-existing weaknesses. Slip is localized along pre-existing joints, an effect that is specific to individual lithostratigraphic zones. Cooling joints are the earliest formed and most pervasive pre-existing weaknesses and are unique to each flow unit. In general, each zone has a characteristic set of joint parameters (preferred orientation of joints, spacing or intensity, trace length) that makes the unit unique in its ability to accommodate extensional strain by distributed slip within the joint network. The result is different geometry in different parts of the stratigraphic section; what may be a discrete break in one part of the section may be a broad zone of distributed deformation in another.
- Fault history and timing of motion. Deformation in the southwestern Nevada volcanic field is spatially and temporally associated with major pyroclastic eruptions. In some cases the timing of fault motion can be documented where certain faults do not penetrate the entire volcanic section. Faults that predate the deposition of the Tiva Canyon Tuff would have no correlative surface structures. Similarly, cooling-related features in a particular flow, even if reactivated later, may not have a correlative surface expression.

3.6.3.9 Structural Evidence for Fast Hydrologic Pathways from Studies of ^{36}Cl

The radioactive isotope ^{36}Cl is present in anomalous concentrations (relative to natural background values, see following paragraphs) in young infiltrating waters. Elevated levels of ^{36}Cl , referred to as bomb-pulse ^{36}Cl , are the result of global fallout from more than 70 atmospheric nuclear tests conducted in the South Pacific between 1952 and 1958 (Glasstone 1962). These anomalous concentrations occur in chloride leached from bulk-rock samples from the Exploratory Studies Facility at Yucca Mountain (Fabryka-Martin et al. 1998). The occurrence of bomb-pulse ^{36}Cl in the Exploratory Studies Facility indicates the presence of flow paths capable of transmitting infiltration from the surface to depths as much as 300 m in less than 50 years (Fabryka-Martin et al. 1998). Detailed characterization of the structural settings of these sample locations and their relationships to structural features and infiltration rates have resulted in a conceptual model for fast pathways at Yucca Mountain (Levy, Sweetkind et al. 1997) that requires that two conditions be met in order to transmit bomb-pulse to the sampled depth within 50 years:

- A continuous structural path must extend from the surface to the sampled depth.

- The magnitude of surface infiltration must be sufficiently high to initiate and sustain at least a small component of fracture flow along the connected fracture path.

Sample localities in the Exploratory Studies Facility in which multiple samples show indications of bomb-pulse ^{36}Cl are generally associated with faults that are correlative with faults mapped at the surface (Barr et al. 1996; Day et al. 1998a). The results of hydrologic modeling highlight the importance of structures as the primary controls on the presence of fast hydrologic pathways through the lithostratigraphic units equivalent to the PTn hydrogeologic unit (Fabryka-Martin et al. 1998). Model simulations required structural disruption of the PTn equivalent units to allow the arrival of at least a small amount of water with the bomb-pulse signature at the middle nonlithophysal zone of the Topopah Spring Tuff (main drift of the Exploratory Studies Facility) in 50 years or less (Fabryka-Martin et al. 1998). Bomb-pulse levels of ^{36}Cl are associated with a variety of fault types, including a block-bounding fault (Bow Ridge fault), a probable strike-slip fault (Drill Hole Wash fault), and smaller, intra-block faults (Sundance fault) (Levy, Sweetkind et al. 1997). In the vicinity of Diabolus Ridge, an elevated $^{36}\text{Cl}/\text{Cl}$ value at the Exploratory Studies Facility sampling location does not correspond to a mapped fault in the Exploratory Studies Facility. However, geologic evidence indicates that the east-dipping reverse fault mapped at the surface (Day et al. 1998a, Central Block Map I-2601 reference) may be projected in the subsurface at a dip of about 30° on the basis of:

- Three-point calculations from the mapped trace of the fault as it crosses Wren Wash
- Attitude of breccia zones observed along the trace of the fault at the surface
- Intersection of a gently dipping fault by borehole USW SD-9 within poorly welded Yucca Mountain Tuff (Engstrom and Rautman 1996)

The projected location in the subsurface where this fault transects the PTn hydrogeologic unit lies almost directly above the Exploratory Studies Facility, where bomb-pulse ^{36}Cl was detected in samples from Stations 26+79 and Stations 27+18. Structural features sampled in the Exploratory Studies Facility that do not have elevated $^{36}\text{Cl}/\text{Cl}$ values either do not have a connected pathway to the surface (see Subsection 5.3.4.1.5; for example, much of the intensely fractured zone) or are faults whose surface traces tend to coincide with areas of low infiltration (for example, the southern part of the Ghost Dance fault as exposed in the Main Drift of the Exploratory Studies Facility) (Levy, Sweetkind et al. 1997).

Additional discussion of results of ^{36}Cl studies can be found in subsections 5.3.4.3.1.3 and 6.2.6.3

3.6.4 Structural Model for Yucca Mountain

To provide a comprehensive summary of the structural geology of Yucca Mountain, the structural description and interpretations presented in the preceding subsections are applied in the construction of a descriptive structural model that illustrates the kinematic and geometric interactions among various structural elements at a variety of scales. Elements of the descriptive structural model then form the basis for a discussion of the genesis of structures, in terms of the relative influences of local stratigraphic control and regional tectonic control.

3.6.4.1 Descriptive Structural Model

A descriptive structural model is illustrated in a series of block diagrams (Figures 3.6-19 through 3.6-23) that together portray a hierarchy of observational scales that span four orders of magnitude, and the fundamental structural elements that were operative at each of these scales. Note that these diagrams are generalized and in part schematic and are not intended to represent all faults and fault relations shown on previous figures. The scales of observation include:

- A subregional scale that portrays the overall structural framework of all of Yucca Mountain
- Intermediate scales that portray intra-block faulting within the potential repository block from the surface to the repository level and below, and the relations between the intra-block and the structure of the block-bounding fault zones
- Small (1,000 m³) volumes of rock, mainly within the Yucca Crest sub-block

Figures 3.6-19 through 3.6-23 illustrate the geometric linkages between structural elements at each of the various scales of observations, and linkages between structural elements at different scales of observation. Figure 3.6-19 illustrates the overall hierarchy of the scales of observation illustrated in the subsequent figures.

Figure 3.6-20 is a block diagram illustrating structural elements that shape the gross aspects of Yucca Mountain structure. The front of this block diagram is a cross section through Yucca Mountain at a northing of N 749,000 (Nevada State coordinate system, in feet). Surface traces of faults are generalized from the site area geologic map of Day et al. (1997), and subsurface geology is taken (with some modification such as addition of second order faults and a more detailed interpretation of the top of the Paleozoic basement) from the Yucca Mountain Project 3-D Geologic Framework Model ISM 2.0 (CRWMS M&O 1997e). The front face illustrates geology in the moderately extended, south-central part of the mountain, and the top (map view) illustrates structural transitions to the less-extended northern part of the mountain. The principle structural issues at this scale are:

- Systems of block-bounding faults that are kinematically and geometrically linked in three dimensions
- The character of hanging-wall and footwall deformation with respect to these large fault systems
- The nature of displacement transfer between individual block-bounding faults along relay fault zones

These are structures and structural patterns that are obvious on maps and cross subsections at scales of 1:24,000 and smaller. Consideration of these issues at the scale of Yucca Mountain involves discussion of the relations among the structural domains defined above, the north-to-south increase in vertical axis rotation, and the north-to-south increase in the magnitude of east-west extension.

The western part of the front face of the block (Figure 3.6-20) shows the geology of the Plug Hill domain (Figure 3.6-5), in which several strands of the Solitario Canyon fault, and the southern continuation of the Boomerang Point fault (the largest intra-block fault in the hanging wall of the Solitario Canyon fault) are buried beneath the surficial deposits of southeastern Crater Flat. Key structural relations include the complex geometry of intersecting fault strands in the Solitario Canyon fault system, the “rollover” style of steepening of stratal dips into the Solitario Canyon fault system, and the steeper dips of intra-block fault planes relative to the block-bounding fault plane.

East of the Plug Hill domain, the front face of the block (Figure 3.6-20) crosses the northern tip of the Southwest domain (Figure 3.6-5), characterized by relay faults and intense footwall deformation, east of the Solitario Canyon fault system. There is a prominent relay fault zone that splays southeast from the Solitario Canyon fault system, crosses the southern part of Yucca Crest, and turns south to become the north-striking Iron Ridge fault just south of the block face. This is a classic example of a relay fault zone distributing displacement between two block-bounding faults. South of this complex relay zone (just south of the front face of this block), the northwest-striking splays developed on the footwall of the Solitario Canyon fault essentially comprise a broad distributed relay zone that transfers displacement between the Solitario Canyon and Iron Ridge faults.

In the vicinity of Abandoned Wash, the front face of the block (Figure 3.6-20) crosses the southern extension of the central block of the structurally simple Central Yucca Mountain domain (Figure 3.6-5). The Abandoned Wash fault, which is interpreted to be the southern extension of the Ghost Dance fault (Day et al. 1998a, 1998b), is shown with the steep dip that is characteristic of intra-block faults, and it merges with a narrow northwest-trending graben that accommodates extension between the Abandoned Wash fault and the Iron Ridge relay fault zone.

The complex Dune Wash domain (Figure 3.6-5) occupies the center of the southern part of the block (Figure 3.6-20) and is clearly more deformed than the blocks that flank it. As stated above, this is not a consistently west-side-down “imbricate zone” as implied by R.B. Scott (1990); instead, it comprises a horst-and-graben complex within a large graben, bounded on the east by the Dune Wash fault. East of there, the diagram illustrates the merging at depth of three block-bounding faults, the Dune Wash, Bow Ridge, and Paintbrush Canyon faults. In this portrayal, the Paintbrush Canyon fault is essentially the “master fault” into which the extensional faults of eastern Yucca Mountain merge, and the Dune Wash domain represents the intense hanging-wall deformation above this system of merging block-bounding faults.

The eastern part of the block (Figure 3.6-20) shows that the Paintbrush Canyon domain (Figure 3.6-5) is a horst at this latitude, bounded on the west by the Paintbrush Canyon fault, and on the east by a buried, unnamed down-to-the-east fault exposed to the south, on the east flank of Busted Butte (Scott, R.B. 1992; Day et al. 1997).

The fundamental pattern illustrated in the southern part of this block (Figure 3.6-20) is that of two large fault systems, each of which contains at least two block-bounding faults, with an intervening little-deformed area. An Iron Ridge-Solitario Canyon fault system has produced a densely faulted and extended tract in the western part of the block, whereas a Paintbrush Canyon-Bow Ridge-Dune Wash fault system, and its impressive hanging-wall deformation represented by the Dune Wash graben, has produced another highly faulted tract. At this latitude, both of these systems are “eating

away” at the central block, which has been reduced from a robust width of 4 km farther north, to a mere 1.5 km at the front face of the block. This tectonic cannibalism of the central block is accomplished by encroachment of hanging-wall deformation from the east, and footwall deformation from the west. To the north, as illustrated on the map view on the top face of the block (Figure 3.6-20) the structure becomes much simpler and the amount of extension and fault offset decreases. Specifically, the myriad faults in the Dune Wash graben lose displacement to the north, merging with the block-margin deformation along the south edge of the central block. The Dune Wash fault itself loses displacement to the north; it dies out in the southeastern part of the central block, where it must transfer its remaining displacement into the block margin deformation in the Bow Ridge fault hanging wall.

The two large fault systems (Iron Ridge-Solitario Canyon fault system and Paintbrush Canyon-Bow Ridge-Dune Wash fault system) converge toward the south end of the block. The Iron Ridge fault becomes a major relay fault that transfers displacement from the western system to the eastern system as it connects the Solitario Canyon fault to the Stagecoach Road fault (Scott, R.B. 1992; Simonds et al. 1995); this effectively merges the deformation associated with the two systems of block-bounding faults into one highly extended, densely faulted domain.

Figure 3.6-21 (A and B) contrasts structural styles in the less-extended northern part of Yucca Mountain with those in the more-extended southern part of the mountain, and includes structures that are apparent at map scales of 1:6,000 to 1:12,000. Figure 3.6-21A is a view of the northern part of the block shown in Figure 3.6-20, and its front face represents a slice through the Yucca Mountain Project 3-D Geologic Framework Model ISM 2.0 (CRWMS M&O 1997e) at a northing of N765,000 (Nevada State coordinate system, in feet). Figure 3.6-21B is a view of a block south of that shown in Figure 3.6-20, and its front face represents a slice through the Yucca Mountain Project 3D Geologic Framework Model (CRWMS M&O 1996a) at a northing of N740,000 (Nevada State coordinate system, in feet). These blocks are at about twice the scale of the block shown in Figure 3.6-20, so they illustrate some of the detailed interactions between the structures shown on that figure, where appropriate. Key structures at the scale used on Figure 3.6-21 are individual block-bounding faults and their associated hanging-wall and footwall deformations.

In Figure 3.6-21A, the front face of the block passes directly through the central block, crossing the Bow Ridge and Solitario Canyon faults. Hanging-wall deformation is shown on the eastern edge of the central block, and the steeper stratal dips and more intense faulting contrast with the gentler dips and lack of significant faulting throughout most of the central block. At this latitude, the Ghost Dance fault and Sundance fault each have very minor offset (less than 5 m in both cases), and a footwall splay of the Solitario Canyon fault is abruptly losing displacement near Yucca Crest. The complex juxtaposition of diverse pieces of the Paintbrush Group stratigraphy in the Solitario Canyon fault system is confined to a narrow zone, west of which is a west-dipping fault-bounded panel, characteristic of this part of the Solitario Canyon fault zone (and of other block-bounding faults such as the Iron Ridge fault).

In Figure 3.6-21B, the front face of the block is situated west of Busted Butte, and crosses the Paintbrush Canyon fault and the Iron Ridge fault, as well as the intervening deformed area. At this latitude, the Paintbrush Canyon fault has gathered displacement from the Bow Ridge and Dune Wash faults, which have merged with the Paintbrush Canyon fault to the north, as seen on the top face of

the block. The 50° dip shown for this fault is characteristic of large-displacement faults, particularly in the southern part of the mountain. In the footwalls of both the Paintbrush Canyon and Iron Ridge faults, there exist footwall deformations in the form of numerous closely spaced splays that have propagated into the footwalls from the principle block-bounding faults. In the case of the Iron Ridge fault, the hanging-wall splays are in the process of dismembering the 0.6 km wide vestige of the central block. At the Earth's surface along the southern edge of the block diagram (Figure 3.6-21B), much of the bedrock is buried beneath surficial cover that blankets low-lying topography. R.B. Scott (1990) inferred the existence of highly faulted tracts beneath this extensive Quaternary cover in the southern part of Yucca Mountain. This is illustrated to a limited degree in Figure 3.6-21B, particularly west of the Paintbrush Canyon fault, where there is almost certainly a buried complex of faults that accomplish hanging-wall extension, as the southern extension of the Dune Wash graben.

The last two figures in this series, Figure 3.6-22 and Figure 3.6-23, focus specifically on the central block. The block diagrams in Figure 3.6-22, which represent about an order of magnitude greater scale of observation than Figure 3.6-21, illustrate the contrast in style between intra-block faults in the geologically simple potential repository volume, relative to the more deformed block-margin subdomain to the east of the potential repository. Figure 3.6-23 illustrates characteristic structural patterns discerned from fractured rock mass investigations of key parts of the stratigraphy underlying the central block.

Figure 3.6-22A portrays an area that includes the Ghost Dance and Sundance faults within the Yucca Crest sub-block of the central block. It illustrates the discontinuous nature of intra-block faults that pass through the Paintbrush Group stratigraphy in the Yucca Crest sub-block, influenced by the specific pre-existing fracture and faulting patterns that are inherent at the each stratigraphic level. The network of northeast- and northwest-striking cooling joints that are well-developed in this part of the central block, and the partial activation of these joints by minor intra-block faults are shown here. Because the joints, which are the fundamental pre-existing planes of weakness available for exploitation by faults, are themselves of limited individual extent, the faults that exploit them are discontinuous as well. Irregular, distributed brecciation is required to accommodate strain transfer between discontinuous fault-activated joint surfaces. In addition, because these small intra-block faults exploit cooling joints, they inherit very steep dips from the cooling joints as well. In this part of the mountain, the presence of pre-existing cooling joints is a powerful influence on both the attitude and the continuity (or lack thereof) of intra-block faults. The Ghost Dance fault is the exception. Although its splays, and the distributed deformation in its vicinity, may be influenced strongly by pre-existing joints, the Ghost Dance has remarkable continuity that is probably controlled to a much greater degree by intra-block stresses (probably bending stresses set up by the block-margin deformation to the east) than by older jointing. It is apparent that the Ghost Dance fault passes through several formations in the Paintbrush Group stratigraphy, whereas smaller faults are clearly confined to specific stratigraphic units, probably because of the specific mechanical properties of those units (as discussed below). The apparent discontinuity in the trace of the Ghost Dance fault on the top surface of the block (Figure 3.6-22A) is a stepover, and the two mis-matching strands are inferred to connect at depth, as described in a preceding part of this subsection. The local strain accommodation within this stepover probably occurs through slip on pre-existing joints.

Figure 3.6-22B shows the nature of block-margin faulting in the hanging wall of the Bow Ridge fault system (Boundary Ridge sub-block of the central block, Figure 3.6-4). Block-margin deformation (3.6-22B) contains closely-spaced north-trending faults that together define horst-and-graben patterns, northwest-trending grabens, and northwest trending miniature relay structures that qualitatively resemble the structures in the extended southern part of Yucca Mountain, such as the Dune Wash graben, though at a different scale. This faulting is more intense than that in the repository area, but the influence of pre-existing cooling joints may still be present, as the narrow northwest trending grabens that are an important element of the block-margin deformation have an orientation parallel to that of a prominent cooling joint set in the relatively undeformed parts of the Tiva Canyon Tuff elsewhere in the mountain. The very small discontinuous faults that are common in the Yucca Crest sub-block are not seen in the Boundary Ridge sub-block.

At the scale of 10 to 50 m (Figure 3.6-23), the fracture network and faults with small displacements are the principle structural elements observable. Representative elements of the fracture network within the Yucca Crest sub-block of the central block are shown at three different stratigraphic levels: the middle portion of Tiva Canyon Tuff, the lithostratigraphic units equivalent to the PTn hydrogeologic unit, and the middle portion of the Topopah Spring Tuff (Figures 3.6-23a,b, and c, respectively). The fracture network subdivides the mountain into innumerable fracture-bounded blocks and forms a pervasive mesoscopic fabric element. Cooling joints act as a significant pre-existing weakness in the rock mass and are the principle control on the style of deformation at this observational scale. Each lithostratigraphic zone has its own characteristic suite of cooling joint attributes (including joint orientation, spacing, trace length) so that each zone has a different fabric of the pre-existing weaknesses. These differences mean that lithostratigraphic zones respond to extensional stresses differently, resulting in a stratigraphic control of structural geometry.

The Tiva Canyon Tuff (Figure 3.6-23a) is characterized by a pervasive network of cooling and tectonic joints. Cooling joints in the crystal-poor upper lithophysal zone and the crystal-rich member are large, steeply dipping, and often form two orthogonal sets. Joints in the underlying middle nonlithophysal zone are more numerous, but are shorter, forming an anastomosing network of curved joints. There is abundant evidence within the Tiva Canyon Tuff for tectonic activation of joints as small faults, including: a) the presence of thin breccia zones along cooling joints, b) slip lineations along fracture surfaces, and c) common small offsets of lithologic contacts. Intra-block faults may exploit the fracture network, and certain intra-block faults may be nothing more than reactivated cooling joints. However, the differences in the nature of the joint network within each lithostratigraphic unit may govern the expression of the intra-block fault. Within the crystal-poor upper lithophysal zone (Tpcpul), extension may be accommodated by slip along a single long cooling joint, whereas in the underlying middle nonlithophysal zone (Tpcpmn) extension may be accommodated as a broad zone of distributed deformation or small amounts of slip on several short joints. Faults, regardless of the amount of offset, commonly occur as zones of brecciation and attendant fracturing many meters wide.

Joints within the lithostratigraphic units that comprise the PTn hydrogeologic unit are much less pervasive than in the surrounding welded units (Figure 3.6-23B). There are no cooling joints in the nonwelded units and few throughgoing joints. Most joints are strata bound and terminate at lithologic contacts. Joints are widely and irregularly spaced, except within welding transitions such as at the base of the Tiva Canyon Tuff (Figure 3.6-23B). Numerous small faults are observed in this

interval, both at the surface and in the Exploratory Studies Facility. Most faults are narrow, sharp breaks, with no attendant brecciation or fracturing.

Similar to the Tiva Canyon Tuff, the Topopah Spring Tuff has a well-developed network of cooling and tectonic joints. Especially in the middle nonlithophysal zone, long cooling joints of various orientations are common (Figure 3.6-23C). There is a distinct difference in fracture intensity between lithophysal and nonlithophysal rock in the Topopah Spring Tuff. Most of the long cooling joints in the middle nonlithophysal zone terminate abruptly at the contact with the underlying lower lithophysal zone (Figure 3.6-23C). In the Exploratory Studies Facility, the middle nonlithophysal zone is dominated by the intensely fractured zone. Joint density more than doubles within this zone of closely spaced northwest striking joints. Similar to the Tiva Canyon Tuff, numerous faulted joints with small displacements are observable in the Topopah Spring Tuff. However, little brecciation along joint surfaces or distributed brecciation is observed within the Topopah Spring Tuff. Fault zones at the level of the Topopah Spring Tuff are narrow. The zone of fault-related fracturing and brecciation is typically only a few meters wide.

3.6.4.2 Genetic Controls on Structural Geometry

From the foregoing descriptive structural model it is clear that the genesis and geometry of the various structural elements may be understood in terms of the relative influence of local stratigraphic control and regional tectonic control (Figure 3.6-24). Local stratigraphic control has a more significant impact on local structures, whereas regional tectonic control will affect structures on a subregional to regional scale. However, nearly all of the structures portrayed in the descriptive structural model draw, to varying degrees, on these two genetic influences.

At the mesoscopic scale, stratigraphic control dominates. Cooling joint attributes are strongly influenced by stratigraphic position within the Paintbrush Group. The above text discussed the preferential development of cooling joints in specific zones of the Tiva Canyon and Topopah Spring Tuffs. This is significant because the subvertical cooling joint sets, which formed concurrently with cooling of the welded tuff units comprise a very important primary fabric that is exploited by fault patterns that develop subsequently in response to tectonic stresses.

Intra-block faults are influenced subequally by local stratigraphic control and regional tectonic control. Closely spaced minor faults on the south slope of Antler Ridge, mapped as intersecting northwest- and northeast-striking structures that are discontinuous in map view (Potter, Dickerson et al. 1995), are almost certainly localized along pre-existing cooling joints in the middle nonlithophysal and upper lithophysal zones of the Tiva Canyon Tuff; minor structures such as these have developed through the superposition of regional tectonic stresses on a pre-existing, stratigraphically controlled network of cooling joints. As discussed above, the Sundance fault is a somewhat larger scale example of this superposition. This fault occupies a well-defined single fault strand where cooling joints are poorly developed (in the crystal-rich member of the Tiva Canyon Tuff on Live Yucca, Purgatory and Dead Yucca Ridges) and distributes its displacement across a broader zone in parts of the stratigraphy where there is a greater abundance of cooling joints (such as near the Tpcpul-Tpcpmn contact in the intervening washes) (Potter, Dickerson et al. 1995).

The largest intra-block faults are influenced only in minor ways by local stratigraphic controls. For example, the Ghost Dance fault has a remarkable continuity when compared with other intra-block faults in the central block; it is mapped as a nearly continuous north-south trace for 4.5 km through the block, and to the south it merges into a larger intra-block fault, the Abandoned Wash fault (Day et al. 1997; Scott, R.B. and Bonk 1984). Its orientation and continuity are largely controlled by its tectonic setting as a prominent zone of strain adjustment within a major tilt block. The minor fault strands that parallel the Ghost Dance fault are not activated cooling joints; they appear to be purely tectonic features. There does, however, appear to be a stratigraphic control in the nature of hanging-wall deformation, and perhaps as cooling joints are activated to locally accommodate strain at stepovers. Similarly, much of the block-margin deformation, which was generated through a hybrid of intra-block faulting and block-bounding fault processes, is largely controlled by the tectonic influences that produced the block-bounding faults, yet elements, such as northwest-trending narrow grabens, may be strongly influenced by stratigraphically-controlled cooling joints.

Block-bounding faults are controlled by regional tectonics, almost completely irrespective of local stratigraphic effects. The strike of block-bounding faults (northerly in the north, to northeast in the south) is a product of the east-west extensional tectonic stress regime that characterized the region during the 13-11 Ma interval, when the magnitude of extension was greatest (Minor 1995; Minor, Hudson et al. 1996; Fridrich et al., *Cenozoic Basins of the Death Valley Region: Late Cenozoic Extension, Vertical-Axis Rotation, and Volcanism in the Crater Flat Basin, Southwest Nevada*, Geological Society of America Special Paper, in press), and the southward-increasing clockwise rotation that affected Yucca Mountain between 13 and 11.45 Ma (mainly between 11.6 and 11.45 Ma) (Rosenbaum et al. 1991; Hudson, M.R. et al. 1996). The latter effects are attributed to a pulse of Walker Lane-related right-lateral deformation (C.J. Fridrich et al., *Cenozoic Basins of the Death Valley Region: Late Cenozoic Extension, Vertical-Axis Rotation, and Volcanism in the Crater Flat Basin, Southwest Nevada*, Geological Society of America Special Paper, in press). Stresses imposed by caldera scale volcanism constitute a second-order influence that affects the specific kinematic characteristics of large faults (Minor 1995; Minor, Hudson et al. 1996). In places, local stratigraphic effects may have had an influence on block-bounding fault systems where major relay fault zones have activated cooling joints, preferentially developed in specific zones of welded tuffs in the footwalls of block-bounding faults.

In summary, the interplay between local stratigraphic and regional tectonic effects is integral to any consideration of the genesis and geometry of structural elements at Yucca Mountain, particularly in the intra-block realm (Figure 3.6-24).

3.7 SITE GEOENGINEERING PROPERTIES

3.7.1 Introduction

This section describes the geoengineering properties of the site with specific focus on the potential repository block (Figure 3.7-1). Geoengineering properties include the physical, mechanical, thermal, thermal/mechanical, and other relevant special properties of the various units of geologic material constituting the site.

The primary emphasis in the description of the geoengineering properties in this section is on the repository block. Investigatory efforts were focused on the stratigraphic horizon proposed as the repository host horizon. However, the planned location of the repository host horizon has been adjusted during the course of design and investigation. Geoengineering properties of near-surface geologic materials have been investigated outside the repository block for the design of surface facilities (Figure 3.7-1). This information also is described in this section.

Data from laboratory testing of borehole samples and in situ testing at larger scales were analyzed to determine the geoengineering properties of the site. Testing and analyses were conducted in the context of other site properties. Experiment measurements are thus the primary source of the geoengineering properties database. Nonqualified existing data have been examined and are presented in this section to supplement qualified data and where qualified data do not exist or are not currently available. Their status as nonqualified data is indicated.

The stratigraphic framework in which the potential repository may be constructed is described in Subsection 3.5, Site Stratigraphy. Surficial Quaternary sedimentary deposits are described in Subsection 3.4, Quaternary Stratigraphy and Surficial Processes. The stratigraphic sequence at the site is generally a series of pyroclastic flow and fallout tephra deposits, as described in Subsection 3.5. Subsection 3.5 also includes criteria for differentiating stratigraphic units, detailed descriptions of all the volcanic units that are exposed or encountered in the subsurface within the study area, an index map showing the distribution of stratigraphic units (Figure 3.5-2), and a stratigraphic table (Tables 3.5-1 and 3.5-2).

Geoengineering data and analysis address the requirements in 10 CFR 60 to describe and assess the geomechanical properties of the subsurface at Yucca Mountain (10 CFR 60.21[c][1][I][C]). Geoengineering information also is needed to evaluate the existence of potentially adverse conditions that would require complex engineering measures to construct a repository (10 CFR 60.122[c][20]) or that would not permit design of stable underground openings (10 CFR 60.122[c][21]). The data and results described below provide the basis for engineering analyses addressing these potentially adverse conditions.

3.7.1.1 Stratigraphic Framework For Testing

The general stratigraphy of the area is illustrated in Table 3.7-1, which has been abstracted from the more extensive stratigraphy shown in Table 3.5-1 and 3.5-2. Rocks that are important to repository design are for the most part within the Paintbrush Group, which comprises welded and nonwelded ashflow deposits of Miocene age. The formations within the Paintbrush Group, as shown in

Table 3.7-1 and described in greater detail in Subsection 3.5, include, in ascending order, the Topopah Spring Tuff, the Pah Canyon Tuff, the Yucca Mountain Tuff, and the Tiva Canyon Tuff. Bedded tuffs are found separating all of the ashflow units of the Paintbrush Group. These tuffs are typically nonwelded and are nonlithified to moderately lithified. They range from 0 to 10 m in thickness and contain a variety of ashflow and ashfall deposits, with minor reworked tuffaceous sandstones. Five of these bedded tuffs are recognized within the Paintbrush Group (Brechtel et al. 1995).

Below the rocks of the Paintbrush Group is the Calico Hills Formation. Overlying the Paintbrush Group in local areas near Exile Hill are younger, nonwelded ashflow and airfall tuffs, including tuff unit "X" and the Rainier Mesa and Ammonia Tanks Tuffs of the Timber Mountain Group.

The late Tertiary and Quaternary surficial sedimentary deposits of the Yucca Mountain area consist of colluvium, fan alluvium, eolian sand sheets, ramps and dunes, or marsh (paludal) sediments, and playa deposits (see Subsection 3.4). These range in age from late Pliocene to Holocene. Surficial deposits are described in greater detail in Subsection 3.7.7, Engineering Properties of Surficial Material.

A thermal/mechanical stratigraphy was developed to provide a systematic basis for characterizing the rock mass in the site area based on geoenvironmental properties of the units of rock at the site and to facilitate analysis of the response of the rock to the repository. It is based on thermal and mechanical rock characteristics that are important to repository design, and was developed by designating lithologic units, in whole or part, or a group of contiguous units, or parts, as thermal/mechanical units. This nomenclature was first proposed by Ortiz et al. (1985) to group rocks with similar thermal and mechanical properties. The stratigraphy was based on the observation (Lappin et al. 1982) that thermal and mechanical properties can be correlated directly to grain density and porosity. The stratigraphy of Ortiz et al. (1985) includes 16 thermal/mechanical units, seven of which are shown on Table 3.7-1. The thermal/mechanical units were originally identified megascopically in terms of their welding and lithophysal cavity content.

The definition of thermal/mechanical units reflects to a large extent the general degree of welding. The thermal/mechanical units do correlate generally with groups of lithostratigraphic units, or in the case of the Topopah Spring Tuff, parts of a lithostratigraphic unit (Tables 3.5-2 and 3.7-1). The upper two Topopah Spring Tuff units, TSw1 and TSw2, are both within the densely welded, devitrified Topopah Spring Tuff. Originally, Ortiz et al. (1985) defined the TSw1 as containing more than 10 percent void space from lithophysal cavities and TSw2 as containing less than 10 percent void space from lithophysal cavities. This difference in lithophysal content was considered for repository design, and the top of the proposed repository host horizon is, in fact, aligned with the horizon below which lithophysal content is less than 10 percent as inferred from borehole geophysical data (CRWMS M&O 1997c). This may be up to 30 m above the Tptpul-Tptpmn lithostratigraphic contact (Spengler, Chornack et al. 1984; Spengler and Fox 1989). However, the change in percentage of lithophysal content does not occur at a consistent stratigraphic position in the crystal-poor upper lithophysal zone, and it can be difficult to identify. For this reason, the Tptpul-Tptpmn lithostratigraphic contact is thus now considered nominally equivalent to and used to define the TSw1-TSw2 thermal/mechanical contact.

Two thermal/mechanical units, the TCw and the TSw1, were further subdivided into the high lithophysal and nonlithophysal zones for Exploratory Studies Facility geotechnical studies (Brechtel et al. 1995; Kicker et al. 1996), to investigate differences in rock structure and rock mass quality within these zones (Brechtel et al. 1995). The zones represent summations of the individual lithophysal and nonlithophysal lithostratigraphic zones for those units. All data presented for the TSw2 thermal/mechanical unit were from the Tptpmn lithostratigraphic unit, and so were not further subdivided.

The uppermost identified thermal/mechanical unit is the undifferentiated overburden unit. This a collection of various rock and soil types that overlie the welded, devitrified Tiva Canyon Tuff. The overburden unit includes alluvium, colluvium, nonwelded, and vitric portions of the Tiva Canyon Tuff, and other tuff units such as the Rainier Mesa Tuff of the Timber Mountain Group, tuff unit "X," and their associated bedded tuff units (see Tables 3.5-2 and 3.7-1).

Most of the Tiva Canyon Tuff is contained in the TCw thermal/mechanical unit. This unit includes rock between and including the densely-welded subzone of the vitric zone of the crystal-rich member and, where it is present, the densely-welded subzone of the vitric zone of the crystal-poor member. Where the crystal-poor, vitric, densely-welded subzone of the Tiva Canyon Tuff does not occur, the contact of the devitrified rocks in the columnar subzone and the vitric rocks in the moderately welded subzone corresponds to the base of the TCw (Buesch, Spengler et al. 1996a). The unit is exposed on top of Yucca Crest and the ridges on the eastern flank.

Below the TCw is the PTn thermal/mechanical unit. This unit consists of partially welded to nonwelded, vitric and, in places, devitrified tuffs. Included in this unit are the nonwelded tuffs at the base of the Tiva Canyon Tuff, the Yucca Mountain Tuff, the Pah Canyon Tuff, the nonwelded tuffs at the top of the Topopah Spring Tuff, and the associated bedded tuffs.

The TSw thermal/mechanical unit underlies the PTn. This unit is subdivided into three subunits based on volume of lithophysal cavities and the identification of the crystal-rich vitrophyre. The top subunit, TSw1, is lithophysae-rich and includes the top vitrophyre (crystal-rich member, vitric zone, densely welded subzone), the nonlithophysal zone, and the upper lithophysal zone. This upper subunit ranges from about 49 m to 113 m thick. The middle subunit, TSw2, is lithophysae-poor and consists of the middle nonlithophysal, lower lithophysal, and lower nonlithophysal zones. The TSw2 subunit ranges in thickness from 175 m to 229 m. The vitrophyre subunit (TSw3) at the base of the TSw is about 7 m to 25 m thick.

Underlying the TSw unit is the CHn. This unit consists of the lower, nonwelded to partially welded portion of the Topopah Spring Tuff, the Calico Hills Formation, the underlying pre-Calico Hills bedded tuff, and the upper, nonwelded portions of the underlying Prow Pass Tuff of the Crater Flat Group.

As shown in Table 3.7-1, the TSw2 thermal/mechanical unit and the lower portion of the TSw1 thermal/mechanical unit have been identified as the proposed repository host horizon (CRWMS M&O 1997c). This includes the lower portion of the Tptpul (upper lithophysal zone) lithostratigraphic unit, and the whole of the Tptpmn (middle nonlithophysal zone), Tptpll (lower lithophysal zone), and Tptpln (lower nonlithophysal zone) lithostratigraphic units.

3.7.1.2 Geographic Distribution of Data

The majority of data presented in this subsection was collected to support the design and construction of the Exploratory Studies Facility and the proposed repository. Figure 3.7-1 shows the location of boreholes and test alcoves that were sources of data used to develop the characterization data. Additional data are presented from ongoing thermal testing in the Exploratory Studies Facility. Figure 3.7-1 also shows a subsurface plan view, showing Exploratory Studies Facility stations, existing boreholes, the repository area, site locations, alcoves, topographic contours, and coordinates of North and South Portals. The primary focus of the data collection program was the lithostratigraphic units constituting the potential repository horizon: the lower portion of the Tptpul (upper lithophysal zone), the Tptpmn (middle nonlithophysal zone), the Tptpll (lower lithophysal zone), and the Tptpln (lower nonlithophysal zone) (CRWMS M&O 1997c). Kicker et al. (CRWMS M&O 1997f) presents data submittals from geologic mapping of the Exploratory Studies Facility. Figures 3.7-2, 3.7-3, and 3.7-4 show a series of geologic cross-sections through the site, and a simplified geologic map of the central block area is presented in Figure 3.6-4.

3.7.1.3 Use of Data for Three-Dimensional Rock Properties Modeling

The 3-D Integrated Site Model of Yucca Mountain, Nevada, version ISM2.0, consists of a geometric representation of selected rock units and structures, a geologic framework model, plus a set of rock properties and mineralogy models and data sets (CRWMS M&O 1997e; Subsection 3.8). The framework model encompasses a 166-square km (64-square mile) rectangle around the Yucca Mountain Conceptual Controlled Area, and includes more than 30 rock units selected to meet the requirements of hydrologic and transport models and to represent the geology of Yucca Mountain. Modeled rock properties included matrix porosity, bulk "lithophysal" porosity, saturated hydraulic conductivity, density, and thermal conductivity. A 3-D model of mineral distributions also was integrated into ISM2.0. Use of data for 3-D rock properties modeling is discussed in greater detail in CRWMS M&O (1997e).

Rautman (1995) and Rautman and McKenna (1997) implemented a 2-D geostatistical model of porosity at Yucca Mountain and developed a correlation between that porosity model and thermal conductivity. The relationship of thermal conductivity to porosity, saturation, and temperature is discussed in Subsection 3.7.3.2. It was assumed for modeling purposes that the spatial continuity of thermal conductivity is identical to those patterns exhibited by lithophysal porosity. This assumption was necessary because there are not enough actual measurements of thermal conductivity from which to develop a spatial continuity model of its own. The result is a suite of thermal conductivity models that exhibit approximately the same cross-variable correlation with porosity as do the few measured data. It is anticipated that such a geostatistical modeling of thermal conductivity based on laboratory data from intact rock may be used in numerical programs to effectively simulate the rock mass thermal conductivity behavior. There may be some uncertainties in scaling thermal conductivity data from small intact rock sample testing to the repository or rock mass scale.

Results of geostatistical modeling of thermal conductivity and a more complete discussion of the correlation of porosity and thermal conductivity are presented in Section 5 and in Rautman (1995), and in Rautman and McKenna (1997). Section 5 further discusses the control of rock material

properties by large-scale geologic processes, the use of porosity as a surrogate for other material properties, the use of empirically observed correlations between selected material properties measured on the same physical specimen, principal sources of rock properties data used for modeling, and the methodological approach and results of rock properties modeling.

3.7.2 Rock Structure

3.7.2.1 Rock Structural Data from Surface Mapping, Underground Mapping, and Geophysical Studies

A description and analysis of rock structural geological data from surface mapping of fractures, detailed line surveys, and underground scanline mapping in the Exploratory Studies Facility is presented in Subsection 3.6, Site Structural Geology. Results of pavement studies conducted at surface exposures, outcrop studies (see also Sweetkind and Williams-Stroud 1996 and Sweetkind 1997), geologic mapping and fracture data from the Exploratory Studies Facility, and fracture data from boreholes are included in that section. The data synthesis includes fracture orientation distributions, trace length distributions, fracture intensity for various stratigraphic units, fracture connectivity, and fracture aperture and mineralization. A brief summary is presented here.

The nature of jointed rock masses requires that both the frequency and characteristics of jointing are assessed along with in situ stress and intact rock strength. Jointing in the rock mass is often the primary factor controlling excavation stability. Joint and fracture data are incorporated into rock mass classifications systems (discussed in Subsection 3.7.4) to estimate tunnel support requirements. Jointing can also have a significant influence on penetration rates of mechanical rock excavation equipment. Frequency and orientation of prominent joint sets are considered when estimating tunnel boring machine penetration rates.

Rock mass discontinuities are subdivided into groups according to their origin because the origin of jointing in the project area has an influence on the characteristics of the joint, such as roughness and planarity.

As discussed in greater detail in Subsection 3.6.3.3, joints within the Paintbrush Group have been subdivided into early cooling joints, later tectonic joints, and joints due to erosional unloading. Each type of joint exhibits different characteristics that may impact trace length, connectivity, and orientation. Cooling joints and tectonic joints are similar in orientation but differ in surface roughness. Joints due to erosional unloading have a different orientation and tend to be cross joints terminating at pre-existing joints (Sweetkind and Williams-Stroud 1996).

Cooling joints are identified in every unit that is at least moderately welded. They occur as two nearly orthogonal sets of steeply dipping joints, with a third, subhorizontal joint set that occurs irregularly. Cooling joints are characterized as having low surface roughness, with a Joint Roughness Coefficient less than 5. Tectonic joints have rougher surfaces (Joint Roughness Coefficient greater than 5) and occur throughout all units of the Paintbrush Group. The predominant strike is also north-south, with less frequent strike trends of northwest and northeast (Sweetkind and Williams-Stroud 1996).

Genetic controls on joint set geometry are discussed in detail in Subsection 3.6.4.2. Joints due to erosional unloading were variably oriented but trended predominantly east-west (Sweetkind and Williams-Stroud 1996). Joint orientations appear to be related primarily to lithology, with a lesser association with major structures. The dominant dip in all lithostratigraphic units was near vertical. This trend was moderated in the undifferentiated overburden, (Tmr, Tpki) and the crystal-rich members of the Tiva Canyon Tuff and Topopah Springs tuff, where fractures with moderate dips were observed (Sweetkind and Williams-Stroud 1996).

Multiple joint sets were well developed in the Tiva Canyon Tuff (U.S. Department of the Interior, Bureau of Reclamation 1995). All lithostratigraphic units in the Tiva Canyon exhibit the subhorizontal joint set to some degree, as well as two sets of near-vertical joints. Nonwelded tuff rocks of the undifferentiated overburden and PTn thermal/mechanical units had fewer joints and generally only a single north-south trending set (Sweetkind and Williams-Stroud 1996). Fracture attributes, including orientation, are summarized in Tables 3.6-1 through 3.6-4.

The subhorizontal joint set occurs in the crystal-rich member of the Topopah Spring Tuff, which corresponds with the upper portion of the TSw1 thermal/mechanical unit. However, it was not observed in the upper lithophysal zone (Tptpul) of the TSw1 (Tables 3.5-2 and 3.7-1). Estimated rock quality in Tptpul was distinctly better than the equivalent unit of the Tiva Canyon Tuff (Tpcpul) due to much less frequent recorded joints as well as fewer joint sets (Sweetkind and Williams-Stroud 1996).

Multiple joint sets occurred in the TSw2 thermal/mechanical unit, with dominant near-vertical joints striking north-south and northwest. The subhorizontal joint set also occurs (Sweetkind and Williams-Stroud 1996).

Very general information on fracture intensity and connectivity indicates that the highest joint frequencies and connectivities occur in the nonlithophysal units of the Tiva Canyon and Topopah Spring Tuffs (see Table 3.6-5 and Subsection 3.6.3.4). Nonwelded tuffs of the PTn had the lowest joint frequencies and lowest observed connectivities.

Geophysical studies augmented bedrock geology structural studies, and contributed to the understanding of the spatial distribution of the geoenvironmental properties of the rocks at Yucca Mountain. Surface and borehole geophysical studies conducted over the period from 1979 to 1996 at Yucca Mountain are synthesized and summarized in the report *Synthesis of Borehole and Surface Geophysical Studies at Yucca Mountain, Nevada and Vicinity*. The synthesis report consists of two volumes, *Volume I: Surface Geophysics* (Majer et al. 1996a), and *Volume II: Borehole Geophysics* (CRWMS M&O 1996d). The interpretations of geophysical data in the above reports are generally consistent with drilling data and have been incorporated in the latest version of the Integrated Site Model, ISM2.0 (CRWMS M&O 1997e).

In general, the geophysical results indicate that the proposed repository at Yucca Mountain is in tuffs that vary in physical properties (Majer et al. 1996a). In addressing the spatial distribution of porosity (fracture porosity and matrix porosity) over the proposed repository volume, the geophysical model indicates that welding, lithophysal character and content, porosity, and mineralogy are variable over scales of tens of meters. The geophysical model is not able to discriminate variation in porosity

caused by fracturing from large scale changes in matrix properties. However, in cases where there is good surface evidence for faulting, it appears that faulting and fracturing are the main causes for the variability in the geophysical data. The general results imply that the subsurface rock is very heterogeneous and complex at a rather small scale (Majer et al. 1996b).

The geophysical synthesis reports also address the amount, type, depth, and continuity of faulting in the proposed repository volume. Vertical seismic profile, surface seismic surveys at four different scales, gravity and magnetic surveys, and magnetotelluric methods were all applied in the Yucca Mountain region. The conclusion was observed that the faulting is a classic example of steeply dipping Basin and Range extensional faulting with cross-faults intersecting the normal faulting. There is abundant evidence of multiple subparallel fracture zones or faults associated with better developed mapped faults. Surface and borehole velocity studies across Yucca Mountain indicated that in addition to local heterogeneity, there is a general trend of increasing seismic velocity to the south, implying increasing porosity to the north (Majer et al. 1996b).

3.7.2.2 Rock Structural Data From Boreholes

Rock structure data presented here were developed primarily from boreholes UE-25 NRG-1, NRG-2, NRG-2A, NRG-3, NRG-4, NRG-5, USW NRG-6, and NRG-7/7A. The Tptpmn was also described by holes USW SD-7, SD-9, SD-12, and UZ-14. Borehole locations are shown in Figure 3.7-1. A detailed description of the structural core logging process is presented in Brechtel et al. (1995).

Structural data developed from the core included core recovery, locations of fractures and vugs, fracture characteristics, hardness, weathering, rock quality designation, and lithophysal and other voids. Lithologic and structural data were presented together with lithologic and stratigraphic units in Geology and Rock Structure Logs. Rock structural data for each hole also were summarized in the Rock Structural Data Summary Log. In this log, data concerning rock weathering, rock hardness, and fracture characteristics were summarized in 3 m (10 feet) intervals and correlated with both lithostratigraphic units and thermal/mechanical units. Variations in rock quality designation also were graphically displayed (CRWMS M&O 1997d).

3.7.2.2.1 Core Recovery

Core recovery can be used as a general indicator of relative rock quality. Substantial amounts of core in all lithostratigraphic units was either lost or recovered as rubble. Combining data from each of the boreholes, the amount of lost core for the Tptpmn lithostratigraphic unit was 15 percent of the total core length, as summarized in the recovery data presented in Table 3.7-2. Rubble zones accounted for 20 percent of the total length. Figure 3.7-5 presents a series of pie charts showing core recovery, lost core, and rubble zones as a percentage of total drilling in the various thermal/mechanical units. Total lost core and rubble ranged from 28.4 percent in the TCw to 49.2 percent in the TSw2 (Brechtel et al. 1995). In the lithophysal-rich portions of TCw and TSw1, the proportion of lost core and rubble zones was 32.6 percent and 51.2 percent, respectively.

The amount of lost core and rubble can also be a general indicator of the quality of the drilling technique. To limit the introduction of water and chemical additives that are typically used in core drilling, a modified method with dry compressed air as the circulating medium was used. The effect

of the non-standard drilling technique on the proportion of lost core and rubble was assessed by Brechtel et al. (1995), who concluded that the amount of lost core and rubble was due to the fractured nature of the welded tuffs and the presence of lithophysal voids, and not due to the drilling technique.

The high proportion of lost core and rubble is attributed to the degree of small-scale fracturing of the welded rocks and the presence of other inhomogeneities such as lithophysae and vapor-phase alteration. Fracturing also may have been induced along a subhorizontal fabric or foliation by drilling. These inhomogeneities had a large influence on core recovery and core quality, but have much less significance at the tunnel scale. Lost core and rubble zones did, however, limit description of core in places where individual features could not be reconstructed.

3.7.2.2.2 Rock Quality Designation

While core recovery is related to the quality of rock encountered in a boring, it also is influenced to some degree by the drilling technique and type and size of core barrel used. The rock quality designation (Deere 1963) is a recovery ratio that provides an alternative estimate of in situ rock quality. This ratio is determined by considering only pieces of core that are at least 100 mm (4 inches) long. The percentage ratio between the total length of such core recovered and the length of core drilled on a given run is the rock quality designation, as follows (Deere 1963):

$$RQD(\%) = \frac{\sum \text{Piece lengths} \geq 100 \text{ mm}}{\text{Interval length}} \times 100 \quad (\text{Eq. 3.7-1})$$

This index has been widely used as general indicator of rock mass quality and is an input for determination of rock mass quality, such as rock mass rating (RMR) and rock mass quality index (Q), discussed later in this report. RMR and Q are indices that consider characteristics of the rock mass such as the degree of jointing, strength, and groundwater condition to classify the rock mass according to rock quality.

The rock quality designation used for geotechnical design purposes considered all breaks in the core, including those identified by geological/geotechnical staff as drilling-induced and those indeterminate as to their natural or drilling-induced origin. Differentiation among types of breaks was difficult because of the general absence of mineralization along fractures and the existence of a subhorizontal fabric similar to foliation in some of the tuff rocks. The resulting rock quality designation, used for subsequent estimations of rock mass quality, is thus considered conservative because it indicates lower rock quality than if only natural fractures had been considered. Attempts were made to filter the effects of drilling-induced fracturing. A parameter called enhanced-rock quality designation (RQD) was calculated (Brechtel et al. 1995), in which the fractures judged to be drilling-induced were not considered in RQD calculations, thus resulting in greater piece lengths. Enhanced-RQD values were 1.5 to 2.2 times higher than RQDs which considered all fractures. However, because of the uncertainty in fracture classification and because of the large proportion of lost core and rubble, the more conservative RQD was used for rock mass quality estimations.

Rock quality designation data are presented graphically in Figure 3.7-6. Rock quality designation was generally not high in any unit, due to the relatively low recovery of intact core, the high frequency of core fractures, and the consideration of drilling-induced mechanical breaks as fractures. Using the relative rock quality descriptions based on rock quality designation developed by Deere (1968), rock quality of core in the Tptpmn stratigraphic zone of the TSw2 thermal/mechanical unit ranges from poor to very poor among the boreholes evaluated. Within the Tptpmn are two intervals of generally higher rock quality designation bounding a lower-rock quality designation interval defined by the lithophysal subzone of the Tptpmn lithostratigraphic unit. The portion of the TSw2 unit cut by the Main Drift is characterized by very low rock quality designations, and these low values are consistent from hole to hole. Based on rock quality designation values, core from the TCw and PTn thermal/mechanical units are classified as poor quality rock, and core from the TSw1 is classified as very poor quality rock (Brechtel et al. 1995). Locally, however, the nonlithophysal portion of the TSw1 was of higher quality and is classified as poor instead of very poor rock.

Based on the minimal tunnel support that was required in the ESF, rock quality is very much higher from an engineering standpoint than indicated by the low borehole RQD. This is due to the inclusion of mechanical and drilling-induced fractures along with natural fractures for RQD calculation, the apparent natural proclivity of the lithophysal zones to produce rubble zones at the core scale that do not significantly affect stability at the tunnel scale, and the use of dry drilling in fairly brittle rocks, which may have produced more fracturing than mud drilling. Because the recovered core was highly fractured, it was difficult to separate features that represented continuous joints from smaller scale incipient cracks and inhomogeneities in the rock (CRWMS M&O 1997d).

Rock mass properties are discussed in Subsection 3.7.4, and as discussed in greater detail in that section, RQD as assessed at the tunnel scale was much higher than borehole RQD. This is in part because the borehole RQD values were artificially low for the reasons listed above and also because the core data included smaller-scale fractures that were not counted at the tunnel scale. Tunnel scanline RQD assessments were made by considering only joints and fractures longer than approximately 30 cm (1 foot) unless their apertures were over 3 mm (SNL Technical Procedure SNL TP-234). Borehole RQD assessments included all fractures longer than the core diameter.

3.7.2.2.3 Rock Weathering

Qualitative rock weathering descriptors were applied to describe the average condition of the core in each core run interval. These standard descriptors are based on recommendations of the International Society for Rock Mechanics (1981) and are listed in Table 3.7-3. The data are presented graphically, by thermal/mechanical unit, in Figure 3.7-7.

All rock from the Tptpmn in the TSw2 unit was either fresh or slightly weathered, constituting 51 and 49 percent, respectively, of the total recovered core (Kicker et al. 1996). A fairly high percentage of the core recovered from other welded tuff units, TCw and TSw1, was also fresh or slightly weathered, constituting approximately 60 to 70 percent. About 20 percent of the core length in the PTn unit was moderately weathered (Brechtel et al. 1995).

3.7.2.2.4 Rock Hardness

Rock hardness is a general descriptor of the strength of the rock material. Estimated rock hardness for recovered core was determined following the procedures in Sandia National Laboratories Technical Procedure TP-233, *Geotechnical Logging of Core from Examination of Core and Video Records*. The estimated hardness classification ratings used are listed in Table 3.7-4. Hardness data are presented graphically, as percentages of total drilling in each thermal/mechanical unit, in Figure 3.7-8. Quantitative hardness measurements on selected samples using Schmidt hammer tests are described in Subsection 3.7.3.3.8.

Rock in the Tptpmn of the TSw2 was generally classified from core logging as almost entirely hard (79 percent) to very hard (16 percent) (Kicker et al. 1996). Most of the rock in the other welded tuff units was estimated to be classified as very hard, hard, or moderately hard, with the highest percentage in the hard category (Brechtel et al. 1995). The nonwelded rock of the PTn unit was much softer than the welded tuffs, and approximately half of the core in this unit was estimated to be in the soft or very soft category (Brechtel et al. 1995).

3.7.2.2.5 Fracture Data

A detailed description of the procedure for logging fracture characteristics in core is presented in Brechtel et al. (1995). Complete data are presented in CRWMS M&O (1997d), Brechtel et al. (1995), and Kicker et al. (1996). Fractures judged to have been induced by drilling generally were oriented normal to the core axis and are believed to have probably formed along subhorizontal planes of incipient weakness (Brechtel et al. 1995). These fractures accounted for 40 to 70 percent of the total fractures depending on the thermal/mechanical unit. Only natural fractures and those indeterminate as to natural or drilling-induced origin were included in evaluations of fracture inclination, frequency, infillings, and roughness. Fractures judged to be drilling-induced were excluded (Brechtel et al. 1995).

Because of testing requirements that the borehole walls be kept dry and clear (i.e., protected from water and mudcake contamination), high-velocity, dry, compressed air was used as the drilling fluid instead of mud for core drilling. The effect of this new drilling technique on fracturing in the core was difficult to establish because of limited data available for comparison (Brechtel et al. 1995). As discussed in Subsection 3.7.2.2.1, Brechtel et al. (1995) concluded that the amount of lost core and rubble was not due to the dry drilling technique but was due to the fractured nature of the welded units and the presence of lithophysal voids. It is possible, however, that due to the brittle nature of these volcanic sequences, dry drilling may have caused increased fracturing from what might have occurred in mud drilling.

When fracture frequencies were corrected for sampling bias due to the relative orientation of the borehole with respect to the fractures, the near-vertical fractures were most numerous. This agreed well with surface mapping observations (Brechtel et al. 1995).

Most fractures were clean, and fracture infillings, when observed, were rated as either "thin" or just "surface sheen." Most frequent infilling materials were identified as white crystalline, white noncrystalline, or black dendritic minerals. Thick infillings have been observed in the Exploratory

Studies Facility excavation but were not sampled effectively by drilling, possibly due to the high velocity compressed air used as the circulation medium (Kicker et al. 1996).

Additional information on fracture mineralization and aperture is presented in Subsection 3.6.3 and in CRWMS M&O (1997d).

Fracture surfaces in core samples were classified predominantly as having an irregular shape. The second most frequent fracture surface shapes were planar. Most fracture surfaces were rated as moderately rough.

3.7.2.3 Potential Key Blocks in Underground Excavations

Key blocks are rock wedges, formed by the intersection of geologic discontinuities and an excavation surface, that are kinematically able to move into the excavation. Key block analyses were performed to verify that ground support being installed in the Exploratory Studies Facility was adequate (SNL Technical Data Information Form No. 305660). Analyses were done prior to excavation of the Exploratory Studies Facility Main Drift to compare the size of potential key blocks that might occur in the North Ramp to the size of blocks projected for the Main Drift alignment, assuming that the joint sets encountered in the North Ramp also would be encountered in the Main Drift. In addition, analyses of a 100 m section of the North Ramp were performed to assess the importance of the subhorizontal vapor-phase parting structure that occurs periodically in the welded units.

The UNWEDGE (University of Toronto Rock Engineering Group 1992) key block stability analysis program was the software used. The purpose of the UNWEDGE program is to rapidly estimate maximum potential key block sizes. The maximum potential key block size is the volume of the largest key block that could potentially form, given an existing excavation configuration and a particular combination of joint set orientations. Specific individual joints cannot be positioned in specific locations. The program is nonprobabilistic, but determines the maximum potential block types and volumes based on the provided joint set data. It is limited to analysis of no more than three joint sets at a time. Input parameters include joint set orientation, joint spacing, cohesion and friction angle of each joint set, and rock unit weight.

The comparative analysis of the potential key blocks in the North Ramp and the Main Drift suggested that given similar rock mass conditions, the Main Drift would have a higher frequency of key blocks due to the orientation of joints relative to the tunnel alignment.

A second analysis was performed to predict the maximum potential size key block that could form based on joint sets observed between stations 12+00 m and 13+00 m in the Exploratory Studies Facility. Although the subhorizontal joints in this interval could have had a negative impact on tunnel stability, most key blocks that were analytically predicted could be supported by the rock bolt support system being installed. Two potential key blocks were found to have sufficient size to exceed the capacity of the rock bolt support system. However, no key blocks of this size were observed in the interval. The key block analysis must be considered conservative because of its inherent assumptions. Observations in the constructed Exploratory Studies Facility indicate that the installed supports are adequate, and no failures of significant rock wedges have been reported.

3.7.3 Laboratory Properties of Intact Rock

3.7.3.1 Physical Properties

Bulk and physical property measurements were performed on specimens of tuff prepared from cores recovered from NRG and SD boreholes. Additional measurements were performed on samples from the Single Heater Test block and the Drift Scale Test block of the Thermal Test Facility of the Exploratory Studies Facility. The data were collected under a qualified quality assurance program and include density, porosity, and mineralogy.

3.7.3.1.1 Density and Porosity

Density, a physical property defined as mass per unit volume at a specific temperature, can vary substantially within a rock mass because of variations in mineralogy, porosity, and welding. Average grain density is controlled by the composition of the rock, and variations in average grain density are attributable to variations in mineralogy and petrology. Porosity is a measure of the volume of voids in a solid material such as rock. It can be calculated from the relationship of average grain density and dry bulk density and also from the relationship of saturated bulk density and dry bulk density. Effective elastic constants, rock fracture, and rock rheological behavior are controlled in large part by the size, shape, and distribution of pores throughout the rock.

Dry bulk density, saturated bulk density, and average grain density measurements were performed on laboratory test specimens of tuff prepared from cores recovered from NRG boreholes. Dry bulk density represents the mass measured in a dry condition divided by the volumetric measurement of the external dimensions of a test specimen. The Sandia National Laboratories procedure, SNL TP-229, *Bulk Properties Determinations of Tuffaceous Rocks: Dry Bulk Density, Saturated Bulk Density, Average Grain Density, and Porosity*, adhered to the American Society for Testing and Materials Standards ASTM D854, *Standard Test Method for Specific Gravity of Soils* and ASTM C135, *Standard Test Method for True Specific Gravity of Materials by Water Immersion*. Test specimens recovered from the NRG boreholes were dried prior to testing, to a constant weight at 110°C and the dry bulk density determined. Heating specimens at 110°C is a deviation from the ASTM recommended procedures, because excessive temperatures may damage the specimen due to differential thermal expansion along grain boundaries. However, a series of thermal diagnostic tests, conducted as part of this study, showed that drying welded tuff specimens at 110°C produced no noticeable damage. This was demonstrated by measuring the compressional and shear wave velocities before and after heating characteristic welded tuff specimens. If microcracks had developed, the velocity would have decreased. The thermal cycling produced no reduction in velocity, indicating that no thermally induced microcracking had occurred.

Once the dry bulk density was measured, each specimen was saturated with distilled water. A two-stage process was used for the saturation. The specimen was first pressure saturated at 10 MPa for a minimum of one hour, followed by a minimum of two vacuum saturation cycles. Once the mass change for successive cycles had stabilized to within ± 0.05 percent, the saturated bulk density was computed (Boyd, Martin et al. 1994; CRWMS M&O 1997d).

The average grain density was measured using the pycnometry method. This technique consists of a two-stage measurement. First, the mass of a dry, powdered specimen was measured. Next, the volume of the powder was determined. These two measurements were combined to compute the average grain density. Detailed procedures for the measurement are presented in Boyd, Martin et al. (1994). Total porosity, ϕ_T , was computed from the grain density, ρ_g , and the dry bulk density, ρ_{db} , using the expression (Boyd, Martin et al. 1994):

$$\phi_T = \frac{\rho_g - \rho_{db}}{\rho_g} \quad (\text{Eq. 3.7-2})$$

Dry and saturated bulk densities, average grain density, and calculated porosity for specimens from the NRG boreholes are presented in CRWMS M&O (1997d); Martin, Price et al. (1994); Boyd, Price et al. (1996a; 1996b); Boyd, Noel et al. (1996) and Martin, Price et al. (1995). The data are summarized by thermal/mechanical unit in Tables 3.7-5, 3.7-6, 3.7-7, and 3.7-8. As shown, nonwelded rocks of the undifferentiated overburden and PTn units have significantly lower bulk density and higher porosity than rocks of welded units TCw, TSw1, and TSw2. Because of the relatively uniform composition of the tuffs, average grain density shows only small variability among different rock units. Mean dry bulk density was 1.28 g/cc in both the nonwelded units undifferentiated overburden and PTn. Mean dry bulk density in the other, welded units was substantially higher and ranged from 2.12 g/cc to 2.35 g/cc.

As part of the pre-heating, ambient characterization of hydrologic properties, density and porosity measurements were also performed on cores from wet-drilled and dry-drilled underground boreholes in the Single Heater Test block and the Drift Scale Test block of the Exploratory Studies Facility. Grab samples from the Observation Drift of the Drift Scale Test were also tested. All tested samples were from the TSw2 thermal/mechanical unit. Complete results and procedures are presented and discussed in CRWMS M&O 1996b and CRWMS M&O 1997f. Results are summarized in Table 3.7-9 and are generally consistent with TSw2 results from surface-based boreholes. As shown, mean bulk density ranged from 2.20 to 2.26 g/cc, mean particle density ranged from 2.49 to 2.51 g/cc, and mean porosity ranged from 9.3 to 12.5 percent.

Porosity, bulk density, and particle density were measured in additional core samples from drill holes SD-7, SD-9, and SD-12 in support of hydrologic measurements. Samples were collected at a nominal 3 feet, regularly spaced sampling interval on core from these boreholes. Results from SD-7, SD-9, and SD-12 are presented in Rautman and Engstrom (1996a), Engstrom and Rautman (1996), and Rautman and Engstrom (1996b), respectively.

3.7.3.1.2 Mineralogy

The mineralogy and petrology of the volcanic sequence at Yucca Mountain has been described extensively in both studies of drill core and outcrop samples (see Geochemistry, Section 6, and Subsection 3.5 for a summary). Mineralogy and petrology affect thermal and mechanical geoenvironmental properties, and thus help characterize the rock mass at the site and predict performance. Because large quantities of heat will be generated by the waste packages, it is

essential that heat transfer properties (such as thermal conductivity, thermal expansion, and thermal heat capacity) be understood so that repository performance can be assessed. Thermal properties are largely a function of mineralogy, and so an understanding of these properties requires that mineralogy be determined.

The abundance of minerals that could affect the thermal/mechanical behavior of the rock at elevated temperatures, is of particular interest. These minerals include cristobalite, which undergoes a phase transition and volume change at elevated temperatures, and smectite and zeolites, that dehydrate at elevated temperatures, with accompanying volume reduction. Other mineralogical effects associated with temperature changes include the dissolution and precipitation of silica and the dehydration of volcanic glass. All these effects in turn affect the thermal and mechanical properties of the rock mass. The purpose of mineralogical and petrological analyses was to evaluate correlations between the thermal/mechanical behavior of rock samples and their mineralogical components and texture. Correlations are discussed in Subsection 3.7.3.2, Thermal Properties. Mineralogy and petrology will also be used as input for modeling heat-induced changes during in situ thermal testing in the Exploratory Studies Facility.

In brief, both the Tiva Canyon Tuff and the Topopah Spring Tuff are zoned ashflow tuffs with crystal-poor rhyolitic units at the base and crystal-rich quartz latite units at the top. Both units have devitrification, welding zones, and secondary crystallization imposed upon their primary features (see Subsection 3.5 for a description of these features). A suite of 97 samples from borehole NRG-6 was studied to understand the mineralogy and petrology of samples tested for thermal expansion, thermal conductivity, and mechanical properties (CRWMS M&O 1997d). Borehole NRG-6 was selected because it provides a relatively complete stratigraphic section from the lower part of the Tiva Canyon Tuff through most of the lower lithophysal zone of the Topopah Spring Tuff of the Paintbrush Group (see Tables 3.5-2 and 3.7-1). Depths ranged from 6.77 to 330.7 m (22.2 to 1,085.0 feet). The data and procedures are summarized here and are presented in detail in Technical Data Information Form 305183, *Petrographic and Mineralogical Characterization of Samples for USW NRG-6*.

Laboratory testing of mineralogy also was performed for the Single Heater Test and the Drift Scale Test of the Thermal Test Facility of the Exploratory Studies Facility, to relate mineralogy to coupled thermal, mechanical, chemical, and hydrological processes. Analyses were performed for 10 samples from the Single Heater Test region of the Thermal Rest Facility. The analyses used the matrix flushing method of Chung (1974) and an internal intensity standard (corundum) to quantify the phases present. These data have been entered into Automated Technical Data Tracking and will be submitted to the Records Processing Center under DTN LL960810704244.016 and DTN LL960810704244.017, and Technical Data Information Form 305620. The Lawrence Livermore National Laboratory Yucca Mountain Project controlled Scientific Notebook No. 00269. Results and procedures are discussed in CRWMS M&O (1996b).

Mineral abundances were also determined for 17 samples from the Drift Scale Test block of the Thermal Test Facility of the Exploratory Studies Facility using the Rietveld method of whole X-ray pattern fitting (Snyder and Bish 1989; Young 1993). Complete procedures and results are described in Roberts and Viani (1997a) and CRWMS M&O (1997g). The method appears to yield better precision than the matrix flushing method of Chung (1974) used for Single Heater Test samples.

These data have been entered into automated Technical Data Tracking and will be submitted to the Records Processing Center under DTN LL970600304244.032 (TBV) and TDIF 306139 (TBV).

Petrographic and mineralogical data from borehole NRG-6 were obtained by an examination of all 97 core samples. Table 3.7-10 shows the summary petrographic characterization of NRG-6 specimens. More detailed mineralogical and chemical analyses were performed for selected samples using different laboratory analytical methods, including optical microscopy of thin-sections with modal point counts of identified constituents to determine composition, X-ray diffraction analysis of prepared powders to identify and estimate proportions of finely crystalline minerals, and whole-rock chemical analysis to determine the chemical composition and water content of samples (CRWMS M&O 1997d).

The most obvious physical divisions are between welded and nonwelded tuff, and these divisions are reflected in the variation in thermal properties discussed later in Subsection 3.7.3.2. Invariably in the samples from NRG-6, the welded intervals show significant compaction, resulting in the destruction of primary porosity. With few exceptions and above the water table, the nonwelded intervals retain their primary glassy or vitric character and retain significant porosity. These intervals rarely correspond to stratigraphic rock unit boundaries because the upper and lower layers of eruptive units (upon which the stratigraphic units are defined) are typically nonwelded while the interiors of the units are welded (CRWMS M&O 1997d).

Minerals identified from X-ray powder diffraction on 23 devitrified samples from NRG-6 included the silica phases (cristobalite, quartz, tridymite), feldspar (plagioclase and sodium- and potassium-rich alkali feldspar), and a clay mineral (primarily illite). Other minerals were noted in thin sections but were not identifiable by X-ray diffraction because of their low abundances. These include small amounts of quartz present as phenocrysts, biotite, amphibole, and iron-titanium oxides (CRWMS M&O 1997d).

As shown in Table 3.7-10, cristobalite is present in virtually all devitrified samples and is the dominant silica phase in most samples. Quartz is absent in all samples shallower than 139.8 m (458.7 feet) and only appears abundantly below 197.7 m (648.6 feet). Tridymite is intermittently present in samples at 129.6 m (425.3 feet) or less in depth and was not identified in any quartz-bearing samples. Clay (illite) is identified in many, but not all, samples in the same interval from which tridymite was identified. It also was noted that silica phase variations tend to cross the lithostratigraphic boundaries defined by Geslin et al. (1995) in their lithostratigraphic classification of rocks from borehole NRG-6. However, in general, the lithostratigraphic classifications assigned by the USGS (Geslin et al. 1995) are consistent with the mineralogical data presented in Table 3.7-10.

Results of laboratory testing of mineral abundances for samples from the Single Heater Test region of the Thermal Test Facility are presented in Table 3.7-11 (CRWMS M&O 1996b). Quartz and cristobalite average about 8 and 19 percent of sample, respectively. Smectite is found in all the samples, but is generally present at less than 3 percent. The greatest variability is shown in the abundances of albite and sanidine. Clinoptilolite was present in small amounts in three of the samples. Because the method used to estimate mineral abundances is not normalized to 100 percent, the total mineral abundances do not sum to 100 percent. The average of the total is 96 ± 4 . This low

value suggests that an unidentified phase may be present. The observed mineralogy is consistent with previous measurements of mineral abundances in core samples of Topopah Spring devitrified tuff (Bish and Chipera 1986).

Results of laboratory testing of mineral abundances for samples from the Drift Scale Test block are summarized in Table 3.7-12 (CRWMS M&O 1997g). All samples were from the TSw2 thermal/mechanical unit. The total abundance of the silica polymorphs is fairly uniform, although the cristobalite component varies from 4 to 31 percent, suggesting potential variability in thermal/mechanical properties at the temperatures at which cristobalite undergoes a phase change. In most samples, albite, sanidine, and cristobalite are the dominant phases, with lesser amounts of quartz. Tridymite is significant in three samples, with cristobalite being less abundant in these samples. Zeolite phases were observed in three samples, clinoptilolite in two samples, and stilbite in one sample. Compared to the analyses of samples from the Single Heater Test block (Roberts and Viani 1997b; Viani and Roberts 1996), these samples show similar total silica polymorph content (between 33 and 41 percent). The quartz and cristobalite contents appear to be inversely related. No samples contained detectable mica phases.

Mineral hardness or abrasivity is commonly used to predict rates of Tunnel Boring Machine cutter wear. Measurements of rock abrasivity, such as the Cercher Abrasivity test, have not been performed on YMP rock samples, but abrasivity can be inferred from mineral composition. The Tunnel Boring Machine disc cutter steel has a hardness of approximately 6.5 on the Moh's scale of hardness. Rock with a large percentage of minerals of hardness equal to or exceeding 6.5 would produce faster cutter wear than rock with a smaller percentage of hard minerals. The percentage of quartz, with a Moh's hardness of 7, is typically used for cutter wear prediction. Generally, a quartz content less than 20 percent would indicate low cutter wear, between 20 and 50 percent would indicate significant cutter wear, and greater than 50 percent would indicate high cutter wear. As shown in Tables 3.7-10, 3.7-11, and 3.7.12, the estimated combined percentage of quartz, cristobalite, and tridymite (which also have hardness of 7) was typically between about 15 and 30 percent for borehole NRG-6 and the Single Heater Test samples and between 33 and 40 for the Drift Scale Test samples. Tables 3.7-10, 3.7-11, and 3.7-12 also include percentages of other hard minerals that could affect cutter wear: the feldspars, which have a Moh's hardness of 6; the mafic minerals, which may not be encountered in significant quantities, but can have Moh's hardness near 6.5.

3.7.3.2 Thermal Properties

Data on the thermal properties of rock consists of thermal conductivity, thermal expansion, and heat capacity.

3.7.3.2.1 Thermal Conductivity

Thermal conductivity is a measure of the ability of a material to transmit heat, and so relates to the ability of the host rock to conduct heat away from waste containers. Thus thermal conductivity is an important parameter for numerically simulating the transient temperature field from heat generated by emplaced radioactive waste.

Characterization of the thermal conductivities of Yucca Mountain Tuffs has been ongoing since 1980 (Lappin 1980). Data published through 1988 were reviewed by Nimick (1989), who summarized only data for which supporting documentation was available. These data were unqualified and from boreholes G-1, G-2, GU-3, and G-4. The reports summarized in Nimick (1989) include Lappin et al. (1982), Lappin and Nimick (1985), Nimick and Lappin (1985), and Nimick et al. (1988). Nimick (1990b) presented analyses of data for the welded, devitrified portion of the Topopah Spring Tuff (units TSw1 and TSw2); experimental results for the units overlying and including CHn2 are analyzed in Nimick (1990a). Additional measurements of thermal conductivity were performed on core specimens from Yucca Mountain by Sass et al. (1988) using a needle probe technique. However, the uncertainty in moisture contents for these specimens is discussed in Nimick (1990a).

Data presented in this report were obtained under a fully qualified quality assurance program for 95 specimens from NRG-4, NRG-5, NRG-6, and NRG-7/7A (Brodsky et al. 1997; CRWMS M&O 1997d). These data also are reported in the Civilian Radioactive Waste Management Technical Database under Technical Data Information Form 305179 (TBV). The test method and test results are described and analyzed in detail in Brodsky et al. (1997). In addition, as part of the geological and geotechnical characterization of the Single Heater Test region of the Exploratory Studies Facility Thermal Test Facility, four specimens were tested for thermal conductivity tests in 1996 (CRWMS M&O 1996b). Specimens for these tests were from boreholes drilled into the Single Heater Test region to accommodate placement of the heater and additional instrumentation. These data have been entered into Automated Technical Data Tracking and will be submitted to the Records Processing Center under DTN SNL22080196001.001 (TBV) and Technical Data Information Form 305593 (TBV). All specimens from the Single Heater Test region were from the TSw2 thermal/mechanical unit and the Tptpmn lithostratigraphic unit.

Twenty specimens from the Drift Scale Test block, all from the TSw2 thermal/mechanical unit, were also measured for thermal conductivity. Specimens for these tests were from boreholes drilled into the Observation Drift to accommodate placement of instrumentation. Results and procedures are described in detail in CRWMS M&O (1997f). These data have been entered into Automated Technical Data Tracking and were submitted to the Records Processing Center under DTN SNL22100196001.001 (TBV) and TDIF 306127 (TBV).

Test specimens were right circular cylinders approximately 12.7 mm in length and 50.8 mm in diameter. Moisture contents were either air dry (as received), oven dry, vacuum saturated, or partially saturated (intermediate between air dry and vacuum saturated). Tests were conducted using the guarded heat flow meter over the temperature range of 30 to 300°C. The test specimen was placed between two heater plates controlled at different temperatures, and the heat flow was measured. Radial heat flow losses were minimized using a cylindrical guard heater. The test procedure is given in SNL TP-202, *Measurement of Thermal Conductivity of Geologic Samples by the Guarded-Heat-Flow Meter Method*. The most applicable ASTM standard, one which relies on the same type of measurement equipment, is ASTM F433-77, *Standard Practice for Evaluating Thermal Conductivity of Gasket Materials*. There were no significant differences between the Sandia National Laboratories and ASTM procedures.

Variation of thermal conductivity with saturation for the NRG boreholes is illustrated for thermal/mechanical units for low temperatures (<100°C) in Table 3.7-13. Variations for high

temperatures ($>100^{\circ}\text{C}$) are shown in Table 3.7-14. The data were compiled in this manner rather than for each 25°C interval because thermal conductivity is not strongly temperature dependent. No data were available for tuff rocks in the UO unit, or for an upper portion of the TCw unit (Tpcrv, Tpcrn, Tpcpul, and Tpcmn). Additional thermal conductivity data from the TSw2 unit (Tptpmn) from the Single Heater Test block is shown in Table 3.7-15. These specimens were all tested in the air dried state, that is, in the as-received condition. Results are consistent with results from the specimens from NRG boreholes. Thermal conductivity data from the TSw2 unit in the Drift Scale Test block is presented in Table 3.7-16. The specimens were all tested in the saturated style, and results are also consistent with specimens from NRG boreholes.

Thermal conductivities are lower for dried specimens and highest for saturated specimens. Thermal conductivities, averaged over all boreholes, ranged, depending on temperature and saturation state, from 1.2 to 1.9 W/(mK) for TCw, from 0.4 to 0.9 W/(mK) for PTn, from 1.0 to 1.7 W/(mK) for TSw1 and from 1.5 to 2.3 W/(mK) for TSw2. The data show distinct differences between the nonwelded tuffs of the PTn and the welded tuffs of the TCw, TSw1, and TSw2. PTn consistently shows the lowest conductivities while the TCw and TSw2 units have the highest values. TSw1 specimens span a larger range of thermal conductivities and are intermediate in value.

Evaluation of the mean values in Tables 3.7-13, 3.7-14, 3.7-15, and 3.7-16 indicates that thermal conductivity was affected by saturation and, to a lesser degree, temperature. Thermal conductivity generally increased with increasing saturation and temperature. Sharp increases in thermal conductivity are observed near 100°C for several oven-dried specimens. These increases are as yet unexplained, but may be associated with a change in instrumentation at 100°C or with the vaporization of remaining water. For Exploratory Studies Facility Single Heater Test block specimens, thermal conductivity appeared to increase sharply at 70°C . This response is probably associated with the change in instrumentation at that temperature. At temperatures above 100°C , thermal conductivity shows little temperature dependence. Decreases in conductivity with increasing temperature observed in saturated specimens are attributed to dehydration (Brodsky et al. 1997).

Comparison of qualified data from NRG-4, NRG-5, NRG-6, and NRG-7 and previous unqualified data from USW G-1, USW G-2, USW G-3, and USW G-4 (Nimick 1989) reported by Brodsky et al. (1997) indicates that the two sets of data compare very well for TSw1 and TSw2. For PTn data, the nonqualified values reported by Nimick (1989) are higher by approximately a factor of two than those reported in Brodsky et al. (1997) and CRWMS M&O (1997d). However, Nimick's database for PTn consisted of only two tests from hole USW G-2, which is almost 3 km from the nearest NRG borehole.

The effective thermal diffusivity, or thermal conductivity divided by the product of density and specific heat, of crushed tuff was measured in two qualified bench-scale tests (Ryder et al. 1996). The first test ran approximately 502 hours and the second 237 hours. In each test, a cylindrical volume (1.58 m^3) was filled with crushed tuff particles ranging in size from 12.5 mm to 37.5 mm (0.5 in to 1.5 in) to form an effective porosity of 0.48. Heat was generated by an axial heater. Temperatures near the heater reached 700°C , with a significant volume of material exceeding 100°C . Thermal diffusivity was estimated post-test using three different analysis methods. Estimates of thermal diffusivity were $5.0 \times 10^{-7}\text{ m}^2/\text{s}$ to $6.6 \times 10^{-7}\text{ m}^2/\text{s}$, of the same order of magnitude as the

thermal diffusivity used for crushed backfill in Total System Performance Assessment 1993 (Wilson et al. 1994).

Attempts have been made to correlate thermal conductivity with an easily measured physical property such as porosity as discussed in Rautman and McKenna (1997). The relationship between thermal conductivity and porosity, saturation, and temperature is discussed in several references. Lappin (1980) documents thermal conductivities of the major silicate phases in tuff and also discusses calculation of matrix conductivities from conductivities of components and measured values of porosity and saturation using the Woodside and Messmer (1961) geometric mean approach. A compilation of data is presented in Nimick (1989). Nimick (1990a) introduces use of the Brailsford and Major (1964) equation for calculating matrix thermal conductivity to replace the geometric mean equation used previously by Lappin (1980), and uses the Brailsford and Major (1964) equation for calculation of matrix porosity. Nimick (1990b) summarizes data for 15 samples of Topopah Spring Tuff and estimates matrix conductivities and in situ thermal conductivities for the TSw1 and TSw2 thermal/mechanical units. The data discussed in this paragraph are unqualified.

The porosities of samples adjacent to many of the NRG borehole thermal conductivity test specimens (from the same original piece of core) were determined. Both the geometric mean equation and the Brailsford and Major (1964) equations were investigated, and based on the measured saturation and porosity of each specimen, the matrix conductivity for each specimen was calculated using each model. These matrix conductivities were then averaged for each model to obtain conductivity at zero porosity. The change in conductivity with increasing porosity was then calculated for each model (CRWMS M&O 1997d). Unfortunately, lithologies also change with increasing porosity, and so it is difficult to isolate the effects of changing one variable. An alternative method of viewing the conductivity versus porosity relationship is reported in Brodsky et al. (1997).

3.7.3.2.2 Thermal Expansion

Thermal expansion is the tendency of a material to undergo a nearly proportional degree of volume or length change as a result of a change in temperature. The coefficient of thermal expansion, is usually recorded as a change in strain (linear dimension per unit original length), per °C. The relationship presented by Weast (1974) is:

$$l_t = l_0(1 + \alpha T) \quad (\text{Eq. 3.7-3})$$

where: l_0 = length at 0°C,

l_t = length at T°C, and
 α = coefficient of linear thermal expansion.

Nonqualified thermal expansion measurements on tuffs correlative with those found in the Exploratory Studies Facility are reported in Lappin (1980) for samples from U#25A#1, Well J-13, and G-tunnel; and in Schwartz, B.M. and Chocas (1992) for 109 specimens from UE-25A#1, USW G-1, USW G-2, USW G-4, and USW GU-3. Seventy-eight of the 109 specimens reported by Schwartz, B.M. and Chocas (1992) were tested unconfined, and 31 were tested at nominally 10 MPa confining pressure.

Data discussed in this section were obtained under a fully qualified quality assurance program. Thermal expansion tests were performed on 120 specimens from NRG-4, NRG-5, NRG-7/7A, and SD-12. The unconfined tests (from NRG boreholes) are reported in Brodsky et al. (1997) and were submitted to the Technical Database under Technical Data Information Form 303181 (TBV). Four SD-12 specimens were tested under confined conditions and are reported in Martin et al. (1997). In addition, nine thermal expansion tests were performed in August 1996 as part of the geological and geotechnical characterization of the Single Heater Test part of the Exploratory Studies Facility Thermal Test Facility (CRWMS M&O 1996b). Specimens for these tests were from boreholes drilled to accommodate placement of the heater and additional instrumentation. These data have been entered into Automated Technical Data Tracking and will be submitted to the Records Processing Center under DTN SNL22080196001.001 and Technical Data Information Form 305593 (TBV). All specimens from the Single Heater Test region were from the TSw2 thermal/mechanical unit and the Tptpmn lithostratigraphic unit. Seventeen TSw2 specimens from the Drift Scale Test block were also measured for thermal expansion as part of the ambient, pre-heating characterization program (CRWMS M&O 1997f). These data have been entered into automated Technical Data Tracking and were submitted to the Records Processing Center under DTN SNL22100196001.001 (TBV) and TDIF 306127 (TBV). Because previous work had shown that for welded tuff, moisture content has no appreciable effect on thermal expansion (Brodsky et al. 1997), all specimens were tested in the air dried state. Measurements were taken through two cycles of heating and cooling. Results of in situ determinations of thermal expansion for the Drift Scale Test are discussed in Subsection 3.7.4.2.

Thermal expansion measurements were made using a push rod dilatometer. Test specimens were right circular cylinders approximately 50.8 mm in length and 25.4 mm in diameter. Moisture contents were either air dry (as received), oven dry, or vacuum saturated. Tests were conducted at ambient pressure over the temperature range of 30°C to over 300°C. Temperature was ramped at 1°C per minute. Specimens under saturated conditions were tested up to 100°C. The test procedure is given in SNL TP-203, *Measurement of Thermal Expansion of Geologic Supplies Using a Push Rod Dilatometer*. The closest applicable ASTM standard is ASTM E228-85, *Standard Test Method for Linear Thermal Expansion of Solid Materials With a Vitreous Silica Dilatometer*. This standard describes equipment similar to that used in SNL TP-203. An additional applicable ASTM standard is ASTM D4535-85, *Standard Test Methods for Measurement of Thermal Expansion of Rock Using a Dilatometer*. The procedures given in ASTM E228-85 and SNL TP-203 do not differ significantly.

Temperature and displacement data were obtained throughout a heating and cooling cycle to determine the coefficient of thermal expansion. Coefficients of thermal expansion change with temperature and so calculations were performed over specified temperature intervals. Mean thermal expansion coefficients were calculated over 25°C intervals from data obtained at the endpoints of the interval. Instantaneous coefficients of thermal expansion were calculated from linear least square fits to data contained within 5°C windows spaced 25°C apart. The instantaneous coefficient of thermal expansion data are given in Brodsky et al. (1997).

Mean coefficients of thermal expansion from surface-based borehole specimens are presented by thermal/mechanical unit and saturation in Table 3.7-17 for heating phases and in Table 3.7-18 for cooling phases. Qualified thermal expansion data only exist for the TCw, PTn, TSw1, and TSw2 thermal/mechanical units. The mean thermal expansion coefficient does show some borehole-to-

borehole variation, which is obscured by the data averaging in these tables: complete data are presented in Brodsky et al. (1997). The mean thermal expansion coefficient was highly temperature dependent and ranged, depending upon temperature and saturation state, from $6.6 \times 10^{-6}/^{\circ}\text{C}$ to $50 \times 10^{-6}/^{\circ}\text{C}$ for TCw, from negative values to $16 \times 10^{-6}/^{\circ}\text{C}$ for PTn, from $6.3 \times 10^{-6}/^{\circ}\text{C}$ to $44 \times 10^{-6}/^{\circ}\text{C}$ for TSw1, and from $6.7 \times 10^{-6}/^{\circ}\text{C}$ to $37 \times 10^{-6}/^{\circ}\text{C}$ for TSw2. Data also are summarized by lithostratigraphic unit and are plotted as strain versus temperature in CRWMS M&O (1997d) and Brodsky et al. (1997). Complete data are presented in Brodsky et al. (1997).

Additional data for TSw2 thermal/mechanical unit (Ttpmn) samples from the Single Heater Test region of the Exploratory Studies Facility Thermal Test Facility are presented in Table 3.7-19. The mean thermal expansion coefficients for these samples ranged from 7.5 to $52 \times 10^{-6}/^{\circ}\text{C}$, and as shown, were temperature dependent during the heating cycle. Complete data and analysis are presented in CRWMS M&O (1996b).

Statistical summaries for mean coefficients of thermal expansion for specimens from the Drift Scale Test block are given in Table 3.7-20 for heating and cooling for each of the two cycles. Complete data and analysis are presented in CRWMS M&O (1997f). Single Heater Test and Drift Scale Test values are generally consistent. There is more variability in the Drift Scale Test data, but that study included a much larger sampling volume. Drift Scale Test mean values are consistently higher than those for the Single Heater Test and are generally higher during cooling. However, the mean Single Heater Test values are typically within one standard deviation of the mean Drift Scale Test values.

The data presented in Tables 3.7-17 through 3.7-20 indicate that at a "transition temperature" of 150 to 200°C , the mean thermal expansion coefficient increases more steeply for the welded tuff but decreases for the nonwelded tuff. A transition is expected in the welded devitrified specimens due to phase changes in tridymite and cristobalite. These minerals occur, with or without quartz, as primary devitrification products in many samples of Yucca Mountain welded tuffs. Phase transitions in synthetic tridymite occur at approximately 117 and 163°C , and in synthetic cristobalite at approximately 272°C (Papike and Cameron 1976), and involve notable changes in volume. Phase transition temperatures have been shown to vary significantly due to lattice variations found in natural occurrences of these minerals which are usually mixed phase material (Thompson and Wennemer 1979). Previous and current work on the mineralogy of welded tuff from TCw, TSw1, TSw2, and TSw3, suggest that these mixed phase assemblages are dominant. Hysteresis is associated with the phase changes because the phases invert at higher temperature during heating than during cooling (Brodsky et al. 1997).

Some specimens that displayed sensitivity to transition temperature were analyzed to assess the role of the maximum test temperature. Specimens from approximately the same depth and same borehole were tested to different temperatures. The results showed that as long as the maximum test temperature remained below the transition temperature, the specimens did not permanently change dimension (Brodsky et al. 1997).

The sharp increase in mean coefficients of thermal expansion beginning at approximately 200°C in welded tuffs is not attributed to thermally induced fracturing or differential expansion, since these behaviors would not be significant during the second heating phase, and the Drift Scale Test test data indicate sharp increases for both cycles. Three specimens from the Drift Scale Test suite of tests did

not show the increase in mean coefficients of thermal expansion at elevated temperature. Two of these specimens appeared to initiate phase changes below 200°C, and one specimen appeared to undergo essentially no phase change. This difference in behavior is attributed to different concentrations of cristobalite and tridymite. Details are presented in CRWMS M&O 1997g.

Thermal expansion was independent of saturation state for welded specimens but did depend on saturation state for the nonwelded specimens. Nonwelded specimens with high moisture contents contracted during testing near 100°C, causing a temporary sharp decrease in mean thermal expansion coefficient at approximately 100°C. This is presumed to be due to reduction of pore water and dehydration of hydrated glass. However, there is insufficient information to determine a mechanism for the shrinkage. The expansion characteristics of the welded specimens, on the other hand, seemed to be independent of saturation state, and the curves for different saturation states are similar (Brodsky et al. 1997).

A suite of confined thermal expansion tests was conducted to determine if strain hysteresis and transition temperature effects would be suppressed by elevated confining pressures. These test results are discussed in detail in Martin et al. (1997). Confining pressure effects for specimens tested between 1 and 30 MPa were very small (Martin et al. 1997), and so data from these pressures were averaged together and compared with data from unconfined tests. At temperatures below approximately 150°C, the coefficient of thermal expansion is slightly lower for unconfined tests than for confined tests. However, at higher temperatures (150 to 250°C), the mean values approach one another and the scatter among the unconfined tests encompasses the results for the confined tests. Over the higher temperature range, coefficients of thermal expansion therefore appear to be independent of confining pressure.

The effect of specimen size was investigated in a nonqualified study using samples from Busted Butte and from boreholes USW G-1, USW G-2, USW GU-3, and USW G-4. Plots of these data are located in the Sandia National Laboratories Participant Data Archive. The original test data were obtained under a qualified YMP quality assurance program, and the test data included five sets of tests that illustrate size effects. For all depths except the Tax unit sampled in USW G-2, mean thermal expansion coefficients are higher for small specimens than for large specimens. However, the difference in mean values is always within the error in the measurement or within one standard deviation of the mean, and data were insufficient to formulate conclusions about size effect.

The correlation between thermal properties and mineralogy was very poor but may be explained in several ways. First, the data set is very limited. Second, the mineralogical analyses were not performed on the test specimens themselves, but on pieces of rock taken from near the test specimens. Third, hysteresis in the thermal expansion data may be influenced by other rock properties besides mineralogy, such as lithophysae content, and a larger database and further analyses would be required to separate the influences of each of these variables (Brodsky et al. 1997).

3.7.3.2.3 Heat Capacity

Heat capacity is the amount of heat required to change the temperature of a substance by a given amount. It is defined (Halliday and Resnick 1974) as:

$$H = \frac{\Delta J}{\Delta T} \quad (\text{Eq. 3.7-4})$$

where ΔJ = Quantity of heat (J) and
 ΔT = Change in temperature (K)

The database for heat capacity measurements consists of theoretical values calculated by Nimick and Connolly (1991) from chemical and mineralogical data, and experimental values reported in Brodsky et al. (1997).

Bulk chemical analyses of 20 tuff samples from Yucca Mountain were used to calculate heat capacities of the solid components of the tuffs as a function of temperature. The data were combined with grain density, matrix porosity, lithophysal-cavity abundance, mineral abundance, in situ saturation, and the properties of water to estimate rock-mass thermal capacitances. Calculations were completed for nine thermal/mechanical units (TCw, PTn, TSw1, TSw2, TSw3, CHn2V, CHn1z, and CHn2z) over the temperature range of 25 to 275°C. Summary mineralogic and chemical data are reported in Connolly and Nimick (1990) and thermal capacitance calculations and results are given in Nimick and Connolly (1991). Data for TSw1 and TSw2 are presented later in this section in comparison with experimentally determined values. These calculations and data are unqualified.

Heat capacity was measured for 10 air-dried specimens from UE-25 NRG-4 and UE-25 NRG-5. The test method and test results are described and analyzed in detail in Brodsky et al. (1997). These data from the NRG boreholes were all obtained under a qualified quality assurance program.

Test specimens were air-dried right circular cylinders approximately 57.0 mm in length and 50.8 mm in diameter. Tests were conducted over the temperature range of 30 to 300°C using an adiabatic pulse calorimeter. This instrument applies a known quantity of electrical energy to a specimen and measures the resulting rise in specimen temperature. The test procedure is presented in SNL-TP-204, *Measurement of Specific Heat of Geologic Samples by Adiabatic Pulse Calorimetry*. The closest applicable ASTM procedure is ASTM D4611, *Standard Practice for Specific Heat of Rock and Soil*. This standard is based on the drop calorimetry and provides less accurate results than the adiabatic calorimeter method given in TP-204.

Thermal capacitance, which is heat capacity multiplied by specimen density, is summarized in Table 3.7-21 and plotted in Figure 3.7-9 along with data from Nimick and Connolly (1991). A complete data presentation is included in Brodsky et al. (1997) and CRWMS M&O (1997d). Thermal capacitance is higher for TSw2 than for TSw1. Mean thermal capacitance ranges from 1.6 J cm⁻³·K⁻¹ to 2.1 J cm⁻³·K⁻¹ for TSw1 and from 1.8 J cm⁻³·K⁻¹ to 2.5 J cm⁻³·K⁻¹ for TSw2 (Table 3.7-21).

Experimentally determined values of heat capacity increased with temperature, reaching a localized peak of 2.4 and 2.1 J/ccK at approximately 150°C to 170°C for the TSw1 and TSw2 units, respectively. This peak may be related to a phase change. However, the data presented here were insufficient to correlate peaks more specifically. The peaks in specific heat at these temperatures do occur at a temperature range associated with the phase change in tridymite (163°C). It also is evident that there were no significant changes in measured specific heat for these air-dried specimens at 100°C, indicating that dehydration effects were minor (Brodsky et al. 1997).

Values of thermal capacitance calculated by Nimick and Connolly (1991) from chemical and mineralogical data are given in Figure 3.7-9 along with the experimental data. For both the theoretical and experimental data, values for TSw2 are higher than for TSw1. The theoretical data show a decrease at 100°C due to the heat of vaporization of water. The test specimens were air dried and showed no comparable decrease. The two sets of data roughly coincide. However, it should be noted that without the decrease at 100°C in the calculated data, the discrepancy between measured and calculated values for TSw1 would be maintained.

3.7.3.3 Mechanical Properties

A comprehensive series of mechanical property measurements was conducted on specimens prepared from cores recovered from NRG and SD boreholes. The measurements included elastic constants, strength, and deformation moduli for specimens from all thermal/mechanical units. One objective of the measurements was to establish a baseline set of properties, to study the vertical and lateral variability of bulk and mechanical properties at Yucca Mountain. Boyd, Price et al. (1996a) noted there was little lateral variability among the NRG boreholes along the axis of the North Ramp as determined from the NRG borehole series. However, there is significant vertical variability due to large differences in lithology, and smaller differences in smaller scale fabric and pore structure characteristics.

Tests were performed on specimens of tuff prepared from cores recovered from NRG and SD boreholes. All data reported were collected under a qualified quality assurance program. The size of the specimen required for each type of measurement was important in the selection of appropriate samples for testing. The other key factor in sample selection was the absence of fractures and large lithophysae, greater than about one centimeter, which could impact test results.

Additional laboratory testing of mechanical properties was performed on 22 samples from the Single Heater Test block of the Exploratory Studies Facility Thermal Test Facility to characterize the area's intact rock properties. Testing and results are described in detail in CRWMS M&O (1996b). Unconfined compression tests were also performed on 16 specimens from the TSw2 thermal/mechanical unit from boreholes in the Drift Scale Test block. Details are presented in CRWMS M&O (1997d).

3.7.3.3.1 Static and Dynamic Elastic Constants

Young's modulus and Poisson's ratio are the primary mechanical deformation indices of rock and are indicators of the elastic response of the rock to stress. Static Young's modulus and Poisson's ratio were computed from the stress-strain data obtained for the specimens tested in confined and

unconfined compression. In addition, dynamic elastic moduli were computed from compressional and shear wave velocities measured under ambient laboratory conditions.

Test procedures for confined and unconfined compression are discussed in the following sections. The test procedure for compressional and shear wave velocity measurements involved measurement of ultrasonic compressional and shear wave velocities both parallel and normal to the core axis of the test specimen. One compressional and two orthogonally polarized shear waves were measured parallel to the axis. One compressional and one polarized shear wave with a vibration direction parallel to the core axis were measured in the radial direction. These data were used to compute the elastic anisotropy of the specimen. In addition, the compressional and shear wave velocity, combined with specimen density, were used to compute dynamic Young's modulus and Poisson's ratio. Details of the test procedure used for the ultrasonic compressional and shear wave velocity measurements are given in Martin et al. (1994).

Detailed results of experiments conducted on specimens from cores recovered from boreholes UE-25 NRG-2, UE-25 NRG-3, UE-25 NRG-4, UE-25 NRG-5, USW NRG-6, and USW NRG-7/7A are presented in Martin et al. (1994), Martin et al. (1995), and Boyd, Price et al. (1996a, 1996b). Tables 3.7-22 and 3.7-23 list the mean and standard deviation of static Young's modulus (elastic modulus) and Poisson's ratio for thermal/mechanical units and for individual lithostratigraphic units. In general, the Young's modulus of the tuff depends on welding. Nonwelded tuff is weak and exhibits low Young's moduli. In contrast, the welded tuffs are stronger and exhibit significantly greater Young's moduli. In borehole NRG-6, for example, the moduli range from less than 1 GPa for the nonwelded units to near 40 GPa for the welded units. The greatest moduli are observed for specimens recovered from units TCw and TSw2. The Young's moduli observed on specimens from TSw1 are somewhat lower than those for the other welded units. The standard deviation in the Young's moduli for each thermal/mechanical unit is large. Specimens separated by very small vertical distances, having nominally the same texture and composition, exhibited large changes in moduli (CRWMS M&O 1997d).

For specimens from the TSw2 thermal/mechanical unit in the Single Heater Test block of the Exploratory Studies Facility Thermal Test Facility, elastic constants calculated from unconfined compression tests were fairly consistent, with a mean Young's modulus of 32.4 GPa and a mean Poisson's ratio of 0.17. Complete test results and analysis are presented in CRWMS M&O (1996b).

Elastic constants calculated from unconfined compression tests on specimens from the TSw2 thermal/mechanical unit (Tptpmn lithostratigraphic unit) in the Drift Scale Test block were slightly higher than values from the Single Heater Test block, but generally consistent with values from NRG borehole samples. The mean Young's modulus was 36.8 GPa and the mean Poisson's ratio 0.201. Standard deviations for both constants were slightly smaller than either of the other two test suites. Complete results and analysis are presented in CRWMS M&O (1997f).

Dynamic Young's moduli were computed from the velocity and density data. Dynamic moduli exceed static moduli. In general, the ratio of dynamic to static moduli is less than two; the difference is greatest at lower moduli, and decreases as the moduli increase.

Compressional and shear wave velocities were measured in the dry and in the saturated condition on each specimen tested in unconfined and confined compression. Table 3.7-24 presents a summary of the velocities measured for wave propagation parallel to the axis of the dry specimens. The compressional and shear wave velocities are greatest in the TCw and TSw2 welded units, and lowest in the nonwelded PTn units (CRWMS M&O 1997d). The compressional wave velocity increases with saturation, and the shear wave velocity decreases. These effects are consistent with theoretical models of seismic waves in porous media.

The elastic anisotropies of specimens tested in unconfined and confined compression were calculated from the ultrasonic velocity data. The anisotropy ranges from less than 5 to 15 percent. Of the densely welded units, the TSw1 unit exhibited the largest anisotropy, probably due to the presence of oriented lithophysae and vapor-phase altered zones.

3.7.3.3.2 Compressive Strength

Compressive strength of a rock is its ability to withstand compressive stress without failure. Compressive strength of intact rock is measured in the laboratory by subjecting a cylindrical test piece to a compressive load parallel to its axis until it fails. Compressive strength is the maximum stress at failure and is computed from the maximum load and the cross-sectional area of the test piece. Confined (or triaxial) compressive strength is determined by subjecting the cylindrical test specimen to a uniform lateral confining pressure in addition to the axial load.

3.7.3.3.3 Unconfined Compressive Strength

Unconfined compressive strength of a wide range of tuff samples from the Yucca Mountain area have been measured and reported by a number of workers (Olsson and Jones 1980; Olsson 1982; Price, R.H. and Jones 1982; Price, R.H. and Nimick 1982; Price, R.H., Jones et al. 1982; Price, R.H., Nimick et al. 1982; Price, R.H. 1983; Price, R.H., Spence et al. 1984; Nimick et al. 1985). Compressive strengths of the various units of the Paintbrush Group from the USW G-1 to G-4 borehole series are given in R.H. Price, Nimick et al. (1985).

For unconfined compression tests described in Brechtel et al. (1995), Kicker et al. (1996), and CRWMS M&O (1997d), ground, right-circular cylindrical specimens of tuff were tested to failure at a constant strain rate of 10^{-5} s⁻¹ under ambient temperature and pressure conditions. Nominal specimen size was 101.6 mm in length and 50.8 mm in diameter. The specimens were saturated with distilled water. Testing was accomplished following the procedures in ASTM D3148, *Standard Test Method for Elastic Moduli of Intact Rock Core Specimens in Uniaxial Compression*, and International Society of Rock Mechanics procedure, *Suggested Methods for Determining Uniaxial Compressive Strength and Deformability of Rock Materials* (Brown, E.T. 1981). Static Young's modulus and Poisson's ratio were computed by performing linear least-squares fits to the stress and strain data collected between 10 and 50 percent of the fracture strength. The reported fracture strength was the maximum stress exerted on the specimen.

Results of unconfined compression tests on specimens from NRG and SD boreholes indicate that the unconfined compressive strengths vary depending on the welding, porosity, and fabric of the rock. Welded tuffs exhibited higher strengths than nonwelded tuffs. Within the welded units, the

variations in strengths are related to the presence and size of lithophysae and vapor-phase altered zones. Table 3.7-25 compares the mean and standard deviation of uniaxial compressive strength for thermal/mechanical units and individual lithostratigraphic units. The data are described in greater detail in CRWMS M&O (1997d).

The modes of fracture in most of the unconfined compression tests were very similar. In most cases, the fractures terminated in the endcaps of the specimens. There often was no evidence of shear cone development in the specimens.

Specimens from TCw typically exhibit the greatest strengths: strengths in excess of 300 MPa are observed for this unit. In contrast, the weakest specimens are from the PTn unit, with strengths generally less than 10 MPa. Large variability is observed for TSw1 and TSw2. The strengths for these units vary from 25 to 250 MPa and show no consistent trend between strength and depth.

In most cases, very little inelastic volumetric strain (dilatancy) is observed in data on the welded TCw, TSw1, and TSw2 tuffs (CRWMS M&O 1997d). Many crystalline rocks begin to dilate at stresses as low as 50 percent of the fracture strength. However, in the welded tuffs, little nonlinearity in the volumetric strain is observed until the specimens are very near failure. The manner in which cracks grow and interact in tuff appears different from that observed in other crystalline rocks in which microcrack porosity is dominant. The data suggest that axial cracks extend without interacting with other cracks until failure is imminent. Similar effects also have been reported by Brace et al. (1966) and Scholz (1968).

Results of unconfined compression tests on TSw2 samples from the Single Heater Test block of the Exploratory Studies Facility Thermal Test Facility (CRWMS M&O 1996b) showed a large scatter in strengths similar to that observed in other testing of Yucca Mountain Tuffs (Brechtel et al. 1995; CRWMS M&O 1997d). Unconfined compressive strengths ranged from 75.1 to 243.8 MPa, with a mean of 143.2 MPa and a standard deviation of ± 50.3 MPa (CRWMS M&O 1996b). Moisture contents for these specimens were not controlled and differences in moisture contents may have contributed to the scatter in strengths. The mode of failure for all specimens was dominated by brittle axial cracking. There was no correlation between strength and mode of failure, and all of the specimens failed explosively (CRWMS M&O 1996b).

Results of unconfined compression tests on 16 samples from the TSw2 thermal/mechanical unit (Tptpmn lithostratigraphic unit) from the Drift Scale Test block of the Exploratory Studies Facility also showed a large scatter in strengths. Complete data and analysis are presented in CRWMS M&O (1997f). Strengths ranged from 71.3 to 324.1 MPa, with a mean value of 176.4 MPa and a standard deviation of ± 66 MPa. The highest and lowest strengths were obtained on specimens that were in relatively close proximity, only 4 m apart. Neither of these two specimens had notable surface features that might predict anomalous behavior. The mean unconfined compressive strength value from the Drift Scale Test block, like the mean values of Young's modulus and Poisson's ratio, is higher than the mean values obtained for samples from the Single Heater Test block. This difference is believed to be at least partly attributable to minor differences in the testing program, although it may be indicative of spatial variability within the Thermal Testing Facility of the Exploratory Studies Facility (CRWMS M&O 1997f).

3.7.3.3.4 Confined Compressive Strength

Confined compression experiments were carried out on cores with a length to diameter ratio of two and nominal diameters of 25.4 or 50.8 mm (Brechtel et al. 1995; Kicker et al. 1996; CRWMS M&O 1997d). All specimens were tested saturated, in a drained condition. The general procedure for testing the specimens was the same as for the unconfined compression tests, except that the specimens were jacketed in copper and deformed in a pressure vessel at a fixed confining pressure. The procedure used for the measurements generally conformed to International Society of Rock Mechanics, *Suggested Methods for Determining the Strength of Rock Materials in Triaxial Compression* (Brown, E.T. 1981) and ASTM D2664-86, *Standard Test Method for Triaxial Compressive Strength of Undrained Rock Core Specimens Without Pore Pressure Measurements*. Deviations from these procedures are discussed in CRWMS M&O (1997d). Measurements were performed at confining pressures of 5 and 10 MPa, and pressure was held constant to ± 0.1 MPa. The instrumented specimens were monotonically loaded to failure at a nominal strain rate of 10^{-5} s $^{-1}$. Young's modulus and Poisson's ratio were computed between 10 and 50 percent of the stress difference at failure. Results of confined compression tests indicate that the axial stress difference at failure increases with increasing confining pressure. Strength parameters calculated from confined compression test results are listed in Table 3.7-26. The specimens tested in confined compression failed in shear; that is, the fractures formed on shear planes with little evidence of axial splitting. In most cases, a visibly evident shear plane developed. However, there was no evidence of conjugate fracture sets forming in any of the specimens.

To examine effects of temperature, seventeen confined compression experiments were also performed at a nominal temperature of 150°C on specimens recovered from borehole USW SD-9 (CRWMS M&O 1997d). All of the measurements were conducted on specimens from thermal/mechanical unit TSw2. Measurements were conducted at effective confining pressures of 1, 5, and 10 MPa, with a pore pressure of 5 MPa. The experiments were performed at a nominal strain rate of 10^{-6} s $^{-1}$. The confining pressure was held constant to ± 0.25 MPa, and the pore pressure was maintained constant at 5.00 ± 0.25 MPa. The elevated temperature was generated by means of band heaters positioned on the outside of the pressure vessel. The temperature was monitored inside the pressure vessel with a thermocouple positioned at the midpoint of the specimen.

The high temperature confined compression test data indicated a clear increase in strength between 1 MPa and 5 MPa (CRWMS M&O 1997d). However, there was no apparent increase in the mean strength of the tuff between 5 and 10 MPa confining pressure. Comparison of room and elevated temperature (150°C) tests suggested that the effect of temperature on the strength of welded tuff from thermal/mechanical units TSw2 was small. Similarly, Young's modulus and Poisson's ratio measured at elevated temperatures (150°C) were not significantly different from those measured at room temperature.

The heterogeneity in the tuff poses a problem in analyzing the effect of pressure on the strength in terms of a Mohr-Coulomb criteria. As seen with the unconfined compression test data, the strengths may vary by as much as a factor of two, even over a limited depth interval. Without a suite of nominally identical specimens, a Mohr-Coulomb failure envelope is difficult to establish. Data are judged to be incomplete for the PTn and CHn1 units.

3.7.3.3.5 Tensile Strength

Indirect tensile strength tests, commonly referred to as Brazilian tests, were carried out using a procedure adhering to ASTM D3967, *Standard Test Method for Splitting Tensile Strength of Intact Rock Core Specimens*. The test is simple in principle. A load is applied to a cylindrical specimen with its axis normal to the loading direction. Tensile stress develops in the center of the cylinder. The force is increased until the specimen fails by an extension fracture along the diametral loading plane. The tensile strength is computed from the force at failure.

Indirect tensile strength tests were performed on specimens from boreholes NRG-2, UE-25 NRG-3, UE-25 NRG-4, USW NRG-6, and USW NRG-7/7A (Brechtel et al. 1995; CRWMS M&O 1997d). Nominal specimen size was 38.1 mm in length and 50.8 mm in diameter. Results are summarized in Table 3.7-27 and presented in greater detail in CRWMS M&O (1997d).

Tensile strengths generally range from between 0.2 and 16 MPa. The weakest specimens are from the nonwelded PTn thermal/mechanical unit. The greatest strengths are observed in the TCw welded tuff. In general, TSw1 is weaker than TSw2. However, there is significant scatter in TSw2 data.

3.7.3.3.6 Shear Strength

Mathematical simulation of the response of rock to mining and drilling requires the use of failure criteria for the rock. One commonly used criteria is the Mohr-Coulomb criterion, which defines the limiting state of stress for static equilibrium with the material at which inelastic deformation begins (Jaeger and Cook 1979). The criteria itself is expressed as follows:

$$\tau = C_0 + \sigma \tan \phi \quad (\text{Eq. 3.7-5})$$

where: τ = shear stress on the failure plane at the onset of failure
 σ = normal stress on the failure plane at the onset of failure
 C_0 = cohesion
 ϕ = angle of internal friction

The shear stress at the onset of failure is also the shear strength of rock, which is defined by its two components, cohesion (C_0) and angle of internal friction (ϕ). Results of unconfined compressive tests and triaxial (confined) compression tests can be used to determine τ and ϕ . As noted in the discussion of compression test results, above, because of the heterogeneity in the tuff, it is difficult to establish a Mohr-Coulomb failure envelope without a suite of nominally identical specimens. Subsection 3.7.4.3 discusses the use of rock mass indices to estimate in situ strength parameters.

3.7.3.3.7 Time-Dependent (Creep) Behavior

If a solid is subjected to a load (stress) within its elastic limit, it instantaneously experiences an amount of deformation (strain), which disappears on the removal of the load. If the load is

maintained at the same level, the solid will continue to deform beyond the instantaneous deformation at a slow rate depending on the level of the applied stress. This continuing deformation with time in spite of no increase in stress is referred to as time-dependent deformation or creep deformation.

Seven creep experiments were performed on right circular cylinders of TSw2 tuff recovered from borehole NRG-77A (CRWMS M&O 1997d). The specimens had a length to diameter ratio of two and a specimen diameter of 50.8 mm. The experiments were performed at a constant confining pressure of 10 MPa and a temperature of 225°C. The procedure used for these measurements was based on ASTM D4406, *Standard Test Method for Creep of Cylindrical Rock Core Specimens in Triaxial Compression*. Measurements were carried out in a compact creep apparatus, described by Martin et al. (1995). The key features of the system included independent controls for the confining pressure, pore pressure, temperature, and axial force producing the differential stress on the sample. Loading continued under constant temperature, differential stress, and confining pressure until the sample failed or the experiment was terminated. The procedure is described in detail in CRWMS M&O (1997d).

Results of creep measurements on specimens from the TSw2 thermal/mechanical unit (Tptpmn lithostratigraphic unit) are presented in Table 3.7-28. The experiments were conducted at nominal differential stresses of 40, 70, 100, and 130 MPa, at a fixed confining pressure of 10 MPa, and at a temperature of 225°C. The duration of the experiments ranged from 2.55×10^6 s to 5.90×10^6 s (30 to 68 days). At higher stress differences, the data show very small increases in the axial strain. The experiments conducted at stress differences between 40 and 100 MPa show smaller strain accumulations, and for the test conducted at a differential stress of 40 MPa, no strain accumulation was observed. Each test was terminated before failure of the specimen.

3.7.3.3.8 Hardness

Schmidt hammer rebound hardness measurements were conducted on samples from the NRG holes to produce early strength estimates and to supplement the rock mechanics test data. The measurements were performed following International Society of Rock Mechanics suggested methods (Brown 1981) and the analysis of the results incorporates suggested improvements to the International Society of Rock Mechanics methods by Goktan and Ayday (1993). Pieces of core were selected on nominal 3 m (10 feet) intervals down hole and clamped in a testing anvil weighing a minimum of 20 kg (44.1 lbs). A group of 20 rebound hardness measurements were then conducted. The data are presented in detail in Brechtel et al. (1995).

Results of Schmidt hammer measurements are summarized in Table 3.7-29.

3.7.3.3.9 Correlations and Parametric Effects for Mechanical Properties

Anisotropy—In general, rock properties often depend on the direction of measurement relative to such characteristics as bedding, schistosity, and dominant orientation of layered silicate minerals. Elastic anisotropy of specimens tested in confined and unconfined compression was calculated from ultrasonic velocity data. The anisotropy ranges from less than 5 to 15 percent. The TSw1 thermal/mechanical unit exhibited the largest anisotropy, probably due to the presence of oriented lithophysae and vapor-phase altered zones. R.H. Price, Spence et al. (1984) found that dynamic

elastic moduli for samples of the densely welded Topopah Spring member from borehole USW GU-3 showed that anisotropy of elastic properties for orientations parallel and perpendicular to the rock fabric is insignificant.

Lithophysae—The units of the Topopah Spring Tuff do contain varying amounts of lithophysae. Lithophysae are described in greater detail in Subsection 3.5, Site Stratigraphy. These are generally spherical to sometimes slightly flattened cavities of up to several tens of centimeters in diameter. The lithophysal cavities often have on their inner wall a thin layer of feldspars, silica minerals, and other vapor-phase mineral deposits (see Figure 3.5-8). The functional porosity, which is the total of lithophysal pore volume, nonlithophysal pore volume, and volume of clay minerals, has been related by Price, R.H. and Bauer (1985) to Young's modulus and unconfined compressive strength.

Porosity—The vertical variability in the elastic and strength properties of the tuffs at Yucca Mountain is large. Even considering the data within thermal/mechanical units, the scatter for each property is large. Variations of a factor of two or more are common. Price, R.H. and Bauer (1985) sorted the elastic and fracture properties of tuff according to porosity in an attempt to compare specimens with similar properties. They observed a good correlation between modulus and porosity. However, there is still significant scatter in the moduli even for similar samples with nearly identical porosities. In spite of the apparent correlation of modulus with porosity for porosities between 8 and 60 percent, it is still difficult to predict modulus based on porosity data (CRWMS M&O 1997d).

A similar correlation exists between ultrasonic wave velocities and porosity. Based on data collected on NRG and SD specimens, compressional and shear wave velocities decrease with increasing porosity, (CRWMS M&O 1997d). However, as with Young's modulus, at each porosity there is large scatter in the measured velocities.

The distribution of strengths observed in unconfined compression tests similarly correlates with porosity, (CRWMS M&O 1997d). As with the elastic properties, the strength decreases with increasing porosity and there is substantial scatter at each porosity. Even within a very narrow range of porosities, and presumably similar composition and distribution of lithophysae and vapor-phase altered zones, the variability in strength is large. Most of this scatter has been attributed to differences in pore distribution (Price, R.H., Martin et al. 1993).

Temperature Effects—The effect of temperature on the TSw2 welded tuff produced somewhat conflicting results (CRWMS M&O 1997d). The application of moderate confining pressure (5 or 10 MPa) resulted in a significant increase in the stress difference at failure. However, comparing data collected at ambient temperature with those at elevated temperature at very low confining pressures indicates that the effect of temperature on strength is small. More data are needed to assess the influence of temperature on strength.

Effect of Sampling on Parametric Studies—The current data set does not adequately isolate parametric effects such as temperature, pressure, and saturation because of the large variability in properties between lithologic units and within lithologic units (CRWMS M&O 1997d). Samples were selected to characterize vertical variability within the thermal/mechanical units. Comparisons were made with samples from different depths in the boreholes, and attempts were made to group properties to define how temperature and confining pressure influence behavior in a specific rock

unit. However, variability between samples may be greater than the parametric effect being investigated.

The data have not been evaluated against the requirements for design and performance assessment and there may be some omissions in the current data set. For example, no confined strength measurements are available for nonwelded tuff units. However, in general, the parametric effects have been investigated in both welded tuffs and nonwelded tuffs.

Scaling Intact Properties—Scaling of baseline data on intact rock properties for site and time may be important for modeling approaches that do not assume an equivalent continuum. In this case, the intact properties of rock blocks between fractures represent an intermediate size between the rock mass and the lab sample. Scaling laws need to be developed based on the requirements of design and performance assessment modeling approaches.

Two important parameters for scaling intact properties are the volume of the rock and the time duration of the applied stress at elevated temperature. R.H. Price (1986) studied the effect of sample size on the unconfined compressive strength and elastic moduli of welded tuff in a nonqualified study conducted on TSw2 welded specimens recovered from Busted Butte, adjacent to Yucca Mountain. The data show a decrease of more than a factor of two in compressive strength as the specimen diameter increases from 25.4 mm to 228.6 mm.

The data pertaining to time dependence reveal an inconsistency. The nonqualified study of strain rate dependence for Busted Butte specimens shows that subcritical crack propagation substantially affects failure strengths. However, failure strengths for SD-12 specimens at room temperature were not different from those of SD-9 at 150°C. Subcritical crack propagation is a thermally activated process and so, if strain rate dependence is observed, it is expected that some temperature dependence also would be observed.

3.7.3.3.10 Mechanical Properties of Fractures

Discontinuities such as joints, bedding planes, faults, and fractures cause the properties of a rock mass in situ to be different from those of intact rock tested in the laboratory. In general, strength and deformational properties of the rock mass will be lower than those measured in the laboratory. An understanding of the mechanical properties of discontinuities is necessary to evaluate their effect on rock mass properties.

Most rock masses contain natural fractures that are called joints if they show little or no visible offset. The presence of these features in the rock mass has important effects on the overall thermal/mechanical and hydro/mechanical response of the rock mass. They can increase the compliance, reduce the strength, alter the thermal conductivity, and act as pathways for fluid movement. Because of their potential importance in design and performance assessment, fracture properties such as normal stiffness, shear stiffness, cohesion, and coefficient of friction are important.

Natural fractures from boreholes UE-25 NRG-4, USW NRG-6, USW NRG-7, USW SD-9, and USW SD-12 were tested for stiffness and strength. Tests are reported in Olsson and Brown (1994,

1995, 1997). These studies used the rotary shear technique for measuring fracture stiffness and shear strength. This technique has been used for at least 20 years and has certain advantages over other configurations for shear testing. Details on implementation of this test technique, along with discussions of its relative advantages and disadvantages and many important results, can be found in a number of papers (Biegel et al. 1992; Christensen et al. 1974; Kutter 1974; Olsson 1987, 1988; Olsson and Brown 1993; Xu and de Frietas 1988; Tullis and Weeks 1986; Weeks, J.D. and Tullis 1985; Yoshioka and Scholz 1989).

In the rotary shear tests, the specimens were composed of two short, hollow tubes of rock that were divided at mid-height by the fracture to be tested. Specimens were prepared from the as-received core by subcoring perpendicular to the fracture. Outer specimen diameters ranged from 44.3 to 82.0 mm (1.74 to 3.22 inches). Test specimens were potted into metal specimen holders with gypsum cement. The metal specimen holders were then bolted into the load-frame. Stress was applied normal to the fracture while the change in fracture aperture was measured with linear variable differential transformers. Torque was then applied to cause sliding on the interface, and shear displacements and shear strength were measured. All samples were sheared at constant normal stress at room temperature and in the air-dry condition. Further details may be found in Olsson (1987), and Olsson and Brown (1997).

For each test, Olsson and Brown (1994, 1995, 1997) reported the normal stress, shear and normal stiffness functions, shear strength, residual shear strength, and dilation angle at peak shear stress. Also, the friction angle, ϕ , and cohesion, C , were reported for each of four thermal/mechanical units. Data are summarized in Tables 3.7-30, 3.7-31, and 3.7-32.

The normal stiffness for Yucca Mountain fractures increases with increasing normal stress, as is typical for interfaces of any type (Olsson and Brown 1994, 1995). However, there is wide variability from fracture to fracture, which is indicated by the large standard deviations in Table 3.7-32. The coefficient of friction seems to be slightly greater for TSw2 than for TSw1, but the one standard deviation band includes essentially all the other values. The small number of tests conducted on TCw and CHn1 do not provide assurance that the data are representative.

There are too few data to draw quantitative conclusions about fracture strengths for TCw and CHn1. For TSw1 and TSw2, where there are more data, the friction angle, expressed as $\tan \phi$, seems to be slightly greater for TSw2 than for TSw1, $0.87 (\phi = 41^\circ) \pm 0.09$ versus $0.77 (\phi = 38^\circ) \pm 0.08$, respectively. The roughness characteristics of the fracture surfaces agree qualitatively with the simple mathematical model of S.R. Brown (1995) derived from fracture data in many other rock types.

3.7.4 Rock Mass Properties

Analyses to support the design of the repository are required to address the potential impacts of seismic, thermal, and mechanical loading. These analyses require knowledge of rock properties at the rock mass scale as inputs. Mechanical properties are known to be very different for strong, jointed, in situ rock masses than for small, intact samples tested in the laboratory. These differences are termed "scale effects" and are attributed to the influence of the size of the rock mass affected and to inhomogeneities such as jointing.

In situ thermal testing is being conducted at the Thermal Test Facility of the Exploratory Studies Facility to better understand rock mass behavior and the coupled thermal, mechanical, hydrological, and chemical processes that may occur due to emplacement of nuclear waste in the rock mass of the potential repository. The Exploratory Studies Facility Thermal Test comprises a Single Heater Test and a long-term Drift Scale Test. Pre-heating characterization studies (CRWMS M&O 1996b; CRWMS M&O 1997f) and early data and analysis from the Single Heater Test (CRWMS 1997g) have contributed significantly to the understanding of rock mass behavior. The Single Heater Test was initiated in August 1996. The heater was deactivated in May 1997, and monitoring continued for an additional nine months during the cool-down period. The Drift Scale Test was initiated in December 1997; test data are not yet available.

For the Single Heater Test, instrumentation was installed within and on the rock mass encompassed by the test block to record measurements during both the heating and cool-down periods. Thermomechanical measurements included temperature measurements using thermocouples, resistance temperature devices, and thermistors. Mechanical instrumentation included multiple-point borehole extensometers, tape extensometers, surface-mounted wire extensometers, load cells on rock bolts, and an NX borehole jack. Additional instrumentation was installed to measure hydrological and chemical properties.

3.7.4.1 Rock Mass Classification

Rock mass quality data were collected in preconstruction exploration boreholes and in the Exploratory Studies Facility. The rock mass quality system (Barton et al. 1974) and the rock mass rating system (Bieniawski 1979) were employed in Exploratory Studies Facility construction activities as the basis of empirical design of excavation ground support and empirical correlation with rock mass properties. These two indices are rock classification methods that consider characteristics of the rock mass such as the degree of jointing, the interaction of joints to form blocks, joint surface frictional characteristics, rock strength, rock stress, and hydrologic conditions. Rock mass quality indices and the parameters used to determine the indices are not primary data, but they are derived from direct observations of rock mass characteristics.

The calculation of rock mass rating requires six parameters that consider the strength of the rock, the rock quality designation, the joint spacing, the condition of joint surfaces, the groundwater environment, and a factor for the adjustment of joint orientation toward the excavation, as shown in the following equation:

$$RMR = C + I_{RQD} + JS + JC + JW + AJO \quad (\text{Eq. 3.7-6})$$

where RMR = a dimensionless number from 0 to 100,
C = the strength parameter,
 I_{RQD} = the rock quality designation parameter,
JS = the joint spacing parameter,
JC = the joint surface condition parameter,
JW = the groundwater parameter, and
AJO = the adjustment for joint orientation.

Table 3.7-33 correlates ranges of rock mass rating with relative descriptions of rock quality. Parameter values are assigned based on classification guidelines presented by Bieniawski (1979). Adjustments for joint orientation can be made to the rock mass rating to account for effects of direction of mining approach. When application of the rock mass rating index is limited to estimation of rock mass mechanical properties in drift design methodology, adjustment for joint orientation is not applied. Borehole estimates of rock mass rating do not include adjustment for joint orientation because joint orientations cannot be determined from core. The scanline data does include the adjustment for joint orientation factor, because joint orientations can in fact be evaluated with respect to the tunnel axis. Borehole rock quality designation was calculated as described in Subsection 3.7.2, while rock mass quality designation was calculated from tunnel scanline data using two methods described in CRWMS M&O (1997d). Rock mass rating values for boreholes and for Exploratory Studies Facility scanlines are presented in Brechtel et al. (1995), Kicker et al. (1996), SNL (1995a), and CRWMS M&O (1997d, 1997f).

The rock mass quality index, as defined by N.R. Barton et al. (1974), is calculated from six parameters:

$$Q = \left(\frac{RQD}{J_n} \right) * \left(\frac{J_r}{J_a} \right) * \left(\frac{J_w}{SRF} \right) \quad (\text{Eq. 3.7-7})$$

The first term (rock quality designation/ J_n) describes the block size, the second term (J_r/J_a) describes interblock shear strength, and the third term (J_w/SRF) describes the effect of the active stress. Relative classes of rock quality based on the overall value of Q have been assigned by N.R. Barton et al. (1974) and are presented in Table 3.7-34.

Data and methodology used to estimate rock mass quality and rock mass rating from the core data are described in Brechtel et al. (1995); Kicker et al. (1996); and CRWMS M&O (1997d). In the methodology, rock mass quality was estimated for every 3 m (10 feet) interval of the core log. Some parameters used to calculate the rock mass quality or rock mass rating index could not be determined from core, and values for each interval were therefore estimated by Monte Carlo simulations from distributions of the parameter that were based on surface mapping and mapping of the North Ramp Starter Tunnel. The approach assumed that the value of each parameter was independent from the other parameters in each interval.

Rock mass quality data were also generated for 5 m (16.4 feet) intervals of the Exploratory Studies Facility, based on scanline observations made on the excavation surface. "Scanline" refers to the determination of parameters along linear traces within the interval, as opposed to a detailed mapping of the features in the interval. The methodology used for the scanline rock mass quality determinations is described in CRWMS M&O (1997d). In addition, rock mass quality data were also determined from full-peripheral field mapping of the Exploratory Studies Facility following the procedure in Beason et al. (1994). Complete data and detailed analysis are presented in CRWMS M&O (1997d, 1997f).

Both the Q and the RMR empirical rock classification systems were applied in the Exploratory Studies Facility. These classification systems were determined in the Exploratory Studies Facility

based on two separate sets of mapping data, including scanline field mapping data collected by Sandia National Laboratories and full-peripheral field mapping data collected by the U. S. Bureau of Reclamation and the USGS. Q and RMR were collected for each 5 m interval of tunnel. To smooth the spatial variability along adjacent 5 m intervals of the Exploratory Studies Facility, a nine-term moving average rock mass property value was determined for each interval, such that the value of a particular interval was averaged together with the values of the four preceding intervals and the four succeeding intervals.

Rock mass quality assessments from the two data sets are shown in Figures 3.7-10 and 3.7-11. RMR data (Figure 3.7-10) typically show higher rock mass quality compared to Q data (Figure 3.7-11). Scanline and full-peripheral data are in very good agreement throughout the Exploratory Studies Facility, with the exception of the TSw1 thermal/mechanical unit in the North Ramp. A comparison of rock mass quality values in the TSw1 shows that the greatest difference between the two data sources occurs over the interval from approximately station 19+00 m to 28+00 m, corresponding primarily to the Topopah Spring crystal-poor upper lithophysal zone (Tptpul). There is an observable structural difference along the tunnel alignment within the Tptpul in the North Ramp such that the rock exposure is significantly smoother and less fractured above the springline compared to below the springline. The scanline Q assessment was conducted above the springline and therefore does not reflect the lower quality rock below the springline.

A new empirical method for assessing the Q system parameter called the stress reduction factor (H.A.D. Kirsten, written discussion of Barton's Rock Mass Quality, p. 85 of ASTM STP 984) was applied to both scanline and full-peripheral data sets in the Exploratory Studies Facility, resulting in the determination of a modified Q value. The method and analysis are described in detail by Kicker et al. (CRWMS M&O 1997f). The Q values calculated by the Kirsten approach, defined as Q_{modified} , are typically higher for both data sets and are generally in closer agreement to the RMR values.

Table 3.7-35 presents a concise statistical description of rock mass quality in the Exploratory Studies Facility. Cumulative frequency of occurrence for each thermal/mechanical unit, from both scanline and full-peripheral data, is shown in Figure 3.7-12 for RMR data, in Figure 3.7-13 for Q data, and in Figure 3.7-14 for Q_{modified} data. This cumulative frequency of occurrence rock mass quality data is summarized in Table 3.7-35, with frequencies of occurrence of 5 percent, 20 percent, 40 percent, 70 percent and 90 percent. These frequencies correspond to the five rock mass quality categories as defined by Hardy and Bauer (1991) and serve as the basis for evaluating the potential range of rock mass conditions. Table 3.7-35 also includes the original borehole values used in the Exploratory Studies Facility ground support design analysis. As shown, these values resulted in conservative estimates of rock mass quality and a conservative ground support system.

Comparison of data obtained from exploratory drilling with early scanline data obtained from the Exploratory Studies Facility to allow the identification of potential biases in the data sets (CRWMS M&O 1997d). The most significant potential sources of bias are directional bias, bias due to the effect of scale (the smaller amount of structural data available from a borehole), and bias due to sample disturbance during borehole drilling. Comparison of rock mass quality projected from boreholes to the scanline assessment data from the Exploratory Studies Facility excavations shows that the borehole data generally produced conservative estimates. The TCw was the only exception,

where the impacts of normal faults on the rock was not well represented in the core data, as the predominantly vertical boreholes did not provide a good sampling of fault impact on the brittle tuff rocks.

Borehole rock quality designation was much lower than the rock quality designation as assessed at the tunnel scale. This is due to the character of the core recovered from drilling. The tuff rocks are extensively fractured at the core scale, which causes a large amount of rubble, lost core, and high fracture frequency. Attempts to filter drilling-induced fractures from the rock quality designation calculations (enhanced-rock quality designation) increases the values by factors of 1.5 to 2.2 for different thermal/mechanical units. However, rock quality designation values from the tunnel scale were still greater by a factor of 1.5 to 3.1. The rock quality designation in the tunnel assessments is based on frequency of fractures that are observed at the tunnel scale, which excludes many fractures that impact the core. In addition, although the extent of rubble or highly fractured intervals was included in the tunnel assessment of rock quality designation, those types of features were much less common than suggested by the core. Joint frequencies were higher in core data because core data included smaller-scale fractures that were not counted at the tunnel scale. This resulted in small values of the joint spacing parameter in the core rock mass rating. Joint set numbers in the core were based on fractures observed in the TCw, which had both more joint sets and higher frequencies of jointing than other units. In values used for the PTn and TSw1 were higher than revealed by the excavation.

As shown in Table 3.7-35, lowest rock mass quality was observed in the TCw thermal/mechanical unit. The TCw also had the greatest variability. Rock mass quality was lowest in the most densely welded lithostratigraphic units, Tpcpul and Tpcpmn, in the Tiva Canyon Tuff (CRWMS M&O 1996d). It was higher in the less densely welded upper and lower portions. This correlates with analysis of the fracture mapping for TCw, which consistently indicates more joint sets and higher joint frequency. In addition, the North Ramp penetrates the TCw in a zone of normal faulting, which contributed to the broken character of the TCw rocks (CRWMS M&O 1996d).

Table 3.7-35 also indicates that the PTn unit showed consistently high rock mass quality ratings. Typically, only one set of joints was evident in the PTn and had very limited impact on the excavation. Rock strength was low in this unit, with some intervals being nonlithified. Shear failures were observed on the sides of the tunnels in some of the weaker PTn materials. However, they were localized and have not affected the long term character of the excavation.

Rock mass quality was higher in the TSw1 unit than in the corresponding portions of the TCw (CRWMS M&O 1996d). Jointing was less well developed. Poor rock mass quality, anticipated in the upper lithophysal zone (Ttpul), was not observed. Jointing was not well developed and was generally limited to one set. The inhomogeneities in the Ttpul caused by large lithophysae and relatively small cracking of the rock had little effect on the rock mass at the excavation scale. Where the middle nonlithophysal zone (Ttpmn) in the TSw2 was exposed in excavations of the Main Drift, rock mass quality was relatively high.

The Exploratory Studies Facility Ground Support Guidelines (CRWMS M&O 1996c) specify ranges of rock mass quality for associated ground support Classes I through V, and based on these guidelines and rock mass quality indices from early Exploratory Studies Facility scanline data,

ground support requirements were projected for each thermal/mechanical unit. Table 3.7-36 presents the recommended ground support with respect to the specified range of rock mass quality values. Classes I and II specify welded wire fabric and rock bolts, with tighter rock bolt spacing for Class II. Class III uses the Class II arrangement of rock bolts and welded wire fabric, but with the addition of shotcrete. However, although called for by design, shotcrete was never used, except in the starter tunnel. Classes IV and V use W8 circular steel sets and lagging, with tighter set spacing and full lagging for Class V.

Table 3.7-37 lists the projected proportion of the tunnel within each thermal/mechanical unit that would require the support suggested by the guidelines. The scanline rock mass quality indices suggested that the majority of tunnel excavation could be supported with rock bolts and welded wire fabric in the undifferentiated overburden, PTn, TSw1, and TSw2 units (CRWMS M&O 1997d). The rock mass quality distribution in the TCw unit, however, projected heavier ground supports than required for the other units. Comparisons of projected and installed ground support were being developed in the construction monitoring activities (CRWMS M&O 1997a) and are discussed in Subsection 3.7.6.2.4 of this report.

3.7.4.2 Rock Mass Thermal Properties

Correlations have been developed or proposed for thermal/mechanical properties at the rock mass scale (Nimick and Connolly 1991). Thermal conductivity at the intact scale has been shown to be a function of porosity, saturation, and temperature. Differences at the rock mass scale are projected to be related to the additional fracture porosity, which should be a small effect. Similarly, the heat capacity of intact rock is expected to be an adequate predictor of heat capacity at the rock mass scale.

Preliminary thermal/mechanical analyses for design have been performed in an attempt to project laboratory thermal expansion data to the rock mass scale, as described in Jung et al. (1993). The preliminary thermal/mechanical analyses indicated a maximum upward displacement of almost 30 cm at the surface, 300 years after waste emplacement. Most of this displacement would originate in the TSw2 unit. The rock in the immediate vicinity of the repository was predicted to be in compression, but the tensile stress nearer the surface (TCw thermal/mechanical unit) was predicted to be relatively high (approximately 5 MPa). This behavior could potentially result in the opening of preferential pathways for water infiltration or gas migration (CRWMS M&O 1997d). However, thermal expansion data for the analyses in Jung et al. (1993) came primarily from borehole laboratory thermal expansion testing results (TDIF 302201 (TBV), DTN SNL01B05059301.002 (TBV) and .005 (TBV)). Data from the in situ thermal tests being conducted in the Exploratory Studies Facility are anticipated to be more representative of rock mass behavior than the laboratory test results and will be used for updating and expanding the three-dimensional thermal/mechanical analysis for the repository. The resulting more realistic material models would probably predict lower stresses (Jung et al. 1993; CRWMS M&O 1997d).

Prior to onset of heating in both the Single Heater Test block and the Drift Scale Test block of the Exploratory Studies Facility Thermal Test Area, baseline laboratory and in situ testing was performed to characterize thermal, mechanical, hydrological, and chemical properties, local geology, in situ hydrology, and local rock mass quality of the area to be tested. (CRWMS M&O 1996b;

CRWMS M&O 1997f). Results of the baseline characterization are generally consistent with results of previous studies in the same thermal/mechanical unit and lithostratigraphic unit.

Data collected from the Single Heater Test through May 1997 (CRWMS M&O 1997g) indicate that the temperature distribution around the heater was radially symmetric and that conduction thus appears to be the primary mode of heat transfer through the rock mass. However, some anomalous temperature gauge readings may indicate convective heat transport in fractures. The available thermal data also indicate the formation of a dry-out zone extending radially outward roughly 1 m from the heater to approximately the 100°C isotherm. Although there is generally good overall agreement between calculated and measured temperatures, numerical simulations of thermal behavior did not accurately predict the observed thermal data. This is likely due to limitations imposed by the equivalent continuum model, which is the conceptual model on which the numerical simulations are based. A complete data presentation and analysis is given in CRWMS M&O (1997g).

The thermal expansion coefficient of the rock mass was determined from selected multi-purpose borehole extensometer displacements and temperatures. The calculated rock mass thermal expansion coefficient ranged from between about 4 and $6 \times 10^{-6}/^{\circ}\text{C}$. Rock mass thermal expansion was calculated from the in situ data, including temperature change for a given axial length from ambient, gage length, and measured thermal displacement over the gage length. Only the data from with multi-purpose borehole extensometers relatively uniform temperature were used (MPBX-1 and MPBX-3). Because of displacement direction reversals after Day 90 of the test, the calculated rock mass thermal expansion coefficients presented in Table 3.7-38 are only for data through Day 90. Analytical calculation of the thermal expansion coefficients for the longest gage lengths available near the end of the heating cycle produced the results presented in Table 3.7-39. A more complete discussion, along with complete data, is given in SNL Level 4 Milestones SP9261M4, SP9271M4, and SP9268M4 and in CRWMS M&O (1997h).

Rock mass thermal expansion coefficients calculated from the Single Heater Test are generally lower than laboratory-determined values for the same TSw2 unit. The observed expansion of the rock mass under heating is not fully explained by elastic continuum models, but it is anticipated that discrete block modeling could be used to significantly advance the understanding of rock mass thermomechanical behavior.

Rautman (1995) developed a correlation between thermal conductivity and a 2-D geostatistical model of porosity at Yucca Mountain. The relationship of laboratory measurements of thermal conductivity to porosity, saturation, and temperature described is summarized in Subsection 3.7.3.2 of this report, and the use of these data for 3-D rock properties modeling is discussed in Subsection 3.7.1.3 of this report. Results of geostatistical modeling of thermal conductivity and a more complete discussion of the correlation of porosity and thermal conductivity are presented in Section 5 of this report and in Rautman (1995).

3.7.4.3 Rock Mass Mechanical Properties

3.7.4.3.1 Rock Mass Strength

Rock mass mechanical properties have been estimated using the approach proposed by Hardy and Bauer (1991). The approach uses laboratory test data and rock mass quality rock mass rating to estimate mechanical properties at the rock mass scale for use in equivalent continuum analyses. The estimated properties are listed in Table 3.7-40 for each thermal/mechanical unit and rock mass rating values at 40 percent cumulative frequency of occurrence. Ranges of the rock mass properties are estimated based on rock mass rating from scanline data and the average of the appropriate intact rock property. Complete analysis is presented in CRWMS M&O (1997d). Two sets of empirical rock mass strength criteria, Yudhbir and Prinzl (1983), and Hoek and Brown (1988), were adopted for the Drift Design Methodology, and an average of the two predicted strengths was used to develop a power law relationship of rock mass strength versus confining pressure. Design parameters for rock mass elastic modulus (Serafim and Pereira 1983), Poisson's ratios, and Mohr-Coulomb strength were developed for each thermal/mechanical unit.

Rock mass strengths based on the empirical strength criteria of Yudhbir and Prinzl (1983) and Hoek and Brown (1988) have been developed for the thermal/mechanical units. Information required for obtaining rock mass strength includes rock mass quality indices, intact rock uniaxial compressive strengths, and the triaxial compressive strength data. The rock mass strength criteria were generated for the five categories of rock mass quality based on frequency of occurrence of 5, 20, 40, 70, and 90 percent, which were presented in Subsection 3.7.4.1.

The equation proposed by Yudhbir and Prinzl (1983) for calculation of rock mass strength is:

$$\sigma_1 = A\sigma_c + B\sigma_c \left(\frac{\sigma_3}{\sigma_c}\right)^\alpha \quad (\text{Eq. 3.7-8})$$

where σ_c = intact rock uniaxial compressive strength
 σ_1 = strength of the rock mass
 σ_3 = confining stress
 A = a dimensionless parameter dependent on the rock mass rating, and
 α, B = rock material constants dependent on rock type.

The value of A for the rock mass is obtained from the design rock mass rating (RMR_D) by the following equation from Yudhbir and Prinzl (1983):

$$A = e^{0.0765(RMR_D) - 7.65} \quad (\text{Eq. 3.7-9})$$

The material constants B and α are related to the rock type and are determined by a curve fitting of the confined compressive strength test results.

Table 3.7-41 lists the value of B and α , as well as σ_c , for each unit. For the TCw thermal mechanical unit, NRG core triaxial test data were used to determine B and α using the method outlined in Hardy and Bauer (1991) and Lin et al. (1993). These data were originally published in Brechtel et al. (1995). For the undifferentiated overburden and PTn thermal/mechanical units, NRG uniaxial compression and Brazilian tensile strength tests were used to determine B and α with modifications of the method suggested by Hardy and Bauer (1991) and Lin et al. (1993). These data were originally published in Brechtel et al. (1995). For the TSw1 and TSw2 thermal/mechanical units, triaxial test data from samples from SD-9 and SD-12 (from data packages Technical Data Information Forms 304623 (TBV) and 304839 (TBV), respectively) were used to determine B and α using the method outlined in Hardy and Bauer (1991) and Lin et al. (1993). Only five data points for each unit were available to evaluate for these constants. Data from the following Technical Data Information Forms (TBV) were used to obtain the values listed in Table 3.7-41: 301485, 301671, 301703, 301785, 301881, 302038, 302071, 302072, 302205, 302231, 302232, 302417, 303003, 303091, 303167, 303340, 303384, and 304095 (Brechtel et al. 1995; Lin et al. 1996).

The Hoek and Brown (1988) rock mass strength criterion is shown in Equation 3.7-10:

$$\sigma_1 = \sigma_3 + \sqrt{m\sigma_c\sigma_3 + s\sigma_c^2} \quad (\text{Eq. 3.7-10})$$

where m = a constant that depends on the properties of the rock, and

$$m = m_i e^{(RMR-100)/28}$$

s = a constant that depends on the extent to which the rock is fractured, and

$$s = e^{(RMR-100)/9}$$

The parameter m_i is the constant for intact rock determined by curve fitting of the confined compressive strength test data. Values for m_i are listed in Table 3.7-41. Data sources and derivations are given in CRWMS M&O (1997d).

The design rock mass strengths for each rock mass quality category were calculated by averaging the strengths determined from both Yudhbir and Prinzi (1983) and Hoek and Brown (1988) criteria, following the procedure of Hardy and Bauer (1991).

A power law relationship of the form

$$\sigma_1 = A + B\sigma_3^C \quad (\text{Eq. 3.7-11})$$

was employed to describe the nonlinear design rock mass strength. The parameters A, B, and C were determined by curve fitting the strength envelopes using a least-square method, and are included in Table 3.7-40 for 40 percent cumulative frequency for each thermal/mechanical unit. The Design Rock Mass Strength Envelopes for the TSw2 unit, based on Exploratory Studies Facility scanline data, is presented in Figure 3.7-15. Complete design rock mass strength envelopes for other thermal/mechanical units and resulting power law constants are given for all rock mass classes in each thermal/mechanical unit in CRWMS M&O (1997d).

The Mohr-Coulomb strength parameters, including cohesion and angle of internal friction, and the dilation angle are commonly used to describe rock mass strength in numerical analysis. The strength parameters were developed from the least-square curve fits of strength data pairs (σ_1 , σ_3) produced using the power law criterion described above and summarized for 40 percent frequency in Table 3.7-40. The linear relation for strength (σ_1) and confining pressure (σ_3) is defined in the form of the following equation:

$$\sigma_1 = \sigma_c + N\sigma_3 \quad (\text{Eq. 3.7-12})$$

where σ_c = uniaxial compressive strength, and
N = confinement factor.

The parameters σ_c and N were then used to create a Mohr-Coulomb failure criterion relating the shear and normal stress on the plane of failure to cohesion and angle of internal friction by the following equation:

$$\tau = C_0 + \sigma_n \tan \phi \quad (\text{Eq. 3.7-13})$$

where C_0 = cohesion and

$$C_0 = \sigma_c / \sqrt{N}$$

ϕ = angle of internal friction and

$$\phi = 2(\tan^{-1} \sqrt{N} - 45^\circ)$$

The least-square best fit was performed over the range of confining pressures from 0 to 3 MPa, which is representative of the projected range in minimum principal stresses near the boundary of the excavations. Table 3.7-40 includes the resulting Mohr-Coulomb strength parameters for 40 percent cumulative frequency of occurrence. Complete results are presented in CRWMS M&O (1997d).

The non-associated flow rule, suggested by Michelis and Brown (1986), which uses a dilation angle equal to half the internal friction angle, was considered suitable for the tuff (Hardy and Bauer 1991), and the resulting values for dilation angles are also listed in Table 3.7-40, with complete results presented in CRWMS M&O (1997d).

Two additional empirical methods were used for assessing rock mass strength properties: the Geological Strength Index (Hoek and Brown 1988) and the Rock Mass Index (Palmstrom 1996a, 1996b). Properties estimated included rock mass elastic modulus, cohesion, friction angle, unconfined compressive strength, and tensile strength and joint cohesion and friction angle. Complete analyses and results are presented in CRWMS M&O (1997f). Results indicated that the original rock mass property assessment methodologies were conservative.

3.7.4.3.2 Rock Mass Elastic Moduli

Serafim and Pereira (1983) developed a correlation between the rock mass rating and rock mass elastic modulus that was recommended for use by Hardy and Bauer (1991). The correlation is shown in the following equation:

$$E = 10^{\frac{(RMR - 10)}{40}} \quad (\text{Eq. 3.7-14})$$

where E is in GPa.

Because the equation does not incorporate the intact rock elastic modulus, the predicted rock mass elastic modulus can exceed the intact rock elastic modulus at high rock mass rating values. An upper bound limit of the rock mass modulus was, therefore, set equal to the intact rock modulus (Table 3.7-41). Calculated rock mass moduli based on design rock mass rating values are shown for 40 percent cumulative frequency of occurrence in Table 3.7-40. Complete results are presented in CRWMS M&O (1997d).

Rock mass moduli determined using Geological Strength Index and Rock Mass Index indices described in Subsection 3.7.4.3.1 above resulted in modulus values that significantly exceeded the mean intact value for the undifferentiated overburden, PTN, and TSw1 thermal/mechanical units based on field mapping data (CRWMS M&O 1997f). The Rock Mass Index empirical methodology applied in this analysis resulted in a significantly smaller range of E values that is more consistent with the intact value for these units. The Rock Mass Index method may be a more appropriate empirical methodology for assessing rock mass modulus for the range of rock mass quality values in the Exploratory Studies Facility (CRWMS M&O 1997f).

Empirical relationships to estimate Poisson's ratio from rock mass quality are not available. The mean values for intact rock Poisson's ratios from the laboratory tests for each thermal/mechanical unit were adopted as the rock mass Poisson's ratios. Table 3.7-40 includes the results. No adjustments for rock mass category are recommended.

Rock mass elastic moduli were also determined in situ as part of the Single Heater Test, using the NX borehole jack (Goodman Jack). Results, procedures, and analysis are described in SNL (1997b) and in CRWMS M&O (1997g). This nonpermanent borehole instrument was periodically inserted into a single borehole drilled roughly horizontal and perpendicular to the Single Heater Test heater and pressurized at various distances along the borehole. Jack pressure and loading platen displacements were monitored, and rock mass modulus was determined from the pressure/displacement curve.

Borehole jack tests were run before heater startup in August 1996 and again in October 1996, November 1996, and March 1997. Temperatures were measured in the borehole for each set of tests prior to insertion of the jack using a portable thermocouple probe at various points, and by manually taking temperature readings using a hand-held thermocouple reader. Jacking tests were run along the borehole at various depths. All borehole jack testing followed ASTM D4971-89, *Standard Test*

Method for Determining the In Situ Modulus of Deformation of Rock Using the Diametrically Loaded 76-mm (3-in.) Borehole Jack, with minor exception.

The NX borehole jack consisted of two hydraulically activated steel loading platens approximately 20.3 cm long, which applied a unidirectional load to a nominal 7.62-cm diameter borehole wall. The maximum jack pressure was 69 MPa, and the maximum platen displacement was 0.63 cm. Jack pressure was applied using an Enerpak hand pump. The jack was inserted into the borehole and platens were slowly expanded until the pressure just began to rise. The resulting linear variable displacement transducer readings represent initial borehole diameter and were used for calculations of borehole wall displacement under pressure. The jack pressure was increased in increments to the desired maximum pressure and then decreased in similar increments. Typically, the jack was pressurized in 3.44 MPa (500 psi) increments to 55.2 MPa (8000 psi), then back to zero, with linear variable displacement transducer readings recorded during both loading and unloading.

Field rock mass moduli from borehole jack testing in the Single Heater Test block are given in Table 3.7-42 along with the rock temperature at the time of the test. Rock modulus values ranged from about 3 to 23 GPa. The data show thermally induced stiffening of the rock mass in the region near the heater, with rock mass moduli in this region increasing from 8 GPa in November 1996 to 23 GPa in March 1997. This modulus increase is likely because of the closing of fractures by rock matrix thermal expansion (CRWMS M&O 1997g).

Ambient in situ rock mass moduli calculated from Single Heater Test borehole jacking are lower than laboratory values determined for intact specimens, which are in turn lower than values determined from Q/RMR rock mass quality estimates. This is consistent with previous in situ experiments conducted in welded tuff in G-tunnel, which indicated that the modulus values for in situ tests were about half the intact laboratory-determined value of about 23 to 35 GPa (Zimmerman and Finley 1987).

3.7.5 In Situ Stress Conditions

Design of the Yucca Mountain repository requires knowledge of the magnitude, direction, and variability of the preconstruction in situ state of stress for the analysis and design of stable underground openings as well as for the prediction of short- and long-term rock mass deformation. Detailed results of in situ stress measurements in tuffs at Yucca Mountain or at Rainier Mesa are contained in several references (Hooker et al. 1971; Haimson et al. 1974; Tyler and Vollendorf 1975; Ellis, W.L. and Ege 1976; Ellis, W.L. and Magner 1980; Warpinski et al. 1981; Zimmerman and Vollendorf 1982; and Stock, J.M. et al. 1984, 1985). These references also discuss details of testing techniques and potential limitations and errors.

Table 3.7-43 presents a summary of the estimated in situ stress at the repository horizon. The direction of the maximum principal stress is vertical, due to lithostatic load. At the repository level, the vertical stress has been assumed to be 7.0 MPa on the average (Stock, J.M. et al. 1984, 1985; CRWMS M&O 1995a). Horizontal stresses are expected to be lower and to range from 3.5 MPa to 4.2 MPa, although the range may be as wide as 2.1 MPa to 7.0 MPa. These in situ stress values were generally confirmed by a stress profile calculated for the Exploratory Studies Facility test area (YMP

1995a), which showed a vertical stress of 6.0 MPa at a depth of 300 m. Horizontal stress for the same depth ranged from 2.1 to 4.2 MPa.

Horizontal in situ stresses at the repository site are expected to be generally low. Consequently, failure modes around underground openings during construction are expected to be primarily controlled by geologic structures. Minimum and maximum horizontal/vertical stress ratios are close, indicating a weak horizontal stress anisotropy. Lateral stresses and their effects would thus be expected to be similar for all drift orientations (CRWMS M&O 1997d).

Hydraulic fracturing tests performed for ambient characterization of the Drift Scale Test block measured in situ stresses in the TSw2 unit (SNL 1997a; CRWMS M&O 1997f). Results were generally consistent but revealed somewhat lower in situ stresses than previously estimated. Tests were conducted in borehole Exploratory Studies Facility-AOD-HDFR#1, drilled from the Thermal Test Facility alcove in the Exploratory Studies Facility, at depths approximately 240 to 249 m below ground surface. The downhole testing equipment consisted of a hydraulic fracturing straddle packer system, which was lowered to predetermined hydraulic fracturing test intervals. An impression packer orienting tool was used to obtain an oriented trace of the induced hydraulic fracture on the borehole wall, and test interval pressure and flow rate were digitally monitored.

A series of five successful hydraulic fracturing tests were conducted in the Drift Scale Test block, but only one test yielded what were considered reliable results. Based on these test results, the principal horizontal stresses around this borehole are estimated to be (SNL 1997a):

$$\sigma_h = 1.7 (\pm 0.1) \text{ MPa acting in the N75}^\circ\text{W } (\pm 14^\circ) \text{ direction} \quad (\text{Eq. 3.7-15})$$

$$\sigma_H = 2.9 (\pm 0.4) \text{ MPa acting in the N15}^\circ\text{E } (\pm 14^\circ) \text{ direction} \quad (\text{Eq. 3.7-16})$$

where σ_h = least horizontal principal stress, and
 σ_H = largest horizontal principal stress.

Because vertical stress was not measured in these tests, it was approximated, as the weight of the overburden at the depth of the tests from the surface, as (SNL 1997a):

$$\sigma_v = 4.7 \text{ MPa} \quad (\text{Eq. 3.7-17})$$

where σ_v = vertical stress.

Although the measured horizontal stresses are only moderately differential, both are smaller than the vertical stress. This measured stress regime, one of low horizontal magnitudes, is in accord with the dominant local normal faults. The north-northeastern maximum horizontal stress direction is subparallel to the average strike of these faults and is supported by previous measurements in the Yucca Mountain area (Zoback and Healy 1984). Additional details of procedures, results, and interpretations are presented in Sandia National Laboratories (1997a) and CRWMS M&O (1997f).

3.7.6 Excavation Characteristics of the Rock Mass

Geotechnical monitoring data were developed during excavation of the North Ramp Starter Tunnel and Upper Tiva Canyon Alcove to provide the basis for design verification (SNL 1995a). The North Ramp Starter Tunnel was constructed to launch the 7.6-m diameter tunnel boring machine being used to construct the Exploratory Studies Facility North Ramp, Main Drift, and South Ramp. Upper Tiva Canyon Alcove was excavated off the North Ramp Starter Tunnel to provide access for site characterization testing. Design verification studies are being performed to monitor and observe the long-term behavior of openings in the range of rock conditions to be encountered in the potential repository host rock, to observe and evaluate the construction of the Exploratory Studies Facility with respect to implications for repository construction and performance, and to collect information for design of the ventilation systems in the repository (DOE 1988b).

Specific safety and health concerns related to rock mass mineralogies at Yucca Mountain include respiratory effects of erionite and silica minerals (including quartz and cristobalite) during daily underground activities. These minerals occur in varying proportions in the different lithologies and geochemical environments at Yucca Mountain as reported in Vaniman, Bish et al. (1996). Hazards include erionite, a carcinogen, and crystalline silica, which can produce respiratory ailments upon becoming airborne and during tunneling operations. Occurrence of these minerals is discussed in detail in Section 6, Geochemistry.

Safety and health concerns for the YMP are currently addressed by the *Safety and Health Plan* (YMP 1995d) which includes respiratory protection. Control measures regarding these mineralogic respiratory hazards are performed according to Harris (M.W. Harris, SAIC, written communication to W.R. Dixon, YMSCO, February 1995) for erionite and McManus (1996) for silica. These measures include monitoring, engineering control, and proper personal protective equipment when tunneling activities are occurring in areas where these minerals are of concern. These measures should also be considered during repository design.

3.7.6.1 Excavation Methods

Both Sandia National Laboratories (1995a) and CRWMS M&O (1997a) address evaluations of mining methods and monitoring of ground support systems and drift stability. Rock mass quality evaluations, an evaluation of as-built mapping data, and blast vibration monitoring are performed as part of the mining methods evaluation. An evaluation of rock structure data from surface and underground mapping is presented in Subsection 3.7.2 of this report, an evaluation of rock mass quality data is presented in Subsection 3.7.4. of this report, and blast monitoring is discussed below and in CRWMS M&O (1997d).

The North Ramp Starter Tunnel, Upper Tiva Canyon Alcove, Alcove 2, and the Thermal Test Facility (Thermal Testing Facility Alcove) were excavated by drilling and blasting. Controlled blasting procedures were implemented to minimize blast-induced damage to the excavation perimeter. Blast damage can result in loosening of the surrounding rock mass which increases ground support requirements and long-term maintenance.

The specific NRC requirement from 10 CFR 60, Subpart E-Technical Criteria 60.133 (f) calls for an "excavation method that will limit the potential for creating a preferential pathway for groundwater or radioactive waste migration to the accessible environment." The Exploratory Studies Facility Design Requirements (YMP 1996) estimated that the rock mass altered by the excavation process will be within 1.5 m of the excavated surface.

Additional criteria for blast vibration limits, based on measurements of peak particle velocity, were developed for the excavation perimeter and nearby structural elements, and are listed in Table 3.7-44. These vibration criteria are specified without reference to the dominant frequency. Application of peak particle velocity-distance relationships is required to obtain estimated peak particle velocity within 1 m of the blast. Far-field monitoring utilized seismic equipment with peak frequency ranges of 250 Hz.

Excavation of the North Ramp Starter Tunnel and Upper Tiva Canyon Alcove produced substantial overbreak on existing structural features, even with the use of perimeter blasting procedures. Monitoring of the blasts indicated that reduced quantities of explosives detonated per delay and long-period delays were successful in controlling peak particle velocities. Observations suggested that measurable blast damage was limited to within 1 m of the excavation perimeter.

During construction of Bow Ridge Fault Alcove and a portion of the Thermal Test Facility (Thermal Testing Facility Alcove), construction monitoring consisted of monitoring ground motion (peak particle velocity), making observations of damage in the rock surrounding the excavation, and making visual observations of the number of borehole half-casts remaining on the excavation perimeter. Half-casts of perimeter trim holes were mapped on the east and west walls of Upper Tiva Canyon Alcove. Half-casts were rare on the east wall. They occurred more frequently on the west wall, but were irregular in occurrence. The half-cast distribution may be attributed to drilling and blasting practices or to structural geologic controls such as joint spacing and orientation (CRWMS M&O 1997a).

Geophones were attached to steel set No. 90, adjacent to the entrance of Upper Tiva Canyon Alcove, and recorded a peak particle velocity of 330 mm/sec (13 in/sec) in the direction of the North Ramp axis during blasts No. 5 and 6. These geophones measured blast vibrations with frequencies below 250 Hz and peak particle velocities well below the 1250 mm/sec criteria in Table 3.7-44.

Visual observations of blasting damage at Upper Tiva Canyon Alcove were made by video borescope records of inspection boreholes at distances of 0.9, 1.5, and 2.5 m from the excavation perimeter. On the basis of observed debris in the holes, rock damage in the holes and overbreak of the excavation, the blasting effects extended up to 1 m from the excavation perimeter. No damage was evident at 1.5 m from the perimeter.

Comparison of Upper Tiva Canyon Alcove far-field blasting results to results obtained during construction of the North Ramp Starter Tunnel Top Heading (SNL 1995a) indicates similar trends.

A similar monitoring program, performed during construction of part of the Thermal Test Facility (Alcove 5), successfully produced both near-field and far-field blasting vibration data. An attenuation relationship was developed by combining the two data groups and was used to project

the peak particle velocity at a distance of 1 m from the excavation perimeter for comparison to the criteria in Table 3.7-44. The calculation indicated that rock 1 m from the excavation perimeter would be most strongly impacted by detonation of the trim holes because they are closest and contain the highest quantity of explosive because of the number of holes. Application of the attenuation relationship predicted peak particle velocities between 703 and 720 mm/sec, which would exceed the criteria of 700 mm/sec at 1 m by a maximum of 3 percent. Data scatter in the peak particle velocities used to develop the attenuation relationship is very large, and it is therefore highly likely that the criteria was not exceeded. Furthermore, the majority of the data are developed from blast holes where the explosive was tamped and fully coupled to the hole perimeter. Trim holes were loaded with decoupled charges (smaller diameter than the hole) and were not tamped. Peak particle velocities predicted for all other holes were well below the 700 mm/sec criteria.

Blast monitoring results at the Thermal Test Facility suggest that damage to the rock was limited to within 1.5 m of the excavation boundary. Peak particle velocities at 1 m from the excavation boundary appeared to satisfy the blast vibration limits. A summary of other observations on drilling and blasting results for the Thermal Test Facility is presented in CRWMS M&O (1997a).

3.7.6.2 Excavation Characteristics

Ground support installed in the Exploratory Studies Facility includes rock bolts, lattice girders, steel fiber reinforced shotcrete, and steel sets (CRWMS M&O 1997d). Wire mesh and channel straps are used to control loose materials between rock bolts. Monitoring of rock bolts was accomplished using rock bolt load cells and instrumented rock bolts. Convergence pins were attached to the lattice girders in the first 10 m of the Exploratory Studies Facility to monitor the displacement of these components of the ground support system. Vibrating wire strain gages and convergence pins were attached to steel sets throughout the Exploratory Studies Facility to monitor the changes in rock loading. Convergence pin arrays and borehole extensometers were installed in rock supported by Swellex bolts (CRWMS M&O 1997d).

3.7.6.2.1 Rock Bolt Load

Rock bolt load cells were installed along the North Ramp Starter Tunnel and on the highwall at the North Ramp portal. Installation procedures are detailed in Sandia National Laboratories (1995a). All bolts had some load bleed-off and have settled into generally stable trends, in which bolt loads are relatively constant. No load increases that would indicate rock loosening were observed from the time of installation to June 1996. Current bolt loads range from 0.1 percent to 16.0 percent of the bolt yield strength (CRWMS M&O 1997d).

Instrumented rock bolts were installed in Upper Tiva Canyon Alcove, as described in Sandia National Laboratories (1995a). Stable bolt loads were similar to those observed in rock bolt load cells. Bolt loads appeared to remain well below the bolt yield strength (SNL 1995a).

Eight rock bolt load cells were also installed as part of the Single Heater Test to evaluate the effects of elevated temperature on bolt performance. Complete data and analysis are presented in Sandia National Laboratories (1997b) and CRWMS M&O (1997h). Four of the rock bolts were installed on the heated side of the thermomechanical alcove below the level of the heater and four additional

bolts were installed on the opposite, cool, side of the alcove. The load cells each contained three strain gages, and the total load acting on the cell was calculated by averaging the measurements from all three.

In Table 3.7-45 (CRWMS M&O 1997h), the Single Heater Test rock bolt load cell data are presented as load and time from the start of heating, or Day zero. As shown, there is a general decrease in load measured in all the load cells, although the decreases are all less than 7 percent of the initial load (CRWMS M&O 1997h). The average percent decrease is 1.37 percent for rock bolts on the ambient (cool) side and 3.45 percent for rock bolts on the heated side. The two largest decreases were measured in the rock bolt load cells that were nearest the heater, RB-1 and RB-2 (CRWMS M&O 1997h).

3.7.6.2.2 Portal Girder Deformation

Deformation of the portal lattice girders embedded in shotcrete was tracked using convergence data collected by a tape extensometer. The deformations have remained fairly constant after the initial settling (SNL 1995a), and the monitoring data from June 1995 to June 1996 showed a continuing trend of no closure (CRWMS M&O 1997a).

3.7.6.2.3 Steel Set Deformation

Vibrating wire strain gages were installed on 33 steel sets from January 1995 through June 1996. The strain gages were attached to the steel sets both prior to and after installation in the tunnel. When the gages were attached prior to installations, stress changes in the web of the steel sets due to jacking loads were monitored during the steel set installation process.

Strain changes that occurred during jacking installation indicated a generally similar pattern of tensile and compressive stress change in the steel. Changes in the crown of the steel set were the most uniform. The measured strain changes during jacking indicated stress changes between 10 and 180 MPa (CRWMS M&O 1997a).

Strain magnitudes remained generally constant after installation was complete and suggested that loading of rock around the steel sets monitored was not occurring. Most of the steel sets were installed in the TCw and in the undifferentiated overburden units. Similar long-term trends indicating no increase of steel set load were observed for steel sets in the PTN, TSw1, and TSw2 units (CRWMS M&O 1997d).

3.7.6.2.4 Installed Ground Support versus Rock Mass Quality Projections

Installed (as-built) ground support has been compared to ground support projected based on the rock mass quality determined for 5 m intervals for the Exploratory Studies Facility (CRWMS M&O 1997d, 1997f). Projected ground support classes were defined as a function of the Q value to provide the recommended ground support to cover the expected range of ground conditions. The as-built, installed ground support classes are shown in Figure 3.7-16, together with the spatial distribution of Q_{modified} values. The installed ground support class was generally in agreement with, or more conservative than, the scanline-based Q_{modified} value (CRWMS M&O 1997f).

3.7.7 Engineering Properties of Surficial Material

3.7.7.1 Surficial Sedimentary Deposits

The late Tertiary and Quaternary surficial sedimentary deposits of the Yucca Mountain area consist of colluvium, fan alluvium, eolian sand sheets, ramps and dunes, or marsh sediments, and playa deposits (see Subsection 3.4). These range in age from late Pliocene to Holocene. The deposits are grouped into eight major units plus locally important eolian and marsh deposits. Quaternary stratigraphy and deposit distribution are described in detail in Subsections 3.4.3.3 and 3.4.3.6, respectively. Distribution of alluvium/colluvium is included in the central block geologic map, Figure 3.6-4.

Late Pliocene and early Pleistocene deposits consist predominantly of debris flows with sparse, bedded fluvial sediments. They occur as dissected fans and fan remnants that are adjacent to bedrock ranges and, less commonly, as isolated outcrops several kilometers from the ranges. These deposits are moderately indurated, coarse, angular, unsorted gravel with minor amounts of sand- to clay-sized material (Wesling et al. 1992; Lundstrom et al., *Preliminary Surficial Deposits Map of the Northwest Quarter of the Busted Butte 7.5-minute Quadrangle*, USGS-OFR-95-133, scale 1:12,000, 1995 in press.).

Middle to late Pleistocene deposits consist of fan alluvium, fluvial and eolian sands, and local lenses of volcanic ash. These deposits generally overlie older alluvial deposits on middle to upper pediment slopes, and they occur in larger stream valleys.

Eolian deposits occur as dunes and sand sheets in and adjacent to the Amargosa Valley. Ramps of fine, well-sorted sand as much as 50 m thick flank many of the hills bordering the Amargosa Valley and near Yucca Mountain at Busted Butte. Fluvial sand sheets occur along major streams and along drainages downstream from dunes.

Holocene deposits in the Yucca Mountain area consist of fluvial sand and gravel and eolian sand. Holocene deposits occur mainly as thin, broad fans downstream from incised stream channels on pediment slopes. Eolian sand deposits consist of well-sorted fine sand that occurs as small dunes and irregularly-shaped sheets in the Amargosa Valley.

3.7.7.2 Surface Soil Investigations

There have been numerous investigations to determine the physical properties of native soils in the site vicinity, primarily the North Portal and the Midway Valley areas. Investigations to assess the surface soils in the vicinity of the Exploratory Studies Facility were conducted primarily between the mid-1980s to the early 1990s. Between 1984 and 1985 Sandia National Laboratories conducted three studies (Neal 1985, 1986; Ho et al. 1986) that addressed surface facilities and soils. Neal's 1985 report presents the general boring logs for eight exploratory borings (UE-25, RF#1 through #8) in the vicinity of Exile Hill. Neal's 1986 report incorporates three additional holes (UE-25, RF#9, #10, and #11) and extends the depth of one of the original holes (UE-25, RF#3). The total depth of penetration ranges from 60 to 301 feet, and detailed logs are presented. In addition, the report contains some of the basic physical properties of the alluvium and cored rock. A Sandia National

Laboratories study in 1986 (Ho et al. 1986) involved four test trenches in the western portion of Midway Valley and south of Exile Hill. The test pits in general corresponded to exploratory boring locations UE-25, RF#1, #2, #3, and #5. The report presents detailed information on shallow (11 to 13 ft) alluvium stratigraphy, physical properties, and engineering characteristics of the native soils.

The U.S. Bureau of Reclamation investigated surficial materials for the North Ramp Surface Facility of the Exploratory Studies Facility (U.S. Department of the Interior Bureau of Reclamation 1992). Their report is based on data from geologic mapping, pavement mapping, 73 test pits, laboratory data from seven test pits, and four drill holes: RF-1, -10, and -11, located in Midway Valley (unqualified data) and UE-25-NRG-1 located at the North Portal start station.

The U.S. Bureau of Reclamation study found that topsoil typically ranges from 0 to 3 ft of silty sand (SM), silty sand with gravel (SM), poorly graded gravel with sand (GP-GM), and silty gravel with sand (GM), is relatively loose, and contains roots. The soil at the site is primarily colluvium and alluvium, generally composed of silty sand (SM) and silty gravels (GM, GP-GM) with fines ranging from 4 to 30 percent. Some clayey sand (SC) and clayey gravel (SC, GC) with fines ranging from 29 to 40 percent are present but in very limited amounts. Physical property data and test pit logs for seven portal pad test pits and 39 road alignment test pits are provided by the U.S. Department of the Interior Bureau of Reclamation (1992). These seven portal pad test pits are representative of materials and foundation conditions for the Exploratory Studies Facility North Ramp Surface Facility. The soil is caliche-cemented from just below the surface to several feet deep adjacent to the hill and decreasing away from the hill.

All the soil in the North Ramp Surface Facility pad area is carbonate-cemented to some degree. The carbonate-cemented soil may be ripped to facilitate excavation. The prevalence of secondary carbonate-cementation throughout the pad area indicates that foundation bearing capacities determined by disturbed sampling methods or physical properties will be conservative. Practical methods to sample and test the gravelly materials at the site do not exist. Soil material had to be jack-hammered for removal for ring-density tests because of the soil cementation. However, in-place and relative densities were determined and can be used to assess the bearing capacity of the material. The material appears to be adequate for founding the relatively temporary, low-load structures contemplated. A suggested design value for bearing capacity is 1.1 ton/ft² per foot of footing width plus 1.9 ton/ft² per foot of depth. Calculations, estimated settlement, and references are contained in U.S. Department of the Interior, Bureau of Reclamation (1992).

Test pits along the road alignments indicate that soils generally consist of poorly graded silty gravel with varying amounts of sand, cobbles, and boulders. Slope recommendations based on natural slopes are that the colluvium and alluvium will stand at 1:1 for temporary slopes and 1 1/2:1 for permanent slopes (U.S. Department of the Interior, Bureau of Reclamation 1992). Occupational Safety and Health Administration requirements may dictate actual slopes used.

Because the material commonly has from 5 to 15 percent fines, initial fill placement tests should be performed using both laboratory compaction and relative density tests in order to establish the appropriate method of construction control. Both testing methods may be needed unless blending of materials is planned, because soils are present with less than and more than 5 to 15 percent fines.

Calcium carbonate cementation is present on the slopes along the base of Exile Hill, but was found to have not developed significantly in the area of the proposed leach field (U.S. Department of the Interior, Bureau of Reclamation 1992). Material excavated from one test pit, MWV-P-32, consisted mostly of gravel with silt and sand and silty sand with gravel.

Between 1988 and 1989 Holmes and Narver conducted two studies of three potential borrow pit areas for the Exploratory Studies Facility (Holmes and Narver 1988, 1989). These reports present estimated quantities of Type I and II aggregate and fill material. A gravel pit exists near the northeast side of Fran Ridge in Nevada Test Site Area 25 (U.S. Department of the Interior, Bureau of Reclamation 1992). The pit supplies select fill, road gravel, and backfill.